

**Modulation of Ca<sub>v</sub>2.3 voltage-gated calcium channels by  
trace metal ions and trace metal chelators.**

Inaugural-Dissertation

zur

Erlangung des Doktorgrades

der Mathematisch-Naturwissenschaftlichen Fakultät

der Universität zu Köln



vorgelegt von

Felix Neumaier

aus Köln

Köln, 2020

**Modulation of Ca<sub>v</sub>2.3 voltage-gated calcium channels by  
trace metal ions and trace metal chelators.**

Inaugural-Dissertation

zur

Erlangung des Doktorgrades

der Mathematisch-Naturwissenschaftlichen Fakultät

der Universität zu Köln

vorgelegt von

Felix Neumaier

aus Köln

Köln, 2020



Berichtersteller/in: Prof. Dr. Ludwig Eichinger  
Prof. Dr. Peter Kloppenburg  
Prof. Dr. Stefan Herzig

Tag der letzten mündlichen Prüfung: 27.04.2020

For Mom, Dad and my brother Moritz.

This thesis presents publications as originally published, reprinted with permission from the corresponding publishers. The introduction and discussion sections contain illustrations from publications 1 and 4, reproduced with permission from the corresponding publishers. The copyright of the original publications is held by the respective copyright holders, see the following copyright notices.

Publication 1: © 2015 Elsevier Ltd. Reprinted with permission. The original publication is available at ScienceDirect (<https://doi.org/10.1016/j.pneurobio.2014.12.003>)

Publication 2: © 2017 John Wiley and Sons. Reprinted with permission. The original publication is available at Wiley Online Library (<https://doi.org/10.1111/apha.12988>)

Publication 3: © 2018 Neumaier et al. The original publication is available at Rockefeller University Press (<https://doi.org/10.1085/jgp.201711880>)

Publication 4: © 2015 Elsevier Ltd. Reprinted with permission. The original publication is available at ScienceDirect (<https://doi.org/10.1016/j.bbamcr.2015.01.001>)

Publication 5: © 2018 John Wiley and Sons. Reprinted with permission. The original publication is available at Wiley Online Library (<https://doi.org/10.1111/jnc.14546>)

Publication 6: © 2020 Neumaier et al. The original publication is available at Rockefeller University Press (<https://doi.org/10.1085/jgp.202012585>)

## Table of contents

Summary .....	6
Zusammenfassung.....	8
1. Introduction.....	10
1.1. Voltage-gated Ca <sup>2+</sup> channels .....	10
1.1.1. Classification and nomenclature.....	10
1.1.2. Subunit composition .....	11
1.1.3. Structure .....	11
1.1.4. Functional properties.....	12
1.2. Ca <sub>v</sub> 2.3 voltage-gated Ca <sup>2+</sup> channels .....	15
1.2.1. Expression and general function.....	16
1.2.2. Role of Ca <sub>v</sub> 2.3 channels in the brain .....	16
1.2.3. Role of Ca <sub>v</sub> 2.3 channels for glucose homeostasis.....	17
1.2.4. Role of Ca <sub>v</sub> 2.3 channels in the vascular system .....	18
1.3. Endogenous trace metal ions.....	18
1.3.1. Trace metal speciation.....	18
1.3.2. Zn <sup>2+</sup> and Cu <sup>2+</sup> signaling in the brain.....	19
1.3.3. Zn <sup>2+</sup> signaling in pancreatic islets.....	20
1.3.4. Metal ion effects on voltage-gated Ca <sup>2+</sup> channels.....	21
1.4. Aims of the present work.....	23
2. Results .....	24
2.1. Publication 1: Progress in Neurobiology 129:1-36.....	24
2.2. Publication 2: Acta Physiologica 222(3): e12988. ....	61
2.3. Publication 3: Journal of General Physiology 150(3): 491-510. ....	80
2.4. Publication 4: Biochimica et Biophysica Acta 1853(5): 953-964. ....	101
2.5. Publication 5: Journal of Neurochemistry 147(3): 310-322. ....	114
2.6. Publication 6: Journal of General Physiology 152(9): e202012585. ....	128
3. Discussion .....	157
3.1. Mechanisms of Ca <sub>v</sub> 2.3 channel modulation by Zn <sup>2+</sup> and Cu <sup>2+</sup> .....	157
3.2. Trace metal chelators as functional Ca <sub>v</sub> 2.3 channel agonists .....	159
3.3. Ca <sub>v</sub> 2.3 channel modulation by endogenous brain Zn <sup>2+</sup> and Cu <sup>2+</sup> .....	159
3.4. Ca <sub>v</sub> 2.3 channels as a target for paracrine Zn <sup>2+</sup> signals in the pancreas.....	160
3.5. Conclusion .....	163
4. References.....	164
5. Declaration .....	179
6. Curriculum vitae .....	180

## Summary

**Background:** The trace metal ions  $Zn^{2+}$  and  $Cu^{2+}$  are increasingly recognized as endogenous modulators of neuronal transmission, hormone secretion and synaptic plasticity.  $Ca_v2.3$ -type voltage-gated  $Ca^{2+}$  channels (VGCCs) are among their most sensitive targets and have an expression pattern that coincides with the spatial distribution of histochemically reactive trace metals in the brain, suggesting that they could represent a main mediator for their reported neuro-modulatory effects. Although non-conserved histidine residues on the external side of domain I have been convincingly implicated in the effects of trace metals on  $Ca_v2.3$  channel gating, the exact mechanisms involved and their (patho)physiological relevance remain incompletely understood.

**Aims:** Aim of the articles compiled in the present thesis was to shed some light on the exact mechanisms of  $Zn^{2+}$ - and  $Cu^{2+}$ -induced  $Ca_v2.3$  channel modulation and their potential relevance under normal and pathophysiological conditions.

**Methods:** In publication 1, crystallographic data of a  $Ca^{2+}$ -selective bacterial model channel was used as a framework to theoretically analyze eukaryotic VGCC structure, function and modulation by inorganic cations. In publication 2, general protocols for preparation and use of metal ion-buffered solutions were developed and a fluorescent  $Zn^{2+}$  sensor was used to illustrate the importance of proper metal ion-buffering. In publication 3, conventional and perforated patch-clamp recordings together with different inhibitors and cytosolic factors were used to study  $Ca_v2.3$  channel run-down during electrophysiological recordings, which was critical to optimize the conditions for experiments performed in publication 6. In publication 4, the effects of intraperitoneal injection of the  $Zn^{2+}$  chelator DEDTC on blood glucose homeostasis, glucose tolerance and peptide hormone secretion in  $Ca_v2.3$ -deficient and -competent mice were analyzed, insulin secretion was examined in isolated islets of Langerhans from both genotypes and the  $Zn^{2+}$ -dependence of DEDTC effects on cloned  $Ca_v2.3$  channels was verified using whole-cell patch-clamp recordings. In publication 5, whole-cell patch-clamp and electroretinographic recordings were used to characterize a receptor-independent but  $Cu^{2+}$ -dependent mechanism of  $Ca_v2.3$  channel modulation by the glutamate-receptor agonist kainic acid (KA). In publication 6, whole-cell patch-clamp recordings were used to characterize  $Zn^{2+}$ -induced changes in  $Ca_v2.3$  channel function and to develop a Markov model for  $Ca_v2.3$  channel gating under control conditions and in the presence of physiological  $Zn^{2+}$  concentrations.

**Results:** Publication 1 provided novel insights into eukaryotic VGCC function and modulation by trace metal ions. Publication 2 demonstrated the critical importance of proper metal ion buffering to avoid deviations between nominal and actual free metal ion concentrations. Publication 3 showed that run-down of  $Ca_v2.3$  channel currents is associated with changes in channel gating and that it can be prevented or delayed by hydrolysable ATP through a mechanism that critically depends on protein phosphorylation by serine/threonine kinases. Publication 4 revealed severe glucose intolerance in  $Zn^{2+}$ -depleted  $Ca_v2.3$ -deficient but not vehicle-treated  $Ca_v2.3$ -deficient or  $Zn^{2+}$ -depleted wildtype mice. In addition, fasting glucose and glucagon levels were significantly higher in  $Ca_v2.3$ -deficient mice, whereas  $Zn^{2+}$  chelation significantly increased blood glucose and glucagon concentrations in wildtype but not  $Ca_v2.3$ -deficient mice. Application of DEDTC significantly stimulated cloned human  $Ca_v2.3$  channels when applied in the presence of  $Zn^{2+}$  but had no effect in the presence of the  $Zn^{2+}$  chelator CaEDTA. Publication 5 uncovered that KA can stimulate cloned human  $Ca_v2.3$  channels in the absence of functional KA receptors by reversing  $Cu^{2+}$ -induced suppression *in vitro*, presumably via formation of stable kainate- $Cu^{2+}$  complexes. When the chelator tricaine was used as a surrogate to study the receptor-independent effects of KA in the isolated bovine retina, it selectively reduced a late ERG b-wave component that was previously shown to be enhanced by

pharmacologic or genetic ablation of  $\text{Ca}_v2.3$  channels. Publication 6 demonstrated that  $\text{Zn}^{2+}$ -induced changes in  $\text{Ca}_v2.3$  channel function are complex and inconsistent with a single mechanisms of action. Computer simulations were used to show that most, but not all of the effects can be reconciled by a simplified Markov model that involves  $\text{Zn}^{2+}$  binding to a first site with an associated electrostatic modification and mechanical slowing of one of the voltage-sensors and  $\text{Zn}^{2+}$ -binding to a second, lower affinity site which blocks the channel and modifies the opening and closing transitions.

Discussion: With regard to  $\text{Zn}^{2+}$ -induced  $\text{Ca}_v2.3$  channel modulation, the results in publication 6 point to an intricate dependence on the prevailing neuronal properties and ionic conditions, which could profoundly influence and even invert the net  $\text{Zn}^{2+}$  action. Thus, due to  $\text{Zn}^{2+}$ -induced parallel changes in activation and inactivation voltage-dependence, the net action is strongly affected by the holding potential, can be either inhibitory or stimulatory and may persist for several minutes after cessation of the  $\text{Zn}^{2+}$  signal. This could conceivably play a role for certain forms of synaptic sensitization or plasticity, and might also be relevant for e.g. the regulation of  $\text{Ca}_v2.3$  channels in pancreatic islets, where sudden cessation of  $\text{Zn}^{2+}$  supply from  $\beta$ -cells is thought to serve as one of the switch-off signals for  $\alpha$ -cell glucagon secretion. In support of the latter notion, the findings in publication 4 provide evidence for an involvement of  $\text{Ca}_v2.3$  channels in the  $\text{Zn}^{2+}$ -mediated suppression of glucagon secretion during hyperglycemia and indicate that  $\text{Ca}_v2.3$  channel dysfunction could lead to severe disturbances in glucose homeostasis, especially under conditions of  $\text{Zn}^{2+}$ -deficiency. Based on the results of publications 5 and 6, a decrease or reversal of  $\text{Zn}^{2+}$  and  $\text{Cu}^{2+}$ -induced  $\text{Ca}_v2.3$  channel suppression by endogenous (i.e. glutamate) or exogenous (i.e. KA) trace metal chelators, moderate acidification or depolarization of the neuronal resting membrane potential could also contribute to the pro-convulsive role of  $\text{Ca}_v2.3$  channels demonstrated in previous investigations, although the pathophysiological relevance of these finding *in vivo* remains to be firmly established. Finally, the findings in publication 3 suggest that protein phosphorylation is required for normal  $\text{Ca}_v2.3$  channel function and that it could modify the normal properties of currents carried by these channels.

Conclusion: The articles compiled in this thesis provide several novel insights into the mechanisms underlying reciprocal  $\text{Ca}_v2.3$  channel modulation by trace metal ions and trace metal chelators as well as first evidence for their importance under (patho)physiological conditions. Moreover, while still far from complete, the model developed in publication 6 provides a quantitative framework for understanding  $\text{Zn}^{2+}$  effects on  $\text{Ca}_v2.3$  channel function and a first step towards the application of computational approaches for predicting the complex action of  $\text{Zn}^{2+}$  on neuronal excitability.

## Zusammenfassung

Hintergrund: Die Spurenmetallkationen  $Zn^{2+}$  und  $Cu^{2+}$  werden zunehmend als endogene Botenstoffe erkannt, welche in die Regulierung von neuronaler Erregbarkeit, Hormonfreisetzung und synaptischer Plastizität involviert sind.  $Ca_v2.3$  spannungsgesteuerte  $Ca^{2+}$  Kanäle gehören zu deren sensibelsten Targets und weisen ein Expressionsmuster auf, das mit der Verteilung von histochemisch reaktiven Spurenmetallkationen im Gehirn übereinstimmt, so dass sie einen Hauptmediator für deren neuro-modulatorischen Effekte darstellen könnten. Obwohl nicht-konservierte Histidinreste auf der extrazellulären Seite von Domäne I nachweislich eine Rolle für Spurenmetall-induzierte Veränderungen im Schaltverhalten von  $Ca_v2.3$  Kanälen spielen, sind viele Fragen bezüglich der zugrundeliegenden Mechanismen und ihrer (patho)physiologischen Relevanz bisher unbeantwortet.

Ziele: Ziel der in dieser Arbeit zusammengestellten Artikel war es, einen besseren Einblick in die exakten Mechanismen der  $Zn^{2+}$ - und  $Cu^{2+}$ -vermittelten Modulation von  $Ca_v2.3$  Kanälen sowie deren potentieller Bedeutung unter normalen und pathophysiologischen Bedingungen zu erhalten.

Methoden: In Publikation 1 wurden auf Basis kristallographischer Daten eines  $Ca^{2+}$ -selektiven bakteriellen Modellkanals die Struktur, Funktion und Modulation von eukaryotischen  $Ca^{2+}$  Kanälen theoretisch analysiert. In Publikation 2 wurden generelle Protokolle für die Herstellung und Verwendung von Spurenmetallionen-gepufferten physiologischen Lösungen erarbeitet und deren praktische Bedeutung mit einem fluoreszenten  $Zn^{2+}$  Indikator untersucht. In Publikation 3 wurden konventionelle und perforierte Ganzzell Patch-clamp Messungen sowie verschiedene Inhibitoren und zytosolische Faktoren verwendet um den Run-down von  $Ca_v2.3$  Kanälen während elektrophysiologischer Messungen zu untersuchen und die Messbedingungen für die Versuche in Publikation 6 zu optimieren. In Publikation 4 wurde untersucht, wie intraperitoneale Injektionen des Komplexbildners DEDTC die Blutglukose-Homöostase, Glukosetoleranz und Peptidhormonfreisetzung in  $Ca_v2.3$ -defizienten und -kompetenten Mäusen beeinflussen. Außerdem wurde die Insulinfreisetzung in isolierten Langerhans Inseln beider Genotypen verglichen sowie die  $Zn^{2+}$ -Abhängigkeit der Effekte von DEDTC auf rekombinante  $Ca_v2.3$  Kanäle in Ganzzell Patch-Clamp Messungen verifiziert. In Publikation 5 wurden Ganzzell Patch-clamp Messungen und elektroretinographische Ableitungen zur Charakterisierung eines Rezeptor-unabhängigen,  $Cu^{2+}$ -abhängigen Mechanismus der  $Ca_v2.3$  Kanal Modulation durch den Glutamaterezeptor Agonisten Kainsäure (KA) untersucht. In Publikation 6 wurden die elektrophysiologischen Effekte von  $Zn^{2+}$  auf rekombinante  $Ca_v2.3$  Kanäle untersucht und ein Markov Model für deren Schaltverhalten unter Kontrollbedingungen sowie in Gegenwart physiologisch relevanter  $Zn^{2+}$  Konzentrationen entwickelt.

Ergebnisse: Publikation 1 erbrachte neue Erkenntnisse zur Funktion eukaryotischer spannungsgesteuerter  $Ca^{2+}$  Kanäle und deren Modulation durch Spurenmetallkationen. Publikation 2 veranschaulichte die Wichtigkeit von Metallionen-Puffern zur Vermeidung von Abweichungen zwischen der nominellen und tatsächlichen freien Metallionenkonzentration in physiologischen Lösungen. Publikation 3 ergab, dass der Run-down von  $Ca_v2.3$  Kanälen mit Veränderungen im Schaltverhalten verbunden ist, dass er durch hydrolysierbares ATP verhindert oder verlangsamt werden kann und dass Serin/Threonin Kinasen kritisch für die protektiven ATP Effekte sind. Publikation 4 ergab, dass Blutglukose und Serum Glukagon Spiegel in  $Ca_v2.3$ -defizienten Mäusen im Vergleich zu  $Ca_v2.3$ -kompetenten Mäusen signifikant erhöht sind, während  $Zn^{2+}$  Depletion mit DEPC zu einem signifikanten Anstieg von Blutglukose und Serum Glukagon Spiegeln in  $Ca_v2.3$ -kompetenten aber nicht in  $Ca_v2.3$ -defizienten Mäusen führt. DEPC Behandlung führte außerdem zu einer schweren Glukoseintoleranz in  $Ca_v2.3$ -defizienten Mäusen, während die Glukosetoleranz in unbehandelten  $Ca_v2.3$ -defizienten sowie behandelten

und unbehandelten Cav2.3-kompetenten Mäusen unbeeinträchtigt war. In *in vitro* Versuchen stimulierte DEPC den Ca<sup>2+</sup> Einfluss durch rekombinante Cav2.3 Kanäle in der Gegenwart von Zn<sup>2+</sup> aber nicht in der Gegenwart des Zn<sup>2+</sup> Komplexbildners CaEDTA. Publikation 5 ergab, dass KA rekombinante Cav2.3 Kanäle durch eine Umkehr Cu<sup>2+</sup>-induzierter Inhibition, die vermutlich auf Bildung stabiler Kainat-Cu<sup>2+</sup> Komplexe beruht, auch in Abwesenheit funktioneller Glutamat Rezeptoren stimulieren könnte. Simulation der Rezeptor-unabhängigen Effekte von KA durch Applikation des Komplexbildners Tricin in der isolierten Rinderretina führte zur selektiven Abnahme in der Amplitude einer späten Komponente der elektroretinographischen b-Welle, für welche in früheren Arbeiten eine Stimulation durch genetische oder pharmakologische Ablation von Cav2.3 Kanälen gezeigt wurde. Publikation 6 ergab, dass die Zn<sup>2+</sup>-induzierten Veränderungen im Schaltverhalten von Cav2.3 Kanälen komplex sind und mehr als einen einzelnen Wirkmechanismus umfassen. Mittels Computersimulationen wurde gezeigt, dass die meisten, aber nicht alle, Effekte durch ein vereinfachtes Modell reproduziert werden können, bei dem Zn<sup>2+</sup> Interaktion mit einer ersten Bindungsstelle zu einer elektrostatischen Modifikation und mechanischen Verlangsamung eines der Spannungssensoren führt und Zn<sup>2+</sup> Interaktion mit einer zweiten Bindungsstelle von niedrigerer Affinität den Kanal blockiert und zu einer Verlangsamung des Öffnungs- und Schließverhaltens führt.

Diskussion: Bezüglich der Zn<sup>2+</sup>-induzierten Modulation von Cav2.3 Kanälen deuten die Ergebnisse aus Publikation 6 auf komplexe Wechselwirkungen mit den vorherrschenden neuronalen und ionischen Bedingungen hin, welche die Zn<sup>2+</sup> Wirkung beeinflussen und sogar umkehren könnten. So hängt der Gesamt Zn<sup>2+</sup> Effekt auf Cav2.3 Kanäle aufgrund paralleler Veränderungen in der Spannungsabhängigkeit von Aktivierung und Inaktivierung stark vom Haltepotential ab, kann sowohl inhibierend als auch stimulierend sein und für mehrere Minuten nach Beendigung des Zn<sup>2+</sup> Signals andauern. Neben einer möglichen Rolle für bestimmte Mechanismen der synaptischen Sensibilisierung und Plastizität könnten diese Effekte für die Regulation von Cav2.3 Kanälen in den Langerhans Inseln des Pankreas relevant sein, wo eine plötzliche Einstellung der Zn<sup>2+</sup> Freisetzung aus  $\beta$ -Zellen als eines der Switch-off Signale für die Glukagon Freisetzung aus  $\alpha$ -Zellen zu dienen scheint. Letztere Annahme wird durch die Ergebnisse in Publikation 4 untermauert, welche erste Belege für eine Rolle von Cav2.3 Kanälen für die Zn<sup>2+</sup>-vermittelte Inhibition der Glukagonfreisetzung unter hyperglykämischen Bedingungen liefern und zeigen, dass Cav2.3 Kanaldysfunktion, besonders in Kombination mit Zn<sup>2+</sup>-Defizienz, zu schweren Störungen der Glukosehomöostase führen könnte. Basierend auf den Ergebnissen der Publikationen 5 und 6 könnte eine Abnahme bzw. Umkehr der Zn<sup>2+</sup> und Cu<sup>2+</sup> vermittelten Inhibition von Cav2.3 Kanälen durch endogene (z.B. Glutamat) oder exogene (z.B. KA) Komplexbildner, mäßige Acidose oder Depolarisation des neuronalen Ruhemembranpotentials möglicherweise auch zur pro-convulsiven Rolle dieser Kanäle beitragen, welche in früheren Arbeiten belegt wurde. Schließlich legen die Ergebnisse aus Publikation 3 nahe, dass Proteinphosphorylierung kritisch für die normale Funktion von Cav2.3 Kanälen ist und ihre elektrophysiologischen Eigenschaften modifizieren könnte.

Konklusion: Die in dieser Arbeit zusammengestellten Artikel liefern verschiedene neue Erkenntnisse über die Mechanismen der reziproken Modulation von Cav2.3 Kanälen durch Spurenmetallkationen und Komplexbildner sowie erste Erkenntnisse zu ihrer möglichen Bedeutung unter (patho)physiologischen Bedingungen. Obwohl das in Publikation 6 erarbeitete Model als vorläufig anzusehen ist, bietet es eine quantitative Grundlage zum Verständnis der Effekte von Zn<sup>2+</sup> auf Cav2.3 Kanäle und einen ersten Schritt in Richtung der Anwendung computerbasierter Methoden zur Prognose der komplexen Wirkung von Zn<sup>2+</sup> auf die neuronale Erregbarkeit.



## 1. Introduction

### 1.1. Voltage-gated Ca<sup>2+</sup> channels

Under physiological conditions, intracellular Ca<sup>2+</sup> levels are tightly controlled and maintained in the low nanomolar concentration range. Ca<sup>2+</sup> can enter the cell through voltage-gated Ca<sup>2+</sup> channels (VGCCs), which shape the electrical properties of excitable cells and represent the key link between electrical signals and non-electrical processes, such as transmitter release, peptide hormone secretion or gene transcription. The following sections will briefly describe their classification, structure and function. A more detailed description that goes beyond a mere recap of the literature is provided in publication 1 (Neumaier et al., 2015).

#### 1.1.1. Classification and nomenclature

Since their first recording in cardiomyocytes (Reuter, 1979, 1967), voltage-dependent Ca<sup>2+</sup> currents in native membranes have been broadly classified into (i) low-voltage activated (LVA) currents which activate at membrane potentials near the resting level and display rapid inactivation kinetics and (ii) high-voltage activated (HVA) currents, which activate at somewhat more depolarized test potentials and display variable but typically less rapid inactivation kinetics (Carbone and Lux, 1984; Nowycky et al., 1985). Based on their biophysical and pharmacological properties, HVA currents were further subdivided into dihydropyridine-sensitive L-type (for long lasting),  $\omega$ -conotoxin GVIA-sensitive N-type (for neuronal or neither T- nor L-type),  $\omega$ -agatoxin IVA-sensitive P/Q-type (for Purkinje neurons) and partly SNX-482-sensitive R-type (for resistant or residual) currents, while LVA currents were assigned to a single group of T-type (for transient) currents (Llinás et al., 1992; Nowycky et al., 1985; Randall and Tsien, 1995; Tsien et al., 1987). Purification (Curtis and Catterall, 1984), reconstitution (Curtis and Catterall, 1986; Flockerzi et al., 1986) and molecular cloning (Tanabe et al., 1987) of the skeletal muscle Ca<sup>2+</sup> channel in the late 1980s and subsequent homology screening of lambda-phage and cDNA libraries firmly established the existence of multiple, distinct Ca<sup>2+</sup> channel  $\alpha_1$ -subunits (Catterall, 2011; Hille, 1992). They were originally named based on an alphabetical nomenclature, which assigned the letter S to the original skeletal muscle channel (i.e.  $\alpha_{1S}$ ) and the letters A-F to subsequently identified  $\alpha_1$ -subunits (Birnbaumer et al., 1994; Snutch et al., 1990; Snutch and Reiner, 1992). Today, VGCCs are classified based on amino acid sequence identity and named according to the same nomenclature used for other voltage-gated ion channels, where a given  $\alpha_1$ -subunit is identified by the principal permeating ion (i.e. Ca for Ca<sup>2+</sup>), the main physiological regulator (i.e. v for voltage) indicated as a subscript (i.e. Ca<sub>v</sub>) and a numerical identifier that corresponds to one of three subfamilies (Ca<sub>v</sub>1 through Ca<sub>v</sub>3) and the order of discovery within that subfamily (Catterall et al., 2003; Ertel et al., 2000). Based on pharmacological and functional criteria, the Ca<sub>v</sub>1 family (Ca<sub>v</sub>1.1 through Ca<sub>v</sub>1.4) has been convincingly linked to native L-type currents, the Ca<sub>v</sub>2 family to native P/Q-type (Ca<sub>v</sub>2.1), N-type (Ca<sub>v</sub>2.2) and R-type (Ca<sub>v</sub>2.3) currents and the Ca<sub>v</sub>3 family (Ca<sub>v</sub>3.1 through Ca<sub>v</sub>3.3) to native T-type currents.

### 1.1.2. Subunit composition

Similar to other voltage-gated ion channels, native HVA channels are multi-subunit complexes comprised of a principal, transmembrane-spanning  $\text{Ca}_v\alpha_1$ -subunit, several auxiliary subunits of lower molecular weight and the ubiquitous intracellular  $\text{Ca}^{2+}$ -sensor calmodulin (CaM), which associates with a CaM-binding domain in the cytoplasmic C-terminal region. Expression levels and the properties of  $\text{Ca}_v\alpha_1$ -subunits vary with co-expression of one of at least four  $\text{Ca}_v\beta$ -subunits, one of at least four  $\text{Ca}_v\alpha_2\delta$ -subunits and in some cases one of several putative  $\text{Ca}_v\gamma$ -subunits. Additional diversity arises from a number of possible splice variants and posttranslational modification of the  $\text{Ca}_v\alpha_1$  or other subunits (Jones, 1998; Lacinová, 2005). LVA channels on the other hand lack the CaM-binding domain and are typically thought to consist only of a pore-forming  $\text{Ca}_v\alpha_1$ -subunit (Lacinová et al., 1999; Lambert et al., 1997; Leuranguer et al., 1998).

### 1.1.3. Structure

As illustrated in Fig. 1,  $\text{Ca}_v\alpha_1$ -subunits are made up of four homologous repeats termed domains I through IV, each comprising six membrane-spanning helical segments (S1-S6) and a pore forming p-loop between S5 and S6 (Zhen et al., 2005). The first four segments of each domain have been shown to form the voltage-sensor modules (VSMs) responsible for coupling changes in membrane potential to channel opening. The remaining two segments make up most of the internal pore lining, with the p-loops forming the extracellular mouth of

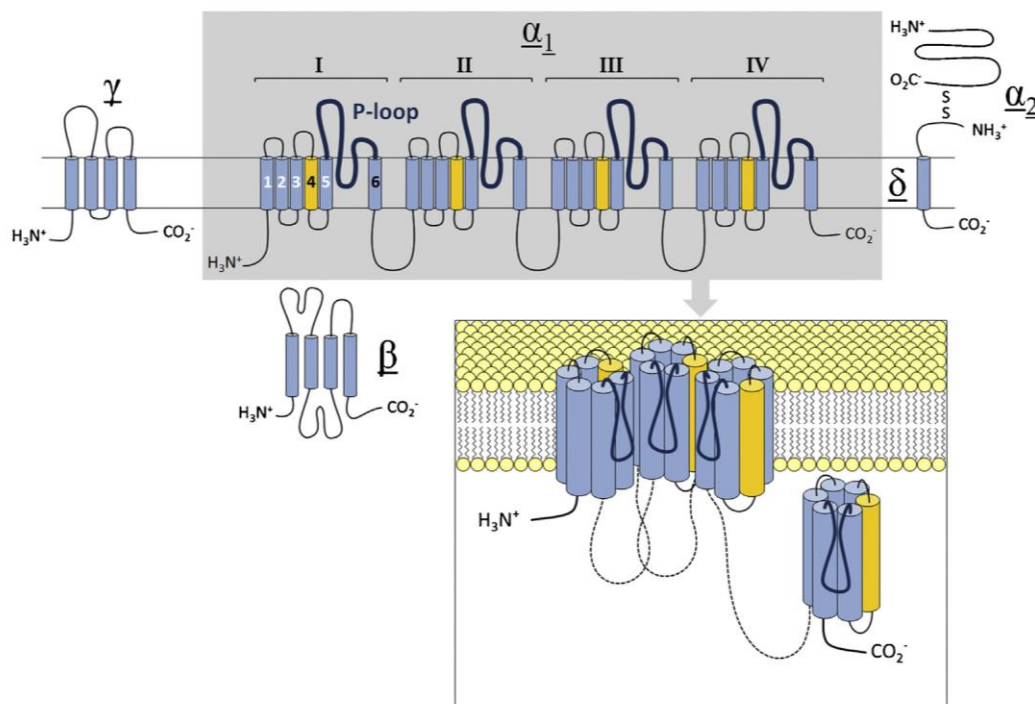


**Figure 1.** Subunit composition and transmembrane topology of high-voltage activated calcium channels. Inset shows quadrameric arrangement of homologous domains of the pore-forming  $\alpha_1$  subunit at the cell membrane. For clarity, domain IV is shown aside from the membrane. Reprinted with permission from (Neumaier et al., 2015).

the pore and the Ca<sup>2+</sup> selective filter region (Kim et al., 1993; Yang et al., 1993). Cav $\beta$ -subunits are intracellular, hydrophilic proteins without transmembrane segments (**Fig. 1**), which bind to a high-affinity site located in the cytoplasmic linker between the first two homologous repeats of the Cav $\alpha$ 1-subunit (Buraei and Yang, 2013). Cav $\alpha$ 2 $\delta$ -subunits are made up of two distinct subunits ( $\alpha$ 2 and  $\delta$ ), formed by post-translational cleavage of a single gene product and associated with each other via disulfide bonds (Ellis et al., 1988). As indicated in **Fig. 1**, the highly glycosylated  $\alpha$ 2-subunit resides on the extracellular side and is thought to be anchored in the plasma membrane by the smaller  $\delta$  protein (Gurnett et al., 1996).

#### **1.1.4. Functional properties**

The classical view of voltage-gated ion channels assumes that transfer of ions across the membrane (permeation) is independent of the transitions between non-conducting and conducting states (gating) and vice versa. This assumption is conceptually useful and often necessary for interpretation of experimental findings, but there is convincing evidence for an interaction between gating and permeation in VGCCs (for details see publication 1).

##### **1.1.4.1. Voltage-dependent activation**

Activation of all voltage-gated ion channels involves charge-moving conformational changes that produce measurable gating currents and have been shown to depend on charged residues in the S2, S3 and especially S4 segments of all four domains (Hille, 1992; Vargas et al., 2012). A possible mechanism for the process based on models for activation of Shaker K<sup>+</sup>-channels is shown in **Fig. 2A & B**. At resting membrane (i.e. hyperpolarized) potentials, the permeation pathway is occluded by parts of the S6 segments, which form a hydrophobic cavity that is inaccessible for ions. Depolarization forces the positively charged S4 segments to rotate or tilt through a protein-lined pathway formed by the rest of the VSM, which leads to relocation of the S5 and S6 segments with formation of a water-filled and ion permeable crevice. Evidence from mutational studies (Beyl et al., 2016; García et al., 1997) and optical tracking of voltage-sensor movement (Pantazis et al., 2014) indicates that activation of only two of the four non-identical VSM may be sufficient to drive channel opening in VGCCs.

##### **1.1.4.2. Voltage- and Ca<sup>2+</sup>-dependent inactivation**

The extent of Ca<sup>2+</sup> entry during prolonged depolarization is limited by voltage- or Ca<sup>2+</sup>-dependent inactivation, which may involve distinct conformational changes and can vary with the exact subunit composition. Voltage-dependent inactivation (VDI) of HVA channels has been linked to parts of the pore-forming segments and intracellular linkers (Hering et al., 2000; Stotz et al., 2000) and proposed to involve a ‘hinged lid’ mechanism, where docking of the I-II linker to the cytoplasmic ends of the S6 segments occludes the inner pore vestibule (**Fig. 2C**)(Stotz et al., 2004, 2000). The process appears to be state- rather than truly voltage-dependent and is subject to modulation by co-expressed Cav $\beta$ -subunits, which may modify mobility of the I-II linker (Stotz et al., 2004). Ca<sup>2+</sup>-dependent inactivation is largely restricted to otherwise non-inactivating (Cav1.1-Cav1.4) or certain neuronal channels (Cav2.1 and Cav2.2) and thought to be induced by formation of Ca<sup>2+</sup>/CaM complexes (Budde et al., 2002).

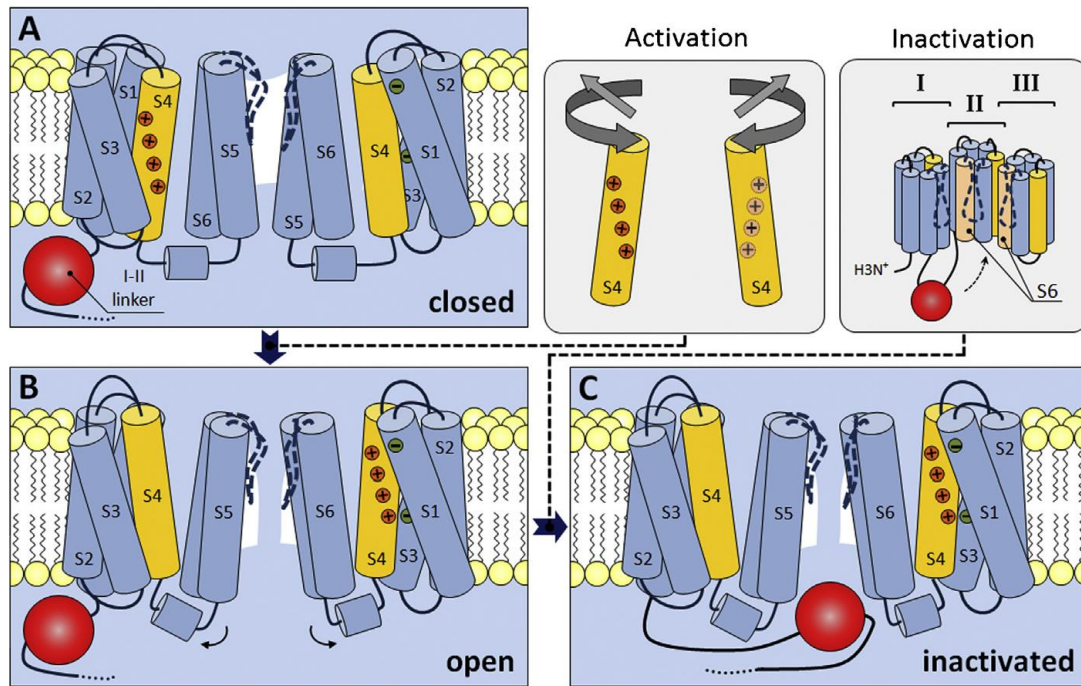


**Figure 2.** Conformational changes during activation and inactivation of VGCCs. Cartoon illustrating possible mechanisms of channel activation and inactivation based on models of activation for Shaker K<sup>+</sup>-channels and fast VDI of Ca<sub>v</sub>2.3 VGCCs. Only two of the four homologous domains are shown. **(A)** At resting membrane potentials, the permeation pathway is occluded by regions of the S6 segments which form parts of the channel lumen, resulting in a hydrophobic cavity that is inaccessible for ions. **(B)** During membrane depolarization, the positively charged S4 segments (yellow) rotate and decrease their tilt (see inset), leading to changes in the relative position of other segments and formation of a water-filled crevice, in which ions can traverse the channel. **(C)** Upon prolonged depolarization, the intracellular linker between domains I and II (highlighted in red) docks to a site composed, in parts, of the S6 segments of domains II and III (see inset), thereby physically occluding the inner vestibule of the channel and terminating the flow of ions. Reprinted with permission from (Neumaier et al., 2015).

#### 1.1.4.3. Selective permeation

Under physiological conditions, VGCCs are almost exclusively selective for Ca<sup>2+</sup>, with estimated rate coefficients for overall Ca<sup>2+</sup> transfer of  $7.5 \times 10^7 \text{ M}^{-1} \text{ s}^{-1}$  for HVA channels (Hess et al., 1986) and  $0.3\text{-}0.5 \times 10^8 \text{ M}^{-1} \text{ s}^{-1}$  for LVA channels (Carbone and Lux, 1987; Lux et al., 1990). Selectivity is mainly conferred by a conserved high-affinity Ca<sup>2+</sup> binding site in the pore region, which is formed by a ring of glutamate (and in LVA channels aspartate) residues located at equivalent positions in each of the four p-loops (EEEE/EEDD-locus) (Cens et al., 2007; Cibulsky and Sather, 2000; Ellinor et al., 1995; Shuba, 2014; Talavera et al., 2001; Tang et al., 1993; Yang et al., 1993). Several mechanisms have been proposed to account for the apparent paradox of high-affinity binding and high conductance, most of which are based on a combination of ion-pore and ion-ion interactions in the permeation pathway. In the classical 'stairstep model', low-affinity binding sites flanking the EEEE/EEDD-locus are thought to allow for stepwise entry and exit of Ca<sup>2+</sup> ions from the pore, thereby lowering the energy required for dissociation from the high-affinity binding site (Dang and McCleskey,

1998). In the ‘car wash model’, the EEEE/EEDD-locus is thought to form a flexible, multi-ion binding site that can accommodate a single  $\text{Ca}^{2+}$  ion with high-affinity or multiple  $\text{Ca}^{2+}$  ions with lower affinity (Yang et al., 1993). Occupation by more than one  $\text{Ca}^{2+}$  ion could destabilize high-affinity binding due to electrostatic repulsion (Almers and McCleskey, 1984; Hess and Tsien, 1984), competition for binding moieties (Armstrong and Neyton, 1991; Yang et al., 1993) and / or conformational changes (Lux et al., 1990; Mironov, 1992). Support for a mechanism akin to the stairstep model has been provided by crystallographic data on the  $\text{Ca}^{2+}$ -selective model channel  $\text{Ca}_v\text{Ab}$ , which was derived from the bacterial sodium channel  $\text{Na}_v\text{AB}$ . In this channel and several related constructs, the selectivity filter is formed by a central high-affinity DDDD-locus and two flanking low-affinity sites (Fig. 3A-C), which are at least partly conserved in human VGCCs (Fig. 3D).

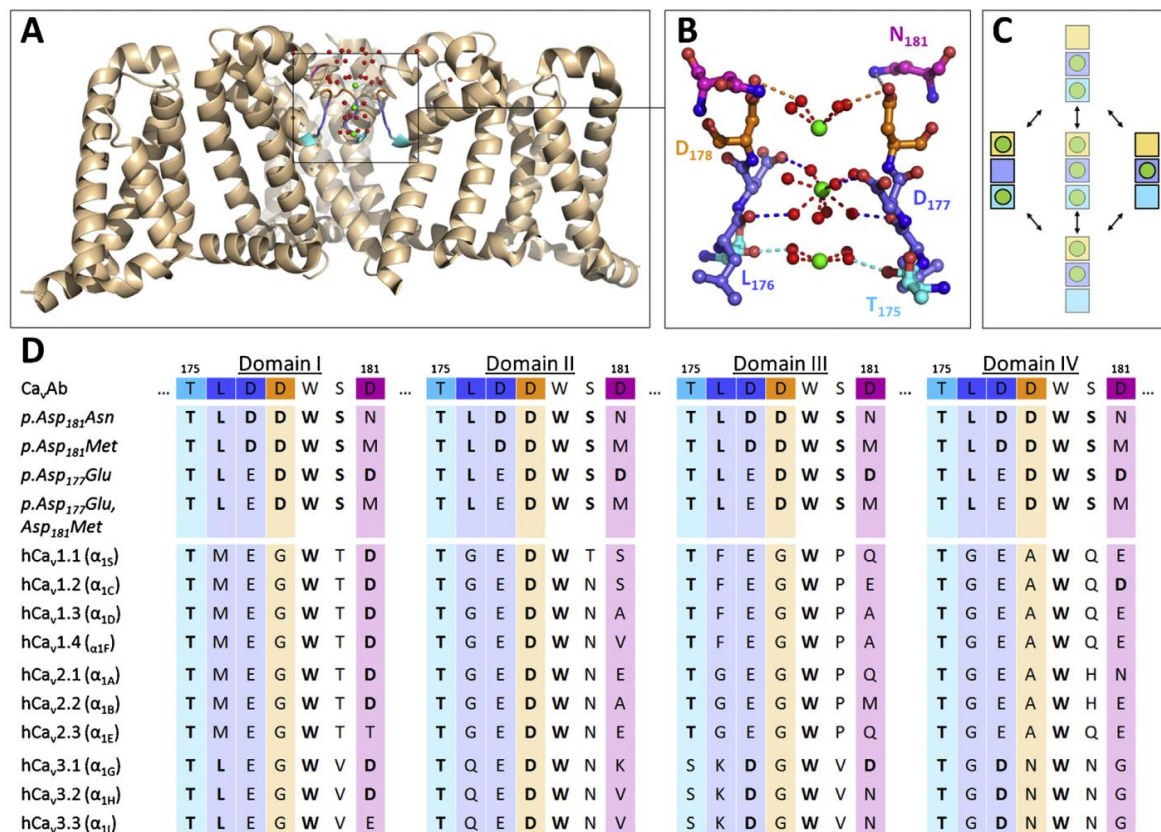


**Figure 3.** Functional organization of the selectivity filter in voltage-gated calcium channels. (A, B) Cartoon representation of the crystal structure of *pAsp181Asn* (a construct closely related to  $\text{Ca}_v\text{Ab}$ ) showing three of the four identical domains with  $\text{Ca}^{2+}$  ions (green) bound to all three coordination sites in the selectivity filter. Note that the crystal structure likely reflects a mixed population of channels, in which either the central or the two flanking coordination sites are occupied. (C) State-diagram showing the two low energy states of occupation and possible intermediates. (D) Sequence alignment of residues making up the selectivity filter in  $\text{Ca}_v\text{Ab}$  and its derivatives with the corresponding residues in cloned human voltage-gated calcium channels. Conserved residues are highlighted in bold. Reprinted with permission from (Neumaier et al., 2015).



#### **1.1.4.4. Run-up and run-down**

Electrophysiological recordings associated with dialysis of the cytoplasm or excision of cell patches are almost invariably hampered by time-dependent changes in voltage-gated ion channel function. The most well-known form of these phenomena is a progressive decline of voltage activated currents after breakthrough into the whole-cell configuration (run-down). The process is typically thought to result from dilution of the cellular contents by the pipette solution and an associated loss of second messengers and intracellular signaling cascades (Becq, 1996). In some cases, run-down is preceded by a transient current facilitation, which could reflect a relief of tonic suppression and / or voltage- and time-dependent repriming (i.e. recovery from inactivation) (Elhamdani et al., 1995, 1994; Tiaho et al., 1993). While they remain a major obstacle for studies on the pharmacology and physiology of voltage-gated channels, these time-dependent changes can also provide insight into the modulation of channels in intact cells. For this reason, the hallmarks and mechanisms of run-down of L-type  $\text{Ca}^{2+}$  currents have been subject to numerous investigations (Belles et al., 1988; Chad and Eckert, 1986; Hao et al., 1999; Hescheler et al., 1988; Martini et al., 2000; McDonald et al., 1994; Mironov and Lux, 1991). Probably owing to their minor contribution to the total  $\text{Ca}^{2+}$  current in many non-neuronal cells, much less work has been devoted to characterizing the process in other HVA VGCCs. For example, native R-type currents, which are mainly mediated by  $\text{Ca}_v2.3$ -type VGCCs, are well known to exhibit both run-up and run-down (Almog and Korngreen, 2009; Benquet et al., 1999; Cota, 1986; Hilaire et al., 1997). Although some findings indicate that run-down may be associated with changes in R-type-like  $\text{Ca}^{2+}$  channel gating (Cota, 1986), the rapid loss of these currents in conventional electrophysiological recordings has generally prevented further characterization of the phenomenon in native cells. Some of the experiments performed in the present work were also hampered by time-dependent changes in  $\text{Ca}_v2.3$  channel currents, which prompted us to investigate the process in more detail. The results of these experiments allowed us to develop experimental conditions that significantly delayed the occurrence of run-down and provided interesting insights into the importance of protein phosphorylation for the normal function of  $\text{Ca}_v2.3$  channels, as described in more detail in publication 3 (Neumaier et al., 2018b).

#### **1.2. $\text{Ca}_v2.3$ voltage-gated $\text{Ca}^{2+}$ channels**

$\text{Ca}_v2.3$ -type VGCCs are the only molecular counterpart of native R-type currents so far identified and remain one of the most enigmatic members of the family of VGCCs, not least because they share biophysical properties with both HVA (high activation threshold; large single channel conductance; rapid deactivation kinetics) and LVA (equal permeability to  $\text{Ca}^{2+}$  and  $\text{Ba}^{2+}$ ; fast inactivation kinetics) channels (Bourinet et al., 1996; Soong et al., 1993; Wakamori et al., 1994). They are resistant towards most commonly used organic  $\text{Ca}^{2+}$  channel antagonists but highly sensitive to certain divalent trace metal ions ( $\text{Zn}^{2+}$ ,  $\text{Cu}^{2+}$  and  $\text{Ni}^{2+}$ ), which has been linked to non-conserved histidine residues on the external side of the domain I VSM (Kang et al., 2007; Shcheglovitov et al., 2012). In addition,  $\text{Ca}_v2.3$  channels are sensitive to the tarantula toxin SNX-482 ( $\text{IC}_{50}$ =20-60 nM), which is a relatively selective inhibitor when

compared to other VGCCs, but has been shown to be even more effective in suppressing A-type  $K^+$ -currents mediated by  $K_v4.3$  channels ( $IC_{50} < 3$  nM) (Kimm and Bean, 2014).

### **1.2.1. Expression and general function**

$Ca_v2.3$  channel expression is most prominent throughout the central and peripheral nervous system (Grabsch et al., 1999; Schneider et al., 1994; Soong et al., 1993; Williams et al., 1994), but has also been detected in neuroendocrine (Grabsch et al., 1999; Pereverzev et al., 2002b; Vajna et al., 1998), cardiovascular (Galetin et al., 2013), reproductive (Cohen et al., 2014; Wennemuth et al., 2000), and gastrointestinal tissues (Grabsch et al., 1999). Insight into the functional roles of  $Ca_v2.3$  channels has been facilitated by the generation of  $Ca_v2.3$ -deficient mice, which exhibit no major pathologies but are characterized by altered spatial memory (Kubota et al., 2001) and nociception (Saegusa et al., 2000), increased anxiety (Lee et al., 2002), cardiac arrhythmias and impaired autonomic control (Galetin et al., 2013; Weiergräber et al., 2005), reduced susceptibility to chemically induced seizures and excitotoxicity (Dibué-Adjei et al., 2017; Weiergräber et al., 2007) and certain alterations in glucose homeostasis (Matsuda et al., 2001; Pereverzev et al., 2002a). Based on this relatively subtle phenotype and their preferential expression in rhythmically active tissues, a general function of  $Ca_v2.3$  channels has been proposed to involve fine-tuning of rhythmogenesis in oscillatory networks (Schneider et al., 2015).

### **1.2.2. Role of $Ca_v2.3$ channels in the brain**

In the CNS, highest densities of  $Ca_v2.3$  channels can be detected in the hippocampus and other limbic regions, in the retina and in cortical neurons (Sochivko et al., 2002; Weiergräber et al., 2006b). They are expressed both presynaptically (Day et al., 1996) and postsynaptically (Day et al., 1996; Yokoyama et al., 1995) and have been shown to be involved in transmitter release and neuronal plasticity (Bloodgood and Sabatini, 2007; Dietrich et al., 2003; Gasparini et al., 2001; Yasuda et al., 2003), somatodendritic integration and action potential burst firing (Christie et al., 1995; Kavalali et al., 1997; Magee and Carruth, 1999; Magee and Johnston, 1995). In addition,  $Ca_v2.3$  channels are the third most extensively phosphorylated ion channels in mouse brain (Cerda et al., 2011) and depolarization has been shown to trigger bulk changes of their phosphorylation state in intact hippocampal slices (Hell et al., 1995). In the retina,  $Ca_v2.3$  channels appear to be involved in GABA-ergic reciprocal inhibition of rod bipolar cells (Siapich et al., 2009), and genetic ablation or pharmacological suppression of these channels have been shown to selectively enhance a late b-wave component of the electroretinogram (ERG) (Alnawaiseh et al., 2011; Lüke et al., 2005; Siapich et al., 2010). The exact physiological relevance of  $Ca_v2.3$  channels in most other brain regions remains elusive, but there is increasing evidence for their involvement in a number of pathophysiological conditions. With regard to human patients, recent findings have implicated de novo gain-of-function mutations in these channels with developmental and epileptic encephalopathies, which are characterized by intractable seizures, abundant epileptiform EEG activity and developmental impairments (Carvill, 2019; Helbig et al., 2018). A pro-ictogenic role of  $Ca_v2.3$  channels in convulsive generalized tonic-clonic and hippocampal seizures has also been

demonstrated in a number of animal studies, where their genetic ablation significantly reduced the susceptibility to kainic acid (KA)-induced seizures and neurodegeneration (Dibué-Adjei et al., 2017; Weiergräber et al., 2007, 2006a). In addition, treatment with the broad-spectrum antiepileptic drugs lamotrigine (LTG) or topiramate (TPM), both of which have been shown to inhibit cloned  $\text{Ca}_v2.3$  channels (Hainsworth et al., 2003; Kuzmiski et al., 2005), significantly reduced KA-induced seizures in wildtype but not  $\text{Ca}_v2.3$ -deficient mice (Dibué-Adjei et al., 2017), suggesting that  $\text{Ca}_v2.3$  channels could be an important target for current antiepileptic treatments.

### **1.2.3. Role of $\text{Ca}_v2.3$ channels for glucose homeostasis**

Animal studies have linked  $\text{Ca}_v2.3$  VGCCs to  $\alpha$ -cell glucagon secretion (Pereverzev et al., 2005),  $\beta$ -cell insulin secretion (Jing et al., 2005; Matsuda et al., 2001; Pereverzev et al., 2002a) and  $\delta$ -cell somatostatin (SST) secretion (Zhang et al., 2007), suggesting that these channels are critically involved in the regulation of blood glucose levels. Under hyperglycemic conditions, glucose homeostasis is primarily maintained by glucose-stimulated insulin secretion (GSIS) from pancreatic  $\beta$ -cells, which is thought to involve a triggering pathway of fast insulin secretion (first phase insulin response), and an amplifying pathway of sustained release (second phase insulin response). The molecular mechanisms underlying fast GSIS are relatively well established and have been shown to involve  $\beta$ -cell glucose uptake and metabolism followed by depolarization due to ATP-dependent closure of  $\text{K}_{\text{ATP}}$  channels, which triggers  $\text{Ca}^{2+}$ -influx through  $\text{Ca}_v1.2$  channels and secretion of a readily releasable pool of insulin vesicles. The sustained insulin response is much less well understood but thought to involve mobilization of a reserve pool of insulin vesicles for release. Genetic or pharmacological ablation of  $\text{Ca}_v2.3$  channels selectively reduces the second phase insulin response in mice (Jing et al., 2005; Pereverzev et al., 2005), suggesting that  $\beta$ -cell  $\text{Ca}_v2.3$  channels are involved in the mobilization of insulin vesicles from the reserve pool. They could also play a role for the paracrine effects of SST released from  $\delta$ -cells, as SST suppresses cloned  $\text{Ca}_v2.3$  channels (Mehrke et al., 1997) and SNX-482 has been shown to prevent SST inhibition of insulin secretion from insulinoma cells (Mergler et al., 2008). According to the intra-islet insulin hypothesis, insulin released into the periportal circulation is carried to nearby  $\alpha$ -cells, where it provides tonic suppression of glucagon secretion during hyperglycemia, while cessation of insulin secretion during hypoglycemia could serve as a switch-off signal that initiates  $\alpha$ -cell glucagon secretion (Banarar et al., 2002; Maruyama et al., 1984). Interestingly,  $\text{Ca}_v2.3$  channels appear to be important for the former (i.e. suppression of glucagon release during hyperglycemia) but not directly involved in the latter (i.e. release of glucagon during hypoglycemia), as glucose-induced suppression of glucagon release is severely impaired or even reversed in  $\text{Ca}_v2.3$ -deficient mice (Jing et al., 2005), isolated islets from  $\text{Ca}_v2.3$ -deficient mice (Jing et al., 2005; Pereverzev et al., 2005) and SNX-482 treated islets from wildtype mice (Göpel et al., 2004; Jing et al., 2005) whereas SNX-482 fails to reduce glucagon secretion from wildtype islets in low glucose. As discussed in more detail in section 1.3.3 and assessed experimentally in publication 4 (section 2.4), there is increasing evidence that  $\text{Zn}^{2+}$  co-released with insulin from pancreatic  $\beta$ -cells could serve as an



additional, non-insulin signal for crosstalk to neighboring  $\alpha$ -cells, which might exert its action in part by suppressing  $\text{Ca}_v2.3$  channels. The pathophysiological relevance of these findings is corroborated by several studies linking variants in the gene encoding  $\text{Ca}_v2.3$  channels to impaired glucose homeostasis in human T2DM patients (Holmkvist et al., 2007; Muller et al., 2007; Trombetta et al., 2012).

#### **1.2.4. Role of $\text{Ca}_v2.3$ channels in the vascular system**

There is also evidence for a role of  $\text{Ca}_v2.3$  channels in the vascular system, although again mainly in the context of certain pathophysiological conditions. For example, hemoglobin, which can be released into the brain extracellular space during hemorrhagic stroke, has been shown to induce up-regulation of  $\text{Ca}_v2.3$  channels in cerebral vessels (Ishiguro et al., 2005) and there is evidence for an involvement of these channels in delayed cerebral vasospasm and ischemia after subarachnoid hemorrhage (Ishiguro and Wellman, 2008). In addition, work from our lab shows that unconjugated bilirubin (UCB), a degradation product of hemoglobin, alters  $\text{Ca}_v2.3$  channel function in a heterologous expression system and attenuates transretinal signaling in the isolated retina from wildtype but not  $\text{Ca}_v2.3$ -deficient when applied at pathophysiologically relevant UCB:albumin molar ratios (Albanna et al., 2019, 2017).

### **1.3. Endogenous trace metal ions**

Trace metal ions like  $\text{Zn}^{2+}$  and  $\text{Cu}^{2+}$  are key structural components of numerous proteins and co-factors for enzymes involved in cellular respiration, catecholamine synthesis and antioxidant defense (Anzellotti and Farrell, 2008; Frederickson et al., 2005). In addition to their established structural and catalytic functions, endogenous  $\text{Zn}^{2+}$  and  $\text{Cu}^{2+}$  are increasingly recognized as potential modulators of neuronal transmission (Frederickson et al., 2005, 2000; Mathie et al., 2006) and synaptic plasticity (Pan et al., 2011). As noted above,  $\text{Zn}^{2+}$  has also been identified as a candidate auto- and / or paracrine signal for intra-islet crosstalk in the pancreas, which could be critically involved in the regulation of blood glucose homeostasis by insulin and glucagon (Ishihara et al., 2003).

#### **1.3.1. Trace metal speciation**

The biological effects of trace metal ions are determined by their chemical speciation, which is defined as the distribution among all free and ligand-bound species in solution (for details see publication 2). Under physiological conditions, the majority of  $\text{Zn}^{2+}$  and  $\text{Cu}^{2+}$  is tightly bound by a range of metalloprotein ligands, so that the pool that remains thermodynamically and kinetically accessible (i.e. loosely-bound) is usually orders of magnitude below the total concentration. This is especially important in the intracellular compartment, where even moderate increases in the loosely-bound  $\text{Zn}^{2+}$  or  $\text{Cu}^{2+}$  level are deleterious and ultimately associated with cell death. A detailed review of the tightly regulated intracellular trace metal homeostasis is beyond the scope of this work and can be found elsewhere (Colvin et al., 2010, 2003; Krężel and Maret, 2006). The present article will focus on the action of extracellular trace metal ions, noting that there is usually a large concentration-gradient favoring their passive entry into postsynaptic neurons. The latter is

under study as potential signaling pathway (Li et al., 2001) and important mechanism that may contribute to hippocampal neurodegeneration under certain pathophysiological conditions (Frederickson et al., 1988; Mathie et al., 2006). With regard to the extracellular compartment, an important implication of chemical speciation is that loosely-bound trace metal concentrations could be subject to modulation by a number of small organic molecules that are capable of acting as trace metal chelators. This is exemplified in publication 5 (Neumaier et al., 2018a), where we provide *in vitro* evidence for a receptor-independent mechanism of Ca<sub>v</sub>2.3 channel modulation by the excitatory amino acid KA that involves reversal of Cu<sup>2+</sup>-induced suppression. Additional implications are that suitable trace metal chelators can be used to antagonize the effects of endogenous trace metals, and that proper metal ion buffering should be used in experiments with metal ion-sensitive targets. The latter is important because even highly purified reagents contain small amounts of trace metal ions, so that estimated levels of Zn<sup>2+</sup>, Cu<sup>2+</sup> and / or other unwanted metal ions in typical physiological solutions are in the nano- to micromolar concentration range (for details see publication 2). As described in one of the later sections, this may be sufficient for significant tonic suppression of certain Ca<sub>v</sub>α<sub>1</sub>-subunits and could therefore also influence experimental findings.

### **1.3.2 Zn<sup>2+</sup> and Cu<sup>2+</sup> signaling in the brain**

While 90% of total brain Zn<sup>2+</sup> is tightly bound to zinc metalloproteins, much of the remaining 10% forms a loosely-bound pool located in the presynaptic vesicles of so-called zinc-enriched neurons (Frederickson et al., 2000; Mathie et al., 2006). These neurons are not associated with a single neurotransmitter and have been shown to release Zn<sup>2+</sup> both spontaneously and in an activity-dependent manner. Similar pools of loosely-bound Cu<sup>2+</sup> that can be released following membrane depolarization have been detected in certain neurons that appear to be primarily associated with glutaminergic or adrenergic transmission (Kardos et al., 1989; Ono and Cherian, 1999; Sato et al., 1994). The distribution of loosely-bound Zn<sup>2+</sup> and Cu<sup>2+</sup> in the brain is not uniform, and highest concentrations are located in specific forebrain areas that include the hippocampus and other limbic regions, the neocortex and the retina (Anastassov et al., 2014, 2013; Charton et al., 1985; Hartter and Barnea, 1988; Kardos et al., 1989). Under physiological conditions, estimated resting or 'tonic' levels in the brain extracellular fluid are in the order of 5-25 nM for loosely-bound Zn<sup>2+</sup> (Frederickson et al., 2006) and 0.1-0.8 μM for loosely-bound Cu<sup>2+</sup> (Mathie et al., 2006). These values are frequently exceeded at mossy fiber synapses, where Zn<sup>2+</sup> concentrations have been estimated to be in excess of 10-20 μM during basal synaptic activity and >100 μM during repetitive electrical stimulation or periods of intense activity (Kardos et al., 1989; Mathie et al., 2006; Vogt et al., 2000). During KA-induced epileptiform (or ictal-like) discharges, Zn<sup>2+</sup> levels in the order of 300 μM have been estimated to be reached in the extracellular space (Assaf and Chung, 1984). Released metal ions could modulate neuronal activity through effects on a variety of voltage- and ligand-gated ion channels (Elinder and Arhem, 2003; Neumaier et al., 2015), which has made it difficult to predict the net action of Zn<sup>2+</sup> and Cu<sup>2+</sup>. As such, their exact functional relevance in the brain remains controversial, although a number of experimental observations indicate that

especially  $Zn^{2+}$  could dampen excitability in limbic regions and serve as an intrinsic anticonvulsant. In mice, synaptic release and extracellular accumulation of  $Zn^{2+}$  have been shown to limit propagation of cortical spreading depression *in vitro* and *in vivo* (Aiba et al., 2012).  $Zn^{2+}$  chelation or deficiency increases the susceptibility to KA-induced seizures (Takeda et al., 2005, 2003) and induces excitotoxicity and convulsions in healthy rats (Blasco-Ibáñez et al., 2004) and rats subjected to non-lesioning over-excitation (Domínguez et al., 2003). In addition,  $Zn^{2+}$  treatment has been shown to reduce dentate granule cell hyperexcitability in epileptic human patients (Williamson and Spencer, 1995). On the other hand, massive release of synaptic  $Zn^{2+}$  and its translocation into postsynaptic neurons has been proposed as a mechanism for hippocampal neurodegeneration, which occurs following seizures, ischemia or traumatic brain injury (Frederickson et al., 1988; Mathie et al., 2006). However, the presynaptic origin of  $Zn^{2+}$  involved in this process remains controversial, since postsynaptic  $Zn^{2+}$  accumulation and cell death after KA-induced seizures or traumatic brain injury were the same or even increased in mice lacking  $Zn^{2+}$  transporter 3 ( $ZnT_3$ ), which are completely devoid of vesicular  $Zn^{2+}$  (Doering et al., 2010; Lee et al., 2000). Because intracellular metal ion buffering and sequestration are tightly coupled to the cells energetic and redox state, deleterious levels of  $Zn^{2+}$  could also be released from metallothioneins and other reservoirs located in damaged postsynaptic neurons themselves. The interpretation of experimental findings is further complicated by the fact that fluorescent probes used for  $Zn^{2+}$  staining have been shown to adhere non-specifically to the membrane of injured neurons (Hawkins et al., 2012). That notwithstanding and considering the many potential targets, it seems reasonable to assume that the effects of  $Zn^{2+}$  (and  $Cu^{2+}$ ) could include both compensatory (i.e. neuroprotective) and causative (i.e. neurotoxic) actions and that a complex interplay of factors determines their respective contribution under pathophysiological conditions. As exemplified in publication 6 (section 2.6), the magnitude and even direction of  $Zn^{2+}$  effects on a single target like  $Ca_v2.3$  channels can be affected by factors such as the resting membrane potential or the exact ionic conditions.

### **1.3.3. $Zn^{2+}$ signaling in pancreatic islets**

It is well known that  $Zn^{2+}$  is present at high (millimolar) concentrations in  $\beta$ -cell insulin secretory vesicles and required for proper insulin biosynthesis, maturation and secretion (Emdin et al., 1980; Li, 2014). During the maturation process, insulin mono- and dimers aggregate in the presence of  $Zn^{2+}$  to form 2Zn-hexameric complexes, which significantly lowers their solubility and causes crystallization within the vesicles (Emdin et al., 1980; Li, 2014). During hyperglycemia, the  $Zn^{2+}$ -insulin complexes are released into the periportal circulation, where the higher pH of blood favors their rapid dissociation into free  $Zn^{2+}$  and insulin monomers (Li, 2014; Robertson et al., 2011). The resulting local  $Zn^{2+}$  concentrations in the extracellular space are estimated to be in the order of several hundred  $\mu M$  (Kim et al., 2000), so that nearby cells are exposed to high levels of unbound  $Zn^{2+}$ . As such,  $Zn^{2+}$  has long been recognized as a candidate signal for non-insulin paracrine crosstalk to neighboring  $\alpha$ -cells (Ishihara et al., 2003), and a number of recent findings provide support to this idea. For example,  $Zn^{2+}$  was reported to suppress pyruvate- or glucose-induced glucagon release in

static secretion and electrophysiological experiments with isolated murine islets and purified  $\alpha$ -cells (Franklin et al., 2005; Gyulxhandanyan et al., 2008). Moreover,  $Zn^{2+}$  but not  $Zn^{2+}$ -free insulin, has been shown to inhibit  $\alpha$ -cell glucagon secretion in the perfused rat pancreas (Robertson et al., 2011; Zhou et al., 2007). It should also be noted however, that some studies failed to detect  $Zn^{2+}$ -induced suppression of glucagon secretion (Ramracheya et al., 2010; Ravier and Rutter, 2005), so that the topic remains a matter of heated debate. Identification of  $Zn^{2+}$  targets expressed in  $\alpha$ -cells and directly involved in glucagon secretion could evidently help to resolve these discrepancies and strengthen understanding of the role of  $Zn^{2+}$  for intra-islet crosstalk. In publication 4, we provide *in vitro* and *in vivo* evidence for a role of  $Ca_v2.3$  channels as targets for the putative  $Zn^{2+}$ -induced suppression of  $\alpha$ -cell glucagon secretion. In addition and consistent with this idea, results obtained in publication 6 indicate that sudden cessation of  $Zn^{2+}$  supply could not only reverse suppression but also transiently stimulate  $Ca^{2+}$  influx through  $Ca_v2.3$  channels under certain conditions.

#### **1.3.4. Metal ion effects on voltage-gated $Ca^{2+}$ channels**

The function of all voltage-gated ion channels is more or less effectively altered by changes in the concentration of divalent cations, although the underlying mechanisms can vary considerably. They may be broadly classified into three general groups, which comprise (i) electrostatic effects of metal ions in the bulk solution (surface charge screening, **Fig. 3A**) or bound to charged regions on the channel surface (surface charge binding, **Fig. 3B**), which alter the local potential sensed by the VSMSs, (ii) blocking effects of metal ions bound to intrapore sites, which physically occlude the permeation pathway (pore block, **Fig. 3C**) and (iii) non-electrostatic effects of metal ions bound to specific metal-binding sites (allosteric modulation, **Fig. 3D**). Under physiological conditions, surface charge effects are mainly of experimental relevance, as they are predicted to become significant only at supra-physiological (i.e. high micro- to millimolar) trace metal concentrations. A notable exception may be the retina, where surface charge effects on VGCCs have been proposed to play a physiological role (Cadetti et al., 2004). The blocking action of  $Zn^{2+}$  and other trace metal ions was investigated in early single-channel studies in mouse myotubes, which found that  $Zn^{2+}$  blocks L-type currents carried by 110 mM  $Ba^{2+}$  in a weakly voltage-dependent manner, with half-maximal inhibition at 0 mV by approximately 500  $\mu$ M nominal  $Zn^{2+}$  (Winegar and Lansman, 1990). Most later studies on the effects of  $Zn^{2+}$  have been done using the whole-cell configuration of the patch-clamp technique, which has the advantage that recordings can be performed with much lower (i.e. near physiological) concentrations of charge carrying ions. However, separation of effects mediated by the different mechanisms of action described above remains a non-trivial task, since all of them may contribute to the net action observed in macroscopic current recordings. In addition, few studies have been performed using metal ion-buffered solutions, and comparison of the available data is further complicated by differences in the experimental conditions, the exact tissue or subunit compositions studied and the electrophysiological parameters used to quantify suppression. For example, nominal  $Zn^{2+}$  concentrations which have been reported to produce half- maximal suppression of

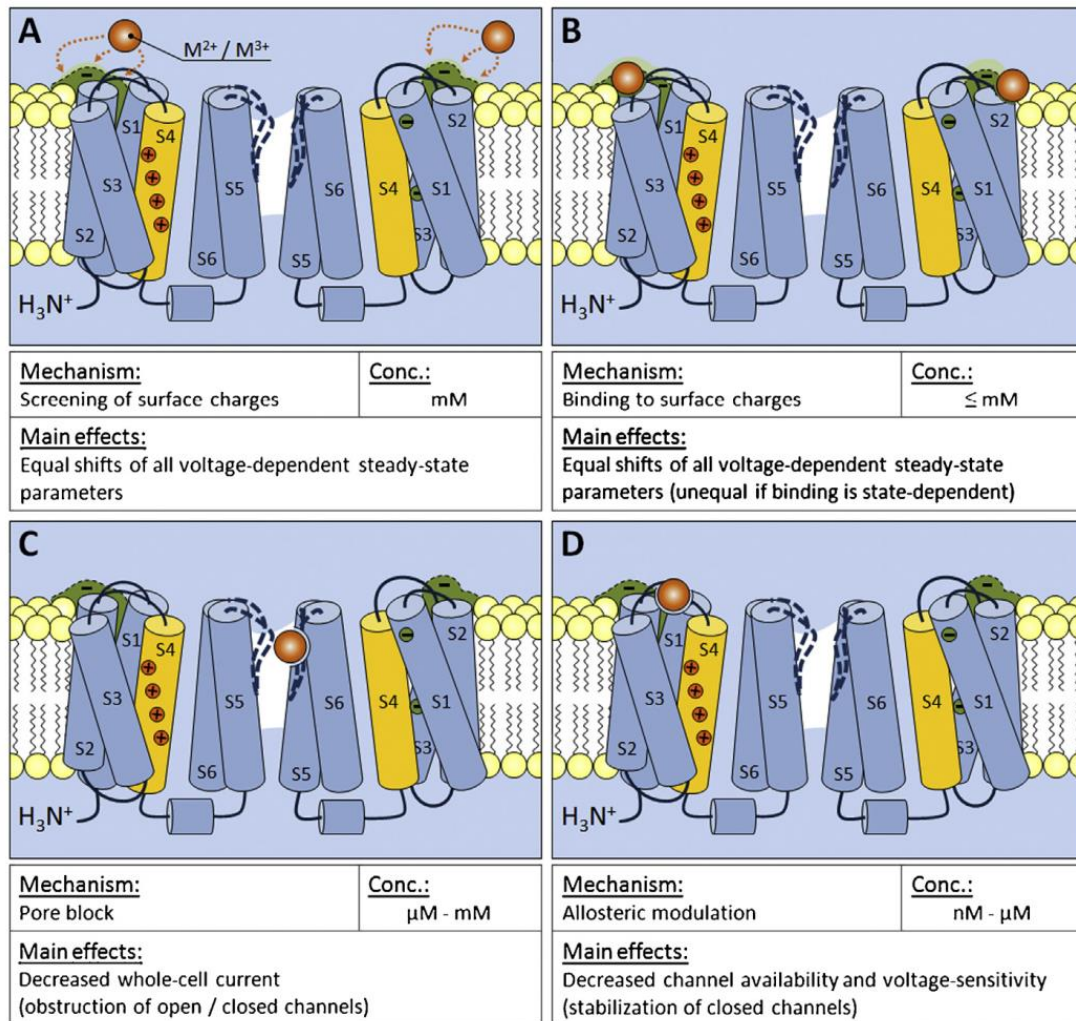


**Figure 4.** Mechanisms of modulation of voltage-gated calcium channels by polyvalent inorganic cations. Sketch of the pore-forming  $\alpha_1$ -subunit in a closed conformation, showing two of the four homologous domains with their voltage-sensor modules (S4 segments highlighted in yellow) and local charges on the channel surface (green). (A) Multivalent cations ( $M^{2+} / M^{3+}$ , orange) in solution can screen charges on the channel surface, thereby electrostatically reducing the local potential sensed by the voltage-sensors (B) Some cations can electrostatically decrease the total surface charge density by directly binding to and neutralizing certain surface charges, producing a more pronounced reduction in the local potential. (C) Most di- and trivalent metal ions can bind to sites at or within the pore region (pore block), thereby physically occluding the permeation pathway. (D) Some VGCCs have been shown to possess high-affinity allosteric metal binding-sites on their domain I voltage-sensor. Reprinted with permission from (Neumaier et al., 2015).

native HVA currents range from 20-30  $\mu\text{M}$  in acutely dissociated cortical neurons (Magistretti et al., 2003) or 70  $\mu\text{M}$  in DRG neurons (Büsselberg et al., 1994) to 210  $\mu\text{M}$  in cultured cortical neurons (Kerchner et al., 2000) or 250  $\mu\text{M}$  in acutely dissociated pelvic neurons (Jeong et al., 2003). The effects of  $\text{Zn}^{2+}$  (and in some cases  $\text{Cu}^{2+}$ ) on individual  $\text{Ca}_v\alpha_1$ -subunits have been studied in a number of recombinant expression studies, which are summarized in detail in publication 1. With regard to cloned  $\text{Ca}_v2.3$  channels, half-maximal suppression of currents carried by 5 mM  $\text{Ca}^{2+}$  was observed at 1.3  $\mu\text{M}$   $\text{Zn}^{2+}$  or 18 nM  $\text{Cu}^{2+}$

when experiments were performed using metal ion-buffered solutions. In addition, (sub)micromolar concentrations of  $Zn^{2+}$ ,  $Cu^{2+}$  and  $Ni^{2+}$  produced depolarizing shifts in channel voltage-dependence, a reduced sensitivity towards depolarization and a pronounced slowing of macroscopic activation (Kang et al., 2007; Shcheglovitov et al., 2012; Zamponi et al., 1996) resembling their action on native R-type currents in cortical (Castelli et al., 2003; Magistretti et al., 2003) and DRG neurons (Shcheglovitov et al., 2012). Molecular cloning studies identified three histidine residues located in the IS1-IS2 (His<sup>111</sup>) and IS3-IS4 (His<sup>179</sup> and His<sup>183</sup>) loops, which are not conserved in other HVA channels and thought to form a high-affinity extracellular binding pocket for certain divalent cations (Kang et al., 2007; Shcheglovitov et al., 2012). Since  $Zn^{2+}$ ,  $Cu^{2+}$  and  $Ni^{2+}$  also alter activation gating in HVA channels lacking critical histidine residues (Castelli et al., 2003; Magistretti et al., 2003; Zamponi et al., 1996), it remains to be determined if additional metal binding sites exist or if the gating changes described above are exclusively related to the putative metal binding site in domain I. This and some other open questions are addressed in publication 6, which provides experimental evidence for the idea that multiple sites are involved in the effects of  $Zn^{2+}$  on  $Ca_v2.3$  channel gating and proposes a model that can account for most, but not all of these effects.

#### **1.4. Aims of the present work**

The general aim of the present work was to shed some light on the exact mechanisms of  $Zn^{2+}$ - and  $Cu^{2+}$ -induced  $Ca_v2.3$  channel modulation and their potential relevance under normal and pathophysiological conditions. In publication 1, we used crystallographic data of the  $Ca^{2+}$ -selective bacterial model channel  $Ca_vAb$  as a framework to analyze eukaryotic VGCC structure, function and modulation by inorganic cations. In publication 2, we assessed the methodical difficulties of metal ion-buffering in physiological solutions, developed general protocols for preparation and use of (multi) metal ion-buffered solutions and experimentally verified the critical importance of proper metal ion-buffering. In publication 3, we used conventional and perforated patch-clamp recordings together with different inhibitors and cytosolic factors to identify signaling cascades involved in  $Ca_v2.3$  channel run-down during cell dialysis, which was critical to improve the stability of recordings for the detailed assessment of  $Zn^{2+}$  effects described in publication 6 (see below). In publication 4, we compared the effects of  $Zn^{2+}$  chelation on glucose homeostasis and peptide hormone secretion in  $Ca_v2.3$ -deficient and wildtype mice to determine if  $Zn^{2+}$ -inhibition of  $Ca_v2.3$  channels contributes to the suppression of glucagon secretion during hyperglycemia. In publication 5, we used whole-cell patch-clamp recordings in stably transfected HEK293 cells and *ex vivo* electroretinographic recordings from the bovine retina to characterize a receptor-independent but  $Cu^{2+}$ -dependent mechanism of  $Ca_v2.3$  channel modulation by KA. Finally, in publication 6, we analyzed the concentration-dependent effects of  $Zn^{2+}$  as a prototype redox-inert trace metal ion on cloned  $Ca_v2.3$  channel function and developed a semi-mechanistic Markov model capable of reproducing most salient features of current through these channels in the absence and presence of physiologically relevant  $Zn^{2+}$  concentrations.

## 2. Results

### 2.1. Publication 1: Progress in Neurobiology 129:1-36.

#### **Voltage-gated calcium channels: Determinants of channel function and modulation by inorganic cations.**

Felix Neumaier, Maxine Dibué-Adjei, Jürgen Hescheler, Toni Schneider

##### **Abstract:**

Voltage-gated calcium channels (VGCCs) represent a key link between electrical signals and non-electrical processes, such as contraction, secretion and transcription. Evolved to achieve high rates of Ca<sup>2+</sup>-selective flux, they possess an elaborate mechanism for selection of Ca<sup>2+</sup> over foreign ions. It has been convincingly linked to competitive binding in the pore, but the fundamental question of how this is reconcilable with high rates of Ca<sup>2+</sup> transfer remains unanswered. By virtue of their similarity to Ca<sup>2+</sup>, polyvalent cations can interfere with the function of VGCCs and have proven instrumental in probing the mechanisms underlying selective permeation. Recent emergence of crystallographic data on a set of Ca<sup>2+</sup>-selective model channels provides a structural framework for permeation in VGCCs, and warrants a reconsideration of their diverse modulation by polyvalent cations, which can be roughly separated into three general mechanisms: (I) long-range interactions with charged regions on the surface, affecting the local potential sensed by the channel or influencing voltage-sensor movement by repulsive forces (electrostatic effects), (II) short-range interactions with sites in the ion-conducting pathway, leading to physical obstruction of the channel (pore block), and in some cases (III) short-range interactions with extracellular binding sites, leading to non-electrostatic modifications of channel gating (allosteric effects). These effects, together with the underlying molecular modifications, provide valuable insights into the function of VGCCs, and have important physiological and pathophysiological implications. Allosteric suppression of some of the pore-forming Ca<sub>v</sub>α<sub>1</sub>-subunits (Ca<sub>v</sub>2.3, Ca<sub>v</sub>3.2) by Zn<sup>2+</sup> and Cu<sup>2+</sup> may play a major role for the regulation of excitability by endogenous transition metal ions. The fact that these ions can often traverse VGCCs can contribute to the detrimental intracellular accumulation of metal ions following excessive release of endogenous Cu<sup>2+</sup> and Zn<sup>2+</sup> or exposure to non-physiological toxic metal ions.

##### **Contributions to Publication 1:**

I independently reviewed the literature and conceptualized the article, performed all sequence alignments, calculations and simulations described in the text and shown in the figures, created all tables and figures, wrote the manuscript and handled the submission and revision process. I was also chosen to create the cover art for the corresponding issue of Progress in Neurobiology.





## Voltage-gated calcium channels: Determinants of channel function and modulation by inorganic cations



Felix Neumaier<sup>a,\*</sup>, Maxine Dibué-Adjei<sup>a,b,c</sup>, Jürgen Hescheler<sup>a</sup>, Toni Schneider<sup>a,\*</sup>

<sup>a</sup> Institute for Neurophysiology, University of Cologne, Robert-Koch-Str. 39, 50931 Cologne, Germany

<sup>b</sup> Department for Neurosurgery, Medical Faculty, Heinrich Heine University, Moorenstraße 5, 40225 Düsseldorf, Germany

<sup>c</sup> Center of Molecular Medicine, Cologne, Germany

### ARTICLE INFO

#### Article history:

Received 14 April 2014

Received in revised form 15 December 2014

Accepted 27 December 2014

Available online 25 March 2015

#### Keywords:

Voltage-gated Ca<sup>2+</sup>-channels

Selective permeation

Endogenous transition metal ions

Pore block

Allosteric modulation

Electrostatic interactions

### ABSTRACT

Voltage-gated calcium channels (VGCCs) represent a key link between electrical signals and non-electrical processes, such as contraction, secretion and transcription. Evolved to achieve high rates of Ca<sup>2+</sup>-selective flux, they possess an elaborate mechanism for selection of Ca<sup>2+</sup> over foreign ions. It has been convincingly linked to competitive binding in the pore, but the fundamental question of how this is reconcilable with high rates of Ca<sup>2+</sup> transfer remains unanswered. By virtue of their similarity to Ca<sup>2+</sup>, polyvalent cations can interfere with the function of VGCCs and have proven instrumental in probing the mechanisms underlying selective permeation. Recent emergence of crystallographic data on a set of Ca<sup>2+</sup>-selective model channels provides a structural framework for permeation in VGCCs, and warrants a reconsideration of their diverse modulation by polyvalent cations, which can be roughly separated into three general mechanisms: (I) long-range interactions with charged regions on the surface, affecting the local potential sensed by the channel or influencing voltage-sensor movement by repulsive forces (electrostatic effects), (II) short-range interactions with sites in the ion-conducting pathway, leading to physical obstruction of the channel (pore block), and in some cases (III) short-range interactions with extracellular binding sites, leading to non-electrostatic modifications of channel gating (allosteric effects). These effects, together with the underlying molecular modifications, provide valuable insights into the function of VGCCs, and have important physiological and pathophysiological implications. Allosteric suppression of some of the pore-forming Ca<sub>v</sub>α<sub>1</sub>-subunits (Ca<sub>v</sub>2.3, Ca<sub>v</sub>3.2) by Zn<sup>2+</sup> and Cu<sup>2+</sup> may play a major role for the regulation of excitability by endogenous transition metal ions. The fact that these ions can often traverse VGCCs can contribute to the detrimental intracellular accumulation of metal ions following excessive release of endogenous Cu<sup>2+</sup> and Zn<sup>2+</sup> or exposure to non-physiological toxic metal ions.

© 2015 Elsevier Ltd. All rights reserved.

### Contents

1. Introduction . . . . .	2
2. Diversity and structure of voltage-gated calcium channels. . . . .	3
2.1. Classification and nomenclature . . . . .	3
2.2. Subunit composition. . . . .	3
2.3. Ca <sub>v</sub> α <sub>1</sub> -subunits . . . . .	4
2.4. Auxiliary subunits. . . . .	4

**Abbreviations:** AMFE, anomalous mole fraction effect; Asp, aspartic acid residue; CaM, calmodulin; CDI, Ca<sup>2+</sup>-dependent inactivation; Glu, glutamic acid residue; Gly, glycine residue; His, histidine residue; HVA, high voltage activated; IV, macroscopic steady-state current–voltage relationship; IIV, macroscopic instantaneous current–voltage relationship; IVA, intermediate voltage activated; LVA, low voltage activated; p-loop, pore loop; VDI, voltage-dependent inactivation; VGCCs, voltage-gated calcium channels.

\* Corresponding authors at: University of Cologne, Institute for Neurophysiology, Robert-Koch-Str. 39, D-50931 Köln, Germany. Tel.: +49 221 4786946;

fax: +49 221 4786965.

E-mail addresses: [felix@neumaier-net.de](mailto:felix@neumaier-net.de) (F. Neumaier), [Toni.Schneider@uni-koeln.de](mailto:Toni.Schneider@uni-koeln.de) (T. Schneider).

<http://dx.doi.org/10.1016/j.pneurobio.2014.12.003>

0301-0082/© 2015 Elsevier Ltd. All rights reserved.



3. Molecular properties . . . . . 5

3.1. Gating behaviour . . . . . 5

3.1.1. Voltage-dependent activation . . . . . 5

3.1.2. Voltage- and Ca<sup>2+</sup>-dependent inactivation . . . . . 5

3.2. Selective permeation . . . . . 6

3.2.1. Continuum models: selection based on charge and size . . . . . 6

3.2.2. Chemical-kinetic models: stepwise changes in affinity . . . . . 7

3.2.3. Molecular models: ion–ion interactions at a flexible binding locus . . . . . 7

3.2.4. Allosteric and electrostatic effects: role of regions outside of the pore . . . . . 7

3.2.5. Structure and function: insights from the bacterial model channel Ca<sub>v</sub>Ab . . . . . 7

3.2.6. Ca<sub>v</sub>Ab as a structural framework: implications for vertebrate channels . . . . . 8

4. Modulation by inorganic cations . . . . . 10

4.1. Electrostatic effects (Fig. 5A and B) . . . . . 10

4.1.1. Classical surface charge theory . . . . . 10

4.1.2. Dynamic binding models . . . . . 13

4.1.3. Validity and relevance of electrostatic models . . . . . 13

4.1.4. Electrostatic interactions in the pore region . . . . . 13

4.2. Pore block (Fig. 5C) . . . . . 14

4.2.1. Voltage-dependence: evidence for binding in the pore . . . . . 14

4.2.2. Association: block provides information about the first step in permeation . . . . . 16

4.2.3. Dissociation: ion–pore interactions are influenced by charge and size . . . . . 17

4.2.4. Translocation: differential ion–ion interactions facilitate exit . . . . . 18

4.2.5. Block from the inside: low-affinity competition at the inner vestibule . . . . . 19

4.2.6. Using transition metal ions to probe translocation . . . . . 19

4.2.7. Structural determinants of pore block . . . . . 25

4.2.8. Permeation: calcium channels as pathway for trace metal entry . . . . . 25

4.3. Allosteric modulation (Fig. 5D) . . . . . 27

4.3.1. Ca<sub>v</sub>3.2 channels . . . . . 27

4.3.2. Ca<sub>v</sub>2.3 channels . . . . . 28

4.3.3. Physiological relevance: role of calcium channels in the control of excitability . . . . . 29

5. Conclusion . . . . . 30

Acknowledgements . . . . . 30

References . . . . . 30

**1. Introduction**

Voltage-gated Ca<sup>2+</sup>-channels (VGCCs) are unique among the superfamily of voltage-gated ion channels, as they are not only involved in electrical signalling but also provide the key link between electrical signals and non-electrical processes, such as transmitter release, muscle contraction and transcription (Table 1) (Catterall, 1998; Hofmann et al., 1999). They respond to membrane potential changes and allow selective influx of Ca<sup>2+</sup>, which can either serve to activate Ca<sup>2+</sup>-dependent intracellular processes or shape the electrical properties of

excitable cells. The diverse functional roles of VGCCs in different tissues are well established and have been reviewed in several excellent articles (Catterall, 2011; Senatore et al., 2012; Hofmann et al., 2014; Simms and Zamponi, 2014), but many fundamental questions regarding the mechanisms by which these channels achieve high rates of voltage-dependent and Ca<sup>2+</sup>-selective flux remain unanswered. Recent construction and crystallographic analysis of the Ca<sup>2+</sup>-selective bacterial model channel Ca<sub>v</sub>Ab provide a structural framework for understanding channel function, and this reveals a mechanism of selective permeation which may be shared by eukaryotic channels. It is

**Table 1**  
Classification of native Ca<sup>2+</sup> currents and cloned α<sub>1</sub>-subunits.

Native current	Organic or polypeptide antagonist <sup>a</sup>	Cloned α <sub>1</sub> -subunit	Proposed cellular functions
L-type	Dihydropyridines Phenylalkylamines Benzothiazepines Calciseptine, FS2	<b>Ca<sub>v</sub>1.1</b> (α <sub>1S</sub> )	Excitation–contraction coupling
		<b>Ca<sub>v</sub>1.2</b> (α <sub>1C</sub> )	Excitation–contraction coupling, excitation–transcription coupling, synaptic integration, hormone release
		<b>Ca<sub>v</sub>1.3</b> (α <sub>1D</sub> )	Cardiac pacemaking, synaptic regulation, excitation–transcription coupling, hormone release, hearing
		<b>Ca<sub>v</sub>1.4</b> (α <sub>1F</sub> )	Transmitter release (photoreceptors)
P/Q-type	ω-Agatoxins IVA & B ω-Conotoxins MVIIC & D	<b>Ca<sub>v</sub>2.1</b> (α <sub>1A</sub> )	Transmitter release, hormone release, dendritic Ca <sup>2+</sup> -transients
N-type	ω-Conotoxins CVIA & D ω-Conotoxin GVIA & MVIIA	<b>Ca<sub>v</sub>2.2</b> (α <sub>1B</sub> )	Transmitter release, hormone release, dendritic Ca <sup>2+</sup> -transients
R-type	SNX-482	<b>Ca<sub>v</sub>2.3</b> (α <sub>1E</sub> )+Ca <sub>v</sub> x?	Pacemaking, transmitter release, LTP, repetitive firing, Ca <sup>2+</sup> -transients
T-type	(+)–ECN (Kurtoxin)	<b>Ca<sub>v</sub>3.1</b> (α <sub>1G</sub> )	Pacemaking, repetitive firing
		<b>Ca<sub>v</sub>3.2</b> (α <sub>1H</sub> )	Pacemaking, repetitive firing
		<b>Ca<sub>v</sub>3.3</b> (α <sub>1I</sub> )	Pacemaking, repetitive firing

Source: McDonough (2004), Snutch et al. (2005), Striessnig and Koschak (2008), Catterall et al. (2013), Schneider et al. (2013).

<sup>a</sup> Note that most of the listed agents are not perfectly selective and affect more than a single type of VGCC, especially at saturating concentrations.

complemented by a vast array of electrophysiological data on the modulation of vertebrate VGCCs by foreign (i.e. non-Ca<sup>2+</sup>) inorganic cations, which have proven instrumental in probing Ca<sup>2+</sup>-selective flux. Many of these ions (Cd<sup>2+</sup>, Ni<sup>2+</sup>, Co<sup>2+</sup>) are prevalent environmental pollutants (He et al., 2005; Mukhtar and Limbeck, 2013), while others (Cu<sup>2+</sup> and Zn<sup>2+</sup>) have been identified as endogenous modulators of neuronal transmission, suggesting that they have important physiological and pathophysiological implications. The scope of the present article is twofold: to provide a comprehensive overview on the modulation of VGCCs by polyvalent cations and to consider possible implications of their actions for the structure–function relationship of these channels. The first part serves to introduce the reader and briefly reviews the classification, structure and subunit composition of VGCCs. The second part summarizes different theoretical concepts to describe channel function and relates them to recent findings on molecular channel structure. With this in mind, the third part compiles the impressive amount of work done on the modulation of VGCCs by polyvalent cations in terms of three general mechanisms, considers different conceptual approaches to explain experimental findings, and compares them to findings in other voltage-gated ion channels. Reference will be made to experimentally, physiologically and pathophysiological relevant aspects, focusing mainly on VGCCs in the brain and their role in neuronal transmission and excitability.

## 2. Diversity and structure of voltage-gated calcium channels

### 2.1. Classification and nomenclature

Following their first recording in cardiomyocytes (Reuter, 1967, 1979), it was quickly realized that multiple distinct Ca<sup>2+</sup> currents exist in several cell types (Nowycky et al., 1985; Bean, 1985; Hagiwara et al., 1975) and different nomenclatures have since evolved to distinguish them from each other (Table 1). Ca<sup>2+</sup> currents in native membranes have been broadly classified into (I) low-voltage activated (LVA) currents, which start to activate at membrane potentials near the resting level (around –60 to –70 mV) and inactivate rapidly, and (II) high-voltage activated (HVA) currents, which start to activate at somewhat more depolarized potentials (above –40 mV) and exhibit variable but typically less rapid inactivation kinetics (Carbone and Lux, 1984; Nowycky et al., 1985). Based mainly on their biophysical and pharmacological properties, HVA currents have been further subclassified into 1,4-dihydropyridine-sensitive L-type (large conductance or long lasting),  $\omega$ -conotoxin GVIA-sensitive N-type (neuronal or neither T- nor L-type),  $\omega$ -agatoxin IVA-sensitive P/Q-type (Purkinje neurons) and partly SNX-482-sensitive R-type (resistant or residual) currents, while LVA currents were assigned to a single group of T-type (tiny conductance or transient) currents (Nowycky et al., 1985; Tsien et al., 1987; Llinás et al., 1992; Randall et al., 1993; Randall and Tsien, 1995). The pharmacology of VGCCs has been reviewed elsewhere (Triggle, 2004; McDonough, 2004; Ertel, 2004), but it should be noted that pharmacological separation of individual currents from a mixed population of structurally related channels inevitably suffers from the lack of perfectly selective antagonist binding (e.g. Hillyard et al., 1992; Grantham et al., 1994) and possible contamination errors due to incomplete block of some channel types (e.g. Newcomb et al., 1998). Adding to the unreliability of traditional Ca<sup>2+</sup> current separation, the biophysical and pharmacological properties of VGCCs can be modified in a complex manner by associated auxiliary subunits or post-translational modification (e.g. Welling et al., 1993; Soldatov et al., 1995).

The first purification of Ca<sup>2+</sup> channel complexes from traverse tubule of skeletal muscle (Curtis and Catterall, 1984, 1986; Flockerzi et al., 1986; Campbell et al., 1988) and molecular cloning of the principal pore-forming  $\alpha_1$ -subunit (Tanabe et al., 1987) in the late 1980s paved the way for a closer biochemical and functional analysis of VGCCs. Subsequent homology screening of lambda-phage and cDNA libraries revealed several additional genes encoding mammalian Ca<sup>2+</sup> channel  $\alpha_1$ -subunits and firmly established that the functional diversity of native Ca<sup>2+</sup> currents arises from multiple distinct types of VGCCs (Hille, 2001; Catterall, 2011). Their naming followed an alphabetical nomenclature, which assigned the letter S to the original skeletal muscle channel (i.e.  $\alpha_{1S}$ ) and the letters A–F to subsequently identified  $\alpha_1$ -subunits (Snutch et al., 1990; Snutch and Reiner, 1992; Birnbaumer et al., 1994). It has since been superseded by a classification into three subfamilies based on amino acid sequence identity and the same numerical nomenclature used for other voltage-gated ion channels (Table 1). A given  $\alpha_1$ -subunit is identified by the principal permeating ion (Ca for Ca<sup>2+</sup>), the main physiological regulator (v for voltage) indicated as a subscript (i.e. Ca<sub>v</sub>) and a numerical identifier, which corresponds to subfamily and order of discovery within the subfamily (Chandy, 1991; Ertel et al., 2000; Catterall et al., 2003). Based on biophysical, pharmacological and functional criteria, the Ca<sub>v</sub>1 family (Ca<sub>v</sub>1.1 through Ca<sub>v</sub>1.4) has been convincingly linked to native L-type currents, the Ca<sub>v</sub>2 family to native N-type (Ca<sub>v</sub>2.1), P/Q-type (Ca<sub>v</sub>2.2) and R-type (Ca<sub>v</sub>2.3) currents, and the Ca<sub>v</sub>3 family (Ca<sub>v</sub>3.1 through Ca<sub>v</sub>3.3) to native T-type currents. Note however that although Ca<sub>v</sub>2.3 is the only molecular counterpart of native R-type currents so far identified and cloned, Ca<sub>v</sub>2.3-deficient mice retain substantial R-type currents in DRG neurons and cerebellar granule cells (Wilson et al., 2000). This could reflect a contribution of yet-to-be identified  $\alpha_1$ -subunits or splice isoforms of known Ca<sup>2+</sup> channel subtypes or result from incomplete block of other channels by applied peptide toxins.

### 2.2. Subunit composition

Similar to other members belonging to the superfamily of voltage-gated ion channels, native HVA channels are heteromeric multi-subunit complexes, consisting of the principal, transmembrane-spanning Ca<sub>v</sub> $\alpha_1$ -subunit, stoichiometrically associated with several auxiliary subunits of lower molecular weight (Fig. 1). The biophysical properties of expressed HVA channel complexes and their trafficking to the cell membrane vary with co-expression of different auxiliary subunits, namely one of at least four  $\beta$ -subunits (Ca<sub>v</sub> $\beta_{1-4}$ ), one of at least four  $\alpha_2\delta$ -subunits (Ca<sub>v</sub> $\alpha_2\delta_{1-4}$ ) and in some cases, one of several putative  $\gamma$ -subunits (Ca<sub>v</sub> $\gamma_{1-8}$ ). Further channel diversity arises from a large number of possible splice variants and posttranslational modifications of the  $\alpha_1$  or other subunits (Jones, 1998; Dolphin, 2006; Lacinova, 2005). In addition to 'classical' auxiliary subunits, HVA channels interact with the ubiquitous intracellular Ca<sup>2+</sup>-sensor calmodulin (CaM), which can bind to a CaM-binding domain in the cytoplasmic C-terminal region, and has been shown to play a major role for feedback regulation by Ca<sup>2+</sup> (Zühlke and Reuter, 1998; Qin et al., 1999; Halling et al., 2005).

LVA channels on the other hand lack the CaM-binding domain and their native counterparts are typically thought to consist only of pore-forming  $\alpha_1$ -subunits (Lambert et al., 1997; Leuranguer et al., 1998; Lacinova et al., 1999), although there is evidence for certain interactions with  $\beta$ - and  $\alpha_2\delta$ -subunits (Lacerda et al., 1994; Wyatt et al., 1998; Dolphin et al., 1999). They share only limited sequence homology with the group of HVA channels (~15% identity at the amino acid level) (Jones, 1998; Perez-Reyes, 2003) and comparison of certain regions, like the proximal C-terminus, in fact reveals a closer structural similarity between HVA Ca<sub>v</sub> $\alpha_1$ -subunits and voltage-gated Na<sup>+</sup> channels than between HVA and LVA Ca<sub>v</sub> $\alpha_1$ -subunits (Yu and Catterall, 2004).



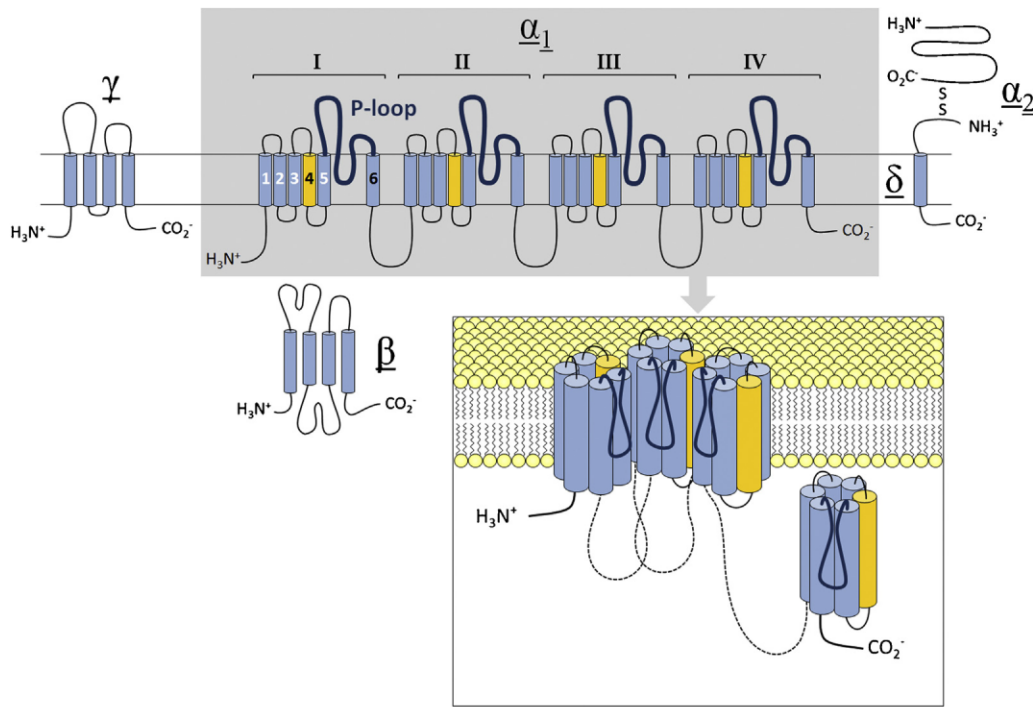


**Fig. 1.** Subunit composition and transmembrane topology of high-voltage activated calcium channels. (A) Native HVA channels are heteromultimeric complexes, consisting of a principal, pore-forming  $\alpha_1$ -subunit and different auxiliary subunits in approximately stoichiometric ratio. Typically,  $\alpha_1$ -subunits are associated with one of four  $\beta$ -subunit isoforms and one of four  $\alpha_2\delta$ -subunit isoforms. In some tissues, additional  $\gamma$ -subunits have been described. Inset: Quadrameric arrangement of homologous domains of the pore-forming  $\alpha_1$  subunit at the cell membrane. For clarity, domain IV is shown aside from the membrane.

### 2.3. $Ca_v\alpha_1$ -subunits

All of the currently known 10  $Ca_v\alpha_1$ -subunits are composed of four homologous repeats (termed domains I through IV), each consisting of six membrane-spanning segments (S1–S6) and a pore-forming P-loop (pore loop) between S5 and S6 (Zhen et al., 2005) (Fig. 1). The first four segments of each domain (S1–S4) are thought to form the voltage-sensing gating machinery which couples channel activity to changes in the membrane potential. The remaining two segments (S5–S6) make up most of the internal pore lining, while the P-loops are thought to fold back into the membrane to form the extracellular mouth of the pore and the molecular basis for high  $Ca^{2+}$  selectivity (Fig. 1 inset) (Kim et al., 1993; Yang et al., 1993). The N- and C-terminal cytoplasmic parts and the three inter-domain linkers (I–II, II–III and III–IV loop) play a role for inactivation and contain sites for association of auxiliary subunits, G-protein interaction and phosphorylation by different protein kinases (Snutch et al., 2005). Taken together,  $\alpha_1$ -subunits seem to possess all molecular components required for channel activity (i.e. a  $Ca^{2+}$  selective pore and a voltage-sensor) and expression of a number of cloned  $\alpha_1$ -subunits alone produces functional  $Ca^{2+}$  channels in *Xenopus* oocytes, albeit in some cases with low membrane expression and abnormal gating properties (Biel et al., 1990; Bosse et al., 1992; Itagaki et al., 1992). It has since been recognized however, that these cells contain an endogenous  $\beta_3$ -like subunit which appears to be both necessary and sufficient for functional expression of at least some HVA  $Ca_v\alpha_1$ -subunits (Singer-Lahat et al., 1992; Tareilus et al., 1997; Canti et al., 2001).

### 2.4. Auxiliary subunits

Not least due to the complications introduced by their endogenous presence in commonly used expression systems, the exact functional relevance of auxiliary subunits is still

controversial. The majority of work has been carried out on  $Ca_v\beta$  subunits, which are intracellular, hydrophilic proteins with no transmembrane segments (Fig. 1). Their association with HVA  $\alpha_1$ -subunits typically leads to substantial increases in the magnitude of  $Ca^{2+}$  current, arising from enhanced channel trafficking, increased expression of functional channel complexes at the plasma membrane and certain modifications of the biophysical properties, which will be addressed in more detail in Section 3.1 (Singer et al., 1991; Josephson and Varadi, 1996; Parent et al., 1997; Birnbaumer et al., 1998; Dolphin, 2003). There are, however, several isoform- and target-specific differences in the impact of  $\beta$ -subunits (De Waard and Campbell, 1995; Walker et al., 1998, 1999; Helton and Horne, 2002) and a number of them have been found to contain potential phosphorylation sites for different protein kinases, indicating that they are also involved in channel regulation (Reuter, 1996; Arikath and Campbell, 2003).

The functional implications of  $\alpha_2\delta$ -subunits are even more diverse, with effects on channel properties depending on the class of  $\alpha_1$ -subunit, the expression system used and in some cases on additional presence of a  $\beta$ -subunit, suggesting that there may be synergistic actions of  $\alpha_2\delta$  with other auxiliary subunits (Gurnett et al., 1996; Klugbauer et al., 1999a). Apart from effects on the biophysical properties, co-expression of  $\alpha_2\delta$ -subunits typically increases the number of channels at the cell surface, suggesting a role for trafficking similar to that of  $\beta$ -subunits (Arikath and Campbell, 2003).  $\alpha_2\delta$ -Subunits consist of two distinct subunits ( $\alpha_2$  and  $\delta$ ), derived from post-translational cleavage of a single gene product and associated with each other via disulfide bonds (Ellis et al., 1988). The  $\alpha_2$  protein is highly glycosylated and resides on the extracellular side whereas the smaller  $\delta$  protein is believed to serve as anchor of the  $\alpha_2\delta$ -dimer in the plasma membrane (Fig. 1) (Gurnett et al., 1996).

In the case of  $\gamma$ -subunits, functional roles are still mostly unresolved, although they have also been shown to modulate the

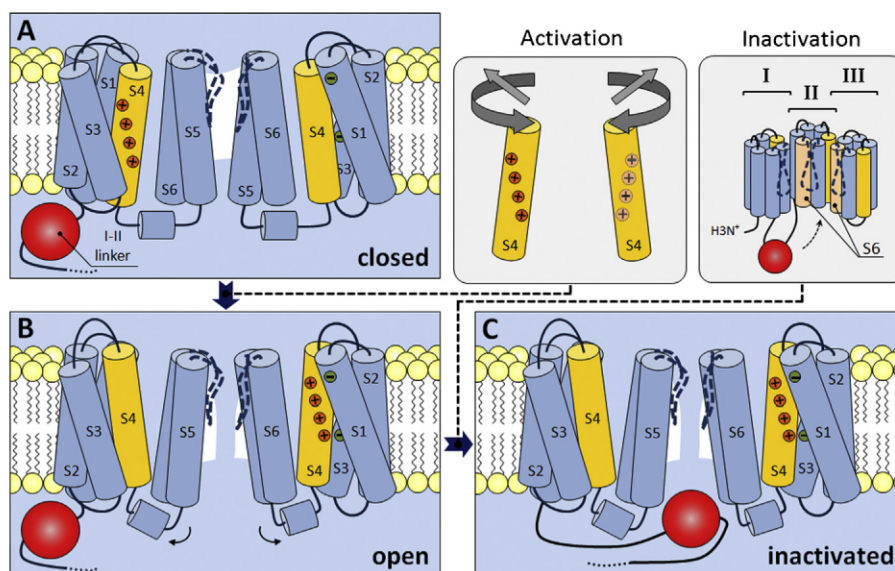


**Fig. 2.** Conformational changes during activation and inactivation of VGCCs. Cartoon illustrating possible mechanisms of channel activation and inactivation based on models of activation for Shaker  $K^+$ -channels and fast VDI of  $Ca_v2.3$  VGCCs. Only two of the four homologous domains are shown. (A) At resting membrane potentials, the permeation pathway is occluded by regions of the S6 segments which form parts of the channel lumen, resulting in a hydrophobic cavity that is inaccessible for ions. (B) During membrane depolarization, the positively charged S4 segments (yellow) rotate and decrease their tilt (see inset), leading to changes in the relative position of other segments and formation of a water-filled crevice, in which ions can traverse the channel. (C) Upon prolonged depolarization, the intracellular linker between domains I and II (highlighted in red) docks to a site composed, in parts, of the S6 segments of domains II and III (see inset), thereby physically occluding the inner vestibule of the channel and terminating the flow of ions.

Redrawn and combined from Bezanilla (2000) and Stotz et al. (2000).

biophysical properties of  $\alpha_1$ -subunits (Wei et al., 1995; Arikath and Campbell, 2003). Unlike  $\beta$ - and  $\alpha_2\delta$ -subunits however, they appear to play no role for trafficking of channels to the cell surface (Arikath and Campbell, 2003; Arikath et al., 2003). To date, a  $\gamma$ -subunit exclusively expressed in skeletal muscle ( $\gamma_1$ ), a neuronal  $\gamma$ -subunit ( $\gamma_2$ ) and a number of  $\gamma$ -like subunits ( $\gamma_3$ – $\gamma_8$ ) have been described and cloned, although in several cases, their classification as actual  $Ca^{2+}$  channel subunits remains controversial (Klugbauer et al., 2000; Chu et al., 2001; Moss et al., 2002).

### 3. Molecular properties

A general assumption first introduced by Hodgkin and Huxley in 1952 and still adopted when characterizing voltage-gated ion channels is that permeation through open channels, as measured by the voltage- and concentration-dependent single-channel (microscopic) current, is independent of channel gating, as measured by the voltage- and time-dependent channel open probability (and vice versa) (Hodgkin and Huxley, 1952a; Hille, 2001; Pusch, 2006). In keeping with this conceptually useful assumption, permeation and gating will be considered separately, noting that the distinction is unlikely to be absolute. As addressed in later sections, ions occupying the pore may affect global protein structure and thus influence channel gating, while conformational rearrangements during gating may conversely lead to structural changes in the pore region and thus modify permeation.

#### 3.1. Gating behaviour

##### 3.1.1. Voltage-dependent activation

Activation and deactivation of VGCCs are tightly coupled to the membrane potential through a process of charge-moving conformational changes, which leads to a sigmoid increase of channel open probability over a relatively narrow voltage-range (Supplementary Fig. 1) and produces measurable gating currents. The underlying mechanism is thought to be similar in all voltage-gated

ion channels and seems to largely depend on charged residues in the S2, S3 and especially S4 segments of all four domains. Based on the crystal structure of bacterial voltage-gated  $Na^+$ - and  $K^+$ -channels, prevailing negative charge in the inside of the cell at resting membrane (i.e. hyperpolarized) potentials is thought to attract the positively charged S4 segments towards the interior of the cell, thereby holding the channel in a closed conformation. Depolarization forces the S4 segments to slide (rotate and/or tilt) through a protein-lined pathway (Fig. 2A and B) (Bezanilla, 2000, 2002; Elinder and Arhem, 2003), a process that may be assisted by formation and braking of salt bridges with neighbouring segments. It seems to be followed by a relatively voltage-independent last step of conformational changes, during which relocation of the S5 and S6 segments produces (in bacterial  $K^+$ - and  $Na^+$ -channels) a total displacement of 8–15 Å, thus opening the channels (Amaral et al., 2012).

In HVA channels, activation gating is subject to modulation by co-expressed  $Ca_v\beta$  subunits, which generally accelerate the time course of macroscopic currents and shift the voltage-dependence of activation towards more hyperpolarized potentials (Lacerda et al., 1991; Mori et al., 1991; Singer et al., 1991; Hullin et al., 1992; Lory et al., 1993; Stea et al., 1993; De Waard and Campbell, 1995; Parent et al., 1997; Jones et al., 1998). Detailed studies of ionic and gating currents indicate that these effects are associated with little change in the kinetics or voltage-dependence of gating charge movement, but may instead involve an improved coupling between voltage-sensors and channel opening (i.e. changes in the final, weakly voltage-dependent closed-to-open transition) (Neely et al., 1993; Josephson and Varadi, 1996; Kamp et al., 1996; Jones et al., 1998).

##### 3.1.2. Voltage- and $Ca^{2+}$ -dependent inactivation

The extent of  $Ca^{2+}$  entry through VGCCs upon prolonged depolarization is limited by transition of activated channels to non-conducting, inactivated states, a process which can proceed through different conformational changes.



Fast voltage-dependent inactivation (VDI) in HVA channels has been linked to residues scattered along the  $\alpha_1$ -subunit, including parts of the pore-forming segments, intracellular linkers and the C-terminal domain (Hering et al., 2000; Stotz et al., 2000). The process could proceed through a 'hinged lid' mechanism involving occlusion of the inner pore vestibule by docking of the intracellular I–II linker to the cytoplasmic ends of the S6 segments (Fig. 2C) (Stotz et al., 2000, 2004; Stotz and Zamponi, 2001). It is thought to primarily arise from a coupling between activation and inactivation (i.e. state-dependent rather than directly voltage-dependent inactivation) (Serrano et al., 1999; Budde et al., 2002; Talavera and Nilius, 2006b) and may be initiated by subtle conformational changes in the S6 segments, which promote interaction with the I–II linker. Fast VDI of HVA channels is markedly affected by co-expressed  $\beta$ -subunits, which associate with a  $\beta$ -subunit interaction domain on the I–II linker and may modify its mobility (Stotz et al., 2004). A general functional pattern observed in heterologous expression studies is that  $\beta_1$  and  $\beta_3$  subunits act primarily to accelerate and  $\beta_2$  and  $\beta_4$  subunits to decelerate macroscopic inactivation of many HVA channel  $\alpha_1$ -subunits (Isom et al., 1994; Qin et al., 1998; Restituito et al., 2000). Interestingly, both fast VDI and  $\beta$ -subunit co-expression also modify binding of organic antagonists and may be relevant for certain effects of inorganic cations as well (but see Section 4.2.6.4).

Even less is known about determinants of fast VDI in LVA channels, although mutations in several regions, including I–II linker, proximal parts of the C-terminal domain and the S6 segment in domain III (Marksteiner et al., 2001; Talavera and Nilius, 2006a), can affect the time course of macroscopic currents. However, it has been pointed out that the strong coupling in LVA channels of macroscopic inactivation to activation (inactivation of single LVA channels is in fact voltage-independent) can complicate analysis of these findings. Thus, modification of LVA channel structure often produces correlated changes of macroscopic activation and inactivation, but closer analysis reveals that inactivation kinetics are in many cases unaffected when measured at depolarized potentials (where macroscopic current decay more accurately reflects microscopic inactivation kinetics) (Talavera and Nilius, 2006a, 2006b). Based on these findings, and the general correlation between activation and inactivation rates in different LVA channel types and mutants, it has been proposed that both activation and inactivation gate may be formed by the same intracellular components of the pore. Enhanced probability for the inactivation transition of the open pore conformation could then couple inactivation to activation gating.

The  $\beta$ -subunit interaction domain in LVA channels is replaced by a rigid helix-loop-helix 'gating brake' structure (Arias-Olguin et al., 2008; Baumgart et al., 2008; Perez-Reyes, 2010; Karmazinova et al., 2011). Interaction of the second helix with parts of the S6 segments has been proposed to slow inactivation and stabilize closed channel states at hyperpolarized potentials, since mutations associated with its disruption result in channels which activate at even more negative membrane potentials and inactivate faster (Karmazinova et al., 2011).

Little is currently known about the slow form of VDI, but some types of VGCCs exhibit rapid  $\text{Ca}^{2+}$ -dependent inactivation (CDI), a negative feedback mechanism directly mediated by  $\text{Ca}^{2+}$  and likely serving to restrict  $\text{Ca}^{2+}$ -influx through otherwise non-inactivating channels ( $\text{Ca}_v1.1$ – $1.4$ ) and channels involved in transmitter release ( $\text{Ca}_v2.1$  and  $\text{Ca}_v2.2$ ). Various factors have been implicated in the induction of CDI, but the major determinant seems to be binding of  $\text{Ca}^{2+}$ /CaM complexes to regions in the C-terminal domain or  $\text{Ca}^{2+}$  binding to constitutively bound CaM respectively (Budde et al., 2002). As discussed in Section 4.2.6.3, CDI may also involve changes in the affinity of the selectivity filter for permeant ions.

### 3.2. Selective permeation

Under physiological conditions, monovalent cations ( $\text{Na}^+$ ,  $\text{K}^+$ ) are present at about 100-fold higher concentrations, yet VGCCs are almost exclusively selective for  $\text{Ca}^{2+}$ , as reflected in permeability ratios of over 1000:1 for  $\text{Ca}^{2+}$  over  $\text{Na}^+$ ,  $\text{K}^+$  or  $\text{Cs}^+$  (Hagiwara and Takahashi, 1967). In its absence however, they become highly permeable to monovalent cations, indicating that selectivity arises from some form of competition between permeant ions. The concentration-dependence of  $\text{Ca}^{2+}$  inward current is non-linear, and saturates as the external  $\text{Ca}^{2+}$  concentration is increased, an effect well described by a Langmuir type expression and traditionally attributed to interaction with sites in the pore (Hagiwara and Takahashi, 1967; Hagiwara et al., 1975; Akaike et al., 1978; Beirao and Lakshminarayanaiah, 1979; Kostyuk, 1980). Also, conductance vs. mole fraction curves measured with mixtures of permeant electrolytes (i.e.  $\text{Ca}^{2+}$  and  $\text{Ba}^{2+}$ ) at a constant total concentration are usually, if not always, non-monotonic and exhibit a minimum (i.e. channel conductance with certain mixtures is less than conductance with the same concentration of either ion alone) (Almers and McCleskey, 1984; Hess and Tsien, 1984; Byerly et al., 1985; McDonald et al., 1986; Friel and Tsien, 1989; Zamponi and Snutch, 1996). This anomalous mole fraction effect (AMFE) is typically taken as evidence for the correlated motion of multiple ions through a narrow, single-file pore with one or more  $\text{Ca}^{2+}$ -binding sites. Mutagenesis studies could eventually link high-affinity  $\text{Ca}^{2+}$  binding in the pore region of HVA channels to a single conserved site (EEEE locus), formed by glutamate residues located at equivalent positions in each of the four  $\alpha_1$  P-loops (Tang et al., 1993; Yang et al., 1993; Ellinor et al., 1995; Cibulsky and Sather, 2000). Detailed structure–function studies show that they all participate in the high-affinity site but make unequal contributions to  $\text{Ca}^{2+}$ -binding and proton block (Kim et al., 1993; Mikala et al., 1993; Yang et al., 1993; Yatani et al., 1994; Bahinski et al., 1997; Ellinor et al., 1995; Parent and Gopalakrishnan, 1995). In LVA channels, two of the four corresponding glutamate residues are substituted by aspartate (EEDD locus), which is associated with some (i.e. low  $\text{Cd}^{2+}$ -sensitivity, lower single channel conductance) but not all of their unique properties (i.e. weak discrimination between different divalent charge carriers, less marked AMFE) (Shuba et al., 1991; Talavera et al., 2001; Cens et al., 2007; Shuba, 2014). In  $\text{Ca}_v3.1$  channels, the contribution of aspartate residues to coordination of divalent cations and proton block appears to be symmetrical (Talavera et al., 2001; Talavera and Nilius, 2006a), whereas in  $\text{Ca}_v3.2$  channels, they differentially affect  $\text{Ca}^{2+}/\text{Ba}^{2+}$  permeability ratio, AMFE and proton block (Park et al., 2013). In the absence of structural data, a number of theoretical models have been developed to account for the apparent paradox of high selectivity and high conductance, differing mainly in their mathematical appearance (i.e. discrete steps in chemical-kinetic models vs. continuous functions in electrodiffusion models) (Miller, 1999) and in the number of assumed pore-localized binding sites. More recent structure-oriented modelling approaches employ molecular dynamics simulations in aqueous phase to reproduce experimental findings based on proposed structural features of VGCCs. As described below, all of these models should be regarded as complementary rather than exclusive, since they demonstrate different general mechanisms of selection, which might well work together and help to guide further structure-based modelling.

#### 3.2.1. Continuum models: selection based on charge and size

Electrodiffusion models like the ion exchange (Nonner et al., 2000) or the resistors-in series model (Gillespie and Boda, 2008) focus on volume-exclusion effects and electrostatic interactions between ions and charged regions of the channel, and assume that

carboxylate groups of the EEEE/EEDD-locus behave like ions in a concentrated bulk solution (i.e. restricted to the selectivity filter but otherwise free to move). They rapidly rearrange to screen permeating cations, creating a liquid-like, spatially confined environment where ions move diffusively and compete for limited space (Gillespie and Boda, 2008). Selectivity arises from the fact that  $\text{Ca}^{2+}$  carries twice as much counter-charge as  $\text{Na}^+$  and other monovalent cations while being of approximately the same size, such that it can neutralize the highly charged carboxylate groups without overcrowding the pore lumen (charge/space competition). Important implications of these models are that discrete binding sites are not necessarily required for selectivity and that the AMFE can, in principle, also occur without single-filing and in channels which contain (on average) less than one ion at a time (Nonner et al., 1998; Gillespie et al., 2005, 2008; Gillespie, 2008).

### 3.2.2. Chemical-kinetic models: stepwise changes in affinity

Chemical kinetic models with two or more pore-localized binding sites have been the most widely considered (Hess and Tsien, 1984; Lansman et al., 1986; Friel and Tsien, 1989; Rosenberg and Chen, 1991; Kuo and Hess, 1993a, 1993c), but several objections have been raised to their use, mainly based on the loss of high-affinity  $\text{Ca}^{2+}$  binding produced by disruption of the EEEE-locus in HVA channels. However, the 'stairstep' model of selective permeation requires only a single high-affinity site to quantitatively reproduce many experimental findings (Dang and McCleskey, 1998). It assumes that flanking low-affinity sites could provide steps of potential energy (i.e. allow for a stepwise entry and exit of ions from the pore), thus lowering the energy required for dissociation from a central high-affinity binding site (Dang and McCleskey, 1998). These steps could be realized by discrete  $\text{Ca}^{2+}$  coordination sites of successively higher/lower affinity, or by a stepwise replacement of water molecules in the inner hydration sphere by ligating pore-residues (i.e. catalysed de- and rehydration) (Eigen and Winkler, 1971; Andersen and Koeppe, 1992). The unequal contribution of EEEE-locus glutamates to  $\text{Ca}^{2+}$ -binding could reflect motif-dependent functionalities, conferred by nearby pore residues. Alternatively, it has been proposed that there may be a set of high-affinity sites separated by low or insignificant energy barriers, at which repulsive interaction between ions, possibly aided by additional low-affinity sites, facilitate high rates of flux (Almers and McCleskey, 1984; Hess and Tsien, 1984; Kuo and Hess, 1993a, 1993b, 1993c). Here, the channel is thought to be occupied almost continually by at least one  $\text{Ca}^{2+}$  ion, such that repulsive ion-ion interactions guard it against permeation by monovalent cations, allow high throughput of  $\text{Ca}^{2+}$  and prevent saturation of the pore (Hess and Tsien, 1984). Simulation of  $\text{Ca}_v3.1$  channels shows that most aspects of permeation through these channels can be described reasonably well by a two-site model with modest repulsion and a low-affinity internal binding site (Lopin et al., 2010).

### 3.2.3. Molecular models: ion-ion interactions at a flexible binding locus

Most current models of selective permeation are based on the assumption that the EEEE/EEDD-locus forms a single, multi-ion binding locus, which can accommodate one  $\text{Ca}^{2+}$ -ion with high affinity or multiple  $\text{Ca}^{2+}$ -ions with lower affinity. Occupation by more than one ion could destabilize the high-affinity site through electrostatic repulsion between ions (Almers and McCleskey, 1984; Hess and Tsien, 1984), competition for binding moieties (Armstrong and Neyton, 1991; Yang et al., 1993) and/or  $\text{Ca}^{2+}$ -induced conformational changes (Lux et al., 1990; Mironov, 1992). The concept of these models is vividly illustrated by molecular dynamics simulations of permeation through L-type channels, carried out based on bacterial  $\text{K}^+$ - and  $\text{Na}^+$ -channels as structural

templates (Lipkind and Fozzard, 2001). Here, in the absence of  $\text{Ca}^{2+}$  or other divalent cations, glutamate oxygens repel each other and retract towards the edge of the selectivity filter, such that organic cations as large as tetramethylammonium ( $\sim 6 \text{ \AA}$ ) can pass the pore (McCleskey and Almers, 1985; Lipkind and Fozzard, 2001; Cataldi et al., 2002). At low micromolar  $\text{Ca}^{2+}$  concentrations, the carboxylate-bearing side chains move towards the centre of the pore and form a pseudo-symmetrical cage around a single dehydrated  $\text{Ca}^{2+}$  ion, thus reducing the apparent diameter of the pore and blocking permeation of monovalent cations. At millimolar  $\text{Ca}^{2+}$  concentrations, they spontaneously interact with additional  $\text{Ca}^{2+}$  ions, such that at least three ions can simultaneously occupy the selectivity filter. In the latter case, no coordination shell is formed, and repulsive interactions enable  $\text{Ca}^{2+}$  ions to overcome the high electrostatic attraction of the selectivity filter and leave the pore.

### 3.2.4. Allosteric and electrostatic effects: role of regions outside of the pore

Selective permeation in VGCCs is not only controlled by intrapore sites, but also by residues located outside of the ion-conducting pathway itself. For instance, an EF-hand<sup>1</sup> like motif present in the p-loop of domain III of all HVA (Feng et al., 2001; Sun et al., 2007) but not LVA channels (Cribbs et al., 1998; Perez-Reyes et al., 1998; Lee et al., 1999a) has been linked to differences in the  $\text{Ca}^{2+}/\text{Ba}^{2+}$  permeability ratio between the two groups (i.e. higher  $\text{Ba}^{2+}$ -permeability of HVA channels vs. approximately equal permeability for  $\text{Ca}^{2+}$  and  $\text{Ba}^{2+}$  of LVA channels). Mutations in this region, which consists of a central glycine residue flanked by acidic amino acids (aspartate and glutamate), enhance  $\text{Ca}^{2+}$  permeability with no effects on  $\text{Ba}^{2+}$  conductance, and produce HVA channels with nearly equal permeability for  $\text{Ca}^{2+}$  and  $\text{Ba}^{2+}$ , suggesting that the intact motif may selectively decrease  $\text{Ca}^{2+}$  permeability (Feng et al., 2001). In addition, all vertebrate VGCCs contain a set of non-conserved (i.e. channel-specific) amino acids, which form a ring of charged residues (divalent cation selection locus or DCS-locus) in the vicinity of the EEEE/EEDD-locus. The DCS-locus has been linked to differences in the  $\text{Ca}^{2+}/\text{Ba}^{2+}$ -permeability ratio of individual HVA and LVA channels, and the LVA-like permeation profile of  $\text{Ca}_v2.3$  channels (Bourinet et al., 1996; Cens et al., 2007), but the exact mechanism by which it exerts its action remains to be elucidated. It has been proposed to form an external low-affinity  $\text{Ca}^{2+}$ -binding site directly involved in permeation, or to provide extra negative charge to electrostatically affect close-range ion-pore and/or ion-ion interactions at the channel entrance (Cens et al., 2007; Shuba, 2014).

### 3.2.5. Structure and function: insights from the bacterial model channel $\text{Ca}_v\text{Ab}$

A structure-based understanding of  $\text{Ca}^{2+}$  channel selectivity and permeation is facilitated by recently published X-ray crystallographic data on the VGCC  $\text{Ca}_v\text{Ab}$  and its derivatives. Created by substitution of up to three amino acids in the selectivity filter of the bacterial voltage-gated  $\text{Na}^+$ -channel  $\text{Na}_v\text{Ab}$  by aspartate residues, these channels possess a pore-motif which is structurally related to vertebrate VGCCs and provide valuable insight into possible mechanisms of selective permeation (Tang et al., 2014). For the following structure-function considerations, all constructs will be designated relative to mutants with all three aspartate-substitutions ( $\text{Ca}_v\text{Ab}$ ), which exhibit the highest degree

<sup>1</sup> It should be noted that the term EF-hand is somewhat misleading, since the affinity of extracellular binding sites for  $\text{Ca}^{2+}$  is usually orders of magnitude lower than that of 'true' EF-hands. Owing to the much higher  $\text{Ca}^{2+}$ -concentration in the extracellular space, they may nevertheless be in their  $\text{Ca}^{2+}$ -bound form most or all of the time (for review see Krebs and Heizmann, 2007).



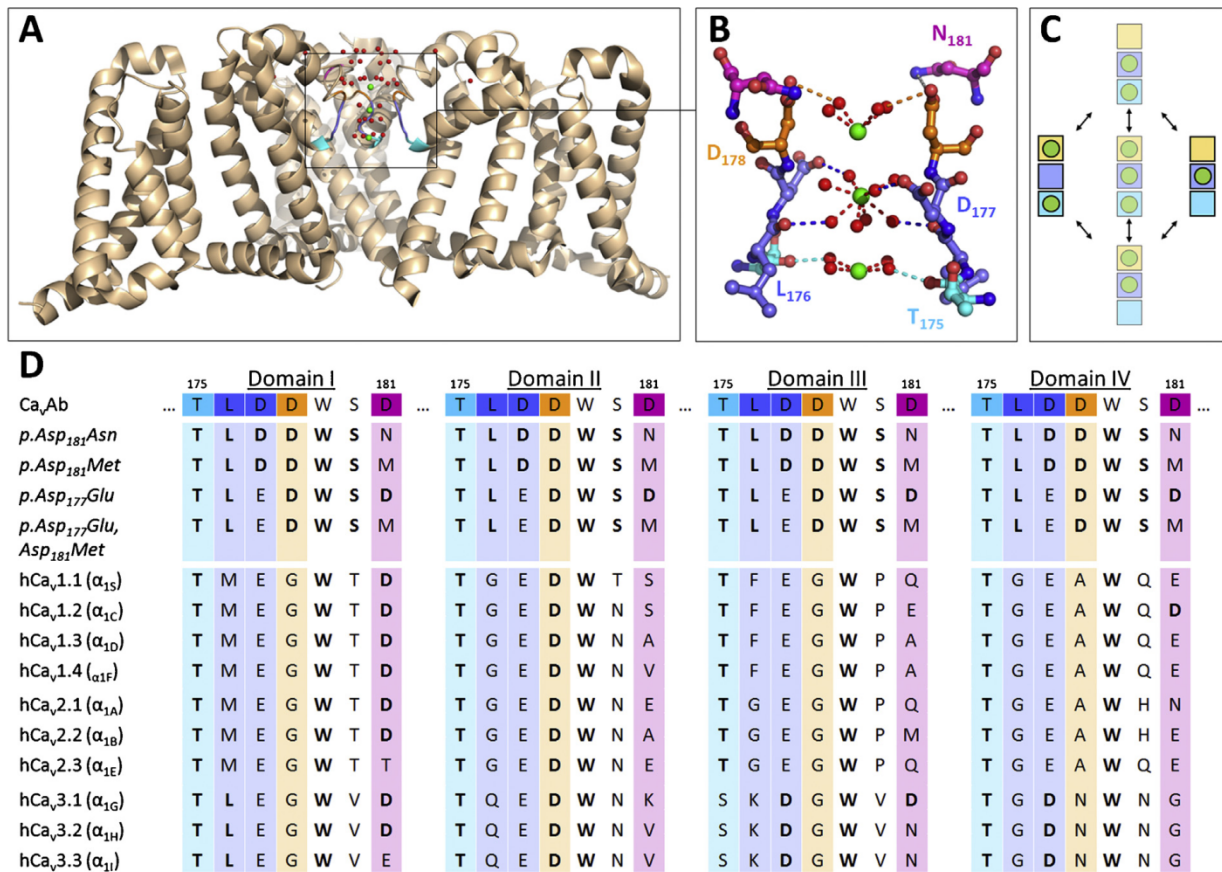


**Fig. 3.** Functional organization of the selectivity filter in Ca<sub>v</sub>Ab and its derivatives. (A, B) Cartoon representation of the crystal structure of pAsp<sub>181</sub>Asn showing three of the four identical domains with Ca<sup>2+</sup> ions (green) bound to all three coordination sites in the selectivity filter. Colour coded regions correspond to residues equivalent to the DCS-locus (magenta), external (orange) and central (blue) high-affinity site and the inner, low-affinity site (cyan). Note that the crystal structure likely reflects a mixed population of channels, in which either the central or the two flanking coordination sites are occupied. (C) State-diagram showing the two low energy states of occupation and possible intermediates. (D) Sequence alignment of residues making up the selectivity filter in Ca<sub>v</sub>Ab, its derivatives and in cloned human VGCCs. Conserved residues are highlighted in bold.

of Ca<sup>2+</sup>-selectivity (permeability ratio >10,000:1 for Ca<sup>2+</sup> over Na<sup>+</sup>) and have the pore motif T<sub>175</sub>LDDWSD<sub>181</sub> (i.e. p.Asp<sub>181</sub>Asn refers to constructs in which, relative to Ca<sub>v</sub>Ab, Asp<sub>181</sub> is replaced by asparagine, but see Fig. 3D). Crystallographic and functional analysis revealed that during passage of these channels, Ca<sup>2+</sup> ions remain stabilized in a hydrated state and interact with a total of three intra-pore binding sites (Fig. 3A and B), although only one of them binds Ca<sup>2+</sup> with sufficient affinity for block. A first external coordination site is formed by a ring of carboxylate oxygens lining the pore entryway, which are provided by aspartate residues (Asp<sub>178</sub>) at the outer edge of the selectivity filter (Fig. 3B). A central coordination site with highest Ca<sup>2+</sup> affinity (site 2) is formed by the concerted action of aspartate residues equivalent to the EEEE/EEDD-locus in vertebrate channels (Asp<sub>177</sub> = site 2a or DDDD-locus), and backbone carbonyl groups of neighbouring leucine residues (Leu<sub>176</sub> = site 2b). Rather than projecting into the pore lumen, carboxylate-bearing side chains of the DDDD-locus are located along the walls of the selectivity filter, thus allowing passage of a single hydrated Ca<sup>2+</sup> ion (Fig. 3B). A third, lower-affinity site (site 3) flanking the central cavity is formed by backbone carbonyl groups of threonine residues (Thr<sub>175</sub>) on the internal side of the selectivity filter (Fig. 3B). The mechanism of flux has been proposed to involve oscillation between two interchangeable low energy states, in which either two Ca<sup>2+</sup> ions simultaneously occupy sites 1 and 3 (state A), or one Ca<sup>2+</sup> ion occupies the central site (state B) (Fig. 3C) (Tang et al., 2014). Transition from state A to state B is thought to occur upon entry of a third ion, which leads to a loss of Ca<sup>2+</sup> from site 3 due to ion-ion

interactions. Taken together, these findings illustrate how the different mechanisms of selection described above might converge and justify a reconsideration of selective permeation in vertebrate VGCCs.

### 3.2.6. Ca<sub>v</sub>Ab as a structural framework: implications for vertebrate channels

Considering their four-domain architecture, vertebrate VGCCs must have evolved to a more complex mechanism of ion transfer, but sequence alignment of the pore motif in Ca<sub>v</sub>Ab with the corresponding region in human channels reveals a number of striking similarities (Fig. 3D). Residues making up the inner low-affinity site in Ca<sub>v</sub>Ab are still present in vertebrate channels (except for repeat III in LVA channels, where threonine residues are substituted by the structurally related amino acid serine), suggesting that the site may be functionally preserved. Of the aspartate residues forming the outer site in Ca<sub>v</sub>Ab, only one in domain II is still present in vertebrate channels, while the equivalent positions in domains I, III and IV are neutral glycine (domains I and III), alanine (domain IV in HVA channels) or asparagine (domain IV in LVA channels) residues (Fig. 3D). A recent investigation by Shaya et al. (2014) nevertheless provides strong evidence that vertebrate channels are also equipped with an outer ion binding site formed by the remaining aspartate residue in domain II. Using hCa<sub>v</sub>1.2 channels expressed in *Xenopus* oocytes, it was found that neutralization of this residue by replacement with asparagine, alanine or glycine reduces apparent Ca<sup>2+</sup> affinity to the same or even greater extent as charge neutralization of the



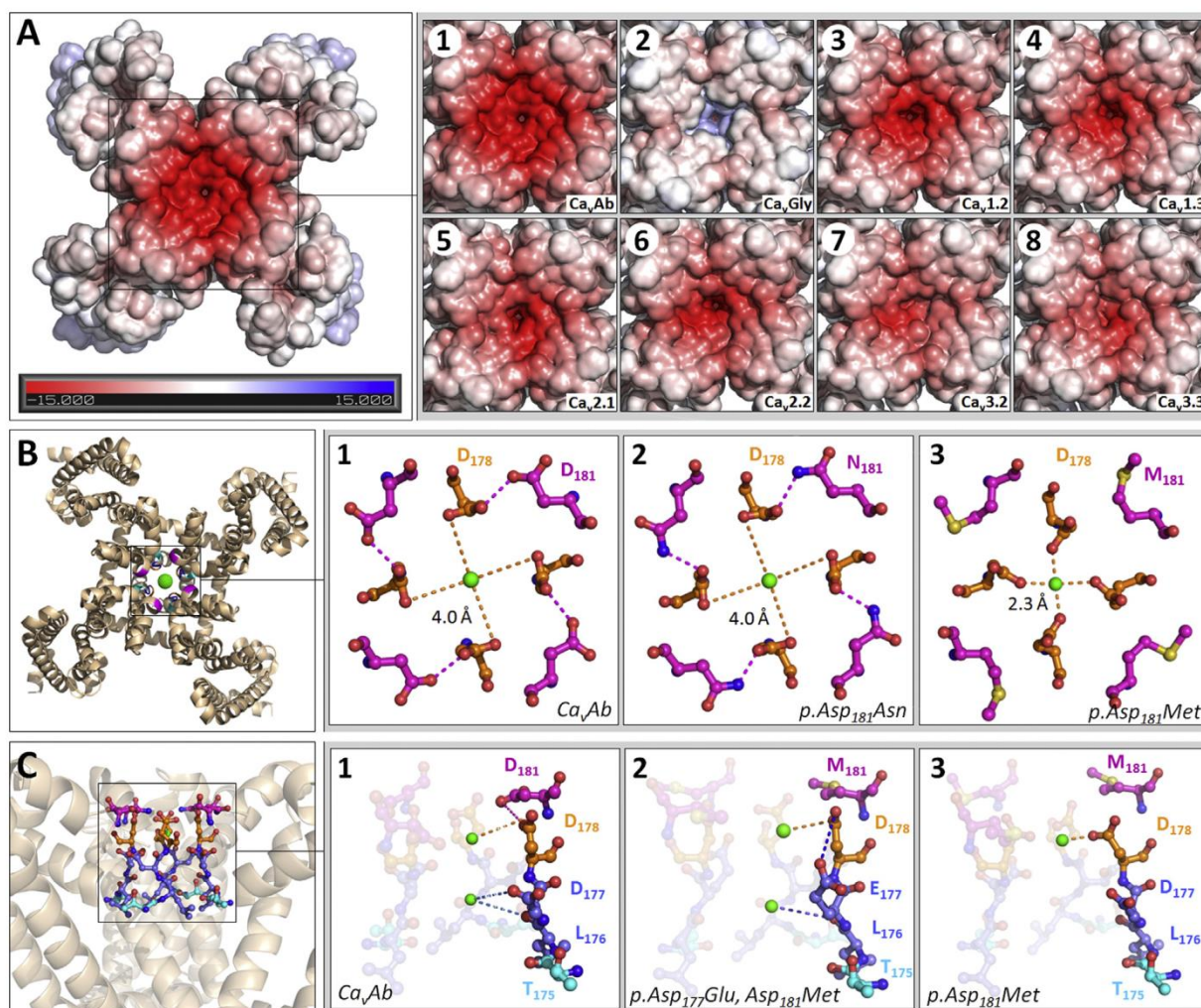


**Fig. 4.** Structure–function relationship of the selectivity filter in  $Ca_vAb$  and its derivatives. (A) Surface representation of electrostatic potentials on solvent-accessible parts at the extracellular channel entrance of  $Ca_vAb$  (A1) and simulated constructs in which the selectivity filter has been replaced by glycine residues ( $Ca_vGly$ ) (A2), or by corresponding residues of the indicated human  $Ca_v\alpha_1$ -subunits (A3–8). Negative and positive charges are coloured in red and blue, respectively. Electrostatic potentials were calculated using PDB2PQR and the adaptive Poisson–Boltzmann solver (APBS). Human channels were simulated by replacement of the corresponding residues in the selectivity filter of  $Ca_vAb$  (positions 175–181 in all four domains) and use of the resulting constructs without further structural optimization. Note how complete replacement of the selectivity filter in  $Ca_vAb$  by glycine abolishes almost all negative charge at the channel entrance and how differences in the DCS-locus shape the distribution of charge in individual human HVA and LVA channels, respectively. (B, C) Ball and sticks representation showing how steric interactions between residues corresponding to the DCS-locus (magenta) and site 1 (orange) produce conductive channels in the case of  $Ca_vAb$  (B1, C1) and  $p.Asp_{181}Asn$  (B2) but not  $p.Asp_{181}Met$  (B3, C3). In constructs with EEEE-locus and  $Met_{181}$  (C2), glutamate residues swing away from the selectivity filter and interact with site 1, such that site 2 is exclusively formed by backbone carbonyl oxygens of  $Leu_{176}$ , but site 1 remains conductive.

neighbouring EEEE-locus glutamate ( $IC_{50}$  for  $Ca^{2+}$  block of  $Li^+$  current approximately 11, 14 and 23  $\mu M$  respectively vs. 2  $\mu M$  in WT and 15  $\mu M$  in EEEE-locus mutants) (Shaya et al., 2014). Point mutations in the EEEE-locus of HVA channels have the largest reported impact on high affinity  $Ca^{2+}$  binding when they target the glutamate residue in domain II (Parent and Gopalakrishnan, 1995; Yang et al., 1993), and since the position of residues corresponding to the outer site in  $Ca_vAb$  is much more exposed to bulk solvent, the effects of their replacement in  $hCa_v1.2$  are thought to reflect ‘true’ changes in the interaction of  $Ca^{2+}$  ions with the pore rather than alterations in the electrostatic environment (Shaya et al., 2014).

It is also worth taking a closer look on  $Asp_{181}$ , which corresponds to the DCS-locus in vertebrate channels and may play a similar role for selective permeation in  $Ca_vAb$ . Here,  $Asp_{181}$  is not directly involved in permeation but a major determinant of the structural arrangement and functional properties of the pore. Its side chains engage site 1, where they influence the degree of  $Ca^{2+}$  selectivity, presumably by fine-tuning the local electric field, as

reflected in the 4–5 times lower  $Ca^{2+}$ -selectivity of aspartate-to-asparagine mutants ( $p.Asp_{181}Asn$ ) (Tang et al., 2014). The net charge density at the channel entrance of  $Ca_vAb$  is mainly determined by its pore motif (Fig. 4A1 and A2), and fine-tuned by residues equivalent to the DCS-locus. In vertebrate channels, the DCS locus is the only structure in the pore motif with truly subunit specific differences in the amino acid sequence (Fig. 3D), suggesting a role of this region in the shaping of specific permeation and/or selectivity profiles of individual channel types. This is vividly illustrated by transfer of the pore motifs of different human  $Ca_v\alpha_1$ -subunits into the structure of  $Ca_vAb$  and computation of the resulting electrostatic potentials at the pore mouth (Fig. 4A3–A8). Since essentially all other charged amino acids in this region are conserved within (but not between) human HVA ( $hCa_v1.1$ – $hCa_v2.3$ ) and LVA ( $hCa_v3.1$ – $hCa_v3.3$ ) channels (Fig. 3D), differences in density and distribution of charge at the pore mouth of individual members of the two subfamilies are almost exclusively determined by the DCS-locus. This comparison ignores the possible



influence of charged regions outside of the pore motif, but previous work on L-type channels suggests that structural differences responsible for the distinct unitary conductance of individual subunits are primarily located in the S5–S6 linkers (Cibulsky and Sather, 2003).

In  $\text{Ca}_v\text{Ab}$  and its derivatives, residues in position 181 moreover sterically interact with pore residues involved in permeation. Thus, formation of carboxylate–carboxylate pairs with ( $\text{Ca}_v\text{Ab}$ ) (Fig. 4B1) or donation of hydrogen bonds to ( $\text{p.Asp}_{181}\text{Asn}$ ) (Fig. 4B2) site 1 seems to be critical for reversible binding of hydrated  $\text{Ca}^{2+}$ -ions. Mutants in which  $\text{Asp}_{181}$  is substituted by hydrophobic methionine residues ( $\text{p.Asp}_{181}\text{Met}$ ) are non-conducting, since the unconstrained amino acid residues of site 1 form an inner sphere coordination compound with  $\text{Ca}^{2+}$  (i.e. tightly bind a dehydrated  $\text{Ca}^{2+}$  ion) (Fig. 4B3 and C3). When the DDDD-locus of  $\text{Ca}_v\text{Ab}$  is replaced with a ring of glutamate residues ( $\text{p.Asp}_{177}\text{Glu}$ ), their side chains move away from the selectivity filter and are firmly held in this position by hydrogen bonds with  $\text{Asp}_{181}$  and  $\text{Ser}_{180}$ . As a consequence, site 2 in  $\text{p.Asp}_{177}\text{Glu}$  is exclusively formed by backbone carbonyls of  $\text{Leu}_{176}$ , and mutants with both EEEE-locus and hydrophobic methionine residues in position 181 ( $\text{p.Asp}_{177}\text{Glu}$ ,  $\text{Asp}_{181}\text{Met}$ ) are conductive, since formation of carboxylate–carboxylate pairs between  $\text{Glu}_{177}$  and  $\text{Asp}_{178}$  prevents binding of dehydrated  $\text{Ca}^{2+}$  ions to site 1 (as in  $\text{p.Asp}_{181}\text{Met}$ ) (Fig. 4C2). Taken together, these findings signify that multiple high-affinity intra-pore sites are not necessarily incompatible with a loss of high  $\text{Ca}^{2+}$  flux produced by disruption of the EEEE-locus in HVA channels.

Looking at the amino acid sequence of human channels, it seems likely that EEEE/EEDD-locus glutamates also interact with nearby residues, although the pseudosymmetrical architecture presumably leads to a domain- and channel-specific pattern. Using analysis of mutant cycles, it has been demonstrated that a channel-specific fine tuning of EEEE-locus glutamates (i.e. site 2a) in HVA channels by their N-terminal neighbour (i.e. site 2b) in repeat III still exists (Williamson and Sather, 1999), which may also contribute to the functional asymmetry of EEEE-locus glutamates. Thus, the picture that emerges is that of a common pore architecture in  $\text{Ca}_v\text{Ab}$  and vertebrate VGCCs, although the mechanism of  $\text{Ca}^{2+}$  selection and conductance is clearly more complex in the latter, evolutionary younger channels. As described in the next chapter, blocking experiments with inorganic cations provide further evidence to support this view, making it tempting to speculate that VGCCs may have evolved through single point mutations in homotetrameric voltage-gated  $\text{Na}^+$ -channels (or vice versa). Gene duplication and adaption of a pseudo-symmetrical architecture could have arisen mainly from a need for diversification (i.e. tuneable  $\text{Ca}^{2+}$ -selectivity and conductance, faster kinetics, voltage- and  $\text{Ca}^{2+}$ -dependent inactivation) as evolutionary pressure.

#### 4. Modulation by inorganic cations

Since several  $\text{Ca}_v\alpha_1$ -subunits and many native  $\text{Ca}^{2+}$  currents are resistant towards small organic  $\text{Ca}^{2+}$  channel antagonist or peptide toxins, but all VGCCs are more or less potently blocked by inorganic cations, these ions have long been used experimentally to inhibit VGCCs. Some of them exhibit little selectivity and effectively suppress all types of VGCCs, while others seem to preferentially inhibit certain  $\text{Ca}_v\alpha_1$ -subunits and have been used to distinguish currents mediated by a particular channel type. The latter is increasingly recognized to depend not only on differences in the degree of block of the ion-conducting pore, but also on subunit-specific additional effects on channel gating. These actions can considerably complicate interpretation of experimental findings,

since often no attempt has been made to separate different mechanisms of action.

The ensuing three parts of the article address the modulatory actions of polyvalent cations in terms of three general mechanisms, (i) electrostatic effects, resulting from long-range interaction with charged regions on or near the channels (Fig. 5A and B), (ii) pore blocking effects, resulting from interaction with regions in the ion-conducting pore (Fig. 5C), and (iii) allosteric effects, resulting from interaction with the gating machinery or regulatory sites (Fig. 5D).

Relevant approaches for the dissection of these mechanisms as well as their potential pitfalls are briefly addressed where it is deemed appropriate. Further information on the analysis of metal-induced effects on VGCCs in electrophysiological recordings can be found in the supplementary materials and elsewhere (Hille, 2001; Pusch, 2006; Abramson and Müller, 1933).

##### 4.1. Electrostatic effects (Fig. 5A and B)

With the understanding of cellular excitability in terms of voltage-dependent conductance changes, it became evident that manipulation of the extracellular salt concentration or composition can produce effects not unlike changes in the membrane potential (e.g. Abramson and Müller, 1933; Brink et al., 1946; Cole, 1949; Brink, 1954). In their pioneering work, Frankenhaeuser, Hagiwara and others noted that the threshold membrane potential for  $\text{Na}^+$  and  $\text{Ca}^{2+}$  spike initiation generally increases with increasing concentration of extracellular polyvalent cations, and demonstrated that this effect is related to depolarizing shifts in the apparent voltage-dependence of  $\text{Na}^+$ -,  $\text{Ca}^{2+}$ - and  $\text{K}^+$ -channel gating (Frankenhaeuser and Hodgkin, 1957; Frankenhaeuser, 1960; Hagiwara and Naka, 1964; Hagiwara and Takahashi, 1967; Kostyuk et al., 1982; Zhou and Jones, 1995). A theoretical mechanism invoked by Frankenhaeuser and Hodgkin to explain this membrane stabilizing action of polyvalent cations is that they interact with diffuse negative charges near the channel surface (surface charges), thus affecting the local electric field sensed by the channels (Frankenhaeuser and Hodgkin, 1957; Andersen and Koeppel, 1992). It is based on the assumption that local potentials (surface potentials), produced by fixed charges close to the channels, effectively offset the voltage-difference measured by the voltage-sensors. Attracted ions of opposite charge can neutralize part of the surface charge and reduce the net charge density, so that effective surface potentials at equilibrium are strongly influenced by changes in the nature or concentration of counter-ions. As they are strictly local phenomena, the effects of surface potentials are invisible for macroscopic electrodes placed in the bulk solution and any manipulation of the ionic conditions associated with a change in surface potential should produce apparent alterations in the voltage-dependence of channel gating (Andersen and Koeppel, 1992; Hille, 2001). The formalism Frankenhaeuser and Hodgkin used makes several simplifying assumptions, but it adequately predicts the effects of polyvalent cations on a variety of voltage-gated ion channels. This has been reviewed in several excellent articles (Henderson, 1983; McLaughlin, 1989) and the present work will focus on its experimental relevance for polyvalent cation-induced changes in VGCC function on the one hand and on the fundamental problem of how to separate it from different mechanisms of cation action on the other. In closing, the role of negative charges in vestibule and pore region will be considered to discuss their possible implications for metal ion effects on the process of ion transfer.

##### 4.1.1. Classical surface charge theory

To quantitatively describe the relationship between surface charge, counter-ions and local potentials, Frankenhaeuser and



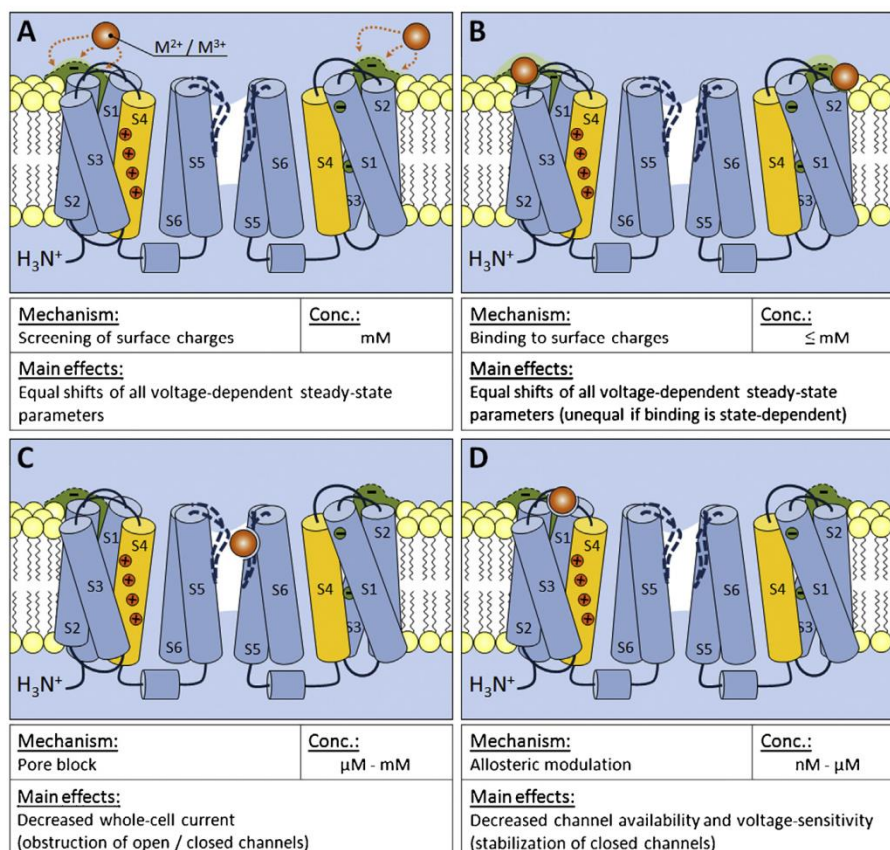


**Fig. 5.** Mechanisms of modulation of voltage-gated calcium channels by polyvalent inorganic cations. Sketch of the pore-forming  $\alpha_1$ -subunit in a closed conformation, showing two of the four homologous domains with their voltage-sensors (S4 segments highlighted in yellow) and local charges on the channel surface (green). (A) Cations ( $M^{2+}$  and  $M^{3+}$ , orange) in solution can screen charges on the channel surface, thereby electrostatically reducing the local potential sensed by the voltage-sensors (see Section 4.1). (B) Some cations can electrostatically decrease the total surface charge density by directly binding to and neutralizing certain surface charges, producing a more pronounced reduction in the local potential. If accessibility of binding sites depends on the conformation (i.e. state-dependent binding), effects on the local potential are state-dependent (see Section 4.1). (C) Most di- and trivalent metal ions can bind to sites at or within the pore region (pore block), thereby physically occluding the permeation pathway (see Section 4.2). (D) Some VGCCs possess high-affinity allosteric metal binding-sites on their domain I voltage-sensor, which certain divalent transition metal ions can occupy, thereby non-electrostatically (i.e. sterically or mechanically) stabilizing closed channel states (see Section 4.3).

Hodgkin employed the Gouy–Chapman theory of electrical double layers, which assumes that charge is uniformly ‘smeared’ across a planar surface and screened (i.e. partially neutralized) by a diffuse layer of attracted counter-ions (Gouy–Chapman diffuse layer) (Fig. 6A) (Gilbert and Ehrenstein, 1969, 1984). The fact that ions often selectively bind to and neutralize certain charged groups is addressed by the Stern-extension, which introduces specific sites, to which ions can bind and neutralize associated charges<sup>2</sup> (Gilbert and Ehrenstein, 1970; Hille et al., 1975). Here, the electrical double layer is assumed to be subdivided into a thin, essentially immobile layer of bound ions (Stern layer) and a zone of mobile (screening) counter-ions extending into the bulk solution (Gouy–Chapman diffuse layer) (Fig. 6B). When applied to voltage-gated ion channels, the Gouy–Chapman–Stern model predicts that changes in the extracellular concentration of counter-ions produce uniform shifts of all voltage-dependent steady-state parameters along the voltage axis, by an amount equal to the resulting change in surface potential (Abramson and Müller, 1933; Grahame, 1947; Gilbert and Ehrenstein, 1969). For a given surface charge density, the efficiency of counter-ions to produce voltage-shifts steeply increases with increasing counter-ion valence and decreases with increasing ionic strength (i.e. decreasing net surface

charge) (Fig. 6D). Ions which appreciably bind to surface charges produce more pronounced voltage-shifts, which additionally depend on the ion-specific equilibrium constant for binding and the density of putative binding sites (Hille et al., 1975; Hille, 2001; Elinder and Arhem, 2003). These predictions have mainly been tested on HVA currents in different native membrane preparations, making it difficult to directly compare experimental findings. However, the general pattern that emerged from these studies is that shifts produced by  $Ba^{2+}$ ,  $Sr^{2+}$  or  $Mg^{2+}$  are quantitatively similar and can usually be adequately described by a Gouy–Chapman screening model, with charge densities of roughly one elemental charge per 80–4000 Å<sup>2</sup> (Ohmori and Yoshii, 1977; Wilson et al., 1983; Cota and Stefani, 1984; Byerly et al., 1985; Kass and Krafte, 1987; Ganitkevich et al., 1988; Becchetti et al., 1992; Smith et al., 1993).  $Ca^{2+}$ -induced shifts on the other hand are typically stronger, and their description with the same surface charge densities necessitates the assumption that  $Ca^{2+}$  binds to certain charges with an equilibrium binding constant of  $K_{Ca} > 1 M^{-1}$  (Cota and Stefani, 1984; Byerly et al., 1985; Kass and Krafte, 1987; Ganitkevich et al., 1988; Smith et al., 1993). It is important to appreciate that experimentally determined surface charge densities are effective charge densities, which depend not only on the exact cell type examined but should also reflect (i) the ionic conditions under which they were determined, as for a given surface charge density, much stronger voltage-shifts may be produced in e.g.

<sup>2</sup> The model assumes that local charges and added polyvalent cations are of equal valence, i.e. each charge is either completely neutralized or free.



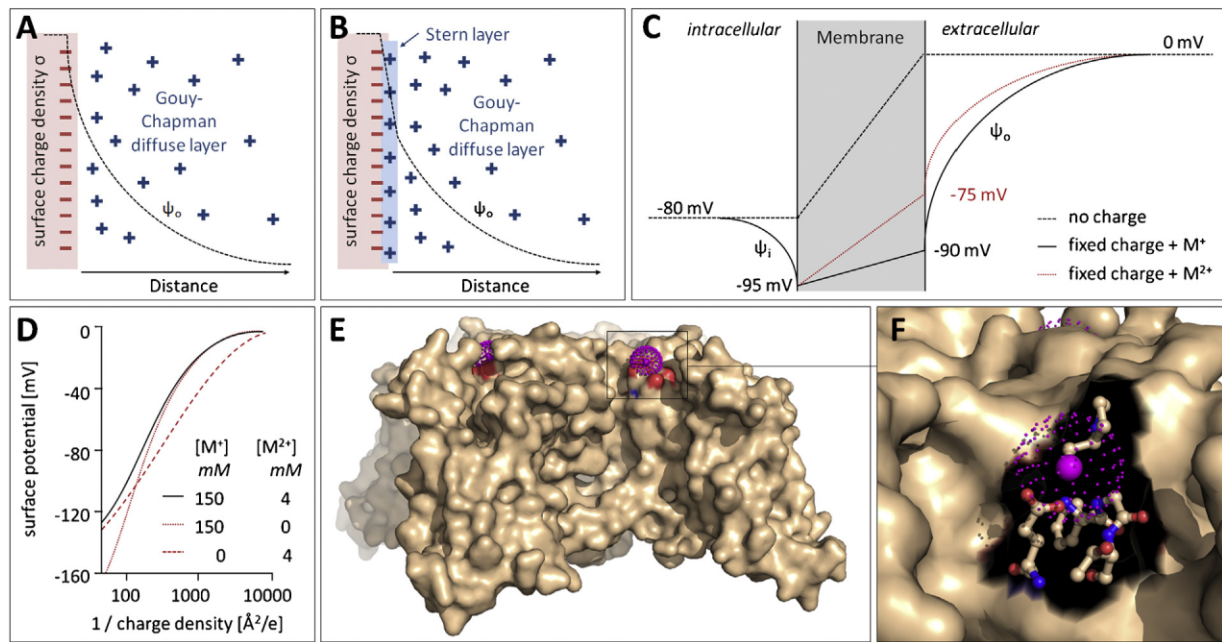


**Fig. 6.** Surface potential hypothesis. (A) The Gouy–Chapman model assumes a uniformly smeared density of fixed charges on the membrane which attracts counter-ions, leading to formation of a diffuse electrical double layer (Gouy–Chapman layer). (B) In the Gouy–Chapman–Stern extension, direct binding of counter-ions to certain charges is assumed to produce a layer of immobile counter-ions (Stern layer) on the surface of the membrane. (C) Both models predict the formation of local potentials at the inner and outer surface of the membrane, which are affected by the nature and concentration of ions in the adjacent solution. Thus, addition of divalent cations reduces the external surface potential (red dotted line) relative to the magnitude in the absence of divalent cations (black solid line). (D) Relationship between local charge density and predicted surface potential under different ionic conditions. (E, F) Surface representation of the crystal structure of Ca<sub>v</sub>Ab viewed from the side, showing Cd<sup>2+</sup> ions (magenta) bound to charged groups on the external channel surface. Negative and positive charges are coloured in red and blue, respectively.

frog ringer (118/2 mM Na<sup>+</sup>/Ca<sup>2+</sup>) vs. artificial sea water (440/60 mM Na<sup>+</sup>/Ca<sup>2+</sup>), and (ii) the assumptions on which the analysis was based, as a given shift may be equally well described by surface charge screening or combined screening and binding (with the latter predicting a higher surface charge density). Likewise, unequal shifts may be equally well explained by selective binding of one ion or differential binding of different ions (with the latter again predicting a higher surface charge density).

Another more serious problem is that cation-induced voltage-shifts have often been quantified based on current–voltage (IV)-relationships, constructed by plotting the peak macroscopic current evoked by step depolarization as a function of the test potential. Interpretation of IV-curves is mechanistically ambiguous, as the underlying steady-state currents (hereinafter designated as IV-currents) depend on both, the voltage-dependence of permeation through open channels and the voltage-dependence of channel gating (Hille, 2001; Pusch, 2006). Changes in shape or position of the IV-curve could therefore result either from surface charge effects or other (non-electrostatic) changes in gating or from voltage-dependent pore block.

Interference from voltage-dependent block can be circumvented by directly measuring the voltage-dependence of activation with an ‘isochronous tail-current’ protocol, consisting of brief conditioning prepulses to a wide range of potentials followed by a fixed hyperpolarizing test pulse. If gating of the channels under investigation is sufficiently slow, the tail currents recorded at the beginning of the fixed test pulse should be proportional to channel open probability at the end of the variable prepulse and since the measurement is carried out at a fixed voltage, voltage-dependent block can be neglected (Pusch, 2006). Using this and other strategies to separate channel gating from permeation it has been convincingly demonstrated that polyvalent cation-induced voltage-shifts are not exclusively determined by voltage-dependent

pore block, although the latter may contribute to changes in the IV-relationship.

At present however, systematic comparison of putative surface charge effects on different cloned vertebrate Ca<sub>v</sub>α<sub>1</sub>-subunits remains unfeasible, as a detailed analysis with different cations has only been done in Ca<sub>v</sub>3.1 channels (Khan et al., 2008; Lopin et al., 2012a, 2012b). Here, Ca<sup>2+</sup>, Ba<sup>2+</sup> and Mg<sup>2+</sup> exert approximately equal effects on channel gating, which are well described by a Gouy–Chapman screening model with assumed surface charge density of 1 e per 98 Å<sup>2</sup> (Khan et al., 2008). Qualitatively similar observations (i.e. a comparable voltage-range of activation measured in Ca<sup>2+</sup> vs. Ba<sup>2+</sup>) have been made in other Ca<sub>v</sub>3 subunits (Klugbauer et al., 1999b; Kaku et al., 2003), suggesting that the apparent lack of Ca<sup>2+</sup> binding may be common to all LVA channels. Certain divalent transition metal ions like Cd<sup>2+</sup> and Fe<sup>2+</sup> conversely produce more pronounced voltage shifts of Ca<sub>v</sub>3.1 channel gating,<sup>3</sup> which can be described by a Gouy–Chapman–Stern model with equilibrium binding constants of K<sub>Cd</sub> = 0.44 M<sup>-1</sup> and K<sub>Fe</sub> = 4.5 M<sup>-1</sup> respectively (Lopin et al., 2012a, 2012b).

Direct evidence for selective binding of polyvalent cations to charged groups on the surface of bacterial channels is provided by crystals of Ca<sub>v</sub>Ab obtained in the presence of Cd<sup>2+</sup> or Mn<sup>2+</sup> (Tang et al., 2014). They show Cd<sup>2+</sup> ions bound to amino acid residues located on the external channel surface (Fig. 6E and F), whereas no such binding is observed in the case of Mn<sup>2+</sup>. Possible effects of extracellular Cd<sup>2+</sup> binding to discrete regions on the surface of Ca<sub>v</sub>Ab remain to be elucidated, but as described in the next section, they may be more complex than predicted by the Gouy–Chapman–Stern model.

<sup>3</sup> 10 mV or 25 mV depolarizing shift of steady-state activation with 1.8 mM Fe<sup>2+</sup> or 2 mM Cd<sup>2+</sup> respectively in Ca<sub>v</sub>3.1 channels.

#### 4.1.2. Dynamic binding models

While the findings described above largely agree with classical surface charge theory, many di- and trivalent cations have been shown to produce differential voltage-shifts of different steady-state parameters and complex kinetic effects on native or cloned VGCCs (Büsselberg et al., 1992, 1994a, 1994b; Castelli et al., 2003; Magistretti et al., 2003; Noh et al., 2010). Most of these effects have either been interpreted in terms of non-electrostatic actions of cation-binding on channel gating or are thought to result from certain intrinsic properties of pore block (but see Sections 4.2 and 4.3). An alternative (and yet complementary) explanation is that the Gouy–Chapman–Stern theory is simply inadequate to predict the complex nature of electrostatic interactions near VGCCs. It has been successfully used for several decades to predict electrostatic potentials near charged lipid bilayers (McLaughlin, 1989; Peitzsch et al., 1995), but clearly fails to consider the discreteness of charges, possible charge heterogeneity and the dynamic, 3-dimensional nature of protein structure (Klapper et al., 1986; McLaughlin, 1989; Cai and Jordan, 1990).

Theoretical reasons and experimental evidence suggest that most negative charge responsible for formation of local potentials near voltage-gated ion channels arises from ionized groups on the channel proteins themselves (Frankenhaeuser et al., 1976; Ohmori and Yoshii, 1977; Bell and Miller, 1984; Cukierman et al., 1988; Worley et al., 1992; Elinder and Arhem, 1999). As a consequence, conformational changes during channel gating could be associated with dynamic changes in the accessibility of charged groups, in which case there may be large differences in the effective surface potential sensed by different conformational states.

This rationale has been employed by Armstrong and Gilly to explain why  $Zn^{2+}$  produces a marked slowing of the activation kinetics, intermediate shifts of the activation curve and almost no effect on the deactivation kinetics of squid axon voltage-gated  $K^+$  and  $Na^+$  channels (Gilly and Armstrong, 1982a, 1982b). They accurately reproduced these effects with a state-dependent model, where  $Zn^{2+}$  ions bound to an external site directly affect a negatively charged element of the voltage-sensors, which resides at the outer membrane surface at rest and moves inward during activation (Gilly and Armstrong, 1982a, 1982b). The difference in voltage-shifts of different steady-state gating parameters predicted by such dynamic models generally decreases as the number of proposed binding sites or the number of metal ions associated with a particular site is increased, or if cooperativity between bound metal ions is assumed (Elinder and Arhem, 2003). Since one may postulate an arbitrary number of binding sites and charge distributions, any combination of (differential) voltage-shifts and kinetic effects can be adequately described and a good fit of experimental data is no proof that a given state-dependent binding model is indeed correct (Hille, 2001).

#### 4.1.3. Validity and relevance of electrostatic models

When interpreting voltage-shifts in terms of electrostatic effects, one should consider all of the available models as theoretical constructs, which are highly simplified and have been invoked to explain experimental findings. They are attractive concepts and the success of classical surface charge theory in explaining many experimental findings supports its general relevance. Dynamic binding models conversely illustrate how deviations between experimental findings and predicted effects could be explained without dismissing the general validity of simplified models. Until surface charge measurements have been compared with molecular channel structure however, they have relatively little informative value and especially dynamic models should not be taken too literal.

An interesting twist to classical electrostatic binding models has been introduced by Armstrong and others, who provided

evidence that polyvalent cation-induced voltage-shifts of  $Na^+$  and  $K^+$  channel gating are closely correlated with pore block by these ions, leading them to propose that ions occupying the pore can electrostatically affect voltage-sensor movement (Armstrong and Lopez-Barneo, 1987; Armstrong and Cota, 1990, 1991, 1999; Pusch, 1990; French et al., 1996; Boccaccio et al., 1998; Armstrong, 1999). They further speculated that  $Ca^{2+}$  binding in the pore may even be required for  $Na^+$  channels to close (Armstrong and Cota, 1991), but it has since been shown that this is not the case (Hong et al., 2001), and that bound ions may instead affect an initial voltage-sensor independent open-to-closed transition through non-electrostatic mechanisms (Gomez-Lagunas et al., 2003). Likewise, conclusive evidence against a purely electrostatic interaction with diffuse surface charge has been presented for differential shifts of cloned  $Ca_v2.1$  channel gating by  $Ca^{2+}$  and  $Ba^{2+}$  (Zamponi and Snutch, 1996). Here, the experimental data were well fit by a model where both ions compete for a single site, possibly in the pore, but only  $Ca^{2+}$  binding produces gating effects by an unidentified non-electrostatic mechanism (Zamponi and Snutch, 1996). Possible gating effects associated with binding of ions in the pore will be addressed in more detail in the context of pore block (but see Section 4.2.6.3). Without wanting to jump ahead to the consideration of these effects, it seems justified to state that electrostatic interactions alone are usually insufficient to completely account for the action of polyvalent cations on VGCC function and that many aspects can be equally well described by alternative mechanisms. Since local potentials inevitably exist, the main challenge is to identify additional, non-electrostatic mechanisms of action, and to separate them from electrostatic effects. Here, simple approximations like the Gouy–Chapman–Stern model can be helpful for estimating the magnitude of electrostatic effects associated with changes in the concentration of extracellular cations.

In closing the discussion of electrostatic gating effects, it remains to be stressed that most organisms maintain more or less constant extracellular divalent cation concentrations, such that surface charge effects are mainly of experimental relevance (Hille, 2001). Given their subtle nature, they are also unlikely to make a significant contribution to the net effect of foreign polyvalent cations at biologically relevant concentrations. Under experimental conditions on the other hand, where high concentrations of metal ions may be used, detectable surface charge effects can occur. They have to be considered especially when working with data obtained under fundamentally different ionic conditions, such as commonly encountered when comparing single-channel measurements (typically carried out with high levels of divalent charge carrier) with recordings acquired under more physiological ionic conditions. As described below, even small changes in the ionic conditions may moreover influence the process of ion transfer through the pore and could thus bias the apparent permeation properties of permeant ions.

#### 4.1.4. Electrostatic interactions in the pore region

Although most of the defining permeation properties of  $Ca^{2+}$  channels (i.e. high  $Ca^{2+}$  selectivity, saturation, AMFE), are typically ascribed to intra-pore binding, they could in principle also partially or entirely be explained by electrostatic effects. Attraction of permeant ions by clusters of negative charge near the channel entrance has been shown to play a role for the permeation properties of other voltage-gated ion channels (Sigworth and Spalding, 1980; Kell and DeFelice, 1988). As electrostatic attraction steeply increases with valence, interfacial accumulation of divalent cations could conceivably also contribute to  $Ca^{2+}$  selective flux. The decline in net charge density associated with raising the external  $Ca^{2+}$  concentration ( $[Ca^{2+}]_o$ ) could conversely diminish the increase of  $[Ca^{2+}]_o$  near the membrane surface relative to the bulk solution and thus contribute to current saturation. Clearly,



voltage-shifts associated with increasing  $[Ca^{2+}]_o$  could also contribute to apparent saturation.

$Ca^{2+}$  current saturation is still observed in the presence of 100 mM extracellular  $Mg^{2+}$  (which should eliminate existing surface potentials and prevents detectable voltage-shifts), supporting the general notion that it arises from ion interactions with intra-pore sites (Hagiwara and Takahashi, 1967; Beirao and Lakshminarayanaiah, 1979). Recordings in a number of different preparations nevertheless indicate a small but detectable surface charge directly associated with the pore region, and Langmuir fits to the concentration-dependence of  $Ba^{2+}$  current can often be improved by correction for the predicted surface  $Ba^{2+}$  concentration (Ohmori and Yoshii, 1977; Wilson et al., 1983; Cota and Stefani, 1984; Byerly et al., 1985; Ganitkevich et al., 1988; Kuo and Hess, 1992; Smith et al., 1993; Zhou and Jones, 1995; Block et al., 1998). Hence, electrostatic effects may contribute to  $Ca^{2+}$  current saturation, although their relevance for permeation under physiological conditions remains a matter of debate (Wilson et al., 1983; Kuo and Hess, 1992; Zhou and Jones, 1995; Block et al., 1998). In any event, the Gouy–Chapman–Stern model is clearly not suited to describe the electrostatic environment at the structurally complex vestibule of VGCCs, let alone that in the narrow pore.

A more elaborate description incorporating finite ion size, discrete charges and a funnel-shaped vestibule of defined size has been used in conjunction with chemical kinetic modelling of a narrow pore to calculate the potential profile along the pore axis of voltage-gated ion channels (Dani, 1986). An important prediction of the work is that binding of cations to charges in the vestibule could reduce the net charge density and the cross-sectional area available for passage of other ions, so that it might impair ion transfer, possibly without complete obstruction of the pore. Since large cations bound in the vestibule can neutralize negative charges less efficiently and may displace other (screening) ions, the net charge density at a given bulk concentration is higher for large vs. small cations (i.e. large cations have higher apparent affinity for binding in the vestibule and their concentration could markedly affect the permeation properties of smaller ions). VGCCs are likely equipped with a shallower, cone-shaped vestibule similar to that in  $Na^+$  and  $K^+$  channels (Fig. 4A), but the above predictions may still apply to some extent. A number of large highly charged polypeptide toxins are thought to act by binding somewhere in the pore vestibule, and their action is strongly but non-competitively affected by the concentration of divalent cations. Among them,  $\omega$ -agatoxin IIIA is unique in that it produces a potent but partial (~70%) inhibition of macroscopic N- and P-type currents (Mintz et al., 1991; Mintz, 1994). The remaining current activates at slightly more depolarized potentials, and non-stationary noise analysis indicates that inhibition is due to reduced single-channel conductance (McDonough et al., 2002; McDonough, 2004), so that toxin binding in the vestibule has been proposed to electrostatically affect permeation (without completely blocking the pore) and (due to the distance only weakly) channel gating. If this is indeed the case, it would also mean that binding of polyvalent cations (which have a much lower charge density) in the pore region is unlikely to have detectable electrostatic effects on voltage-sensor movement (note that this does not refer to possible allosteric effects of intra-pore binding). That said, organic cations like N-methyl-D-glucamine (NMDG<sup>+</sup>) (which is often used to replace  $Na^+$  in  $Ca^{2+}$  current recordings), appear to weakly interfere with permeation through VGCCs as well, although this has not been analysed in detail (Lopin et al., 2012b; Kuo and Hess, 1993b). Whether NMDG<sup>+</sup> acts by binding somewhere in the vestibule, and whether inorganic cations can affect VGCC permeation by a similar mechanism remains to be elucidated, but these findings vividly illustrate that even the choice of 'inert' electrolytes has to be carefully considered when performing or interpreting  $Ca^{2+}$  current recordings.

#### 4.2. Pore block (Fig. 5C)

Block of the ion-conducting pore of VGCCs by polyvalent cations is thought to be governed by the same processes that underlie selective permeation and has been extensively studied to get insight into the mechanisms of selection. By competitive binding in the pore, blocking ions<sup>4</sup> could interfere with flux of permeant ions through open channels, so that the whole-cell current in response to depolarization is reduced, even if the same number of channels is activated. This is typically described in terms of a reversible binding reaction, where (i) fractional occupancy of the intra-pore blocking site at equilibrium is a saturating function of blocker concentration and (ii) blocker residence time at the site a function of binding affinity (Hille, 2001). Block of macroscopic currents at different membrane potentials can be quantified by the use of instantaneous current–voltage (IIV)–relationships. Channels are first activated by a fixed pre-pulse, which is followed by repolarization to a wide range of test potentials. As long as blocker equilibration with the pore is instantaneous relative to the recording bandwidth and gating of the channels under investigation sufficiently slow, the instantaneous macroscopic currents measured at the beginning of each repolarization step (hereinafter termed IIV-currents) should reflect the voltage-dependence of current through a fixed number of channels opened during the pre-pulse (Hodgkin and Huxley, 1952b; Pusch, 2006). Any difference between IIV-currents measured in the presence and absence of a given metal ion should then exclusively reflect changes in permeation and is usually attributed to pore block, although additional data may still be required to exclude alternative mechanisms. As outlined throughout the following sections, pore block can in practice seldom be accurately described in terms of a simple binding reaction, and the inherent assumptions of using IIV-currents are not always met, so that they have to be considered when interpreting electrophysiological data. What adds further to the complexity of pore block is the lack of absolute dichotomy between blocking and permeant ions and a number of ion-specific intrinsic properties, which can produce apparent changes in the time- or voltage-dependence of channel gating and complicate analysis in terms of macroscopic IIV- and especially IV-currents. As mentioned before and discussed in more detail in Section 4.2.6.3, occupation of the selectivity filter or nearby sites in the pore may also lead to blocker-specific effects on channel gating, either due to electrostatic effects on the voltage-sensors or through local or global deformations. All of these factors shape the specific profile of a given blocker and its appearance in electrophysiological recordings, and can often be exploited to assess various aspects of pore block and permeation. The following sections are devoted to the factors determining if an ion is predominantly blocking or permeant, to the intrinsic properties of pore block by inorganic cations and to possible interactions between selectivity filter (i.e. occupation of the pore) and gating machinery of VGCCs. The main focus will be on the different mechanisms proposed to account for experimental findings, and their possible implications for the structure–function relationship of selective permeation in vertebrate channels.

##### 4.2.1. Voltage-dependence: evidence for binding in the pore

The degree of steady-state  $Ca^{2+}$ -block of monovalent currents (Fukushima and Hagiwara, 1985; Lux et al., 1990; Carbone et al., 1997; Shcheglovitov et al., 2007; Khan et al., 2008) and of steady-state block of  $Ca^{2+}$  or  $Ba^{2+}$  currents by  $Cd^{2+}$  (Lansman et al., 1986; Rosenberg et al., 1988; Huang et al., 1989; Lacinova et al., 2000;

<sup>4</sup> It should be noted that the term blocker is commonly used in the literature as a general term for inhibitors, but will herein be used in its strict sense (i.e. to identify ions which physically obstruct the pore of target channels).

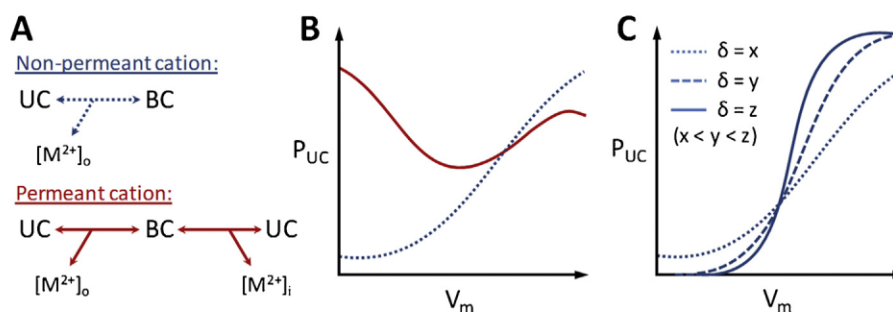


**Fig. 7.** Woodhull model of voltage-dependent pore block. (A) State diagrams for block by non-permeant (top) and permeant (bottom) external divalent cations. In both cases, external cations ( $M^{2+}_o$ ) bind to unblocked open channels (OC) to give blocked channels (BC). Non-permeant ions can only exit the pore to the extracellular side, while permeant ions can also escape into the intracellular compartment. (B) Hypothetical voltage-dependence of block for the two cases illustrated in A. Shown is the probability  $P_{UC}$ , for a given channel to be in an unblocked state as a function of the membrane potential. For non-permeant cations (blue), block is strongest at negative potentials and decreases with increasing depolarization, as ions are propelled back into the external solution. With permeant cations (red), block is strongest at intermediate potentials, while strong de- or hyperpolarization can drive cations back into the external solution or through the channel and into the intracellular compartment respectively. (C) Influence of the relative position of target sites within the electric field on the shape of the voltage-dependence of block by non-permeant cations. The steepness increases with increasing apparent electrical distance ( $\delta$ ) from the bulk solution.

Diaz et al., 2005), most divalent transition metal ions (Winegar and Lansman, 1990; Winegar et al., 1991; Diaz et al., 2005; Lopin et al., 2012a) and trivalent lanthanoid ions (Lansman, 1990) changes as a function of the membrane potential, suggesting some kind of interaction between blocking ions and the membrane electric field.

These observations can be described in terms of the Woodhull model of voltage-dependent block (Woodhull, 1973; Hille, 2001), which assumes that charged particles interact with a single site located sufficiently deep within the cell membrane to experience a fraction of the membrane electric field. The theory describes both, concentration and voltage-dependence of block in terms of two parameters: intrinsic binding energy at zero voltage and apparent electrical distance of the binding site from the bulk solution (i.e. fraction of the electric field an ion traverses to reach its binding site) (Woodhull, 1973). Woodhull assumed that block by charged particles capable to fully traverse a channel is most effective at intermediate potentials, since strong depolarization relieves block by propelling blocking ions back into the extracellular compartment, while strong hyperpolarization relieves block by driving them through the pore and into the cell (Fig. 7A and B). The resulting biphasic voltage-dependence of steady-state block is characteristic for  $Ca^{2+}$  block of monovalent currents (Fukushima and Hagiwara, 1985; Lux et al., 1990; Carbone et al., 1997; Shcheglovitov et al., 2007; Khan et al., 2008), as well as block of divalent currents by  $Cd^{2+}$ , lanthanoids (Lansman et al., 1986; Lansman, 1990; Williams et al., 1994; Williamson and Sather, 1999; Diaz et al., 2005; Rosenberg et al., 1988; Huang et al., 1989; Lacinova et al., 2000) and most divalent transition metal ions (Ochi, 1975; Fukuda and Kawa, 1977; Anderson, 1983; Lansman et al., 1986; Nelson, 1986; Lansman, 1990; Winegar et al., 1991; Castelli et al., 2003; Lopin et al., 2012a), suggesting that all of these ions can in principle traverse VGCCs.

Steady-state block of  $Ca^{2+}$  or  $Ba^{2+}$  currents by  $Ni^{2+}$  and  $Mg^{2+}$  on the other hand decreases monotonically with voltage, such that the degree of block is reduced by depolarization but enhanced rather than relieved by strong hyperpolarization (Fukushima and Hagiwara, 1985; Hess et al., 1986; Lansman et al., 1986; Winegar et al., 1991; Diaz et al., 2005; Khan et al., 2008; Obejero-Paz et al., 2008). This can be reconciled by the Woodhull model for impermeant blocking ions, which predicts the voltage-dependence of block to be monotonic since exit of blocking ions from the pore is only possible by return into the extracellular space (Fig. 7A and B).

The apparent electrical distance is reflected in the slope of the voltage-dependence (Fig. 7C), and provides a rough estimate for the relative location of target sites in the membrane electric field. For instance, the degree of  $Ca^{2+}$  block of monovalent currents

through both HVA and LVA channels changes roughly e-fold per 25 mV, which corresponds to an electrical distance of  $\sim 0.5$ , or 50% of the voltage-drop from the bulk solution (Fukushima and Hagiwara, 1985; Lux et al., 1990; Carbone et al., 1997; Shcheglovitov et al., 2007; Khan et al., 2008). No inference can be made about the physical location of target sites in the pore, since the width of the electric field may differ from the width of the membrane and since the model does not address the relation between electrical and physical distance. The apparent electrical distance can however help to recognize blockers which target the same binding site. Thus,  $Cd^{2+}$  and lanthanoid block of divalent currents exhibit almost the same voltage-dependence as  $Ca^{2+}$  block of monovalent currents (Lansman et al., 1986; Rosenberg et al., 1988; Huang et al., 1989; Lansman, 1990; Lacinova et al., 2000; Diaz et al., 2005), suggesting a common site of action. Most divalent transition metal ions on the other hand exhibit a relatively shallow voltage-dependence of block, with electrical distances corresponding to  $\sim 6$ –20% of the voltage-drop from the bulk solution (Winegar and Lansman, 1990; Winegar et al., 1991; Diaz et al., 2005; Lopin et al., 2012a). This is only one of many findings indicating that these ions act by a somewhat different mechanism, which is discussed in more detail in Section 4.2.6.

It is important to appreciate however, that strictly speaking the Woodhull model only applies to block of pores which are empty most of the time and that it does not consider interactions (i.e. competition, repulsion) between blocking and permeant ions (Tikhonov and Magazanik, 1998; Hille, 2001). Ion–ion interactions play a major role for flux through VGCCs and can strongly contribute to the apparent dependence of block on the membrane potential. The distinct voltage-dependence of block by transition metal ions could therefore reflect differences in the location of target sites relative to the electric field (i.e. a ‘true’ difference in the voltage-dependence), or differences in the degree or nature of ion–ion interactions at the same principal site (i.e. a difference in the current-dependence).

It should also be mentioned that an apparent lack of clear voltage-dependence is not necessarily evidence for an action outside of the membrane electric field, but may also result if, for example, the voltage-range examined is simply too narrow to detect voltage-dependent changes in the degree of block (e.g. Hess and Tsien, 1984). Likewise, when working with low blocker concentrations, equilibration of blocking ions with the pore may be too slow for the brief pre-pulses employed in the IIV-protocol to produce detectable changes in the degree of resting block. This is especially problematic with rapidly inactivating channels (where time-dependent gating processes may prohibit the use of longer



**Table 2**  
Physical and chemical properties and binding characteristics of selected inorganic cations.

	Ion	Effective radius (Å) <sup>a</sup>	Hydrated diameter (Å) <sup>b</sup>	Water exchange rate at 298 K (s <sup>-1</sup> ) <sup>a,c</sup>	Apparent affinity	Binding (entry rate) (M <sup>-1</sup> s <sup>-1</sup> ) <sup>p</sup>	Unbinding (exit rate) (s <sup>-1</sup> ) <sup>p</sup>	Donor atom preference
Alkaline earth metal ions	Mg <sup>2+</sup>	0.72	8	6.7 × 10 <sup>5</sup>	Low	Slow (2 × 10 <sup>5</sup> ) <sup>d</sup>	Slow (10 <sup>3</sup> –10 <sup>4</sup> ) <sup>d</sup>	Oxygen donor groups
	Ca <sup>2+</sup>	1.00	6	5 × 10 <sup>8</sup>	High	Rapid (1–5 × 10 <sup>8</sup> ) <sup>d,j</sup>	Rapid	
	Str <sup>2+</sup>	1.18	5	~10 <sup>9</sup>				
	Ba <sup>2+</sup>	1.35	5	~10 <sup>9</sup>				
Transition metal ions	Ni <sup>2+</sup>	0.69	6	3.2 × 10 <sup>4</sup>	High	Slow (10 <sup>4</sup> –10 <sup>6</sup> ) <sup>e,f,h,k</sup>	Very slow (100) <sup>e</sup>	Nitrogen donor groups
	Cu <sup>2+</sup>	0.73	6	4.4 × 10 <sup>9</sup>	Intermediate	Rapid (10 <sup>6</sup> –10 <sup>8</sup> ) <sup>f,k</sup>	Rapid (1.6 × 10 <sup>4</sup> ) <sup>e,l</sup>	
	Co <sup>2+</sup>	0.74	6	3.2 × 10 <sup>6</sup>				
	Zn <sup>2+</sup>	0.74	6	~10 <sup>7</sup>				
	Fe <sup>2+</sup>	0.78	6	4.4 × 10 <sup>6</sup>				
	Mn <sup>2+</sup>	0.83	6	2.1 × 10 <sup>7</sup>				
	Cd <sup>2+</sup>	0.95	5	~10 <sup>8</sup>	Very high	Rapid (10 <sup>7</sup> –10 <sup>8</sup> ) <sup>d,f,g,m</sup>	Very slow (50–1000) <sup>d,m,g</sup>	
Lanthanoid ions	Yb <sup>3+</sup>	0.86		4.1 × 10 <sup>7</sup>	Very high	Rapid (10 <sup>6</sup> –10 <sup>9</sup> ) <sup>m,n,o</sup>	Very slow (10–250) <sup>m,n,o</sup>	Oxygen donor groups
	Gd <sup>3+</sup>	0.93		1.0 × 10 <sup>9</sup>				
	Nd <sup>3+</sup>	0.98	9	5 × 10 <sup>8</sup>				
	Ce <sup>3+</sup>	1.01	9					
	La <sup>3+</sup>	1.03	9					

<sup>a</sup>Shannon (1976); <sup>b</sup>Kielland (1937); <sup>c</sup>Helm and Merbach (1999); Southwood-Jones et al. (1980); Cossy et al. (1987); Bleuzen et al. (1997); Powell and Merbach (1994); <sup>d</sup>Lansman et al. (1986); <sup>e</sup>Winegar et al. (1991); <sup>f</sup>Diaz et al. (2005); <sup>g</sup>Thevenod and Jones (1992); <sup>h</sup>Lee et al. (1999b); <sup>i</sup>Khan et al. (2008); <sup>j</sup>Lux et al. (1990); <sup>k</sup>Obejero-Paz et al. (2008); <sup>l</sup>Winegar and Lansman (1990); <sup>m</sup>Block et al. (1998); <sup>n</sup>Lansman (1990); <sup>o</sup>Babich et al. (2007a, 2007b); <sup>p</sup>Entry and exit rates vary with concentration of blocker and permeant ions, temperature and the affected subunits.

pre-pulses) and could explain claims that lanthanoid block of LVA channels is voltage-independent (e.g. Mlinar and Enyeart, 1993).

Altogether, the Woodhull model is nevertheless a valuable tool to predict the general shape of the relationship between apparent blocker affinity and membrane potential, and can be very useful to approximate the contribution of voltage-dependent block to the net effect of drugs with multiple mechanisms of action.

#### 4.2.2. Association: block provides information about the first step in permeation

When Li<sup>+</sup> currents are blocked by external Ca<sup>2+</sup>, the blocker on-rate should provide a reasonable lower limit for the process of association or entry, during which Ca<sup>2+</sup> ions transition from the bulk solution to the channel entrance. As illustrated in Table 2, Ca<sup>2+</sup> block of inward monovalent currents is characterized by on-rates close to values expected for a diffusion-limited reaction,<sup>5</sup> suggesting that the initial transition step for Ca<sup>2+</sup> entry takes place at an easily accessible site. Likewise, almost all foreign metal ions, such as Cd<sup>2+</sup>, lanthanoid ions and most divalent transition metal ions, rapidly block inward currents carried by Ca<sup>2+</sup> or Ba<sup>2+</sup> (Table 2) and Cd<sup>2+</sup>-block of inward Li<sup>+</sup>-currents through HVA channels can be up to 5 times faster than the predicted diffusion-controlled limit (Cloues et al., 2000). Apparently, the high-affinity coordination site is either located close to the pore entrance, or there must be an additional, lower-affinity site at the extracellular face of the channel, where incoming Ca<sup>2+</sup>-ions are transiently stabilized before entering the pore. The latter is supported by the following experimental observations. In frog skeletal muscle, block of inward Ca<sup>2+</sup> currents through VGCCs by Co<sup>2+</sup> is approximately as effective as block of inward Na<sup>+</sup> currents through the same channels ( $K_d \sim 1$  mM) (Almers et al., 1984, 1985). Block by competition for a site with much higher affinity for Ca<sup>2+</sup> than for Na<sup>+</sup> should be vastly more effective against currents carried by Na<sup>+</sup>, so Co<sup>2+</sup> cannot compete with Ca<sup>2+</sup> for the high-affinity site. Similar observations of low-affinity competition between monovalent cations and Ca<sup>2+</sup> at the outer vestibule have been made with N-type channels in chick sensory neurons (Polo-Parada and Korn, 1997) and T-type like currents in mouse neoplastic B lymphocytes (Yamashita et al., 1990). Further evidence for an initial interaction

<sup>5</sup> Estimated diffusion-controlled limit for association between Ca<sup>2+</sup> and L-type VGCCs  $\sim 10^9$  M<sup>-1</sup> s<sup>-1</sup> (Kuo and Hess, 1992).

of permeant and blocking ions with a superficial binding site is provided by detailed kinetic analyses of the voltage-dependence of block, which show that on-rates are in most cases (Ca<sup>2+</sup>, Cd<sup>2+</sup>, lanthanoid and most divalent transition metal ions) unaffected by the test potential, consistent with an initial stabilization of ions at the pore mouth (i.e. in the initial portion or outside of the membrane electric field) (Hess et al., 1986; Lansman et al., 1986; Lansman, 1990; Lux et al., 1990; Rosenberg and Chen, 1991; Mlinar and Enyeart, 1993; Carbone et al., 1997; Khan et al., 2008). Off-rates on the other hand are in most cases strongly affected by the membrane potential and essentially determine the voltage-dependence of steady-state block, suggesting that the actual blocking site is located deeper in the membrane electric field (Lansman et al., 1986; Khan et al., 2008).

Direct evidence for an initial stabilization of Ca<sup>2+</sup> ions near the selectivity filter is provided by crystallographic data of Ca<sub>v</sub>Ab and its derivatives (Tang et al., 2014). They frequently contain Ca<sup>2+</sup> ions in the vicinity of the pore mouth, which seem to be stabilized by interaction with the channel through water molecules from their inner hydration sphere (Fig. 8A–E). These findings illustrate that initial ion interactions with the channel are unlikely to involve binding in the strict sense, but rather formation of an ‘encounter complex’ with the channel mouth (Andersen and Koeppe, 1992). Interestingly, the exact position of stabilized Ca<sup>2+</sup> ions relative to the selectivity filter depends on its state of occupation, suggesting some kind of interaction with ions already occupying the pore. Thus, when the external intra-pore site is occupied, Ca<sup>2+</sup> ions are located several Å away from the pore entrance, possibly due to repulsive interactions (Fig. 8B and C). If it is unoccupied, Ca<sup>2+</sup> ions are dragged close to the pore entrance, such that formation of an outer sphere complex may be facilitated (Fig. 8D and E). Hence ions already occupying the pore can apparently interact with incoming ions, which is consistent with the experimental observation that blocking rates strongly depend on the nature and concentration of permeant ions. For example, Cd<sup>2+</sup> blocks inward currents through HVA channels carried by Li<sup>+</sup> 400-times faster than inward currents carried by Ba<sup>2+</sup> (which binds to the pore  $\sim 10^8$  times more tightly than Li<sup>+</sup>) (Cloues et al., 2000) and in both cases on-rates decrease with increasing concentration of charge carrier (Kuo and Hess, 1993b, 1993c). It follows that the second order rate constant for block of foreign currents must somewhat underestimate ‘true’ association rates. A better measure for entry in the absence of



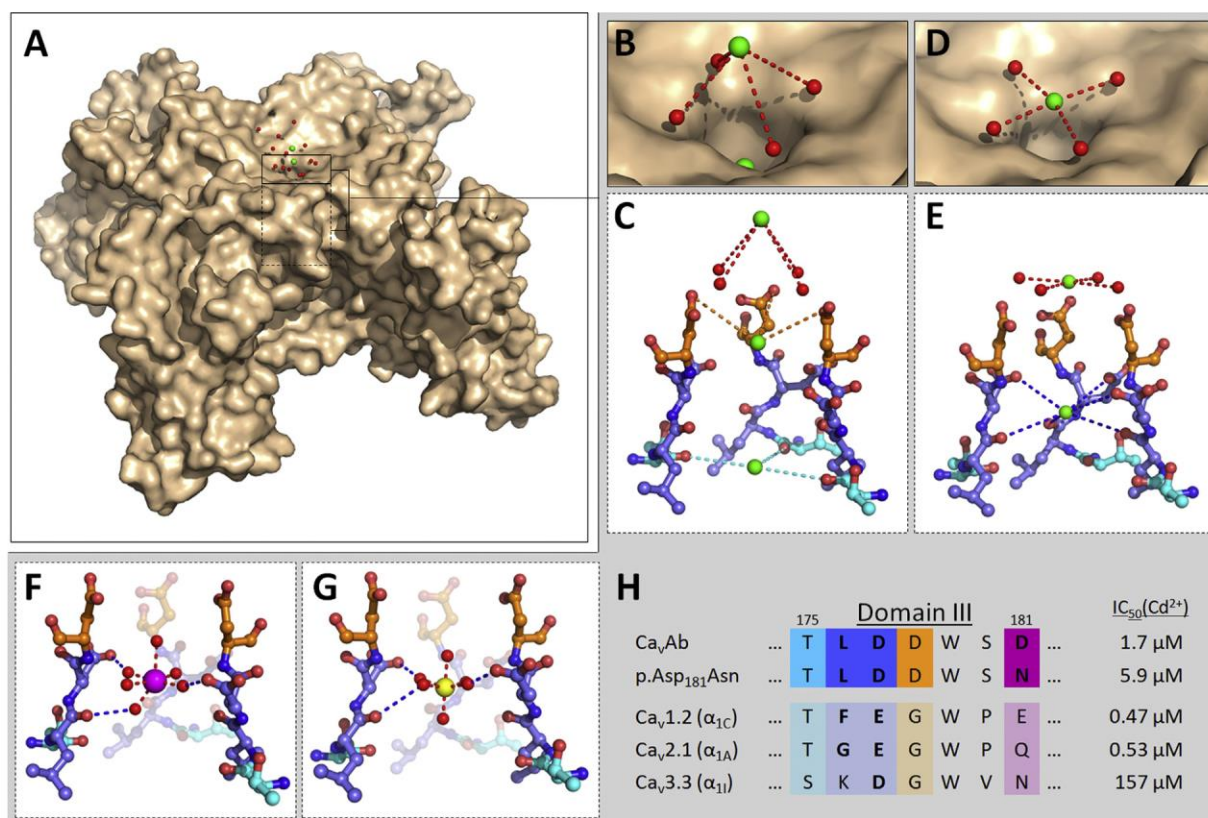


**Fig. 8.** Interactions of polyvalent inorganic cations with sites at or within the pore of VGCCs. (A) Surface representation of the crystal structure of Ca<sub>v</sub>Ab with multiple Ca<sup>2+</sup> ions in the vicinity of the channel entrance. (B) Close up view and (C) ball and stick representation of the situation at a doubly occupied channel. The external binding site (orange) is occupied and a ‘waiting’ Ca<sup>2+</sup> ion (green) can be seen several Å away from the channel entrance, but associated to the channel through water molecules from its inner hydration sphere (red). (D) Close up view and (E) ball and stick representation of the situation at a singly occupied channel. As the external binding site is unoccupied, the waiting Ca<sup>2+</sup> ion is dragged close to the pore entrance. (F) and (G) ball and stick representations of crystallographic data of Ca<sub>v</sub>Ab obtained in the presence of 100 mM Cd<sup>2+</sup> (magenta) or Mn<sup>2+</sup> (yellow) respectively. Both ions block the channel by binding to the central high-affinity site (blue) formed by DDDD-locus and neighbouring leucine residues, while remaining stabilized by their inner hydration sphere (red). (H) Structural determinants of Cd<sup>2+</sup> block in bacterial and vertebrate VGCCs. Sequence alignment of the selectivity filter in domain III and Cd<sup>2+</sup> sensitivity of the indicated channel types with residues directly involved in Cd<sup>2+</sup> binding or shown to influence block highlighted in bold.

ion–ion interactions has been obtained from the relationship between rate of block and concentration of current carrying ions. Thus, fitting the data for Ca<sup>2+</sup> block of inward Li<sup>+</sup> currents yields on-rates of around  $1.8 \times 10^9 \text{ M}^{-1} \text{ s}^{-1}$  at 0 mM Li<sup>+</sup> activity, which correspond well to the estimated diffusion-limited maximum association rate (Kuo and Hess, 1993b, 1993c).

#### 4.2.3. Dissociation: ion–pore interactions are influenced by charge and size

Analogous to the above considerations on entry, the rate-constant for Ca<sup>2+</sup> unblock of inward Li<sup>+</sup> currents (off-rate) should provide a first approximation for the unimolecular translocation step (i.e. passage of Ca<sup>2+</sup> ions through the channel), although it lumps together all individual transitions between possible intrapore binding sites. In a simple blocking-unblocking scheme, rates of dissociation should be equivalent to the product of on-rates and equilibrium binding affinity ( $K_d$  for block). Since Ca<sup>2+</sup> blocks monovalent currents with high on-rates and high affinity ( $K_d \sim 1\text{--}3 \mu\text{M}$  at intermediate potentials) (Fukushima and Hagiwara, 1985; Lansman et al., 1986; Carbone and Lux, 1987; Lux et al., 1990; Khan et al., 2008), predicted rates for Ca<sup>2+</sup> exit hardly exceed  $\sim 1000 \text{ s}^{-1}$ . Considering that estimated rate coefficients for overall Ca<sup>2+</sup> transfer under physiological conditions are  $7.5 \times 10^7 \text{ M}^{-1} \text{ s}^{-1}$  for HVA channels (Hess et al., 1986) and  $0.3\text{--}0.5 \times 10^8 \text{ M}^{-1} \text{ s}^{-1}$  for LVA channels respectively (Carbone and Lux, 1987; Lux et al., 1990), Ca<sup>2+</sup> flux through VGCCs clearly cannot be described in

terms of a simple binding reaction. Trivalent lanthanoid ions on the other hand rapidly enter the pore, have very low rates of unbinding (Table 2) and produce discrete, long lasting blocking events, typically already at submicromolar concentrations (Biagi and Enyeart, 1990; Lansman, 1990; Mlinar and Enyeart, 1993; Beedle et al., 2002; Obejero-Paz et al., 2004; Babich et al., 2007b). Like Ca<sup>2+</sup>, these ions preferentially interact with oxygen donor groups (Nieboer, 1975; Dos Remedios, 1981) and appear to be the main high-affinity coordination site in the pore, as reflected in the similar voltage-dependence of steady-state block. However, in stark contrast to Ca<sup>2+</sup> or Ba<sup>2+</sup>, their exit rates are much more consistent with a simple blocking-unblocking scheme.

The effective ionic radii of lanthanoid ions decrease across the series in steps of less than 0.1 Å (lanthanoid contraction), making them well suited to study the effects of ion size on the degree and kinetics of block (Beedle et al., 2002). In both HVA and LVA channels, steady-state lanthanoid block increases with decreasing effective ionic radius and approaches a maximum for radii equal to or slightly smaller than Ca<sup>2+</sup> (Triggle and Triggle, 1976; Lansman, 1990; Mlinar and Enyeart, 1993; Beedle et al., 2002). Comparative analysis of lanthanoid blocking kinetics has only been done for HVA channels, where both on- and off-rates increase with decreasing non-hydrated radius but off-rates change little for the smaller trivalent species (Lansman, 1990). To understand these findings, it is useful to view binding of ions to ligating groups in terms of a competition between ion–ligand and ion–water



interactions, both being dominated by coulombic forces. The work required to remove an ion from surrounding water molecules, which screen its strong electric field, is compensated by some energetically favourable interaction with the ligand. Little is known about actual ion–ligand interactions, but interaction of ions with water molecules has been extensively characterized and is known to depend on valence and ionic radius (which together determine an ion's charge density). Smaller ions have a higher net surface charge and can approach the negatively charged oxygen groups of water molecules more closely. Since coulomb interaction energy is inversely proportional to the distance between two charges, they hold water molecules from their inner hydration sphere more tightly and exhibit higher energies of interaction with charged groups. Smaller cations are therefore preferentially bound by high-field-strength sites like the EEEE/EEDD-locus, at which ion–pore electrostatic interaction energy is high compared to dehydration energy. This view is highly simplified but consistent with selection by the main binding-locus for divalent (trivalent) over monovalent (divalent) cations and with the increase of HVA channel conductance in the order  $\text{Cd}^{2+}$  (0.95 Å) <  $\text{Ca}^{2+}$  (1 Å) <  $\text{Sr}^{2+}$  (1.18) <  $\text{Ba}^{2+}$  (1.35). LVA channels exhibit essentially equal apparent permeability for  $\text{Ca}^{2+}$  and  $\text{Ba}^{2+}$  (Bean, 1985; Fukushima and Hagiwara, 1985; Carbone and Lux, 1987; Huguenard, 1996) and currents carried by  $\text{Ca}^{2+}$  can even exceed  $\text{Ba}^{2+}$ -currents (Serrano et al., 2000), yet  $\text{Mg}^{2+}$ -block of  $\text{Ca}_v3.1$  channels is 7-fold more potent in  $\text{Ba}^{2+}$  relative to  $\text{Ca}^{2+}$ , suggesting that the EEDD-locus binds  $\text{Ca}^{2+}$  more tightly as well (Serrano et al., 2000). As a consequence of differential  $\text{Mg}^{2+}$ -block,  $\text{Ca}^{2+}$ -currents are larger than  $\text{Ba}^{2+}$ -currents if measured in the presence of physiological concentrations of  $\text{Mg}^{2+}$ , but comparable in its absence (Serrano et al., 2000).

Apparently, smaller ions bind to the selectivity filter more tightly and block other currents, but they also leave the channel at a lower rate. That other factors influence ion–ligand interactions as well can be seen in the shallow relationship between blocking affinity and ionic radius for smaller lanthanoid ions (<1 Å) and the much weaker action of the smallest members of this group, like  $\text{Sc}^{3+}$  (0.74 Å) (Beedle et al., 2002; Lansman, 1990). It is reasonable to assume that steric effects within a three-dimensional site limit binding of small ions, which necessitate a closer association of donor groups. Hence, the lack of further decrease in unbinding rates observed for lanthanoid ions smaller than  $\text{Ca}^{2+}$  as well as the low apparent affinity of both HVA and LVA channels for  $\text{Mg}^{2+}$  (0.72 Å) could be related to a limited flexibility of the EEEE/EEDD-locus. Likewise, less effective selection for  $\text{Ca}^{2+}$  over  $\text{Ba}^{2+}$  by LVA relative to HVA channels could be interpreted in terms of a more rigid binding locus formed by the EEDD-locus.

On-rates for lanthanoid block as well as for block by most other metal ions on the other hand usually increase with increasing ion size (i.e. ions with low dehydration energy enter faster), which is opposite to what would be expected for binding at a high-field-strength site. This loose inverse correlation between rates of entry and rates of water loss has traditionally been ascribed to slower dehydration of small ions. An alternative explanation is that ions initially interact with a low-field-strength site, affinity of which for different ions should mainly depend on their water exchange rate constants (i.e. ion size). This concept would be consistent with the findings described in the previous section and with the distribution of negative charge in the vicinity of the selectivity filter over a relatively large surface area at the channel mouth (Fig. 4A3–8).

What makes it difficult to appraise the role of these aspects however, is the fundamental question if ions traverse vertebrate VGCCs in a hydrated state, as observed in  $\text{Ca}_v\text{Ab}$ , or if water molecules from their inner hydration sphere are substituted by ligating pore residues.

Considering that smaller ions attract more water molecules to their inner hydration sphere (i.e. hydrated diameter and rates of water exchange are typically inversely proportional to the effective non-hydrated radius<sup>6</sup>), one could also argue that lanthanoid ions, due to their greater ionic potential and thus hydrated diameter, have to dehydrate more completely than  $\text{Ca}^{2+}$  to fit into the pore, which might in turn lead to tighter ion–pore interactions.

The available data are insufficient to draw a definite conclusion, but the mechanism of hydrated cation transfer observed in  $\text{Ca}_v\text{Ab}$  and its derivatives demonstrates that highly  $\text{Ca}^{2+}$  selective flux is possible even without the time-consuming step of complete water loss. Catalysed dehydration by pore residues would allow for an even more efficient selection of  $\text{Ca}^{2+}$  over foreign ions, but from an evolutionary point of view, a complex mechanism like this seems unlikely if single point-mutations in bacterial voltage-gated sodium channels suffice to achieve high  $\text{Ca}^{2+}$  selectivity without dehydration.

Regardless of the exact mechanism underlying selective permeation, ion–pore interactions as described above certainly involve additional determinants, like coordination number, donor atom preference or polarizability. Likewise, ion size may be important for volume-exclusion effects in the spatially confined pore. Modelling of VGCCs in fact shows that, depending on entropic, electrostatic, and dehydration forces, a high-field-strength site like the EEEE/EEDD-locus can also preferentially bind larger ions (Krauss et al., 2011). Even more importantly, ion–pore interactions alone can explain selective binding, but not the high rates of  $\text{Ca}^{2+}$ -flux achieved by VGCCs.

#### 4.2.4. Translocation: differential ion–ion interactions facilitate exit

Consistent with a requirement for ion–ion interactions to overcome the limitations associated with high-affinity binding, microscopic and macroscopic electrophysiological evidence demonstrates that  $\text{Ca}^{2+}$  unblock of monovalent currents is slow at nanomolar  $\text{Ca}^{2+}$  concentrations ( $\sim 30 \text{ s}^{-1}$  in LVA channels with 100 nM  $\text{Ca}^{2+}$ ), intermediate at micromolar  $\text{Ca}^{2+}$  concentrations ( $\sim 3000 \text{ s}^{-1}$  in LVA channels with 100  $\mu\text{M}$   $\text{Ca}^{2+}$ ) and typically beyond the maximum temporal resolution at millimolar  $\text{Ca}^{2+}$  concentrations (Lansman et al., 1986; Khan et al., 2008).

When  $\text{Li}^+$  inward or outward currents through HVA channels are blocked by micromolar concentrations of  $\text{Ca}^{2+}$ , blocking  $\text{Ca}^{2+}$  ions always leave the pore with the  $\text{Li}^+$  current and not against it, supporting the notion that ions traverse the pore in a single file and cannot move independently from each other (flux coupling) (Kuo and Hess, 1993b, 1993c). The existence of flux coupling suggests that the single-file region of the pore must contain a composite coordination site or a set of sites separated by insignificant energy barriers, where ion–ion interactions can take place. Here, occupation of a particular site by an ion can facilitate exit of other ions from nearby sites (enhancement or knock-off effect), which appears to be one of the main strategies used by VGCCs to overcome the limitations brought about by high-affinity  $\text{Ca}^{2+}$  binding. Thus, when monovalent inward currents are blocked by micromolar concentrations of  $\text{Ca}^{2+}$ , the  $\text{Ca}^{2+}$  off-rates are linearly correlated with the external concentration of monovalent cations ( $[\text{M}^+]_o$ ) and extrapolate to the origin, indicating that  $\text{Ca}^{2+}$  exit from the pore under these experimental conditions would be negligible without the enhancement effect (Kuo and Hess, 1993b). A qualitatively similar relationship between blocker off-rate and permeant ion concentration has been observed for other alkaline earth metal ions ( $\text{Ba}^{2+}$ ,  $\text{Mg}^{2+}$ ),  $\text{Cd}^{2+}$  and lanthanoid ions (Lansman

<sup>6</sup> It should be anticipated that this is still a highly simplified view, as the extent of hydration may change through very short time scales (i.e. the hydration shell is dynamic) and bigger ions may in fact be in direct contact with more water molecules than smaller ions, but they bind them less tightly (Hille, 2001).

et al., 1986; Kuo and Hess, 1993b; Mlinar and Enyeart, 1993; Cloues et al., 2000). Repulsion is steeply valence-dependent (Almers and McCleskey, 1984), but the enhancement effect is not solely determined by electrostatic repulsion, since it can markedly differ between ions of the same charge. For example, off-rates for  $Mg^{2+}$  block of  $Li^+$  currents are much less affected by the concentration of  $Li^+$  than off-rates for  $Ca^{2+}$  block of  $Li^+$  currents, and a clear enhancement of  $Mg^{2+}$  unblock is only observed at very hyperpolarized potentials or high  $Li^+$  concentrations (Kuo and Hess, 1993a). In other words, the apparent  $K_d$  for  $Li^+$  occupation of an enhancement site is high ( $\sim 2\text{--}3\text{ M}$ ) when a neighbouring site is occupied by  $Ca^{2+}$  (two charges, high affinity) and much lower ( $\sim 300\text{ mM}$ ) when the neighbouring site is occupied by  $Mg^{2+}$  (two charges, lower affinity). Likewise,  $Cd^{2+}$  (two charges, very high affinity) has more effect on  $Ba^{2+}$  occupation of the enhancement site than  $Ba^{2+}$  itself (two charges, high affinity) (Kuo and Hess, 1993b). Apparently, the magnitude of ion–ion interactions at the high-affinity site depends more on affinity (and possibly additional mechanisms such as local deformations) than on electrostatic repulsion between ions. As mentioned before, the enhancement effect has important implications for the voltage-dependence of unblock, and its interpretation in terms of apparent electrical distances. Since occupation of nearby enhancement sites by permeant ions facilitates blocker exit, the overall voltage-dependence of unblock is not only determined by the translocation of blocker (i.e. the energy profile of blocking ions in the pore) but also by permeant ion occupancy of the enhancement site. In other words, ‘clearing’ of the permeation pathway by permeant ions can lead to a relief of block by depolarization and produce apparently voltage- but essentially current-dependent off-rates (Lansman et al., 1986). In support of the Woodhull model, voltage-dependent  $La^{3+}$ ,  $Mg^{2+}$ ,  $Ni^{2+}$  and  $Cd^{2+}$ -unblock is still demonstrable in the absence of permeant ions, excluding ion–ion interactions as the sole mechanism for these observations (Thevenod and Jones, 1992; Carbone et al., 1997; Block et al., 1998; Lee et al., 1999b). Yet fractional  $Ni^{2+}$ -unblock of outward currents through  $Ca_v3.1$  and  $Ca_v3.3$  channels is markedly stronger in the presence of permeant ions (Lee et al., 1999b), suggesting that the current-dependence of block due to ion movements can add up to the voltage-dependence of block resulting from blocker entry into the membrane electric field. Thus, unless all potential sources of voltage-dependence are included in the calculation or experimentally eliminated, apparent electrical distances cannot accurately reflect actual electrical distances relative to the membrane electric field. Moreover, the voltage-dependence of  $Ca^{2+}$  unblock changes as a function of  $[Li^+]_o$  (Kuo and Hess, 1993b). At high  $[Li^+]_o$ ,  $Ca^{2+}$  exit to the internal site is enhanced and hyperpolarization increases the off-rate (i.e. relieves block). At low  $[Li^+]_o$ ,  $Ca^{2+}$  exit is essentially unenhanced and takes place into both directions. In this case, hyperpolarization still increases the rates of  $Ca^{2+}$  exit to the inside, but at the expense of exit rates to the outside, such that the absolute off-rate changes little with voltage. The situation is different in the case of  $Mg^{2+}$ , which has much lower affinity for the blocking site and can leave the pore at rates in the order of  $200\text{--}400\text{ s}^{-1}$  even when no (enhancing)  $Li^+$  ions are present (Kuo and Hess, 1993a). Since the tendency for enhanced exit is very small, there is also little contribution of  $Li^+$  to  $Mg^{2+}$  unblock, which may explain part of the shallow voltage-dependence of steady-state  $Mg^{2+}$  block. A lack of enhancement is presumably also the reason for the inefficiency of  $Mg^{2+}$  as permeant ion relative to  $Ca^{2+}$  despite the much tighter binding of  $Ca^{2+}$  ions to intra-pore sites. It has been shown that most features of permeation and block of  $Ca_v3.1$  channels by  $Ca^{2+}$ ,  $Ba^{2+}$ ,  $Na^{2+}$  and  $Mg^{2+}$  can be described reasonably well by a two-site model with strong ion–ion interactions (Lopin et al., 2010; Khan et al., 2008). The calculations interestingly predict preferential binding of  $Ca^{2+}$  ions to the outer and of  $Ba^{2+}$  ions to the inner

intra-pore site (Lopin et al., 2010), which could explain the stronger blocking action of most metal ions in  $Ba^{2+}$  vs.  $Ca^{2+}$  (i.e. the magnitude of effects of ion–ion interactions on entry may also depend on the preferential target site of blocking ions in the pore). Of note however, the data can be described almost equally well by a model with weak repulsion and both models fail to accurately describe the block of IIV-currents by external  $Mg^{2+}$ , suggesting that the actual mechanism is more complex (Lopin et al., 2010).

#### 4.2.5. Block from the inside: low-affinity competition at the inner vestibule

In contrast to the rapid block of  $Li^+$  currents by external  $Ca^{2+}$ , block of inward  $Li^+$  currents through HVA channels by internal  $Ca^{2+}$  is very slow, suggesting that  $Li^+$  current flow in this experimental configuration strongly affects the movement of  $Ca^{2+}$  to its blocking site (Kuo and Hess, 1993c). Also,  $Ca^{2+}$  unblock of inward  $Li^+$  currents decreases if the internal  $Li^+$  concentration is raised (Kuo and Hess, 1993b). In a single-file, multi-ion pore, this can be explained by the lock-in effect, which denotes that occupation of a particular site by an ion prevents entry of other ions into this site, and thus passage through the channel (Kuo and Hess, 1993b). In other words, there must be at least one lower-affinity site in the internal single-file region of the pore, such that raising the concentration of intracellular  $Li^+$  increases the probability that this site is occupied by  $Li^+$ , and that blocking  $Ca^{2+}$  ions have to wait for them to leave the site before they can exit the pore. Further evidence for the existence of an internal low-affinity site is provided by the observation that internal, but not external, millimolar  $Mg^{2+}$  produces a decrease of unitary inward  $Li^+$  currents through HVA channels (Kuo and Hess, 1993a), presumably reflecting rapid (unresolved)  $Mg^{2+}$  block via an internal, low-affinity site. Likewise, outward currents through LVA channels are also weakly blocked by internal  $Mg^{2+}$  (Serrano et al., 2000).

#### 4.2.6. Using transition metal ions to probe translocation

Divalent transition metal ions are the most inhomogeneous group of blocking ions, and exhibit potencies ranging from very strong block with complete inhibition of currents at low micromolar concentrations, to relatively weak block, which is effective only at higher concentrations. One end of the spectrum is represented by  $Cd^{2+}$ , a very potent blocker of HVA ( $IC_{50} < 1\text{ }\mu\text{M}$ ) and to a lesser extent, LVA channels ( $IC_{50} = >50\text{ }\mu\text{M}$ ), which produces discrete blocking events with a voltage-dependence similar to that of  $Ca^{2+}$ - or lanthanoid-block (Lansman et al., 1986; Lansman, 1990; Williams et al., 1994; Williamson and Sather, 1999; Diaz et al., 2005; Rosenberg et al., 1988; Huang et al., 1989; Lacinova et al., 2000). The other end of the spectrum is represented by  $Mn^{2+}$ , a weak blocker of VGCCs which produces an intermediate to rapid block and can carry significant inward currents (Hagiwara and Nakajima, 1966; Ochi, 1970, 1975, 1976; Yamagish, 1973; Delahayes, 1975; Fukuda and Kawa, 1977; Hagiwara and Miyazaki, 1977; Okamoto et al., 1977; Palade and Almers, 1978; Anderson, 1983; Nelson, 1986). Most other transition metal ions ( $Co^{2+}$ ,  $Cu^{2+}$ ,  $Zn^{2+}$ ,  $Fe^{2+}$ ) are much less permeant, but they also have high rates of unblock and produce a flickering block of single-channel currents (Table 2) (Ochi, 1975; Fukuda and Kawa, 1977; Kawa, 1979; Anderson, 1983; Lansman et al., 1986; Nelson, 1986; Lansman, 1990; Winegar et al., 1991; Castelli et al., 2003; Lopin et al., 2012a). Several characteristics of their effects seem to suggest that they act by a mechanism distinct from  $Ca^{2+}$ -block of monovalent currents, including (i) the relatively shallow voltage-dependence of block (Winegar and Lansman, 1990; Winegar et al., 1991; Diaz et al., 2005; Lopin et al., 2012a), (ii) the markedly subunit-dependent apparent blocker affinity (Table 3) and (iii) the diverse, ion- and subunit-dependent alterations in the time-course of residual macroscopic currents and/or the voltage-dependence of channel



**Table 3**  
Suppression of recombinant calcium channels by selected polyvalent cations.

Metal ion	Charge carrier (mM)	Test potential (mV)	IC <sub>50</sub> (μM)						Reference		
			Ca <sub>v</sub> 1.2	Ca <sub>v</sub> 2.1	Ca <sub>v</sub> 2.2	Ca <sub>v</sub> 2.3	Ca <sub>v</sub> 3.1	Ca <sub>v</sub> 3.2		Ca <sub>v</sub> 3.3	
Ni <sup>2+</sup>	2 Ca <sup>2+</sup>	−30					133–148		184	a,b	
	5 Ca <sup>2+</sup>	40						1.9/1350		c	
	20 Ca <sup>2+</sup>	−10					1130			d	
	10 Ba <sup>2+</sup>	−40					250	12	216	e,f	
	10 Ba <sup>2+</sup>	−30					167	5.7	87	e	
	10 Ba <sup>2+</sup>	−20					280	7		p	
	10 Ba <sup>2+</sup>	0				14.2				g	
	10 Ba <sup>2+</sup>	G <sub>max</sub>		127.6	535	1337.6	303				h
	15 Ba <sup>2+</sup>	?				27.4		6.6			i,j
Zn <sup>2+</sup>	2 Ca <sup>2+</sup>	−30						81.7	0.78	158.6	q
	5 Ca <sup>2+</sup>	−20					1.3				k
	5 Ca <sup>2+</sup>	+20					8.1				k
	10 Ca <sup>2+</sup>	−30						135	2.3	470	l
	10 Ba <sup>2+</sup>	−20						82.2	3		m
	20 Ca <sup>2+</sup>	−20			1210			132.8			n
	20 Ba <sup>2+</sup>	−20		10.9	110	98	31.8	196.5	24.1	152.2	n
	Cu <sup>2+</sup>	5 Ca <sup>2+</sup>	−20				0.018				
5 Ca <sup>2+</sup>		+20				0.27					k
10 Ca <sup>2+</sup>		−30						22	0.9	26	l,r
Co <sup>2+</sup>	2 Ca <sup>2+</sup>	−40					335	122	345	f	
Cd <sup>2+</sup>	2 Ca <sup>2+</sup>	−40					128	65	157	f	
	5 Ca <sup>2+</sup>	+40						218			c
	~10 Ba <sup>2+</sup>	+20	0.47	0.53							o
	15 Ba <sup>2+</sup>	?				0.8		104			i,j
	20 Ca <sup>2+</sup>	−10					658				d
20 Ba <sup>2+</sup>	−10					162				d	

<sup>a</sup>Monteil et al. (2000a); <sup>b</sup>Monteil et al. (2000b); <sup>c</sup>Perchenet et al. (2000); <sup>d</sup>Lacinova et al. (2000); <sup>e</sup>Lee et al. (1999b); <sup>f</sup>Diaz et al. (2005); <sup>g</sup>Kang et al. (2007); <sup>h</sup>Zamponi et al. (1996); <sup>i</sup>Williams et al. (1994); <sup>j</sup>Williams et al. (1999); <sup>k</sup>Shcheglovitov et al. (2012); <sup>l</sup>Jeong et al. (2003); <sup>m</sup>Kang et al. (2010); <sup>n</sup>Sun et al. (2007); <sup>o</sup>Williamson and Sather (1999); <sup>p</sup>Perez-Reyes et al. (1999); <sup>q</sup>Traboulsie et al. (2007); <sup>r</sup>Nelson et al. (2007a).

gating they produce. Due to the lack of comprehensive single-channel data or knowledge of molecular channel structure, numerous mechanisms have been suggested to account for these complex actions, the most important of which will be summarized in the following sections. As with all models, they have to be interpreted with care, keeping in mind that they are based on several assumptions and can at best provide a partial or provisional truth. Used sensibly however, they may provide insight into channel function and serve as valuable guides to new experiments.

**4.2.6.1. Ni<sup>2+</sup> block of Ca<sub>v</sub>3.1 channels – successive action at multiple sites?** Steady-state Ni<sup>2+</sup> block of both HVA and LVA channels is similar to Mg<sup>2+</sup>-block in that it decreases monotonically with voltage, such that block is enhanced rather than relieved by strong hyperpolarization (Fukushima and Hagiwara, 1985; Hess et al., 1986; Lansman et al., 1986; Winegar et al., 1991; Diaz et al., 2005; Khan et al., 2008; Obejero-Paz et al., 2008). In HVA channels Ni<sup>2+</sup> has been demonstrated to produce discrete blocking events, with estimated exit rates about one order of magnitude slower than Cd<sup>2+</sup> exit, yet steady-state Ni<sup>2+</sup> block is much weaker, suggesting a somewhat different mechanism of action (Lansman et al., 1986; Winegar et al., 1991). Suppression of LVA channels by Ni<sup>2+</sup> has been particularly well studied, since this metal ion was long regarded as selective T-type antagonists. It is now understood that Ca<sub>v</sub>3.2 channels are the only members of the group potently suppressed by low micromolar Ni<sup>2+</sup> concentrations and that this is mainly due to allosteric effects via non-pore residues addressed in Section 4.3.1. In Ca<sub>v</sub>3.1 and Ca<sub>v</sub>3.3 channels on the other hand, much higher Ni<sup>2+</sup> concentrations are required for a similar degree of inhibition, which is associated with prominent changes in the time-course of residual macroscopic currents and a shift of the IV-curve towards more positive potentials (Lacinova et al., 2000; Diaz

et al., 2005; Kang et al., 2006; Obejero-Paz et al., 2008; Nosal et al., 2013). These effects are either absent or much weaker in Ca<sub>v</sub>3.2 channels, probably because the concentrations required for detectable kinetic effects already produce almost complete inhibition by the allosteric mechanism (Diaz et al., 2005).

The Ni<sup>2+</sup>-induced voltage shift of currents through Ca<sub>v</sub>3.1 channels has been interpreted in terms of allosteric effects on activation gating (Lacinova et al., 2000), but several studies have since shown that it is more likely a consequence of voltage-dependent block (Lee et al., 1999b; Diaz et al., 2005; Obejero-Paz et al., 2008). Interestingly, Ni<sup>2+</sup>-induced suppression of these channels can be separated into a rapid, low-affinity and a slower high-affinity component with differential ion- and voltage-dependencies, suggesting interaction with more than a single site. The rapid component can be quantified as weakly voltage- or current-dependent, low-affinity ( $K_d \sim 1\text{--}3$  mM, depending on charge carrier) reduction of macroscopic IIV-currents (Obejero-Paz et al., 2008). The slow component has been inferred from a number of findings, including a biphasic concentration-dependence of Ni<sup>2+</sup>-block, stronger suppression of macroscopic IV-compared to IIV-currents, accelerated deactivation at negative potentials, slower inactivation of inward currents at intermediate potentials, slower activation and inactivation of outward Na<sup>+</sup>-currents at very positive potentials and a delayed partial release of inhibition during strongly depolarizing voltage-steps (Diaz et al., 2005; Obejero-Paz et al., 2008; Nosal et al., 2013; Lee et al., 1999b). Both components are sensitive to changes in the nature and concentration of permeant ions, indicating an action at sites normally occupied by Ca<sup>2+</sup> (Obejero-Paz et al., 2008; Nosal et al., 2013). However, while slow suppression is 2–3 times faster in Ba<sup>2+</sup> vs. Ca<sup>2+</sup> and ~10 times faster with 2 vs. 110 mM Ca<sup>2+</sup> or Ba<sup>2+</sup> as the charge carrier, the rapid low-affinity component is much less

affected by the ionic conditions, so that its contribution to net block increases with increasing concentration of permeant ions and with increasing affinity of permeant ions for the high-affinity site (Obejero-Paz et al., 2008; Nosal et al., 2013). Based on these findings, it has been proposed that  $\text{Ni}^{2+}$  could rapidly interact with an outer low-affinity site, accessible at near diffusion-limited rates, followed by a slower development of block at the high-affinity EDD locus deeper within the pore (Obejero-Paz et al., 2008). In this view, stronger suppression of IV-currents could arise from time-dependent block, accelerated tail-current decay from voltage- and time-dependent reblock of open channels, slower activation of outward currents from voltage- and time-dependent relief of resting block and slower inactivation from voltage- and time-dependent unblock during the test pulse. Others have interpreted the low-affinity, voltage-independent component in terms of direct  $\text{Ni}^{2+}$ -effects on channel gating, homologous to high-affinity allosteric modulation of  $\text{Ca}_v3.2$  channels via extracellular trace metal binding sites (Nosal et al., 2013). What argues against this view is that increased occupation of the low-affinity site at high  $\text{Ni}^{2+}$ -concentrations can lock in block (i.e. reduce unblock) at the high-affinity site, indicating that both sites are located close to each other and supporting a two-site blocking model (Obejero-Paz et al., 2008). Moreover, both low- and high-affinity  $\text{Ni}^{2+}$ -block depend on current and/or voltage and on the nature of permeant ions (Obejero-Paz et al., 2008), while high-affinity allosteric  $\text{Ni}^{2+}$  suppression of  $\text{Ca}_v3.2$  channels is essentially current- and voltage-independent and not affected by the nature of permeant ions (Diaz et al., 2005; Kang et al., 2006), suggesting a fundamentally different interaction. This is also supported by the fact that  $\text{Ca}_v3.1$  as well as  $\text{Ca}_v3.3$  channels lack critical residues in domain I (Gly<sup>190</sup> and His<sup>191</sup>) required for high-affinity extracellular trace metal binding (but see Section 4.3.1). However, substitution in  $\text{Ca}_v3.1$  of the glutamine residue corresponding to His<sup>191</sup> by histidine selectively decreases the  $\text{Ni}^{2+}$ -concentration required for low-affinity block (Nosal et al., 2013), so that some remaining affinity of the site in relatively  $\text{Ni}^{2+}$ -insensitive  $\text{Ca}_v3.1$  and  $\text{Ca}_v3.3$  channels may still be present. Nosal et al. (2013) proposed that  $\text{Ni}^{2+}$ -binding to this site might produce allosteric effects on both, channel gating and ion-channel interactions in the pore. This could in turn suggest a certain degree of functional coupling between the pore region and one or more of the gating modules, as discussed in Section 4.2.6.3.

In any event, slow  $\text{Ni}^{2+}$ -transition from an external binding site to the selectivity filter would be consistent with the relatively weak nature of steady-state  $\text{Ni}^{2+}$ -block despite low rates of unbinding. Nosal et al. (2013) found that only 20–30% of  $\text{Ni}^{2+}$ -induced suppression of  $\text{Ca}_v3.1$  channels can be attributed to high-affinity interactions, whereas 70–80% appears to be due to low-affinity interactions. In terms of traditional permeation models involving partial or complete dehydration, rates of transition deeper into the pore could be limited by the low water exchange rate of  $\text{Ni}^{2+}$  ions. Considering that  $\text{Ni}^{2+}$ -dehydration is 100–1000-fold slower than that of other transition metal ions and about 10-fold slower than  $\text{Mg}^{2+}$ -dehydration (Diebler et al., 1969), it seems conceivable that slow dehydration, together with frequent displacement by permeant ions during the longer sojourn at the pore mouth, might be the rate-limiting step for  $\text{Ni}^{2+}$ -entry into the pore. If on the other hand permeant ions traverse the channels without complete dehydration, slow entry could reflect appreciable  $\text{Ni}^{2+}$  binding to residues involved in the (transient) stabilization of permeant ions, possibly due to its preference for nitrogen over oxygen donor groups (Table 2). Said differently, favourable ion-ligand interactions at the pore mouth could be associated with a more complete replacement by ligating groups of water molecules in the hydration sphere of  $\text{Ni}^{2+}$  relative to permeant ions, so that the energy required for further transition in the pore might be comparatively high. Considering the asymmetric pore

structure (Fig. 3D) and unequal charge distribution on their vestibule (Fig. 4A3–8), it seems likely that stabilization of permeant ions in vertebrate VGCCs takes place on lateral aspects of the vestibule rather than directly in front of the narrow pore (as observed in  $\text{Ca}_v\text{Ab}$ ). In this case, bound  $\text{Ni}^{2+}$  ions could conceivably reduce current through affected channels without completely plugging the pore.

Once  $\text{Ni}^{2+}$  reaches the intra-pore sites, the energy required for inward exit could be simply too high, so that net unblock is almost exclusively to the outside, where it may be energetically more favourable. This could explain the non-permeant nature of  $\text{Ni}^{2+}$ , and the fact that increased  $\text{Ni}^{2+}$ -occupation of the low-affinity site can lock-in block at the high-affinity site (i.e.  $\text{Ni}^{2+}$  ions stabilized or bound at the pore mouth might interfere with exit of  $\text{Ni}^{2+}$  ions already in the pore). However, the monotonic voltage-dependence of  $\text{Ni}^{2+}$  block in both LVA and HVA channels arises, at least in part, from the fact that on-rates for the slow component are markedly voltage-dependent (electrical distance  $\sim 0.2$ – $0.4$ ) (Winegar et al., 1991; Obejero-Paz et al., 2008). As a consequence, there is little or no apparent effect of hyperpolarization on steady-state  $\text{Ni}^{2+}$  block, since both on- and off-rates increase with increasingly negative potentials (Winegar et al., 1991; Obejero-Paz et al., 2008). This in turn suggests that  $\text{Ni}^{2+}$  can, in principle, traverse VGCCs, although apparently at negligibly low rates (see also Section 4.2.8).

**4.2.6.2. Relating  $\text{Ni}^{2+}$  block to other findings.**  $\text{Ni}^{2+}$ -block of HVA channels is less well characterized, but findings in several different preparations appear to support the concept of multiple interaction sites. For example, in mouse myotubes  $\text{Ni}^{2+}$  produces not only discrete block of single DHP-sensitive  $\text{Ca}^{2+}$ -currents but also a reduction of unitary conductance (Winegar et al., 1991). The latter could be due to screening of negative charge near the pore mouth, but given that the recordings were carried out with high concentrations (120 mM) of divalent charge carrier, it more likely reflects a rapid, unresolved component of block by  $\text{Ni}^{2+}$  binding somewhere in the vestibule (or allosteric effects of  $\text{Ni}^{2+}$  binding to a non-pore site). Two distinct types of  $\text{Ni}^{2+}$  block associated with a prominent slowing of macroscopic activation and slightly accelerated tail-current decay have also been described for P/Q-type like  $\text{Ca}^{2+}$ -currents in squid giant fibre lobe neurons (McFarlane and Gilly, 1998). Here the second type of block was identified as time- and voltage-dependent increase in the inhibition of IIV-currents upon extended depolarization (i.e. a stronger suppression of tail-current amplitudes with increasing prepulse duration). In cloned  $\text{Ca}_v1.2$  and  $\text{Ca}_v2$  channels,  $\text{Ni}^{2+}$ -block reduces the maximum macroscopic conductance determined from the IV-curve, shifts the IV-curve to more depolarized potentials and reduces the voltage-sensitivity of half-maximal current activation (Zamponi et al., 1996). The latter two effects are closely correlated with each other and quantitatively similar in all but  $\text{Ca}_v2.3$ -type channels, which have since been shown to be subject to high-affinity trace metal modulation via sites outside of the pore region (but see Section 4.3.2).  $\text{Ni}^{2+}$  effects on the remaining three subunits observed in the study are nevertheless difficult to interpret, since only IV-currents were analysed. If  $\text{Ca}_v2.3$  channels are excluded, the results are largely consistent with a combination of voltage-dependent pore block and electrostatic surface charge effects, although none of these mechanisms can account for the reduced voltage-sensitivity and the available data are clearly insufficient to exclude additional mechanisms of action. Of note however,  $\text{Ni}^{2+}$  block of  $\text{Ca}_v2.1$  channels is markedly affected by the identity of coexpressed  $\beta$ -subunits and almost completely abolished in the absence of a  $\beta$ -subunit (Zamponi et al., 1996). This could point at a role of fast VDI for  $\text{Ni}^{2+}$ -induced suppression (suggesting a functional coupling between the pore and inactivation gating, as addressed in Section



4.2.6.4) or simply reflect the distinct functional consequences of co-expressing different  $\beta$ -subunits. For example, differential shifts of channel gating along the voltage-axis produced by different  $\beta$ -subunits could obviously affect the degree of voltage-dependent pore block. A later study on native R-type and non-R-type HVA currents in guinea-pig cortical neurons found stronger  $\text{Ni}^{2+}$ -induced suppression of IV- relative to IIV-currents and significantly slowed activation kinetics of residual currents, but tail-current decay at intermediate potentials was slowed rather than accelerated (Magistretti et al., 2001). Differential effects of voltage- and time-dependent block on LVA and HVA channel tail-current kinetics are to be expected, considering that different step protocols have to be used since HVA channels deactivate much faster and at different membrane potentials. For example, in the voltage-range examined by Magistretti et al. (2001), HVA channel deactivation can be faster than  $\text{Ni}^{2+}$ -reblock in  $\text{Ca}_v3.1$  channels, so that gating may simply be too fast to detect time-dependent reblock. This cannot, however, explain the slowing of macroscopic deactivation, which was increased with longer prepulse durations and proposed to reflect allosteric effects of  $\text{Ni}^{2+}$ -binding to one of its blocking sites (but see Section 4.2.6.3).

In view of the similar dehydration energies of  $\text{Ni}^{2+}$  and  $\text{Mg}^{2+}$ , and the comparable voltage-dependence of block, it is interesting to note that several other characteristics of  $\text{Ni}^{2+}$ -block have also been reported for  $\text{Mg}^{2+}$ -block of  $\text{Ca}_v3.1$  channels. Thus,  $\text{Mg}^{2+}$  produces rapid block of IIV-currents, stronger suppression of IV- vs. IIV-currents, a depolarizing shift of the IV-curve and accelerated macroscopic deactivation (Serrano et al., 2000). In contrast to the rapid component of  $\text{Ni}^{2+}$ -block however,  $\text{Mg}^{2+}$ -induced suppression of IIV-currents is markedly voltage-dependent. Considering the somewhat faster dehydration of  $\text{Mg}^{2+}$  relative to  $\text{Ni}^{2+}$  (Diebler et al., 1969) and its more  $\text{Ca}^{2+}$ -like preference for oxygen donor groups (Table 2), this could simply reflect a faster transition into the pore, so that part of the voltage-dependent fraction of block is already detected by the IIV-protocol. Thus estimated bimolecular blocking rates for  $\text{Mg}^{2+}$  ( $\sim 10^7 \text{ M}^{-1} \text{ s}^{-1}$  for 1 mM  $\text{Mg}^{2+}$  in 2 mM  $\text{Ba}^{2+}$ ) are almost two orders of magnitude higher than blocking rates for the slow component of  $\text{Ni}^{2+}$ -block ( $\sim 3 \times 10^5 \text{ M}^{-1} \text{ s}^{-1}$  for 3 mM  $\text{Ni}^{2+}$  in 2 mM  $\text{Ba}^{2+}$ ) (Serrano et al., 2000; Obejero-Paz et al., 2008).  $\text{Cd}^{2+}$ -block of  $\text{Ca}_v3.1$  channels may be even faster, so that reblock upon repolarization to negative potentials is essentially instantaneous relative to the speed of the voltage-clamp and not detectable as a change in the time-course of tail-current decay (Diaz et al., 2005). However, it is also important to consider differences in the voltage-dependence of block.  $\text{Cd}^{2+}$ -block of  $\text{Ca}_v3.1$  and  $\text{Ca}_v3.3$  channels has a non-monotonic voltage-dependence and no clear effect on the position of the IV-curve and unlike  $\text{Ni}^{2+}$ ,  $\text{Cd}^{2+}$  significantly affects the apparent reversal potential of these channels (Lacinova et al., 2000; Diaz et al., 2005). This is consistent with a relatively permeant nature of  $\text{Cd}^{2+}$ , in which case the Woodhull model predicts the voltage-dependence of block to be biphasic. As a consequence, voltage-steps to strongly depolarized potentials and repolarization to very negative potentials may be associated with little change in the degree of block or (depending on the prepulse voltage) even with slower tail-current decay due to slow unblock upon repolarization, as it has been described in native HVA channels (Taylor, 1988). Thus, Lacinova et al. (2000), using repolarization to intermediate potentials (where  $\text{Cd}^{2+}$  block should be strongest), observed a  $\text{Cd}^{2+}$ -induced acceleration of  $\text{Ca}_v3.1$  macroscopic deactivation for  $\text{Ca}^{2+}$ - but not  $\text{Ba}^{2+}$ -currents. Likewise, time-dependent reblock of open  $\text{Ca}_v3.1$  channels by  $\text{Ca}^{2+}$  as well as  $\text{Co}^{2+}$  can be demonstrated as fast component of tail-current decay, but this is usually only possible in a very narrow window of concentration and voltage (Diaz et al., 2005; Khan et al., 2008). Different voltage-dependencies of  $\text{Cd}^{2+}$  vs.  $\text{Ni}^{2+}$  block could also explain why  $\text{Cd}^{2+}$ , in contrast

to  $\text{Ni}^{2+}$ , slightly accelerates inactivation of inward currents at intermediate potentials (Diaz et al., 2005), since block would in this case increase rather than decrease during the test pulse.

A similar explanation could apply to the significant acceleration of macroscopic inactivation associated with trivalent cation block of HVA but apparently not LVA channels (Biagi and Enyeart, 1990; Mlinar and Enyeart, 1993; Beedle et al., 2002; Obejero-Paz et al., 2004; Babich et al., 2007b). Here, it is important to keep in mind the concentration-dependence of blocker on-rates and the distinct gating properties of the two channel families. Due to their high potency, trivalent cations are commonly used at submicromolar concentrations, in which case the on-rates for block can be slower than channel gating (Obejero-Paz et al., 2004). Therefore, block of additional channels upon depolarization to intermediate potentials may markedly accelerate the slow decay of current during the voltage-step in HVA channels, yet contribute little to the rapid decay of current in LVA channels. As illustrated in case of  $\text{Ni}^{2+}$ , time- and voltage-dependent block of LVA channels may also be missed or underestimated by analysis of IIV-currents, since brief depolarization is insufficient for a detectable change in the level of steady-state block, while longer depolarization is already associated with significant inactivation. As a consequence, block of these channels by nanomolar  $\text{Y}^{3+}$  appears to be unaffected by depolarization to physiological voltages ( $-40$  to  $+40$  mV), yet a voltage-dependence can be demonstrated by very strong depolarization to  $+200$  mV, where block is almost completely relieved (Obejero-Paz et al., 2004). This has been reaffirmed by calculation of the time course of fractional block (i.e. the ratio of current traces recorded in the presence and absence of  $\text{Y}^{3+}$ ), which reveals that block is initially strong, but changes with a nearly exponential time course so that at strongly depolarized potentials, the current ratios approach unity (i.e. complete relieve of block) (Obejero-Paz et al., 2004). It remains to be elucidated if relief of  $\text{Y}^{3+}$  block by strong depolarization is due to a true voltage-dependence or simply due to clearing of the permeation pathway by outward-current.

To recapitulate the previous two sections, many of the distinct metal blocking effects could be accounted for by quantitative differences in the energetics and kinetics of ion-interaction with sites in the permeation pathway (as opposed to actions mediated by distinct, ion-specific sites). Firstly, permeation and block of monovalent currents by alkaline earth metal ions can be explained in terms of a two-site model, where ion-ion interactions influence entry- and exit-rates and subtle differences in affinity and enhancement (determinants of which remain to be elucidated) result in distinct permeability and blocking properties. The same likely applies to lanthanoid ions and  $\text{Cd}^{2+}$ , entry rates of which are also affected by the nature of ions already occupying the pore. Due to their very high apparent affinity, these ions nevertheless rapidly enter the pore and tightly bind to one of the intra-pore sites to produce discrete block, but they can still be driven out of the pore and into the cell by strong hyperpolarization.  $\text{Ni}^{2+}$  (and to a lesser extent  $\text{Mg}^{2+}$ ) appears to deviate from this general pattern mainly in that it has considerable difficulties reaching the intra-pore sites. This could produce rapid block or reduce the single-channel conductance by interfering with stabilization of  $\text{Ca}^{2+}$ -ions at the vestibule, both of which could explain the low-affinity component of inhibition and should be relatively insensitive to permeant ion concentration and membrane potential. Transition of  $\text{Ni}^{2+}$  to the nearby external intra-pore site (i.e. into the pore) produces discrete block, but is opposed by ion-ion interactions (i.e. competition), ion-pore interactions (i.e. slow dehydration) and/or other factors. The predicted preference of  $\text{Ba}^{2+}$  to bind at the putative internal intra-pore site of  $\text{Ca}_v3.1$  channels (Lopin et al., 2010) could in this view explain why slow  $\text{Ni}^{2+}$ -block is 2–3 times faster in  $\text{Ba}^{2+}$  vs.  $\text{Ca}^{2+}$  (Obejero-Paz et al., 2008). Once at the external intra-pore site, the tendency for  $\text{Ni}^{2+}$ -transition to the internal site or for enhanced

$\text{Ni}^{2+}$ -exit from the internal site into the cell might be negligible and binding might be too tight for 'intrinsic' inward exit (i.e. exit without enhancement effect), so that unlike  $\text{Mg}^{2+}$ , net exit into the cell is below the limits for detection. Other divalent cations like  $\text{Co}^{2+}$  seem to have less difficulty reaching the intra-pore sites (i.e. faster on-rates), but they also bind there less tightly, so that rates of intrinsic inward exit are sufficient for detectable entry into the cell (i.e. faster off-rates). Considering their preference for nitrogen over oxygen donor groups (Diebler et al., 1969; Martin, 1988), this interpretation could provide a clue about the identity of residues involved in the initial stabilization of permeant ions at the pore mouth, as discussed in more detail in Section 4.2.7.

Altogether, the picture that emerges is that of a pore with multiple binding sites, where all polyvalent cations may interact with most or all of these sites, although the time-scale of interaction might in some cases make this difficult to demonstrate. That said, the true mechanisms of pore block are likely to be more complex, and as described in the following sections, several findings argue for certain 'true' effects of blocking ions on channel gating, which could explain the differential  $\text{Ni}^{2+}$ -effects on tail-current decay in LVA vs. HVA channels. These effects and the proposed mechanisms of action are not necessarily incompatible with the above considerations, but may rather necessitate an extension of models based on the intrinsic properties of block to include certain gating effects, arising from ion-channel interactions at the pore mouth or at one of the putative intra-pore binding sites.

**4.2.6.3. The selectivity filter as a channel gate.** There is ample evidence that the nature and concentration of permeant ions can affect channel gating by a mechanism distinct from surface charge effects. For example, macroscopic activation and deactivation of  $\text{Ca}^{2+}$ -channels in the ciliate *Paramecium* as well as mean open and closed times of single  $\text{Ca}^{2+}$ -channels in *Aplysia* neurons have been shown to be markedly affected by the nature of permeant ions (Saimi and Kung, 1982; Chesnoy-Marchais, 1985). Likewise, a consistent observation in studies on native vertebrate HVA and LVA channels reconstituted in planar lipid bilayers is that mean open times are correlated with the permeability of charge carrying ions (Nelson et al., 1984; Nelson, 1986; Shuba et al., 1991). For obvious reasons, these findings may be relevant for blocker-induced changes in channel gating, but unfortunately, the available data concerning gating effects of pore occupation by blocking ions is currently limited to macroscopic recordings.

Noh et al. (2010) characterized effects of  $\text{Zn}^{2+}$  on cloned  $\text{Ca}_v3.1$  channels and native  $\text{Ca}_v3.1$ -like currents in rat thalamic neurons. They found that  $\text{Zn}^{2+}$ -block is associated with significantly faster macroscopic deactivation and recovery from inactivation, moderate but significant depolarizing shifts of steady-state inactivation and activation (the latter measured with a tail-current protocol) and selective slowing of macroscopic inactivation around the activation threshold. Block is unaffected by depolarization to physiological voltages but relieved by strong depolarization (i.e. by outward current) and inversely related to the holding potential (i.e. block decreases with increasingly positive holding potentials), suggesting that both permeant ions and inactivation interfere with inhibition. The peak tail-current inhibition was moreover independent of the prepulse potential, indicating that  $\text{Zn}^{2+}$  reblock of open channels upon repolarization is essentially instantaneous with respect to the recording bandwidth and should not contribute to tail-current decay. To account for these findings, they proposed a model where  $\text{Zn}^{2+}$ -binding to a superficial intra-pore site, accessible only after channel activation, could block the channel and accelerate return of the activation gate to its closed state. Since LVA channels recover from inactivation by a deactivation-first pathway (Kuo and Yang, 2001; Burgess et al., 2002), faster

deactivation could conceivably also accelerate the process of recovery. Slowing of macroscopic inactivation near the activation threshold was proposed to arise from a coupling between deactivation and inactivation (i.e. faster deactivation leads to slower inactivation and vice versa), as it has been previously described for  $\text{Ca}_v3.3$  channels (Warre and Randall, 2000).

Somewhat contradictory findings have been reported by Troubousie et al. (2007), who observed a  $\text{Zn}^{2+}$ -induced hyperpolarizing shift of  $\text{Ca}_v3.1$  steady-state inactivation and IV-curve, accelerated macroscopic activation, slower macroscopic inactivation at negative potentials and a moderate but insignificant speeding of macroscopic deactivation. They suggested that  $\text{Zn}^{2+}$  preferentially binds to and stabilizes inactivated channel states, possibly via an extracellular allosteric site. Inconsistencies between different studies can be due to diverse experimental conditions, step protocols and expression systems used, although in this case, both investigations employed essentially the same experimental conditions (i.e. same holding potential,  $\text{Zn}^{2+}$  concentration and extracellular solution with 3 vs. 2 mM  $\text{Ca}^{2+}$  as the charge carrier) and very similar expression systems (HEK-293 vs. HEK-293/tsA-201 cells). It is thus very difficult to interpret these findings, although it is noteworthy that the effects observed by Noh et al. (2010) closely resemble the functional consequences of point mutations in the selectivity filter of LVA channels. In particular, it has been shown that aspartate-to-glutamate substitutions in the EEDD-locus markedly increase the rates of macroscopic deactivation and recovery from inactivation, shift activation and steady-state inactivation to more positive potentials and slow the time-course of macroscopic inactivation at voltages close to the activation threshold (Talavera et al., 2001, 2003). Since this produces mutants with HVA-like fast deactivation kinetics, it has been proposed that the divergent selectivity filter of LVA and HVA channels may be involved in their distinct deactivation behaviour and that it may form part of a gate controlling lifetime of the open state (Talavera and Nilius, 2006a). A concept like this could account for certain effects of other blocking ions which are difficult to explain in terms of voltage- and time-dependent block. For example,  $\text{Zn}^{2+}$ ,  $\text{Co}^{2+}$ ,  $\text{Cu}^{2+}$  and  $\text{Mn}^{2+}$  suppress macroscopic currents through native HVA channels with little apparent voltage-dependence, but at the same time, they produce a marked slowing of both macroscopic activation and deactivation (Büsselberg et al., 1992, 1994a, 1994b; Castelli et al., 2003). As pointed out by Castelli et al. (2003), in a properly implemented kinetic model, block and gating effects mediated via the same principle intra-pore site are not necessarily inconsistent with the fact that only unblocked channels should contribute to macroscopic current. However, in the absence of additional data, one can only speculate that ion-specific allosteric effects via intra-pore sites could, for example, contribute to and modify the kinetic features of voltage- and time-dependent block.

There is also evidence that voltage-dependent gating may conversely affect pore occupation by regulating the affinity of the selectivity filter for permeant ions. Most notably, activation of  $\text{Ca}_v1.2$  channels is associated with a 10-fold increase in the on-rates of  $\text{Gd}^{3+}$  block, whereas CDI can conversely prevent  $\text{Gd}^{3+}$  block (Babich et al., 2007a, 2007b). Exclusive block of open channels can be ruled out as the underlying mechanism, since sub-threshold depolarization produces a similar rise in the efficiency of block (Babich et al., 2007b). From these observations, it has been deduced that depolarization may be associated with pre-opening conformational changes in the pore region, which transiently lower the affinity for  $\text{Ca}^{2+}$ , thereby increasing the rates of  $\text{Ca}^{2+}$  exit from the pore. This could facilitate permeation of  $\text{Ca}^{2+}$  upon activation and, due to reduced competition, enhance  $\text{Gd}^{3+}$  block during depolarization. Increased affinity of the selectivity filter for  $\text{Ca}^{2+}$  (so that it blocks the channel) might conversely serve as a



mechanism of CDI, promoting termination of flux and preventing  $Gd^{3+}$ -binding (Babich et al., 2007a). Consistent with such a model,  $Ca^{2+}$ -dependent inactivation of  $Ca_v1.2$  channels has no effect on permeation of monovalent cations (Babich et al., 2005), and substitution of the EEEE-locus glutamate in repeat III by glutamine abolishes  $Ca^{2+}$ -dependent inactivation in these channels (Zong et al., 1994). This may also provide an alternative explanation for the effects of trivalent cations on macroscopic inactivation in HVA channels as well as for their absence in LVA channels, which exhibit no CDI (Biagi and Enyeart, 1990; Mlinar and Enyeart, 1993; Beedle et al., 2002; Obejero-Paz et al., 2004; Babich et al., 2007b). Taken together, the findings described in this section are reminiscent of the situation in voltage-gated sodium and potassium channels, where certain forms of channel gating are thought to involve conformational changes in the selectivity filter (Lopez-Barneo et al., 1993; Liu et al., 1996; Benitah et al., 1999; Ong et al., 2000; Hilber et al., 2001; Xiong et al., 2003; Cordero-Morales et al., 2006a, 2006b). In sodium channels, gating transitions in the pore region appear to be coupled to the domain IV voltage sensor, since ‘trapping’ of the pore in a certain state (by TTX-binding or cross-bridging of residues at the pore mouth) selectively interferes with its return to the resting state and reduces OFF-gating currents by about 25% (Capes et al., 2012). In other words, functional coupling of the pore region to one or more of the gating modules could establish a reciprocal pathway, so that gating may fine-tune permeation and vice versa. This has two important implications: On the one hand, structural alterations in the pore region during channel gating could produce dynamic changes in the affinity of intra-pore sites and result in a complex state-dependence of block (i.e. channel gating may affect pore block). On the other hand, binding of blocking ions to intra-pore sites could interfere with or promote local conformational changes, and thus influence movement of the voltage-sensors (i.e. pore block may affect channel gating). It seems reasonable to assume that subtle differences in the spatial arrangement of the pore region could be associated with differential and even opposite effects of occupation by a given blocker on channel gating. Likewise, variations in the size of different blocking ions or the distance they travel within the pore before they are stabilized could translate into distinct effects on local conformational changes and thus channel gating. Since  $Gd^{3+}$ -block of  $Ca_v1.2$  channels has no measurable effects on gating currents, it remains to be elucidated whether there is a similar link to voltage-dependent movements of the S4 segments or if structural rearrangements in the permeation pathway of VGCCs are instead controlled by independent voltage-sensors, such as charged residues in the pore region (Babich et al., 2007b).

**4.2.6.4. Role of fast voltage-dependent inactivation.** Polyvalent cations have traditionally been regarded as open channel blockers (Nelson, 1986; Lansman, 1990; Winegar et al., 1991), but different investigations in HVA and LVA channels suggest that they can block both open and closed channel states (Swandulla and Armstrong, 1989; Chow, 1991; Thevenod and Jones, 1992; Obejero-Paz et al., 2004; Babich et al., 2007b). Thus, the primary activation gate seems to be located on the intracellular side of the permeation pathway and does apparently not interfere with entry of extracellular blockers into the pore (Obejero-Paz et al., 2004; Babich et al., 2007b). Moreover, electrophysiological evidence suggests that both channel families can usually close while occupied by blocking ions and that blocked channels can still activate and rapidly unblock upon opening at high-hyperpolarized potentials (i.e. blocking ions have to wait for channel opening to leave towards the intracellular side) (Chow, 1991; Obejero-Paz et al., 2004; Diaz et al., 2005; Babich et al., 2007b; Traboulsie et al., 2007). A notable exception are  $Ca_v3.3$  channels, in which  $Cd^{2+}$ - and

$Zn^{2+}$ -block produce a marked slowing of macroscopic tail-current decay, suggesting that they cannot close while the pore is occupied by these ions (Diaz et al., 2005; Traboulsie et al., 2007). However, the effect seems to be ion-specific, since other transition metal ions such as  $Ni^{2+}$  and  $Co^{2+}$  accelerate tail-current decay like they do in other  $Ca_v3$  channels (Diaz et al., 2005). Hence, the peculiar slowing of  $Ca_v3.3$  channel tail-current decay by  $Cd^{2+}$  and  $Zn^{2+}$  could in principle also arise from differences in their effects on putative conformational changes in the pore region as described in the previous section.

Given the strong electrostatic forces in the pore, the above findings imply that under physiological conditions, closed channels might permanently contain a permeant  $Ca^{2+}$ -ion.

This could in turn not only provide an alternative explanation for the dependence of single-channel open and closed times on the nature of permeant ions, but also for certain state-dependent changes in the apparent affinity, since blocking ions would have to wait for slow exit of bound ions to the outside before they can block a closed channel. The latter hypothesis has been derived from findings on  $Y^{3+}$ -block of  $Ca_v3.1$  channels, which affects both open and closed channel states, yet is 8-fold slower for closed compared to open channels (Obejero-Paz et al., 2004). Replacement of  $Ca^{2+}$  with  $Ba^{2+}$  as the charge carrier selectively accelerates closed but not open channel block, suggesting that the reduced on-rate for  $Y^{3+}$  block of closed states arises from ion–ion interactions in the pore. Similar findings have been reported for HVA channels, where on- and off-rates for  $Cd^{2+}$ -block of closed vs. open states can differ by more than 100-fold (Thevenod and Jones, 1992). The higher apparent blocker affinity for open channels, together with a voltage-dependent increase in the degree of block and slow on-rates, could explain the trivalent-cation induced acceleration of macroscopic inactivation in HVA channels as a time-dependent increase in the fraction of blocked channels, which may be less evident in rapidly inactivating LVA channels. However, manipulations which interfere with fast VDI are interestingly associated with opposite effects on peak current inhibition and speeding of macroscopic inactivation by trivalent cations. Thus, coexpression of ‘inactivation decelerating’  $\beta_{2a}$ -subunits as well as structural modification of the I–II-linker increase apparent blocking affinity but virtually abolish  $Y^{3+}$ -induced acceleration of  $Ca_v2.1$  channel inactivation, suggesting that trivalent cations promote entry into the inactivated state (Beedle et al., 2002). The exact mechanism of action remains to be elucidated, but it is well known that point-mutations in the pore-lining S6 segments of L-type channels can also produce marked alterations in fast VDI, presumably by influencing the conformational changes required for docking of the I–II-linker to their cytoplasmic ends (Kraus et al., 2000; Berjukow et al., 2001; Stotz and Zamponi, 2001). Hence, occupation of the pore by trivalent cations may promote inactivation by exerting similar effects, or there may be an external regulatory site, which is allosterically coupled to the inactivation machinery. The latter seems more likely, considering that  $Y^{3+}$  block takes place at a site external to the primary activation gate, while the molecular components responsible for fast inactivation are located in the intracellular compartment and presumably not directly accessible for blocking  $Y^{3+}$  ions. This is also supported by differences in the concentration–response relationship and in the effect of permeant ions on blocking vs. kinetic effects of  $Y^{3+}$  (Beedle et al., 2002).

Once again, the situation appears to be similar in certain voltage-gated sodium channels, where polyvalent cations bind to a site in the pore, at which they produce both block and a dramatic slowing of fast inactivation (Kuo et al., 2004). The site seems to be located in the outer portion of the pore but within the single-file region, since both block and gating effects are relatively insensitive to changes in the membrane potential but strongly affected by the direction of current flow (Kuo et al., 2004). It is thought to be

accessible in both open and closed channel states, but subject to imperative conformational rearrangements during inactivation gating. Binding of metal ions interferes with these conformational changes and stabilizes non-inactivated channel states to a degree well correlated with the extent of pore block (Kuo et al., 2004).

Since LVA channels exhibit fast VDI as well, one could ask why the kinetic effects of trivalent cations seem to be absent in  $\text{Ca}_v3$  channels. The most obvious explanation is differences in the mechanism of fast VDI, which could be insensitive to binding of polyvalent cations in LVA channels. However, macroscopic inactivation of vertebrate  $\text{Ca}_v3.1$  channels is accelerated by 30–35% in  $\text{Ba}^{2+}$  vs.  $\text{Na}^+$  and  $\text{Ca}^{2+}$ , an effect which is correlated with the degree of  $\text{Ba}^{2+}$ -block of monovalent current, indicating that it is a direct consequence of pore occupancy (Klugbauer et al., 1999b; Serrano et al., 2000; Khan et al., 2008). Another possible explanation for the lack of trivalent cation-induced changes in macroscopic inactivation may be that their equilibration with a putative regulatory site is simply too slow for detectable kinetic effects on rapidly-inactivating channels.

#### 4.2.7. Structural determinants of pore block

Structural determinants of pore block are best characterized in the case of  $\text{Cd}^{2+}$ , which has been used together with mutational approaches to uncover the mechanisms underlying selective permeation. Consistent with the interpretation of functional data,  $\text{Cd}^{2+}$  appears to target glutamate residues of the high-affinity binding locus, since aspartate-to-glutamate substitutions in the EEDD-locus of LVA channels increase  $\text{Cd}^{2+}$  sensitivity (Talavera et al., 2001), while mutations of glutamate residues in the EEEE-locus of HVA channels diminish  $\text{Cd}^{2+}$  block (Ellinor et al., 1995). However, the determinants must be more complex, as  $\text{Cd}^{2+}$  block in  $\text{Ca}_v\text{Ab}$  (DDDD-locus:  $\text{IC}_{50} = 1.7 \mu\text{M}$ ) is almost as potent as in HVA channels (EEEE-locus) (Tang et al., 2014). X-ray crystallographic data of  $\text{Ca}_v\text{Ab}$  obtained in the presence of high  $\text{Cd}^{2+}$  (100 mM) shows binding of hydrated  $\text{Cd}^{2+}$  ions to the composite high-affinity site formed by DDDD-locus (site 2a) and its N-terminal neighbours (site 2b) (Fig. 8F and H) (Tang et al., 2014). In vertebrate HVA channels, residues corresponding to site 2b in repeat III directly influence  $\text{Cd}^{2+}$  sensitivity and determine the effect of mutations in neighbouring EEEE-locus glutamates (i.e. residues corresponding to site 2a) (Williamson and Sather, 1999), suggesting a similar mechanism of action.  $\text{Cd}^{2+}$  block in  $\text{Ca}_v\text{Ab}$  is moreover influenced by the DCS-locus, since replacement of the corresponding aspartate residues with asparagine produces a moderate reduction of  $\text{Cd}^{2+}$  sensitivity (p.Asp<sub>181</sub>Asn:  $\text{IC}_{50} = 5.9 \mu\text{M}$ ) (Tang et al., 2014). Considering the 4–5-fold lower  $\text{Ca}^{2+}$ -selectivity of p.Asp<sub>181</sub>Asn mutants, these findings support the notion that  $\text{Cd}^{2+}$  block takes place at the main  $\text{Ca}^{2+}$ -coordination site and that it is governed by the same factors that determine  $\text{Ca}^{2+}$  binding.

Crystals of  $\text{Ca}_v\text{Ab}$  obtained in the presence of  $\text{Mn}^{2+}$  show binding to the same principal blocking site ( $\text{IC}_{50} = 526 \mu\text{M}$ ) (Fig. 8G), but interestingly, the degree of  $\text{Mn}^{2+}$ -block is enhanced rather than decreased by replacement of residues corresponding to the DCS-locus with asparagine (p.Asp<sub>181</sub>Asn:  $\text{IC}_{50} = 388 \mu\text{M}$ ) (Tang et al., 2014). This is consistent with a distinct mechanism of block and may reflect the preference of most transition metal ions for nitrogen over oxygen donor groups. It is peculiar that position 180 in repeat II and IV of all vertebrate VGCCs (except for  $\text{Ca}_v1.1$ ) is made up of nitrogen-containing amino acids and that most channels contain additional nitrogen-bearing residues in outer parts of the selectivity filter, such as the DCS-locus (Fig. 3D) which has been proposed to serve as an external low-affinity binding site in these channels. Considering the high blocker concentrations used in the experiments with  $\text{Ca}_v\text{Ab}$  and the high permeability of  $\text{Mn}^{2+}$  relative to most other polyvalent cations, it will be interesting to see whether similar results are obtained with lower

$\text{Mn}^{2+}$  concentrations and with other transition metal ions. Likewise, electrophysiological techniques coupled with mutational approaches promise further insight into the role of DCS-locus and other residues in the vicinity of the EEEE/EEDD-locus for block by metal ions. To date, this aspect has received little attention, although the DCS-locus has been implicated in differential  $\text{Mg}^{2+}$  block of  $\text{Ca}_v2.1/\text{Ca}_v2.3$  and  $\text{Ca}_v3.1/\text{Ca}_v3.2$  channels (Cens et al., 2007). An involvement of the region in permeation and block of vertebrate channels may contribute to the lower sensitivity of LVA channels towards  $\text{Cd}^{2+}$ , since these channels typically possess less oxygen donor groups in their DCS-locus. Given its location and apparently strong influence on the electrostatic potential at the pore mouth of vertebrate VGCCs (e.g. Fig. 4A), the DCS-locus could play a role for the stabilization of ions in the vicinity of the channels. Depending on an ions donor atom preference, further entry into the pore may be more or less energetically favourable. As the putative outer binding site in vertebrate channels is made up of a single glutamate residue in domain II, it may also be important where exactly an ion is stabilized relative to this residue.

However, it has been shown that regions outside of the ion-conducting pore itself can affect metal-induced block of vertebrate HVA channels as well. In particular,  $\text{Zn}^{2+}$ -induced suppression of  $\text{Ca}_v2.2$  but not  $\text{Ca}_v3.1$  channels is approximately 10 times stronger with  $\text{Ba}^{2+}$  instead of  $\text{Ca}^{2+}$  as a charge carrier (Table 3), an effect partly reversed by disruption of the putative EF-hand-like binding site in domain III of HVA channels (Sun et al., 2007). This has been interpreted in terms of differential effects of  $\text{Ca}^{2+}/\text{Ba}^{2+}$  binding to the site on  $\text{Zn}^{2+}$ -block, consistent with the proposed role of the motif for  $\text{Ca}^{2+}/\text{Ba}^{2+}$  selection. While key residues of the site are conserved among all HVA channels (Sun et al., 2007), their relative positions (i.e. the number and nature of additional residues) differ between individual subunits, which could explain subtle differences in the characteristics of block of different HVA channels. Its absence in LVA channels may conversely account for some of the functional variation between block of HVA and LVA channels.

Considering the conservation of residues forming the internal low-affinity site in  $\text{Ca}_v\text{Ab}$  among the family of vertebrate VGCCs, they represent the most likely candidates for an internal binding site in vertebrate channels as well. In LVA channels, threonine residues in repeat III are substituted by serine residues, but it seems likely that the principal site is still intact, especially since outward currents through LVA channels are also weakly blocked by internal  $\text{Mg}^{2+}$  (Serrano et al., 2000).

#### 4.2.8. Permeation: calcium channels as pathway for trace metal entry

As mentioned in the preceding sections, most inorganic cations can, in principle, traverse VGCCs and end up in the intracellular compartment, as reflected in their biphasic voltage-dependence of block. This has been confirmed by Shibuya and Douglas (1992, 1993) in rat melanotrophs injected with the  $\text{Ca}^{2+}$ -sensitive fluorescent probe fura-2 and exposed to extracellular  $\text{Mn}^{2+}$ ,  $\text{Co}^{2+}$ ,  $\text{Ni}^{2+}$ ,  $\text{Cd}^{2+}$  or  $\text{La}^{3+}$ . In cell-free solution, all of these divalent cations bind to fura-2 with higher apparent affinity than  $\text{Ca}^{2+}$  and either quench fluorescence ( $\text{Mn}^{2+}$ ,  $\text{Co}^{2+}$  and  $\text{Ni}^{2+}$ ) or produce changes in the ratio of fluorescence measured with different excitation wavelengths ( $\text{Cd}^{2+}$  and  $\text{La}^{3+}$ ), so that cellular entry should be detectable as a change in fluorescence (Shibuya and Douglas, 1992). In fura-2 loaded cells and under resting conditions, addition of  $\text{Mn}^{2+}$ ,  $\text{Co}^{2+}$  or  $\text{Cd}^{2+}$  (0.3–5 mM) produced concentration-dependent, TTX-insensitive changes in fluorescence, which were slowed by lowering external  $\text{K}^+$  (i.e. by hyperpolarization) and accelerated by raising external  $\text{K}^+$  (i.e. by depolarization) or by lowering external  $\text{Ca}^{2+}$  (Shibuya and Douglas, 1992).  $\text{Ni}^{2+}$  and  $\text{La}^{3+}$  had no effects on fluorescence under resting conditions but lowered basal intracellular  $\text{Ca}^{2+}$  levels and competitively suppressed the effects of other divalent cations, with  $\text{La}^{3+}$  being



50–100-fold more potent than  $\text{Ni}^{2+}$ . In high external  $\text{K}^+$  solution,  $\text{La}^{3+}$  produced fluorescence changes as well, indicating that it can in principle also enter the cells, while  $\text{Ni}^{2+}$  only quenched fluorescence after addition of the cationophore ionomycin. Interestingly, the same  $\text{Ni}^{2+}$  concentration abolished both  $\text{Mn}^{2+}$ -induced fluorescence quenching under resting conditions and in high external  $\text{K}^+$ , while  $\text{Cd}^{2+}$ -concentrations sufficient to suppress the response in high external  $\text{K}^+$  failed to affect the response under resting conditions (Shibuya and Douglas, 1993). Taken together, these findings suggest that most divalent transition metal ions can gain access into these cells through a TTX- and relatively  $\text{Cd}^{2+}$ -insensitive pathway at or near the resting membrane potential as well as through a TTX-insensitive but  $\text{Cd}^{2+}$ -sensitive pathway during depolarization. Considering that rat melanotrophs display L-, N- and T-type like voltage-gated  $\text{Ca}^{2+}$  channels (Cota, 1986; Taleb et al., 1986; Williams et al., 1990), it seems likely that the two pathways for entry reflect LVA and HVA VGCCs channels respectively. More specifically and consistent with their functional properties, LVA channels, which activate at negative potentials, are relatively  $\text{Cd}^{2+}$ -insensitive and exhibit prominent window-currents, might mediate metal uptake under resting conditions, while HVA channels, which activate at more positive membrane potentials and are very  $\text{Cd}^{2+}$ -sensitive, may mainly mediate metal ion entry during depolarization.

Despite great interest into VGCCs as pathways for cellular metal uptake however, few studies have directly assessed and quantified entry of metal ions through specific  $\text{Ca}_v\alpha_1$ -subunits in recombinant expression. Lopin et al. (2012b) carried out a throughout characterization of  $\text{Cd}^{2+}$  permeation through  $\text{Ca}_v3.1$  channels stably transfected in HEK293 cells. They found that  $\text{Cd}^{2+}$  added in the presence of  $\text{Ca}^{2+}$  affects the reversal potential, that block saturates at 80–85% and that 50–60% of the remaining current is apparently carried by  $\text{Cd}^{2+}$ . In the absence of  $\text{Ca}^{2+}$ , 2 mM  $\text{Cd}^{2+}$  carried small IV- and much larger IIV-currents, which corresponded to 5–17% of the currents carried by  $\text{Ca}^{2+}$ . Incubation with  $^{109}\text{Cd}^{2+}$  for 30 min demonstrated a concentration-dependent increase in intracellular  $\text{Cd}^{2+}$  in transfected but not untransfected cells, which was blocked by the preferential T-type inhibitor NNC 55-0396 (Lopin et al., 2012b). Using a two-site model for permeation and block,  $\text{Cd}^{2+}$  entry rates through a single open channel at physiologically relevant concentrations (1–10 nM) were estimated to be close to  $1 \text{ s}^{-1}$  at  $-20 \text{ mV}$  and to increase with increasingly negative membrane potentials (due to increasing driving force). Taking into account the voltage-dependence of channel open probability and electrochemical driving force, steady-state  $\text{Cd}^{2+}$  entry through single  $\text{Ca}_v3.1$  channels is maximal at potentials of around  $-60 \text{ mV}$  ( $\sim 0.05 \text{ s}^{-1}$  with 10 nM), sharply reduced at more negative potentials ( $\sim 0.005 \text{ s}^{-1}$  with 10 nM at  $-80 \text{ mV}$ ), where channel open probability decreases and less sharply reduced at more positive potentials ( $\sim 0.04 \text{ s}^{-1}$  with 10 nM at  $-40 \text{ mV}$ ), where the driving force decreases (Lopin et al., 2012b). Similar findings have been reported for  $\text{Fe}^{2+}$ -permeation through  $\text{Ca}_v3.1$  channels, where the entry rates through open channels have been estimated to be in the order of  $20 \text{ s}^{-1}$  at  $-60 \text{ mV}$  and  $1 \mu\text{M}$   $\text{Fe}^{2+}$  (Lopin et al., 2012a). Thus, while rates of metal ion entry through VGCCs may in many cases be negligible, they can in some instances clearly reach levels sufficient to acquire experimental (i.e. use of  $\text{Mn}^{2+}$ -entry as a probe for VGCC activity, see Section 4.2.8.1), physiological (i.e.  $\text{Zn}^{2+}$  entry into post-synaptic neurons, see Section 4.2.8.2) and/or pathophysiological (i.e. cellular entry and accumulation of  $\text{Cd}^{2+}$  and other toxic metals, see above and Section 4.2.8.2) relevance.

**4.2.8.1.  $\text{Mn}^{2+}$  as a probe for  $\text{Ca}^{2+}$ -dependent neuronal activity.**  $\text{Mn}^{2+}$  is an essential trace metal ion required for a number of enzymes, but chronic exposure to supra-physiological levels is associated

with a clinical picture (manganism) sharing several features with certain extrapyramidal motor disorders, most notably Parkinson's disease (Olanow, 2004; Santamaria, 2008). The role of VGCCs for the underlying accumulation of  $\text{Mn}^{2+}$  in discrete brain regions has not been studied, but the cellular entry of  $\text{Mn}^{2+}$  via VGCCs is widely utilized by its use as a MRI contrast agent for anatomical and functional neuroimaging. More specifically, activation-induced  $\text{Mn}^{2+}$ -enhanced MRI is based on the specific patterns of  $\text{Mn}^{2+}$  accumulation observed during neuronal activation, which are thought to arise from the opening of VGCCs associated with transmitter release and can be visualized *in vivo* as a positive contrast enhancement in  $T_1$ -weighted MRI measurements (Lin and Koretsky, 1997; Aoki et al., 2002, 2004a; Hsu et al., 2007; Yu et al., 2008). After entry into neurons,  $\text{Mn}^{2+}$  is transported by microtubule-based axonal transport to the synaptic terminals, where it is released and taken up by postsynaptic neurons. This in turn makes possible the use of  $\text{Mn}^{2+}$ -enhanced MRI for longitudinal *in vivo* trans-synaptic tract tracing (Pautler et al., 2003; Aoki et al., 2004b).

**4.2.8.2. Role of calcium channels for trace metal toxicity.** Unlike conventional neurotransmitters, synaptically released  $\text{Zn}^{2+}$  can enter postsynaptic neurons, where it may function as an intracellular second messenger (Li et al., 2001). While little is known about the physiological relevance of cellular  $\text{Zn}^{2+}$ -uptake, neurotoxicity due to excessive  $\text{Zn}^{2+}$  entry into neurons is becoming increasingly recognized (Frederickson et al., 1989; Koh et al., 1996; Enger and Kang, 1999; Kim et al., 1999; Suh et al., 2000; Lee et al., 2002). Under normal conditions, neurons contain sub-nanomolar concentrations of free cytosolic  $\text{Zn}^{2+}$  (Frederickson, 1989; Sensi et al., 1997), and a marked rise can lead to displacement of other metal ions from important intracellular binding-sites, oxidative injury, mitochondrial dysfunction and ultimately cell death (Enger and Kang, 1999). Seizures, cerebral ischaemia and traumatic brain injury all lead to a translocation of free  $\text{Zn}^{2+}$  from pre- into post-synaptic neurons, and cell death under these conditions is preceded by accumulation of  $\text{Zn}^{2+}$  in degenerating neurons (Frederickson et al., 1989; Koh et al., 1996; Suh et al., 2000; Lee et al., 2002).  $\text{Zn}^{2+}$  uptake and toxicity appear to be closely correlated with the membrane potential, such that in the presence of a membrane-depolarizing stimulus (high  $\text{K}^+$ -solution, glutamate, kainate or AMPA), cultured cortical cells are much more susceptible to  $\text{Zn}^{2+}$  toxicity, with 5 min of exposure to concentrations as low as  $100 \mu\text{M}$  producing an immediate rise in intracellular  $\text{Zn}^{2+}$  level sufficient to kill most cells (Weiss et al., 1993; Sensi et al., 1997). Both  $\text{Zn}^{2+}$  entry into neurons and neuronal injury can be reduced by raising extracellular  $\text{Ca}^{2+}$  levels (Weiss et al., 1993; Koh and Choi, 1994) or by addition of N-type  $\text{Ca}^{2+}$ -channel antagonists ( $\omega$ -conotoxin GVIA) (Sensi et al., 1997; Kerchner et al., 2000) and almost completely blocked by L-type  $\text{Ca}^{2+}$ -channel antagonists (DHPs) or non-selective inorganic  $\text{Ca}^{2+}$ -channel blockers ( $\text{Gd}^{3+}$ ) (Atar et al., 1995; Sensi et al., 1997). HVA VGCCs may therefore represent a major pathway for depolarization-dependent cellular entry of  $\text{Zn}^{2+}$ ,  $\text{Cu}^{2+}$  and foreign metal ions, although other divalent cation-permeable channels (NMDA-receptors, kainate-receptors) have been shown to be involved as well (Jia et al., 2002). More direct evidence for the involvement of VGCCs comes from whole cell voltage-clamp recordings in cultured cortical neurons, which demonstrate that L- and N-type channels can mediate substantial  $\text{Zn}^{2+}$ -currents both in the absence and presence of  $\text{Ca}^{2+}$  (Kerchner et al., 2000). Interestingly, decreased extracellular pH reduces  $\text{Ca}^{2+}$ -currents (presumably due to screening of surface charges by  $\text{H}^+$ ) but enhances  $\text{Zn}^{2+}$  currents (possibly due to reduced electrostatic  $\text{Zn}^{2+}$ -effects) (Kerchner et al., 2000), which may play an important role in certain pathophysiological conditions, such as epileptic seizures and hypoxic ischaemia, which are often associated with brain acidosis (Siesjo, 1982;

Siesjo et al., 1985; von Hanwehr et al., 1986). Postsynaptic VGCCs are primarily located outside of the synapse and postsynaptic entry of  $Zn^{2+}$  under physiological conditions has been shown to be mainly mediated by AMPA/kainate receptors (Li et al., 2001). Excessive release of  $Zn^{2+}$  under pathophysiological conditions on the other hand, is likely associated with massive extrasynaptic spillover, which is to some extent already observed during physiological activation (Ueno et al., 2002). Coupled with supra-physiological neuronal activation, this could promote  $Zn^{2+}$  permeation through VGCCs as (i) a large concentration gradient for  $Zn^{2+}$  is established, (ii) the fraction of open channels is greatly increased, (iii) extracellular pH may be lowered (i.e. acidosis) and (iv) extracellular  $Ca^{2+}$  levels are often markedly reduced (Nilsson et al., 1993; Kristian and Siesjo, 1998; Amzica et al., 2002). The majority of depolarization-dependent  $Zn^{2+}$  entry through VGCCs seems to be mediated by HVA channels (Kerchner et al., 2000), which is consistent with their higher conductance and slower inactivation kinetics relative to LVA channels. L-type channels, which produce pronounced, long lasting currents, likewise appear to be the most important HVA channels for  $Zn^{2+}$  entry (Sensi et al., 1997; Kerchner et al., 2000). This may also be related to the fact that L-type channels mainly inactivate via CDI as opposed to VDI. Hence, currents through these channels mediated by  $Zn^{2+}$  do not significantly inactivate and currents mediated by  $Ca^{2+}$  and  $Zn^{2+}$  exhibit reduced inactivation upon prolonged depolarization (Kerchner et al., 2000). LVA channels on the other hand are characterized by their hyperpolarized and overlapping voltage-range for activation and inactivation, leading to well defined inward currents at resting membrane potentials (Serrano et al., 1999; Lopin et al., 2012b). Since the driving force for divalent cation entry at these potentials is high, T-type channels could allow for a significant influx of divalent cations near resting membrane potentials and may contribute to the persistent  $Zn^{2+}$  accumulation observed following the acute phase of seizures or cerebral ischaemia (Weiss et al., 2000), the cumulative effects of repeated exposure to toxic metals such as cadmium, and the intracellular accumulation of metal ions during ageing or in certain neurodegenerative diseases (Lopin et al., 2012a, 2012b).

#### 4.3. Allosteric modulation (Fig. 5D)

Some divalent transition metal ions cannot only affect VGCCs by electrostatic effects or block of the channel pore, but also non-electrostatically (allosterically) interfere with extracellular parts of the gating machinery of certain  $Ca_v\alpha_1$ -subunits (Fig. 5D). As already illustrated in the preceding sections, extracellular binding sites for divalent cations appear to be a common structural feature of VGCCs (Nosal et al., 2013), but their possible interaction with foreign ions has only been characterized in some cases. In particular, allosteric metal binding sites, which are not conserved among the family of VGCCs, have been identified in the domain I gating modules of  $Ca_v2.3$  and  $Ca_v3.2$  channels (Kang et al., 2006, 2010; Nelson et al., 2007a, 2007b; Shcheglovitov et al., 2012). When occupied by certain divalent metal ions ( $Cu^{2+}$ ,  $Zn^{2+}$ ,  $Ni^{2+}$ ), these sites mediate a tonic suppression of channel gating, presumably by stabilizing closed channel conformations. There are however, several differences in the qualitative and quantitative nature of effects and the proposed binding sites are structurally distinct.

##### 4.3.1. $Ca_v3.2$ channels

As mentioned before,  $Ni^{2+}$  was long regarded as selective blocker of LVA channels but it has since been shown that  $Ca_v3.2$  is the only member of this group selectively suppressed by low micromolar  $Ni^{2+}$  concentrations (Lee et al., 1999b; Jeong et al., 2003; Traboulsie et al., 2007) and that  $Ca_v2.3$ -type HVA channels

are almost as potently inhibited as  $Ca_v3.2$  channels. The pattern of inhibition of  $Ca_v3.2$  by endogenous transition metal ions ( $Zn^{2+}$ ,  $Cu^{2+}$ ) and  $Ni^{2+}$  differs from that observed in other LVA channels in that it is unaffected by the membrane potential or the nature of permeant ions (Mlinar and Enyeart, 1993; Lee et al., 1999b; Traboulsie et al., 2007; Kang et al., 2010; Shcheglovitov et al., 2012), indicating an action at target sites outside of the membrane electric field. In addition,  $Ca_v3.2$  channels are much more sensitive towards these ions, so that  $Zn^{2+}$ - or  $Ni^{2+}$ -induced suppression can be orders of magnitude stronger than in other  $Ca_v3$  channels (Williams et al., 1999; Lee et al., 1999b; Jeong et al., 2003; Traboulsie et al., 2007).

Molecular cloning studies have identified a histidine residue ( $His^{191}$ ) in the extracellular loop between segments 3 and 4 of domain I (IS3–IS4) as the most critical determinant for high  $Ni^{2+}$ -sensitivity of  $Ca_v3.2$  channels. Thus, substitution of  $His^{191}$  by glutamine ( $Ca_v3.2His^{191}Gln$ ) or alanine ( $Ca_v3.2His^{191}Ala$ ) reduces  $Zn^{2+}$ - and  $Ni^{2+}$ -sensitivity of these channels to the level observed for  $Ca_v3.1$  channels (Kang et al., 2006, 2010) (Fig. 9A and B). Reverse mutation of the corresponding glutamine residue in  $Ca_v3.1$  channels to histidine ( $Ca_v3.1Gln^{172}His$ ) conversely increases  $Zn^{2+}$ - and  $Ni^{2+}$ -sensitivity by a factor of 2 and 5 respectively, but is not sufficient to confer the same trace metal sensitivity as observed in  $Ca_v3.2$  channels (Kang et al., 2006, 2010) (Fig. 9B). This suggested that additional residues are required for coordinated interaction with divalent cations, most of which have been identified by sequence comparison, systematic mutation of individual amino acid residues and construction of chimeric channels. Using these approaches, it was shown that high-affinity modulation of  $Ca_v3.2$  by  $Zn^{2+}$  and  $Ni^{2+}$  critically depends on a sequence of aspartate ( $Asp^{189}$ ), glycine ( $Gly^{190}$ ) and histidine ( $His^{191}$ ) (Asp-Gly-His motif) in the IS3–IS4 loop (Kang et al., 2006, 2010; Nelson et al., 2007a, 2007b) (Fig. 9B). Introduction of both  $His^{191}$  and  $Gly^{190}$  into the corresponding regions in  $Ca_v3.1$  channels ( $Ca_v3.1Gln^{172}His + Leu^{171}Gly$ ) brings  $Zn^{2+}$ -sensitivity close to that of  $Ca_v3.2$  channels (Fig. 9B). Substitution of the preceding  $Asp^{189}$  in  $Ca_v3.2$  by a neutral alanine residue ( $Ca_v3.2Asp^{189}Ala$ ) reduces  $Zn^{2+}$ -sensitivity by a factor of 10, while substitution by glutamate ( $Ca_v3.2Asp^{189}Glu$ ) increases it by about 3-fold (Kang et al., 2010), suggesting that the carboxylate-group of  $Asp^{189}$  is directly involved in metal binding. In view of these findings, the importance of  $Gly^{190}$  for metal binding has been related to its provision of a deprotonated amide nitrogen atom and to its high flexibility relative to other amino acids, which may be required for optimal interaction of the flanking residues  $His^{191}$  and  $Asp^{189}$  with metal ions. A single negatively charged residue in the outer portion of IS2 appears to contribute to metal binding in  $Ca_v3.2$  channels as well, since substitution of  $Asp^{140}$  by neutral alanine ( $Ca_v3.2Asp^{140}Ala$ ) results in a moderate but significant reduction of  $Zn^{2+}$ -sensitivity, while substitution by acidic glutamate ( $Ca_v3.2Asp^{140}Glu$ ) has no such effect. Interestingly, placement of an additional aspartate residue downstream of  $Asp^{140}$  ( $Ca_v3.2Ala^{141}Asp$ ) to mimic the situation in  $Ca_v3.1$  and  $Ca_v3.3$  channels significantly reduces  $Zn^{2+}$ -sensitivity by a factor of 4, while substitution of the corresponding aspartate residue in  $Ca_v3.1Gln^{172}His + Leu^{171}Gly$  mutants by neutral alanine ( $Ca_v3.1Gln^{172}His + Leu^{171}Gly + Asp^{122}Ala$ ) conversely increases their  $Zn^{2+}$ -sensitivity by a factor of 4. The exact mechanism by which metal ions interact with the putative binding site formed by these residues is still not fully understood, but based on preferential inhibition of closed channel states by  $Zn^{2+}$ , it has been proposed to involve immobilization of the domain I voltage-sensor in a closed position (Fig. 9A) (Kang et al., 2010). Consistent with this hypothesis, saturating concentrations of  $Zn^{2+}$  (10  $\mu M$ ) reduce  $Ca_v3.2$  gating currents by about 25% (Kang et al., 2010).



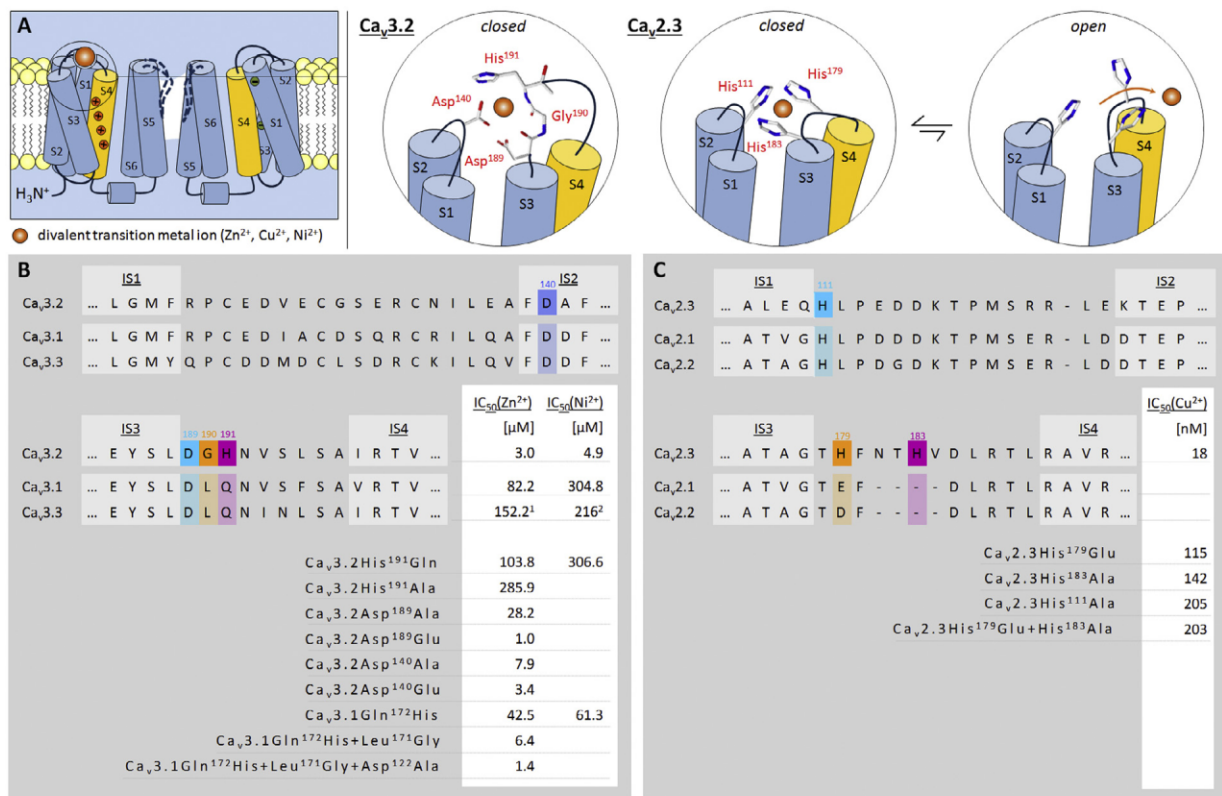


**Fig. 9.** Allosteric modulation of VGCCs by divalent transition metal ions ( $Cu^{2+}$ ,  $Zn^{2+}$  and  $Ni^{2+}$ ). (A) Cartoon illustrating possible mechanisms of allosteric modulation of Cav3.2 and Cav2.3 channels by trace metal binding to the domain I voltage-sensor. Regions involved in the interaction with metal ions are shown as individual amino acid residues, with carbon, nitrogen and oxygen atoms highlighted in white, blue and red respectively. In Cav3.2 channels, the metal binding site consists of a single aspartate residue on the IS1-IS2 loop (Asp<sup>140</sup>) and an Asp-Gly-His motif on the IS3-IS4 loop. In Cav2.3 channels, three histidine residues on the extracellular loops between IS1-IS2 (His<sup>111</sup>) and IS3-IS4 (His<sup>179</sup> and His<sup>183</sup>) form the high-affinity allosteric trace metal binding site only when channels reside in a closed conformation, whereas conformational changes during opening lead to disruption of the binding pocket and rapid unbinding of bound metal ions. [Structural models redrawn and combined from (Shcheglovitov et al., 2012) and (Kang et al., 2010).] (B) Sequence alignment of relevant regions in Cav3.2 and other Cav3 channels and comparison of  $Zn^{2+}$  and  $Ni^{2+}$  sensitivity among the three  $\alpha_1$ -subunits and different mutants created by single, double, or triple point mutations. Data are from Kang et al. (2006, 2010) except for <sup>1</sup>(Sun et al., 2007) and <sup>2</sup>(Lee et al., 1999b; Diaz et al., 2005). (C) Sequence alignment of relevant regions in Cav2.3 and other Cav2 channels and comparison of  $Cu^{2+}$  sensitivity among the three  $\alpha_1$ -subunits and different mutants created by single or double point mutations. Data are from Shcheglovitov et al. (2012).

Substitution of Asp<sup>140</sup> and other negatively charged amino acids in the outer portion of IS2 with neutral residues is also associated with decreased functional expression of Cav3 channels and positive shifts in the voltage-dependence of activation and inactivation (Kang et al., 2010), suggesting a role for the structural conformation of these channels. In voltage-gated  $K^+$ -channels, a residue corresponding to Asp<sup>140</sup> has been shown to be involved in channel folding and trafficking to the cell membrane as well (Planells-Cases et al., 1995; Tiwari-Woodruff et al., 1997; Kang et al., 2010), so that it remains to be elucidated if Asp<sup>140</sup> simply serves as an additional ligand for high-affinity metal binding or plays a more complex, regulatory role.

#### 4.3.2. Cav2.3 channels

Cav2.3 channels exhibit a similar susceptibility to allosteric suppression by endogenous transition metal ions as Cav3.2 channels and represent the most sensitive molecular target of  $Cu^{2+}$  currently known (Shcheglovitov et al., 2012). Low nanomolar concentrations suffice to tonically inhibit these channels and to markedly shift voltage-dependent gating towards more depolarized potentials. This exceptionally high sensitivity has been traced back to two histidine residues (His<sup>179</sup> and His<sup>183</sup>) in the IS3-IS4 loop and a third one (His<sup>111</sup>) located in the IS1-IS2 loop of the  $\alpha_1$ -subunit (Kang et al., 2007; Shcheglovitov et al., 2012). All three residues have been proposed to reside in close spatial proximity when the channels are in a closed conformation,

thus forming a high-affinity extracellular binding pocket for divalent cations (Fig. 9A). Channel opening is thought to translocate ligating residues away from each other, thereby disrupting the binding pocket, while bound transition metal ions can hold it intact and stabilize one or more closed channel states. Substitution of His<sup>111</sup> by alanine interestingly reduces  $Cu^{2+}$  sensitivity to the same extent as substitution of both His<sup>179</sup> by glutamate and His<sup>183</sup> by alanine residues (Fig. 9C), suggesting that both interventions may abolish high-affinity binding. Single point mutations of His<sup>179</sup> or His<sup>183</sup> produce a similar but less marked reduction of  $Cu^{2+}$  sensitivity. Consistent with a qualitative picture in which metal ions stabilize closed channel states,  $Zn^{2+}$ ,  $Cu^{2+}$  and  $Ni^{2+}$  all markedly decrease the rate of macroscopic activation (Zamponi et al., 1996; Shcheglovitov et al., 2012) and the degree of inhibition is more pronounced in closed channels. Strong depolarization can conversely reverse a significant fraction of inhibition, presumably due to rapid metal unbinding upon physical disruption of the binding pocket during channel opening (Shcheglovitov et al., 2012). All of these findings could, in principle, reflect voltage-dependent block, increased non-electrical work required to open the channel or alterations in the movement of gating charges (Hille, 2001). The latter mechanism seems most likely, given that  $Cu^{2+}$  and  $Zn^{2+}$  inhibition is associated with reduced sensitivity of Cav2.3 channels towards depolarization (as reflected in a decreased slope of the activation curve) and a slower decay of gating currents, while it does not appear to affect the total

gating charge transferred across the membrane (Shcheglovitov et al., 2012). Hence and in contrast to  $\text{Ca}_v3.2$  channels, bound metal ions seem to decelerate gating charge transition into the ON-position without completely immobilizing parts of the voltage-sensors. To obtain a rough estimate of the relative contribution of pore block and allosteric modulation to the overall effects of  $\text{Cu}^{2+}$  and  $\text{Zn}^{2+}$  on recombinant  $\text{Ca}_v2.3$  channels, Shcheglovitov et al. (2012) compared changes in the amplitude of whole-cell currents recorded in response to voltage-steps to  $-20$  mV and  $+20$  mV respectively. This approach can clearly not provide an absolute separation of permeation and gating and has to be interpreted with care. However, measurements carried out close to the voltage of half-maximal activation for these channels (i.e. at  $-20$  mV) should mostly detect effects on activation gating, while measurements at a potential sufficiently far on the plateau of the activation curve (i.e.  $+20$  mV) should be unaffected by shifts in activation gating and thus primarily detect effects on whole-cell conductance (i.e. pore-block). Shcheglovitov et al. (2012) found that both cations exert approximately 10-fold stronger effects on activation gating than on conductance, with  $\text{Cu}^{2+}$  being about 100 times more potent than  $\text{Zn}^{2+}$ . Zamponi et al. (1996) compared  $\text{Ni}^{2+}$ -induced shifts of the IV-curve with the effects on whole-cell conductance (estimated from the IV-curve as well). Consistent with the data by Shcheglovitov et al., they found that the concentration required to reduce macroscopic conductance by 50% is approximately ten times higher than the concentration required to produce half-maximal shifts of the IV-curve and concluded the blocking effect of  $\text{Ni}^{2+}$  on  $\text{Ca}_v2.3$  to be relatively weak compared to the combined blocking and gating effects. The approach they used is susceptible to overestimation of the gating component due to voltage-dependent block, yet given the negligible  $\text{Ni}^{2+}$  blocking action compared to its allosteric effects on  $\text{Ca}_v2.3$  channels, it seems unlikely that the resulting error is large. Nevertheless, the exact contribution of pore block and gating effects remains to be elucidated by means of suitable macroscopic recording protocols and ultimately, by microscopic analysis of permeation and gating. That said, the influence of permeant ions on allosteric modulation of  $\text{Ca}_v2.3$  by  $\text{Cu}^{2+}$  or  $\text{Zn}^{2+}$  has not been assessed, but given the unusually high affinity of the target site for  $\text{Cu}^{2+}$ , and the proposed role of  $\text{Cu}^{2+}$  as a neuronal signalling molecule, it may serve as a specific binding-site for endogenous metal ions not normally occupied by  $\text{Ca}^{2+}$ . Since  $\text{Ca}_v2.3$  channels are thought to play a role in synaptic transmission, integration and plasticity, they may be of major importance for the modulatory role of endogenous  $\text{Cu}^{2+}$  and  $\text{Zn}^{2+}$  in the brain as described below.

#### 4.3.3. Physiological relevance: role of calcium channels in the control of excitability

Endogenous  $\text{Zn}^{2+}$  and  $\text{Cu}^{2+}$  are increasingly recognized to be involved in central neurotransmission although their exact role remains ambiguous. Both can be released spontaneously or in an activation-dependent manner from certain populations of neurons located primarily in limbic regions (hippocampus, amygdala), in the cerebral cortex and in the retina (Charton et al., 1985; Hartter and Barnea, 1988; Kardos et al., 1989; Anastassov et al., 2013, 2014). They affect numerous voltage- and ligand-gated channels involved in excitatory and inhibitory signalling (for review see Mathie et al., 2006), suggesting an important role in the regulation of neuronal excitability. Consistent with such a role, alterations in  $\text{Cu}^{2+}$  or  $\text{Zn}^{2+}$  homeostasis have been linked to a number of pathophysiological conditions, including different forms of epilepsy, ischaemia and neurodegenerative disease (Frederickson et al., 2005). The diversity and number of their molecular targets makes it difficult to predict the net effect of endogenous transition metal ions and in most pathological cases it remains a matter of debate whether they play a compensatory (i.e. neuroprotective, anticonvulsive) or causative (i.e. neurotoxic, proconvulsive) role. Resting

concentrations of extracellular free or loosely bound (i.e. chelatable)  $\text{Cu}^{2+}$  and  $\text{Zn}^{2+}$  in the brain are not clearly established, but have been estimated to be in the order of 100–800 nM for  $\text{Cu}^{2+}$  (Mathie et al., 2006) and 5–25 nM for  $\text{Zn}^{2+}$  (Frederickson et al., 2006) respectively. To date, only  $\text{Ca}_v2.3$  and  $\text{Ca}_v3.2$ -type VGCCs and certain NMDA-type ionotropic glutamate receptors have been shown to be tonically suppressed by sub-micromolar concentration of endogenous  $\text{Cu}^{2+}$  and  $\text{Zn}^{2+}$ , suggesting that these channels are among the main targets and primary mediators of their effects. This is supported by the expression pattern of  $\text{Ca}_v2.3$  channels, which coincides with the spatial distribution of loosely bound transition metal ions in the brain, as highest densities of these channels occur in the hippocampus and other limbic regions, in the retina and in cortical neurons (Sochivko et al., 2002; Weiergräber et al., 2006). On the cellular level,  $\text{Ca}_v2.3$  channels are localized both presynaptically (Day et al., 1996), where they have been shown to be involved in synaptic transmission and neuronal plasticity (Gasparini et al., 2001; Dietrich et al., 2003; Yasuda et al., 2003; Bloodgood and Sabatini, 2007) and postsynaptically (Yokoyama et al., 1995; Day et al., 1996), where they are thought to contribute to action potential burst firing and oscillatory activity (Christie et al., 1995; Magee and Johnston, 1995; Kavalali et al., 1997; Magee and Carruth, 1999). Less is known about the role of  $\text{Ca}_v3.2$  channels, but they appear to be critically involved in  $\text{Ca}^{2+}$ -dependent low-threshold rebound spikes, which trigger bursts of  $\text{Na}^+$ -dependent APs and contribute to the formation of sustained synchronous network discharges (Jahnson and Llinas, 1984; Kim et al., 2001). Tonic inhibition of  $\text{Ca}_v2.3$  and  $\text{Ca}_v3.2$  channels by  $\text{Zn}^{2+}$  and  $\text{Cu}^{2+}$  as well as more or less unspecific pore-block of other VGCCs could accordingly suppress neurotransmission under resting conditions and possibly serve as a mechanism to prevent transition to abnormal patterns of excitation generation, conduction and/or integration. This is supported by a number of experimental observations which indicate that endogenous  $\text{Zn}^{2+}$  and possibly  $\text{Cu}^{2+}$  dampen overall excitability in limbic regions, thereby serving as intrinsic anticonvulsants. Thus, in hippocampal slices,  $\text{Zn}^{2+}$  can enhance synchronized release of GABA, increase the responsiveness of GABA-receptors and inhibit excitatory synaptic transmission (Xie et al., 1993; Xie and Smart, 1993a, 1993b, 1994). Complete chelation of synaptic transition metal ions in the hippocampus conversely induces excitotoxicity and convulsions in healthy rats (Blasco-Ibanez et al., 2004) and in rats subjected to non-lesioning over-excitation (Dominguez et al., 2003). Similarly,  $\text{Zn}^{2+}$  deficient mice are more susceptible to kainate-induced seizures and neurotoxicity (Takeda et al., 2003a, 2005) and exhibit increased post-ictal levels of glutamate and decreased levels of GABA in their extracellular hippocampal fluid compared to control mice (Takeda et al., 2003b). With regard to the allosteric component, such a mechanism would be very effective at or near resting membrane potentials, where most channels are closed and available for inhibition. Excessive depolarization, as observed during seizures or after traumatic brain injury, on the other hand could shift the equilibrium in favour of open channel states and greatly reduce the fraction of channels available for inhibition. Under these conditions, even high levels of released  $\text{Zn}^{2+}$  could fail to markedly inhibit VGCCs and instead lead to neurotoxic effects due to excessive inflow of  $\text{Zn}^{2+}$  into neurons, as described in Section 4.2.8.2. This could explain why exogenous administration of zinc salts can trigger seizure activity and neurotoxicity in animal models (Pei et al., 1983) and why brief exposure (15 min) of cultured cortical cells to  $\text{Zn}^{2+}$  concentrations exceeding 300  $\mu\text{M}$  is associated with extensive neuronal death (Yokoyama et al., 1986). Also, massive synaptic release of  $\text{Zn}^{2+}$  has been linked to delayed cell death observed following seizures (Frederickson et al., 1989), transient focal or global ischaemia (Koh et al., 1996; Lee et al., 2002) and traumatic brain injury (Suh et al., 2000).



## 5. Conclusion

VGCCs possess elaborate mechanisms to allow for selective permeation and voltage-dependent gating, which are still only partly understood. Their multifactorial modulation and permeation by polyvalent inorganic cations complicates analysis of experimental findings but may also contribute to current understanding of molecular channel structure and function. While theoretical models can still not completely account for the diverse effects of polyvalent cations, they help to understand experimental findings, exemplify different possible mechanisms of action, and provide a starting point for further studies. The present analysis of experimental data has barely scratched the surface of the topic, but reveals several striking similarities in the action of polyvalent cations on VGCCs compared to other voltage-gated channels. They indicate that  $\text{Ca}^{2+}$  transfer through the pore of vertebrate VGCCs could proceed through a mechanism not unlike that in bacterial voltage-gated  $\text{Na}^+$  channels and that there may be a complex interrelationship between pore region and gating machinery of VGCCs, just as it has been described in  $\text{Na}^+$  channels. Ultimately however, only crystallographic data of vertebrate VGCCs will allow for a validation of current models based on actual structural data. For now, investigators should keep in mind that multiple mechanisms have to be taken into account when interpreting the effects of metal ions on VGCCs, and that previous investigations may have over- or under-estimated some of these mechanisms at the cost of other factors. The high sensitivity of certain channels also raises the possibility that traces of metal contaminants may have affected the determination of dose-response characteristics, as already uncovered in a number of cases.<sup>7</sup> Likewise, future work with said channels will require rigorous exclusion of contaminated external solutions, which could otherwise profoundly bias the observed effects.

## Conflict of interest

The authors declare no conflicts of interest.

## Acknowledgement

The work was financially supported by the Köln Fortune Program (259/2013)/Faculty of Medicine, University of Cologne.

## Appendix A. Supplementary data

Supplementary data associated with this article can be found, in the online version, at <http://dx.doi.org/10.1016/j.pneurobio.2014.12.003>.

## References

- Abramson, H.A., Müller, H., 1933. The influence of salts on the electric charge of surfaces in liquids. *Cold Spring Harb. Symp. Quant. Biol.* 1, 29–33.
- Akaïke, N., Lee, K.S., Brown, A.M., 1978. The calcium current of Helix neuron. *J. Gen. Physiol.* 71, 509–531.
- Almers, W., McCleskey, E.W., 1984. Non-selective conductance in calcium channels of frog muscle: calcium selectivity in a single-file pore. *J. Physiol.* 353, 585–608.
- Almers, W., McCleskey, E.W., Palade, P.T., 1984. A non-selective cation conductance in frog muscle membrane blocked by micromolar external calcium ions. *J. Physiol.* 353, 565–583.
- Almers, W., McCleskey, E.W., Palade, P.T., 1985. Ca channels in vertebrate skeletal muscle. In: Rubin, R.P., Weiss, G.B., Putney, Jr., J.W. (Eds.), *Calcium in Biological Systems*. Springer US, New York, pp. 321–330.
- Amaral, C., Carnevale, V., Klein, M.L., Treptow, W., 2012. Exploring conformational states of the bacterial voltage-gated sodium channel NavAb via molecular dynamics simulations. *Proc. Natl. Acad. Sci. U. S. A.* 109, 21336–21341.
- Amzica, F., Massimini, M., Manfredi, A., 2002. Spatial buffering during slow and paroxysmal sleep oscillations in cortical networks of glial cells in vivo. *J. Neurosci.* 22, 1042–1053.
- Anastassov, I., Ripps, H., Chappell, R.L., 2014. Cytoprotection by endogenous zinc in the vertebrate retina. *J. Neurochem.* 129, 249–255.
- Anastassov, I., Shen, W., Ripps, H., Chappell, R.L., 2013. Zinc modulation of calcium activity at the photoreceptor terminal: a calcium imaging study. *Exp. Eye Res.* 112, 37–44.
- Andersen, O.S., Koeppe II, R.E., 1992. Molecular determinants of channel function. *Physiol. Rev.* 72 (Suppl.), S89–S158.
- Anderson, M., 1983. Mn ions pass through calcium channels. A possible explanation. *J. Gen. Physiol.* 81, 805–827.
- Aoki, I., Naruse, S., Tanaka, C., 2004a. Manganese-enhanced magnetic resonance imaging (MEMRI) of brain activity and applications to early detection of brain ischemia. *NMR Biomed.* 17, 569–580.
- Aoki, I., Tanaka, C., Takegami, T., Ebisu, T., Umeda, M., Fukunaga, M., Fukuda, K., Silva, A.C., Koretsky, A.P., Naruse, S., 2002. Dynamic activity-induced manganese-dependent contrast magnetic resonance imaging (DAIM MRI). *Magn. Reson. Med.* 48, 927–933.
- Aoki, I., Wu, Y.J., Silva, A.C., Lynch, R.M., Koretsky, A.P., 2004b. In vivo detection of neuroarchitecture in the rodent brain using manganese-enhanced MRI. *Neuroimage* 22, 1046–1059.
- Arias-Olguin, I.I., Vitko, I., Fortuna, M., Baumgart, J.P., Sokolova, S., Shumilin, I.A., Van Deusen, A., Soriano-Garcia, M., Gomora, J.C., Perez-Reyes, E., 2008. Characterization of the gating brake in the I-II loop of Ca(v)3.2 T-type Ca(2+) channels. *J. Biol. Chem.* 283, 8136–8144.
- Arikkath, J., Campbell, K.P., 2003. Auxiliary subunits: essential components of the voltage-gated calcium channel complex. *Curr. Opin. Neurobiol.* 13, 298–307.
- Arikkath, J., Chen, C.C., Ahern, C., Allamand, V., Flanagan, J.D., Coronado, R., Gregg, R.G., Campbell, K.P., 2003. Gamma 1 subunit interactions within the skeletal muscle L-type voltage-gated calcium channels. *J. Biol. Chem.* 278, 1212–1219.
- Armstrong, C.M., 1999. Distinguishing surface effects of calcium ion from pore-occupancy effects in  $\text{Na}^+$  channels. *Proc. Natl. Acad. Sci. U. S. A.* 96, 4158–4163.
- Armstrong, C.M., Cota, G., 1990. Modification of sodium channel gating by lanthanum. Some effects that cannot be explained by surface charge theory. *J. Gen. Physiol.* 96, 1129–1140.
- Armstrong, C.M., Cota, G., 1991. Calcium ion as a cofactor in Na channel gating. *Proc. Natl. Acad. Sci. U. S. A.* 88, 6528–6531.
- Armstrong, C.M., Cota, G., 1999. Calcium block of  $\text{Na}^+$  channels and its effect on closing rate. *Proc. Natl. Acad. Sci. U. S. A.* 96, 4154–4157.
- Armstrong, C.M., Lopez-Barneo, J., 1987. External calcium ions are required for potassium channel gating in squid neurons. *Science* 236, 712–714.
- Armstrong, C.M., Neyton, J., 1991. Ion permeation through calcium channels: a one-site model. *Ann. N. Y. Acad. Sci.* 635, 18–25.
- Atar, D., Backx, P.H., Appel, M.M., Gao, W.D., Marban, E., 1995. Excitation–transcription coupling mediated by zinc influx through voltage-dependent calcium channels. *J. Biol. Chem.* 270, 2473–2477.
- Babich, O., Isaev, D., Shirokov, R., 2005. Role of extracellular  $\text{Ca}^{2+}$  in gating of CaV1.2 channels. *J. Physiol.* 565, 709–715.
- Babich, O., Matveev, V., Harris, A.L., Shirokov, R., 2007a.  $\text{Ca}^{2+}$ -dependent inactivation of CaV1.2 channels prevents Gd3+ block: does  $\text{Ca}^{2+}$  block the pore of inactivated channels? *J. Gen. Physiol.* 129, 477–483.
- Babich, O., Reeves, J., Shirokov, R., 2007b. Block of CaV1.2 channels by Gd3+ reveals preopening transitions in the selectivity filter. *J. Gen. Physiol.* 129, 461–475.
- Bahinski, A., Yatani, A., Mikala, G., Tang, S.Q., Yamamoto, S., Schwartz, A., 1997. Charged amino acids near the pore entrance influence ion-conduction of a human L-type cardiac calcium channel. *Mol. Cell. Biochem.* 166, 125–134.
- Baumgart, J.P., Vitko, I., Bidaud, I., Kondratskiy, A., Lory, P., Perez-Reyes, E., 2008. I–II loop structural determinants in the gating and surface expression of low voltage-activated calcium channels. *PLoS ONE* 3, e2976.
- Bean, B.P., 1985. Two kinds of calcium channels in canine atrial cells. *J. Gen. Physiol.* 86, 1–30.
- Becchetti, A., Arcangeli, A., Del Bene, M.R., Olivetto, M., Wanke, E., 1992. Intra and extracellular surface charges near  $\text{Ca}^{2+}$  channels in neurons and neuroblastoma cells. *Biophys. J.* 63, 954–965.
- Beedle, A.M., Hamid, J., Zamponi, G.W., 2002. Inhibition of transiently expressed low- and high-voltage-activated calcium channels by trivalent metal cations. *J. Membr. Biol.* 187, 225–238.
- Beirao, P.S., Lakshminarayanaiah, N., 1979. Calcium carrying system in the giant muscle fibre of the barnacle species, *Balanus nubilus*. *J. Physiol.* 293, 319–327.
- Bell, J.E., Miller, C., 1984. Effects of phospholipid surface charge on ion conduction in the  $\text{K}^+$  channel of sarcoplasmic reticulum. *Biophys. J.* 45, 279–287.
- Benitah, J.P., Chen, Z., Balsler, J.R., Tomaselli, G.F., Marban, E., 1999. Molecular dynamics of the sodium channel pore vary with gating: interactions between P-segment motions and inactivation. *J. Neurosci.* 19, 1577–1585.
- Berjukow, S., Marksteiner, R., Sokolov, S., Weiss, R.G., Margreiter, E., Hering, S., 2001. Amino acids in segment IVS6 and beta-subunit interaction support distinct conformational changes during Ca(v)2.1 inactivation. *J. Biol. Chem.* 276, 17076–17082.
- Bezanilla, F., 2000. The voltage sensor in voltage-dependent ion channels. *Physiol. Rev.* 80, 555–591.
- Bezanilla, F., 2002. Voltage sensor movements. *J. Gen. Physiol.* 120, 465–473.
- Biagi, B.A., Enyeart, J.J., 1990. Gadolinium blocks low- and high-threshold calcium currents in pituitary cells. *Am. J. Physiol. Cell Physiol.* 259, C515–C520.

<sup>7</sup> For examples see Paoletti et al. (1997), Thio and Zhang (2006) and Shcheglovitov et al. (2012).

- Biel, M., Ruth, P., Bosse, E., Hullin, R., Stühmer, W., Flockerzi, V., Hofmann, F., 1990. Primary structure and functional expression of a high voltage activated calcium channel from rabbit lung. *FEBS Lett.* 269, 409–412.
- Birnbaumer, L., Campbell, K.P., Catterall, W.A., Harpold, M.M., Hofmann, F., Horne, W.A., Mori, Y., Schwartz, A., Snutch, T.P., Tanabe, T., Tsien, R.W., 1994. The naming of voltage-gated calcium channels. *Neuron* 13, 505–506.
- Birnbaumer, L., Qin, N., Olcese, R., Tareilus, E., Platano, D., Costantin, J., Stefani, E., 1998. Structures and functions of calcium channel  $\beta$  subunits. *J. Bioenerg. Biomembr.* 30, 357–375.
- Blasco-Ibanez, J.M., Poza-Aznar, J., Crespo, C., Marques-Mari, A.I., Gracia-Llanes, F.J., Martinez-Guijarro, F.J., 2004. Chelation of synaptic zinc induces overexcitation in the hilar mossy cells of the rat hippocampus. *Neurosci. Lett.* 355, 101–104.
- Bleuzen, A., Helm, L., Merbach, A.E., 1997. Water exchange on magnesium(II) in aqueous solution: a variable temperature and pressure  $^{17}\text{O}$  NMR study. *Magn. Reson. Chem.* 35, 765–773.
- Block, B.M., Stacey, W.C., Jones, S.W., 1998. Surface charge and lanthanum block of calcium current in bullfrog sympathetic neurons. *Biophys. J.* 74, 2278–2284.
- Bloodgood, B.L., Sabatini, B.L., 2007. Nonlinear regulation of unitary synaptic signals by  $\text{CaV}(2.3)$  voltage-sensitive calcium channels located in dendritic spines. *Neuron* 53, 249–260.
- Boccaccio, A., Moran, O., Conti, F., 1998. Calcium dependent shifts of  $\text{Na}^+$  channel activation correlated with the state dependence of calcium-binding to the pore. *Eur. Biophys. J.* 27, 558–566.
- Bosse, E., Bottlender, R., Kleppisch, T., Hescheler, J., Welling, A., Hofmann, F., Flockerzi, V., 1992. Stable and functional expression of the calcium channel  $\alpha_1$  subunit from smooth muscle in somatic cell lines. *EMBO J.* 11, 2033–2038.
- Bourinet, E., Zamponi, G.W., Stea, A., Soong, T.W., Lewis, B.A., Jones, L.P., Yue, D.T., Snutch, T.P., 1996. The  $\alpha_{1E}$  calcium channel exhibits permeation properties similar to low-voltage-activated calcium channels. *J. Neurosci.* 16, 4983–4993.
- Brink, F., 1954. The role of calcium ions in neural processes. *Pharmacol. Rev.* 6, 243–298.
- Brink, F., Bronk, D.W., Larrabee, M.G., 1946. Chemical excitation of nerve. *Ann. N. Y. Acad. Sci.* 47, 457–485.
- Budde, T., Meuth, S., Pape, H.C., 2002. Calcium-dependent inactivation of neuronal calcium channels. *Nat. Rev. Neurosci.* 3, 873–883.
- Burgess, D.E., Crawford, O., Delisle, B.P., Satin, J., 2002. Mechanism of inactivation gating of human T-type (low-voltage activated) calcium channels. *Biophys. J.* 82, 1894–1906.
- Büsselberg, D., Michael, D., Evans, M.L., Carpenter, D.O., Haas, H.L., 1992. Zinc ( $\text{Zn}^{2+}$ ) blocks voltage gated calcium channels in cultured rat dorsal root ganglion cells. *Brain Res.* 593, 77–81.
- Büsselberg, D., Pekel, M., Michael, D., Platt, B., 1994a. Mercury ( $\text{Hg}^{2+}$ ) and zinc ( $\text{Zn}^{2+}$ ): two divalent cations with different actions on voltage-activated calcium channel currents. *Cell. Mol. Neurobiol.* 14, 675–687.
- Büsselberg, D., Platt, B., Michael, D., Carpenter, D.O., Haas, H.L., 1994b. Mammalian voltage-activated calcium channel currents are blocked by  $\text{Pb}^{2+}$ ,  $\text{Zn}^{2+}$ , and  $\text{Al}^{3+}$ . *J. Neurophysiol.* 71, 1491–1497.
- Byerly, L., Chase, P.B., Stimers, J.R., 1985. Permeation and interaction of divalent cations in calcium channels of snail neurons. *J. Gen. Physiol.* 85, 491–518.
- Cai, M., Jordan, P.C., 1990. How does vestibule surface charge affect ion conduction and toxin binding in a sodium channel? *Biophys. J.* 57, 883–891.
- Campbell, K.P., Leung, A.T., Sharp, A.H., 1988. The biochemistry and molecular biology of the dihydropyridine-sensitive calcium channel. *Trends Neurosci.* 11, 425–430.
- Canti, C., Davies, A., Berrow, N.S., Butcher, A.J., Page, K.M., Dolphin, A.C., 2001. Evidence for two concentration-dependent processes for beta-subunit effects on  $\alpha_1\text{B}$  calcium channels. *Biophys. J.* 81, 1439–1451.
- Capes, D.L., Arcisio-Miranda, M., Jarecki, B.W., French, R.J., Chanda, B., 2012. Gating transitions in the selectivity filter region of a sodium channel are coupled to the domain IV voltage sensor. *Proc. Natl. Acad. Sci. U. S. A.* 109, 2648–2653.
- Carbone, E., Lux, H.D., 1984. A low voltage-activated, fully inactivating Ca channel in vertebrate sensory neurones. *Nature* 310, 501–502.
- Carbone, E., Lux, H.D., 1987. Single low-voltage-activated calcium channels in chick and rat sensory neurones. *J. Physiol.* 386, 571–601.
- Carbone, E., Lux, H.D., Carabelli, V., Aicardi, G., Zucker, H., 1997.  $\text{Ca}^{2+}$  and  $\text{Na}^+$  permeability of high-threshold  $\text{Ca}^{2+}$  channels and their voltage-dependent block by  $\text{Mg}^{2+}$  ions in chick sensory neurones. *J. Physiol.* 504 (Pt 1), 1–15.
- Castelli, L., Tanzi, F., Taglietti, V., Magistretti, J., 2003.  $\text{Cu}^{2+}$ ,  $\text{Co}^{2+}$ , and  $\text{Mn}^{2+}$  modify the gating kinetics of high-voltage-activated  $\text{Ca}^{2+}$  channels in rat palaeocortical neurons. *J. Membr. Biol.* 195, 121–136.
- Cataldi, M., Perez-Reyes, E., Tsien, R.W., 2002. Differences in apparent pore sizes of low and high voltage-activated  $\text{Ca}^{2+}$  channels. *J. Biol. Chem.* 277, 45969–45976.
- Catterall, W.A., 1998. Structure and function of neuronal  $\text{Ca}^{2+}$  channels and their role in neurotransmitter release. *Cell Calcium* 24, 307–323.
- Catterall, W.A., 2011. Voltage-gated calcium channels. *Cold Spring Harb. Perspect. Biol.* 3, 1–23.
- Catterall, W.A., Perez-Reyes, E., Snutch, T.P., Striessnig, J., 2013. Voltage-gated calcium channels. IUPHAR database (IUPHAR-DB). <http://www.iuphar-db.org/DATABASE/FamilyMenuForward?familyId=80> (last modified 05.02.13; accessed 18.07.13).
- Catterall, W.A., Striessnig, J., Snutch, T.P., Perez-Reyes, E., 2003. International Union of Pharmacology. XL. Compendium of voltage-gated ion channels: calcium channels. *Pharmacol. Rev.* 55, 579–581.
- Cens, T., Rousset, M., Kajava, A., Charnet, P., 2007. Molecular determinant for specific Ca/Ba selectivity profiles of low and high threshold  $\text{Ca}^{2+}$  channels. *J. Gen. Physiol.* 130, 415–425.
- Chandy, K.G., 1991. Simplified gene nomenclature. *Nature* 352, 26.
- Charton, G., Rovira, C., Ben Ari, Y., Leviev, V., 1985. Spontaneous and evoked release of endogenous  $\text{Zn}^{2+}$  in the hippocampal mossy fiber zone of the rat in situ. *Exp. Brain Res.* 58, 202–205.
- Chesnoy-Marchais, D., 1985. Kinetic properties and selectivity of calcium-permeable single channels in *Aplysia* neurones. *J. Physiol.* 367, 457–488.
- Chow, R.H., 1991. Cadmium block of squid calcium currents. Macroscopic data and a kinetic model. *J. Gen. Physiol.* 98, 751–770.
- Christie, B.R., Eliot, L.S., Ito, K., Miyakawa, H., Johnston, D., 1995. Different  $\text{Ca}^{2+}$  channels in soma and dendrites of hippocampal pyramidal neurons mediate spike-induced  $\text{Ca}^{2+}$  influx. *J. Neurophysiol.* 73, 2553–2557.
- Chu, P.J., Robertson, H.M., Best, P.M., 2001. Calcium channel gamma subunits provide insights into the evolution of this gene family. *Gene* 280, 37–48.
- Cibulsky, S.M., Sather, W.A., 2000. The EEEE Locus is the sole high-affinity  $\text{Ca}^{2+}$  binding structure in the pore of a voltage-gated  $\text{Ca}^{2+}$  channel. Block by  $\text{Ca}^{2+}$  entering from the intracellular pore entrance. *J. Gen. Physiol.* 116, 349–362.
- Cibulsky, S.M., Sather, W.A., 2003. Control of ion conduction in L-type  $\text{Ca}^{2+}$  channels by the concerted action of S5–6 regions. *Biophys. J.* 84, 1709–1719.
- Cloues, R.K., Cibulsky, S.M., Sather, W.A., 2000. Ion interactions in the high-affinity binding locus of a voltage-gated  $\text{Ca}^{2+}$  channel. *J. Gen. Physiol.* 116, 569–586.
- Cole, K.S., 1949. Dynamic electrical characteristics of the squid axon membrane. *Arch. Sci. Physiol. (Paris)* 3, 253–258.
- Cordero-Morales, J.F., Cuello, L.G., Perozo, E., 2006a. Voltage-dependent gating at the KcsA selectivity filter. *Nat. Struct. Mol. Biol.* 13, 319–322.
- Cordero-Morales, J.F., Cuello, L.G., Zhao, Y., Jogini, V., Cortes, D.M., Roux, B., Perozo, E., 2006b. Molecular determinants of gating at the potassium-channel selectivity filter. *Nat. Struct. Mol. Biol.* 13, 311–318.
- Cossy, C., Helm, L., Merbach, A.E., 1987. Water exchange kinetics on lanthanide(III) ions: a variable temperature and pressure  $^{17}\text{O}$  NMR study. *Inorg. Chim. Acta* 139, 147–149.
- Cota, G., 1986. Calcium channel currents in pars intermedia cells of the rat pituitary gland. Kinetic properties and washout during intracellular dialysis. *J. Gen. Physiol.* 88, 83–105.
- Cota, G., Stefani, E., 1984. Saturation of calcium channels and surface charge effects in skeletal muscle fibres of the frog. *J. Physiol.* 351, 135–154.
- Cribbs, L.L., Lee, J.-H., Yang, J., Satin, J., Zhang, Y., Daud, A., Barclay, J., Williamson, M.P., Fox, M., Rees, M., Perez-Reyes, E., 1998. Cloning and characterization of  $\alpha_1\text{H}$  from human heart, a member of the T-type calcium channel gene family. *Circ. Res.* 83, 103–109.
- Cukierman, S., Zinkand, W.C., French, R.J., Krueger, B.K., 1988. Effects of membrane surface charge and calcium on the gating of rat brain sodium channels in planar bilayers. *J. Gen. Physiol.* 92, 431–447.
- Curtis, B.M., Catterall, W.A., 1984. Purification of the calcium antagonist receptor of the voltage-sensitive calcium channel from skeletal muscle transverse tubules. *Biochemistry* 23, 2113–2117.
- Curtis, B.M., Catterall, W.A., 1986. Reconstitution of the voltage-sensitive calcium channel purified from skeletal muscle transverse tubules. *Biochemistry* 25, 3077–3083.
- Dang, T.X., McCleskey, E.W., 1998. Ion channel selectivity through stepwise changes in binding affinity. *J. Gen. Physiol.* 111, 185–193.
- Dani, J.A., 1986. Ion-channel entrances influence permeation. Net charge, size, shape, and binding considerations. *Biophys. J.* 49, 607–618.
- Day, N.C., Shaw, P.J., McCormack, A.L., Craig, P.J., Smith, W., Beattie, R., Williams, T.L., Ellis, S.B., Ince, P.G., Harpold, M.M., Lodge, D., Volsen, S.G., 1996. Distribution of  $\alpha_1\text{A}$ ,  $\alpha_1\text{B}$  and  $\alpha_1\text{E}$  voltage-dependent calcium channel subunits in the human hippocampus and parahippocampal gyrus. *Neuroscience* 71, 1013–1024.
- De Waard, M., Campbell, K.P., 1995. Subunit regulation of the neuronal  $\alpha_{1A}$   $\text{Ca}^{2+}$  channel expressed in *Xenopus* oocytes. *J. Physiol. (Lond.)* 485, 619–634.
- Delahayes, J.F., 1975. Depolarization-induced movement of Mn<sup>2+</sup> cations across the cell membrane in the guinea pig myocardium. *Circ. Res.* 36, 713–718.
- Diaz, D., Bartolo, R., Delgadillo, D.M., Higueldo, F., Gomora, J.C., 2005. Contrasting effects of  $\text{Cd}^{2+}$  and  $\text{Co}^{2+}$  on the blocking/unblocking of human Cav3 channels. *J. Membr. Biol.* 207, 91–105.
- Diebler, H.M., Eigen, G., Illgenfritz, G., Maas, G., Winkler, R., 1969. Kinetics and mechanism of reactions of main group metal ions with biological carriers. *Pure Appl. Chem.* 20, 93–115.
- Dietrich, D., Kirschstein, T., Kukley, M., Pereverzev, A., von der Brölie, C., Schneider, T., Beck, H., 2003. Functional specialization of presynaptic Cav2.3  $\text{Ca}^{2+}$  channels. *Neuron* 39, 483–496.
- Dolphin, A.C., 2003. Beta subunits of voltage-gated calcium channels. *J. Bioenerg. Biomembr.* 35, 599–620.
- Dolphin, A.C., 2006. A short history of voltage-gated calcium channels. *Br. J. Pharmacol.* 147 (Suppl. 1), S56–S62.
- Dolphin, A.C., Wyatt, C.N., Richards, J., Beattie, R.E., Craig, P., Lee, J.-H., Cribbs, L.L., Volsen, S.G., Perez-Reyes, E., 1999. The effect of  $\alpha_2$ -delta and other accessory subunits on expression and properties of the calcium channel  $\alpha_1\text{G}$ . *J. Physiol. (Lond.)* 519, 35–45.
- Dominguez, M.I., Blasco-Ibanez, J.M., Crespo, C., Marques-Mari, A.I., Martinez-Guijarro, F.J., 2003. Zinc chelation during non-lesioning overexcitation results in neuronal death in the mouse hippocampus. *Neuroscience* 116, 791–806.
- Dos Remedios, C.G., 1981. Lanthanide ion probes of calcium-binding sites on cellular membranes. *Cell Calcium* 2, 29–51.
- Eigen, M., Winkler, R., 1971. Carriers and specificity in membranes. II. Characteristics of carriers. Alkali ion carriers: specificity, architecture, and mechanisms: an essay. *Neurosci. Res. Progr. Bull.* 9, 330–338.



- Elinder, F., Arhem, P., 1999. Role of individual surface charges of voltage-gated K channels. *Biophys. J.* 77, 1358–1362.
- Elinder, F., Arhem, P., 2003. Metal ion effects on ion channel gating. *Q. Rev. Biophys.* 36, 373–427.
- Ellinor, P.T., Yang, J., Sather, W.A., Zhang, J.F., Tsien, R.W., 1995.  $\text{Ca}^{2+}$  channel selectivity at a single locus for high-affinity  $\text{Ca}^{2+}$  interactions. *Neuron* 15, 1121–1132.
- Ellis, S.B., Williams, M.E., Ways, N.R., Brenner, R., Sharp, A.H., Leung, A.T., Campbell, K.P., McKenna, E., Koch, W.J., Hui, A., et al., 1988. Sequence and expression of mRNAs encoding the alpha 1 and alpha 2 subunits of a DHP-sensitive calcium channel. *Science* 241, 1661–1664.
- Enger, M.D., Kang, Y.J., 1999. Cellular and molecular mechanisms of metal toxicities. In: *Handbook of Human Toxicology* CRC Press, Massaro, pp. 189–284.
- Ertel, E.A., 2004. Pharmacology of  $\text{Ca}_v3$  (T-type) channels. In: McDonough, S.I. (Ed.), *Calcium Channel Pharmacology*. Kluwer Academic/Plenum Publishers, New York, pp. 183–236.
- Ertel, E.A., Campbell, K.P., Harpold, M.M., Hofmann, F., Mori, Y., Perez-Reyes, E., Schwartz, A., Snutch, T.P., Tanabe, T., Birnbaumer, L., Tsien, R.W., Catterall, W.A., 2000. Nomenclature of voltage-gated calcium channels. *Neuron* 25, 533–535.
- Feng, Z.-P., Hamid, J., Doering, C., Jarvis, S.E., Bosey, G.M., 2001. Amino acid residues outside of the pore region contribute to N-type calcium channel permeation. *J. Biol. Chem.* 276, 5726–5730.
- Flockerzi, V., Oeken, H.J., Hofmann, F., Pelzer, D., Cavalie, A., Trautwein, W., 1986. Purified dihydropyridine-binding site from skeletal muscle t-tubules is a functional calcium channel. *Nature* 323, 66–68.
- Frankenhaeuser, B., 1960. Sodium permeability in toad nerve and in squid nerve. *J. Physiol.* 152, 159–166.
- Frankenhaeuser, B., Hodgkin, A.L., 1957. The action of calcium on the electrical properties of squid axons. *J. Physiol.* 137, 218–244.
- Frankenhaeuser, B., Ryan, K.J., Arhem, P., 1976. The effects of neuraminidase and protamine chloride on potential clamp parameters of the node of Ranvier (*Xenopus laevis*). *Acta Physiol. Scand.* 96, 548–557.
- Frederickson, C.J., 1989. Neurobiology of zinc and zinc-containing neurons. *Int. Rev. Neurobiol.* 31, 145–238.
- Frederickson, C.J., Giblin, L.J., Krezel, A., McAdoo, D.J., Mueller, R.N., Zeng, Y., Balaji, R.V., Masalha, R., Thompson, R.B., Fierke, C.A., Sarvey, J.M., de Valdenebro, M., Prough, D.S., Zornow, M.H., 2006. Concentrations of extracellular free zinc ( $\text{pZn}$ ) in the central nervous system during simple anesthetization, ischemia and reperfusion. *Exp. Neurol.* 198, 285–293.
- Frederickson, C.J., Hernandez, M.D., McGinty, J.F., 1989. Translocation of zinc may contribute to seizure-induced death of neurons. *Brain Res.* 480, 317–321.
- Frederickson, C.J., Koh, J.Y., Bush, A.I., 2005. The neurobiology of zinc in health and disease. *Nat. Rev. Neurosci.* 6, 449–462.
- French, R.J., Prusak-Sochaczewski, E., Zamponi, G.W., Becker, S., Kularatna, A.S., Horn, R., 1996. Interactions between a pore-blocking peptide and the voltage sensor of the sodium channel: an electrostatic approach to channel geometry. *Neuron* 16, 407–413.
- Friel, D.D., Tsien, R.W., 1989. Voltage-gated calcium channels: direct observation of the anomalous mole fraction effect at the single-channel level. *Proc. Natl. Acad. Sci. U. S. A.* 86, 5207–5211.
- Fukuda, J., Kawa, K., 1977. Permeation of manganese, cadmium, zinc, and beryllium through calcium channels of an insect muscle membrane. *Science* 196, 309–311.
- Fukushima, Y., Hagiwara, S., 1985. Currents carried by monovalent cations through calcium channels in mouse neoplastic B lymphocytes. *J. Physiol.* 358, 255–284.
- Ganitkevich, V.Y., Shuba, M.F., Smirnov, S.V., 1988. Saturation of calcium channels in single isolated smooth muscle cells of guinea-pig taenia caeci. *J. Physiol.* 399, 419–436.
- Gasparini, S., Kasyanov, A.M., Pietrobon, D., Voronin, L.L., Cherubini, E., 2001. Presynaptic R-type calcium channels contribute to fast excitatory synaptic transmission in the rat hippocampus. *J. Neurosci.* 21, 8715–8721.
- Gilbert, D.L., Ehrenstein, G., 1969. Effect of divalent cations on potassium conductance of squid axons: determination of surface charge. *Biophys. J.* 9, 447–463.
- Gilbert, D.L., Ehrenstein, G., 1970. Use of a fixed charge model to determine the pK of the negative sites on the external membrane surface. *J. Gen. Physiol.* 55, 822–825.
- Gilbert, D.L., Ehrenstein, G., 1984. Membrane surface charge. *Curr. Top. Membr. Transp.* 22, 407–421.
- Gillespie, D., 2008. Energetics of divalent selectivity in a calcium channel: the ryanodine receptor case study. *Biophys. J.* 94, 1169–1184.
- Gillespie, D., Boda, D., 2008. The anomalous mole fraction effect in calcium channels: a measure of preferential selectivity. *Biophys. J.* 95, 2658–2672.
- Gillespie, D., Boda, D., He, Y., Apel, P., Siwy, Z.S., 2008. Synthetic nanopores as a test case for ion channel theories: the anomalous mole fraction effect without single filing. *Biophys. J.* 95, 609–619.
- Gillespie, D., Xu, L., Wang, Y., Meissner, G., 2005. (De)constructing the ryanodine receptor: modeling ion permeation and selectivity of the calcium release channel. *J. Phys. Chem. B* 109, 15598–15610.
- Gilly, W.F., Armstrong, C.M., 1982a. Divalent cations and the activation kinetics of potassium channels in squid giant axons. *J. Gen. Physiol.* 79, 965–996.
- Gilly, W.F., Armstrong, C.M., 1982b. Slowing of sodium channel opening kinetics in squid axon by extracellular zinc. *J. Gen. Physiol.* 79, 935–964.
- Gomez-Lagunas, F., Melischuk, A., Armstrong, C.M., 2003. Block of Shaker potassium channels by external calcium ions. *Proc. Natl. Acad. Sci. U. S. A.* 100, 347–351.
- Grahame, D.C., 1947. The electrical double layer and the theory of electrocapillarity. *Chem. Rev.* 41, 441–501.
- Grantham, C.J., Bowman, D., Bath, C.P., Bell, D.C., Bleakman, D., 1994. Omega-conotoxin MVIC reversibly inhibits a human N-type calcium channel and calcium influx into chick synaptosomes. *Neuropharmacology* 33, 255–258.
- Gurnett, C.A., De Waard, M., Campbell, K.P., 1996. Dual function of the voltage-dependent  $\text{Ca}^{2+}$  channel alpha 2 delta subunit in current stimulation and subunit interaction. *Neuron* 16, 431–440.
- Hagiwara, S., Miyazaki, S., 1977. Ca and Na spikes in egg cell membrane. *Prog. Clin. Biol. Res.* 15, 147–158.
- Hagiwara, S., Naka, K.I., 1964. The initiation of spike potential in barnacle muscle fibers under low intracellular  $\text{Ca}^{++}$ . *J. Gen. Physiol.* 48, 141–162.
- Hagiwara, S., Nakajima, S., 1966. Differences in Na and Ca spikes as examined by application of tetrodotoxin, procaine, and manganese ions. *J. Gen. Physiol.* 49, 793–806.
- Hagiwara, S., Ozawa, S., Sand, O., 1975. Voltage clamp analysis of two inward current mechanisms in the egg cell membrane of a starfish. *J. Gen. Physiol.* 65, 617–644.
- Hagiwara, S., Takahashi, K., 1967. Surface density of calcium ions and calcium spikes in the barnacle muscle fiber membrane. *J. Gen. Physiol.* 50, 583–601.
- Halling, D.B., Aracena-Parks, P., Hamilton, S.L., 2005. Regulation of voltage-gated  $\text{Ca}^{2+}$  channels by calmodulin. *Sci. STKE* 2005, re15.
- Harterter, D.E., Barnea, A., 1988. Evidence for release of copper in the brain: depolarization-induced release of newly taken-up  $^{67}\text{Cu}$ . *Synapse* 2, 412–415.
- He, Z.L.L., Yang, X.E., Stoffella, P.J., 2005. Trace elements in agroecosystems and impacts on the environment. *J. Trace Elem. Med. Biol.* 19, 125–140.
- Helm, L., Merbach, A.E., 1999. Water exchange on metal ions: experiments and simulations. *Coord. Chem. Rev.* 187, 151–181.
- Helton, T.D., Horne, W.A., 2002. Alternative splicing of the beta4 subunit has alpha1 subunit subtype-specific effects on  $\text{Ca}^{2+}$  channel gating. *J. Neurosci.* 22, 1573–1582.
- Henderson, D., 1983. Recent progress in the theory of the electric double-layer. *Prog. Surf. Sci.* 13, 197–224.
- Hering, S., Berjukow, S., Sokolov, S., Marksteiner, R., Weiss, R.G., Kraus, R., Timin, E.N., 2000. Molecular determinants of inactivation in voltage-gated  $\text{Ca}^{2+}$  channels. *J. Physiol.* 528 (Pt 2), 237–249.
- Hess, P., Lansman, J.B., Tsien, R.W., 1986. Calcium channel selectivity for divalent and monovalent cations. Voltage and concentration dependence of single channel current in ventricular heart cells. *J. Gen. Physiol.* 88, 293–319.
- Hess, P., Tsien, R.W., 1984. Mechanism of ion permeation through calcium channels. *Nature* 309, 453–456.
- Hilber, K., Sandtner, W., Kudlacek, O., Glaaser, I.W., Weisz, E., Kyle, J.W., French, R.J., Fozzard, H.A., Dudley, S.C., Todt, H., 2001. The selectivity filter of the voltage-gated sodium channel is involved in channel activation. *J. Biol. Chem.* 276, 27831–27839.
- Hille, B., 2001. *Ionic channels of excitable membranes*. Sinauer Assoc. Inc., Sunderland, MA.
- Hille, B., Woodhull, A.M., Shapiro, B.I., 1975. Negative surface charge near sodium channels of nerve: divalent ions, monovalent ions, and pH. *Philos. Trans. R. Soc. Lond. B: Biol. Sci.* 270, 301–318.
- Hillyard, D.R., Monje, V.D., Mintz, I.M., Bean, B.P., Nadasdi, L., Ramachandran, J., Miljanich, G., Azimi-Zoonooz, A., McIntosh, J.M., Cruz, L.J., 1992. A new Conus peptide ligand for mammalian presynaptic  $\text{Ca}^{2+}$  channels. *Neuron* 9, 69–77.
- Hodgkin, A.L., Huxley, A.F., 1952a. A quantitative description of membrane current and its application to conduction and excitation in nerve. *J. Physiol. (Lond.)* 117, 500–544.
- Hodgkin, A.L., Huxley, A.F., 1952b. The components of membrane conductance in the giant axon of *Loligo*. *J. Physiol.* 116, 473–496.
- Hofmann, F., Flockerzi, V., Kahl, S., Wegener, J.W., 2014. L-type  $\text{Ca}_v1.2$  calcium channels: from in vitro findings to in vivo function. *Physiol. Rev.* 94, 303–326.
- Hofmann, F., Lacinova, L., Klugbauer, N., 1999. Voltage-dependent calcium channels: from structure to function. *Rev. Physiol. Biochem. Pharmacol.* 139, 33–87.
- Hong, K.H., Armstrong, C.M., Miller, C., 2001. Revisiting the role of  $\text{Ca}^{2+}$  in shaker  $\text{K}^+$  channel gating. *Biophys. J.* 80, 2216–2220.
- Hsu, Y.H., Lee, W.T., Chang, C., 2007. Multiparametric MRI evaluation of kainic acid-induced neuronal activation in rat hippocampus. *Brain* 130, 3124–3134.
- Huang, Y., Quayle, J.M., Worley, J.F., Standen, N.B., Nelson, M.T., 1989. External cadmium and internal calcium block of single calcium channels in smooth muscle cells from rabbit mesenteric artery. *Biophys. J.* 56, 1023–1028.
- Huguenard, J.R., 1996. Low-threshold calcium currents in central nervous system neurons. *Annu. Rev. Physiol.* 58, 329–348.
- Hullin, R., Singer-Lahat, D., Freichel, M., Biel, M., Dascal, N., Hofmann, F., Flockerzi, V., 1992. Calcium channel  $\beta$  subunit heterogeneity: functional expression of cloned cDNA from heart, aorta and brain. *EMBO J.* 11, 885–890.
- Isom, L.L., De Jongh, K.S., Catterall, W.A., 1994. Auxiliary subunits of voltage-gated ion channels. *Neuron* 12, 1183–1194.
- Itagaki, K., Koch, W.J., Bodi, I., Klöckner, U., Sligh, D.F., Schwartz, A., 1992. Native-type DHP-sensitive calcium channel currents are produced by cloned rat aortic smooth muscle and cardiac  $\alpha_1$  subunits expressed in *Xenopus laevis* oocytes and are regulated by  $\alpha_2$ - and  $\beta$ -subunits. *FEBS Lett.* 297, 221–225.
- Jahnsen, H., Llinas, R., 1984. Electrophysiological properties of guinea-pig thalamic neurones: an in vitro study. *J. Physiol.* 349, 205–226.
- Jeong, S.W., Park, B.G., Park, J.Y., Lee, J.W., Lee, J.H., 2003. Divalent metals differentially block cloned T-type calcium channels. *Neuroreport* 14, 1537–1540.

- Jia, Y., Jeng, J.M., Sensi, S.L., Weiss, J.H., 2002. Zn<sup>2+</sup> currents are mediated by calcium-permeable AMPA/kainate channels in cultured murine hippocampal neurones. *J. Physiol.* 543, 35–48.
- Jones, L.P., Wei, S.K., Yue, D.T., 1998. Mechanism of auxiliary subunit modulation of neuronal  $\alpha_{1E}$  calcium channels. *J. Gen. Physiol.* 112, 125–143.
- Jones, S.W., 1998. Overview of voltage-dependent calcium channels. *J. Bioenerg. Biomembr.* 30, 299–312.
- Josephson, I.R., Varadi, G., 1996. The beta subunit increases Ca<sup>2+</sup> currents and gating charge movements of human cardiac L-type Ca<sup>2+</sup> channels. *Biophys. J.* 70, 1285–1293.
- Kaku, T., Lee, T.S., Arita, M., Hadama, T., Ono, K., 2003. The gating and conductance properties of Cav3.2 low-voltage-activated T-type calcium channels. *Jpn. J. Physiol.* 53, 165–172.
- Kamp, T.J., Pérez-García, M.T., Marban, E., 1996. Enhancement of ionic current and charge movement by coexpression of calcium channel  $\beta_{1A}$  subunit with  $\alpha_{1C}$  subunit in a human embryonic kidney cell line. *J. Physiol. (Lond.)* 492, 89–96.
- Kang, H.W., Moon, H.J., Joo, S.H., Lee, J.H., 2007. Histidine residues in the IS3–IS4 loop are critical for nickel-sensitive inhibition of the Cav2.3 calcium channel. *FEBS Lett.* 581, 5774–5780.
- Kang, H.W., Park, J.Y., Jeong, S.W., Kim, J.A., Moon, H.J., Perez-Reyes, E., Lee, J.H., 2006. A molecular determinant of nickel inhibition in Cav3.2 T-type calcium channels. *J. Biol. Chem.* 281, 4823–4830.
- Kang, H.W., Vitko, I., Lee, S.S., Perez-Reyes, E., Lee, J.H., 2010. Structural determinants of the high affinity extracellular zinc binding site on Cav3.2 T-type calcium channels. *J. Biol. Chem.* 285, 3271–3281.
- Kardos, J., Kovacs, I., Hajos, F., Kalman, M., Simonyi, M., 1989. Nerve endings from rat brain tissue release copper upon depolarization. A possible role in regulating neuronal excitability. *Neurosci. Lett.* 103, 139–144.
- Karmazinova, M., Baumgart, J.P., Perez-Reyes, E., Lacinova, L., 2011. The voltage dependence of gating currents of the neuronal CA(v)3.3 channel is determined by the gating brake in the I-II loop. *Pflügers Arch.* 461, 461–468.
- Kass, R.S., Krafte, D.S., 1987. Negative surface charge density near heart calcium channels. Relevance to block by dihydropyridines. *J. Gen. Physiol.* 89, 629–644.
- Kavalali, E.T., Zhuo, M., Bito, H., Tsien, R.W., 1997. Dendritic Ca<sup>2+</sup> channels characterized by recordings from isolated hippocampal dendritic segments. *Neuron* 18, 651–663.
- Kawa, K., 1979. Zinc-dependent action potentials in giant neurons of the snail, *Euhadra quaestia*. *J. Membr. Biol.* 49, 325–344.
- Kell, M.J., DeFelice, L.J., 1988. Surface charge near the cardiac inward-rectifier channel measured from single-channel conductance. *J. Membr. Biol.* 102, 1–10.
- Kerchner, G.A., Canzoniero, L.M.T., Yu, S.P., Ling, C., Choi, D.W., 2000. Zn<sup>2+</sup> current is mediated by voltage-gated Ca<sup>2+</sup> channels and enhanced by extracellular acidity in mouse cortical neurones. *J. Physiol. (Lond.)* 528, 39–52.
- Khan, N., Gray, I.P., Obejero-Paz, C.A., Jones, S.W., 2008. Permeation and gating in Cav3.1 (alpha1G) T-type calcium channels effects of Ca<sup>2+</sup>, Ba<sup>2+</sup>, Mg<sup>2+</sup>, and Na<sup>+</sup>. *J. Gen. Physiol.* 132, 223–238.
- Kielland, J., 1937. Individual activity coefficients of ions in aqueous solutions. *J. Am. Chem. Soc.* 59, 1675–1678.
- Kim, D., Song, I., Keum, S., Lee, T., Jeong, M.J., Kim, S.S., McEnery, M.W., Shin, H.S., 2001. Lack of the burst firing of thalamocortical relay neurons and resistance to absence seizures in mice lacking  $\alpha_{1C}$  T-type Ca<sup>2+</sup> channels. *Neuron* 31, 35–45.
- Kim, E.Y., Koh, J.Y., Kim, Y.H., Sohn, S., Joe, E., Gwag, B.J., 1999. Zn<sup>2+</sup> entry produces oxidative neuronal necrosis in cortical cell cultures. *Eur. J. Neurosci.* 11, 327–334.
- Kim, M.-S., Morii, T., Sun, L.-X., Imoto, K., Mori, Y., 1993. Structural determinants of ion selectivity in brain calcium channel. *FEBS Lett.* 318, 145–148.
- Klapper, I., Hagstrom, R., Fine, R., Sharp, K., Honig, B., 1986. Focusing of electric fields in the active site of Cu–Zn superoxide dismutase: effects of ionic strength and amino-acid modification. *Proteins* 1, 47–59.
- Klugbauer, N., Dai, S.P., Specht, V., Lacinová, L., Marais, E., Bohn, G., Hofmann, F., 2000. A family of gamma-like calcium channel subunits. *FEBS Lett.* 470, 189–197.
- Klugbauer, N., Lacinová, L., Marais, E., Hobom, M., Hofmann, F., 1999a. Molecular diversity of the calcium channel  $\alpha_{2\delta}$  subunit. *J. Neurosci.* 19, 684–691.
- Klugbauer, N., Marais, E., Lacinová, L., Hofmann, F., 1999b. A T-type calcium channel from mouse brain. *Pflügers Arch.* 437, 710–715.
- Koh, J.Y., Choi, D.W., 1994. Zinc toxicity on cultured cortical neurons: involvement of N-methyl-D-aspartate receptors. *Neuroscience* 60, 1049–1057.
- Koh, J.Y., Suh, S.W., Gwag, B.J., He, Y.Y., Hsu, C.Y., Choi, D.W., 1996. The role of zinc in selective neuronal death after transient global cerebral ischemia. *Science* 272, 1013–1016.
- Kostyuk, P.G., 1980. Calcium ionic channels in electrically excitable membrane. *Neuroscience* 5, 945–959.
- Kostyuk, P.G., Mironov, S.L., Doroshenko, P.A., Ponomarev, V.N., 1982. Surface charges on the outer side of mollusc neuron membrane. *J. Membr. Biol.* 70, 171–179.
- Kraus, R.L., Sinnegger, M.J., Koschak, A., Glossmann, H., Stenirri, S., Carrera, P., Striessnig, J., 2000. Three new familial hemiplegic migraine mutants affect P/Q-type Ca<sup>2+</sup> channel kinetics. *J. Biol. Chem.* 275, 9239–9243.
- Krauss, D., Eisenberg, B., Gillespie, D., 2011. Selectivity sequences in a model calcium channel: role of electrostatic field strength. *Eur. Biophys. J.* 40, 775–782.
- Krebs, J., Heizmann, C.W., 2007. Calcium-binding proteins and the EF-hand principle. In: Krebs, J., Michalak, M. (Eds.), *Calcium: A Matter of Life or Death*. Elsevier, pp. 51–93.
- Kristian, T., Siesjö, B.K., 1998. Calcium in ischemic cell death. *Stroke* 29, 705–718.
- Kuo, C.C., Chen, W.Y., Yang, Y.C., 2004. Block of tetrodotoxin-resistant Na<sup>+</sup> channel pore by multivalent cations: gating modification and Na<sup>+</sup> flow dependence. *J. Gen. Physiol.* 124, 27–42.
- Kuo, C.-C., Hess, P., 1992. A functional view of the entrances of L-type Ca<sup>2+</sup> channels: estimates of the size and surface potential at the pore mouths. *Neuron* 9, 515–526.
- Kuo, C.-C., Hess, P., 1993a. Block of the L-type Ca<sup>2+</sup> channel pore by external and internal Mg<sup>2+</sup> in rat pheochromocytoma cells. *J. Physiol. (Lond.)* 466, 683–706.
- Kuo, C.-C., Hess, P., 1993b. Characterization of the high-affinity Ca<sup>2+</sup> binding sites in the L-type Ca<sup>2+</sup> channel pore in rat pheochromocytoma cells. *J. Physiol. (Lond.)* 466, 657–682.
- Kuo, C.-C., Hess, P., 1993c. Ion permeation through the L-type Ca<sup>2+</sup> channel in rat pheochromocytoma cells: two sets of ion binding sites in the pore. *J. Physiol. (Lond.)* 466, 629–655.
- Kuo, C.-C., Yang, S., 2001. Recovery from Inactivation of T-type Ca<sup>2+</sup> channels in rat thalamic neurons. *J. Neurosci.* 21 (6), 1884–1892.
- Lacerda, A.E., Kim, H.S., Ruth, P., Perez Reyes, E., Flockerzi, V., Hofmann, F., Birnbaumer, L., Brown, A.M., 1991. Normalization of current kinetics by interaction between the alpha 1 and beta subunits of the skeletal muscle dihydropyridine-sensitive Ca<sup>2+</sup> channel. *Nature* 352, 527–530.
- Lacerda, A.E., Perez-Reyes, E., Wei, X., Castellano, A., Brown, A.M., 1994. T-type and N-type calcium channels of *Xenopus* oocytes: evidence for specific interactions with  $\beta$  subunits. *Biophys. J.* 66, 1833–1843.
- Lacinova, L., 2005. Voltage-dependent calcium channels. *Gen. Physiol. Biophys.* 24 (Suppl. 1), 1–78.
- Lacinova, L., Klugbauer, N., Hofmann, F., 1999. Absence of modulation of the expressed calcium channel alpha1G subunit by alpha2delta subunits. *J. Physiol.* 516 (Pt 3), 639–645.
- Lacinova, L., Klugbauer, N., Hofmann, F., 2000. Regulation of the calcium channel alpha(1G) subunit by divalent cations and organic blockers. *Neuropharmacology* 39, 1254–1266.
- Lambert, R.C., Maulet, Y., Mouton, J., Beattie, R., Volsen, S., De Waard, M., Feltz, A., 1997. T-type Ca<sup>2+</sup> current properties are not modified by Ca<sup>2+</sup> channel  $\beta$  subunit depletion in nodosus ganglion neurons. *J. Neurosci.* 17, 6621–6628.
- Lansman, J.B., 1990. Blockade of current through single calcium channels by trivalent lanthanide cations. Effect of ionic radius on the rates of ion entry and exit. *J. Gen. Physiol.* 95, 679–696.
- Lansman, J.B., Hess, P., Tsien, R.W., 1986. Blockade of current through single calcium channels by Cd<sup>2+</sup>, Mg<sup>2+</sup>, and Ca<sup>2+</sup>. Voltage and concentration dependence of calcium entry into the pore. *J. Gen. Physiol.* 88, 321–347.
- Lee, J.H., Daud, A.N., Cribbs, L.L., Lacerda, A.E., Pereverzev, A., Klöckner, U., Schneider, T., Perez-Reyes, E., 1999a. Cloning and expression of a novel member of the low voltage-activated T-type calcium channel family. *J. Neurosci.* 19, 1912–1921.
- Lee, J.H., Gomora, J.C., Cribbs, L.L., Perez-Reyes, E., 1999b. Nickel block of three cloned T-type calcium channels: low concentrations selectively block  $\alpha_{1H}$ . *Biophys. J.* 77, 3034–3042.
- Lee, J.M., Zipfel, G.J., Park, K.H., He, Y.Y., Hsu, C.Y., Choi, D.W., 2002. Zinc translocation accelerates infarction after mild transient focal ischemia. *Neuroscience* 115, 871–878.
- Leuranguer, V., Bourinet, E., Lory, P., Nargeot, J., 1998. Antisense depletion of  $\beta$ -subunits fails to affect T-type calcium channels properties in a neuroblastoma cell line. *Neuropharmacology* 37, 701–708.
- Li, Y., Hough, C.J., Suh, S.W., Sarvey, J.M., Frederickson, C.J., 2001. Rapid translocation of Zn(2+) from presynaptic terminals into postsynaptic hippocampal neurons after physiological stimulation. *J. Neurophysiol.* 86, 2597–2604.
- Lin, Y.J., Koretsky, A.P., 1997. Manganese ion enhances T1-weighted MRI during brain activation: an approach to direct imaging of brain function. *Magn. Reson. Med.* 38, 378–388.
- Lipkind, G.M., Fozzard, H.A., 2001. Modeling of the outer vestibule and selectivity filter of the L-type Ca<sup>2+</sup> channel. *Biochemistry* 40, 6786–6794.
- Liu, Y., Jurman, M.E., Yellen, G., 1996. Dynamic rearrangement of the outer mouth of a K<sup>+</sup> channel during gating. *Neuron* 16, 859–867.
- Linás, R., Sugimori, M., Hillman, D.E., Cherksey, B., 1992. Distribution and functional significance of the P-type, voltage-dependent Ca<sup>2+</sup> channels in the mammalian central nervous system. *Trends Neurosci.* 15, 351–355.
- Lopez-Barneo, J., Hoshi, T., Heinemann, S.H., Aldrich, R.W., 1993. Effects of external cations and mutations in the pore region on C-type inactivation of Shaker potassium channels. *Recept. Channels* 1, 61–71.
- Lopin, K.V., Gray, I.P., Obejero-Paz, C.A., Thevenod, F., Jones, S.W., 2012a. Fe(2)(+) block and permeation of Cav3.1 (alpha1G) T-type calcium channels: candidate mechanism for non-transferrin-mediated Fe(2)(+) influx. *Mol. Pharmacol.* 82, 1194–1204.
- Lopin, K.V., Obejero-Paz, C.A., Jones, S.W., 2010. Evaluation of a two-site, three-barrier model for permeation in Ca(V)3.1 (alpha1G) T-type calcium channels: Ca(2+), Ba(2+), Mg(2+), and Na(+). *J. Membr. Biol.* 235, 131–143.
- Lopin, K.V., Thevenod, F., Page, J.C., Jones, S.W., 2012b. Cd<sup>2+</sup> block and permeation of Cav3.1 (alpha1G) T-type calcium channels: candidate mechanism for Cd<sup>2+</sup> influx. *Mol. Pharmacol.* 82, 1183–1193.
- Lory, P., Varadi, G., Sligh, D.F., Varadi, M., Schwartz, A., 1993. Characterization of  $\beta$  subunit modulation of a rabbit cardiac L-type Ca<sup>2+</sup> channel  $\alpha_1$  subunit as expressed in mouse L cells. *FEBS Lett.* 315, 167–172.
- Lux, H.D., Carbone, E., Zucker, H., 1990. Na<sup>+</sup> currents through low-voltage-activated Ca<sup>2+</sup> channels of chick sensory neurones: block by external Ca<sup>2+</sup> and Mg<sup>2+</sup>. *J. Physiol. (Lond.)* 430, 159–188.



- Magee, J.C., Carruth, M., 1999. Dendritic voltage-gated ion channels regulate the action potential firing mode of hippocampal CA1 pyramidal neurons. *J. Neurophysiol.* 82, 1895–1901.
- Magee, J.C., Johnston, D., 1995. Characterization of single voltage-gated Na<sup>+</sup> and Ca<sup>2+</sup> channels in apical dendrites of rat CA1 pyramidal neurons. *J. Physiol. (Lond.)* 487, 67–90.
- Magistretti, J., Brevi, S., de Curtis, M., 2001. Ni<sup>2+</sup> slows the activation kinetics of high-voltage-activated Ca<sup>2+</sup> currents in cortical neurons: evidence for a mechanism of action independent of channel-pore block. *J. Membr. Biol.* 179, 243–262.
- Magistretti, J., Castelli, L., Taglietti, V., Tanzi, F., 2003. Dual effect of Zn<sup>2+</sup> on multiple types of voltage-dependent Ca<sup>2+</sup> currents in rat palaeocortical neurons. *Neuroscience* 117, 249–264.
- Marksteiner, R., Schurr, P., Berjukow, S., Margreiter, E., Perez-Reyes, E., Hering, S., 2001. Inactivation determinants in segment IIIIS6 of Ca<sub>v</sub>3.1. *J. Physiol. (Lond.)* 537, 27–34.
- Martin, R.B., 1988. Nickel ion binding to amino acids and peptides. In: Sigel, H. (Ed.), *Metal Ions in Biological Systems*. Vol. 23: Nickel and its Role in Biology. Marcel Dekker Inc., New York, pp. 123–164.
- Mathie, A., Sutton, G.L., Clarke, C.E., Veale, E.L., 2006. Zinc and copper: pharmacological probes and endogenous modulators of neuronal excitability. *Pharmacol. Ther.* 111, 567–583.
- McCleskey, E.W., Almers, W., 1985. The Ca channel in skeletal muscle is a large pore. *Proc. Natl. Acad. Sci. U. S. A.* 82, 7149–7153.
- McDonald, T.F., Cavalie, A., Trautwein, W., Pelzer, D., 1986. Voltage-dependent properties of macroscopic and elementary calcium channel currents in guinea pig ventricular myocytes. *Pflügers Arch.* 406, 437–448.
- McDonough, S.I., 2004. Peptide toxin inhibition of voltage gated calcium channels. In: McDonough, S.I. (Ed.), *Selectivity and Mechanisms*. Calcium Channel Pharmacology. Kluwer Academic/Plenum Publishers, New York, pp. 95–142.
- McDonough, S.I., Boland, L.M., Mintz, I.M., Bean, B.P., 2002. Interactions among toxins that inhibit N-type and P-type calcium channels. *J. Gen. Physiol.* 119, 313–328.
- McFarlane, M.B., Gilly, W.F., 1998. State-dependent nickel block of a high-voltage-activated neuronal calcium channel. *J. Neurophysiol.* 80, 1678–1685.
- McLaughlin, S., 1989. The electrostatic properties of membranes. *Annu. Rev. Biophys. Biophys. Chem.* 18, 113–136.
- Mikala, G., Bahinski, A., Yatani, A., Tang, S., Schwartz, A., 1993. Differential contribution by conserved glutamate residues to an ion-selectivity site in the L-type Ca<sup>2+</sup> channel pore. *FEBS Lett.* 335, 265–269.
- Miller, C., 1999. Perspective – ionic hopping defended. *J. Gen. Physiol.* 113, 783–787.
- Mintz, I.M., 1994. Block of Ca channels in rat central neurons by the spider toxin omega-Aga-IIIa. *J. Neurosci.* 14, 2844–2853.
- Mintz, I.M., Venema, V.J., Adams, M.E., Bean, B.P., 1991. Inhibition of N- and L-type Ca<sup>2+</sup> channels by the spider venom toxin omega-Aga-IIIa. *Proc. Natl. Acad. Sci. U. S. A.* 88, 6628–6631.
- Mironov, S.L., 1992. Conformational model for ion permeation in membrane channels: a comparison with multi-ion models and applications to calcium channel permeability. *Biophys. J.* 63, 485–496.
- Mlinar, B., Eneart, J.J., 1993. Block of current through T-type calcium channels by trivalent metal cations and nickel in neural rat and human cells. *J. Physiol.* 469, 639–652.
- Monteil, A., Chemin, J., Bourinet, E., Mennessier, G., Lory, P., Nargeot, J., 2000a. Molecular and functional properties of the human alpha(1G) subunit that forms T-type calcium channels. *J. Biol. Chem.* 275, 6090–6100.
- Monteil, A., Chemin, J., Leuranguer, V., Altier, C., Mennessier, G., Bourinet, E., Lory, P., Nargeot, J., 2000b. Specific properties of T-type calcium channels generated by the human alpha 1I subunit. *J. Biol. Chem.* 275, 16530–16535.
- Mori, Y., Friedrich, T., Kim, M.-S., Mikami, A., Nakai, J., Ruth, P., Bosse, E., Hofmann, F., Flockerzi, V., Furuichi, T., Mikoshiba, K., Imoto, K., Tanabe, T., Numa, S., 1991. Primary structure and functional expression from complementary DNA of a brain calcium channel. *Nature* 350, 398–402.
- Moss, F.J., Viard, P., Davies, A., Bertaso, F., Page, K.M., Graham, A., Cantì, C., Plumpton, M., Plumpton, C., Clare, J.J., Dolphin, A.C., 2002. The novel product of a five-exon *stargazin*-related gene abolishes Ca<sub>v</sub>2.2 calcium channel expression. *EMBO J.* 21, 1514–1523.
- Mukhtar, A., Limbeck, A., 2013. Recent developments in assessment of bio-accessible trace metal fractions in airborne particulate matter: a review. *Anal. Chim. Acta* 774, 11–25.
- Neely, A., Wei, X., Olcese, R., Birnbaumer, L., Stefani, E., 1993. Potentiation by the beta subunit of the ratio of the ionic current to the charge movement in the cardiac calcium channel. *Science* 262, 575–578.
- Nelson, M.T., 1986. Interactions of divalent cations with single calcium channels from rat brain synaptosomes. *J. Gen. Physiol.* 87, 201–222.
- Nelson, M.T., French, R.J., Krueger, B.K., 1984. Voltage-dependent calcium channels from brain incorporated into planar lipid bilayers. *Nature* 308, 77–80.
- Nelson, M.T., Joksovic, P.M., Su, P., Kang, H.W., Van Deusen, A., Baumgart, J.P., David, L.S., Snutch, T.P., Barrett, P.Q., Lee, J.H., Zorumski, C.F., Perez-Reyes, E., Todorovic, S.M., 2007a. Molecular mechanisms of subtype-specific inhibition of neuronal T-type calcium channels by ascorbate. *J. Neurosci.* 27, 12577–12583.
- Nelson, M.T., Woo, J., Kang, H.W., Vitko, I., Barrett, P.Q., Perez-Reyes, E., Lee, J.H., Shin, H.S., Todorovic, S.M., 2007b. Reducing agents sensitize C-type nociceptors by relieving high-affinity zinc inhibition of T-type calcium channels. *J. Neurosci.* 27, 8250–8260.
- Newcomb, R., Szoke, B., Palma, A., Wang, G., Chen, X.H., Hopkins, W., Cong, R., Miller, J., Urge, L., Tarczy-Hornoch, K., Loo, J.A., Dooley, D.J., Nadasdi, L., Tsien, R.W., Lemos, J., Miljanich, G., 1998. Selective peptide antagonist of the class E calcium channel from the venom of the tarantula *Hysteroecrates gigas*. *Biochemistry* 37, 15353–15362.
- Nieboer, E., 1975. The lanthanide ions as structural probes in biological and model systems. *Struct. Bond.* 22, 1–47.
- Nilsson, P., Hillered, L., Olsson, Y., Sheardown, M.J., Hansen, A.J., 1993. Regional changes in interstitial K<sup>+</sup> and Ca<sup>2+</sup> levels following cortical compression contusion trauma in rats. *J. Cereb. Blood Flow Metab.* 13, 183–192.
- Noh, J., Kim, M.K., Chung, J.M., 2010. A novel mechanism of zinc block on alpha1G-like low-threshold T-type Ca<sup>2+</sup> channels in a rat thalamic relay neuron. *Neurosci. Res.* 66, 353–358.
- Nonner, W., Catacuzzeno, L., Eisenberg, B., 2000. Binding and selectivity in L-type calcium channels: a mean spherical approximation. *Biophys. J.* 79, 1976–1992.
- Nonner, W., Chen, D.P., Eisenberg, B., 1998. Anomalous mole fraction effect, electrostatics, and binding in ionic channels. *Biophys. J.* 74, 2327–2334.
- Nosal, O.V., Lyubanova, O.P., Naidenov, V.G., Shuba, Y.M., 2013. Complex modulation of Ca(v)3.1 T-type calcium channel by nickel. *Cell. Mol. Life Sci.* 70, 1653–1661.
- Nowicky, M.C., Fox, A.P., Tsien, R.W., 1985. Three types of neuronal calcium channel with different calcium agonist sensitivity. *Nature* 316, 440–443.
- Obejero-Paz, C.A., Gray, I.P., Jones, S.W., 2004. Y<sup>3+</sup> block demonstrates an intracellular activation gate for the alpha1G T-type Ca<sup>2+</sup> channel. *J. Gen. Physiol.* 124, 631–640.
- Obejero-Paz, C.A., Gray, I.P., Jones, S.W., 2008. Ni<sup>2+</sup> block of Cav3.1 (alpha1G) T-type calcium channels. *J. Gen. Physiol.* 132 (2), 239–250.
- Ochi, R., 1970. The slow inward current and the action of manganese ions in guinea-pig's myocardium. *Pflügers Arch.* 316, 81–94.
- Ochi, R., 1975. Manganese action potentials in mammalian cardiac muscle. *Experientia* 31, 1048–1049.
- Ochi, R., 1976. Manganese-dependent propagated action potentials and their depression by electrical stimulation in guinea-pig myocardium perfused by sodium-free media. *J. Physiol.* 263, 139–156.
- Ohmori, H., Yoshii, M., 1977. Surface potential reflected in both gating and permeation mechanisms of sodium and calcium channels of the tunicate egg cell membrane. *J. Physiol.* 267, 429–463.
- Okamoto, H., Takahashi, K., Yamashita, N., 1977. Ionic currents through the membrane of the mammalian oocyte and their comparison with those in the tunicate and sea urchin. *J. Physiol.* 267, 465–495.
- Olanow, C.W., 2004. Manganese-induced parkinsonism and Parkinson's disease. *Ann. N. Y. Acad. Sci.* 1012, 209–223.
- Ong, B.H., Tomaselli, G.F., Balsler, J.R., 2000. A structural rearrangement in the sodium channel pore linked to slow inactivation and use dependence. *J. Gen. Physiol.* 116, 653–662.
- Palade, P.T., Almers, W., 1978. Slow Na and Ca currents across membrane of frog skeletal-muscle fibers. *Biophys. J.* 21, A168.
- Paoletti, P., Ascher, P., Neyton, J., 1997. High-affinity zinc inhibition of NMDA NR1–NR2A receptors. *J. Neurosci.* 17, 5711–5725.
- Parent, L., Gopalakrishnan, M., 1995. Glutamate substitution in repeat IV alters divalent and monovalent cation permeation in the heart Ca<sup>2+</sup> channel. *Biophys. J.* 69, 1801–1813.
- Parent, L., Schneider, T., Moore, C.P., Talwar, D., 1997. Subunit regulation of the human brain alpha1E calcium channel. *J. Membr. Biol.* 160, 127–140.
- Park, H.J., Park, S.J., Ahn, E.J., Lee, S.Y., Seo, H., Lee, J.H., 2013. Asp residues of the Glu-Glu-Asp-Asp pore filter contribute to ion permeation and selectivity of the Ca(v)3.2 T-type channel. *Cell Calcium* 54, 226–235.
- Pautler, R.G., Mongeau, R., Jacobs, R.E., 2003. In vivo trans-synaptic tract tracing from the murine striatum and amygdala utilizing manganese enhanced MRI (MEMRI). *Magn. Reson. Med.* 50, 33–39.
- Pei, Y., Zhao, D., Huang, J., Cao, L., 1983. Zinc-induced seizures: a new experimental model of epilepsy. *Epilepsia* 24, 169–176.
- Peitzsch, R.M., Eisenberg, M., Sharp, K.A., McLaughlin, S., 1995. Calculations of the electrostatic potential adjacent to model phospholipid bilayers. *Biophys. J.* 68, 729–738.
- Perchenet, L., Bérardeau, A., Ertel, E.A., 2000. Pharmacological properties of Ca<sub>v</sub>3.2, a low voltage-activated Ca<sup>2+</sup> channel cloned from human heart. *Naunyn-Schmiedeberg's Arch. Pharmacol.* 361, 590–599.
- Perez-Reyes, E., 2003. Molecular physiology of low-voltage-activated T-type calcium channels. *Physiol. Rev.* 83, 117–161.
- Perez-Reyes, E., 2010. Characterization of the gating brake in the I–II loop of Cav3 T-type calcium channels. *Channels (Austin)* 4, 453–458.
- Perez-Reyes, E., Cribbs, L.L., Daud, A., Lacerda, A.E., Barclay, J., Williamson, M.P., Fox, M., Rees, M., Lee, J.-H., 1998. Molecular characterization of a neuronal low voltage-activated T-type calcium channel. *Nature* 391, 896–900.
- Perez-Reyes, E., Lee, J.-H., Cribbs, L.L., 1999. Molecular characterization of two members of the T-type calcium channel family. *Ann. N. Y. Acad. Sci.* 868, 131–143.
- Planells-Cases, R., Ferrer-Montiel, A.V., Patten, C.D., Montal, M., 1995. Mutation of conserved negatively charged residues in the S2 and S3 transmembrane segments of a mammalian K<sup>+</sup> channel selectively modulates channel gating. *Proc. Natl. Acad. Sci. U. S. A.* 92, 9422–9426.
- Polo-Parada, L., Korn, S.J., 1997. Block of N-type calcium channels in chick sensory neurons by external sodium. *J. Gen. Physiol.* 109, 693–702.
- Powell, D.H., Merbach, A.E., 1994. Water exchange on the light lanthanide aqua ions [Pr(H<sub>2</sub>O)<sub>9</sub>]<sup>3+</sup> and [Nd(H<sub>2</sub>O)<sub>9</sub>]<sup>3+</sup>: a variable temperature and magnetic field <sup>17</sup>O NMR study. *Magn. Reson. Chem.* 32, 739–745.
- Pusch, M., 1990. Divalent cations as probes for structure–function relationships of cloned voltage-dependent sodium channels. *Eur. Biophys. J.* 18, 327–333.



- Pusch, M., 2006. Analysis of electrophysiological data. In: Clare, J.J., Trezise, D.J. (Eds.), *Expression and Analysis of Recombinant Ion Channels*. Wiley-VCH, Weinheim, pp. 111–144.
- Qin, N., Olcese, R., Bransby, M., Lin, T., Birnbaumer, L., 1999.  $\text{Ca}^{2+}$ -induced inhibition of the cardiac  $\text{Ca}^{2+}$  channel depends on calmodulin. *Proc. Natl. Acad. Sci. U. S. A.* 96, 2435–2438.
- Qin, N., Platano, D., Olcese, R., Costantin, J.L., Stefani, E., Birnbaumer, L., 1998. Unique regulatory properties of the type 2a  $\text{Ca}^{2+}$  channel  $\beta$  subunit caused by palmitoylation. *Proc. Natl. Acad. Sci. U. S. A.* 95, 4690–4695.
- Randall, A., Tsien, R.W., 1995. Pharmacological dissection of multiple types of  $\text{Ca}^{2+}$  channel currents in rat cerebellar granule neurons. *J. Neurosci.* 15, 2995–3012.
- Randall, A.D., Wendland, B., Schweizer, F., Miljanich, G., Adams, M.E., Tsien, R.W., 1993. Five pharmacologically distinct high voltage- $\text{Ca}^{2+}$  channels in cerebellar granule cells. *Soc. Neurosci. Abstr.* 19, 1478.
- Restituito, S., Cens, T., Barrere, C., Geib, S., Galas, S., De Waard, M., Charnet, P., 2000. The  $[\beta\text{eta}]2\alpha$  subunit is a molecular groom for the  $\text{Ca}^{2+}$  channel inactivation gate. *J. Neurosci.* 20, 9046–9052.
- Reuter, H., 1967. The dependence of slow inward current in Purkinje fibres on the extracellular calcium-concentration. *J. Physiol.* 192, 479–492.
- Reuter, H., 1979. Properties of two inward membrane currents in the heart. *Annu. Rev. Physiol.* 41, 413–424.
- Reuter, H., 1996. Diversity and function of presynaptic calcium channels in the brain. *Curr. Opin. Neurobiol.* 6, 331–337.
- Rosenberg, R.L., Chen, X.H., 1991. Characterization and localization of two ion-binding sites within the pore of cardiac L-type calcium channels. *J. Gen. Physiol.* 97, 1207–1225.
- Rosenberg, R.L., Hess, P., Tsien, R.W., 1988. Cardiac calcium channels in planar lipid bilayers. L-type channels and calcium-permeable channels open at negative membrane potentials. *J. Gen. Physiol.* 92, 27–54.
- Saimi, Y., Kung, C., 1982. Are ions involved in the gating of calcium channels? *Science* 218, 153–156.
- Santamaria, A.B., 2008. Manganese exposure, essentiality & toxicity. *Indian J. Med. Res.* 128, 484–500.
- Schneider, T., Dibué, M., Hescheler, J., 2013. How “pharmacoresistant” is Cav2.3, the major component of voltage-gated R-type  $\text{Ca}^{2+}$  channels? *Pharmaceuticals* 6, 759–776.
- Senatore, A., Zhorov, B.S., Spafford, J.D., 2012.  $\text{Ca}_v3$  T-type calcium channels. *WIREs Membr. Transp. Signal.* 1, 467–491.
- Sensi, S.L., Canzoniero, L.M., Yu, S.P., Ying, H.S., Koh, J.Y., Kerchner, G.A., Choi, D.W., 1997. Measurement of intracellular free zinc in living cortical neurons: routes of entry. *J. Neurosci.* 17, 9554–9564.
- Serrano, J.R., Dashti, S.R., Perez-Reyes, E., Jones, S.W., 2000.  $\text{Mg}(2+)$  block unmasks  $\text{Ca}(2+)/\text{Ba}(2+)$  selectivity of  $\alpha 1\text{G}$  T-type calcium channels. *Biophys. J.* 79, 3052–3062.
- Serrano, J.R., Perez-Reyes, E., Jones, S.W., 1999. State-dependent inactivation of the  $\alpha 1\text{G}$  T-type calcium channel. *J. Gen. Physiol.* 114, 185–201.
- Shannon, R.D., 1976. Revised effective ionic radii and systematic studies of interatomic distances in halides and chalcogenides. *Acta Crystallogr. Sect. A* 32, 751–767.
- Shaya, D., Findeisen, F., Abderemane-Ali, F., Arrigoni, C., Wong, S., Nurva, S.R., Loussouarn, G., Minor Jr., D.L., 2014. Structure of a prokaryotic sodium channel pore reveals essential gating elements and an outer ion binding site common to eukaryotic channels. *J. Mol. Biol.* 426, 467–483.
- Shcheglovitov, A., Kostyuk, P., Shuba, Y., 2007. Selectivity signatures of three isoforms of recombinant T-type  $\text{Ca}^{2+}$  channels. *Biochim. Biophys. Acta* 1768, 1406–1419.
- Shcheglovitov, A., Vitko, I., Lazarenko, R.M., Orestes, P., Todorovic, S.M., Perez-Reyes, E., 2012. Molecular and biophysical basis of glutamate and trace metal modulation of voltage-gated  $\text{Ca}(v)2.3$  calcium channels. *J. Gen. Physiol.* 139, 219–234.
- Shibuya, I., Douglas, W.W., 1992. Calcium channels in rat melanotrophs are permeable to manganese, cobalt, cadmium, and lanthanum, but not to nickel: evidence provided by fluorescence changes in fura-2-loaded cells. *Endocrinology* 131, 1936–1941.
- Shibuya, I., Douglas, W.W., 1993. Indications from Mn-quenching of Fura-2 fluorescence in melanotrophs that dopamine and baclofen close Ca channels that are spontaneously open but not those opened by high  $[\text{K}^+]_0$ ; and that Cd preferentially blocks the latter. *Cell Calcium* 14, 33–44.
- Shuba, Y.M., 2014. Models of calcium permeation through T-type channels. *Pflügers Arch.* 466, 635–644.
- Shuba, Y.M., Teslenko, V.I., Savchenko, A.N., Pogorelaya, N.H., 1991. The effect of permanent ions on single calcium channel activation in mouse neuroblastoma cells: ion-channel interaction. *J. Physiol. (Lond.)* 443, 25–44.
- Siesjo, B.K., 1982. Lactic acidosis in the brain: occurrence, triggering mechanisms and pathophysiological importance. *Ciba Found. Symp.* 87, 77–100.
- Siesjo, B.K., von Hanwehr, R., Nergelius, G., Nevander, G., Ingvar, M., 1985. Extra- and intracellular pH in the brain during seizures and in the recovery period following the arrest of seizure activity. *J. Cereb. Blood Flow Metab.* 5, 47–57.
- Sigworth, F.J., Spalding, B.C., 1980. Chemical modification reduces the conductance of sodium channels in nerve. *Nature* 283, 293–295.
- Simms, B.A., Zamponi, G.W., 2014. Neuronal voltage-gated calcium channels: structure, function, and dysfunction. *Neuron* 82, 24–45.
- Singer, D., Biel, M., Lotan, I., Flockerzi, V., Hofmann, F., Dascal, N., 1991. The roles of the subunits in the function of the calcium channel. *Science* 253, 1553–1557.
- Singer-Lahat, D., Lotan, I., Itagaki, K., Schwartz, A., Dascal, N., 1992. Evidence for the existence of RNA of  $\text{Ca}^{2+}$  channel  $\alpha 2\delta$  subunit in *Xenopus* oocytes. *Biochim. Biophys. Acta Mol. Cell Res.* 1137, 39–44.
- Smith, P.A., Ashcroft, F.M., Fewtrell, C.M.S., 1993. Permeation and gating properties of the L-type calcium channel in mouse pancreatic  $\beta$  cells. *J. Gen. Physiol.* 101, 767–797.
- Snutch, T.P., Leonard, J.P., Gilbert, M.M., Lester, H.A., Davidson, N., 1990. Rat brain expresses a heterogeneous family of calcium channels. *Proc. Natl. Acad. Sci. U. S. A.* 87, 3391–3395.
- Snutch, T.P., Pelouquin, J., Mathews, E., McRory, J.E., 2005. Molecular properties of voltage-gated calcium channels. In: Zamponi, G.W. (Ed.), *Voltage-Gated Calcium Channels*. Landes Bioscience, Georgetown, TX, pp. 61–79.
- Snutch, T.P., Reiner, P.B., 1992.  $\text{Ca}^{2+}$  channels: diversity of form and function. *Curr. Opin. Neurobiol.* 2, 247–253.
- Sochivko, D., Pereverzev, A., Smyth, N., Gissel, C., Schneider, T., Beck, H., 2002. The  $\alpha 1\text{E}$  calcium channel subunit underlies R-type calcium current in hippocampal and cortical pyramidal neurons. *J. Physiol.* 542, 699–710.
- Soldatov, N.M., Bouron, A., Reuter, H., 1995. Different voltage-dependent inhibition by dihydropyridines of human  $\text{Ca}^{2+}$  channel splice variants. *J. Biol. Chem.* 270, 10540–10543.
- Southwood-Jones, R.V., Earl, W.L., Newman, K.E., Merbach, A.E., 1980. Oxygen-17 NMR and EPR studies of water exchange from the first coordination sphere of gadolinium(III) aquoion and gadolinium(III) propylenediaminetetra-acetate. *J. Chem. Phys.* 73, 5909.
- Stea, A., Dubel, S.J., Pragnell, M., Leonard, J.P., Campbell, K.P., Snutch, T.P., 1993. A  $\beta$ -subunit normalizes the electrophysiological properties of a cloned N-type  $\text{Ca}^{2+}$  channel  $\alpha 1$ -subunit. *Neuropharmacology* 32, 1103–1116.
- Stotz, s.c., Hamid, J., Spaetgens, R.L., Jarvis, S.E., Zamponi, G.W., 2000. Fast inactivation of voltage-dependent calcium channels. A hinged-lid mechanism? *J. Biol. Chem.* 275, 24575–24582.
- Stotz, S.C., Jarvis, S.E., Zamponi, G.W., 2004. Functional roles of cytoplasmic loops and pore lining transmembrane helices in the voltage-dependent inactivation of HVA calcium channels. *J. Physiol.* 554, 263–273.
- Stotz, S.C., Zamponi, G.W., 2001. Structural determinants of fast inactivation of high voltage-activated  $\text{Ca}^{2+}$  channels. *Trends Neurosci.* 24, 176–181.
- Striessnig, J., Koschak, A., 2008. Exploring the function and pharmacotherapeutic potential of voltage-gated  $\text{Ca}^{2+}$  channels with gene knockout models. *Channels (Austin)* 2, 233–251.
- Suh, S.W., Chen, J.W., Motamedi, M., Bell, B., Listiak, K., Pons, N.F., Danscher, G., Frederickson, C.J., 2000. Evidence that synaptically-released zinc contributes to neuronal injury after traumatic brain injury. *Brain Res.* 852, 268–273.
- Sun, H.S., Hui, K., Lee, D.W., Feng, Z.P., 2007.  $\text{Zn}^{2+}$  sensitivity of high- and low-voltage activated calcium channels. *Biophys. J.* 93, 1175–1183.
- Swandulla, D., Armstrong, C.M., 1989. Calcium channel block by cadmium in chicken sensory neurons. *Proc. Natl. Acad. Sci. U. S. A.* 86, 1736–1740.
- Takeda, A., Hirate, M., Tamano, H., Nisibaba, D., Oku, N., 2003a. Susceptibility to kainate-induced seizures under dietary zinc deficiency. *J. Neurochem.* 85, 1575–1580.
- Takeda, A., Hirate, M., Tamano, H., Oku, N., 2003b. Release of glutamate and GABA in the hippocampus under zinc deficiency. *J. Neurosci. Res.* 72, 537–542.
- Takeda, A., Tamano, H., Nagayoshi, A., Yamada, K., Oku, N., 2005. Increase in hippocampal cell death after treatment with kainate in zinc deficiency. *Neurochem. Int.* 47, 539–544.
- Talavera, K., Janssens, A., Klugbauer, N., Droogmans, G., Nilius, B., 2003. Pore structure influences gating properties of the T-type  $\text{Ca}^{2+}$  channel  $\alpha 1\text{G}$ . *J. Gen. Physiol.* 121, 529–540.
- Talavera, K., Nilius, B., 2006a. Biophysics and structure-function relationship of T-type  $\text{Ca}^{2+}$  channels. *Cell Calcium* 40, 97–114.
- Talavera, K., Nilius, B., 2006b. Evidence for common structural determinants of activation and inactivation in T-type  $\text{Ca}^{2+}$  channels. *Pflügers Arch.* 453, 189–201.
- Talavera, K., Staes, M., Janssens, A., Klugbauer, N., Droogmans, G., Hofmann, F., Nilius, B., 2001. Aspartate residues of the Glu-Glu-Asp-Asp (EEDD) pore locus control selectivity and permeation of the T-type  $\text{Ca}^{2+}$  channel  $\alpha 1\text{G}$ . *J. Biol. Chem.* 276, 45628–45635.
- Taleb, O., Trouslard, J., Demeneix, B.A., Feltz, P., 1986. Characterization of calcium and sodium currents in porcine pars intermedia cells. *Neurosci. Lett.* 66, 55–60.
- Tanabe, T., Takeshima, H., Mikami, A., Flockerzi, V., Takahashi, H., Kangawa, K., Kojima, M., Matsuo, H., Hirose, T., Numa, S., 1987. Primary structure of the receptor for calcium channel blockers from skeletal muscle. *Nature* 328, 313–318.
- Tang, L., Gamal El-Din, T.M., Payandeh, J., Martinez, G.Q., Heard, T.M., Scheuer, T., Zheng, N., Catterall, W.A., 2014. Structural basis for Ca selectivity of a voltage-gated calcium channel. *Nature* 500, 56–61.
- Tang, S., Mikala, G., Bahinski, A., Yatani, A., Varadi, G., Schwartz, A., 1993. Molecular localization of ion selectivity sites within the pore of a human L-type cardiac calcium channel. *J. Biol. Chem.* 268, 13026–13029.
- Tareilus, E., Roux, M., Qin, N., Olcese, R., Zhou, J.M., Stefani, E., Birnbaumer, L., 1997. A *Xenopus* oocyte  $\beta$  subunit: evidence for a role in the assembly/expression of voltage-gated calcium channels that is separate from its role as a regulatory subunit. *Proc. Natl. Acad. Sci. U. S. A.* 94, 1703–1708.
- Taylor, W.R., 1988. Permeation of barium and cadmium through slowly inactivating calcium channels in cat sensory neurons. *J. Physiol.* 407, 433–452.
- Thevenod, F., Jones, S.W., 1992. Cadmium block of calcium current in frog sympathetic neurons. *Biophys. J.* 63, 162–168.
- Thio, L.L., Zhang, H.X., 2006. Modulation of inhibitory glycine receptors in cultured embryonic mouse hippocampal neurons by zinc, thiol containing redox agents and carnosine. *Neuroscience* 139, 1315–1327.

- Tikhonov, D.B., Magazanik, L.G., 1998. Voltage dependence of open channel blockade: onset and offset rates. *J. Membr. Biol.* 161, 1–8.
- Tiwari-Woodruff, S.K., Schulteis, C.T., Mock, A.F., Papazian, D.M., 1997. Electrostatic interactions between transmembrane segments mediate folding of Shaker K<sup>+</sup> channel subunits. *Biophys. J.* 72, 1489–1500.
- Traboulsi, A., Chemin, J., Chevalier, M., Quignard, J.F., Nargeot, J., Lory, P., 2007. Subunit-specific modulation of T-type calcium channels by zinc. *J. Physiol.* 578, 159–171.
- Triggle, C.R., Triggle, D.J., 1976. An analysis of the action of cations of the lanthanide series on the mechanical responses of guinea-pig ileal longitudinal muscle. *J. Physiol.* 254, 39–54.
- Triggle, D.J., 2004. Pharmacology of Cav1 (L-type) channels. In: McDonough, S.I. (Ed.), *Calcium Channel Pharmacology*. Kluwer Academic/Plenum Publishers, New York, pp. 21–72.
- Tsien, R.W., Fox, A.P., Hess, P., McCleskey, E.W., Nilius, B., Nowycky, M.C., Rosenberg, R.L., 1987. Multiple types of calcium channel in excitable cells. *Soc. Gen. Physiol. Ser.* 41, 167–187.
- Ueno, S., Tsukamoto, M., Hirano, T., Kikuchi, K., Yamada, M.K., Nishiyama, N., Nagano, T., Matsuki, N., Ikegaya, Y., 2002. Mossy fiber Zn<sup>2+</sup> spillover modulates heterosynaptic N-methyl-D-aspartate receptor activity in hippocampal CA3 circuits. *J. Cell Biol.* 158, 215–220.
- von Hanwehr, R., Smith, M.L., Siesjö, B.K., 1986. Extra- and intracellular pH during near-complete forebrain ischemia in the rat. *J. Neurochem.* 46, 331–339.
- Walker, D., Bichet, D., Campbell, K.P., De Waard, M., 1998. A  $\beta_4$  isoform-specific interaction site in the carboxyl-terminal region of the voltage-dependent Ca<sup>2+</sup> channel  $\alpha_{1A}$  subunit. *J. Biol. Chem.* 273, 2361–2367.
- Walker, D., Bichet, D., Geib, S., Mori, E., Cornet, V., Snutch, T.P., Mori, Y., De Waard, M., 1999. A new  $\beta$  subtype-specific interaction in  $\alpha_{1A}$  subunit controls P/Q-type Ca<sup>2+</sup> channel activation. *J. Biol. Chem.* 274, 12383–12390.
- Warre, R., Randall, A., 2000. Modulation of the deactivation kinetics of a recombinant rat T-type Ca<sup>2+</sup> channel by prior inactivation. *Neurosci. Lett.* 293, 216–220.
- Wei, X.Y., Pan, S., Lang, W.H., Kim, H.Y., Schneider, T., Perez-Reyes, E., Birnbaumer, L., 1995. Molecular determinants of cardiac Ca<sup>2+</sup> channel pharmacology – subunit requirement for the high affinity and allosteric regulation of dihydropyridine binding. *J. Biol. Chem.* 270, 27106–27111.
- Weiergräber, M., Kamp, M.A., Radhakrishnan, K., Hescheler, J., Schneider, T., 2006. The Ca<sub>v</sub>2.3 voltage-gated calcium channel in epileptogenesis. Shedding new light on an enigmatic channel. *Neurosci. Biobehav. Rev.* 30, 1122–1144.
- Weiss, J.H., Hartley, D.M., Koh, J.Y., Choi, D.W., 1993. AMPA receptor activation potentiates zinc neurotoxicity. *Neuron* 10, 43–49.
- Weiss, J.H., Sensi, S.L., Koh, J.Y., 2000. Zn(2+): a novel ionic mediator of neural injury in brain disease. *Trends Pharmacol. Sci.* 21, 395–401.
- Welling, A., Kwan, Y.W., Bosse, E., Flockerzi, V., Hofmann, F., Kass, R.S., 1993. Subunit-dependent modulation of recombinant L-type calcium channels: molecular basis for dihydropyridine tissue selectivity. *Circ. Res.* 73, 974–980.
- Williams, M.E., Marubio, L.M., Deal, C.R., Hans, M., Brust, P.F., Philipson, L.H., Miller, R.J., Johnson, E.C., Harpold, M.M., Ellis, S.B., 1994. Structure and functional characterization of neuronal  $\alpha_{1E}$  calcium channel subtypes. *J. Biol. Chem.* 269, 22347–22357.
- Williams, M.E., Washburn, M.S., Hans, M., Urrutia, A., Brust, P.F., Prodanovich, P., Harpold, M.M., Stauderman, K.A., 1999. Structure and functional characterization of a novel human low-voltage activated calcium channel. *J. Neurochem.* 72, 791–799.
- Williams, P.J., MacVicar, B.A., Pittman, Q.J., 1990. Electrophysiological properties of neuroendocrine cells of the intact rat pars intermedia: multiple calcium currents. *J. Neurosci.* 10, 748–756.
- Williamson, A.V., Sather, W.A., 1999. Nonglutamate pore residues in ion selection and conduction in voltage-gated Ca<sup>2+</sup> channels. *Biophys. J.* 77, 2575–2589.
- Wilson, D.L., Morimoto, K., Tsuda, Y., Brown, A.M., 1983. Interaction between calcium ions and surface charge as it relates to calcium currents. *J. Membr. Biol.* 72, 117–130.
- Wilson, S.M., Toth, P.T., Oh, S.B., Gillard, S.E., Volsen, S., Ren, D., Philipson, L.H., Lee, E.C., Fletcher, C.F., Tessarollo, L., Copeland, N.G., Jenkins, N.A., Miller, R.J., 2000. The status of voltage-dependent calcium channels in alpha1E knock-out mice. *J. Neurosci.* 20, 8566–8571.
- Winegar, B.D., Kelly, R., Lansman, J.B., 1991. Block of current through single calcium channels by Fe, Co, and Ni. Location of the transition metal binding site in the pore. *J. Gen. Physiol.* 97, 351–367.
- Winegar, B.D., Lansman, J.B., 1990. Voltage-dependent block by zinc of single calcium channels in mouse myotubes. *J. Physiol.* 425, 563–578.
- Woodhull, A.M., 1973. Ionic blockage of sodium channels in nerve. *J. Gen. Physiol.* 61, 687–708.
- Worley III, J.F., French, R.J., Pailthorpe, B.A., Krueger, B.K., 1992. Lipid surface charge does not influence conductance or calcium block of single sodium channels in planar bilayers. *Biophys. J.* 61, 1353–1363.
- Wyatt, C.N., Page, K.M., Berrow, N.S., Brice, N.L., Dolphin, A.C., 1998. The effect of overexpression of auxiliary Ca<sup>2+</sup> channel subunits on native Ca<sup>2+</sup> channel currents in undifferentiated mammalian NG108-15 cells. *J. Physiol. (Lond.)* 510, 347–360.
- Xie, X., Gerber, U., Gahwiler, B.H., Smart, T.G., 1993. Interaction of zinc with ionotropic and metabotropic glutamate receptors in rat hippocampal slices. *Neurosci. Lett.* 159, 46–50.
- Xie, X., Smart, T.G., 1993a. Giant GABAB-mediated synaptic potentials induced by zinc in the rat hippocampus: paradoxical effects of zinc on the GABAB receptor. *Eur. J. Neurosci.* 5, 430–436.
- Xie, X., Smart, T.G., 1993b. Properties of GABA-mediated synaptic potentials induced by zinc in adult rat hippocampal pyramidal neurones. *J. Physiol.* 460, 503–523.
- Xie, X., Smart, T.G., 1994. Modulation of long-term potentiation in rat hippocampal pyramidal neurons by zinc. *Pflügers Arch.* 427, 481–486.
- Xiong, W., Li, R.A., Tian, Y., Tomaselli, G.F., 2003. Molecular motions of the outer ring of charge of the sodium channel: do they couple to slow inactivation? *J. Gen. Physiol.* 122, 323–332.
- Yamagishi, S., 1973. Manganese-dependent action potentials in intracellularly perfused squid giant axons. *Proc. Jpn. Acad.* 49, 218–222.
- Yamashita, N., Ciani, S., Hagiwara, S., 1990. Effects of internal Na<sup>+</sup> on the Ca channel outward current in mouse neoplastic B lymphocytes. *J. Gen. Physiol.* 96, 559–579.
- Yang, J., Ellinor, P.T., Sather, W.A., Zhang, J.F., Tsien, R.W., 1993. Molecular determinants of Ca<sup>2+</sup> selectivity and ion permeation in L-type Ca<sup>2+</sup> channels. *Nature* 366, 158–161.
- Yasuda, R., Sabatini, B.L., Svoboda, K., 2003. Plasticity of calcium channels in dendritic spines. *Nat. Neurosci.* 6, 948–955.
- Yatani, A., Bahinski, A., Mikala, G., Yamamoto, S., Schwartz, A., 1994. Single amino acid substitutions within the ion permeation pathway alter single-channel conductance of the human L-type cardiac Ca<sup>2+</sup> channel. *Circ. Res.* 75, 315–323.
- Yokoyama, C.T., Westenbroek, R.E., Hell, J.W., Soong, T.W., Snutch, T.P., Catterall, W.A., 1995. Biochemical properties and subcellular distribution of the neuronal class E calcium channel  $\alpha_1$  subunit. *J. Neurosci.* 15, 6419–6432.
- Yokoyama, M., Koh, J., Choi, D.W., 1986. Brief exposure to zinc is toxic to cortical neurons. *Neurosci. Lett.* 71, 351–355.
- Yu, F.H., Catterall, W.A., 2004. The VGL-chonome: a protein superfamily specialized for electrical signaling and ionic homeostasis. *Sci. STKE* 2004, re15.
- Yu, X., Zou, J., Babb, J.S., Johnson, G., Sanes, D.H., Turnbull, D.H., 2008. Statistical mapping of sound-evoked activity in the mouse auditory midbrain using Mn-enhanced MRI. *Neuroimage* 39, 223–230.
- Zamponi, G.W., Bourinet, E., Snutch, T.P., 1996. Nickel block of a family of neuronal calcium channels: subtype- and subunit-dependent action at multiple sites. *J. Membr. Biol.* 151, 77–90.
- Zamponi, G.W., Snutch, T.P., 1996. Evidence for a specific site for modulation of calcium channel activation by external calcium ions. *Eur. J. Physiol.* 431, 470–472.
- Zhen, X.G., Xie, C., Fitzmaurice, A., Schoonover, C.E., Orenstein, E.T., Yang, J., 2005. Functional architecture of the inner pore of a voltage-gated Ca<sup>2+</sup> channel. *J. Gen. Physiol.* 126, 193–204.
- Zhou, W., Jones, S.W., 1995. Surface charge and calcium channel saturation in bullfrog sympathetic neurons. *J. Gen. Physiol.* 105, 441–462.
- Zong, S., Zhou, J., Tanabe, T., 1994. Molecular determinants of calcium-dependent inactivation in cardiac L-type calcium channels. *Biochem. Biophys. Res. Commun.* 201, 1117–1123.
- Zühlke, R.D., Reuter, H., 1998. Ca<sup>2+</sup>-sensitive inactivation of L-type Ca<sup>2+</sup> channels depends on multiple cytoplasmic amino acid sequences of the  $\alpha_{1C}$  subunit. *Proc. Natl. Acad. Sci. U. S. A.* 95, 3287–3294.

## 2.2. Publication 2: Acta Physiologica 222(3): e12988.

### A practical guide to the preparation and use of metal ion-buffered systems for physiological research.

Felix Neumaier, Serdar Alpdogan, Jürgen Hescheler, Toni Schneider

#### **Abstract:**

Recent recognition that mobile pools of  $Zn^{2+}$  and  $Cu^{2+}$  are involved in the regulation of neuronal, endocrine and other cells has stimulated the development of tools to visualize and quantify the level of free trace metal ions. Most of the methods used to measure or control loosely bound metals require reference media that contain exactly defined free concentrations of the target ions. Despite the central importance of proper metal ion buffering, there is still a lack of international standards and beginners in the field may have difficulties finding a coherent description of how to prepare trace metal ion buffers, especially when experiments are to be performed in multimetal systems. To close this gap, we provide a guide for the design, preparation and use of metal ion buffered systems that facilitate immediate application under physiologically relevant ionic conditions. Thermodynamic and kinetic concepts of chemical speciation as well as general protocols and specific examples are outlined for the accurate preparation of single- and dual-metal ion buffers. In addition, experiments have been performed with FluoZin-3 to illustrate that metal ion-buffered systems are required for reliable preparation of nanomolar  $Zn^{2+}$  solutions and that dual-metal ion buffers can be used to calibrate suitable fluorescent  $Zn^{2+}$  sensors in the presence of millimolar  $Ca^{2+}$  concentrations. Together, the information provided should sensitize readers to the many potential pitfalls and uncertainties that exist when working with physiologically relevant concentrations of trace metal ions and enable them to formulate their own metal ion buffers for most *in vitro* applications.

#### **Contributions to Publication 2:**

I independently reviewed the literature and conceptualized the article, developed the protocols and performed the experiments with FluoZin-3, created all tables and figures, wrote the manuscript and handled the submission and revision process.



## REVIEW

# A practical guide to the preparation and use of metal ion-buffered systems for physiological research

F. Neumaier  | S. Alpdogan | J. Hescheler | T. Schneider

Institute for Neurophysiology, University of Cologne, Cologne, Germany

**Correspondence**

F. Neumaier, Institute of Neurophysiology, University of Cologne, Cologne, Germany.  
Email: felix@neumaier-net.de

**Funding information**

This work was financially supported by the Deutsche Forschungsgemeinschaft (DFG, SCHN 387/21-1).

**Abstract**

Recent recognition that mobile pools of  $Zn^{2+}$  and  $Cu^{2+}$  are involved in the regulation of neuronal, endocrine and other cells has stimulated the development of tools to visualize and quantify the level of free trace metal ions. Most of the methods used to measure or control loosely bound metals require reference media that contain exactly defined free concentrations of the target ions. Despite the central importance of proper metal ion buffering, there is still a lack of international standards and beginners in the field may have difficulties finding a coherent description of how to prepare trace metal ion buffers, especially when experiments are to be performed in multimetal systems. To close this gap, we provide a guide for the design, preparation and use of metal ion-buffered systems that facilitate immediate application under physiologically relevant ionic conditions. Thermodynamic and kinetic concepts of chemical speciation as well as general protocols and specific examples are outlined for the accurate preparation of single- and dual-metal ion buffers. In addition, experiments have been performed with FluoZin-3 to illustrate that metal ion-buffered systems are required for reliable preparation of nanomolar  $Zn^{2+}$  solutions and that dual-metal ion buffers can be used to calibrate suitable fluorescent  $Zn^{2+}$  sensors in the presence of millimolar  $Ca^{2+}$  concentrations. Together, the information provided should sensitize readers to the many potential pitfalls and uncertainties that exist when working with physiologically relevant concentrations of trace metal ions and enable them to formulate their own metal ion buffers for most in vitro applications.

**KEYWORDS**

endogenous mobile zinc and copper pools, fluorescent detection of trace metals, loosely bound or free trace metals, polyaminopolycarboxylate chelator, thermodynamic stability constants, tricine

## 1 | INTRODUCTION

It is increasingly recognized that pools of loosely bound zinc ( $Zn^{2+}$ ) and copper ( $Cu^{2+}$ ) ions exist in the brain, which have been implicated in synaptic transmission and linked to several pathophysiological conditions. These and other findings have led to an impressive growth in attention and stimulated the development of new tools for studying

trace metal biology. Physiologically relevant concentrations of loosely bound metal ions span several orders of magnitude. They range from less than one  $Cu^{2+}$  molecule per cell<sup>1</sup> and picomolar  $Zn^{2+}$  in the intracellular compartment<sup>2,3</sup> to nanomolar extracellular levels, which may transiently rise to (high) micromolar concentrations.<sup>4,5</sup> This wide range of very low concentrations provides many sources of potential error and necessitates the use of



suitable metal ion buffers. For example, most methods used to measure or control the level of a given trace metal require reference media that contain exactly defined free concentrations of this ion. The central importance of proper metal ion buffering is well established, but there is still a lack of international standards for physiological  $\text{Zn}^{2+}$ ,  $\text{Cu}^{2+}$  and other metal ions,<sup>6,7</sup> such as are available for calibration of pH electrodes.<sup>8</sup> Moreover, while buffers containing specified free  $\text{Ca}^{2+}$  levels based on calculated values are available from several suppliers, the preparation of trace metal ion buffers is still much more empirically. Unfortunately, beginners in the field may have difficulties finding a coherent description of how to prepare trace metal ion buffers themselves, especially when experiments are to be performed in the presence of other divalent cations. As a consequence, many of the solutions reported in the literature are not adequately buffered, and significant differences may exist between assumed and actual free metal ion concentrations.<sup>9</sup> Aim of this article is to provide an introduction into the theory and practice of trace metal ion buffering, with a focus on the physiologically relevant range of free  $\text{Zn}^{2+}$  and  $\text{Cu}^{2+}$  concentrations. Particular emphasis is placed on the preparation and use of dual-metal ion buffers, which allow for the control of free  $\text{Zn}^{2+}$  or  $\text{Cu}^{2+}$  at a fixed concentration of  $\text{Ca}^{2+}$  or  $\text{Mg}^{2+}$ . To this end, section 2 will briefly familiarize the reader with the concept of metal ion buffering, summarize the general requirements for construction of well-defined buffer systems, and discuss problems associated with the calculation of free metal ion concentrations and with the lack of a simple method for their verification. The third section deals with practical aspects, such as the choice of reagents and labware or general sample handling techniques, and provides a step-by-step guide on the preparation of single- and dual-metal ion buffers with minimal experimental uncertainty. Calibration of the fluorescent probe FluoZin-3 with nanomolar  $\text{Zn}^{2+}$  in the presence of millimolar  $\text{Ca}^{2+}$  concentrations is used to exemplify both the application of dual-metal ion buffers and the consequences of improper trace metal ion buffering.

## 2 | THEORY OF TRACE METAL ION BUFFERING

A thorough understanding of chemical speciation is crucial for all experiments involving physiologically relevant free trace metal concentrations, but the complexity of the topic prevents an exhaustive treatment in this article. Instead, we will provide a brief introduction into the topic and then focus on aspects relevant for the design of metal ion-buffered systems and for estimation of free metal ion concentrations in complex solutions.

### 2.1 | Chemical speciation and metal ion buffering

In complex media such as cytoplasm or extracellular fluid, trace metals become bound by a range of ligands, which include inorganic anions, small organic molecules like amino acids and large biomolecules like proteins. As some of them bind metal ions very tightly, the amount that remains thermodynamically and kinetically accessible (ie the free or loosely bound pool) can be orders of magnitude below the total concentration. The biological effects of metal ions are thus greatly affected by their chemical speciation, which is defined to be the distribution among all possible (free and ligand-bound) species in solution. Even under more defined conditions, like in artificial saline solutions, free metal ion concentrations can markedly deviate from the nominal concentration. This is because at physiologically relevant (ie pico- to micromolar) concentrations, processes like metal ion hydrolysis, surface adsorption or binding by buffer constituents may significantly influence the free metal ion concentration.<sup>10</sup> To circumvent this problem and to reduce the impact of contamination with unwanted metal ions, free  $\text{Zn}^{2+}$  and  $\text{Cu}^{2+}$  concentrations should be buffered with appropriate trace metal chelators. By providing a reservoir of metal complex to replenish ions that have been removed from the system, these ligands can effectively maintain free metal ion concentrations at a constant level. Numerous naturally occurring or synthetic molecules can act as ligands, and there is extensive literature on metal ion-ligand interactions. To be useful for metal buffering, a chelator should be well-characterized in terms of its binding properties, exhibit sufficient specificity for the cation to be buffered and sufficient buffering capacity for the desired concentration range. Additional considerations that are of importance when working in biological systems are chelator mobility across the cell membrane and possible effects not related to metal-ion buffering. Lipophilic chelators (like TPEN, cupral or dithizone) and ionophores (like pyrithione) should generally be avoided, as they can cross the membrane and interfere with intracellular trace metal homeostasis. The same applies to certain naturally occurring ligands like citrate, which may exert metal ion buffering-independent effects.<sup>11</sup> Most of the chelators useful for biological research belong to the group of glycine-derived polyaminopolycarboxylates (PAPCs). Thanks to their relevance for a wide variety of environmental, chemical and medical applications, numerous PAPC ligands have been described and there is a large literature on the topic. Here, we will focus on ethylenediaminetetraacetic acid (EDTA), ethyleneglycol-bis(aminoethylether)-N,N,N',N'-tetraacetic acid (EGTA) and N-(2-hydroxyethyl) ethylenediamine-N,N',N'-triacetic acid (HEDTA), three of the most widely used PAPCs which have been extensively

**TABLE 1** Protonation constants for selected trace metal chelators

Protonation constants $H_x$ (at 20°C & $I = 0.1$ mol/L) and enthalpy values $\Delta H_x$ [kcal/mol]								
	$H_1$	$ \Delta H_1$	$H_2$	$ \Delta H_2$	$H_3$	$ \Delta H_3$	$H_4$	$ \Delta H_4$
EDTA <sup>13</sup>	10.3	-5.6	6.2	-4.2	2.7	1.5	2.0	0.3
EGTA <sup>13</sup>	9.5	-5.9	8.9	-5.8	2.7	-2.6	1.9	-0.4
HEDTA <sup>13</sup>	9.9	-6.6	5.4	-3.1	2.6	1.1		
Tricine <sup>98</sup>	8.0	7.6	2.4	1.4				

characterized in terms of their protonation (Table 1) and metal-binding constants (Table 2). They are representative for most other members of the group in that their anion species act as strong hexadentate ligands for  $Zn^{2+}$  or  $Cu^{2+}$ , giving rise to 1:1 molar complexes where the metal ion is coordinated by six donor groups of the chelator (Figure 1A). Ligands of lower denticity (ie with less donor groups), such as the closely related

**TABLE 2** Stability constants for selected 1:1 metal ion-ligand complexes

Stability constants $\log K_{ML}$ (at 20°C at $I = 0.1$ mol/L) and enthalpy values $\Delta H_x$ [kcal/mol]								
	$Ca^{2+}$	$ \Delta H$	$Mg^{2+}$	$ \Delta H$	$Zn^{2+}$	$ \Delta H$	$Cu^{2+}$	$ \Delta H$
EDTA <sup>13</sup>	10.7	-6.1	8.7	3.4	16.6	-4.7	18.9	-8.2
EGTA <sup>13</sup>	10.9	-8.4	5.2	5.2	12.7	-4.3	17.8	-11.0
HEDTA <sup>13</sup>	8.2	-6.5	6.9	3.4	14.7	-8.4	17.5	-9.4
Tricine <sup>99,100</sup>	2.4	n.a.	1.2	n.a.	5.2	-7.9	7.8	-9.8

(monoaminopolycarboxylic) nitrilotriacetic acid (NTA), can interact with metal ions in multiple stoichiometries (ie multiple ligand molecules can bind to a single metal ion). The same applies to N-[tris(hydroxymethyl)methyl] glycine (tricine), a glycine-derived zwitterionic proton buffer and tridentate ligand for  $Zn^{2+}$  and  $Cu^{2+}$  (Figure 1B), which exhibits very low affinity for  $Ca^{2+}$  and  $Mg^{2+}$ . As described in more detail in sections 2.2 through 2.4, binding in multiple stoichiometries can complicate speciation modelling and the construction of well-defined buffer systems.<sup>12</sup> Depending on the cations present, use of tricine-based buffers can be further complicated by the lack of comprehensive thermodynamic and/or kinetic data on its metal ion binding properties (but see section 2.4). As it remains one of the few compounds that can effectively maintain nano- to micromolar free  $Zn^{2+}$  and  $Cu^{2+}$  concentrations in the presence of physiological  $Ca^{2+}$  or  $Mg^{2+}$  levels however, tricine has been widely used for  $Zn^{2+}$  and  $Cu^{2+}$  buffering in biological systems and will be discussed in this article as well.

## 2.2 | Estimation of free metal ion concentrations

The chemical equilibria between ligands (L), metal ions (M) and the corresponding metal complexes (ML) can be described in terms of thermodynamic stability constants (Figure 2). They provide a measure for the strength of metal ion-ligand interactions and can be used to estimate

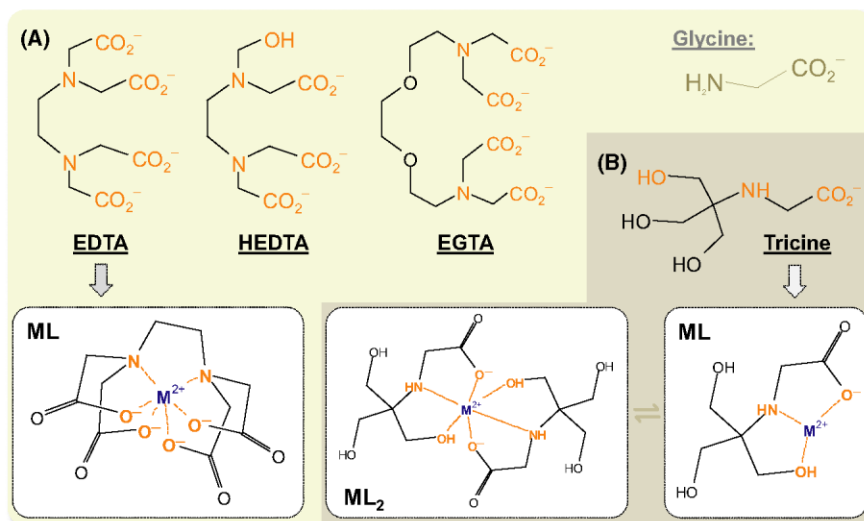


**FIGURE 1** Structure of glycine-derived trace metal chelators and some of their metal complexes. A, The deprotonated species of polyaminopolycarboxylic acids like EDTA are strong hexadentate ligands for  $Zn^{2+}$ ,  $Cu^{2+}$  and most other divalent cations. Because all amino and carboxylate donor groups (indicated in orange) are coordinated to the metal ion, these ligands form very stable 1:1 complexes, in which the metal is surrounded by a total of five chelate rings. B, The zwitterionic proton buffer tricine acts as a lower affinity tridentate ligand for  $Zn^{2+}$  and  $Cu^{2+}$  that can form both 1:1 and 1:2 metal ion-ligand complexes containing two or four chelate rings respectively

the composition of a system at equilibrium. Published constants have been determined at specific conditions for temperature and ionic strength (usually 20-25°C and  $I = 0.1$  mol/L) and are typically expressed on a log scale, where one unit change corresponds to a 10-fold change in the respective constant. A number of critically evaluated compilations (like the NIST,<sup>13</sup> IUPAC<sup>14</sup> or JESS<sup>15</sup> stability constant databases, reviewed in detail in<sup>16,17</sup>) are available, which provide access to internally consistent sets of thermodynamic constants for thousands of metal ion-ligand reactions. To account for differences in the experimental conditions, they can be converted to apparent or conditional constants, provided that the molar enthalpy changes for the reactions are known (for temperature correction) and non-thermodynamic assumptions are used to calculate the relevant single ion activity coefficients (for ionic strength correction). In principle, conditional constants can be used to solve, by manual (algebraic) techniques, the complexation equilibria in simple systems.<sup>12</sup> As illustrated in Figure 2 however, additional reactions must usually be taken into account. When protonated forms of the ligand ( $H_xL$ ) do not significantly contribute to complex formation (ie if there is competition for binding between metal ions

and protons), the fraction of chelator species able to form the complex is a function of proton concentration (ie pH) and of the corresponding protonation constants (Figure 2A). Depending on the exact chelator(s) and metal ion(s) present, further reactions may take place, which can include (i) interaction of metal ions with some of the protonated forms of the ligand or of complexes with protons (ie formation of protonated complexes like MHL in Figure 2B1), (ii) interaction of metal ions or complexes with hydroxide ions or of metal ion hydroxides with the ligand (ie formation of hydroxo species like MOHL in Figure 2B2), (iii) interaction of multiple ligands with a single metal ion or of multiple metal ions with a single ligand (ie deviation from 1:1 stoichiometry and formation of species like  $ML_2$  or  $M_2L$  in Figure 2B3) and (iv) interaction of different metal ions with a single ligand or of different ligands with a single metal ion (ie formation of mixed metal ion-ligand complexes, not shown in Figure 2). As all of these reactions are connected through thermodynamic laws and may mutually affect each other, a mathematical treatment of chemical speciation in complex systems yields nonlinear equations, which have to be solved simultaneously using computer-based iterative approaches.<sup>18</sup> Various

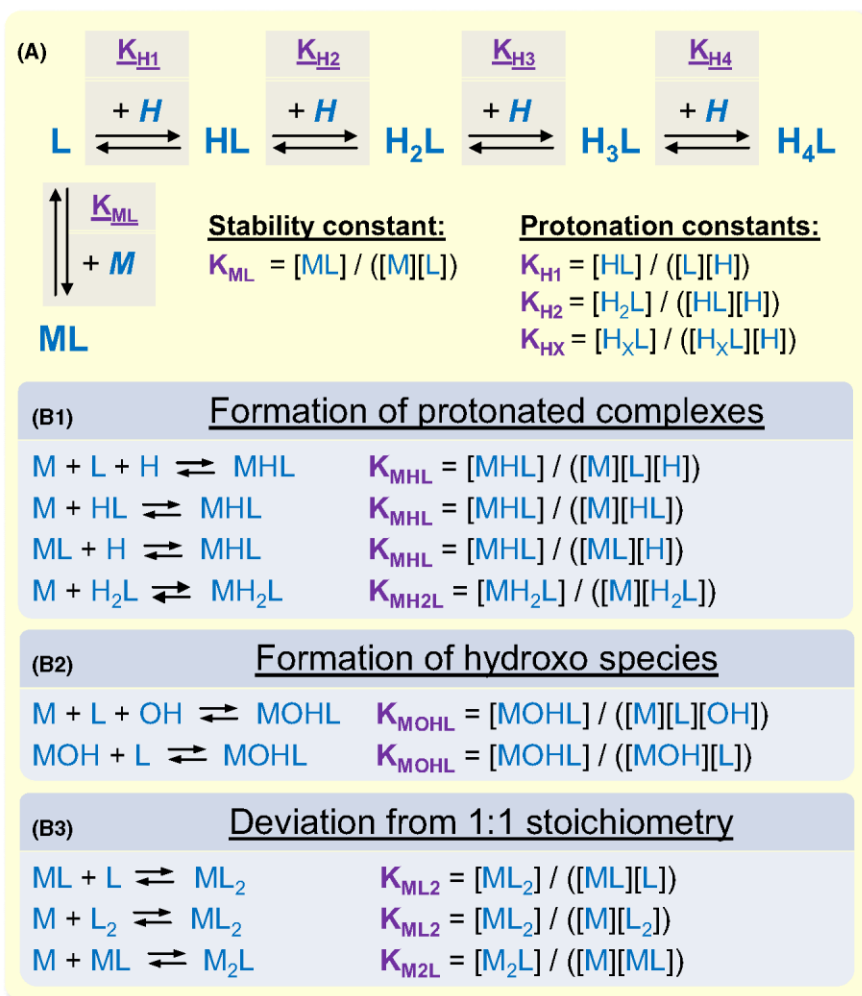


**FIGURE 2** Overview of reactions that may be relevant for trace metal speciation. Shown are various reactions which can alter the species distribution at equilibrium and may thus have to be considered for calculation of free metal ion concentrations. Note that the list is not exhaustive and that charges have been omitted for clarity. A, Equilibrium speciation of a metal ion species (M) in the presence of complexing ligand species (L) and non-complexing, protonated forms of the ligand ( $H_xL$ ) is controlled by the concentration of reactants, the protonation constants of the ligand and the stability constant for the complexes (ML) formed. B, In some cases, additional reactions may take place, such as formation of complexes that contain one or more protons ( $MH_xL$ ) (B1) or hydroxide ions ( $MOH_xL$ ) (B2) or that deviate from a simple 1:1 stoichiometry ( $M_xL$  or  $ML_x$ ) (B3). Not shown is the formation of ternary complexes, which contain two different ligands bound to the same metal ion or vice versa



free or commercial speciation programs exist for speciation calculations over a wide range of experimental conditions (ionic strength  $<0.5$  mol/L, pH = 4-10 and temperature  $<50^{\circ}\text{C}$ ), the specific capabilities and limitations of which have been reviewed in detail elsewhere.<sup>19</sup> Depending on the requirements, we have used the free programs MaxChelator/WinMax (available at<sup>20</sup>) or Visual MINTEQ (available at<sup>21</sup>), both of which have been employed over a long period by many users. Provided that all relevant metal and proton binding constants and the corresponding enthalpy changes are known, the WinMax software can be used to calculate pH-, temperature- and ionic strength-corrected free metal ion concentrations in solutions containing up to 6 metals and ligands. Default conditions for data entry are  $20^{\circ}\text{C}$  and  $0.1$  mol/L ionic strength so that most constants reported in the literature can be used with little or no further adjustment. The software can model metal ion-ligand ( $M + L \leftrightarrow ML$ ), proton-ligand ( $H + H_xL \leftrightarrow H_{x+1}L$ ) and metal ion-protonated ligand interactions ( $M + HL \leftrightarrow MHL$ ) so that it is well suited for estimation of free metal ion concentrations in PAPC-based buffers, where other reactions can often be neglected. Calculation of the equilibria in more complex systems usually needs to be performed using general-purpose speciation software like MINEQL+ (Environmental Research Software, Hallowell, ME, USA), Visual MINTEQ (Stockholm Royal Institute of Technology (KTH), Stockholm, Sweden) or GEOCHEM-EZ (USDA-Agricultural Research Service, Ithaca, NY, USA). All of these programs allow for incorporation of numerous additional reactions, such as formation of mixed metal ion-ligand complexes or metal ion hydrolysis and precipitation. However, the default conditions for data entry are usually much less intuitive and prone to error, because they are based on stepwise formation constants at infinite dilution (ie adjusted to zero ionic strength), which need to be expressed in terms of the reactions specified by the software.<sup>22,23</sup> Although most programs are already supplied with a standard thermodynamic database, there can be substantial errors in the exact values so that they have to be checked against constants from critically reviewed compilations.<sup>22,23</sup> The latter is not always straightforward, as it may also require reformulation of reactions in terms of the components specified by the software. Considering the many sources of potential error associated with the use of general-purpose speciation software, especially beginners in the field are advised to first familiarize with the more user-friendly MaxChelator/WinMax software, which is much less prone to operating errors.

### 2.3 | Choice of ligand concentrations

In a typical experiment, a fixed concentration of some ligand is combined with increasing concentrations of a metal ion to produce a series of solutions that contain different free concentrations of that ion.<sup>24-26</sup> For strong

ligands like the examples shown in Figure 1A, predicted free concentrations increase almost linearly with the total metal concentration as long as (i) all other parameters (ie pH, temperature and ionic strength) remain constant, (ii) only 1:1 mononuclear complexes are formed and (iii) the concentration of free ligand never drops to below 5%-10% of the total metal concentration. Because the ligand-bound to free metal ion ratio increases as a function of ligand molecules present, higher total ligand concentrations provide more effective buffering and reduce the sensitivity to trace metal contamination. They also accelerate the responsiveness of the buffer to perturbations in the species distribution (but see section 2.5). On the other hand however, high chelator concentrations may abstract protein-bound metal ions from catalytic or structural sites and can be toxic to some species.<sup>27</sup> In addition, it has been reported that even membrane-impermeable high-affinity ligands applied extracellularly may alter intracellular trace metal homeostasis, presumably by establishing a steep gradient for efflux of ions like  $\text{Zn}^{2+}$ .<sup>28,29</sup> For these and other reasons, the concentration of strong ligands should be kept as low as possible when metal ion-buffered systems are used in living tissues or cells. Provided that steps are taken to reduce the initial amount of contaminating metal ions present,  $1$  mmol/L of a PAPC ligand is often sufficient for effective buffering and reduction in background  $\text{Zn}^{2+}$  contamination below the threshold for detection with indicators like FluoZin-3 (but see section 3.4). The same does not apply to tricine, which has much lower trace metal affinities and can interact with divalent cations in multiple stoichiometries. In this case, the total to free metal ion relationship is only linear when the total ligand concentration remains significantly larger than the total metal concentration.<sup>12,19,30</sup> This in turn means that tricine needs to be used in much higher concentrations (typically  $10$  mmol/L), which has the advantage that it also serves as a hydrogen ion buffer, with a useful pH range of 7.4-8.8. The latter obviates the need for additional pH buffers (which can interfere with metal ion buffering, but see section 3.3) and makes this ligand much more resistant to changes in the concentration of protons.

### 2.4 | Single- and dual-metal ion buffers

To illustrate the general characteristics of different metal ion buffers, we will consider a situation where  $1$  mmol/L of a strong ligand (EDTA, HEDTA or EGTA) or  $10$  mmol/L tricine are titrated with  $0.1$ - $0.9$  mmol/L total  $\text{Zn}^{2+}$  (Figure 3) or  $\text{Cu}^{2+}$  (Figure 4) at a pH of 7.4,  $20^{\circ}\text{C}$  and  $I = 0.16$  mol/L. Figures 3A and 4A plot the range of predicted free  $\text{Zn}^{2+}$  and  $\text{Cu}^{2+}$  levels in terms of pmol/L

values (ie the negative logarithm of free ion concentration), such that every increase by one unit corresponds to a 10-fold decrease in concentration. For comparison, vertical bars in Figure 3A indicate the estimated range of loosely bound brain  $Zn^{2+}$  concentrations at rest (intracellular  $pZn = 8.8-9.4$  or  $400-1600$  pmol/L; extracellular  $pZn = 7.6-8.3$  or  $5-25$  nmol/L)<sup>2,3,5</sup> and during phasic  $Zn^{2+}$  release (extracellular  $pZn = 4.0-6.0$  or  $1-100$   $\mu$ mol/L).<sup>4,5</sup>

### 2.4.1 | Polyaminopolycarboxylate-based systems

As can be seen by comparison with the data in Table 2, the useful concentration range for metal ion buffering in single-metal systems (ie in the absence of competing metal ions, indicated by black bars in Figures 3A and 4A) is primarily determined by chelator affinity for the target ions.

Because PAPC ligands bind trace metals very tightly, the range is typically situated far below physiologically relevant levels (Figure 3A). Moreover, as protons are strong competitors even for strongly complexing metals like  $Zn^{2+}$  and  $Cu^{2+}$ , chelator affinity may be fairly sensitive to small changes in pH. The latter can be a problem in experiments which require constant free metal ion concentrations over a range of pH values (ie kinetic studies on the pH dependence of enzymes) or involve changes in pH due to for example biological processes. It is also problematic as addition of metals to PAPC-based buffers can result in uncontrolled pH changes, which may in turn significantly alter their buffering capacity.<sup>9</sup> This is because the major fraction of these ligands at near neutral pH is protonated, such that metal ion binding results in a displacement of protons. To effectively reduce ligand protonation in this pH range, a secondary metal ion (like  $Ca^{2+}$  or  $Mg^{2+}$ ) can be

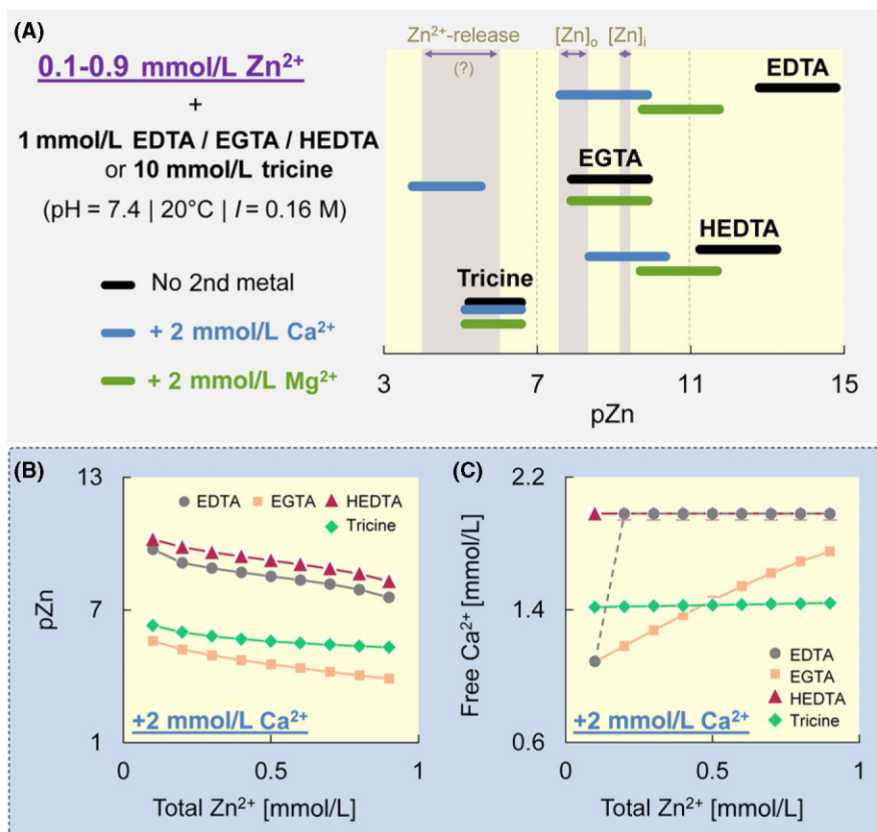
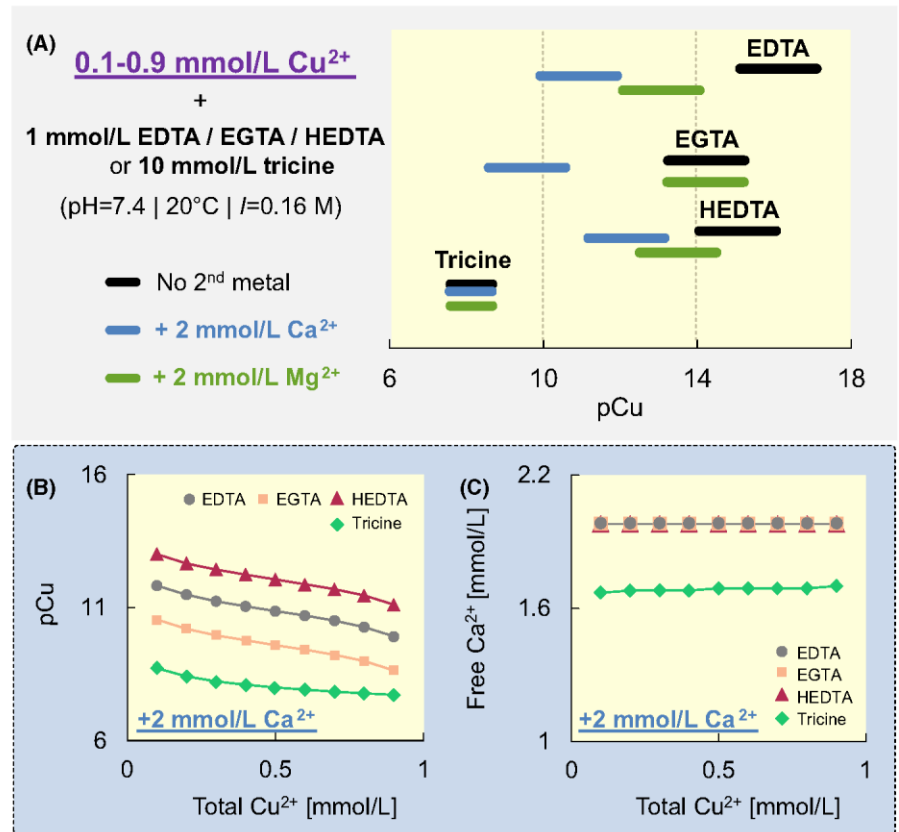


**FIGURE 3** Properties of selected single- and dual-metal ion  $Zn^{2+}$ -buffered systems. A, Overview of predicted free  $Zn^{2+}$ -concentrations for titration of the indicated ligands with 0.1-0.9 mmol/L total  $Zn^{2+}$  in the absence of secondary metal ions (black bars) and in the presence of 2 mmol/L total  $Ca^{2+}$  (blue bars) or  $Mg^{2+}$  (green bars). Calculations were performed with Visual MINTEQ (for tricine) or WinMax (for all other ligands) as described in more detail in the Supplementary Methods. To allow for comparison over the whole range of concentrations, free  $Zn^{2+}$  levels are expressed in terms of pZn values. Also indicated are estimated resting concentrations of loosely bound  $Zn^{2+}$  in the intracellular ( $[Zn]_i$ ) and extracellular ( $[Zn]_o$ ) compartment and the range of extracellular free  $Zn^{2+}$  concentrations that could be envisioned to result from physiological or pathophysiological cellular release ( $Zn^{2+}$ -release; for details and references, see main text). B, Dependence of predicted free  $Zn^{2+}$  levels on the total  $Zn^{2+}$  concentration for the indicated ligands under the same experimental conditions as in A with 2 mmol/L total  $Ca^{2+}$  as the secondary ion. For numerical values, see Table S1. C, Dependence of predicted free  $Ca^{2+}$  levels on the total  $Zn^{2+}$  concentration for the same systems as in B

**FIGURE 4** Properties of selected single- and dual-metal ion  $\text{Cu}^{2+}$ -buffered systems. A, Overview of predicted free  $\text{Cu}^{2+}$  concentrations for titration of the indicated ligands with 0.1-0.9 mmol/L total  $\text{Cu}^{2+}$  in the absence of secondary metal ions (black bars) and in the presence of 2 mmol/L total  $\text{Ca}^{2+}$  (blue bars) or  $\text{Mg}^{2+}$  (green bars). Calculations were performed with Visual MINTEQ (for tricine) or WinMax (for all other ligands) as described in more detail in the Supplementary Methods. To allow for comparison over the whole range of concentrations, free  $\text{Cu}^{2+}$  levels are expressed in terms of pCu values. B, Dependence of predicted free  $\text{Cu}^{2+}$  levels on the total  $\text{Cu}^{2+}$  concentration for the indicated ligands under the same experimental conditions as in A with 2 mmol/L total  $\text{Ca}^{2+}$  as the secondary ion. For numerical values, see Table S1. C, Dependence of predicted free  $\text{Ca}^{2+}$  levels on the total  $\text{Cu}^{2+}$  concentration for the same systems as in B



added to compete with protons and with the primary metal ion.<sup>31-33</sup> If the secondary ion is present at sufficient concentration and bound with much lower affinity than the primary ion, the pH dependence of the resulting dual-metal systems is markedly reduced. More specifically, the buffering capacity can be shown to remain constant between about pH 6 and 10, if the affinity of the chelator for the secondary metal ion is (i) at most 100 times smaller than the affinity for the first proton (ie if  $K_{\text{H1}}:K_{\text{ML}} \leq 100$ , see Table 3) and (ii) not higher than the square root of the product of affinity for the first and second proton (ie if  $\sqrt{K_{\text{H1}}K_{\text{H2}}}:K_{\text{ML}} \leq 1$ , see Table 3).<sup>32,33</sup> In practice, even ligand-secondary metal ion combinations that do not satisfy the above criteria can be used, provided that the pH does not need to be changed and is fixed by a suitable proton buffer.

More importantly, addition of secondary metal ions also alters the buffering capacity and/or effective concentration range for buffering of the primary ion, in a manner that varies with primary:secondary metal ion affinity ratio of the ligand. For example, addition of 2 mmol/L total  $\text{Ca}^{2+}$  or  $\text{Mg}^{2+}$  to the above single-metal ion buffers (indicated by blue or green bars in Figures 3A and 4A) results in ligand- and ion-specific changes of the predicted free trace metal concentrations. Because all three PAPC ligands exhibit high affinity for  $\text{Ca}^{2+}$  but even higher affinity for  $\text{Zn}^{2+}$  and  $\text{Cu}^{2+}$  (Table 2), addition of the former ion invariably

**TABLE 3** Proton:secondary metal ion affinity ratios for selected PAPC ligands

	Proton:secondary metal ion affinity ratios (20°C at $I = 0.1 \text{ mol/L}$ )			
	$K_{\text{H1}}:K_{\text{CaL}}$	$\sqrt{K_{\text{H1}}K_{\text{H2}}}:K_{\text{CaL}}$	$K_{\text{H1}}:K_{\text{MgL}}$	$\sqrt{K_{\text{H1}}K_{\text{H2}}}:K_{\text{MgL}}$
EDTA	$4.0 \times 10^{-1}$	$3.5 \times 10^{-3}$	$4.0 \times 10^1$	$3.5 \times 10^{-1}$
EGTA	$4.0 \times 10^{-2}$	$2.0 \times 10^{-2}$	$2.0 \times 10^4$	$1.0 \times 10^4$
HEDTA	$5.0 \times 10^1$	$2.8 \times 10^{-1}$	$1.0 \times 10^3$	5.6

increases the level of free  $\text{Zn}^{2+}$  (Figure 3A) or  $\text{Cu}^{2+}$  (Figure 4A). However, the magnitude of this effect varies and it can be accompanied by an increase (EDTA), a decrease (EGTA) or no change (HEDTA) in  $\text{Zn}^{2+}$  buffering capacity.  $\text{Mg}^{2+}$  affinity on the other hand is typically much lower (Table 2), so that addition of  $\text{Mg}^{2+}$  ions is either less effective (EDTA, HEDTA) or ineffective (EGTA) in altering free  $\text{Zn}^{2+}$  (Figure 3A) or  $\text{Cu}^{2+}$  (Figure 4A) levels. While these two biologically relevant cations serve to exemplify the general properties of dual-metal ion buffers, data on various systems containing other secondary metal ions (and/or ligands) can be found in the literature.<sup>24,25,32</sup> In addition, custom buffers containing two (or more) metals can be easily assessed using WinMax and correct constants as described in section 2.2. By choosing a suitable chelator



and secondary metal ion, dual-metal ion systems can thus be used to buffer free trace metals over a wide range of concentrations. The almost linear relationship between free and total concentrations of  $Zn^{2+}$  and  $Cu^{2+}$  is exemplified in Figures 3B and 4B for systems containing 2 mmol/L  $Ca^{2+}$  (for numerical values see Table S1). Provided that the affinity ratio is sufficiently high, dual-metal ion buffers have the added advantage to allow for manipulation of free  $Zn^{2+}$  or  $Cu^{2+}$  levels at a fixed free secondary ion concentration, an important requirement for many applications. Figures 3C and 4C show the relationship between total  $Zn^{2+}$  or  $Cu^{2+}$  and free  $Ca^{2+}$  concentration with different ligands and 2 mmol/L total  $Ca^{2+}$ . In EDTA- and HEDTA-buffered systems ( $K_{ZnL}:K_{CaL} > 10^5$ ;  $K_{CuL}:K_{CaL} > 10^8$ ), the predicted free  $Ca^{2+}$  concentration is essentially equal to the total amount of  $Ca^{2+}$  present ( $\sim 2$  mmol/L, except at the lowest total  $Zn^{2+}$  concentration with EDTA) and independent of the total amount of  $Zn^{2+}$  or  $Cu^{2+}$  added. As such, they provide an excellent choice for in vitro extracellular  $Zn^{2+}$  or  $Cu^{2+}$  buffering at or near physiological resting concentrations, which may be required for for example dose-response experiments with  $Ca^{2+}$ -permeable channels or calibration of fluorescent probes. Importantly however, this does not apply to all metal ion-ligand combinations. For example, according to Figure 3A, EGTA would appear to be a candidate ligand for buffering micromolar extracellular  $Zn^{2+}$  concentrations in the presence of  $Ca^{2+}$ . Because it has a much lower  $Zn^{2+}:Ca^{2+}$  affinity ratio ( $K_{ZnL}:K_{CaL} = 63$ ) however, EGTA- $Ca^{2+}$  interactions at low total  $Zn^{2+}$  strongly reduce the free  $Ca^{2+}$  concentration (Figure 3C). When the total  $Zn^{2+}$  concentration is increased,  $Ca^{2+}$  ions are displaced from the ligand, resulting in a corresponding increase in the free  $Ca^{2+}$  concentration (ie a strong dependence of free  $Ca^{2+}$  on total  $Zn^{2+}$ ). This means that a fixed concentration of free  $Ca^{2+}$  while varying total  $Zn^{2+}$  could only be maintained by additional changes in the buffer to adjust for the effects of  $Ca^{2+}$  binding and displacement. When the primary metal ion is  $Cu^{2+}$  on the other hand, EGTA ( $K_{CuL}:K_{CaL} > 10^6$ ) behaves much like the two other PAPC ligands with  $Zn^{2+}$  in that the free  $Ca^{2+}$  level is more or less equal to the total  $Ca^{2+}$  and independent of the total  $Cu^{2+}$  concentration (Figure 4C). It is therefore also useful for buffering of picomolar to low nanomolar (ie physiologically relevant) free  $Cu^{2+}$  concentrations.

### 2.4.2 | Tricine-based systems

Even in the presence of competing metal ions, the affinity of PAPC ligands for trace metals is typically too high to be useful for buffering of for example micromolar  $Zn^{2+}$  (Figure 3A) or nanomolar  $Cu^{2+}$  (Figure 4A) concentrations. Because these concentrations may be reached during

phasic release in the brain, investigators have instead resorted to the use of tricine. As evident in Figures 3A and 4A, the lower  $Zn^{2+}$  and  $Cu^{2+}$  affinity of tricine relative to stronger ligands like EDTA means that the useful range for buffering of these ions is at much higher concentrations. Also, in contrast to PAPC ligands, trace metal ion buffering by tricine is essentially unaffected by addition of  $Ca^{2+}$  or  $Mg^{2+}$  (Figure 3A and 4A), reflecting its very low affinity for alkaline earth metal ions (Table 2). Because of the high total concentration of tricine present, some binding of secondary ions by the ligand may still occur, which can be seen by the difference between total and free  $Ca^{2+}$  levels in Figures 3C and 4C. This effect is essentially independent of the total trace metal concentration, however, so that it can simply be compensated by the use of a higher total  $Ca^{2+}$  concentration. Finally, a major disadvantage of tricine that we have touched upon before is the lack of (critically evaluated) thermodynamic data (ie stability constants and especially enthalpy values) for many cations. As reported constants have typically been determined at or near room temperature, this can be especially problematic when experiments are to be performed at physiological temperatures (30-37°C). Considering the growing interest in trace metal homeostasis and the progress made in analytic techniques however, it seems likely that more extensive data on tricine will become available in the near future.

## 2.5 | Complexation kinetics: validity of the equilibrium assumption

According to thermodynamic models, equilibrium speciation is controlled by the concentration of metal ion and ligand species present and the stability constants for all complex species formed. If the system is perturbed by changes in the nature or concentration of species present, a new equilibrium will be attained. Not included in most models is the finite amount of time required for equilibration, which depends on the initial species distribution and the rate of complexation and exchange reactions involved. As slow exchange reactions can retard the responsiveness of metal ion buffers to changes in the conditions, they may introduce significant kinetic uncertainty. A throughout discussion of coordination kinetics and how they may be implemented into speciation calculations is beyond the scope of this article and can be found elsewhere.<sup>34-36</sup> Here, we will focus on practical implications for the choice of ligand concentration in dual-metal ion buffers and briefly discuss the relevance for applications like interception of synaptic  $Zn^{2+}$  in for example brain slices.

In the absence of competition, metal ion binding by small-molecule ligands with significant affinity for their target ion is intrinsically rapid,<sup>34,37,38</sup> so that equilibration of single-metal ion buffers is effectively instantaneous. The

same may not apply to more complex systems containing multiple metal ion species, because the rate-limiting steps for metal-exchange reactions (ie dissociation of the pre-bound metal or formation/dissociation of a di-nuclear intermediate complex) can be orders of magnitude slower than metal ion binding by the free ligand.<sup>34,39,40</sup> For example, alkaline earth metal complexes of high-affinity ligands like EDTA exhibit relatively small rates of dissociation and exchange with transition metals so that they are also much slower in binding these metals than the free ligand.<sup>27,39</sup> This means that trace metal speciation at very low (ie nano- to micromolar) EDTA and substantially higher (ie 1-10 mmol/L) alkaline earth metal concentrations may be extremely slow, with equilibration times in the order of hours to days.<sup>27,39,40</sup> At higher (ie millimolar) ligand concentrations, trace metal complexation occurs on a much faster timescale (ie seconds to minutes, see also section 3.5).<sup>41-44</sup> This may still be too slow for some applications, such as capture of endogenous transition metals in the synaptic cleft. Here, binding must occur within <100 ms to effectively prevent all postsynaptic actions, which can be achieved with specifically designed ligands like ZX1.<sup>45,46</sup> Tricine binding of  $Zn^{2+}$  and  $Cu^{2+}$  is also rapid both in the presence and absence of  $Ca^{2+}$  or  $Mg^{2+}$  so that it has been employed for interception of synaptic  $Zn^{2+}$  as well.<sup>47,48</sup> Here, it is important to consider the lower  $Zn^{2+}$  affinity of tricine, which means that it may be unable to effectively prevent  $Zn^{2+}$  binding to very high-affinity target sites.<sup>46</sup> While this can complicate comparison of experimental findings, it might also provide a way to separate effects of phasic  $Zn^{2+}$  release mediated by high- vs low-affinity target sites.

## 2.6 | Additional uncertainties and direct speciation measurements

Despite well-established thermodynamic models, predicted free metal ion concentrations can be associated with significant uncertainty, introduced mainly by the choice of constants, ambiguities concerning their correction and the lack of international standards or clearly defined protocols for metal ion buffer preparation. This is exemplified by experimental and modelling studies on traditional  $Ca^{2+}$  and  $Mg^{2+}$  buffers,<sup>6,7,35,49,50</sup> which identified several sources of uncertainty and potential error. They comprise (i) the use of empirically derived thermodynamic constants and the frequent lack of enthalpy values for proper temperature correction, (ii) the use of non-thermodynamic conventions to calculate single ion activity coefficients for ionic strength correction, (iii) errors in the conversion between measured pH (ie  $H^+$  activity) and proton concentration due to liquid junction potential changes at the reference pH electrode<sup>51</sup> and (iv) uncertainties with regard to ligand purity,<sup>52,53</sup>

pipetting errors and the level of contaminating metal ions present. As a consequence of these uncertainties, results obtained by calculation may show considerable variation, and there is currently no simple way to determine which of the predictions is correct, creating a classical catch 22 situation.<sup>6</sup> Thus, until appropriate international standards become available, calculated free metal concentrations can only be validated by direct speciation measurements, which are often expensive and require significant instrumentation, complexity and/or equilibration times.<sup>35</sup> A method of choice to confirm speciation calculations and to directly determine apparent constants in  $Ca^{2+}$  and  $Mg^{2+}$  buffers is the ligand optimization method, which was introduced by Lüthi et al<sup>54</sup> and has since been refined by McGuigan and co-workers.<sup>55-57</sup> It is based on ion-selective electrodes (ISEs), calibrated (in the Nernstian response range) with standards set out by dilution, and uses the Nicolsky-Eisenman equation to account for the influence of the lumped interference on the slope of the electrode in the non-Nernstian buffer range (for details see<sup>54-58</sup>). At present, commercial electrodes for most trace metals (including  $Zn^{2+}$  and  $Cu^{2+}$ ) are either unavailable or lack sufficient sensitivity<sup>59-62</sup> so that their use for trace metal speciation purposes remains limited. Given that there is now a clear need and the field is rapidly expanding, suitable electrodes or other simple means to confirm speciation calculations will almost certainly become available in the near future. In the meantime, it remains important to establish clearly defined protocols for buffer preparation, so as to minimize uncertainties introduced by experimental error, which can neither be evaluated nor corrected retrospectively. While this does still not allow for strict determination of absolute concentrations, a number of previous studies show that at least in well-defined systems, there is usually reasonable agreement between predicted and measured values.<sup>35,63-68</sup>

## 3 | PREPARATION AND USE OF METAL ION BUFFERS

Lacking a simple method to verify speciation calculations, it becomes especially important to accurately simulate the system under study, and to prevent unwanted reactions or uncontrolled changes in the experimental conditions. This entails use of critically evaluated and correctly adjusted constants, as well as an accurate account of the experimental conditions and the exact speciation calculations performed. Even more important are steps to exclude uncertainties with regard to metal ion and ligand purity, pipetting errors and pH changes secondary to metal ion-ligand interactions.<sup>6,7,50</sup> To this end, the rest of this article will provide instructions and a general protocol for the preparation of single- and dual-metal ion buffers, which is



based on the same principle used in commercial kits for calibration of  $\text{Ca}^{2+}$  indicators, but can be used for metal ion buffering in most background solutions of choice. Finally, the application and importance of proper metal ion buffering will be illustrated and some useful applications of fluorescent sensors for a literature comparison of custom buffer performance and/or detection of contaminating metal ions will be outlined.

### 3.1 | Reagents, labware and sample handling techniques

Major determinants for the background level of trace metal contamination in physiological solutions are the purity of reagents and type of labware used for their preparation and storage as well as the general sample handling procedures. Initial contamination can be reduced using type I ultrapure water (UPW) dispensed from a high-grade purification system and reagents of the highest purity available (preferably trace metal grade). Chemicals and solutions should be transferred using Teflon-coated spatula and metal-free pipette tips, respectively, avoiding even transient contact with any metal surface. Because borosilicate glass contains high levels of trace metals and has a tendency to adsorb metal ions from the sample,<sup>41</sup> use of standard laboratory glass should also be avoided. Instead, solutions are usually prepared and stored in containers made from one of various synthetic polymers (polymethylpentene, polypropylene or fluoropolymers like Teflon).<sup>69</sup> Initial trace metal impurities in these materials may vary based on the exact manufacturing process or environment so that comprehensive cleaning procedures should always be applied. Depending on the material and metal ion species to be investigated, various cleaning protocols have been reported in the analytical literature. Table 4 outlines a general procedure for cleaning all types of containers, which involves rinses with alcohol to remove organic contaminants, soaking in dilute hydrochloric and nitric acid (which leach various elements with different efficiencies<sup>69</sup>) and extensive washes with UPW to remove residual acid. During cleaning and storage of containers, precautions should be taken to minimize airborne contamination by dust particles, which can introduce significant amounts of trace metal contaminants. Finally, investigators should be aware that even nominally metal-free solutions prepared with the most highly purified salts and under strict adherence to the above precautions will likely contain nano- to micromolar amounts of trace metal contaminants.<sup>70</sup> They can be detected by inductively coupled plasma mass spectrometry (ICP-MS), which is also useful to assay, where possible, the total metal content in for example stock solutions. Steps that can be taken to further reduce contamination to negligible levels are described in section 3.3.

### 3.2 | Preparation of chelator-metal ion stock solutions

Calibration of fluorescent sensors or dose-response experiments require reference media which contain different concentrations of free  $\text{Zn}^{2+}$  or  $\text{Cu}^{2+}$  at a fixed pH and ionic strength. In practice, preparation of these solutions can prove to be a non-trivial task, because of complications that include the formation and precipitation of colloidal hydroxo polymers in neutral  $\text{Zn}^{2+}$ -containing solutions,<sup>71,72</sup> the uncontrolled pH changes that can result from proton release during chelator-metal ion interactions<sup>9</sup> and uncertainties with regard to pipetting errors and chelator or metal ion purity.<sup>9,73</sup> A convenient solution to most of these problems is to prepare two concentrated stock solutions containing the chelator + metal ion and the chelator only, respectively, which can be diluted into a “background” solution of choice (but see section 3.3) and mixed in appropriate proportions to give specific concentrations of the free metal ion (Figure 5A). For dual-metal ion buffers, a fixed amount of the secondary ion is added to both stocks so that all solutions produced by the above cross-dilution technique contain the same final concentration of that ion. This is illustrated in Figure 5B for an EDTA- $\text{Zn}^{2+}$ - $\text{Ca}^{2+}$  buffer system, which gives final concentrations of 1 mmol/L total EDTA, 2 mmol/L total  $\text{Ca}^{2+}$  and 0.1-0.9 mmol/L total  $\text{Zn}^{2+}$ . Using the MaxChelator software and constants from Tables 1 and 2, the free  $\text{Zn}^{2+}$  (and  $\text{Ca}^{2+}$ ) concentrations in the solutions obtained can be calculated (Figure 5, B4). To

**TABLE 4** Initial and routine cleaning of plastic labware

<i>Reagents</i>
10% HCl solution, 10% nitric acid, 2-propanol, type I ultrapure water (UPW)
<i>Experimental</i>
1. Rinse the complete surface with 2-propanol to remove traces of organic contaminants (Note 1) followed by UPW to remove residual alcohol
2. Fill with 10% HCl solution and leave to soak at room temperature for at least 48 h (Note 2)
3. Empty and rinse with UPW, then fill with 10% nitric acid and leave to soak at room temperature for at least 48 h
4. Empty and rinse with UPW, then fill with fresh UPW and leave to soak at room temperature for several days, while changing the water periodically to ensure continued cleaning
5. For storage or use, empty and allow to dry in a particle- and dust-free environment or rinse with the solution to be used in the container

Note 1: Greases, oils and other organic contaminants often present can contribute to trace metal absorption and may exert unwanted biological effects.

Note 2: While a soak in 10% hydrochloric acid is recommended for the initial cleaning of labware, we have typically omitted this step for routine cleaning.



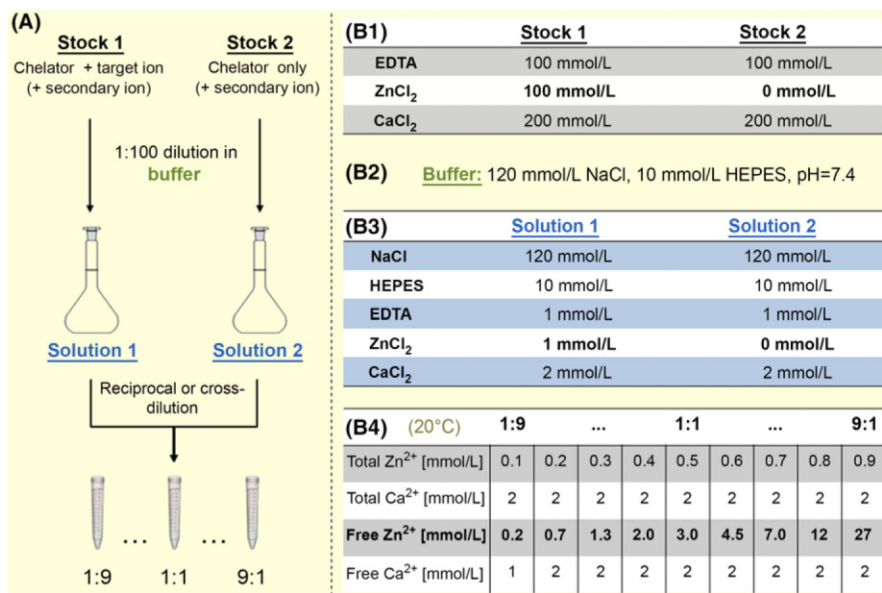


**FIGURE 5** Preparation of single- and dual-metal ion buffers. A, Cartoon depicting a general approach for the preparation of metal ion-buffered systems. Two stocks containing a fixed amount of a strong chelator (+ secondary ion if desired) in the presence and absence of equimolar concentrations of the target ion are diluted into an appropriate background buffer. The resulting solutions can be mixed by reciprocal or cross-dilution to obtain various concentrations of the target ion. B, Application of the approach in A for the preparation of an EDTA-based Zn<sup>2+</sup> buffer with 2 mmol/L total Ca<sup>2+</sup> as the secondary ion. The two stock solutions (B1) can be stored frozen and are diluted (1:100) into a suitable, proton-buffered background solution (B2) to obtain two solutions of the desired ionic strength that contain 0 and 1 mmol/L total Zn<sup>2+</sup> (B3). Using the constants from Tables 1 and 2, the free Zn<sup>2+</sup> (and Ca<sup>2+</sup>) concentrations obtained by cross-dilution of these solutions can be predicted with WinMax (B4) or other speciation software. Note that a wide range of more complex background solutions can be used, provided that they conform to the requirements detailed in section 3.3 (and that the free metal concentrations given in B4 are re-calculated accordingly)

avoid large error at the endpoints of the cross-dilution (ie 0.1 and 0.9 mmol/L total Zn<sup>2+</sup> in Figure 5B), it is critical that the stock solution with chelator + target ion contains an exact 1:1 ratio of the two components. This can be achieved by pH-metric titration of the chelator with the metal ion, an approach previously used for the preparation of CaEGTA solutions.<sup>74,75</sup> It is based on the proton release from PAMP ligands during metal ion binding, which should cease as the chelator:metal ion ratio approaches 1:1. As exemplified in Table 5 for the EDTA-Zn<sup>2+</sup>-Ca<sup>2+</sup> buffer described above, the process involves titration of a solution containing excess chelator with small portions of the metal ion until the resulting change in pH per unit of metal ion added decreases abruptly. Although precise control of the pH is not essential, the titration should be performed in a range where the di-protonated form of the ligand is predominant (ie below the second-highest protonation constant) so that metal ion binding releases two equivalents of protons. In closing this section, it should be noted again that, due to its distinct protonation behaviour compared to PAMP ligands, tricine is much less problematic to handle. To avoid uncertainties due to pipetting errors, a cross-dilution approach like the above may still be preferable for applications that involve very small

sample volumes (like eg sensor calibrations). For electrophysiological recordings with large sample volumes on the other hand, we have prepared tricine-based buffers by direct addition of tricine and metal ion stock solutions to the Chelex-treated buffer of choice. In this case, no titration is performed and the pH needs to be readjusted anyway, so that metal ions should be added from commercially available (atomic absorption) standards containing a pre-assayed metal ion concentration in dilute acid.

### 3.3 | Other components of the system

In choosing the background solution for dilution of the above stocks, it is important to consider potential interactions between the metal ions or ligands and any of the other components present. For example, phosphate anions (ie PO<sub>4</sub><sup>3-</sup>) precipitate Zn<sup>2+</sup>, while other phosphate species present at physiological pH can form complexes with Zn<sup>2+</sup> and Cu<sup>2+</sup>.<sup>19,76</sup> Several commonly used hydrogen ion buffers containing organic amines, such as TRIS<sup>77-81</sup> and most of the zwitterionic Good's buffers,<sup>82-86</sup> have also been shown to exhibit significant metal ion binding (reviewed in detail in<sup>87</sup>). Although these interactions can be incorporated

**TABLE 5** Preparation of metal-chelator stock solutions

Reagents
EDTA, KOH, ZnCl <sub>2</sub> , 1 mol/L CaCl <sub>2</sub> solution, 45% KOH solution, 35% HCl solution, Chelex-treated UPW
Experimental
Stock 1: [EDTA] <sub>total</sub> = 0.1 mol/L; [Zn <sup>2+</sup> ] <sub>total</sub> = 0.1 mol/L; [Ca <sup>2+</sup> ] <sub>total</sub> = 0.2 mol/L
1. In a 100 mL metal-free plastic beaker equipped with a Teflon-coated stir bar, a solution is prepared by dissolving into ~30 mL Chelex-treated type I ultrapure water: 2.922 g EDTA (=10 mmol) 1.226 g ZnCl <sub>2</sub> (=9 mmol) 2.46 g KOH The pH of the solution is adjusted by addition of KOH or HCl until the pH~5 (Note 1)
2. The exact pH of the solution is noted, and 200 μL of a freshly prepared ~0.5 mol/L ZnCl <sub>2</sub> solution (Note 2) is added. The resulting pH is again noted, and the two pH values are used to calculate ΔpH and ΔpH/ΔZn
3. The above step is repeated, and the pH readjusted to ~5 with 45% KOH solution if necessary. For maximal precision, the volume of the ZnCl <sub>2</sub> additions may be reduced as the amount of Zn <sup>2+</sup> added approaches 1 mmol (Note 3). Complete titration is indicated by a sharp decrease in ΔpH/ΔZn to below half of its initial value
4. 20 mL of 1 mol/L CaCl <sub>2</sub> solution (=20 mmol) is added with stirring, and the resulting mixture is transferred into a 100-mL volumetric flask. To effect complete transfer, the beaker is repeatedly rinsed with small portions of Chelex-treated type I ultrapure water and the washes are combined with the solution in the volumetric flask until the total volume reaches 100 mL
Stock 2: [EDTA] <sub>total</sub> = 0.1 mol/L; [Ca <sup>2+</sup> ] <sub>total</sub> = 0.2 mol/L
1. In a 100-mL metal-free plastic beaker equipped with a Teflon-coated stir bar, a solution is prepared by dissolving into ~30 mL Chelex-treated type I ultrapure water: 2.922 g EDTA (=10 mmol) 2.46 g KOH The pH of solution is noted (it should be around 10.5), and 20 mL of 1 mol/L CaCl <sub>2</sub> solution (=20 mmol) is added
2. The pH of the solution is again noted (should be around 4) and 20 μL aliquots of 45% aq. KOH are added until pH ~7 (Note 4)
3. The resulting mixture is transferred into a 100-mL volumetric flask. To effect complete transfer, the beaker is washed with several small portions of Chelex-treated type I ultrapure water, which are combined with the solution in the volumetric flask until the total volume reaches 100 mL

Note 1: The preferred pH range is below the second-highest protonation constant of the ligand and may be different for other chelators (see Table 1).

Note 2: The exact concentration of the ZnCl<sub>2</sub> stock solution is not critical, but it should be prepared immediately prior to the titration to avoid hydrolysis and precipitation.

Note 3: The maximum final deviation between EDTA and Zn<sup>2+</sup> concentration is determined by the volume of the last metal addition and decreases from approx. 1% for 200 μL to 0.25% for 50 μL additions of the 0.5 mol/L ZnCl<sub>2</sub> stock solution.

Note 4: At higher Ca<sup>2+</sup> concentrations, this can result in precipitation of CaOH.

into the calculation of free metal ion concentrations, it is usually preferable to use alternative pH buffers. Compounds suitable for buffering at physiological pH values that have been shown or are thought to be non-complexing include HEPES, PIPES and MOPS.<sup>81,88-91</sup> Also, a series of non-complexing tertiary amine buffers has been proposed, which covers the entire range of pH 3-11.<sup>72,92</sup> To assess possible metal ion interactions with other organic components, investigators should consult the databases mentioned in section 2.2. It is also worth noting that some common organic reagents, such as glucose, may be difficult to obtain in trace metal grade. This is usually not a problem, because appropriate steps should be taken in any case to reduce contamination with trace metals. For preparation of metal-free reference solutions, contamination can often be reduced to negligible levels by adding small amounts of a strong ligand like EDTA or diethylenetriaminepentaacetic

acid. For preparation of actual metal ion buffers on the other hand, all solutions should be pre-treated (before the addition of multivalent cations or chelators) with a metal-chelating ion-exchange resin like Chelex, which contains immobilized iminodiacetate moieties that scavenge adventitious metals without altering the concentration of non-metallic ions.<sup>70</sup> As this can markedly affect the pH of the solution, it is prudent to always measure and readjust it afterwards.

### 3.4 | Calibration of fluorescent indicators

The panoply of new fluorescent indicators with minimal interfering Ca<sup>2+</sup> and Mg<sup>2+</sup> sensitivity has made it possible to visualize and quantify low levels of free Zn<sup>2+</sup> or Cu<sup>2+</sup> in the presence of physiologically relevant concentrations of other divalent cations.<sup>30,93</sup> Calibration of these

indicators under user-specific conditions is a prerequisite for valid experimental findings and provides a good example for the application of dual-metal ion buffers. Table 6 outlines a general procedure for calibration of the widely used  $Zn^{2+}$  sensor FluoZin-3, which can be performed with the stock solutions described in section 3.2 or adapted for use with different solutions and/or indicators. To minimize pipetting and indicator concentration errors, it uses a reciprocal dilution method similar to that in commercial kits for calibration of  $Ca^{2+}$  indicators.<sup>94</sup> Briefly, a background solution containing the desired indicator concentration is used to dilute the two stocks (ie chelator + metal ion & chelator only) and prepare a pair of matched solutions containing 0 and 1 mmol/L total  $Zn^{2+}$ . Fluorescence signals corresponding to different total  $Zn^{2+}$  concentrations at a fixed indicator and chelator (+ secondary ion) concentration are obtained by varying the ratio of the two solutions as described in section 3.2. To ensure complete equilibration, measurements should only be performed after the signal no longer changes (but see section 3.5). Signals may be corrected for background fluorescence by subtracting the values recorded with 0 mmol/L total  $Zn^{2+}$  solution and normalized to the signal obtained by addition of saturating  $Zn^{2+}$  concentrations or with 1 mmol/L total  $Zn^{2+}$  solution (which contains  $>1 \mu\text{mol/L}$  free  $Zn^{2+}$  and should also produce a maximum sensor response). Figure 6 compares the titration curves thus obtained for different calibrations performed in our laboratory with FluoZin-3, using either EDTA-based  $Zn^{2+}$  buffers (prepared according to the above procedures with 2 or 5 mmol/L total  $Ca^{2+}$ ) or unbuffered  $Zn^{2+}$  solutions (prepared by direct addition of a  $10 \mu\text{mol/L}$   $ZnCl_2$  solution<sup>a</sup> to the same HEPES-based background buffer with 5 mmol/L  $Ca^{2+}$ ). With adequate  $Zn^{2+}$  buffering and in the presence of 2-5 mmol/L total  $Ca^{2+}$ , the titration curves yield Hill coefficients close to 1 (Figure 6A,B), which is consistent with 1:1  $Zn^{2+}$  binding to the probe. The data also confirm that FluoZin-3 remains responsive to nanomolar  $Zn^{2+}$  even in the presence of (supra)physiological  $Ca^{2+}$  levels. Thus, relative to  $K_m$  values of 9-15 nmol/L previously determined under similar conditions but in the nominal absence of  $Ca^{2+}$ ,<sup>95,96</sup> apparent  $Zn^{2+}$  affinity is reduced only slightly to give  $K_m$  values of 19-23 nmol/L (for 3 titrations with 2 mmol/L  $Ca^{2+}$ ) and 36-40 nmol/L (for 4 titrations with 5 mmol/L  $Ca^{2+}$ ) respectively (Figure 6B). When calibrations are performed using unbuffered  $Zn^{2+}$  solutions on the other hand, fluorescence responses are either absent or strongly reduced (Figure 6A,B). As a consequence, very poor titration curves are obtained that only fit to improbable Hill coefficients close to 1.4 and yield much higher and more variable  $K_m$  values of 118-186 nmol/L (for 3 titrations with 5 mmol/L  $Ca^{2+}$ ) (Figure 6B). A corollary to these observations is that the use of submicromolar  $Zn^{2+}$  concentrations

**TABLE 6** Calibration of FluoZin-3

Reagents
1 mmol/L FluoZin-3 stock solution in Chelex-treated UPW, Stock 1 (EDTA-Zn-Ca) and Stock 2 (EDTA-Ca) prepared according to Table 5, ~40 mL of a Chelex-treated background solution (120 mmol/L NaCl + 10 mmol/L HEPES, pH = 7.4)
Experimental
1. For a typical calibration, 20 $\mu\text{L}$ of the FluoZin-3 stock solution is added to 40 mL of the background solution and vortexed to give a final concentration of 0.5 $\mu\text{mol/L}$ FluoZin-3 (Note 1)
2. 200 $\mu\text{L}$ of Stock 1 (EDTA/ $Ca^{2+}$ / $Zn^{2+}$ ) is added to 20 mL of the resulting background buffer with FluoZin-3 to prepare a solution containing 0.5 $\mu\text{mol/L}$ FluoZin-3, 2 mmol/L total $Ca^{2+}$ , 1 mmol/L total EDTA and 1 mmol/L total $Zn^{2+}$ (=“1 mmol/L total $Zn^{2+}$ solution”)
3. 100 $\mu\text{L}$ of Stock 2 (EDTA/ $Ca^{2+}$ ) is added to 10 mL of the resulting background buffer with FluoZin-3 to prepare a matched solution containing 0.5 $\mu\text{mol/L}$ FluoZin-3, 2 mmol/L total $Ca^{2+}$ , 1 mmol/L total EDTA and no $Zn^{2+}$ (=“0 mmol/L total $Zn^{2+}$ solution”)
4. 3 mL of the 0 mmol/L total $Zn^{2+}$ solution is added into a new, clean fluorimeter cuvette, and the fluorescence intensity is recorded to obtain an estimate of the analytical blank ( $R_{\text{min}}$ ) (Note 2)
5. 300 $\mu\text{L}$ is removed from the cuvette and replaced by an equal volume of 1 mmol/L total $Zn^{2+}$ solution to give a final concentration of 0.1 mmol/L total $Zn^{2+}$ . The solution is mixed by repeatedly pipetting up and down and allowed to equilibrate completely before the response is obtained as the mean of three consecutive measurements (Note 3)
6. The above step is repeated by removing the volumes given below and replacing them by an equal volume of the 1 mmol/L total $Zn^{2+}$ solution to give the indicated final concentrations: 0.20 mmol/L total $Zn^{2+}$ : 333 $\mu\text{L}$ 0.30 mmol/L total $Zn^{2+}$ : 375 $\mu\text{L}$ 0.40 mmol/L total $Zn^{2+}$ : 429 $\mu\text{L}$ 0.50 mmol/L total $Zn^{2+}$ : 500 $\mu\text{L}$ 0.60 mmol/L total $Zn^{2+}$ : 600 $\mu\text{L}$ 0.70 mmol/L total $Zn^{2+}$ : 750 $\mu\text{L}$ 0.80 mmol/L total $Zn^{2+}$ : 1000 $\mu\text{L}$ 0.90 mmol/L total $Zn^{2+}$ : 1500 $\mu\text{L}$ 0.95 mmol/L total $Zn^{2+}$ : 2000 $\mu\text{L}$
7. The cuvette is emptied and rinsed once with “1 mmol/L total $Zn^{2+}$ solution.” 3 mL of fresh “1 mmol/L total $Zn^{2+}$ solution” is then added, and the fluorescence intensity is recorded to obtain the maximum sensor response (Note 4)

Note 1: As long as they are protected from light and stored at room temperature, working solutions of FluoZin-3 should be stable for at least 12 h.<sup>101</sup>

Note 2: The contribution of contaminating  $Zn^{2+}$  or other metal ions to background fluorescence can be assessed by measuring the fluorescence after addition of 25  $\mu\text{mol/L}$  TPEN.

Note 3: For more details, see sections 3.4 and 3.5 in the main text.

Note 4: Conditions in the 1 mmol/L total  $Zn^{2+}$  solution should overwhelm the EDTA buffering capacity so that the free  $Zn^{2+}$  concentration is much higher than 1  $\mu\text{mol/L}$ .

without adequate buffering is futile, because significant differences may exist between nominal and actual free  $Zn^{2+}$  levels.



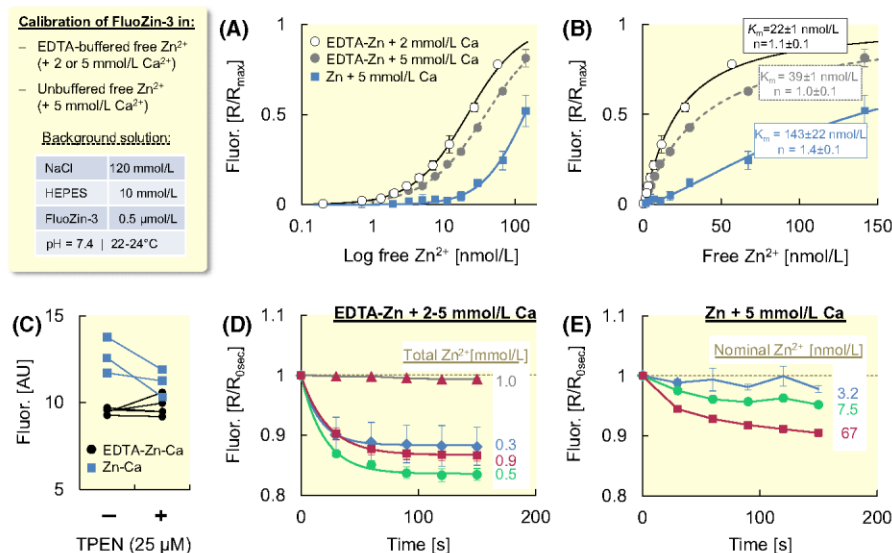


**FIGURE 6** Influence of Zn<sup>2+</sup> buffering and Ca<sup>2+</sup> ions on FluoZin-3 calibration with nanomolar Zn<sup>2+</sup>. Fluorescence intensities at 515 nm were recorded with a Jenway Model 6280 fluorimeter under the experimental conditions indicated in the upper left corner (for more details see Supplementary Methods). Signals have been normalized to the full-scale response obtained with saturating (>1 μmol/L) free Zn<sup>2+</sup> concentrations ( $R_{max}$ ) for the titration curves or to the initial response obtained immediately after sample preparation ( $R_{0sec}$ ) for the kinetic experiments as indicated. All values are given as mean ± SEM for the indicated number of independent experiments. A, Semi-logarithmic plots of sensor response as a function of free Zn<sup>2+</sup>, recorded in EDTA-buffered Zn<sup>2+</sup> solutions containing 2 mmol/L (open circles,  $n = 4$ ) or 5 mmol/L (black circles,  $n = 4$ ) Ca<sup>2+</sup> or with an unbuffered Zn<sup>2+</sup> solution containing 5 mmol/L Ca<sup>2+</sup> (orange squares,  $n = 3$ ). B, Same data as in A, but plotted on a linear scale and shown with the  $K_m$  values and Hill coefficients obtained by nonlinear regression analysis. C, Effect of TPEN addition on sensor responses (raw fluorescence units) recorded under nominally Zn<sup>2+</sup>-free conditions in EDTA-buffered (pooled data for 2-5 mmol/L Ca<sup>2+</sup>) or unbuffered (with 5 mmol/L Ca<sup>2+</sup>) solutions. D, Time course of changes in sensor response recorded immediately after preparation of the indicated total Zn<sup>2+</sup> concentrations by combination and mixing in different proportions of 0 and 1 mmol/L total Zn<sup>2+</sup> EDTA-buffered background solution (pooled data for 2-5 mmol/L Ca<sup>2+</sup>). E, Time course of changes in sensor response recorded immediately after preparation of the indicated nominal free Zn<sup>2+</sup> concentrations by addition and mixing of different amounts of 10 μmol/L ZnCl<sub>2</sub> solution (freshly prepared by dilution of a 0.1 mol/L stock solution) to unbuffered background solution containing 5 mmol/L Ca<sup>2+</sup>

### 3.5 | Testing effectiveness and timescale of metal ion buffering

The approach described in the preceding section (ie calibration of a suitable sensor and comparison of the  $K_m$  values obtained with the literature) is an excellent way to verify that the calculated free metal ion concentrations are accurate. To test the effectiveness of buffering in the nominal absence of the target ion, one can compare the fluorescence recorded before and after addition of a very strong chelator to the indicator-containing solution of interest. This is exemplified in Figure 6C for the EDTA-buffered (pooled data from the experiments with 2 or 5 mmol/L Ca<sup>2+</sup>) and unbuffered (with 5 mmol/L Ca<sup>2+</sup>) solutions described above. Note that the background fluorescence without adequate buffering is higher and that the strong Zn<sup>2+</sup> chelator TPEN (25 μmol/L) tends to reduce it in unbuffered but not EDTA-buffered systems. Together, these findings indicate that variable amounts of Zn<sup>2+</sup> and/or other metal ions capable of eliciting a fluorescence response are present and contribute to background fluorescence in the unbuffered solution. More importantly, they also show that this can be

avoided by the use of an adequately buffered system. Note, however, that the absence of fluorescence changes should not be taken as evidence for complete elimination of trace metal contamination, as metal ions may be present that are either not bound by the indicator (or TPEN) or simply elicit no fluorescence response.

Metal complexation by TPEN is rapid so that the time course of abstraction of metal ions from the sensor could only be resolved by more elaborate methods. When the underlying reactions occur on a slower timescale, equilibration may be visualized by following changes in sensor response over time. For example, Figure 6D shows the time course of changes in fluorescence, recorded immediately after combination and throughout mixing of the 0 mmol/L and 1 mmol/L Zn<sup>2+</sup> solutions to give the indicated final total Zn<sup>2+</sup> concentrations (pooled data from the experiments with EDTA and 2 or 5 mmol/L Ca<sup>2+</sup>). Due to the slow exchange kinetics of CaEDTA (which is present at high levels in the 0 mmol/L Zn<sup>2+</sup> solution), Zn<sup>2+</sup> speciation is initially dominated by FluoZin-3,<sup>b</sup> even though it has much lower Zn<sup>2+</sup> affinity.<sup>41,42</sup> Subsequent re-equilibration to give the thermodynamically favoured ZnEDTA

complex is associated with  $Zn^{2+}$  removal from the sensor, which can be seen in Figure 6D as a decrease in initial fluorescence by up to 15% for all but the highest total  $Zn^{2+}$  concentration (ie 1 mmol/L). The latter reflects the fact that, if only 1 mmol/L total  $Zn^{2+}$  solution is present (ie no pre-formed CaEDTA is added), equilibrium should already be attained prior to “mixing” and start of the recordings. For comparison, Figure 6E shows results from the experiments with unbuffered  $Zn^{2+}$  solution, which were performed in the same manner except that samples were prepared by direct addition of  $ZnCl_2$  to the cuvette containing background solution with 5 mmol/L  $Ca^{2+}$ . As initial fluorescence under these conditions should correspond to the nominal  $Zn^{2+}$  concentration, the progressive decline of the signals indicates loss of free  $Zn^{2+}$  ions from the solution. The lack of changes at the lowest nominal  $Zn^{2+}$  concentrations is presumably because most or all of the added  $Zn^{2+}$  ions are already lost from solution before the first measurement can be obtained (ie during preparation and mixing).

## 4 | CONCLUSIONS

Meaningful studies on the biochemical effects of trace metals require a solid understanding of chemical speciation and, due to the lack of international standards, the ability to prepare solutions containing exactly defined free metal ion concentrations. We have reviewed the design, preparation and use of single- and dual-metal ion buffers, described the many potential pitfalls and exemplified the consequences of using unbuffered trace metal solutions. Although the focus has been on  $Zn^{2+}$  and  $Cu^{2+}$  buffering in the presence of  $Ca^{2+}$  or  $Mg^{2+}$ , the instructions given in the second section should enable readers to do their own calculations for systems containing any combination of metal ions and ligands. Because the metal ion binding properties of many simple organic compounds are well established, accurate estimates of the species distribution at equilibrium may thus be obtained even for relatively complex systems. As a large number of ligands has been designed by modification of the prototype PAPCs discussed herein,<sup>97</sup> there may also be more suitable chelators for some systems. Unfortunately, equilibrium and especially physiological studies typically lag far behind the description of new ligands so that thermodynamic and toxicity data for these compounds is often sparse. Given the emerging demand for metal ion buffering over a wide range of concentrations and experimental conditions, objectives of future work will be to close these gaps and to identify or design optimal ligands for individual applications. Even more importantly, there is an urgent need for routine confirmation of predicted free metal concentrations,

preferably by simple and cost-effective approaches like ion-selective electrodes. The protocols described herein provide a starting point for buffer preparation in physiological background solutions that gives results consistent with previous studies, indicating that the estimated free metal concentrations are in reasonable agreement with the literature. For absolute quantification of free metal ion concentrations in a way that can be directly compared among different laboratories, it will clearly be necessary to go one step further and to establish international standards for  $Zn^{2+}$ ,  $Cu^{2+}$  and other metal ions that can be used for sensor calibration and verification of speciation calculations.

## AUTHOR CONTRIBUTIONS

F.N., T.S. and S.A. conceived the article, F.N. and S.A. performed the experiments, F.N. interpreted the data, prepared the figures and tables and wrote the manuscript. F.N., S.A., T.S. and J.H. participated in drafting of the manuscript.

## CONFLICT OF INTEREST

The authors declare no conflict of interests.

## ENDNOTES

<sup>a</sup>Prepared immediately prior to the measurements by dilution of a 0.1 mol/L stock.

<sup>b</sup>Any free  $Zn^{2+}$  ions introduced (together with  $Zn^{2+}$ -saturated FluoZin-3) by the 1 mmol/L total  $Zn^{2+}$  solution are rapidly bound by  $Zn^{2+}$ -free FluoZin-3 molecules introduced by 0 mmol/L total  $Zn^{2+}$  solution.

## ORCID

F. Neumaier  <http://orcid.org/0000-0002-6376-6391>

## REFERENCES

1. Rae TD, Schmidt PJ, Pufahl RA, Culotta VC, O'Halloran TV. Undetectable intracellular free copper: the requirement of a copper chaperone for superoxide dismutase. *Science*. 1999;284:805-808.
2. Krężel A, Maret W. Zinc-buffering capacity of a eukaryotic cell at physiological pZn. *JBIC, J Biol Inorg Chem*. 2006;11:1049-1062.
3. Colvin RA, Holmes WR, Fontaine CP, Maret W. Cytosolic zinc buffering and muffling: their role in intracellular zinc homeostasis. *Metallomics*. 2010;2:306.
4. Frederickson CJ, Suh SW, Silva D, Frederickson CJ, Thompson RB. Importance of zinc in the central nervous system: the zinc-containing neuron. *J Nutr*. 2000;130:1471S-1483S.
5. Frederickson CJ, Giblin LJ, Krężel A, et al. Concentrations of extracellular free zinc (pZn)<sub>e</sub> in the central nervous system

- during simple anesthetization, ischemia and reperfusion. *Exp Neurol*. 2006;198:285-293.
6. McGuigan JAS, Kay J, Elder H. Why are the problems associated with the lack of international standards for  $\text{Ca}^{2+}/\text{Mg}^{2+}$  buffers still being ignored? *Physiol News*. 2016;103:26-29.
  7. McGuigan JAS, Kay JW, Elder HY. Ionised concentrations in calcium and magnesium buffers: standards and precise measurement are mandatory. *Prog Biophys Mol Biol*. 2017;126:48-64.
  8. Bates RG. *Determination of pH: Theory and Practice*. New York: John Wiley & Sons, Inc.; 1964.
  9. Patton C, Thompson S, Epel D. Some precautions in using chelators to buffer metals in biological solutions. *Cell Calcium*. 2004;35:427-431.
  10. Haase H, Hebel S, Engelhardt G, Rink L. The biochemical effects of extracellular  $\text{Zn}^{2+}$  and other metal ions are severely affected by their speciation in cell culture media. *Metallomics*. 2014;7:102-111.
  11. Bers DM, Hryshko LV, Harrison SM, Dawson DD. Citrate decreases contraction and Ca current in cardiac muscle independent of its buffering action. *Am J Physiol*. 1991;260:C900-C909.
  12. Baker JO. Metal-buffered systems. *Methods Enzymol*. 1988;158:33-55.
  13. Martell AE, Smith RM, Motekaitis RJ. *NIST Critically Selected Stability Constants of Metal Complexes Database*. Gaithersburg: National Institute of Standards and Technology; 2003.
  14. IUPAC. *Stability Constants Database and Mini-SCDatabase*. London: International Union of Pure and Applied Chemistry; 2005.
  15. May PM, Murray K. Database of chemical reactions designed to achieve thermodynamic consistency automatically. *J Chem Eng Data*. 2001;46:1035-1040.
  16. Popov KI, Wanner H. Stability constants data sources: critical evaluation and application for environmental speciation. *ACS Symp Ser*. 2005;910:50-73. <https://doi.org/10.1021/bk-2005-0910.ch003>.
  17. Popov K, Pletnev I, Wanner H, Vendilo A. Stability constants data sources, reliability, algorithms and a software for the data verification. *Proceedings of the 1st International Proficiency Testing Conference 2007 in Sinaia (Romania)*, 324-334; 2007.
  18. Brooks SP, Storey KB. Bound and determined: a computer program for making buffers of defined ion concentrations. *Anal Biochem*. 1992;201:119-126.
  19. Aslamkhan AG, Aslamkhan A, Ahearn GA. Preparation of metal ion buffers for biological experimentation: a methods approach with emphasis on iron and zinc. *J Exp Zool*. 2002;292:507-522.
  20. Patton C. MaxChelator/WinMax homepage. [maxchelator.stanford.edu](http://maxchelator.stanford.edu) Accessed February 11, 2017.
  21. Gustafsson JP. Visual MINTEQ homepage. 2000. <https://vminteq.lwr.kth.se/> Accessed February 16, 2017.
  22. Serkiz SM, Allison JD, Perdue EM, Allen HE, Brown DS. Correcting errors in the thermodynamic database for the equilibrium speciation model MINTEQA2. *Water Res*. 1996;30:1930-1933.
  23. Twiss MR, Errécalde O, Fortin C, et al. Coupling the use of computer chemical speciation models and culture techniques in laboratory investigations of trace metal toxicity. *Chem Speciat Bioavailab*. 2001;13:9-24.
  24. Qin Y, Dittmer PJ, Park JG, Jansen KB, Palmer AE. Measuring steady-state and dynamic endoplasmic reticulum and Golgi  $\text{Zn}^{2+}$  with genetically encoded sensors. *Proc Natl Acad Sci*. 2011;108:7351-7356.
  25. Dittmer PJ, Miranda JG, Gorski JA, Palmer AE. Genetically encoded sensors to elucidate spatial distribution of cellular zinc. *J Biol Chem*. 2009;284:16289-16297.
  26. Loas A, Radford RJ, Lippard SJ. Addition of a second binding site increases the dynamic range but alters the cellular localization of a red fluorescent probe for mobile zinc. *Inorg Chem*. 2014;53:6491-6493.
  27. Raspor B, Nürnberg HW, Valenta P, Branica M. Kinetics and mechanism of trace metal chelation in sea water. *J Electroanal Chem Interfacial Electrochem*. 1980;115:293-308.
  28. Frederickson CJ, Suh SW, Koh J-Y, et al. Depletion of intracellular zinc from neurons by use of an extracellular chelator in vivo and in vitro. *J Histochem Cytochem*. 2002;50:1659-1662.
  29. Ollig J, Kloubert V, WeBels I, Haase H, Rink L. Parameters influencing zinc in experimental systems in vivo and in vitro. *Metals (Basel)*. 2016;6:71.
  30. Westerberg N, Thompson R, Cramer M, et al. *Fluorescence Sensors and Biosensors*. Boca Raton, FL: CRC Press; 2005. <https://doi.org/10.1201/9781420028287.ch14>
  31. Park JG, Palmer AE. Quantitative measurement of  $\text{Ca}^{2+}$  and  $\text{Zn}^{2+}$  in mammalian cells using genetically encoded fluorescent biosensors. *Methods Mol Biol*. 2014;29-47. [https://doi.org/10.1007/978-1-62703-622-1\\_3](https://doi.org/10.1007/978-1-62703-622-1_3).
  32. Wolf HU. Divalent metal ion buffers with low pH-sensitivity. *Experientia*. 1973;29:241-249.
  33. Perrin DD, Dempsey B. *Buffers for pH and Metal Ion Control*. Dordrecht, The Netherlands: Springer; 1979. <https://doi.org/10.1007/978-94-009-5874-6>
  34. Margerum DW, Cayley GR, Weatherburn DC, Pagenkopf GK. Kinetics and mechanisms of complex formation and ligand exchange. In: *Coordination Chemistry, Vol. 2, ACS Monograph 174*. Washington: American Chemical Society; 1978.
  35. VanBriesen JM, Small M, Weber C, Wilson J. In: Hanrahan G, ed. *Modelling chemical speciation: Thermodynamics, kinetics and uncertainty*. Hertfordshire, England: ILM Publications; 2010:133-149.
  36. VanBriesen JM, Rittmann BE. Modeling speciation effects on biodegradation in mixed metal/chelate systems. *Biodegradation*. 1999;10:315-330.
  37. Eigen M, Wilkins RG. The kinetics and mechanism of formation of metal complexes. In Kleinberg J, et al., eds. *Mechanisms of Inorganic Reactions*. New York: American Chemical Society; 1965:55-80.
  38. McAuley A, Hill J. Kinetics and mechanism of metal-ion complex formation in solution. *Q Rev Chem Soc*. 1969;23:18.
  39. Hering JG, Morel FMM. Kinetics of trace metal complexation: role of alkaline-earth metals. *Environ Sci Technol*. 1988;22:1469-1478.
  40. Hering JG, Morel FMM. Slow coordination reactions in seawater. *Geochim Cosmochim Acta*. 1989;53:611-618.
  41. Kay AR. Detecting and minimizing zinc contamination in physiological solutions. *BMC Physiol*. 2004;4:4.
  42. Zhao J, Bertoglio BA, Gee KR, Kay AR. The zinc indicator FluoZin-3 is not perturbed significantly by physiological levels of calcium or magnesium. *Cell Calcium*. 2008;44:422-426.
  43. Khurram MS, Shahzad K, Haider AAR, Ghauri M. Kinetic study of metal-EDTA complex formation and metal-to-metal exchange. *J Pakistan Inst Chem Eng*. 2014;42:91-99.



44. Kuempel JR, Schaap WB. Cyclic voltammetric study of the rate of ligand exchange between cadmium ion and calcium ethylenediaminetetraacetate. *Inorg Chem.* 1968;7:2435-2442.
45. Pan E, Zhang X, Huang Z, et al. Vesicular zinc promotes presynaptic and inhibits postsynaptic long term potentiation of mossy fiber-CA3 synapse. *Neuron.* 2011;71:1116-1126.
46. Anderson CT, Radford RJ, Zastrow ML, et al. Modulation of extrasynaptic NMDA receptors by synaptic and tonic zinc. *Proc Natl Acad Sci USA.* 2015;112:E2705-E2714.
47. Vergnano AM, Rebola N, Savtchenko LP, et al. Zinc dynamics and action at excitatory synapses. *Neuron.* 2014;82:1101-1114.
48. Zhang Y, Keramidas A, Lynch JW. The free zinc concentration in the synaptic cleft of artificial glycinergic synapses rises to at least 1  $\mu\text{M}$ . *Front Mol Neurosci.* 2016;9:88.
49. McGuigan JAS, Stumpff F. Calculated and measured  $[\text{Ca}^{2+}]$  in buffers used to calibrate  $\text{Ca}^{2+}$  macroelectrodes. *Anal Biochem.* 2013;436:29-35.
50. McGuigan JAS, Kay JW, Elder HY, Lüthi D. Comparison between measured and calculated ionised concentrations in  $\text{Mg}^{2+}/\text{ATP}$ ,  $\text{Mg}^{2+}/\text{EDTA}$  and  $\text{Ca}^{2+}/\text{EGTA}$  buffers; influence of changes in temperature, pH and pipetting errors on the ionised concentrations. *Magnes Res.* 2007;20:72-81.
51. Illingworth JA. A common source of error in pH measurements. *Biochem J.* 1981;195:259-262.
52. Miller DJ, Smith GL. EGTA purity and the buffering of calcium ions in physiological solutions. *Am J Physiol.* 1984;246:C160-C166.
53. Bers DM. A simple method for the accurate determination of free  $[\text{Ca}]$  in Ca-EGTA solutions. *Am J Physiol.* 1982;242:C404-C408.
54. Lüthi D, Spichiger U, Forster I, McGuigan JAS. Calibration of  $\text{Mg}(2+) - \text{selective}$  macroelectrodes down to 1  $\mu\text{mol l}^{-1}$  in intracellular and  $\text{Ca}(2+) - \text{containing}$  extracellular solutions. *Exp Physiol.* 1997;82:453-467.
55. McGuigan JAS, Kay JW, Elder HY. An improvement to the ligand optimisation method (LOM) for measuring the apparent dissociation constant and ligand purity in  $\text{Ca}^{2+}$  and  $\text{Mg}^{2+}$  buffer solutions. *Prog Biophys Mol Biol.* 2014;116:203-211.
56. McGuigan JAS, Kay JW, Elder HY. Critical review of the methods used to measure the apparent dissociation constant and ligand purity in  $\text{Ca}^{2+}$  and  $\text{Mg}^{2+}$  buffer solutions. *Prog Biophys Mol Biol.* 2006;92:333-370.
57. Kay JW, Steven RJ, McGuigan JAS, Elder HY. Automatic determination of ligand purity and apparent dissociation constant ( $K_{\text{app}}$ ) in  $\text{Ca}^{2+}/\text{Mg}^{2+}$  buffer solutions and the  $K_{\text{app}}$  for  $\text{Ca}^{2+}/\text{Mg}^{2+}$  anion binding in physiological solutions from  $\text{Ca}^{2+}/\text{Mg}^{2+}$ -macroelectrode measurements. *Comput Biol Med.* 2008;38:101-110.
58. Kay J. <http://www.stats.gla.ac.uk/jim/ligopt.html>. 1999. Accessed September 20, 2017.
59. Rimal IRS, Praseetha PK. Zinc(II) ion selective electrodes. *Int J Pharm Sci Rev Res.* 2016;38:41-50.
60. Westall JC, Morel FMM, Hume DN. Chloride interference in cupric ion selective electrode measurements. *Anal Chem.* 1979;51:1792-1798.
61. Metrohm AG. Manual\_Ion-selective electrodes (ISE). 2013;24.
62. Du Laing G. *Trace Elements in Soils*. Chichester, UK: John Wiley & Sons, Ltd.; 2010. <https://doi.org/10.1002/9781444319477.ch5>
63. Chito D, Weng L, Galceran J, et al. Determination of free  $\text{Zn}^{2+}$  concentration in synthetic and natural samples with AGNES (Absence of Gradients and Nernstian Equilibrium Stripping) and DMT (Donnan Membrane Technique). *Sci Total Environ.* 2012;421-422:238-244.
64. Kalis EJ, Weng L, Temminghoff EJM, van Riemsdijk WH. Measuring free metal ion concentrations in multicomponent solutions using the Donnan membrane technique. *Anal Chem.* 2007;79:1555-1563.
65. Waska H, Koschinsky A, Dittmar T. Fe- and Cu-complex formation with artificial ligands investigated by ultra-high resolution fourier-transform ion cyclotron resonance mass spectrometry (FT-ICR-MS): implications for natural metal-organic complex studies. *Front Mar Sci.* 2016;3:119.
66. Temminghoff EJM, Plette ACC, Van Eck R, Van Riemsdijk WH. Determination of the chemical speciation of trace metals in aqueous systems by the Wageningen Donnan Membrane Technique. *Anal Chim Acta.* 2000;417:149-157.
67. Cloutier-Hurteau B, Sauvé S, Courchesne F. Comparing WHAM 6 and MINEQL+ 4.5 for the chemical speciation of  $\text{Cu}^{2+}$  in the rhizosphere of forest soils. *Environ Sci Technol.* 2007;41:8104-8110.
68. Harrison SM, Bers DM. Correction of proton and Ca association constants of EGTA for temperature and ionic strength. *Am J Physiol.* 1989;256:C1250-C1256.
69. Moody JR, Lindstrom RM. Selection and cleaning of plastic containers for storage of trace element samples. *Anal Chem.* 1977;49:2264-2267.
70. Buettner GR, Jurkiewicz BA. Catalytic metals, ascorbate and free radicals: combinations to avoid. *Radiat Res.* 1996;145:532-541.
71. Peacock JC, Peacock BLD. Some observations on the dissolving of zinc chloride and several suggested solvents. *J Am Pharm Assoc.* 1918;7:689-697.
72. Stumm W, Morgan JJ. *Aquatic Chemistry: Chemical Equilibria and Rates in Natural Waters*. New York: John Wiley & Sons, Inc.; 1995.
73. McGuigan JAS, Lüthi D, Buri A. Calcium buffer solutions and how to make them: a do it yourself guide. *Can J Physiol Pharmacol.* 1991;69:1733-1749.
74. Smith GL, Miller DJ. Potentiometric measurements of stoichiometric and apparent affinity constants of EGTA for protons and divalent ions including calcium. *Biochim Biophys Acta.* 1985;839:287-299.
75. Tsien R, Pozzan T. Measurement of cytosolic free  $\text{Ca}^{2+}$  with quin2. *Methods Enzymol.* 1989;172:230-262.
76. Collier HB. Binding of  $\text{Zn}^{2+}$  by buffers. *Clin Chem.* 1979;25:495-496.
77. Hanlon DP, Watt DS, Westhead EW. The interaction of divalent metal ions with tris buffer in dilute solution. *Anal Biochem.* 1966;16:225-233.
78. Peña MJ, Arevalillo A, Rucandio I, Jiménez JS. Complex species of Zn(II) and Cu(II) in tris buffer solutions—I. Zn(II). *Electrochim Acta.* 1990;35:673-677.
79. Arevalillo A, Pena MJ. Complex species of Zn(II) and Cu(II) in tris buffer solution—II Cu(II). *Electrochim Acta.* 1993;38:957-962.
80. Fischer BE, Häring UK, Tribolet R, Sigel H. Metal ion/buffer interactions: stability of binary and ternary complexes containing 2-amino-2-(hydroxymethyl)-1,3-propanediol (Tris) and adenosine 5'-triphosphate (ATP). *Eur J Biochem.* 1979;94:523-530.

81. Benitez MJ, Company M, Arevalillo A, Jiménez JS. Comparative study of various hydrogen ion buffers to assay Zn(2+) -dependent beta-lactamases. *Antimicrob Agents Chemother.* 1991;35:1517-1519.
82. Nakon R. Free metal ion depletion by 'Good's' buffers. I. N-(2-acetamido)iminodiacetic acid 1:1 complexes with calcium(II), magnesium(II), zinc(II), manganese(II), cobalt(II), nickel(II), and copper(II). *Anal Biochem.* 1979;95:527-532.
83. Pope JM, Stevens PR, Angotti MT, Nakon R. Free metal ion depletion by 'Good's' buffers. II. N-(2-acetamido)-2-aminoethanesulfonic acid (ACESH): complexes with calcium(II), magnesium(II), manganese(II), cobalt(II), zinc(II), nickel(II), and copper(II). *Anal Biochem.* 1980;103:214-221.
84. Lance EA, Rhodes CW, Nakon R. Free metal ion depletion by 'Good's' buffers. III. N-(2-acetamido)iminodiacetic acid, 2:1 complexes with zinc(II), cobalt(II), nickel(II), and copper(II); amide deprotonation by Zn(II), Co(II), and Cu(II). *Anal Biochem.* 1983;133:492-501.
85. Krishnamoorthy CR, Nakon R. Free metal ion depletion by Good's buffers. IV. Bicine 1:1 and 2:1 Complexes with Mg(II), Ca(II), Mn(II), Co(II), Ni(II), Cu(II) and Zn(II). *J Coord Chem.* 1991;23:233-243.
86. Yu Q, Kandedgedara A, Xu Y, Rorabacher DB. Avoiding interferences from Good's buffers: a contiguous series of noncomplexing tertiary amine buffers covering the entire range of pH 3–11. *Anal Biochem.* 1997;253:50-56.
87. Ferreira CMH, Pinto ISS, Soares EV, Soares HMVM. (Un)suitability of the use of pH buffers in biological, biochemical and environmental studies and their interaction with metal ions – a review. *RSC Adv.* 2015;5:30989-31003.
88. Renganathan M, Bose S. Inhibition of photosystem II activity by Cu<sup>++</sup> ion. Choice of buffer and reagent is critical. *Photosynth Res.* 1990;23:95-99.
89. Soares HMVM, Pinho SC, Barros MGRM. Influence of N-substituted aminosulfonic acids with a morpholinic ring pH buffers on the redox processes of copper or zinc ions: a contribution to speciation studies. *Electroanalysis.* 1999;11:1312-1317.
90. Mash HE, Chin Y-P, Sigg L, Hari R, Xue H. Complexation of copper by zwitterionic aminosulfonic (Good) buffers. *Anal Chem.* 2003;75:671-677.
91. Vasconcelos MTS, Almeida CMR. Electrochemical study of proton ionisation, copper(II) complexation and surfactant properties of piperazine-N-N'-bis[2-hydroxypropanesulfonic acid] pH buffer – comparison with other N-substituted aminosulfonic acids pH buffers. *Anal Chim Acta.* 1998;369:115-122.
92. Kandedgedara A, Rorabacher DB. Noncomplexing tertiary amines as 'better' buffers covering the range of pH 3–11. Temperature dependence of their acid dissociation constants. *Anal Chem.* 1999;71:3140-3144.
93. Thompson R, Peterson D, Mahoney W, et al. Fluorescent zinc indicators for neurobiology. *J Neurosci Methods.* 2002;118:63-75.
94. Molecular Probes. Calcium Calibration Buffer Kits [Product Information Sheet]. 2014. [https://tools.thermofisher.com/content/sfs/manuals/CalciumCalibrationBufferKits\\_PI.pdf](https://tools.thermofisher.com/content/sfs/manuals/CalciumCalibrationBufferKits_PI.pdf) Accessed March 5, 2017.
95. Gee KR, Zhou Z-L, Qian W-J, Kennedy R. Detection and imaging of zinc secretion from pancreatic  $\beta$ -cells using a new fluorescent zinc indicator. *J Am Chem Soc.* 2002;124:776-778.
96. Marszałek I, Krężel A, Goch W, Zhukov I, Paczkowska I, Bal W. Revised stability constant, spectroscopic properties and binding mode of Zn(II) to FluoZin-3, the most common zinc probe in life sciences. *J Inorg Biochem.* 2016;161:107-114.
97. Martell AE. Chelating agents for metal buffering and analysis in solution. *Pure Appl Chem.* 1978;50:813-829.
98. Goldberg RN, Kishore N, Lennen RM. Thermodynamic quantities for the ionization reaction of buffers. *J Phys Chem Ref Data.* 2002;31:231-370.
99. El-Roudi OM, Abdel-Latif SA. Effect of ionic strength, aquo-organic solvents, and temperature on the stabilities of N-[Tris(hydroxymethyl)methyl]glycine + metal complexes. *J Chem Eng Data.* 2004;49:1193-1196.
100. Good NE, Douglas Winget G, Winter W, Connolly TN, Izawa S, Singh RMM. Hydrogen ion buffers for biological research. *Biochemistry.* 1966;5:467-477.
101. Grand M, Oliveira HM, Ruzicka J, Measures C. Determination of dissolved zinc in seawater using micro-Sequential Injection lab-on-valve with fluorescence detection. *Analyst.* 2011; 136:2747.

## SUPPORTING INFORMATION

Additional Supporting Information may be found online in the supporting information tab for this article.

**How to cite this article:** Neumaier F, Alpdogan S, Hescheler J, Schneider T. A practical guide to the preparation and use of metal ion-buffered systems for physiological research. *Acta Physiol.* 2017;e12988. <https://doi.org/10.1111/apha.12988>

### 2.3. Publication 3: Journal of General Physiology 150(3): 491-510.

#### Protein phosphorylation maintains the normal function of cloned human Ca<sub>v</sub>2.3 channels.

Felix Neumaier, Serdar Alpdogan, Jürgen Hescheler, and Toni Schneider

##### **Abstract:**

R-type currents mediated by native and recombinant Ca<sub>v</sub>2.3 voltage-gated Ca<sup>2+</sup> channels (VGCCs) exhibit facilitation (run-up) and subsequent decline (run-down) in whole-cell patch-clamp recordings. A better understanding of the two processes could provide insight into constitutive modulation of the channels in intact cells, but low expression levels and the need for pharmacological isolation have prevented investigations in native systems. Here, to circumvent these limitations, we use conventional and perforated-patch-clamp recordings in a recombinant expression system, which allows us to study the effects of cell dialysis in a reproducible manner. We show that the decline of currents carried by human Ca<sub>v</sub>2.3+β<sub>3</sub> channel subunits during run-down is related to adenosine triphosphate (ATP) depletion, which reduces the number of functional channels and leads to a progressive shift of voltage-dependent gating to more negative potentials. Both effects can be counteracted by hydrolysable ATP, whose protective action is almost completely prevented by inhibition of serine/threonine but not tyrosine or lipid kinases. Protein kinase inhibition also mimics the effects of run-down in intact cells, reduces the peak current density, and hyperpolarizes the voltage dependence of gating. Together, our findings indicate that ATP promotes phosphorylation of either the channel or an associated protein, whereas dephosphorylation during cell dialysis results in run-down. These data also distinguish the effects of ATP on Ca<sub>v</sub>2.3 channels from those on other VGCCs because neither direct nucleotide binding nor PIP<sub>2</sub> synthesis is required for protection from run-down. We conclude that protein phosphorylation is required for Ca<sub>v</sub>2.3 channel function and could directly influence the normal features of current carried by these channels. Curiously, some of our findings also point to a role for leupeptin-sensitive proteases in run-up and possibly ATP protection from run-down. As such, the present study provides a reliable baseline for further studies on Ca<sub>v</sub>2.3 channel regulation by protein kinases, phosphatases, and possibly proteases.

##### **Contributions to Publication 3:**

I independently conceptualized and performed all experiments, analyzed and interpreted the data, prepared all of the figures, wrote the manuscript and handled the submission and revision process.



COMMUNICATION

# Protein phosphorylation maintains the normal function of cloned human Ca<sub>v</sub>2.3 channels

Felix Neumaier<sup>1</sup>, Serdar Alpdogan, Jürgen Hescheler, and Toni Schneider<sup>1</sup>

R-type currents mediated by native and recombinant Ca<sub>v</sub>2.3 voltage-gated Ca<sup>2+</sup> channels (VGCCs) exhibit facilitation (run-up) and subsequent decline (run-down) in whole-cell patch-clamp recordings. A better understanding of the two processes could provide insight into constitutive modulation of the channels in intact cells, but low expression levels and the need for pharmacological isolation have prevented investigations in native systems. Here, to circumvent these limitations, we use conventional and perforated-patch-clamp recordings in a recombinant expression system, which allows us to study the effects of cell dialysis in a reproducible manner. We show that the decline of currents carried by human Ca<sub>v</sub>2.3+β<sub>3</sub> channel subunits during run-down is related to adenosine triphosphate (ATP) depletion, which reduces the number of functional channels and leads to a progressive shift of voltage-dependent gating to more negative potentials. Both effects can be counteracted by hydrolysable ATP, whose protective action is almost completely prevented by inhibition of serine/threonine but not tyrosine or lipid kinases. Protein kinase inhibition also mimics the effects of run-down in intact cells, reduces the peak current density, and hyperpolarizes the voltage dependence of gating. Together, our findings indicate that ATP promotes phosphorylation of either the channel or an associated protein, whereas dephosphorylation during cell dialysis results in run-down. These data also distinguish the effects of ATP on Ca<sub>v</sub>2.3 channels from those on other VGCCs because neither direct nucleotide binding nor PIP<sub>2</sub> synthesis is required for protection from run-down. We conclude that protein phosphorylation is required for Ca<sub>v</sub>2.3 channel function and could directly influence the normal features of current carried by these channels. Curiously, some of our findings also point to a role for leupeptin-sensitive proteases in run-up and possibly ATP protection from run-down. As such, the present study provides a reliable baseline for further studies on Ca<sub>v</sub>2.3 channel regulation by protein kinases, phosphatases, and possibly proteases.

## Introduction

Electrophysiological recordings from excised cell patches or dialyzed cells are almost invariably hampered by time-dependent changes in voltage-gated ion channel function. The most common form of these phenomena, termed run-down or washout, is a progressive decline of ionic currents and is thought to reflect changes in intracellular signaling cascades, which occur secondary to the loss or dilution of cytosolic factors (Beccq, 1996). It can be preceded by a transient current facilitation (run-up), which may reflect voltage- and time-dependent repriming (i.e., recovery from inactivation) or modification of signaling cascades that tonically inhibit these currents (Tiaho et al., 1993; Elhamdani et al., 1994, 1995). Although run-down remains a major obstacle for studies on voltage-gated Ca<sup>2+</sup> channel (VGCC) function, it has also provided insight into the manifold regulation of these channels in intact cells. For example, the decline of L-type Ca<sup>2+</sup> currents has been linked to several interrelated processes, which

may include loss of ATP and other cytoplasmic factors, progressive protein dephosphorylation, decoupling of guanosine-5'-triphosphate (GTP)-binding proteins, and possibly increased proteolysis of the channels (Chad et al., 1987; McDonald et al., 1994; Kepplinger and Romanin, 2005; Xu et al., 2016; Yu et al., 2016). In P/Q-, N-, and certain neuronal L-type Ca<sup>2+</sup> channels on the other hand, run-down appears to involve depletion of membrane PIP<sub>2</sub>, a mechanism also thought to mediate M<sub>1</sub> muscarinic receptor-dependent inhibition of these channels (Wu et al., 2002; Suh et al., 2010). Much less is known about the run-down of "pharmacoresistant" R-type currents, which are mainly mediated by Ca<sub>v</sub>2.3-type VGCCs. R-type and R-type-like currents have been shown to exhibit both run-up and run-down (Cota, 1986; Hilaire et al., 1997; Benquet et al., 1999; Almog and Korngreen, 2009), but low expression levels and the need for pharmacological isolation have generally prevented further characterization of the

.....  
 Institute for Neurophysiology, University of Cologne, Cologne, Germany.

Correspondence to Felix Neumaier: [felix@neumaier-net.de](mailto:felix@neumaier-net.de).

© 2018 Neumaier et al. This article is distributed under the terms of an Attribution–Noncommercial–Share Alike–No Mirror Sites license for the first six months after the publication date (see <http://www.rupress.org/terms/>). After six months it is available under a Creative Commons License (Attribution–Noncommercial–Share Alike 4.0 International license, as described at <https://creativecommons.org/licenses/by-nc-sa/4.0/>).



two processes in native cells. The human embryonic kidney (HEK-293) cell line is widely used for heterologous expression of recombinant ion channels and receptors because it contains few endogenous channels, whereas most signaling pathways for regulation and posttranslational processing are operational (Toth et al., 1996; Thomas and Smart, 2005; Clare, 2006). Apart from circumventing the need for R-type current isolation, HEK-293 cells have a simple and uniform shape, which facilitates reproducible manipulation of their intracellular milieu. We therefore used conventional and perforated-patch-clamp recordings together with different inhibitors and cytosolic factors to study the effects of cell dialysis in a stably transfected HEK-293 cell line expressing human  $\text{Ca}_v2.3+\beta_3$  channel subunits. Our findings show that the decline of macroscopic currents during run-down can partly be accounted for by changes in channel voltage dependence and that it can be prevented or slowed down by provision of intracellular ATP and in perforated-patch recordings. Protection from run-down depended on ATP-hydrolysis and was not related to lipid kinase-mediated  $\text{PIP}_2$  synthesis or phosphorylation of tyrosine residues but was sensitive to inhibition of serine/threonine kinases. Protein kinase inhibition in intact cells also reduced peak current densities and reproduced the effects of run-down on channel voltage-dependence. Together, these findings indicate that run-down involves constitutive dephosphorylation of sites on the channels themselves or an associated protein and that ATP promotes phosphorylation of these sites by one or more endogenous kinases. Interestingly, our findings also indicate that the current facilitation during run-up could involve activation of leupeptin (Leu)-sensitive proteases, which may also influence the protective action of ATP.

## Materials and methods

### Cell culture

Human embryonic kidney (HEK-293) cells stably transfected with human  $\text{Ca}_v2.3d$  and  $\beta_3 \text{Ca}^{2+}$  channel subunits (Nakashima et al., 1998) were cultured under normal growth conditions (37°C and 5%  $\text{CO}_2$ ) in Dulbecco's modified Eagle medium (DMEM; Sigma-Aldrich) supplemented with 10% FCS and antibiotics (1% penicillin-streptomycin and selection markers: 1 mg/ml geneticin [G-418] and 200  $\mu\text{g}/\text{ml}$  hygromycin B). Cells were routinely passaged twice a week by using 0.05% trypsin/0.02% EDTA. For electrophysiological recordings, cells were seeded on nitric acid-washed glass coverslips and used within 24–48 h after plating.

### Electrophysiological recordings

Cells were voltage-clamped by using the whole-cell configuration of the patch-clamp technique (Hamill et al., 1981). Pipettes were prepared from thick-walled borosilicate glass capillaries (1.5/0.84-mm-outside/inside diameter; World Precision Instruments) by using a P97 Micropipette puller (Sutter Instruments). Resistance of the resulting electrodes was between 1.5 and 6.5  $\text{M}\Omega$  (mean =  $3.8 \pm 0.1 \text{ M}\Omega$  in 339 recordings) when filled with standard internal solution. The bath was connected to ground via 140 mM sodium chloride agar bridges. Currents were sampled at 20 or 50 kHz and filtered at 10 kHz by using an EPC9 amplifier (HEKA) controlled with HEKA's Pulse software. Leak and

capacitive currents were subtracted online by use of a  $-P/5$  protocol. Recordings obtained with voltage ramps were leak-corrected by a linear fit to the current recorded between  $-80$  and  $-50 \text{ mV}$ , which was extrapolated to  $+60 \text{ mV}$  and subtracted from the whole recording. Series resistance ( $R_s$ ) was compensated electronically by up to 90% (mean  $R_s$  after compensation =  $2.7 \pm 0.1 \text{ M}\Omega$ ) and continuously monitored throughout the measurements. The charging time-constant after compensation was always  $\leq 100 \mu\text{s}$  (mean =  $38 \pm 1 \mu\text{s}$ ), and the maximum uncompensated  $R_s$ -error at the time of peak current was  $\leq 2.5 \text{ mV}$  (mean =  $0.82 \pm 0.04 \text{ mV}$ ). All experiments were performed at room temperature, from a holding potential of  $-80 \text{ mV}$  and, unless noted otherwise, in cells with a whole-cell capacitance ( $C_s$ ) between 5 and 25 pF (mean =  $15 \pm 1 \text{ pF}$ ), as estimated from the slow capacitance compensation of the amplifier. Perforated patch recordings were performed by using  $\beta$ -escin, which was dissolved in type I ultrapure water to prepare a 25 mM stock solution, protected from light and stored at  $-20^\circ\text{C}$  for up to 2 wk. Before the recordings, aliquots of the stock solution were diluted in standard internal solution and vortex-mixed for 1 min to give a final escin concentration of 40  $\mu\text{M}$ . After patch formation, gradual perforation was observed as a progressive increase in the speed and amplitude of capacitive transients during 5-ms voltage-steps to  $-75 \text{ mV}$ . Cells showing signs of spontaneous patch rupture (i.e., sudden increase in the amplitude and speed of capacitive transients) were omitted or used as control recordings to exclude that  $\beta$ -escin itself affected the channel properties or the time course of changes in  $I_{\text{Ba}}$ .

### Recording solutions and drugs

All solutions for electrophysiological experiments were prepared by using type 1 ultrapure water (Milli-Q by Millipore Corporation or Purelab Flex 2 by ELGA Labwater) and, unless noted otherwise, reagents purchased from Sigma-Aldrich. During the recordings, cells were constantly perfused with external solution containing (mM) 120 NaCl, 5  $\text{BaCl}_2$  or  $\text{CaCl}_2$ , 5 KCl, 1  $\text{MgCl}_2$ , 20 TEA chloride, 10 glucose, 10 HEPES, and 0.1 BaEDTA with the pH adjusted to 7.4 by using NaOH and osmolarity of 300–320 mOsm. The solution was filtered through 0.2- $\mu\text{m}$  polyethersulfone membranes and applied to cells at a rate of  $\sim 2\text{--}4 \text{ ml}/\text{min}$  by using a gravity-driven perfusion system controlled by manual precision flow regulators (Sarstedt). The standard intracellular solution was composed of (mM) 130 CsCl, 5 oxaloacetic acid, 5 creatine, 5 pyruvic acid, 10 EGTA, and 10 HEPES with the pH adjusted to 7.3 by using CsOH and osmolarity of 275–295 mOsm. It was stored at  $-20^\circ\text{C}$ , thawed on the day of the experiments, filtered through 0.2- $\mu\text{m}$  surfactant-free cellulose acetate membranes (Corning), and kept on ice between the recordings. The liquid junction potential between internal and external solution (calculated by using the JPCalc algorithm in pClamp 10; Molecular Devices) was  $\sim 5.5 \text{ mV}$ . Because no correction for the liquid junction potential was done, all voltages shown were actually 5.5 mV more negative.

Nucleotide triphosphates (NaATP, MgATP, and MgGTP) were dissolved in 10 mM HEPES to prepare 100 mM stock solutions (pH = 7.3), stored at  $-20^\circ\text{C}$  and diluted in standard internal solution immediately before the recordings. Calmodulin (CaM) was dissolved in type I ultrapure water to prepare a 100  $\mu\text{M}$  stock solution and stored at  $-20^\circ\text{C}$ . AMP-PNP was used as the lithium



salt and dissolved directly in the standard internal solution. Deltamethrin, wortmannin, U73122, genistein, and staurosporine (stauro) were dissolved in DMSO to prepare 2–50 mM stock solutions, protected from light and stored at  $-20^{\circ}\text{C}$ . Before the experiments, they were diluted in standard internal solution, and the same amount of DMSO (0.1–0.25% vol/vol) without drug was added to the internal solution used for parallel control recordings. To account for the short half-life in aqueous media, all solutions containing wortmannin were discarded after a maximum of 20 min after its dilution into standard internal or external solution, respectively. Cytosolic extract was prepared on the day of the experiments by freeze/thaw lysis of  $\sim 2.1 \times 10^7$  cells in 1.5 ml ice-cold pipette solution. After centrifugation at  $0^{\circ}\text{C}$  for 5 min, the supernatant was filtered through a  $0.2\text{-}\mu\text{m}$  surfactant-free cellulose membrane (Corning), an aliquot was removed for quantification of the protein concentration, and the rest was immediately used for the recordings.

### Whole-cell protocols

Unless noted otherwise, time-course recordings were performed by repetitive application at 0.03 Hz of a 30-ms test pulse to +10 mV followed by 10-ms repolarization at  $-50$  mV to record well resolved tail-currents. In some experiments, a 50-ms voltage ramp from  $-80$  mV to +60 mV (2.8 V/s) was used instead of the voltage steps to monitor changes in the quasi steady-state voltage dependence. Because recordings with drugs added to the internal solution could not be used as their own control, we always performed parallel control recordings with standard internal solution. To study changes in current immediately after establishing the whole-cell configuration, cells were clamped at the holding potential of  $-80$  mV before disruption of the patch. After patch rupture, capacitance was quickly compensated by using the auto function of the amplifier, and stimulation started after a delay of no more than 10 s. Because initial current amplitudes were small and several seconds were often required for  $R_s$  to stabilize completely, the first response was always recorded without  $R_s$  compensation. We then stopped stimulation, adjusted the  $R_s$  compensation of the amplifier to achieve maximal compensation without ringing, and restarted the stimulation protocol. To reduce variation introduced by differences in the time required for stabilization of  $R_s$ , initial values ( $I_{\text{start}}$ ) for statistical comparison were always calculated as the average of the first two responses, which also provided a compromise between the lack of  $R_s$  compensation during acquisition of the first response and the time that had already evolved when the second response was recorded. To construct steady-state current-voltage (IV) relationships, peak currents recorded with a protocol consisting of 25-ms test pulses to potentials between  $-80$  mV and +60 mV (10-mV increments at 0.1 Hz) were normalized by the maximum current amplitude at time 0 and plotted as a function of the test-pulse potential. Instantaneous IV (IIV) relationships were obtained with a protocol consisting of a fixed 10-ms prepulse to +60 mV followed by 40-ms test pulses to potentials between  $-80$  mV and +60 mV (10-mV increments at 0.1 Hz). Instantaneous (tail) current amplitudes recorded during the test pulses were normalized by the maximum tail current amplitude at time 0 and plotted as a function of the prepulse potential. The voltage dependence of

activation was assessed by a protocol consisting of 25-ms prepulses to potentials between  $-80$  mV and +60 mV (10-mV increments at 0.1 Hz) followed by a fixed 10-ms test pulse to  $-50$  mV. Tail-current amplitudes recorded during the test pulse were normalized to the maximum tail-current amplitude and plotted as a function of the prepulse potential to construct isochronous activation curves. The fraction of channels available for activation from different holding potentials was assessed by a protocol consisting of 3-s conditioning prepulses at potentials between  $-120$  mV and +10 mV (10-mV increments at 0.1 Hz) followed by a fixed 35-ms test pulse to +10 mV. To construct prepulse inactivation curves, peak current amplitudes recorded during the test pulse were normalized by the maximum amplitude and plotted as a function of the prepulse potential.

### Data analysis and statistics

Leak-subtracted current traces were directly analyzed with PulseFit (HEKA) or exported for further processing with Microsoft Excel 2010 and OriginLab Pro (version 9; OriginLab).

Time-course recordings were quantified in terms of the current increase during run-up, the duration of run-up, and the residual current after 7 min of run-down, as detailed in the results section. To compare the effect of various test solutions, each of these parameters was also normalized by the mean value observed in parallel control recordings according to Eq. 1:

$$\Delta p_t = p_t - \bar{p}_c \quad (1)$$

where  $p_t$  is the value of parameter  $p$  measured in a cell with test solution  $t$ ,  $\bar{p}_c$  is the mean value of  $p$  in parallel control recordings, and  $\Delta p_t$  is the normalized value of  $p$ , which should provide an estimate for the amount of change over control.

IV relationships were fitted with a combined Ohm-Boltzmann equation (Eq. 2):

$$I = (V_m - V_{\text{rev}}) * g_{IV} / (1 + \exp(-(V_m - V_{0.5})/k)), \quad (2)$$

where  $I$  is the (normalized) peak current density measured at the test potential  $V_m$ ,  $V_{\text{rev}}$  is the apparent reversal potential,  $g_{IV}$  is the maximum slope conductance,  $V_{0.5}$  is the voltage eliciting half-maximal inward currents, and  $k$  is the slope factor. Isochronous activation and prepulse inactivation curves were fitted with single Boltzmann equations (Eq. 3):

$$I/I_{\text{max}} = A_2 + (A_1 - A_2) / (1 + \exp((V_m - V_{0.5})/k)), \quad (3)$$

where  $I/I_{\text{max}}$  is the normalized current at the prepulse potential  $V_m$ ,  $V_{0.5}$  is the voltage of half-maximal activation ( $V_{0.5\text{act}}$ ) or inactivation ( $V_{0.5\text{inact}}$ ),  $k$  is the activation ( $k_{\text{act}}$ ) or inactivation ( $k_{\text{inact}}$ ) slope factor, and  $A_1$  and  $A_2$  are the initial and final values, respectively. All fits were performed by using the Levenberg-Marquardt least-squares algorithm, and the goodness of fit was judged based on residual plots and adjusted  $\chi^2$  values. Smooth curves in the figures represent fits to average data whereas values given in the text are average data from fits to individual measurements. Values in the text and figures are expressed as mean  $\pm$  SEM based on the number of independent experiments. Statistical significance was assessed with OriginLab Pro 9 by using a repeated-measures ANOVA followed by Bonferroni's post hoc analysis when comparing mean values from



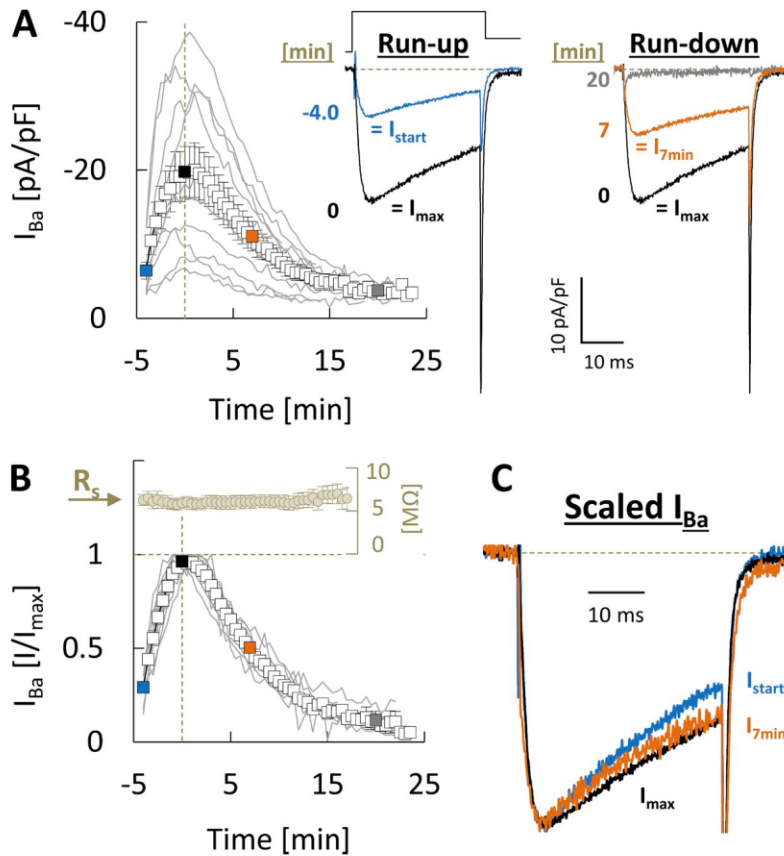


**Figure 1. Evolution and run-down of  $\text{Ca}_v2.3$  channel currents carried by 5 mM  $\text{Ba}^{2+}$ .** (A) Time course of changes in peak whole-cell currents evoked by repetitive step depolarization to 10 mV every 30 s ( $n = 10$ ). For consistency with the later figures, time 0 is defined as the time of maximum inward current ( $I_{\text{max}}$ ). Gray lines in the background indicate time course of changes in individual recordings. Also shown are mean current traces corresponding to the time points indicated next to the traces and by filled symbols in the graph. (B) Same data as in A but normalized to the maximum peak current amplitude ( $I_{\text{max}}$ ). Gray lines in the background indicate the time course of changes in individual recordings. Also shown above is the lack of spontaneous changes in  $R_s$  over the time course of the recordings. (C) Same current traces as in A but scaled to their maximum amplitude to visualize changes in their shape. Values are expressed as mean  $\pm$  SEM.

the same cells or a one-way ANOVA followed by Bonferroni's post hoc analysis when comparing multiple independent mean values. Homogeneity of variances between groups was tested by using Levene's test for equality of variances on the squared deviations. In the case of heteroscedastic data ( $P < 0.05$  in Levene's test and ratio of largest-to-smallest variance  $\geq 4$ ), statistical significance was assessed with Minitab (version 17; Minitab Inc.) by using Welch's ANOVA and the Games-Howell multiple-comparison method. The secondary  $\text{Ca}_v2.3$  channel structure in Fig. 14 was visualized by using the web-based tool Protter for interactive protein feature visualization (available at <http://wlab.ethz.ch/protter/start/>; Omasits et al., 2014). Phosphorylation sites in the same figure were predicted at the highest threshold with the Group-based Prediction Software for Prediction of Kinase-specific Phosphorylation Sites 3.0 (available at <http://gps.biocuckoo.org>; Xue et al., 2008).

## Results

### Evolution and run-down of cloned $\text{Ca}_v2.3$ channel currents

Fig. 1 summarizes changes over time in macroscopic  $\text{Ca}_v2.3$  channel currents carried by 5 mM  $\text{Ba}^{2+}$  and evoked by voltage-steps to 10 mV in dialyzed HEK-293 cells. Peak current amplitudes recorded immediately after establishing the whole-cell configuration ( $I_{\text{start}}$ ) were small and tended to increase for several minutes (run-up) until they reached a maximum value ( $I_{\text{max}}$ ). This was invariably followed by a progressive but somewhat slower current decline (run-down), so that the response that remained

7 min after complete run-up ( $I_{7\text{min}}$ ) amounted to approximately half of the maximum current amplitude (Fig. 1, A and B).

We quantified the time course of changes by estimating (1) the time required after patch rupture for currents to reach  $I_{\text{max}}$  (= time to  $I_{\text{max}}$ ), (2) the ratio between  $I_{\text{max}}$  and  $I_{\text{start}}$  (= increase), and (3) the ratio between  $I_{7\text{min}}$  and  $I_{\text{max}}$  (= remaining  $I_{\text{Ba}}$ ). Under standard recording conditions (Fig. 1), with mean  $R_s$  and  $C_s$  values of  $6 \pm 1 \text{ M}\Omega$  and  $14 \pm 1 \text{ pF}$ , respectively ( $n = 10$ ), run-up took  $4 \pm 1 \text{ min}$  and was associated with a  $2.7 \pm 0.2$ -fold increase of peak  $I_{\text{Ba}}$  at 10 mV, whereas the residual current amplitude after partial run-down amounted to  $42 \pm 4\%$  of its maximum value.

As illustrated by inspection of scaled current traces (Fig. 1 C), the initial increase of currents was paralleled by a decrease of fractional inactivation during the 30-ms test-pulses from  $53 \pm 4\%$  immediately after establishing the whole-cell configuration to  $40 \pm 4\%$  ( $P < 0.001$ ) after complete run-up. On the other hand, run-down tended to increase inactivation, although quantification of this effect was often confounded by the reduced signal-to-noise ratio due to current decline (but see also Fig. 13 E).

The general time course of changes was very similar among cells with different peak current densities, not attributable to voltage loss or  $R_s$  variation (Fig. 1 B) and unaffected by inclusion of two 3-min resting periods without stimulation (not depicted).

### Factors involved in run-up and run-down

Increased mechanical tension associated with fluid flow has been shown to cause run-up and functional alterations in some other VGCCs (Peng et al., 2005; Park et al., 2007), but the time-dependent

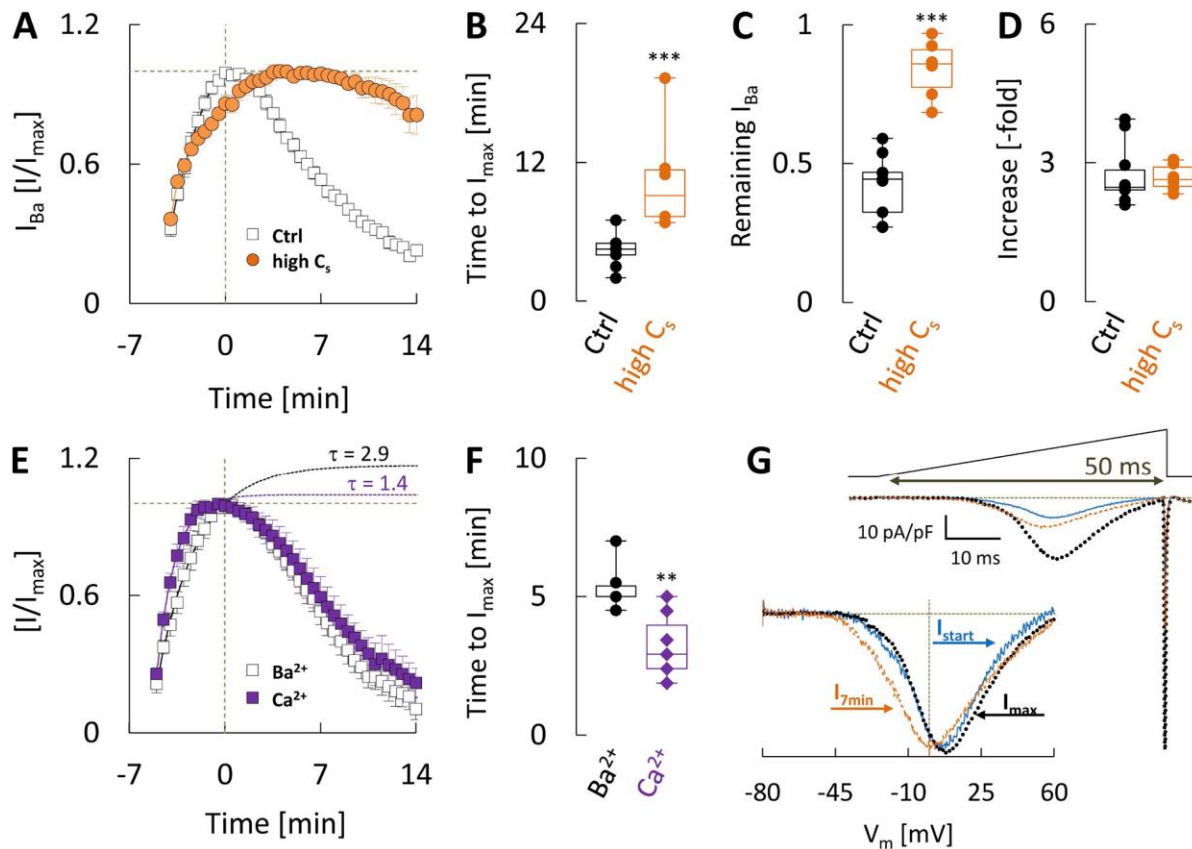


**Figure 2. Dependence of run-up and run-down on cell dialysis,  $\text{Ca}^{2+}$ , and voltage.** (A) Comparison of time-course recordings performed under standard recording conditions (Ctrl, with  $R_s = 6 \pm 1 \text{ M}\Omega$  and  $C_s = 14 \pm 1 \text{ pF}$ ; same data as in Fig. 1) or with high-resistance pipettes ( $R_s = 12 \pm 1 \text{ M}\Omega$ ) in large cells ( $C_s = 29 \pm 6 \text{ pF}$ ) to retard cytosolic dilution (high  $C_s$ ,  $n = 6$ ). (B) Comparison of the run-up duration, determined as the time required for currents to reach their maximum amplitude (same cells as in A). (C) Comparison of the residual current after partial run-down, determined as the ratio between current amplitudes after 7 min of run-down and at time 0 (same cells as in A). (D) Comparison of the current increase during run-up, determined as the ratio between maximum and initial current amplitude (same cells as in A). (E) Comparison of time-course recordings performed with 5 mM  $\text{Ba}^{2+}$  ( $n = 5$ ) or  $\text{Ca}^{2+}$  ( $n = 5$ ) as the charge carrier. Dotted lines are extrapolated single exponential fits to the evolution of currents during run-up, which yielded the time-constant indicated above. (F) Comparison of the run-up duration observed with  $\text{Ba}^{2+}$  or  $\text{Ca}^{2+}$  as the charge carrier (same cells as in E). (G) Mean current traces evoked by a 50-ms voltage ramp from  $-80 \text{ mV}$  to  $60 \text{ mV}$  immediately after establishing the whole-cell configuration ( $I_{\text{start}}$ , blue solid line), at the time of maximum  $I_{\text{Ba}}$  ( $I_{\text{max}}$ , black solid line) and after 7 min of run-down ( $I_{7\text{min}}$ , orange broken line;  $n = 7$ ). Inset: Same current traces but scaled to their maximum value to illustrate the lack of changes in position and shape during run-up and subsequent left shift of the curve during run-down. \*\*,  $P < 0.01$ ; \*\*\*,  $P < 0.001$  vs. Ctrl in B and C or vs.  $\text{Ba}^{2+}$  in F (one-way ANOVA with Bonferroni post-hoc correction). Values are expressed as mean  $\pm$  SEM.

changes in  $\text{Ca}_v2.3$  channel current were still observed when recordings were performed under static (i.e., without perfusion) conditions ( $n = 3$ ; not depicted). As would be expected for a process that involves diffusion-controlled depletion of metabolic substrates or other cytosolic factors on the other hand, the time course but not magnitude of changes in  $I_{\text{Ba}}$  depended on the absolute values of  $R_s$  (i.e., cell-pipette coupling) and  $C_s$  (i.e., cell size), so that combined use of smaller pipette tip diameters ( $R_s = 12 \pm 1 \text{ M}\Omega$ ) and larger cells ( $C_s = 29 \pm 6 \text{ pF}$ ) resulted in a significant slowing of run-up and run-down compared with standard recording conditions (Fig. 2, A–D). Unless noted otherwise, the following experiments were all performed under standard recording conditions to facilitate fast and reproducible cell dialysis.

As shown in Fig. 2 E, the characteristic sequence of changes was also observed when recordings were performed with 5 mM  $\text{Ca}^{2+}$  as the charge carrier (Fig. 2 E), although run-up was significantly faster (Fig. 2 F) and appeared to be more complete when

compared with parallel recordings with 5 mM  $\text{Ba}^{2+}$ . Moreover,  $I_{\text{start}}$  (but not  $I_{\text{max}}$  or  $I_{7\text{min}}$ ) was significantly larger in recordings performed with  $\text{Ca}^{2+}$ , suggesting that run-up but not run-down may be initiated or facilitated by a  $\text{Ca}^{2+}$ -dependent mechanism.

Because changes in the ionic conditions during cell dialysis could affect currents by altering the driving force, we also examined the quasi-steady-state voltage dependence of  $I_{\text{Ba}}$  with a 50-ms voltage-ramp from  $-80$  to  $60 \text{ mV}$  (Fig. 2 G). Run-up was similar over the whole voltage range and not associated with changes in the apparent reversal potential ( $V_{\text{rev}}$ ), so that initial ( $I_{\text{start}}$ , blue solid line) and run-up ( $I_{\text{max}}$ , black solid line) currents overlapped almost completely when scaled to their maximum amplitude (Fig. 2 G, inset). Currents recorded after partial run-down ( $I_{7\text{min}}$ , orange dotted line) still had the same  $V_{\text{rev}}$  but were shifted to more negative stimulus voltages, suggesting that their decline is not the result of a change in driving force but influenced by the test potential.



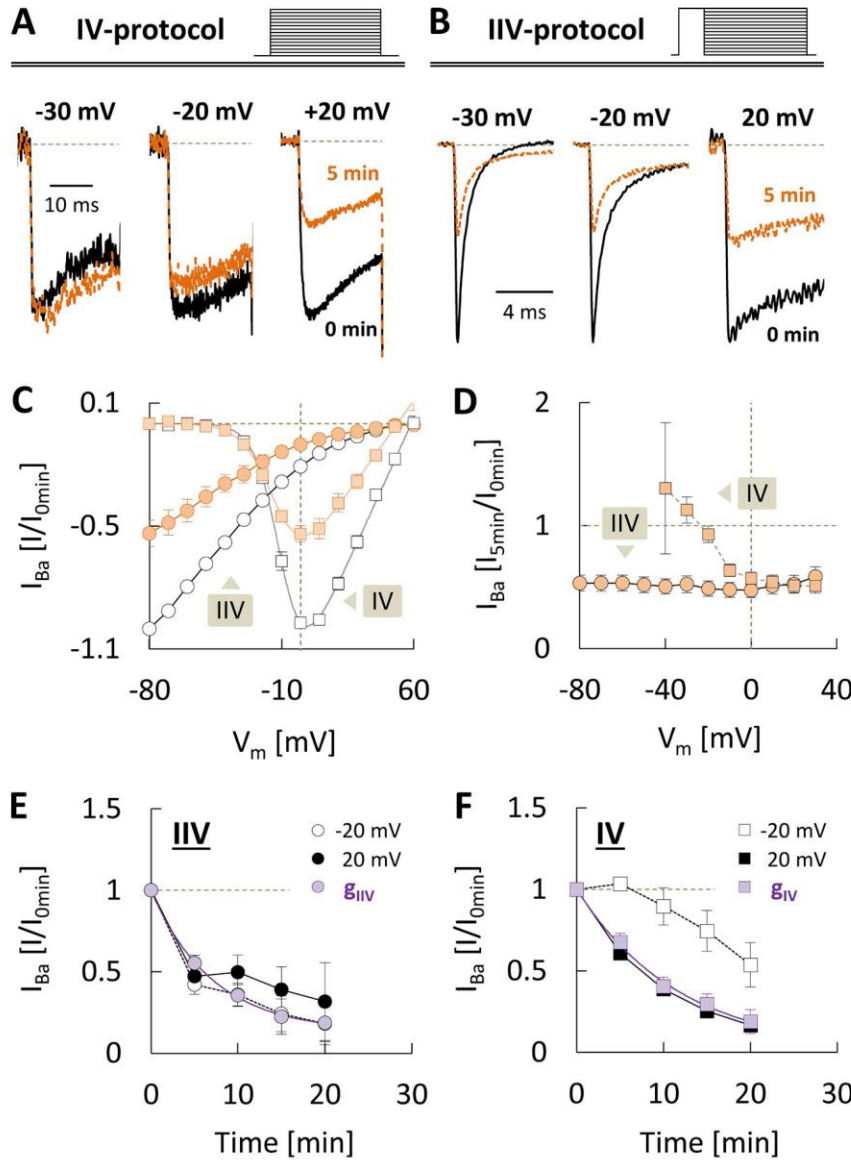


**Figure 3. Voltage dependence of steady-state and instantaneous current decline.** (A) Mean steady-state (IV) currents ( $n = 6$ ) recorded at the indicated test potentials before (black lines) and after 5 min of run-down (orange lines). To allow for comparison of the relative change at different test potentials, they have been normalized to the peak current amplitude observed at each voltage before run-down. (B) Mean instantaneous (IIV) currents recorded from the same cells as in A before (black lines) and after 5 min of run-down (orange lines). To allow for comparison of the relative change at different test potentials, they have been normalized as in A. (C) Comparison of steady-state IV (squares) and IIV (circles) relationships, determined immediately after complete run-up (open symbols) and after 5 min of run-down (orange symbols; same cells as in A and B). (D) Voltage dependence of the fraction of IV (squares) and IIV (circles) current remaining after 5 min of run-down, determined as the ratio between current amplitudes after 5 min of run-down and current amplitudes at time 0 (same cells as in A–C). (E) Mean changes over time in the fraction of IIV current recorded at  $-20$  mV (open circles with dotted line) and  $+20$  mV (black circles with solid line) and in the slope conductance ( $g_{IV}$ ) between  $-80$  and  $0$  mV (same cells as in A–D). (F) Mean changes over time in the fraction of IV current recorded at  $-20$  mV (open squares with dotted line) and  $+20$  mV (black squares with solid line) and in the maximum slope conductance ( $g_{IV}$ ) determined from IV relationships (same cells as in A–E). Values are expressed as mean  $\pm$  SEM.

**Run-down involves separable changes in gating and maximum conductance**

The macroscopic conductance of a uniform population of voltage-gated channels can be approximated by the product of (1) the voltage- and time-dependent channel open probability ( $P_O$ ), (2) the holding potential-dependent availability for activation ( $P_F$ ), and (3) the voltage-independent maximum macroscopic conductance ( $G_{max}$ ), which depends on single-channel conductance ( $\gamma$ ), the total number of channels ( $N$ ), and the maximum values of  $P_O$  ( $P_{O,max}$ ) and  $P_F$  ( $P_{F,max}$ ). In this framework, run-down could involve reduced activation, increased inactivation, and/or an intrinsically voltage-dependent decrease of  $G_{max}$ . In a first attempt to distinguish between these possibilities, we compared steady-state (IV) and instantaneous (IIV) current-voltage relationships, determined at the onset of run-down and in 5-min intervals thereafter (Fig. 3, A–C). Because IIV currents were recorded immediately after a brief prepulse to open most channels available for activation,

they should be little affected by changes in the voltage-dependence of  $P_O$ . Fig. 3 D plots the fraction of IV and IIV currents that remained after partial run-down for 5 min as a function of the test potential. The decline of steady-state currents increased with voltage but reached voltage-independent values at positive test potentials (where  $P_O$  approaches  $P_{O,max}$ ), which is consistent with the shift of ramp-evoked currents (Fig. 2 G). When measured with the IIV protocol on the other hand, run-down was about the same at different test potentials and similar to IV-current decline at depolarized voltages (Fig. 3 D). The same pattern was observed at the later time points examined, so that the kinetics of IIV-current run-down were well represented by the exponential decline in slope conductance between  $-80$  and  $0$  mV ( $\tau = 7 \pm 2$  min,  $g_{IIV}$  in Fig. 3 E). The time course of IV-current decline was markedly delayed during weak depolarization but similar when it was measured at sufficiently positive test potentials ( $\tau = 9 \pm 1$  min) or in terms of the maximum slope conductance ( $\tau = 10 \pm 2$  min,



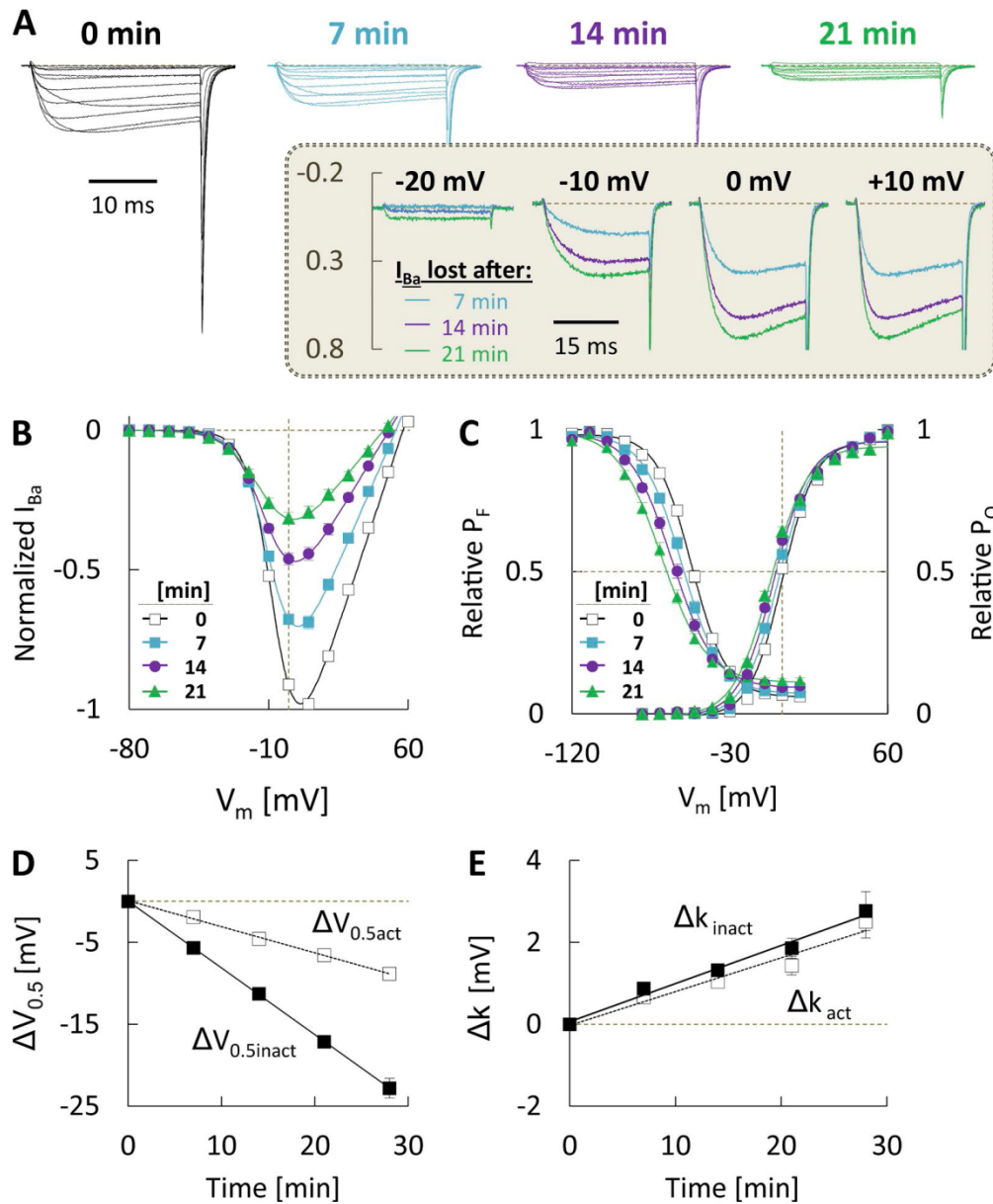
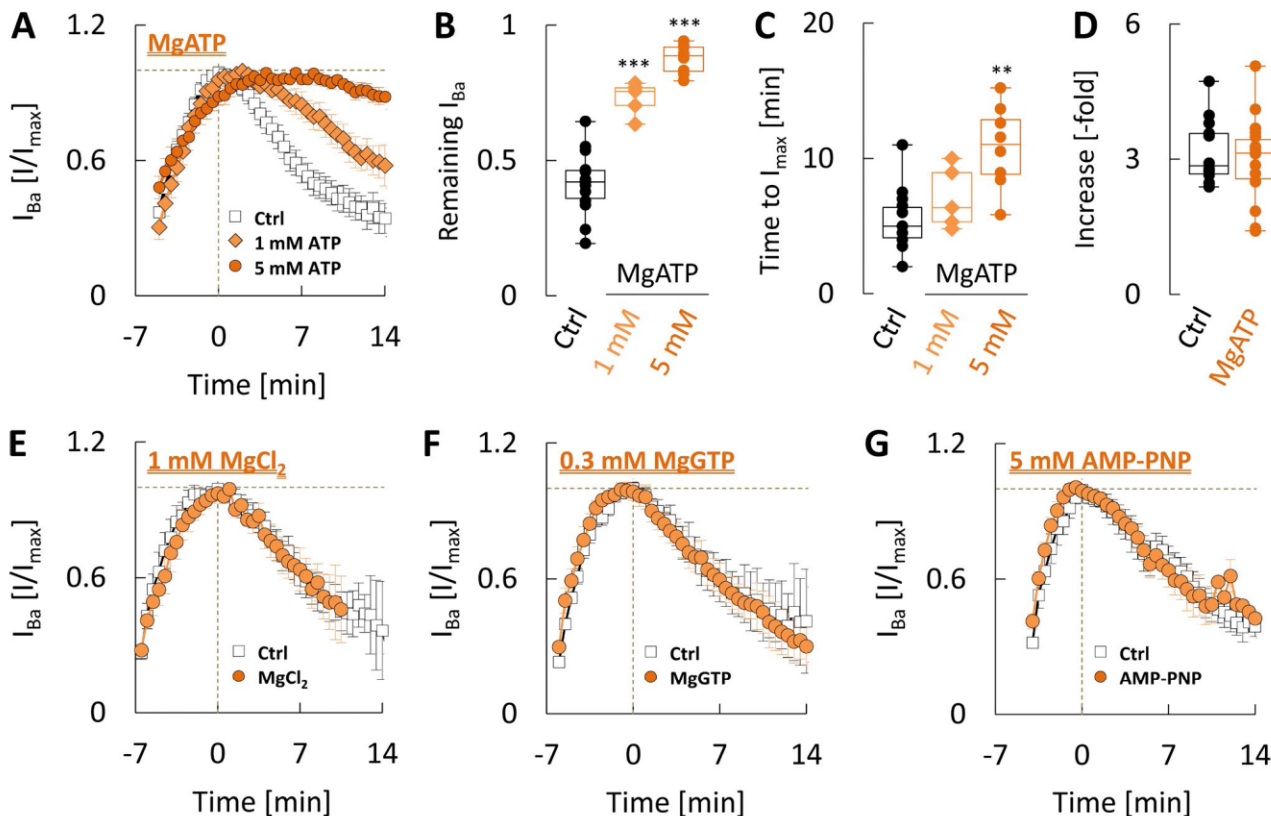


Figure 4. **Changes in channel voltage dependence during run-down.** (A) Families of mean IV currents ( $n = 8$ ) evoked by 25 ms voltage steps to test potentials between  $-80$  mV and  $+60$  mV at the onset of run-down (0 min) and in 7-min intervals thereafter. They have been normalized to the maximum peak  $I_{Ba}$  at time 0. Inset: Current lost to run-down at the indicated test potentials, determined by subtracting from the normalized current traces recorded at time 0 the corresponding traces recorded after 7 (orange lines), 14 (purple lines), and 21 min (green lines) of run-down. (B) Mean IV relationships measured at the same time points as in A and normalized to the maximum peak current amplitude recorded at time 0 ( $n = 49$ ). (C) Voltage dependence of activation (right) and prepulse inactivation (left), determined at the same time points as in A (same cells as in B). (D) Time course of changes in the half-activation ( $V_{0.5act}$ ) and half-inactivation ( $V_{0.5inact}$ ) voltages, determined from single Boltzmann fits to the data in C. (E) Time course of changes in the activation ( $k_{act}$ ) and inactivation ( $k_{inact}$ ) slope factors, determined from single Boltzmann fits to the data in C. Values are expressed as mean  $\pm$  SEM.

$g_{IV}$  in Fig. 3 F). Based on these findings, the decrease of macroscopic conductance by itself was independent of the test-pulse potential and had an approximately exponential time course, so the apparent voltage-dependence must have derived from changes in the voltage dependence of  $P_O$ , which (partly) counteracted IV-current decline and even caused some transient stimulation at negative test potentials.

### Run-down is paralleled by changes in channel voltage dependence

To assess how changes in the voltage dependence of  $P_O$  and  $P_F$  are involved in current decline, we compared IV, activation, and prepulse inactivation curves (for details on the voltage protocols see Materials and methods), determined at different time points after the onset of run-down. Fig. 4 summarizes the results



**Figure 5. Hydrolysable ATP provides protection from  $Ca_v2.3$  channel run-down.** Comparison between time-course recordings performed with the indicated test substances and parallel control recordings with standard internal solution. **(A)** Mean data from 5 recordings with 1 mM MgATP (orange squares), 8 recordings with 5 mM MgATP (orange circles), and 13 parallel control recordings (open squares). **(B)** Comparison of the residual  $I_{Ba}$  after 7 min of run-down under control conditions and with 1 or 5 mM MgATP in the pipette solution (same cells as in A). **(C)** Comparison of the run-up duration under control conditions and with 1 or 5 mM MgATP in the pipette solution (same cells as in A). **(D)** Comparison of the current increase under control conditions and with 1–5 mM MgATP in the pipette solution (same cells as in A). **(E)** Mean data from five recordings with 1 mM  $MgCl_2$  (orange squares) and seven parallel control recordings (open squares). **(F)** Mean data from six recordings with 0.3 mM MgGTP (orange squares) and five parallel control recordings (open squares). **(G)** Mean data from eight recordings with 5 mM AMP-PNP (orange squares) and seven parallel control recordings (open squares). \*\*,  $P < 0.01$ ; \*\*\*,  $P < 0.001$  vs. Ctrl (one-way ANOVA with Bonferroni post hoc correction). Values are expressed as mean  $\pm$  SEM.

obtained in a total of 49 cells ( $C_{slow} = 29 \pm 2$  pF), from which meaningful currents could be recorded for at least 21 min. The shape of IV current lost to run-down (Fig. 4 A, inset), was essentially identical to the shape at time 0 and contained a prominent ON-gating current component, suggesting that run-down reduced the total number of active channels (i.e.,  $P_F$  at  $-80$  mV,  $P_{F,max}$ , and/or  $N$ ). It was paralleled by progressive but unequal hyperpolarizing shifts of activation and prepulse inactivation, which are illustrated in Fig. 4 (C and D). The half-activation voltage ( $V_{0.5act}$ ) significantly decreased from  $0 \pm 1$  mV at time 0 to  $-6 \pm 1$  mV ( $P < 0.001$ ) after 21 min of run-down, corresponding to a shift by roughly  $-6$  mV. In the same time, the half-inactivation voltage ( $V_{0.5inact}$ ) significantly decreased from  $-52 \pm 1$  mV to  $-69 \pm 1$  mV ( $P < 0.001$ ), corresponding to a shift by roughly  $-17$  mV. In both cases, the rate of shift in individual recordings could be well described by linear fits to the changes in half-point as a function of time, with slopes of  $-0.33 \pm 0.02$  mV/min (adjusted  $R^2 = 0.90 \pm 0.02$ ) for activation and  $-0.82 \pm 0.03$  mV/min (adjusted  $R^2 = 0.95 \pm 0.01$ ) for inactivation. Based on these findings,  $P_F$  at  $-80$  mV was reduced by  $\sim 5, 12,$  and  $19\%$  after 7, 14, and 21 min of run-down, respectively (Fig. 4 C), which corresponds to a constant rate of roughly  $1\%$

min. In the same time,  $g_{IV}$  declined by  $\sim 25, 47,$  and  $61\%$ , so that reduced availability for activation alone could only explain part of the IV-current decline at positive test potentials (Fig. 4 B). Together with a complete loss of gating currents during run-down, these findings suggested that the decline in conductance involves additional (holding potential-independent) changes in the number of active channels (i.e.,  $N$  and/or  $P_{F,max}$ ). This was also evident in time-course recordings where the holding potential after partial run-down was made more negative, which led to considerable but incomplete recovery of the current at 10 mV (not depicted).

In addition to the shift, run-down reduced the steepness of both curves in Fig. 4 C, which was reflected in a gradual increase of the activation and inactivation slope factors ( $k_{act}$  and  $k_{inact}$ ) from  $9.0 \pm 0.2$  and  $9.2 \pm 0.1$  mV/e-fold change at time 0 to  $10.5 \pm 0.3$  ( $P < 0.001$ ) and  $11.1 \pm 0.3$  ( $P < 0.001$ ) mV/e-fold change after 21 min of run-down, respectively (Fig. 4 E).

#### Hydrolysable ATP provides protection from run-down

Because one of the most common reasons for “washout” of ionic currents is a decrease in the level of intracellular high-energy

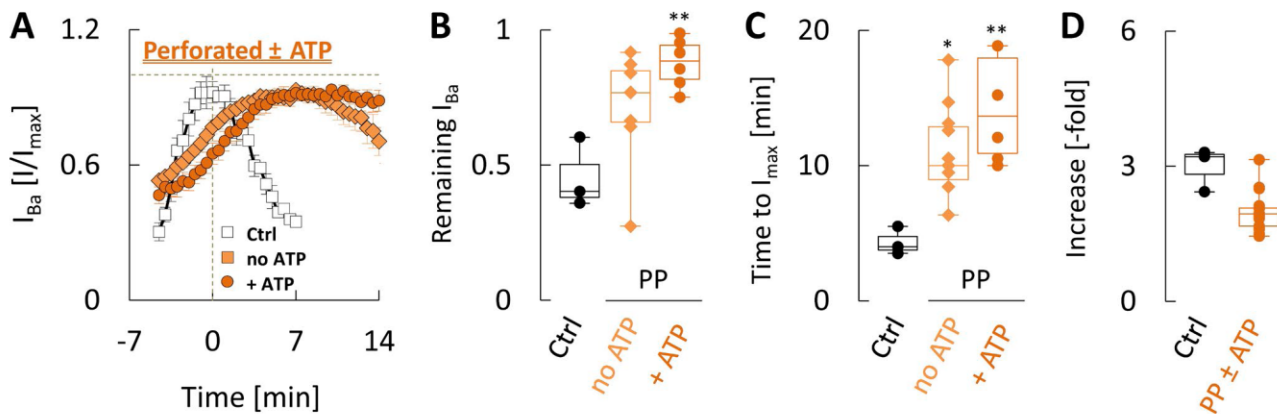


**Figure 6. ATP protection from run-down is reproduced by perforated-patch recordings.** Comparison of time-course recordings with 40  $\mu\text{M}$   $\beta$ -escin in the absence and presence of MgATP. **(A)** Mean data from 11 perforated-patch recordings with standard internal solution (orange diamonds), 6 perforated-patch recordings with 5 mM MgATP (orange circles), and 3 perforated-patch recordings with standard internal solution in which the patch ruptured during perforation (open squares). All recordings were performed with 40  $\mu\text{M}$   $\beta$ -escin as the perforating agent. **(B)** Comparison of the residual  $I_{\text{Ba}}$  after 7 min of run-down in recordings with patch rupture and in perforated recordings without or with 5 mM MgATP (same cells as in A). **(C)** Comparison of the run-up duration in recordings with patch rupture and in perforated recordings without or with 5 mM MgATP (same cells as in A). **(D)** Comparison of the current increase in recordings with patch rupture and in perforated recordings without or with 5 mM MgATP (same cells as in A). \*,  $P < 0.05$ ; \*\*,  $P < 0.01$  vs. Ctrl (one-way ANOVA with Bonferroni post hoc correction). Values are expressed as mean  $\pm$  SEM.

compounds or other cytosolic factors, we next tested if different forms and concentrations of nucleotide triphosphates, a cytosolic extract, and/or perforated-patch recordings are effective in altering run-down. To this end, the time course of changes in peak  $I_{\text{Ba}}$  under various experimental conditions was quantified as described above and compared with parallel control recordings performed with standard internal solution (Figs. 5 and 6). To facilitate comparison of effects between the different experiments, Fig. 7 summarizes mean changes expressed relative to the corresponding control recordings (i.e.,  $\Delta$  Increase,  $\Delta$  Time to  $I_{\text{max}}$ , and  $\Delta$  Remaining  $I_{\text{Ba}}$ ), which were determined by subtracting from each individual value with the indicated test solutions the mean value determined in parallel control recordings (for details see Materials and methods). As can be seen in Fig. 5, addition of 1–5 mM MgATP to the pipette solution significantly increased the current fraction that remained after 7 min of run-down compared with parallel control recordings (Fig. 5, A and B) and produced a concentration-dependent slowing of run-up (Fig. 5, A and C). These effects were not attributable to changes in intracellular free  $\text{Mg}^{2+}$  ( $\sim 0.4$  mM with 5 mM MgATP) because addition of 1 mM  $\text{MgCl}_2$  alone ( $\sim 0.5$  mM free  $\text{Mg}^{2+}$ ) to the standard internal solution affected neither run-up nor run-down (Fig. 5 E). Moreover, with a pipette solution containing 5 mM NaATP and no added free  $\text{Mg}^{2+}$ , there was still a significant slowing of run-up and a significant increase of the current fraction remaining after 7 min of run-down (Fig. 7, A and C).

ATP protection from run-down was about the same with different charge carriers (i.e.,  $\text{Ba}^{2+}$  vs.  $\text{Ca}^{2+}$ ) and not altered when the nucleotide was combined with 3  $\mu\text{M}$  CaM (Fig. 7 C). Supplementation of the pipette solution with 0.3 mM MgGTP (Fig. 5 F) or 5 mM of the nonhydrolyzable ATP-analogue AMP-PNP (Fig. 5 G) on the other hand affected neither run-up nor run-down (Fig. 7). Together, these findings argue against a role of direct nucleotide binding and indicate a requirement for ATP-hydrolysis and transfer of the phosphate group.

Note also that (with  $\text{Ba}^{2+}$  as the charge carrier) none of the manipulations tested significantly altered the magnitude of run-up (Figs. 5 B and 7 B) or the absolute values of  $I_{\text{max}}$  (not depicted), suggesting that ATP can slow but not prevent the processes underlying run-up. The apparent increase in the magnitude of run-up by ATP observed with  $\text{Ca}^{2+}$  as the charge carrier (Fig. 7 B) was also not related to a more pronounced up-regulation of  $I_{\text{Ca}}$  per se because absolute values of  $I_{\text{max}}$  were the same as in parallel control recordings (not depicted). Although there was a tendency for  $I_{\text{start}}$  to be smaller in recordings with ATP, this effect could hardly be ascribed to an action of the nucleotide. Because the faster run-up kinetics in  $\text{Ca}^{2+}$  hampered accurate determination of  $I_{\text{start}}$ , it might instead have resulted from small differences between groups in the time required for  $R_s$  to stabilize after patch-rupture.

#### ATP protection is reproduced by perforated-patch recordings

In principle, exogenous ATP might counteract run-down by preventing a decrease of cytosolic nucleotide levels or by increasing them above the normal value in intact cells, thereby stimulating the channels through an unrelated mechanism. To distinguish between these two possibilities, we performed perforated-patch recordings with  $\beta$ -escin, diluted into the same internal recording solution as in ruptured-patch experiments. ATP-diffusion through  $\beta$ -escin pores has been demonstrated, but perforating efficiency is concentration and time dependent, so washout should be considerably slower than in ruptured-patch recordings (Arnould et al., 1996; Fan and Palade, 1998; Fu et al., 2003). As illustrated in Fig. 6 A and summarized in Fig. 7, the time course of changes during perforated recordings was very similar to that observed in ruptured recordings with ATP. Importantly, and consistent with a role of ATP-depletion for the current decline, perforated recordings were almost as effective in reducing run-down as provision of ATP in ruptured recordings. Moreover, the protective



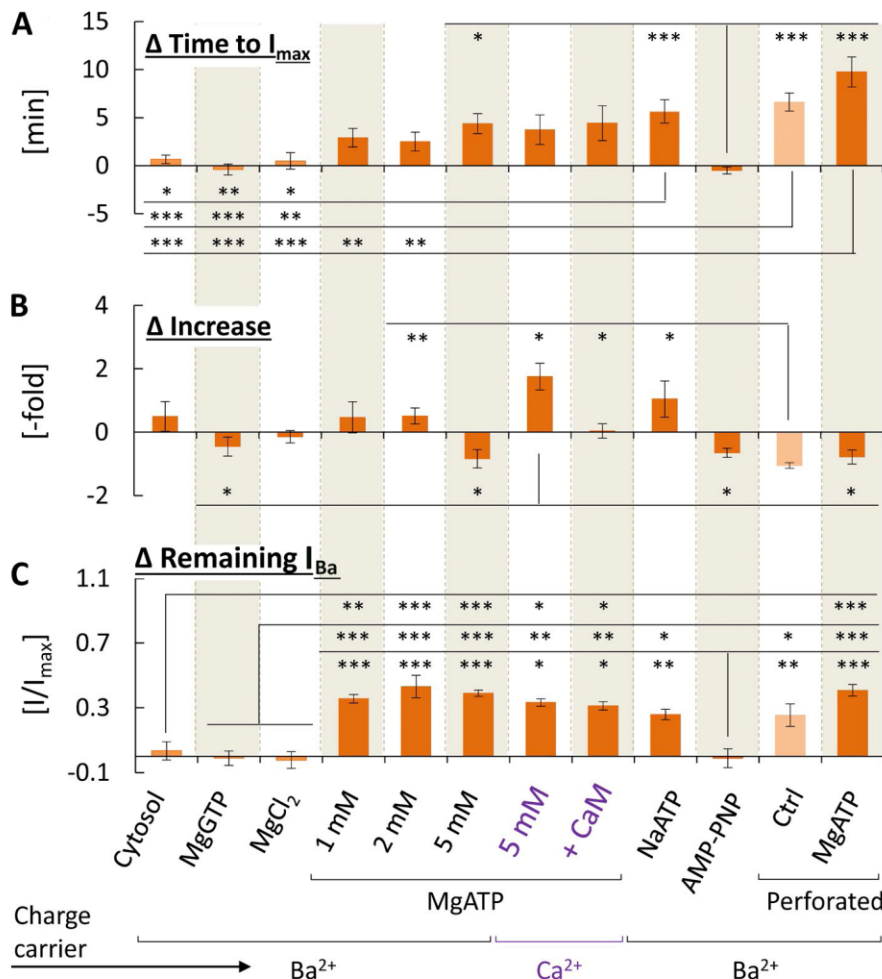


Figure 7. Overview of changes in run-up and run-down observed under various experimental conditions. Data are from the same cells as in Figs. 5 and 6 with additional data from 7 recordings with cytosolic extract (Cytosol) and 6 parallel control recordings, 9 recordings with 5 mM NaATP and 7 parallel control recordings, and 13 recordings performed with Ca<sup>2+</sup> as the charge carrier and 5 mM MgATP in the presence or absence of 3 μM CaM plus 5 parallel control recordings. For comparison between the different experimental conditions, all values obtained with a given test solution were normalized by subtracting the mean value observed in parallel control recordings and then averaged, so the derived parameters provide a measure for the mean change relative to control (for details see Materials and methods). Symbols for statistical significance refer to the comparison of normalized values between different experimental conditions. (A) Comparison of mean changes relative to parallel control recordings in the duration of run-up (Δ Time to I<sub>max</sub>). (B) Comparison of mean changes relative to parallel control recordings in the magnitude of run-up (Δ Increase). (C) Comparison of mean changes relative to parallel control recordings in the residual current after 7 min of run-down (Δ Remaining I<sub>Ba</sub>). \*, P < 0.05; \*\*, P < 0.01; \*\*\*, P < 0.001 (one-way ANOVA with Bonferroni post hoc correction in A and C or Welch's ANOVA with the Games-Howell multiple-comparison method in B). Values are expressed as mean ± SEM.

effects of perforated recordings and ATP were not additive, so that provision of 5 mM MgATP in perforated recordings produced the same effects as in ruptured recordings (Figs. 6 B and 7 C). Collectively, these findings indicate that both, perforated recording and/or provision of ATP reduced run-down by preventing depletion of the nucleotide during the recordings. This is in contrast to the effects on run-up duration, which were much more pronounced in perforated recordings and further increased in the presence of ATP (Figs. 6 C and 7 A). Moreover, because our measurements were started only after R<sub>o</sub> had reached values ≤15 MΩ, we most likely missed part of the run-up process, so these results may still underestimate the true slowing of run-up in perforated recordings. Thus, the initial but not maximum peak current density was significantly larger in perforated recordings (not depicted), and this was reflected in a reduced magnitude of run-up (Figs. 6 D and 7 B). Together, these observations point to the involvement of additional cytosolic factors during run-up, which are more effectively retained in perforated-patch recordings. However, a cytosolic extract prepared in standard internal solution (4.32 mg protein/ml) was ineffective in altering run-up or run-down (Fig. 7), possibly because these factors depend on the additional presence of ATP.

#### ATP stabilizes channel gating and maximum conductance

All the above findings supported the assumption that Ca<sub>v</sub>2.3 channel run-down and, to some extent, run-up in dialyzed cells are related to a depletion of cytosolic ATP. Because it was of interest how ATP affects the different alterations associated with run-down, we reexamined the changes in channel voltage dependence during current decline with a pipette solution supplemented with 5 mM MgATP. As illustrated in Fig. 8 A, inclusion of ATP completely abolished the early phase of current decline, so that on average, g<sub>IV</sub> after 7 min of run-down amounted to 97 ± 7% of its initial value (n = 6). In addition, the stabilizing action of ATP was associated with an almost complete prevention of time-dependent changes in channel voltage dependence and sensitivity (Fig. 8, B-E), suggesting that basal ATP-dependent modulation alters channel-gating behavior and is required for maintaining it in a functional state.

#### The effects of ATP are not related to lipid kinase-mediated PIP<sub>2</sub> synthesis

Because run-down of several neuronal VGCCs and its reversal by MgATP have been linked to depletion and resynthesis of membrane PIP<sub>2</sub>, respectively (Wu et al., 2002; Suh et al., 2010), we next examined the effects of wortmannin (WM), a potent and

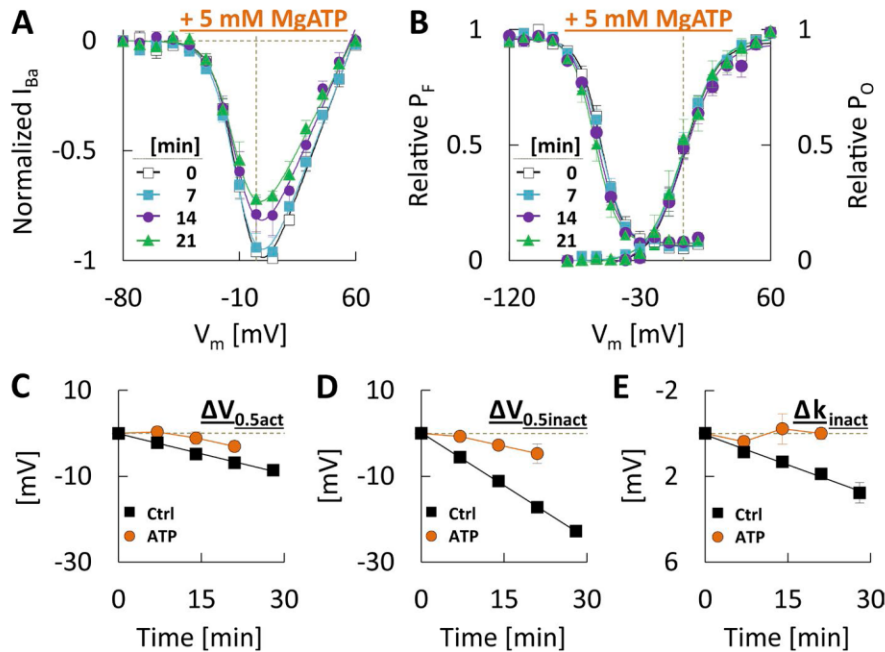


Figure 8. **Hydrolysable ATP stabilizes  $Ca_v2.3$  channel gating and function.** (A) Mean IV relationships measured at the onset of run-down and in 7-min intervals thereafter with a pipette solution containing 5 mM MgATP ( $n = 6$ ). (B) Voltage dependence of activation (right) and pre-pulse inactivation (left), determined at the same time points as in A (same cells as in A). (C) Time course of changes in the half-activation voltage during run-down observed in the absence (black squares, same cells as in Fig. 4) and presence (orange circles, same cells as in A) of 5 mM MgATP. (D) Time course of changes in the half-inactivation voltage during run-down observed in the absence (black squares, same cells as in Fig. 4) and presence (orange circles, same cells as in A) of 5 mM MgATP. (E) Time course of changes in the inactivation slope factor during run-down observed in the absence (black squares, same cells as in Fig. 4) and presence (orange circles, same cells as in A) of 5 mM MgATP. Values are expressed as mean  $\pm$  SEM.

irreversible lipid kinase inhibitor (Wipf and Halter, 2005). When MgATP in the pipette solution was combined with 10  $\mu$ M WM (ATP+WM in Fig. 9, A-D), it still significantly increased the current fraction remaining after 7 min of run-down (Fig. 9 B) and markedly slowed run-up (Fig. 9 C). Relative to recordings with MgATP alone, WM actually tended to enhance the protective effects (Fig. 10 C), suggesting that it increased ATP availability because of reduced consumption by lipid kinases. Likewise, pretreatment of cells by incubation in extracellular solution containing 10  $\mu$ M WM for 15 min (ATP+WM PT in Fig. 9, A-D) did not significantly impair the stabilizing action of MgATP (Fig. 9 B) nor did it alter the time course of changes observed in parallel control recordings. Unlike acute treatment (i.e., ATP+WM) however, WM pretreatment markedly enhanced the ATP-induced slowing of run-up in a subset of cells (Fig. 9 C), so that on average, the latter effect was stronger but also more variable (Fig. 10 A). A similar modification of ATP-induced changes in the duration of run-up was observed in only one of seven recordings with ATP+WM (Fig. 9 C), suggesting that PIP<sub>2</sub> depletion rather than acute inhibition of its resynthesis may be required to modify ATP-effects on run-up. Brief application of WM inhibits PIP<sub>2</sub> replenishment without affecting PIP<sub>2</sub> hydrolysis (Zhang et al., 2003), so the variable effectiveness of WM pretreatment might have been related to differences in lipid turnover and degree of actual PIP<sub>2</sub> depletion between cells. Regardless of the exact effects on run-up however, the protection by ATP against run-down was clearly unaffected by WM, suggesting that it was not related to lipid kinase-mediated mechanisms and arguing against a role of PIP<sub>2</sub> depletion for  $Ca_v2.3$  channel run-down in our system.

Another line of reasoning has been that not PIP<sub>2</sub> depletion itself, but rather accumulation of one of its fatty acid cleavage products, arachidonic acid (AA), is responsible for run-down of some neuronal VGCCs (Liu et al., 2001, 2006; Liu and Rittenhouse, 2003). However, neither 1 mg/ml of the AA-scavenger BSA (Fig. 9 E) nor 5  $\mu$ M of the phospholipase C inhibitor

U73122 (Fig. 9 F) affected the time course of run-up or run-down when they were added to the (ATP-free) internal solution (Fig. 10, A-C).

#### The effects of ATP depend on protein kinase-mediated phosphorylation

We next examined the role of changes in protein phosphorylation and dephosphorylation, which may result from ATP-depletion and have been implicated in the run-down of L-type high-voltage-activated  $Ca^{2+}$  channels (Armstrong and Eckert, 1987; Hilgemann, 1997). As summarized in Fig. 10 (A-C), the effects of MgATP were well preserved and again even somewhat enhanced when it was combined with 100  $\mu$ M of the protein tyrosine kinase inhibitor genistein (GS). Combination with 10  $\mu$ M of the broad-spectrum serine/threonine kinase inhibitor stauro on the other hand completely abolished MgATP effects on the duration of run-up, so the time to  $I_{max}$  with MgATP+stauro was not significantly different from the time course in parallel control recordings (Fig. 11, A-C; and Fig. 10 A). Moreover, although MgATP in the presence of stauro still significantly increased the fraction of current remaining after 7 min of run-down relative to parallel control recordings (Fig. 11, A and B), the net effect was significantly reduced when compared with that observed in other recordings with MgATP. Thus, expressed relative to the corresponding control recordings, MgATP+stauro was significantly less effective in increasing the current fraction after 7 min of run-down than MgATP alone, MgATP+WM, or MgATP+GS (Fig. 10 C).

There was no evident effect of stauro in the absence of ATP (Fig. 11, A-C), indicating that it acted by reducing ATP-protection from run-down. From these findings it follows that the ATP-induced slowing of run-up and most but not all the protection from run-down must have involved protein kinase-mediated phosphorylation of serine/threonine residues. On the other hand, run-down in the absence of ATP might reflect a progressive



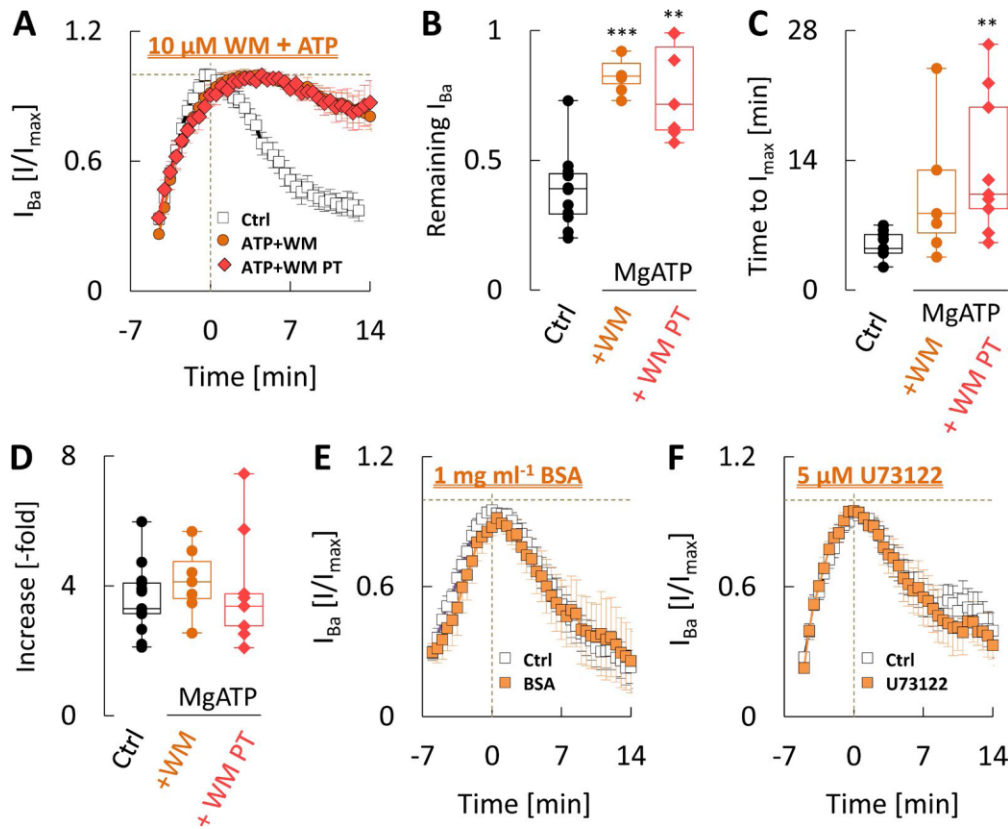


Figure 9. **ATP protection from run-down is not related to increased PIP<sub>2</sub> synthesis.** (A) Mean data from seven recordings with 5 mM MgATP and 10  $\mu$ M WM (ATP + WM), nine recordings with 5 mM MgATP after WM pretreatment (ATP + WM PT), and 13 parallel control recordings. (B) Comparison of the residual  $I_{Ba}$  after 7 min of run-down under control conditions, with ATP and WM and with ATP after WM pretreatment (same cells as in A). (C) Comparison of the run-up duration under control conditions, with ATP and WM and with ATP after WM pretreatment (same cells as in A). (D) Comparison of the current increase under control conditions, with ATP and WM and with ATP after WM pretreatment (same cells as in A). (E) Mean data from five recordings with 1 mg/ml BSA and nine parallel control recordings. (F) Mean data from six recordings with 5  $\mu$ M U73122 and eight parallel control recordings. \*\*,  $P < 0.01$ ; \*\*\*,  $P < 0.001$  vs. Ctrl (one-way ANOVA with Bonferroni post hoc correction). Values are expressed as mean  $\pm$  SEM.

decrease of channel phosphorylation because of changes in the balance between constitutive de- and rephosphorylation. To test this assumption, we examined the effects of a sustained (30–60-min) incubation of cells in extracellular solution containing 1  $\mu$ M stauro, which should mimic run-down by reducing basal protein phosphorylation. Consistent with (partial) run-down of the channels before establishment of the recordings, stauro pretreatment increased the number of cells lacking macroscopic currents and significantly reduced both  $I_{start}$  and  $I_{max}$  in the remaining cells (Fig. 11, D–F). Interestingly, it also significantly increased the magnitude and duration of run-up (Fig. 11, G–I), although the latter effect may have been related to the appearance of a plateau phase with little change in current amplitudes for several minutes. Subsequently, run-down proceeded with a normal time course, so the decrease of currents after 7 min was essentially the same as in parallel control recordings.

To assess how these effects were related to the ATP-sensitive gating changes, we also examined the effects of stauro pretreatment on channel voltage dependence (Fig. 12). As illustrated in Fig. 12 (B and C), activation and prepulse inactivation curves recorded in pretreated cells before the onset of run-down showed a significant shift to more negative test potentials

when compared with the results obtained in untreated cells, although the voltage-sensitivity (i.e.,  $k_{act}$  and  $k_{inact}$ ) was similar (not depicted).

In addition, stauro pretreatment tended to accelerate the voltage shifts during run-down (Fig. 12, D and E), although comparison of the exact time course is confounded by differences in cell size between the experiments, so no firm conclusions can be drawn from this finding. Interestingly however, it also effectively prevented the decrease in activation voltage sensitivity during run-down (Fig. 12 F) without altering the changes in inactivation voltage sensitivity (not depicted), possibly pointing to the involvement of multiple mechanisms at distinct sites.

Because the serine/threonine phosphatase calcineurin has been shown to interact with neuronal VGCCs (Chad and Eckert, 1986; Fomina and Levitan, 1997) and implicated in the run-down of certain K<sup>+</sup> channels (Horváth et al., 2002), we also tested the effects of pretreating cells with a 60-min incubation in extracellular solution containing 10  $\mu$ M of the membrane-permeable calcineurin-inhibitor deltamethrin (DM). However, the time course of changes in  $I_{Ba}$  observed in DM-pretreated cells (recorded with ATP-free pipette solution) was not significantly different from that in parallel control recordings (Fig. 10).



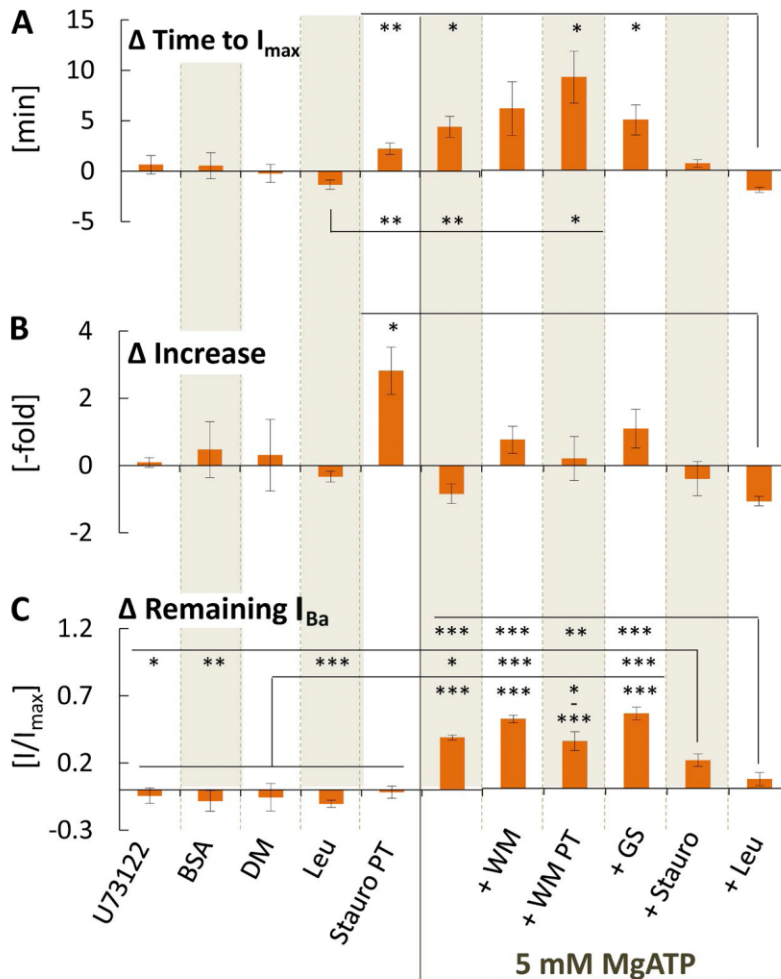


Figure 10. **Overview of changes in run-up and run-down observed under various experimental conditions.** Data are from the same cells as in Figs. 9, 11, and 13 with additional data from six recordings with 5 mM MgATP + 100  $\mu$ M GS (+GS) and four parallel control recordings and three recordings after a 60-min pretreatment with 10  $\mu$ M DM and five parallel control recordings. For comparison between the different experimental conditions, all values obtained with a given test solution were normalized as described in Fig. 7 and Materials and methods. Symbols for statistical significance refer to the comparison of normalized values between different experimental conditions. (A) Comparison of mean changes relative to parallel control recordings in the duration of run-up ( $\Delta$  Time to  $I_{max}$ ). (B) Comparison of mean changes relative to parallel control recordings in the magnitude of run-up ( $\Delta$  Increase). (C) Comparison of mean changes relative to parallel control recordings in the residual current after 7 min of run-down ( $\Delta$  Remaining  $I_{Ba}$ ). \*,  $P < 0.05$ ; \*\*,  $P < 0.01$ ; \*\*\*,  $P < 0.001$  (one-way ANOVA with Bonferroni post hoc correction in A and C or Welch's ANOVA with the Games-Howell multiple-comparison method in B). Values are expressed as mean  $\pm$  SEM.

**Run-up may involve activation of Leu-sensitive proteases**

Finally, we performed experiments with Leu, a protease inhibitor that has been shown to prevent an irreversible ATP-resistant component of run-down in L-type VGCCs (Chad and Eckert, 1986; Elhamdani et al., 1994). Unexpectedly, and in contrast to all other manipulations tested, MgATP+100  $\mu$ M Leu significantly decreased the magnitude of run-up (Fig. 13, A–C), so that  $I_{start}$  was similar but  $I_{max}$  was approximately half of the value observed in parallel control recordings. In addition, Leu not only abolished the MgATP-dependent slowing of run-up but actually produced a significant decrease of the time to  $I_{max}$  when it was combined with ATP (Fig. 13 D). Apart from altering the time course and net increase of currents, ATP+Leu reduced cell-to-cell variability in the magnitude of run-up (variance = 0.89 in control recordings vs. 0.16 with MgATP+Leu,  $P < 0.05$ ) and diminished the initial slowing of inactivation (Fig. 13 C), indicating that both processes may be related to activation of Leu-sensitive proteases and influenced by variable endogenous protease and/or protease inhibitor levels.

Curiously, Leu also suppressed the protective effect of MgATP against run-down (Fig. 13 A), so that expressed relative to the corresponding control recordings, MgATP+Leu was significantly less effective against rundown than MgATP alone, MgATP+WM, MgATP after WM pretreatment, or MgATP+GS (Fig. 10 C). When

the same concentration of Leu (100  $\mu$ M) was used in the absence of MgATP, it had similar but quantitatively much less marked effects on run-up (Fig. 13, A–D) and no effect on the degree of run-down (Fig. 10 C) or the inactivation changes during run-up (Fig. 13 E).

**Discussion**

In the present study, we used conventional and perforated-patch-clamp recordings in a recombinant expression system to assess changes in  $Ca_v2.3$  channel currents during cell dialysis. Our findings recapitulate studies about their native counterparts and show that dialysis with ATP-free internal solutions produces a characteristic sequence of run-up and run-down, the time-course of which depends on  $R_o$ , cell size, and recording configuration. The exponential decline in conductance during run-down by itself was voltage independent but paralleled by a progressive shift of channel voltage dependence to more negative test potentials. The voltage-shift reduced channel availability at the holding potential (i.e.,  $P_F$ ) but proceeded at a constant rate and could only partly account for the complete loss of gating currents during run-down. Therefore, most of the decline in conductance was related to changes in the total number of functional channels (i.e.,  $N$  and/or  $P_{F,max}$ ) and possibly to other factors (i.e., decrease of  $\gamma$  or  $P_{O,max}$ ). Run-down and all the associated

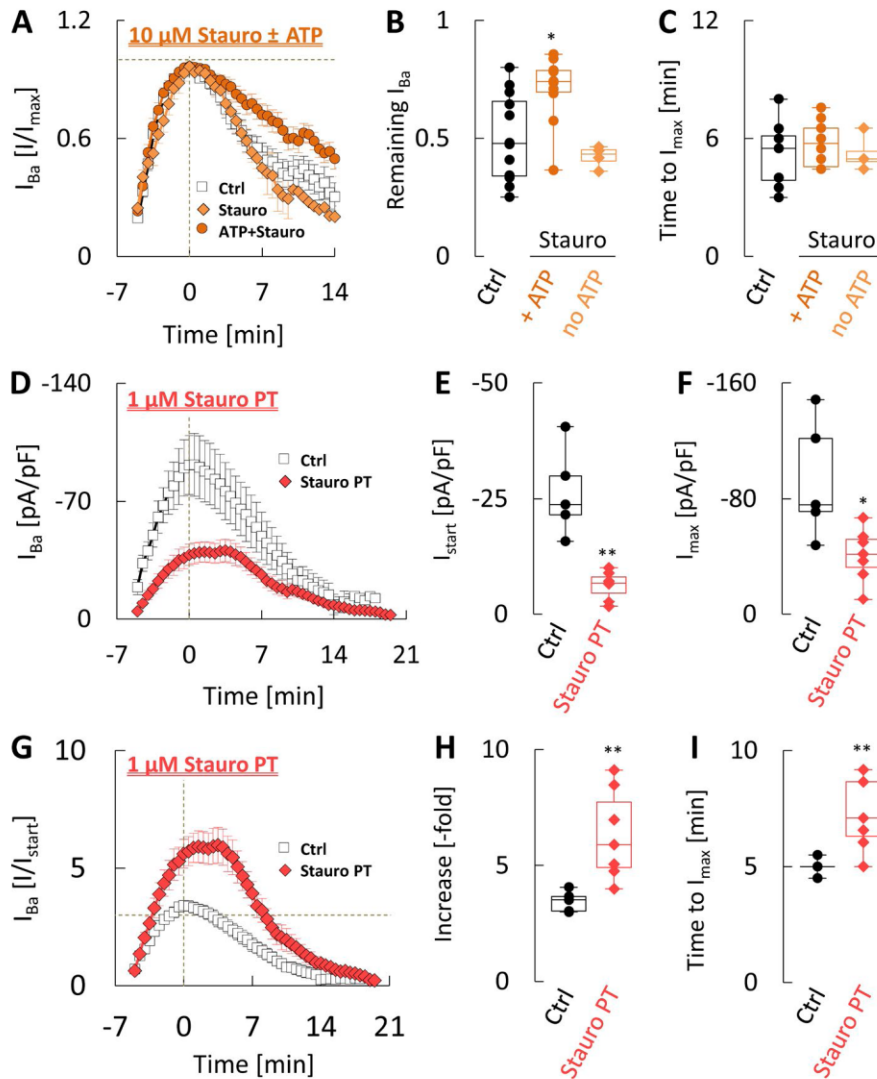


**Figure 11. ATP protection from run-down involves serine/threonine phosphorylation.** (A) Mean data from 10 recordings with 5 mM MgATP and 10  $\mu$ M stauro (ATP+Stauro), 4 recordings with 10  $\mu$ M stauro only (Stauro), and 12 parallel control recordings (Ctrl). (B) Comparison of the residual  $I_{Ba}$  after 7 min of run-down in recordings with Stauro or ATP+Stauro and in parallel control recordings (same cells as in A). (C) Comparison of the run-up duration in recordings with Stauro or ATP+Stauro and in parallel control recordings (same cells as in A). (D) Mean data from seven recordings after pretreatment with 1  $\mu$ M stauro (Stauro PT) and five parallel control recordings (Ctrl). Note that current amplitudes are expressed in pA/pF to illustrate the reduced peak current densities after stauro pretreatment. (E) Comparison of the initial peak current densities observed after stauro pretreatment and in parallel control recordings (same cells as in D). (F) Comparison of the maximum peak current densities observed after stauro pretreatment and in parallel control recordings (same cells as in D). (G) Same data as in D but normalized to the initial current amplitudes to illustrate changes in the magnitude of run-up. (H) Comparison of the current increase during run-up after stauro pretreatment and in parallel control recordings (same cells as in D). (I) Comparison of the run-up duration after stauro pretreatment and in parallel control recordings (same cells as in D). \*,  $P < 0.05$ ; \*\*,  $P < 0.01$  (one-way ANOVA with Bonferroni post hoc correction). Values are expressed as mean  $\pm$  SEM.

biophysical changes could be slowed or prevented by provision of ATP, and this protective action was almost completely abolished by inhibition of serine/threonine kinases. Protein kinase inhibition also mimicked the effects of run-down in intact cells, so it reduced overall peak current densities and hyperpolarized the voltage dependence of gating relative to untreated cells. The effects of ATP could be replicated neither by a nonhydrolyzable ATP analogue nor by GTP, which argues against a role of direct nucleotide binding or G-protein interactions but is consistent with the reported selectivity of protein kinases for ATP (Becher et al., 2013). Finally, run-down was not influenced by dialysis with a PLC inhibitor or the AA scavenger BSA, and the effects of ATP were unaffected by inhibition of lipid kinases, suggesting that run-down was not related to PIP<sub>2</sub> hydrolysis, or accumulation of its cleavage product AA. Based on these findings, we conclude that (1) ATP-protects from Ca<sub>v</sub>2.3 channel run-down by maintaining phosphorylation of serine/threonine residues on the channels themselves or an associated protein, (2) constitutive dephosphorylation of these sites in dialyzed cells affects channel gating and reduces the total number of functional channels, and (3) (de-)phosphorylation of at least some of the sites can

also regulate channel function in intact cells. In addition, some of our findings point to a role of Leu-sensitive proteases for Ca<sub>v</sub>2.3 channel up-regulation during run-up and for the effects of protein phosphorylation on run-down.

#### Comparison with run-down in other voltage-gated Ca<sup>2+</sup> channels

Since its first description, Ca<sup>2+</sup> channel run-down has been consistently linked to diffusion-controlled dilution of ATP and other cytosolic components, but the underlying processes seem to differ among channels. ATP-induced protection from L-type Ca<sup>2+</sup> channel run-down involves several interrelated processes, which may include changes in lipid turnover (Wu et al., 2002; Kaur et al., 2015), direct nucleotide binding (Feng et al., 2014), and phosphorylation of the channels by PKA, CaMKII and possibly other kinases (Wang et al., 2009; Xu et al., 2016). The latter counteracts constitutive dephosphorylation by opposing protein phosphatases and has been proposed to stabilize conformations that can be reprimed by voltage, CaM, or calpastatin and/or are more resistant to proteolytic degradation (Chad et al., 1987; Wang et al., 2009; Sun et al., 2014). This is in contrast to the situation

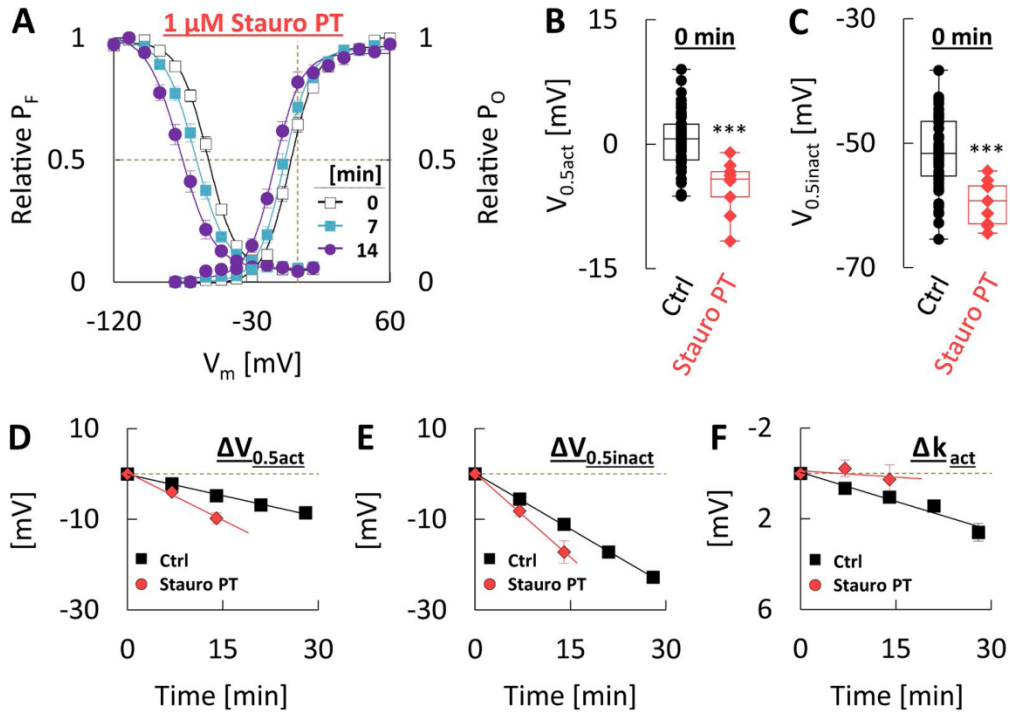


Figure 12. **Protein kinase inhibition in intact cells reproduces the gating changes during run-down in dialyzed cells.** (A) Voltage dependence of activation (right) and prepulse inactivation (left), determined at the onset of run-down (time 0) and in 7-min intervals thereafter in nine cells pretreated with 1  $\mu$ M stauro for 30–60 min. (B) Comparison of half-activation voltages at the onset of run-down in cells pretreated with 1  $\mu$ M stauro (same cells as in A) and under control conditions (same cells as in Fig. 4). (C) Comparison of half-inactivation voltages at the onset of run-down in cells pretreated with 1  $\mu$ M stauro and under control conditions (same cells as in B). (D) Time-course of changes in half-activation voltages during run-down observed in cells pretreated with 1  $\mu$ M stauro and under control conditions (same cells as in B). (E) Time course of changes in half-inactivation voltages during run-down observed in cells pretreated with 1  $\mu$ M stauro and under control conditions (same cells as in B). (F) Time course of changes in activation slope factors during run-down observed in cells pretreated with 1  $\mu$ M stauro and under control conditions (same cells as in B). \*\*\*,  $P < 0.001$  vs. Ctrl (one-way ANOVA with Bonferroni post hoc correction). Values are expressed as mean  $\pm$  SEM.

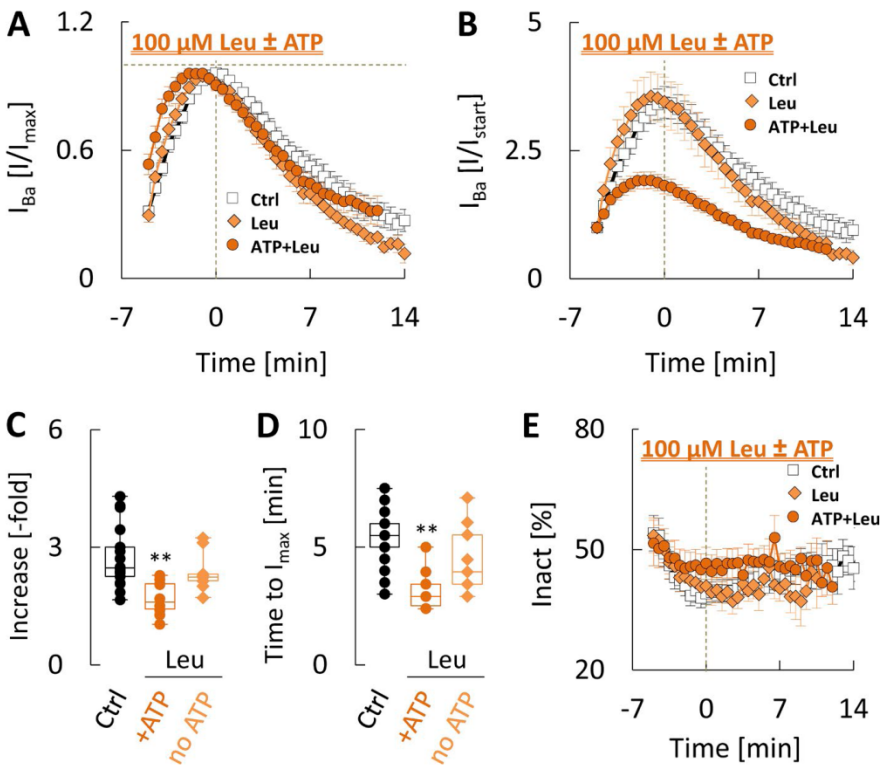


Figure 13. **Run-up may involve activation of Leu-sensitive proteases.** (A) Mean data from 10 recordings with 5 mM MgATP and 100  $\mu$ M Leu (ATP+Leu), 9 recordings with 100  $\mu$ M Leu only (Leu), and 17 parallel control recordings (Ctrl). (B) Same data as in A but normalized to the initial current amplitude to illustrate differences in the magnitude of run-up. (C) Comparison of the current increase during run-up with ATP+Leu, Leu only, and in parallel control recordings (same cells as in A). (D) Comparison of the run-up duration with ATP+Leu, Leu only, and in parallel control recordings (same cells as in A). (E) Time course of changes in inactivation during the 30-ms test pulses with ATP+Leu, Leu only, and in parallel control recordings (same cells as in A). \*\*,  $P < 0.01$  (one-way ANOVA with Bonferroni post hoc correction in D or Welch's ANOVA with the Games-Howell multiple-comparison method in C). Values are expressed as mean  $\pm$  SEM.



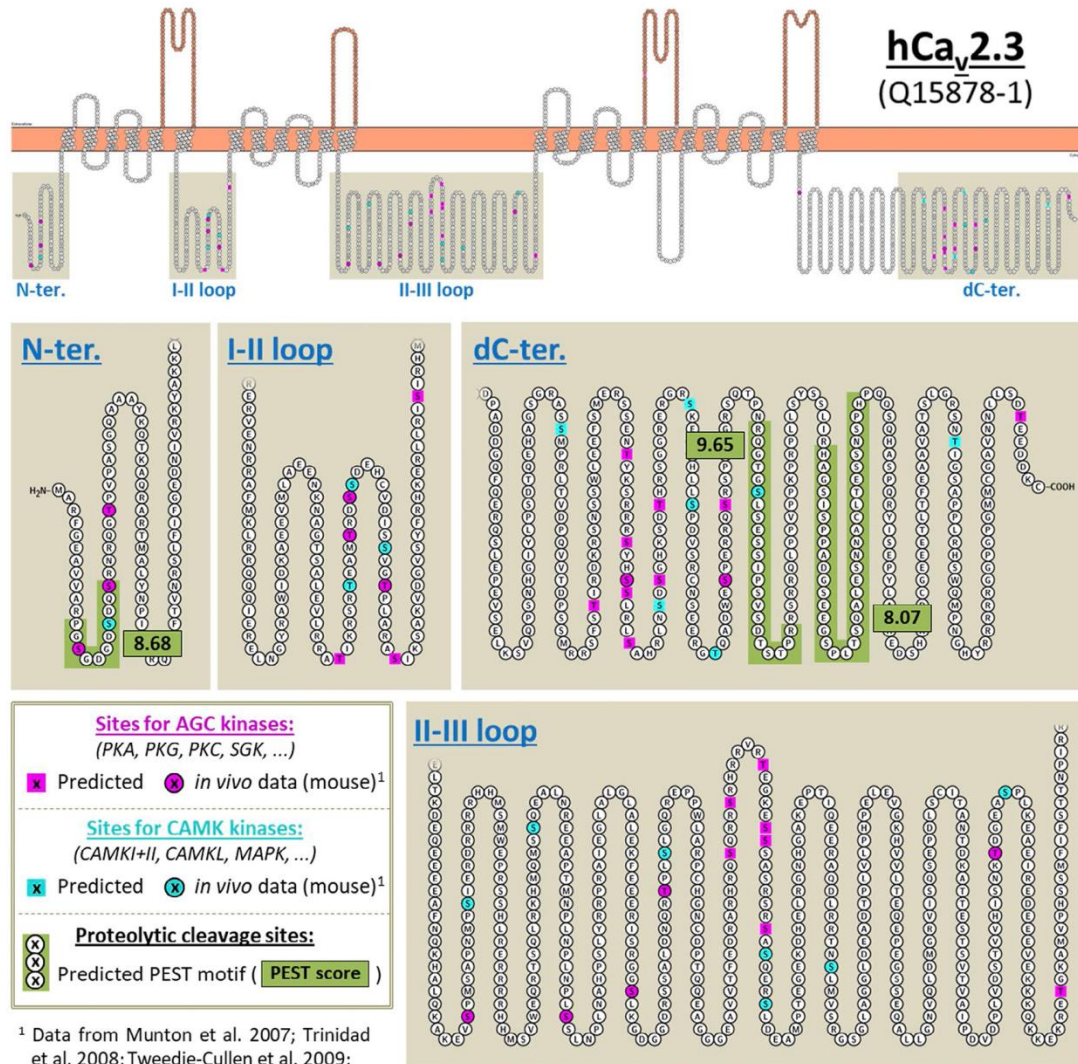


Figure 14. **Phosphorylation sites and potential PEST regions in human Ca<sub>v</sub>2.3 channels.** The secondary structure was visualized with Protter based on the human protein database entry Q15878, which includes exon 19 and exon 45 encoded stretches of the full-length Ca<sub>v</sub>2.3d-splice variant. Predictions were performed at the highest threshold by using the Group-based System Software for Prediction of Kinase-specific Phosphorylation Sites 3.0 and at a threshold score of +5.0 by using epestfind for detection of potential proteolytic cleavage sites, respectively. CAMKI, Ca<sup>2+</sup>/CaM-dependent protein kinase I; CAMKII, Ca<sup>2+</sup>/CaM-dependent protein kinase II; CAMKL, Ca<sup>2+</sup>/CaM-dependent protein kinase-like kinases; MAPK, mitogen-activated protein kinase; SGK, serum and glucocorticoid-regulated kinase 1; ter, terminal.

in Ca<sub>v</sub>2.1 and Ca<sub>v</sub>2.2 channels, where run-down has been linked to constitutive hydrolysis of membrane PIP<sub>2</sub>, which can be prevented by ATP through lipid kinase-mediated PIP<sub>2</sub> resynthesis (Wu et al., 2002; Suh et al., 2010). Although we have not directly tested the effects of PIP<sub>2</sub>, our present findings demonstrate that lipid kinases are not involved in ATP-induced protection from Ca<sub>v</sub>2.3 channel run-down and that the current decline is not related to accumulation of AA. Together with a previous study, where PIP<sub>2</sub>-depletion had no effect on Ca<sub>v</sub>2.3 channels (Suh et al., 2010), these findings argue against a major role of PIP<sub>2</sub> hydrolysis for Ca<sub>v</sub>2.3 channel run-down. Instead, ATP appears to maintain Ca<sub>v</sub>2.3 channel function through increased phosphorylation of sites on the channels themselves or an associated protein, which may be required to counteract constitutive dephosphorylation. It has been shown that HEK-293 cells contain endogenous kinases

and phosphatases, which can regulate the activity of transfected Ca<sup>2+</sup> channels (Perez-Reyes et al., 1994; Johnson et al., 1997; Fuller et al., 2010; Aita et al., 2011; Blesneac et al., 2015). In addition, Ca<sub>v</sub>2.3 channels are a well-known substrate for phosphorylation by various protein kinases (Fig. 14), at least some of which can be constitutively active in HEK-293 cells (Perez-Reyes et al., 1994; Crump et al., 2006). Although no firm conclusions can be drawn with regard to the exact sites or kinases involved in Ca<sub>v</sub>2.3 channel maintenance, our findings provide a reliable baseline for further studies. They also raise the question how protein phosphorylation might be involved in the maintenance Ca<sub>v</sub>2.1 and Ca<sub>v</sub>2.2 channels, which still exhibit significant rundown in the presence of exogenous PIP<sub>2</sub> (Gamper et al., 2004) or with mutations that reduce PIP<sub>2</sub> sensitivity (Zhen et al., 2006). Because there can be cross talk with lipid signaling (Wu et al., 2002) and



PIP<sub>2</sub>-hydrolysis partially inhibited Ca<sub>v</sub>2.3 channels after full activation by PKC (Jeong et al., 2016), it will also be interesting to examine the exact relevance of lipid turnover for this form of regulation.

### Molecular mechanisms and potential implications

Very little is known about the molecular and structural mechanisms of Ca<sup>2+</sup> channel run-down, but possibilities that have been considered include disruption of the linkage between voltage sensors and activation gate, entry into a permanent but existing inactivated state, and spontaneous drops in the total number of channels due to internalization or degradation. Our results do not resolve the exact processes underlying Ca<sub>v</sub>2.3 channel run-down but do argue against a significant decoupling between voltage-sensors and activation gate because run-down abolished both ionic and gating currents. In addition, Leu was ineffective against run-down and actually reduced the protective effects of ATP, suggesting that the current decline was not directly related to increased proteolytic degradation (but see next section). Together, these findings contrast with studies that L-type-channel gating currents are not diminished by run-down (Hadley and Lederer, 1991; Costantin et al., 1999) and that Leu prevents an irreversible component of run-down in these channels (Chad et al., 1987). We can only speculate that dephosphorylation of Ca<sub>v</sub>2.3 channels themselves or an interacting protein induces a conformational change that leads to terminal inactivation and/or facilitates their removal from the membrane.

More importantly, our findings reveal that part of the current decline can be attributed to a gradual development of inactivation due to changes in channel voltage dependence. Based on the lack of saturation or concurrent changes in  $V_{rev}$ , these effects may have been related to changes in the fraction of applied membrane voltage sensed by the channels. Interestingly, and in contrast to the exponential decline in conductance, the gating changes occurred at a constant rate, which is difficult to reconcile in terms of a conformational change. An attractive hypothesis that remains to be substantiated is that progressive dephosphorylation could shift channels among their states in a simple manner, such as altering the internal surface charge. It has been quantitatively demonstrated that the bulk electrostatic effects of dephosphorylation are sufficient to produce hyperpolarizing voltage shifts during run-down of other voltage-gated ion channels (Perozo and Bezanilla, 1990, 1991). Regardless of the exact mechanism, our findings document a close relationship between protein phosphorylation and channel voltage dependence, which may influence the basal features of current carried by cloned Ca<sub>v</sub>2.3 channels. Based on previous studies about their native counterparts, it seems reasonable to propose that this is also relevant under physiological conditions. Thus, Ca<sub>v</sub>2.3 channels are the third most extensively phosphorylated ion channels in mouse brain (Cerdeza et al., 2011; Fig. 14), and depolarization of intact hippocampal slices has been shown to induce bulk changes in their phosphorylation state (Hell et al., 1995).

### Run-up and the role of calpain-like proteases

Unexpectedly, our findings also indicate that Ca<sub>v</sub>2.3 channel run-up may involve activation of calpain-like proteases (CLPs)

and that it can be slowed but not prevented by ATP through increased protein phosphorylation. The process started immediately upon patch rupture, which can hardly be accounted for by ATP depletion but might reflect the loss of small cytosolic protease inhibitors because it was much slower in perforated recordings. In addition, run-up was observed with Ba<sup>2+</sup> as the charge carrier but significantly faster and more complete with Ca<sup>2+</sup>, which is consistent with studies that show that Ba<sup>2+</sup> can partially substitute for Ca<sup>2+</sup> in activating CLPs (DeMartino and Croall, 1985; McDonald et al., 1994; Seydl et al., 1995). That phosphorylation suppresses most CLPs (Shiraha et al., 2002; Smith et al., 2003), while PIP<sub>2</sub> is well known to be required for activation and may considerably lower their Ca<sup>2+</sup> requirement (Tompa et al., 2001; Leloup et al., 2010), could explain why (1) ATP, but not AMP-PNP or ATP+stauro, slowed run-up and (2) pretreatment with WM (i.e., partial depletion of membrane PIP<sub>2</sub>) further increased the ATP-induced slowing in some cells. Dialysis or pretreatment with stauro alone had no effect or even increased run-up, suggesting that the process was not related to proteolytic activation of protein kinases. With this in mind and considering its fast onset, we can only speculate that run-up might involve partial proteolysis of the channels themselves and/or associated Ca<sub>v</sub>β<sub>3</sub> subunits. Both proteins contain several PEST motifs or PEST-like regions in their C and N termini (Fig. 14), and there is convincing evidence for a functional relevance of these sites as potential cleavage sites. For example, deletion of PEST-like regions in the Ca<sub>v</sub>β<sub>3</sub> subunit increased its half-life, stimulated currents mediated by coexpressed Ca<sub>v</sub>2.2 channels, and reduced voltage-dependent inactivation in HEK-293 cells (Sandoval et al., 2006). Likewise, intracellular protease application has been shown to produce strong stimulation of VGCCs and a partial loss of fast voltage-dependent inactivation, which has been linked to C-terminal cleavage of a conserved autoinhibitory region in the pore-forming Ca<sub>v</sub>α<sub>1</sub> subunit (Wei et al., 1994; Klöckner et al., 1995; Gao et al., 2001; Mikala et al., 2003). Given that C-terminal truncation of L-, N- and P/Q-type VGCCs by endogenous proteases has been demonstrated before in HEK-293 cells (Kubodera et al., 2003; Gomez-Ospina et al., 2006) and in vivo (Gerhardstein et al., 2000; Abele and Yang, 2012), it seems not so far off that the structural determinants for Ca<sub>v</sub>2.3 channel run-up could also be located in this region. With regard to the Leu effects on run-down, it may be important that L-type channels can also be cleaved at PEST regions within the core of the Ca<sub>v</sub>α<sub>1</sub> subunit, which has been shown to disrupt channel function (Groth et al., 2014; Michailidis et al., 2014). That Ca<sub>v</sub>2.3 channels lack such regions might account for the inability of Leu to sustain ATP-induced protection. On the other hand, this cannot explain the puzzling finding that Leu actually impaired the protective effects of ATP on run-down. We can only speculate that the latter might be related to differential phosphorylation of long and short forms or changes in the accessibility of certain sites. Because Leu could also alter the effects of ATP in some other way, further studies will clearly be required to delineate the underlying processes. However, our finding that protein kinase inhibition alone replicated most of the gating changes during run-down in intact cells leads us to conclude that proteolysis is either not required for these effects or that it does also occur in intact cells.

## Conclusion

In summary, our findings show that run-down of cloned  $Ca_v2.3$  channels in dialyzed cells is associated with progressive changes in channel voltage-dependence and a decrease in the total number of functional channels, which can be prevented by ATP through maintained protein phosphorylation and replicated by protein kinase inhibition in intact cells. These findings distinguish the process from run-down in other  $Ca_v2$  channels and suggest that one or more sites on the channels themselves or an associated protein must be phosphorylated to maintain them in a functional state. In addition, changes in the phosphorylation of a subset of sites may directly influence channel gating, possibly through bulk electrostatics. Although additional studies will be required to delineate the underlying mechanisms and their relevance in native cells, our results provide a reliable baseline that could stimulate further work on  $Ca_v2.3$  channel regulation by protein kinases, phosphatases, and possibly proteases.

## Acknowledgments

We thank Tobias Pook for technical help and supply of software for facilitated analysis and Mrs. Renate Clemens for her excellent and permanent assistance.

This work was financially supported by the Deutsche Forschungsgemeinschaft (SCHN 387/21-1).

The authors declare no competing financial interests.

Author contributions: F. Neumaier contributed to the conception and design of the work, performed the experiments, analyzed and interpreted the data, prepared the figures, wrote the first draft of the manuscript, and coordinated its critical revision. T. Schneider contributed to the conception and design of the work, interpretation of the data, and critical revision of the manuscript. S. Alpdogan and J. Hescheler contributed to analysis and interpretation of the data and drafting of the manuscript. All authors have approved the final version of the manuscript and agree to be accountable for all aspects of the work. All persons designated as authors qualify for authorship, and all those who qualify for authorship are listed. Experiments were carried out in the Institute for Neurophysiology at the University of Cologne, Germany.

Sharona E. Gordon served as editor.

Submitted: 14 August 2017

Revised: 22 December 2017

Accepted: 24 January 2018

## References

- Abele, K., and J. Yang. 2012. Regulation of voltage-gated calcium channels by proteolysis. *Sheng Li Xue Bao.* 64:504–514.
- Aita, Y., N. Kurebayashi, S. Hirose, and A.D. Maturana. 2011. Protein kinase D regulates the human cardiac L-type voltage-gated calcium channel through serine 1884. *FEBS Lett.* 585:3903–3906. <https://doi.org/10.1016/j.febslet.2011.11.011>
- Almog, M., and A. Korngreen. 2009. Characterization of voltage-gated  $Ca^{2+}$  conductances in layer 5 neocortical pyramidal neurons from rats. *PLoS One.* 4:e4841. <https://doi.org/10.1371/journal.pone.0004841>
- Armstrong, D., and R. Eckert. 1987. Voltage-activated calcium channels that must be phosphorylated to respond to membrane depolarization. *Proc. Natl. Acad. Sci. USA.* 84:2518–2522. <https://doi.org/10.1073/pnas.84.8.2518>
- Arnould, T., D. Janssens, C. Michiels, and J. Remacle. 1996. Effect of aescine on hypoxia-induced activation of human endothelial cells. *Eur. J. Pharmacol.* 315:227–233. [https://doi.org/10.1016/S0014-2999\(96\)00645-0](https://doi.org/10.1016/S0014-2999(96)00645-0)
- Becher, I., M.M. Savitski, M.F. Savitski, C. Hopf, M. Bantscheff, and G. Drewes. 2013. Affinity profiling of the cellular kinome for the nucleotide cofactors ATP, ADP, and GTP. *ACS Chem. Biol.* 8:599–607. <https://doi.org/10.1021/cb3005879>
- Becq, F. 1996. Ionic channel rundown in excised membrane patches. *Biochim. Biophys. Acta.* 1286:53–63. [https://doi.org/10.1016/0304-4157\(96\)00002-0](https://doi.org/10.1016/0304-4157(96)00002-0)
- Benquet, P., J.L. Guen, G. Dayanithi, Y. Pichon, and F. Tiago. 1999. omega-Aga1-VA-sensitive (P/Q-type) and -resistant (R-type) high-voltage-activated  $Ba(2+)$  currents in embryonic cockroach brain neurons. *J. Neurophysiol.* 82:2284–2293. <https://doi.org/10.1152/jn.1999.82.5.2284>
- Blesneac, I., J. Chemin, I. Bidaud, S. Huc-Brandt, F. Vandermoere, and P. Lory. 2015. Phosphorylation of the  $Ca_v3.2$  T-type calcium channel directly regulates its gating properties. *Proc. Natl. Acad. Sci. USA.* 112:13705–13710. <https://doi.org/10.1073/pnas.1511740112>
- Cerda, O., J.-H. Baek, and J.S. Trimmer. 2011. Mining recent brain proteomic databases for ion channel phosphosite nuggets. *J. Gen. Physiol.* 137:3–16. <https://doi.org/10.1085/jgp.201010555>
- Chad, J.E., and R. Eckert. 1986. An enzymatic mechanism for calcium current inactivation in dialyzed *Helix* neurones. *J. Physiol.* 378:31–51. <https://doi.org/10.1113/jphysiol.1986.sp016206>
- Chad, J., D. Kalman, and D. Armstrong. 1987. The role of cyclic AMP-dependent phosphorylation in the maintenance and modulation of voltage-activated calcium channels. *Soc. Gen. Physiol. Ser.* 42:167–186.
- Clare, J.J. 2006. Functional expression of ion channels in mammalian systems. *In Expression and Analysis of Recombinant Ion Channels.* J.J. Clare and D.J. Trezise, editors. Wiley-VCH, Weinheim, Germany. 79–109.
- Costantin, J.L., N. Qin, M.N. Waxham, L. Birnbaumer, and E. Stefani. 1999. Complete reversal of run-down in rabbit cardiac  $Ca^{2+}$  channels by patch-cramming in *Xenopus* oocytes; partial reversal by protein kinase A. *Pflugers Arch.* 437:888–894. <https://doi.org/10.1007/s004240050859>
- Cota, G. 1986. Calcium channel currents in pars intermedia cells of the rat pituitary gland. Kinetic properties and washout during intracellular dialysis. *J. Gen. Physiol.* 88:83–105. <https://doi.org/10.1085/jgp.88.1.83>
- Crump, S.M., R.N. Correll, E.A. Schroder, W.C. Lester, B.S. Finlin, D.A. Andres, and J. Satin. 2006. L-type calcium channel alpha-subunit and protein kinase inhibitors modulate Rem-mediated regulation of current. *Am. J. Physiol. Heart Circ. Physiol.* 291:H1959–H1971. <https://doi.org/10.1152/ajpheart.00956.2005>
- DeMartino, G.N., and D.E. Croall. 1985. Calcium-dependent proteases from liver and heart. *Prog. Clin. Biol. Res.* 180:117–126.
- Elhamdani, A., J.-L. Bossu, and A. Feltz. 1994. Evolution of the  $Ca^{2+}$  current during dialysis of isolated bovine chromaffin cells: effect of internal calcium. *Cell Calcium.* 16:357–366. [https://doi.org/10.1016/0143-4160\(94\)90029-9](https://doi.org/10.1016/0143-4160(94)90029-9)
- Elhamdani, A., J.-L. Bossu, and A. Feltz. 1995. ATP and G proteins affect the runup of the  $Ca^{2+}$  current in bovine chromaffin cells. *Pflugers Arch.* 430:410–419. <https://doi.org/10.1007/BF00373917>
- Fan, J.-S., and P. Palade. 1998. Perforated patch recording with beta-escin. *Pflugers Arch.* 436:1021–1023. <https://doi.org/10.1007/PL00008086>
- Feng, R., J. Xu, E. Minobe, A. Kameyama, L. Yang, L. Yu, L. Hao, and M. Kameyama. 2014. Adenosine triphosphate regulates the activity of guinea pig  $Ca_v1.2$  channel by direct binding to the channel in a dose-dependent manner. *Am. J. Physiol. Cell Physiol.* 306:C856–C863. <https://doi.org/10.1152/ajpcell.00368.2013>
- Fomina, A.F., and E.S. Levitan. 1997. Control of  $Ca^{2+}$  channel current and exocytosis in rat lactotrophs by basally active protein kinase C and calcineurin. *Neuroscience.* 78:523–531. [https://doi.org/10.1016/S0306-4522\(96\)00571-4](https://doi.org/10.1016/S0306-4522(96)00571-4)
- Fu, L.-Y., F. Wang, X.-S. Chen, H.-Y. Zhou, W.-X. Yao, G.-J. Xia, and M.-X. Jiang. 2003. Perforated patch recording of L-type calcium current with beta-escin in guinea pig ventricular myocytes. *Acta Pharmacol. Sin.* 24:1094–1098.
- Fuller, M.D., M.A. Emrick, M. Sadilek, T. Scheuer, and W.A. Catterall. 2010. Molecular mechanism of calcium channel regulation in the fight-or-flight response. *Sci. Signal.* 3:ra70. <https://doi.org/10.1126/scisignal.2001152>
- Gamper, N., V. Reznikov, Y. Yamada, J. Yang, and M.S. Shapiro. 2004. Phosphatidylinositol [correction] 4,5-bisphosphate signals underlie

Neumaier et al.

Phosphorylation prevents  $Ca_v2.3$  channel run-down

Journal of General Physiology

<https://doi.org/10.1085/jgp.201711880>



- receptor-specific Gq/11-mediated modulation of N-type Ca<sup>2+</sup> channels. *J. Neurosci.* 24:10980–10992. <https://doi.org/10.1523/JNEUROSCI.3869-04.2004>
- Gao, T., A.E. Cuadra, H. Ma, M. Bunemann, B.L. Gerhardstein, T. Cheng, R.T. Eick, and M.M. Hosey. 2001. C-terminal fragments of the alpha 1C (Ca<sub>v</sub>1.2) subunit associate with and regulate L-type calcium channels containing C-terminal-truncated alpha 1C subunits. *J. Biol. Chem.* 276:21089–21097. <https://doi.org/10.1074/jbc.M008000200>
- Gerhardstein, B.L., T. Gao, M. Bunemann, T.S. Puri, A. Adair, H. Ma, and M.M. Hosey. 2000. Proteolytic processing of the C terminus of the alpha(1C) subunit of L-type calcium channels and the role of a proline-rich domain in membrane tethering of proteolytic fragments. *J. Biol. Chem.* 275:8556–8563. <https://doi.org/10.1074/jbc.275.12.8556>
- Gomez-Ospina, N., F. Tsuruta, O. Barreto-Chang, L. Hu, and R. Dolmetsch. 2006. The C terminus of the L-type voltage-gated calcium channel Ca<sub>v</sub>1.2 encodes a transcription factor. *Cell.* 127:591–606. <https://doi.org/10.1016/j.cell.2006.10.017>
- Goswami, T., X. Li, A.M. Smith, E.M. Luderowski, J.J. Vincent, J. Rush, and B.A. Ballif. 2012. Comparative phosphoproteomic analysis of neonatal and adult murine brain. *Proteomics.* 12:2185–2189. <https://doi.org/10.1002/pmic.201200003>
- Groth, R.D., N.N. Tirko, and R.W. Tsien. 2014. Ca<sub>v</sub>1.2 calcium channels: Just cut out to be regulated? *Neuron.* 82:939–940. <https://doi.org/10.1016/j.neuron.2014.05.030>
- Hadley, R.W., and W.J. Lederer. 1991. Properties of L-type calcium channel gating current in isolated guinea pig ventricular myocytes. *J. Gen. Physiol.* 98:265–285. <https://doi.org/10.1085/jgp.98.2.265>
- Hamill, O.P., A. Marty, E. Neher, B. Sakmann, and F.J. Sigworth. 1981. Improved patch-clamp techniques for high-resolution current recording from cells and cell-free membrane patches. *Pflügers Arch.* 391:85–100. <https://doi.org/10.1007/BF00656997>
- Hell, J.W., C.T. Yokoyama, L.J. Breeze, C. Chavkin, and W.A. Catterall. 1995. Phosphorylation of presynaptic and postsynaptic calcium channels by cAMP-dependent protein kinase in hippocampal neurons. *EMBO J.* 14:3036–3044.
- Hilaire, C., S. Diochot, G. Desmadryl, S. Richard, and J. Valmier. 1997. Toxin-resistant calcium currents in embryonic mouse sensory neurons. *Neuroscience.* 80:267–276. [https://doi.org/10.1016/S0304-4522\(97\)00101-2](https://doi.org/10.1016/S0304-4522(97)00101-2)
- Hilgemann, D.W. 1997. Cytoplasmic ATP-dependent regulation of ion transporters and channels: Mechanisms and messengers. *Annu. Rev. Physiol.* 59:193–220. <https://doi.org/10.1146/annurev.physiol.59.1.193>
- Horváth, F., L. Erdei, B. Wodala, U. Homann, and G. Thiel. 2002. Deltamethrin rescues run down of K<sup>+</sup> outward rectifying channels in *Vicia faba* guard cells. *Acta Biol. Szeged.* 46:19–20.
- Huttlin, E.L., M.P. Jedrychowski, J.E. Elias, T. Goswami, R. Rad, S.A. Beausoleil, J. Villén, W. Haas, M.E. Sowa, and S.P. Gygi. 2010. A tissue-specific atlas of mouse protein phosphorylation and expression. *Cell.* 143:1174–1189. <https://doi.org/10.1016/j.cell.2010.12.001>
- Jeong, J.-Y., H.-J. Kweon, and B.-C. Suh. 2016. Dual regulation of R-type Cav2.3 channels by M<sub>1</sub> muscarinic receptors. *Mol. Cells.* 39:322–329. <https://doi.org/10.14348/molcells.2016.2292>
- Johnson, B.D., J.P. Brousal, B.Z. Peterson, P.A. Gallombardo, G.H. Hockerman, Y. Lai, T. Scheuer, and W.A. Catterall. 1997. Modulation of the cloned skeletal muscle L-type Ca<sup>2+</sup> channel by anchored cAMP-dependent protein kinase. *J. Neurosci.* 17:1243–1255.
- Kaur, G., A. Pinggera, N.J. Ortner, A. Lieb, M.J. Sinnegger-Brauns, V. Yarov-Yarovoy, G.J. Obermair, B.E. Flucher, and J. Striessnig. 2015. A polybasic plasma membrane binding motif in the I-II linker stabilizes voltage-gated Ca<sub>v</sub>1.2 calcium channel function. *J. Biol. Chem.* 290:21086–21100. <https://doi.org/10.1074/jbc.M115.645671>
- Kepplinger, K.J.F., and C. Romanin. 2005. The run-down phenomenon of Ca<sup>2+</sup> channels. In *Voltage-Gated Calcium Channels*. Springer, Boston. 219–230.
- Klöckner, U., G. Mikala, M. Varadi, G. Varadi, and A. Schwartz. 1995. Involvement of the carboxyl-terminal region of the α<sub>1</sub> subunit in voltage-dependent inactivation of cardiac calcium channels. *J. Biol. Chem.* 270:17306–17310. <https://doi.org/10.1074/jbc.270.29.17306>
- Kubodera, T., T. Yokota, K. Ohwada, K. Ishikawa, H. Miura, T. Matsuoka, and H. Mizusawa. 2003. Proteolytic cleavage and cellular toxicity of the human α1A calcium channel in spinocerebellar ataxia type 6. *Neurosci. Lett.* 341:74–78. [https://doi.org/10.1016/S0304-3940\(03\)00156-3](https://doi.org/10.1016/S0304-3940(03)00156-3)
- Leloup, L., H. Shao, Y.H. Bae, B. Deasy, D. Stolz, P. Roy, and A. Wells. 2010. m-Calpain activation is regulated by its membrane localization and by its binding to phosphatidylinositol 4,5-bisphosphate. *J. Biol. Chem.* 285:33549–33566. <https://doi.org/10.1074/jbc.M110.123604>
- Liu, L., and A.R. Rittenhouse. 2003. Arachidonic acid mediates muscarinic inhibition and enhancement of N-type Ca<sup>2+</sup> current in sympathetic neurons. *Proc. Natl. Acad. Sci. USA.* 100:295–300. <https://doi.org/10.1073/pnas.0136826100>
- Liu, L., C.F. Barrett, and A.R. Rittenhouse. 2001. Arachidonic acid both inhibits and enhances whole cell calcium currents in rat sympathetic neurons. *Am. J. Physiol. Cell Physiol.* 280:C1293–C1305. <https://doi.org/10.1152/ajpcell.2001.280.5.C1293>
- Liu, L., R. Zhao, Y. Bai, L.F. Stanish, J.E. Evans, M.J. Sanderson, J.V. Bonventre, and A.R. Rittenhouse. 2006. M<sub>1</sub> muscarinic receptors inhibit L-type Ca<sup>2+</sup> current and M-current by divergent signal transduction cascades. *J. Neurosci.* 26:11588–11598. <https://doi.org/10.1523/JNEUROSCI.2102-06.2006>
- Lundby, A., A. Secher, K. Lage, N.B. Nordsborg, A. Dmytriiev, C. Lundby, and J.V. Olsen. 2012. Quantitative maps of protein phosphorylation sites across 14 different rat organs and tissues. *Nat. Commun.* 3:876. <https://doi.org/10.1038/ncomms1871>
- McDonald, T.F., S. Pelzer, W. Trautwein, and D.J. Pelzer. 1994. Regulation and modulation of calcium channels in cardiac, skeletal, and smooth muscle cells. *Physiol. Rev.* 74:365–507. <https://doi.org/10.1152/physrev.1994.74.2.365>
- Michailidis, I.E., K. Abele-Henckels, W.K. Zhang, B. Lin, Y. Yu, L.S. Geyman, M.D. Ehlers, E.A. Pnevmatikakis, and J. Yang. 2014. Age-related homeostatic midchannel proteolysis of neuronal L-type voltage-gated Ca<sup>2+</sup> channels. *Neuron.* 82:1045–1057. <https://doi.org/10.1016/j.neuron.2014.04.017>
- Mikala, G., I. Bodi, U. Klöckner, M. Varadi, G. Varadi, S.E. Koch, and A. Schwartz. 2003. Characterization of auto-regulation of the human cardiac α<sub>1</sub> subunit of the L-type calcium channel: importance of the C-terminus. *Mol. Cell. Biochem.* 250:81–89. <https://doi.org/10.1023/A:1024910605389>
- Munton, R.P., R. Tweedie-Cullen, M. Livingstone-Zatceh, F. Weinandy, M. Waidelich, D. Longo, P. Gehrig, F. Potthast, D. Rutishauser, B. Gerrits, et al. 2007. Qualitative and quantitative analyses of protein phosphorylation in naive and stimulated mouse synaptosomal preparations. *Mol. Cell. Proteomics.* 6:283–293. <https://doi.org/10.1074/mcp.M600046-MCP200>
- Nakashima, Y.M., S.M. Todorovic, A. Pereverzev, J. Hescheler, T. Schneider, and C.J. Lingle. 1998. Properties of Ba<sup>2+</sup> currents arising from human α1E and α1Ebata3 constructs expressed in HEK293 cells: Physiology, pharmacology, and comparison to native T-type Ba<sup>2+</sup> currents. *Neuropharmacology.* 37:957–972. [https://doi.org/10.1016/S0028-3908\(98\)00097-5](https://doi.org/10.1016/S0028-3908(98)00097-5)
- Omasits, U., C.H. Ahrens, S. Müller, and B. Wollscheid. 2014. Protter: Interactive protein feature visualization and integration with experimental proteomic data. *Bioinformatics.* 30:884–886. <https://doi.org/10.1093/bioinformatics/btt607>
- Park, S.W., D. Byun, Y.M. Bae, B.H. Choi, S.H. Park, B. Kim, and S.I. Cho. 2007. Effects of fluid flow on voltage-dependent calcium channels in rat vascular myocytes: fluid flow as a shear stress and a source of artifacts during patch-clamp studies. *Biochem. Biophys. Res. Commun.* 358:1021–1027. <https://doi.org/10.1016/j.bbrc.2007.05.024>
- Peng, S.Q., R.K. Hajela, and W.D. Atchison. 2005. Fluid flow-induced increase in inward Ba<sup>2+</sup> current expressed in HEK293 cells transiently transfected with human neuronal L-type Ca<sup>2+</sup> channels. *Brain Res.* 1045:116–123. <https://doi.org/10.1016/j.brainres.2005.03.039>
- Perez-Reyes, E., W. Yuan, X. Wei, and D.M. Bers. 1994. Regulation of the cloned L-type cardiac calcium channel by cyclic-AMP-dependent protein kinase. *FEBS Lett.* 342:119–123. [https://doi.org/10.1016/0014-5793\(94\)80484-2](https://doi.org/10.1016/0014-5793(94)80484-2)
- Perozo, E., and F. Bezanilla. 1990. Phosphorylation affects voltage gating of the delayed rectifier K<sup>+</sup> channel by electrostatic interactions. *Neuron.* 5:685–690. [https://doi.org/10.1016/0896-6273\(90\)90222-2](https://doi.org/10.1016/0896-6273(90)90222-2)
- Perozo, E., and F. Bezanilla. 1991. Phosphorylation of K<sup>+</sup> channels in the squid giant axon. A mechanistic analysis. *J. Bioenerg. Biomembr.* 23:599–613. <https://doi.org/10.1007/BF00785813>
- Rinschen, M.M., M.-J. Yu, G. Wang, E.S. Boja, J.D. Hoffert, T. Pisitkun, and M.A. Knepper. 2010. Quantitative phosphoproteomic analysis reveals vasopressin V2-receptor-dependent signaling pathways in renal collecting duct cells. *Proc. Natl. Acad. Sci. USA.* 107:3882–3887. <https://doi.org/10.1073/pnas.0910646107>
- Sandoval, A., N. Oviedo, A. Tadmouri, T. Avila, M. De Waard, and R. Felix. 2006. Two PEST-like motifs regulate Ca<sup>2+</sup>/calpain-mediated cleavage of the CaVbeta3 subunit and provide important determinants for neuronal Ca<sup>2+</sup> channel activity. *Eur. J. Neurosci.* 23:2311–2320. <https://doi.org/10.1111/j.1460-9568.2006.04749.x>

- Seydl, K., J.-O. Karlsson, A. Dominik, H. Gruber, and C. Romanin. 1995. Action of calpastatin in prevention of cardiac L-type  $\text{Ca}^{2+}$  channel run-down cannot be mimicked by synthetic calpain inhibitors. *Pflugers Arch.* 429:503–510. <https://doi.org/10.1007/BF00704155>
- Shiraha, H., A. Glading, J. Chou, Z. Jia, and A. Wells. 2002. Activation of m-calpain (calpain II) by epidermal growth factor is limited by protein kinase A phosphorylation of m-calpain. *Mol. Cell. Biol.* 22:2716–2727. <https://doi.org/10.1128/MCB.22.8.2716-2727.2002>
- Smith, S.D., Z. Jia, K.K. Huynh, A. Wells, and J.S. Elce. 2003. Glutamate substitutions at a PKA consensus site are consistent with inactivation of calpain by phosphorylation. *FEBS Lett.* 542:115–118. [https://doi.org/10.1016/S0014-5793\(03\)00361-2](https://doi.org/10.1016/S0014-5793(03)00361-2)
- Suh, B.-C., K. Leal, and B. Hille. 2010. Modulation of high-voltage activated  $\text{Ca}^{2+}$  channels by membrane phosphatidylinositol 4,5-bisphosphate. *Neuron.* 67:224–238. <https://doi.org/10.1016/j.neuron.2010.07.001>
- Sun, W., R. Feng, H. Hu, F. Guo, Q. Gao, D. Shao, D. Yin, H. Wang, X. Sun, M. Zhao, et al. 2014. The  $\text{Ca}^{2+}$ -dependent interaction of calpastatin domain L with the C-terminal tail of the  $\text{Ca}_v1.2$  channel. *FEBS Lett.* 588:665–671. <https://doi.org/10.1016/j.febslet.2014.01.019>
- Thomas, P., and T.G. Smart. 2005. HEK293 cell line: A vehicle for the expression of recombinant proteins. *J. Pharmacol. Toxicol. Methods.* 51:187–200. <https://doi.org/10.1016/j.vascn.2004.08.014>
- Tiaho, F., J. Nargeot, and S. Richard. 1993. Repriming of L-type calcium currents revealed during early whole-cell patch-clamp recordings in rat ventricular cells. *J. Physiol.* 463:367–389. <https://doi.org/10.1113/jphysiol.1993.sp019599>
- Tompa, P., R. Tóth-Boconádi, and P. Friedrich. 2001. Frequency decoding of fast calcium oscillations by calpain. *Cell Calcium.* 29:161–170. <https://doi.org/10.1054/ceca.2000.0179>
- Toth, P.T., L.R. Shekter, G.H. Ma, L.H. Philipson, and R.J. Miller. 1996. Selective G-protein regulation of neuronal calcium channels. *J. Neurosci.* 16:4617–4624.
- Trinidad, J.C., A. Thalhammer, C.G. Specht, A.J. Lynn, P.R. Baker, R. Schoepfer, and A.L. Burlingame. 2008. Quantitative analysis of synaptic phosphorylation and protein expression. *Mol. Cell. Proteomics.* 7:684–696. <https://doi.org/10.1074/mcp.M700170-MCP200>
- Trinidad, J.C., D.T. Barkan, B.F. Gullledge, A. Thalhammer, A. Sali, R. Schoepfer, and A.L. Burlingame. 2012. Global identification and characterization of both O-GlcNAcylation and phosphorylation at the murine synapse. *Mol. Cell. Proteomics.* 11:215–229. <https://doi.org/10.1074/mcp.O112.018366>
- Tweedie-Cullen, R.Y., J.M. Reck, and I.M. Mansuy. 2009. Comprehensive mapping of post-translational modifications on synaptic, nuclear, and histone proteins in the adult mouse brain. *J. Proteome Res.* 8:4966–4982. <https://doi.org/10.1021/pr9003739>
- Wang, W.-Y., L.-Y. Hao, E. Minobe, Z.A. Saud, D.-Y. Han, and M. Kameyama. 2009. CaMKII phosphorylates a threonine residue in the C-terminal tail of  $\text{Ca}_v1.2$   $\text{Ca}^{2+}$  channel and modulates the interaction of the channel with calmodulin. *J. Physiol. Sci.* 59:283–290. <https://doi.org/10.1007/s12576-009-0033-y>
- Wei, X., A. Neely, A.E. Lacerda, R. Olcese, E. Stefani, E. Perez-Reyes, and L. Birnbaumer. 1994. Modification of  $\text{Ca}^{2+}$  channel activity by deletions at the carboxyl terminus of the cardiac  $\alpha_1$  subunit. *J. Biol. Chem.* 269:1635–1640.
- Wipf, P., and R.J. Halter. 2005. Chemistry and biology of wortmannin. *Org. Biomol. Chem.* 3:2053–2061. <https://doi.org/10.1039/b504418a>
- Wiśniewski, J.R., N. Nagaraj, A. Zougman, F. Gnäd, and M. Mann. 2010. Brain phosphoproteome obtained by a FASP-based method reveals plasma membrane protein topology. *J. Proteome Res.* 9:3280–3289. <https://doi.org/10.1021/pr1002214>
- Wu, L., C.S. Bauer, X.-G. Zhen, C. Xie, and J. Yang. 2002. Dual regulation of voltage-gated calcium channels by  $\text{PtdIns}(4,5)\text{P}_2$ . *Nature.* 419:947–952. <https://doi.org/10.1038/nature01118>
- Xu, J., L. Yu, E. Minobe, L. Lu, M. Lei, and M. Kameyama. 2016. PKA and phosphatases attached to the  $\text{Ca}_v1.2$  channel regulate channel activity in cell-free patches. *Am. J. Physiol. Cell Physiol.* 310:C136–C141. <https://doi.org/10.1152/ajpcell.00157.2015>
- Xue, Y., J. Ren, X. Gao, C. Jin, L. Wen, and X. Yao. 2008. GPS 2.0, a tool to predict kinase-specific phosphorylation sites in hierarchy. *Mol. Cell. Proteomics.* 7:1598–1608. <https://doi.org/10.1074/mcp.M700574-MCP200>
- Yu, L., J. Xu, E. Minobe, A. Kameyama, L. Yang, R. Feng, L. Hao, and M. Kameyama. 2016. Role of protein phosphatases in the run down of guinea pig cardiac  $\text{Ca}_v1.2$   $\text{Ca}^{2+}$  channels. *Am. J. Physiol. Cell Physiol.* 310:C773–C779. <https://doi.org/10.1152/ajpcell.00199.2015>
- Zhang, H., L.C. Craciun, T. Mirshahi, T. Rohács, C.M. Lopes, T. Jin, and D.E. Logothetis. 2003.  $\text{PIP}_2$  activates KCNQ channels, and its hydrolysis underlies receptor-mediated inhibition of M currents. *Neuron.* 37:963–975. [https://doi.org/10.1016/S0896-6273\(03\)00125-9](https://doi.org/10.1016/S0896-6273(03)00125-9)
- Zhen, X.-G., C. Xie, Y. Yamada, Y. Zhang, C. Doyle, and J. Yang. 2006. A single amino acid mutation attenuates rundown of voltage-gated calcium channels. *FEBS Lett.* 580:5733–5738. <https://doi.org/10.1016/j.febslet.2006.09.027>

## 2.4. Publication 4: *Biochimica et Biophysica Acta* 1853(5): 953-964.

### Diethyldithiocarbamate-mediated zinc ion chelation reveals role of Ca<sub>v</sub>2.3 channels in glucagon secretion.

Irina Drobinskaya\*, Felix Neumaier\*, Alexey Pereverzev, Jürgen Hescheler, Toni Schneider

\* equal contribution

#### **Abstract:**

Peptide-hormone secretion is partially triggered by Ca<sup>2+</sup> influx through voltage-gated Ca<sup>2+</sup> channels (VGCCs) and gene inactivation of Zn<sup>2+</sup>-sensitive Ca<sub>v</sub>2.3-type VGCCs is associated with disturbed glucose homeostasis in mice. Zn<sup>2+</sup> has been implicated in pancreatic islet cell crosstalk and recent findings indicate that sudden cessation of Zn<sup>2+</sup> supply during hypoglycemia triggers glucagon secretion in rodents. Here we show that diethyldithiocarbamate (DEDTC), a chelating agent for Zn<sup>2+</sup> and other group IIB metal ions, differentially affects blood glucose and serum peptide hormone level in wild-type mice and mice lacking the Ca<sub>v</sub>2.3-subunit. Fasting glucose and glucagon level were significantly higher in Ca<sub>v</sub>2.3-deficient compared to wild-type mice, while DEDTC Zn<sup>2+</sup>-chelation produced a significant and correlated increase of blood glucose and serum glucagon concentration in wild-type but not Ca<sub>v</sub>2.3-deficient mice. Glucose tolerance tests revealed severe glucose intolerance in Zn<sup>2+</sup>-depleted Ca<sub>v</sub>2.3-deficient but not vehicle-treated Ca<sub>v</sub>2.3-deficient or Zn<sup>2+</sup>-depleted wildtype mice. Collectively, these findings indicate that Ca<sub>v</sub>2.3 channels are critically involved in the Zn<sup>2+</sup>-mediated suppression of glucagon secretion during hyperglycemia. Especially under conditions of Zn<sup>2+</sup> deficiency, ablation or dysfunction of Ca<sub>v</sub>2.3 channels may lead to severe disturbances in glucose homeostasis.

#### **Contributions to Publication 4:**

I conceptualized and performed the whole-cell patch-clamp recordings, analyzed and interpreted the data from all experiments, prepared all tables and figures, wrote the manuscript and handled the submission and revision process.





## Diethyldithiocarbamate-mediated zinc ion chelation reveals role of Ca<sub>v</sub>2.3 channels in glucagon secretion

Irina Drobinskaya<sup>1</sup>, Felix Neumaier<sup>\*1</sup>, Alexey Pereverzev<sup>2</sup>, Jürgen Hescheler, Toni Schneider<sup>\*</sup>

Institute for Neurophysiology, University of Cologne, Robert-Koch-Str. 39, D-50931 Köln, Germany

### ARTICLE INFO

#### Article history:

Received 3 September 2014  
Received in revised form 28 December 2014  
Accepted 3 January 2015  
Available online 17 January 2015

#### Keywords:

Peptide hormone release  
Gene inactivation  
Toxin-resistant current  
Pharmacoresistant Ca<sup>2+</sup> channel

### ABSTRACT

Peptide-hormone secretion is partially triggered by Ca<sup>2+</sup> influx through voltage-gated Ca<sup>2+</sup> channels (VGCCs) and gene inactivation of Zn<sup>2+</sup>-sensitive Ca<sub>v</sub>2.3-type VGCCs is associated with disturbed glucose homeostasis in mice. Zn<sup>2+</sup> has been implicated in pancreatic islet cell crosstalk and recent findings indicate that sudden cessation of Zn<sup>2+</sup> supply during hypoglycemia triggers glucagon secretion in rodents. Here we show that diethyldithiocarbamate (DEDTC), a chelating agent for Zn<sup>2+</sup> and other group IIB metal ions, differentially affects blood glucose and serum peptide hormone level in wild-type mice and mice lacking the Ca<sub>v</sub>2.3-subunit. Fasting glucose and glucagon level were significantly higher in Ca<sub>v</sub>2.3-deficient compared to wild-type mice, while DEDTC Zn<sup>2+</sup>-chelation produced a significant and correlated increase of blood glucose and serum glucagon concentration in wild-type but not Ca<sub>v</sub>2.3-deficient mice. Glucose tolerance tests revealed severe glucose intolerance in Zn<sup>2+</sup>-depleted Ca<sub>v</sub>2.3-deficient but not vehicle-treated Ca<sub>v</sub>2.3-deficient or Zn<sup>2+</sup>-depleted wildtype mice. Collectively, these findings indicate that Ca<sub>v</sub>2.3 channels are critically involved in the Zn<sup>2+</sup>-mediated suppression of glucagon secretion during hyperglycemia. Especially under conditions of Zn<sup>2+</sup> deficiency, ablation or dysfunction of Ca<sub>v</sub>2.3 channels may lead to severe disturbances in glucose homeostasis.

© 2015 Elsevier B.V. All rights reserved.

### 1. Introduction

Ionic zinc (Zn<sup>2+</sup>) is required for proper formation, processing and crystallization of insulin in β-cell secretory granules [1,2], and co-secreted with insulin during hyperglycemia [3]. In addition to its role for β-cell function, Zn<sup>2+</sup> is increasingly recognized as a possible auto- and paracrine signaling molecule involved in pancreatic islet cell crosstalk. Zn<sup>2+</sup> concentrations co-released into the extracellular space during hyperglycemia are estimated to be in the order of several hundred μmol/l [3], so that nearby cells are exposed to high levels of unbound Zn<sup>2+</sup>. A number of *in vitro* and *in vivo* studies have implicated Zn<sup>2+</sup> in the feedback regulation of β-cell insulin secretion, but the exact physiological relevance of these findings remains a matter of debate. Recent results moreover demonstrate that sudden cessation of Zn<sup>2+</sup> supply during glucose deprivation triggers glucagon release in isolated mouse and rat islets and in living rats, suggesting that Zn<sup>2+</sup> serves as a switch-off signal for glucagon secretion during hypoglycaemia [4–6].

Zn<sup>2+</sup>-induced changes in α- and β-cell function have been shown or proposed to involve activation of ATP-sensitive K<sup>+</sup> (K<sub>ATP</sub>) channels [4–7], but the relevance of other zinc-binding targets in endocrine cells has not been established. Besides weakly blocking all voltage-gated Ca<sup>2+</sup> channels (VGCCs) [8], Zn<sup>2+</sup> is a potent allosteric antagonist of certain Ca<sub>v</sub>α<sub>1</sub> subunits (Ca<sub>v</sub>2.3 and Ca<sub>v</sub>3.2), which possess extracellular metal binding sites with nanomolar to low micromolar Zn<sup>2+</sup> affinity [9–13]. Since Ca<sub>v</sub>2.3 VGCCs have been linked to insulin [14–16], glucagon [17], and somatostatin (SST) release in mice [18], we compared the effects of Zn<sup>2+</sup> chelation on glucose homeostasis and peptide hormone release in Ca<sub>v</sub>2.3-deficient and control mice. Due to an unexpectedly high glucose-tolerance of Ca<sub>v</sub>2.3-deficient mice, we also reassessed glucose tolerance and glucose-stimulated insulin secretion (GSIS) *in vivo* and in isolated islets of Langerhans.

### 2. Materials & methods

#### 2.1. Animals

Mice were housed at a constant temperature (22 °C–23 °C), with light on from 7 a.m. to 7 p.m. and ad libitum access to food and water as described previously [15]. They were fed a breeding diet containing 22.5% crude protein, 5% crude fat, and 4.5% crude fiber (Altromin, Lage, Germany).

The *cacna1e* gene encoding Ca<sub>v</sub>2.3 was disrupted *in vivo* by agouti-colored Ca<sub>v</sub>2.3(fl<sup>+</sup>) and delete mice expressing Cre-recombinase

\* Corresponding authors. Tel.: +49 221 478 6946; fax: +49 221 478 6965.  
E-mail addresses: [felix@neumaier-net.de](mailto:felix@neumaier-net.de) (F. Neumaier), [toni.schneider@uni-koeln.de](mailto:toni.schneider@uni-koeln.de) (T. Schneider).

<sup>1</sup> I. Drobinskaya and F. Neumaier are co-first authors and contributed equally to the paper.

<sup>2</sup> Present address: Department of Physiology and Pharmacology, Faculty of Medicine and Dentistry, University of Western Ontario, London, Ontario N6A 5C1, Canada.

constitutively [15]. Thus, exon 2 was deleted by Cre-mediated recombination.  $Ca_v2.3$ -deficient mice were fertile, exhibited no obvious behavioral abnormalities and had the same lifespan as control mice. Parallel breeding of parental inbred mouse lines of  $Ca_v2.3$ -deficient and control mice ensured their identical background. Number, age and mean body weight of mice used in the different experiments are summarized in Table 1.

During the experiments mice were fasted with free access to water. The animal experimentation described in the text was approved by the institutional committee on animal care and conducted in accordance with accepted standards of humane animal care, as described in the UFAW handbook on the care and management of laboratory animals.

## 2.2. Glucose tolerance tests and serum insulin measurements

After a 14 h fasting period, glucose tolerance tests were performed in 5 and 10 weeks old mice by a single intraperitoneal (i.p.) injection of glucose (2 mg/g body weight) and sampling of glucose levels in tail vein blood obtained by small tail cuts immediately before and 15 min, 30 min, 60 min, and 120 min after the glucose injection. Blood glucose concentration was determined using the Glucometer Elite (Bayer Diagnostics GmbH, Germany). In 10 week old animals, serum insulin level was quantified in blood samples taken immediately before (=time point 0) and 2 min, 5 min, 15 min, 30 min, 60 min and 120 min after the glucose injection by the enzyme-linked immunosorbent assay (ELISA) kit from Crystal Chem Inc. (Chicago, USA) using mouse insulin as a reference. To investigate the effects of  $Zn^{2+}$ -chelation on glucose tolerance, 14–17 week old mice were fasted for 7.25 h and i.p. injections of the  $Zn^{2+}$  chelator diethyldithiocarbamate (DEDTC, sodium salt trihydrate, 0.15 mg/g; Sigma Aldrich) or 0.9% NaCl (Berlin-Chemie AG, Berlin, Germany) were carried out 75 min, 105 min, 165 min, 195 min and 285 min after the start of the fasting period. Glucose was injected 150 min after the last DEDTC treatment and blood glucose concentration measured as described above using the GlucoMen Glyc6 (Berlin-Chemie AG, Germany).

## 2.3. Isolation of islets of Langerhans for insulin secretion assays

17–24 week old mice were anesthetized by intraperitoneal injection of ketamine/xylazine. A mixture of 2 ml ketamine stock solution (25 mg/ml) and 0.25 ml 2% xylazine, diluted with 3 ml 0.9% NaCl, was injected intraperitoneally (0.01 ml per gram body weight). The mixture was stored at 4 °C for maximal ten days. Pancreatic islets were isolated by a collagenase digestion protocol modified after Gotoh et al. [19]. Briefly, the pancreas was removed after slow ductal injection of 3 ml collagenase (3 mg/ml) in cold Hanks buffered salt solution (HBSS) containing (in mM) 137 NaCl, 5 KCl, 0.8  $MgSO_4$ , 0.34  $Na_2HPO_4$ , 0.44  $KH_2PO_4$ , 4.2  $NaHCO_3$ , 1.26  $CaCl_2$ , 2 D-glucose, and 10 HEPES (pH = 7.25) and supplemented with 6.26 mM  $CaCl_2$ . After 19 min incubation at 37 °C in 0.5 ml HBSS, digestion was stopped

**Table 1**

Gender, age and body weight of mice used in the different experiments. Data are mean values  $\pm$  SEM. GTT, glucose tolerance tests; II, islet isolation.

Gender	Age [weeks]	Genotype	Body weight [g]	n	Experiment
Female	14–17	Wildtype	20.7 $\pm$ 1.5	25	DEDTC
		$Ca_v2.3(-/-)$	24.5 $\pm$ 1.7	27	DEDTC
Male	5	Wildtype	21.5 $\pm$ 1.5	8	GTT
		$Ca_v2.3(-/-)$	18.7 $\pm$ 1.3	8	GTT
	10	Wildtype	25.9 $\pm$ 1.2	8	GTT
		$Ca_v2.3(-/-)$	23.8 $\pm$ 0.9	8	GTT
	14–17	Wildtype	24.5 $\pm$ 0.9	9	DEDTC
		$Ca_v2.3(-/-)$	25.9 $\pm$ 1.4	8	DEDTC
	17–24	Wildtype	27.9 $\pm$ 0.5	8	II
		$Ca_v2.3(-/-)$	29.5 $\pm$ 1.8	7	II

by addition of 30 ml cold HBSS supplemented with 0.3% BSA. Following mechanical disruption at 4 °C and removal of undigested tissue, islets were transferred on ice, collected under a dissection microscope and allowed to recover for 22 h in RPMI culture medium supplemented with 10% FBS, 1 mM L-glutamine, 100 U/ml penicillin, 100  $\mu$ g/ml streptomycin and 0.1% BSA at 37 °C and 5%  $CO_2$ .

Insulin secretion was investigated in static batch incubations of three to five islet sets per mouse. Each set contained the same number of size-matched islets, consisting of one large (200–250  $\mu$ m), six to ten intermediate (110–170  $\mu$ m) and one small (70–90  $\mu$ m) islet. After a 30 min equilibration period, islets were incubated for 55 min at 37 °C in Krebs–Ringer buffer (KRB) containing (in mM) 120 NaCl, 4.2 KCl, 1.2  $KH_2PO_4$ , 25  $NaHCO_3$ , 1.2  $MgSO_4$ , 2.5  $CaCl_2$ , 2.8 D-glucose and 10 HEPES (pH = 7.4). The medium was removed and stored at –20 °C pending basal insulin secretion measurements, while the islets were incubated for another 55 min at 37 °C in 0.5 ml KRB containing 20 mM D-glucose. Following recovery of the medium for glucose-stimulated insulin secretion measurements, islets were lysed by incubation for 15 min at 37 °C in 0.5 ml PBS containing 1% (v/v) Igepal CA-630, 0.5% (w/v) Na-deoxycholate and 0.1% (w/v) SDS, and the resulting extract used for quantification of total protein and insulin content.

Insulin was quantified by the Insulin (Mouse) ELISA Kit from DRG Instruments (Marburg, Germany) and total protein content by the BCA Protein Assay Kit from Perbio Science Deutschland (Bonn, Germany) using BSA as a reference.

## 2.4. Whole-cell patch clamp recordings

Human embryonic kidney (HEK-293) cells stably transfected with human  $Ca_v2.3d$  and  $\beta_3$  subunits were cultured under normal growth conditions (37 °C and 5%  $CO_2$ ) in Dulbecco's modified Eagle medium (Sigma-Aldrich) supplemented with 10% fetal calf serum and antibiotics (1% penicillin–streptomycin and selection markers G-418 and hygromycin B). For electrophysiological recordings, cells were seeded on nitric acid-washed glass coverslips and used within 1 to 3 days after plating. All recordings were performed at room temperature using the whole-cell configuration of the patch clamp technique [20]. Briefly, cells were voltage-clamped with an EPC9 amplifier (HEKA, Germany) controlled by HEKA's Pulse software. Leak and capacitive currents were subtracted online by use of a –P/5 protocol and series resistance (5–15 M $\Omega$ ) compensated electronically by 65–85%. Pipettes were prepared from thick-walled borosilicate glass capillaries (World Precision Instruments) and had a resistance of 2–5 M $\Omega$  when filled with internal solution. The standard external solution contained (in mM) 120 NaCl, 5  $BaCl_2$ , 5 KCl, 1  $MgCl_2$ , 20 tetraethylammonium chloride, 10 glucose, 0.01  $ZnCl_2$  and 10 HEPES (pH = 7.4). It was applied to cells at a rate of 1–2 ml  $min^{-1}$  using a gravity-driven 2-barreled perfusion system with two separate inlets, and the bath was connected to ground by a 120 mM NaCl agar bridge. The internal solution contained (in mM) 130 CsCl, 5 oxaloacetic acid, 5 creatine, 5 pyruvic acid, 10 ethyleneglycol-bis( $\beta$ -aminoethylether)-N,N,N',N'-tetraacetic acid (EGTA) and 10 HEPES (pH = 7.3). All voltages were corrected for the liquid junction potential of 5.5 mV (calculated using the JPCalc algorithm in pClamp 10; Molecular Devices, Sunnyvale, CA) between internal and external solution. DEDTC was prepared as 5 mM stock solution and added to the standard external solution prior to recordings to make the final concentration given in the text. Currents were evoked by brief voltage-steps from a holding potential of –80 mV to potentials between –60 and 60 mV. Current–voltage (IV)-relationships were constructed by plotting peak current amplitudes as a function of the test potential and fitted with a combined Ohm–Boltzmann equation:

$$I = (V_m - V_{rev}) * G_{max} / (1 + \exp((-V_m - V_{0.5})/dV))$$

where  $V_m$  is the test potential,  $I$  the peak current measured at the corresponding potential,  $V_{rev}$  the apparent reversal potential,  $G_{max}$  the



maximum slope conductance,  $V_{0.5}$  the voltage of half-maximal current activation and  $dV$  the slope factor. The voltage-dependence of activation was determined from tail currents produced upon repolarization from different test potentials to  $-60$  mV. Relative tail current amplitude ( $I/I_{max}$ ) was plotted as a function of the test potential and fitted with a single Boltzmann equation:

$$I/I_{max} = 1/(1 + \exp((-V_m - V_{0.5act})/dV_{act}))$$

where  $V_{0.5act}$  is the voltage of half-maximal activation and  $dV_{act}$  the activation slope factor. All fits were performed with OriginLab Pro 9 (OriginLab, Northampton, MA) using the Levenberg–Marquardt least-squares algorithm. Smooth curves in the figures represent fits to average data, while values given in the text are average data from fits to individual measurements.

### 2.5. Blood glucose homeostasis during DEDTC $Zn^{2+}$ chelation

During a 5.25 h fasting period, three i.p. DEDTC injections (0.025 mg/g body weight each) were carried out 75 min, 105 min and 165 min after the start of the fasting period in 14–17 week old mice. Blood glucose level was monitored in blood samples obtained from the tail vein by small tail cuts collected immediately before the first DEDTC injection (= time point 0) and 30 min, 60 min, 120 min and 180 min thereafter. In some experiments, blood glucose was additionally measured 90 min after the first DEDTC injection. Whenever DEDTC injections and blood collection were performed at the same time point, the blood sample was obtained prior to the injection.

### 2.6. Peptide hormone homeostasis during DEDTC $Zn^{2+}$ chelation

During a 3.25 h fasting period, two i.p. DEDTC injections (0.025 mg/g body weight each) were carried out 75 min and 105 min after of the fasting period. Blood samples for quantification of glucose and serum peptide hormones were obtained from the tail vein by small tail cuts collected immediately before the first and 30 min after the second DEDTC injection. Serum insulin was quantified as described above, glucagon and SST were quantified using the Glucagon EIA kit (YK090) from Yanaihara Institute Inc. (Awakura, Japan) and the extraction-free somatostatin-14 EIA kit from Bachem Ltd. (St. Helens, Merseyside, UK) respectively. Optical density in samples during the ELISA/EIA tests was measured with the automatic microplate reader  $\mu$ Quant (Bio-Tek Instruments, Germany). Data analysis based on the 4-parameter curve fit was performed using the KC4 2.5 software (Bio-Tek Instruments).

### 2.7. Statistical data analysis

All values mentioned in the text and shown in the figures and tables are expressed as mean  $\pm$  standard error of the mean (SEM), based on  $n$  the number of independent experiments. Smooth curves in Fig. 3 represent fits to average data as described in Section 2.4. Statistical significance was calculated using Student's unpaired t-test (or Student's paired t-test for electrophysiological recordings). Levels of  $p < 0.05$  were considered as statistically significant (\*), and levels of  $p < 0.001$  as statistically highly significant (\*\*).

## 3. Results

### 3.1. $Ca_v2.3$ -deficient mice have preserved glucose tolerance despite impaired peripheral insulin response

Intraperitoneal glucose tolerance tests were performed in fasted (14 h), 5 week old  $Ca_v2.3$ -deficient mice and aged-matched wild-type mice with identical genetic background ( $n = 8$  for both genotypes) (Fig. 1A). As illustrated in Fig. 1B, fasting blood glucose level was significantly lower in  $Ca_v2.3$ -deficient mice ( $p < 0.001$ ), but it reached

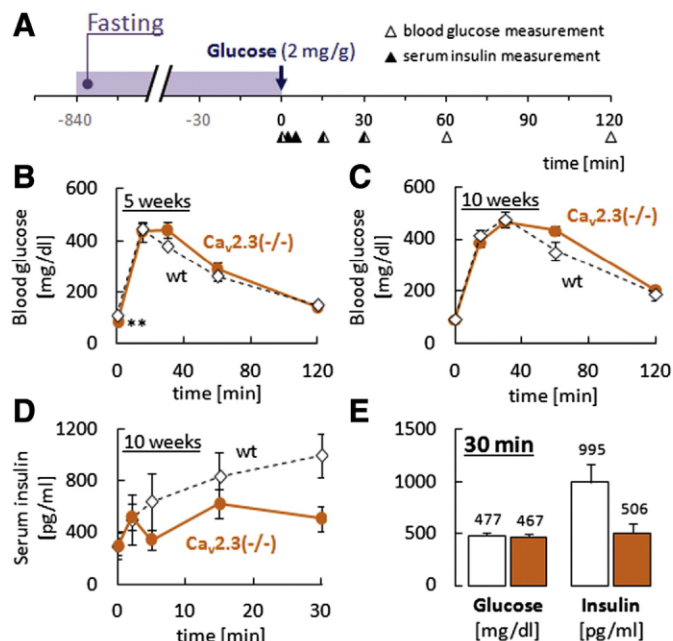


**Fig. 1.** Effects of  $Ca_v2.3$  channel ablation on glucose tolerance and insulin secretion *in vivo*. A. Experimental protocol: Intraperitoneal glucose (2 mg/g) tolerance tests were performed on 14 h fasted  $Ca_v2.3$ -deficient and wildtype mice. Blood glucose and serum insulin level were quantified in blood samples taken from the tail vein immediately prior to glucose challenge (time point 0) and at the indicated time points thereafter. B. Time course of blood glucose disposal in 5 weeks old  $Ca_v2.3$ -deficient and wild-type mice ( $n = 8$  for both genotypes). C. Same as in B, but measured in 10 weeks old mice ( $n = 8$  for both genotypes). D. Time course of changes in serum insulin level of 10 weeks old  $Ca_v2.3$ -deficient and wild-type mice (same animals as in C). E. Comparison of blood glucose and serum insulin level in 10 weeks old wild-type and  $Ca_v2.3$ -deficient mice 30 min after glucose injection (same data as in C and D). Statistically significant differences are indicated by footnotes and are by unpaired Student's t-test (\*\*,  $p < 0.001$ ; \*,  $p < 0.05$ ).

comparable values in both genotypes 15 min after glucose injection. Thereafter, absolute glucose excursion was similar in the two genotypes, although the area under the curve (AUC) above baseline glucose was approximately 25% higher in  $Ca_v2.3$ -deficient mice. When the experiment was repeated with the same number of 10 weeks old mice, neither basal blood glucose level nor absolute glucose excursion (Fig. 1C) or AUC above baseline glucose differed between the two genotypes, possibly indicating age-dependent metabolic changes in one of the two groups. However, serum insulin measurements revealed that ablation of  $Ca_v2.3$  channels was in fact associated with a markedly diminished sustained insulin response in 10 weeks old mice, so that 30 min after glucose injection, serum insulin level had significantly increased to 335% of the basal level ( $p < 0.05$ ) in wild-type mice but only to 175% ( $p > 0.05$ ) in  $Ca_v2.3$ -deficient animals (Fig. 1D). This impairment had surprisingly little effect on glucose tolerance (Fig. 1E), suggesting that it is either masked by other effects of  $Ca_v2.3$ -deficiency or offset by compensatory functional changes.

### 3.2. Isolated islets from $Ca_v2.3$ -deficient mice exhibit normal GSIS but basal hyperinsulinemia and reduced insulin content

The lower peripheral insulin response in  $Ca_v2.3$ -deficient mice could result from reduced  $\beta$ -cell GSIS, increased peripheral insulin clearance or changes in the extrinsic regulation of  $\beta$ -cell function. Therefore, basal and glucose-stimulated insulin secretion was also characterized in 55-min static batch incubations of isolated islets of Langerhans. In seven independent experiments, islets were isolated from 17 to 22 week old male wild-type and  $Ca_v2.3$ -deficient mice, and insulin secretion, insulin content and total protein content measured in three to five sets of size-matched islets per animal (Fig. 2A). Total protein



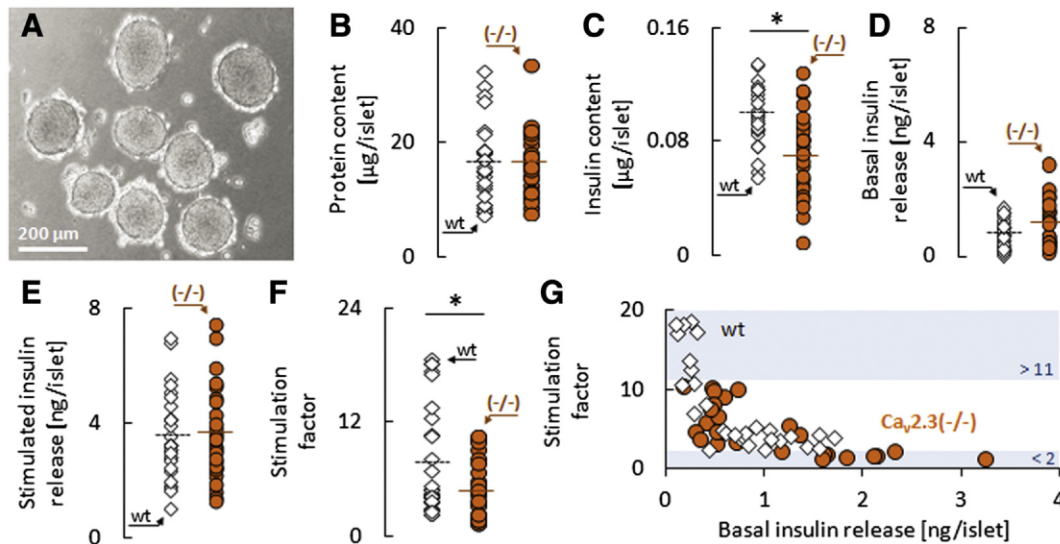


**Fig. 2.** Effects of  $Ca_v2.3$  channel ablation on insulin content, basal insulin secretion and glucose-stimulated insulin secretion in isolated islets of Langerhans. Sets of size-matched islets were isolated from wild-type and  $Ca_v2.3$ -deficient mice, and characterized in 55-min static batch incubations. A. Representative set of isolated islets. B. Distribution of total protein content in islets from  $Ca_v2.3$ -deficient ( $n = 26$  assays in islets from 7 animals) and wild-type mice ( $n = 29$  assays in islets from 7 animals). C. Distribution of total insulin content in islets from  $Ca_v2.3$ -deficient and wild-type mice (same islets as in B). D. Distribution of basal insulin secretion in islets from  $Ca_v2.3$ -deficient and wild-type mice measured in the presence of 2.8 mM glucose (same islets as in B & C). E. Distribution of glucose-stimulated insulin secretion in islets from  $Ca_v2.3$ -deficient and wild-type mice measured in the presence of 20 mM glucose (same islets as in B–D). F. Stimulation factor, calculated as the ratio of data in D and E. G. Same data as in F, but plotted as a function of basal insulin secretion. Statistically significant differences are indicated by footnotes and are by unpaired Student's *t*-test (\*,  $p < 0.05$ ).

content in islets from the two genotypes was essentially the same (Fig. 2B), but insulin content was significantly lower ( $p < 0.05$ ) in islets from  $Ca_v2.3$ -deficient mice, which had a mean insulin content corresponding to approximately 74% of the insulin content in wild-type islets (Fig. 2C). Surprisingly, insulin secretion in the presence of low glucose (2.8 mM) also tended to be higher in islets from  $Ca_v2.3$ -deficient mice (Fig. 2D), indicating that they exhibit basal insulin hypersecretion. This difference was abolished when the glucose concentration was raised to 20 mM (Fig. 2E), so that the stimulation factor, calculated as the ratio of insulin release in high vs. low glucose, was significantly higher ( $p < 0.05$ ) in islets from wild-type mice (Fig. 2F).

The stimulation factor in individual islet assays from both genotypes varied inversely with basal insulin secretion, so that the response to glucose stimulation was stronger in islets with lower basal insulin secretion (Fig. 2G). Ablation of  $Ca_v2.3$  channels enhanced basal islet insulin secretion by 57% relative to wild-type mice, thereby increasing the fraction of islets with low response (i.e. 7 vs. 0 islets with stimulation factor  $< 2$  in  $Ca_v2.3$ -deficient vs wild-type mice; lower blue area in Fig. 2G) and decreasing the fraction of islets with high response (i.e. 0 vs. 6 islets with stimulation factor  $> 11$  in  $Ca_v2.3$ -deficient vs. wild-type mice; upper blue area in Fig. 2G). Thus,  $Ca_v2.3$ -channel ablation attenuated the ability of glucose to increase insulin secretion in isolated islets mainly by increasing basal insulin secretion, while absolute secretion capacity in high glucose was similar for islets from both genotypes (indicating normal glucose responsiveness).

The lower peripheral insulin response of  $Ca_v2.3$ -deficient mice *in vivo* is apparently not related to reduced  $\beta$ -cell insulin secretion per se, and may instead result from  $\beta$ -cell desensitization, changes in the extrinsic regulation of  $\beta$ -cell function or increased peripheral insulin clearance (but see discussion).

### 3.3. DEDTC $Zn^{2+}$ chelation reverses tonic suppression of $Ca_v2.3$ channels *in vitro*

A number of previous studies have implicated  $Zn^{2+}$  in the paracrine regulation of  $\beta$ -cell function [21–24], and insulin hypersecretion in  $ZnT8$ -deficient mice has been linked to insufficient suppression of

$\beta$ -cells due to reduced  $Zn^{2+}$  release [7]. In view of their exceptional  $Zn^{2+}$  sensitivity ( $IC_{50}(Zn^{2+}) = 1–10 \mu M$ ) [12], we hypothesized that a lack of  $\beta$ -cell  $Ca_v2.3$  channels may have similar functional consequences and result in impaired feedback inhibition of insulin secretion. To investigate the role of  $Ca_v2.3$  channels for  $Zn^{2+}$  modulation of glucose homeostasis *in vivo*, we used DEDTC, which is a relatively nontoxic (doses up to 1 mg/g b.w. are tolerated well [25]) chelator routinely used for experimental  $Zn^{2+}$  depletion in rodents. Effects of DEDTC  $Zn^{2+}$  chelation were also characterized *in vitro* using whole-cell patch clamp recordings in HEK293 cells stably transfected with human  $Ca_v2.3d$  and  $\beta_3$ -subunits. As illustrated in Fig. 3A–C, addition of 100  $\mu M$  DEDTC to the extracellular solution containing 10  $\mu M$   $Zn^{2+}$  potently stimulated  $Ba^{2+}$  inward currents over the whole voltage-range examined without changing the apparent reversal potential. Consistent with a reversal of allosteric suppression by chelation of extracellular  $Zn^{2+}$  [12,13], DEDTC effects were associated with a significant ( $p < 0.001$ ) hyperpolarizing shift of the half-maximal activation voltage (Fig. 3C & D), they were rapid (Fig. 3E) and fully reversible upon washout (Fig. 3B–E). When the same recordings were performed in presence of the selective  $Zn^{2+}$ -chelator  $Ca^{2+}$ -EDTA (100  $\mu M$ ), all of the above effects were abolished (Fig. 3F–H), confirming that the action of DEDTC was mediated by chelation of  $Zn^{2+}$  in the extracellular solution.

### 3.4. $Zn^{2+}$ -depletion stimulates glucose mobilization and impairs glucose tolerance in $Ca_v2.3$ -deficient mice

The *in vivo* effect of  $Zn^{2+}$  chelation on glucose tolerance was assessed by intraperitoneal glucose challenge (2 mg/g body weight) after five consecutive intraperitoneal injections of 0.15 mg/g b.w. DEDTC in female, fasted mice (Fig. 4A). As illustrated in Fig. 4B, DEDTC treatment had no effect on the kinetics of blood glucose disposal in wild-type mice. Likewise, glucose tolerance was not significantly affected by ablation of  $Ca_v2.3$  channels alone (i.e. see vehicle-treated  $Ca_v2.3$ -deficient mice in Fig. 4B & C). In contrast, DEDTC pre-treatment of  $Ca_v2.3$ -deficient mice was associated with severe glucose intolerance, reflected in significantly higher ( $p < 0.05$ ) blood glucose levels relative

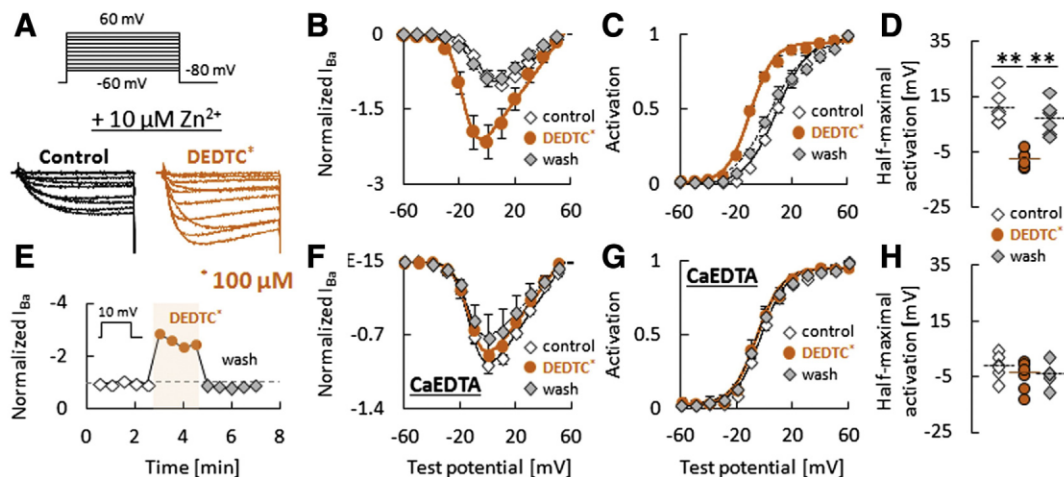


**Fig. 3.** Effects of  $Zn^{2+}$ -chelation on whole-cell  $Ba^{2+}$  currents through recombinant  $Ca_v2.3$  channels recorded in the presence of  $10 \mu M Zn^{2+}$ . Whole-cell currents were recorded with  $5 mM Ba^{2+}$  as the charge carrier from perfused HEK-293 cells stably transfected with human  $Ca_v2.3d$  and  $\beta_3$  subunits. All recordings were performed in the presence of  $10 \mu M$  nominal  $Zn^{2+}$  and from a holding potential of  $-80 mV$ . A. Representative families of current traces recorded in response to the protocol depicted above before (black) and after (orange) addition of  $100 \mu M$  DEDTC. B. Peak current–voltage (IV)-relationships obtained by the protocol depicted in A before (control) and after addition of  $100 \mu M$  DEDTC and after washout. Values are normalized to the maximum peak current observed under control conditions ( $n = 6$ ). C. Voltage-dependence of steady-state activation, obtained by recording tail-current amplitudes upon repolarization from the indicated potentials to  $-60 mV$  before (control) and after addition of  $100 \mu M$  DEDTC and after washout (same cells as in B). D. Voltages of half-maximal activation, obtained from Boltzmann fits to the data in C. E. Time-course of acute DEDTC effects on peak whole-cell currents evoked by step depolarization to  $10 mV$ . F. IV-relationships obtained as in B but in the continued presence of the selective  $Zn^{2+}$  chelator Ca-EDTA ( $n = 7$ ). G. Voltage-dependence of steady-state activation obtained as in C but in the continued presence of the selective  $Zn^{2+}$  chelator Ca-EDTA (same cells as in F but  $n = 6$ ). H. Voltages of half-maximal activation, obtained from Boltzmann fits to the data in G. Statistically significant differences are indicated by footnotes and are by paired Student's *t*-test (\*\*,  $p < 0.001$ ).

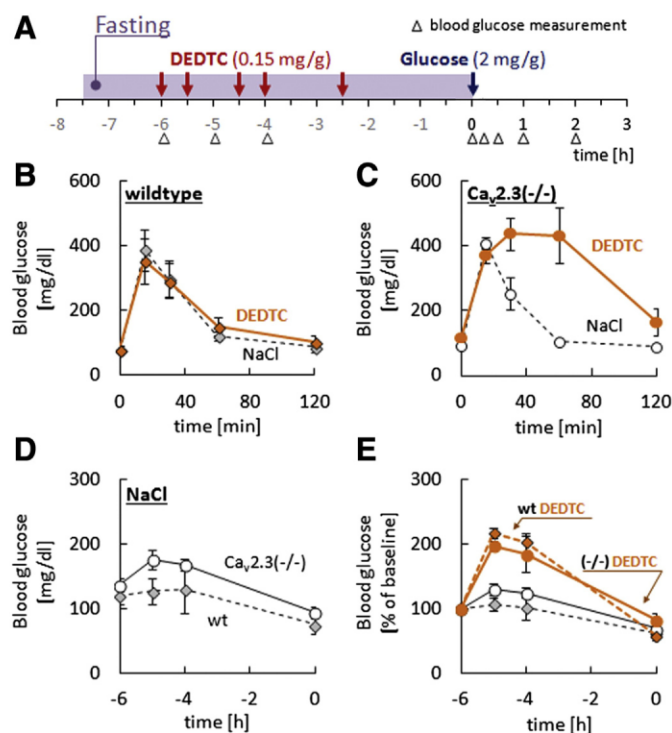


**Fig. 4.** Effects of  $Zn^{2+}$ -depletion on glucose tolerance in  $Ca_v2.3$ -deficient and wild-type mice. A. Experimental protocol: After 6 h of fasting and pre-treatment with DEDTC ( $5 \times 0.15 mg/g$ , i.p., red arrows), animals received a single injection of D-glucose ( $2 mg/g$ , i.p., blue arrow). Blood glucose level was quantified in blood samples taken from the tail vein immediately prior to glucose challenge (time point 0) and at the indicated time points thereafter. B. Time course of glucose excursion in DEDTC- and vehicle-treated wild-type mice ( $n = 5$  for both groups). C. Time course of glucose excursion in DEDTC- ( $n = 6$ ) and vehicle-treated ( $n = 4$ )  $Ca_v2.3$ -deficient mice. D. Time course of changes in blood glucose level during the fasting period before glucose injection in vehicle-treated wild-type and  $Ca_v2.3$ -deficient mice (same mice as in B & C). E. Time course of changes in blood glucose level during the fasting period before glucose injection in DEDTC-treated wild-type and  $Ca_v2.3$ -deficient mice. Values are normalized to the baseline level and data from vehicle-treated littermates are also shown for comparison (same mice as in B & C).

to vehicle-treated littermates 30 and 60 min after glucose challenge (Fig. 4C). When the number of DEDTC injections was reduced to three, this effect was less pronounced but still evident (data not shown).

Throughout the whole fasting period before glucose injection, blood glucose concentration was markedly higher in vehicle-treated  $Ca_v2.3$ -deficient compared to vehicle-treated wild-type mice (Fig. 4D), further supporting the concept of age-dependent metabolic changes in one of the two genotypes. However, this discrepancy with the above findings (i.e. reduced or normal fasting glucose in 5 and 10 weeks old  $Ca_v2.3$ -deficient mice respectively) could also be related to gender-specific differences, as addressed later. In any event, DEDTC-treatment appeared to potentially stimulate glucose mobilization in both genotypes, and this effect was more pronounced in wild-type mice (Fig. 4E). Within the following 6 h, only wild-type mice were capable to lower their blood glucose after DEDTC treatment to the level observed in vehicle-treated littermates, while it was still markedly increased immediately prior to glucose injection in DEDTC-compared to vehicle-treated  $Ca_v2.3$ -deficient mice (Fig. 4E).

Assuming that  $Zn^{2+}$  chelation produces both,  $Ca_v2.3$ -dependent and unspecific effects, additional experiments were carried out with lower doses of DEDTC. To account for possible gender-specific differences, these experiments were performed in parallel with age-matched male and female mice of both genotypes.

### 3.5. Ablation of $Ca_v2.3$ channels is associated with changes in the gender-specific metabolic response to $Zn^{2+}$ -chelation

During treatment with three consecutive injections of  $0.025 mg/g$  b.w. DEDTC (Fig. 5A), blood glucose level still increased in both genotypes, but the effect was significantly more pronounced in wild-type mice after 30 ( $p < 0.05$  for both male and female mice) and 60 min ( $p < 0.05$ , only female mice) (Fig. 5B–G). Thereafter, blood glucose level started to decline again and after 120 and 180 min, similar values were reached in both genotypes. Strikingly, the lower dose DEDTC treatment also revealed a marked gender-specific difference in the effects of  $Zn^{2+}$  chelation, as the relative increase of blood glucose level was much more transient and less pronounced in male mice (Fig. 5B &



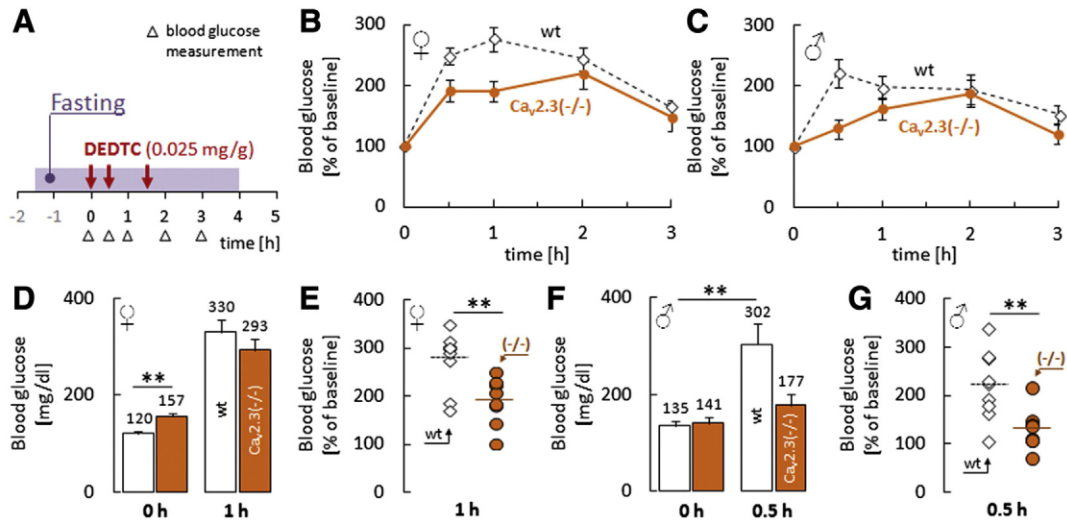


**Fig. 5.** Effects of  $Zn^{2+}$  chelation on fasting blood glucose level in  $Ca_v2.3$ -deficient and wild-type mice. **A.** Experimental protocol: Under conditions of starvation, three injections of DEDTC (0.025 mg/g, i.p.) were carried out at the indicated time points and glucose levels in blood samples taken from the tail vein were monitored over a period of 3 h. **B.** Time course of changes in blood glucose level during DEDTC treatment in female  $Ca_v2.3$ -deficient ( $n = 8$ ) and wild-type ( $n = 9$ ) mice. Values are normalized to the blood glucose level measured immediately before the first DEDTC injection. **C.** Time course of changes in blood glucose level during DEDTC treatment in male  $Ca_v2.3$ -deficient ( $n = 8$ ) and wild-type ( $n = 9$ ) mice. Values are normalized to the blood glucose level measured before the first DEDTC injection. **D.** Comparison of blood glucose levels before (left) and 1 h after (right) the first DEDTC injection in female  $Ca_v2.3$ -deficient and wild-type animals (same data as in B). Note the significant difference between baseline glucose levels in the two genotypes. **E.** Comparison of individual normalized blood glucose levels 1 h after the first DEDTC injection in female wild-type (left) and  $Ca_v2.3$ -deficient (right) mice (same data as in B and D). Mean values are indicated by vertical bars. **F.** Comparison of blood glucose levels before (left) and 1 h after (right) the first DEDTC injection in male  $Ca_v2.3$ -deficient and wild-type animals (same data as in C). **G.** Comparison of individual normalized blood glucose levels 1 h after the first DEDTC injection in male wild-type (left) and  $Ca_v2.3$ -deficient (right) mice (same data as in C and F). Mean values are indicated by vertical bars. Statistically significant differences are indicated by footnotes and are by unpaired Student's t-test (\*\*,  $p < 0.001$ ).

**C.)** Moreover, basal blood glucose level (i.e. before the first DEDTC treatment) of female (Fig. 5D) but not male (Fig. 5F)  $Ca_v2.3$ -deficient mice was significantly higher than in wild-type animals. To further investigate the phenomenon, female mice were chosen to study the effects of DEDTC on peptide hormone release, and the observation period was limited to the initial 60 min after the start of the DEDTC treatment, where significant differences in glucose homeostasis were observed.

### 3.6. $Zn^{2+}$ chelation produces a glucagon response in wild-type but not $Ca_v2.3$ -deficient mice

One hour after starting DEDTC treatment in fasted female mice (Fig. 6A), blood glucose level again reached a significantly higher level in wild-type mice ( $p < 0.05$ ), while basal glucose level (i.e. before DEDTC-treatment) was significantly higher in  $Ca_v2.3$ -deficient mice

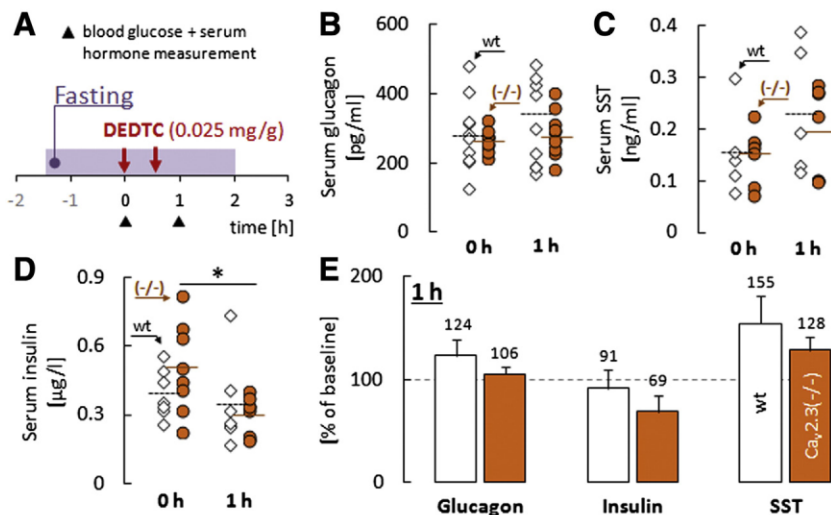


**Fig. 6.** Effects of  $Zn^{2+}$  chelation on fasting serum peptide hormone level in  $Ca_v2.3$ -deficient and wild-type mice. **A.** Experimental protocol: Under conditions of starvation, two injections of DEDTC (0.025 mg/g, i.p.) were carried out at the indicated time points and peptide hormone content was quantified in blood samples taken from the tail vein immediately before the first (0 h) and 0.5 h after the second (1 h) DEDTC injection. **B.** Comparison of individual serum glucagon levels before (left) and after (right) DEDTC treatment in  $Ca_v2.3$ -deficient and wild-type mice ( $n = 10$  for both genotypes). Mean values are indicated by vertical bars. **C.** Comparison of individual serum somatostatin (SST) levels before (left) and after (right) DEDTC treatment in  $Ca_v2.3$ -deficient ( $n = 7$ ) and wild-type ( $n = 5$ ) mice. Mean values are indicated by vertical bars. **D.** Comparison of individual serum insulin levels before (left) and after (right) DEDTC treatment in  $Ca_v2.3$ -deficient ( $n = 8$ ) and wild-type ( $n = 7$ ) mice. Mean values are indicated by vertical bars. **E.** Comparison of normalized serum glucagon (left), insulin (middle), and SST (right) levels after DEDTC treatment in  $Ca_v2.3$ -deficient and wild-type mice (same data as in B–D). Statistically significant differences are indicated by footnotes and are by unpaired Student's t-test (\*,  $p < 0.05$ ).



( $p < 0.05$ ).  $Ca_v2.3$ -deficient mice also displayed a higher basal insulin level relative to wild-type mice (Fig. 6D & E) indicating that insulin hypersecretion detected in isolated islets from  $Ca_v2.3$ -deficient mice was not or not entirely due to a lack of neurally mediated effects. DEDTC  $Zn^{2+}$  chelation conversely decreased serum insulin level in both genotypes, but this effect was much more pronounced and statistically significant only in  $Ca_v2.3$ -deficient mice ( $p < 0.05$ ).  $Zn^{2+}$  potentially suppresses hepatic insulin uptake [7], so that the insulin lowering effect of DEDTC  $Zn^{2+}$  chelation in both genotypes was presumably mainly due to increased insulin clearance. However, serum insulin level is also affected by the degree of SST-suppression of insulin secretion, and  $\delta$ -cell SST-release has been shown to involve  $Ca_v2.3$  channels. As illustrated in Fig. 6C, there was no difference in basal SST level and DEDTC stimulated SST secretion in both genotypes, but this effect was reduced by approximately half in  $Ca_v2.3$ -deficient mice (Fig. 6C & E). Thus, increased SST suppression of insulin secretion likely contributed to reduced serum insulin level in both genotypes, but it couldn't account for the stronger insulin lowering effect of DEDTC in  $Ca_v2.3$ -deficient mice (and may in fact even have led to an underestimation of the difference between the two genotypes). Glucagon conversely stimulates insulin secretion [26], and DEDTC increased serum glucagon level by 24% in wild-type and only 6% in  $Ca_v2.3$ -deficient mice (Fig. 6B). Hence, part of the genotype-dependent difference in DEDTC effects on insulin level could have been secondary to the stronger glucagon increasing effects of DEDTC in wild-type mice. As  $Zn^{2+}$  disinhibition of glucagon secretion requires both, low blood glucose levels and pre-existing inhibition of glucagon release [6,27–29] this could explain the transient nature of DEDTC effects on blood glucose level (Fig. 5B & C). Thus,  $Zn^{2+}$  chelation was most effective during the first treatment, where both conditions (i.e. low blood glucose and pre-existing  $Zn^{2+}$  inhibition) were still met. It could also account for the much more pronounced effects in female mice, which exhibit larger  $\alpha$ -cell mass and glucagon content relative to male mice [30,31] and a more pronounced glucagon response to hypoglycemic stress [32].

The difference between the two genotypes did not reach statistical significance, possibly due to its small magnitude and the relatively high variability of serum glucagon level in wild-type mice (Fig. 6B). Since even small changes in glucagon secretion can markedly affect

**Table 2**

Effect of DEDTC-mediated  $Zn^{2+}$  chelation on blood glucose concentration under conditions of starvation. Data are pooled mean  $\pm$  SEM values from the experiments shown in Figs. 5–7. Statistically significant differences between wild-type and  $Ca_v2.3$ -deficient mice are indicated by footnotes and are by unpaired Student's t-test (\*\*,  $p < 0.01$ ; \*,  $p < 0.05$ ).

Gender	Genotype	Time [h]	Blood glucose		
			[mg/dl]	[% of baseline]	n
Female	Wild type	0	104 $\pm$ 2**	100	27
		0.5	294 $\pm$ 18**	273 $\pm$ 18**	15
		1	312 $\pm$ 12**	302 $\pm$ 15**	25
	$Ca_v2.3(-/-)$	3	193 $\pm$ 11**	178 $\pm$ 12**	15
		0	127 $\pm$ 4**	100	27
		0.5	292 $\pm$ 14**	224 $\pm$ 14**	17
		1	292 $\pm$ 12**	232 $\pm$ 10**	27
		3	248 $\pm$ 16**	189 $\pm$ 13**	17
		3	135 $\pm$ 9**	100	9
Male	Wild type	0	135 $\pm$ 9**	100	9
		0.5	302 $\pm$ 42**	221 $\pm$ 23**	9
		1	266 $\pm$ 30**	197 $\pm$ 18**	9
	$Ca_v2.3(-/-)$	3	211 $\pm$ 30**	153 $\pm$ 15**	9
		0	141 $\pm$ 13**	100	8
		0.5	177 $\pm$ 24**	129 $\pm$ 15**	8
		1	225 $\pm$ 32**	161 $\pm$ 17**	8
		3	169 $\pm$ 24**	120 $\pm$ 16**	8
		3	169 $\pm$ 24**	120 $\pm$ 16**	8

glucose homeostasis, additional experiments were carried out with 15 female mice per genotype to obtain a more reliable estimate of DEDTC effects on  $\alpha$ -cell function.

Consistent with our suspicion, basal glucose and glucagon level in the larger sample were both significantly higher in  $Ca_v2.3$ -deficient compared to wild-type mice ( $p < 0.001$  and  $p < 0.05$  respectively), whereas DEDTC effects on serum glucagon level were significantly ( $p = 0.012$ ) more pronounced in wild-type animals (Fig. 7A–D) (see also Tables 2 and 3 for pooled data obtained from different experimental sets). Thus, ablation of  $Ca_v2.3$  channels as well as  $Zn^{2+}$  chelation in wild-type (and to a significantly lesser extent also in  $Ca_v2.3$ -deficient) mice appeared to stimulate glucagon secretion, suggesting that  $Ca_v2.3$  channels mediate part of the paracrine  $Zn^{2+}$  inhibition of  $\alpha$ -cell glucagon secretion. To corroborate these findings, a correlation analysis was carried out by plotting individual values of normalized blood glucose

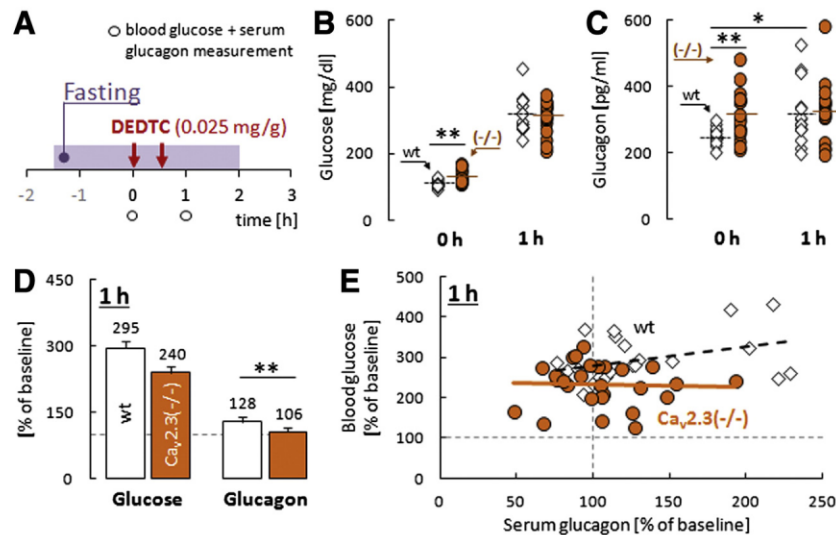


**Fig. 7.** Relationship between blood glucose and serum glucagon level in  $Ca_v2.3$ -deficient and wild-type mice. A. Experimental protocol: Under conditions of starvation, two injections of DEDTC (0.025 mg/g, i.p.) were carried out at the indicated time points and glucose and glucagon levels were quantified in blood samples taken from the tail vein immediately before the first (0 h) and 0.5 h after the second (1 h) DEDTC injection. B. Comparison of blood glucose levels before (left) and 1 h after (right) DEDTC treatment in wild-type ( $n = 15$ ) and  $Ca_v2.3$ -deficient ( $n = 17$ ) mice. C. Comparison of serum glucagon levels before (left) and after (right) DEDTC treatment in  $Ca_v2.3$ -deficient and wild-type mice (same animals as in B). D. Comparison of normalized blood glucose (left) and serum glucagon (right) levels after DEDTC treatment in  $Ca_v2.3$ -deficient and wild-type mice (same data as in B and C). E. Relationship between blood glucose and serum glucagon levels in  $Ca_v2.3$ -deficient and wild-type mice. Linear correlation analysis revealed a correlation with a  $R^2$ -value of 0.137 in wild-type animals but no positive correlation with slightly negative slope and a low  $R^2$ -value of 0.002 in  $Ca_v2.3$ -deficient animals. Statistically significant differences are indicated by footnotes and are by unpaired Student's t-test (\*\*,  $p < 0.001$ ; \*,  $p < 0.05$ ).

**Table 3**  
Effect of DEDTC-mediated  $Zn^{2+}$  chelation on serum peptide hormones under conditions of starvation. Data are pooled mean  $\pm$  SEM values from the experiments shown in Figs. 6 and 7. Statistically significant differences between wild-type and  $Ca_v2.3$ -deficient mice are indicated by footnotes and are by unpaired Student's t-test (\*,  $p < 0.05$ ).

Genotype	Time [h]	Serum glucagon			Serum insulin			Serum somatostatin		
		[mg/dl]	[% of baseline]	n	[ $\mu$ g/l]	[% of baseline]	n	[mg/dl]	[% of baseline]	n
Wild type	0	267 $\pm$ 14	100	25	0.40 $\pm$ 0.04*	100	7	0.16 $\pm$ 0.04	100	5
	1	238 $\pm$ 9*	127 $\pm$ 9	25	0.34 $\pm$ 0.07*	91 $\pm$ 19	7	0.24 $\pm$ 0.06	155 $\pm$ 27	5
$Ca_v2.3(-/-)$	0	312 $\pm$ 18	100	27	0.51 $\pm$ 0.07*	100	8	0.15 $\pm$ 0.02	100	7
	1	311 $\pm$ 16	104 $\pm$ 5	27	0.30 $\pm$ 0.03*	69 $\pm$ 16	8	0.19 $\pm$ 0.03	128 $\pm$ 13	7

concentration after DEDTC treatment as a function of the corresponding serum glucagon concentration. As shown in Fig. 7E, there was a positive correlation between DEDTC effects on glucose and glucagon level in wild-type ( $R^2 = 0.14$ ) but not in  $Ca_v2.3$ -deficient mice ( $R^2 < 0.002$ ), confirming that the DEDTC-induced increase of blood glucose level in wild-type mice was related to enhanced glucagon secretion, and that this effect was not present in  $Ca_v2.3$ -deficient mice.

#### 4. Discussion

Immunohistochemical and functional studies indicate that  $Zn^{2+}$  sensitive  $Ca_v2.3$  channels are involved in peptide hormone secretion and that their ablation is associated with a complex metabolic phenotype [14–18]. We investigated the role of  $Zn^{2+}$  for glucose homeostasis and peptide hormone secretion in wild-type and  $Ca_v2.3$ -deficient mice. Our most important findings are (i) that glucose tolerance is preserved in  $Ca_v2.3$ -deficient mice but highly sensitive to  $Zn^{2+}$  depletion, (ii) that isolated islets from  $Ca_v2.3$ -deficient mice exhibit increased basal insulin secretion and (iii) that  $Zn^{2+}$  chelation with low concentrations of DEDTC evokes a marked glucagon response in wild-type but not  $Ca_v2.3$ -deficient mice *in vivo*. Altered  $Zn^{2+}$  homeostasis evidently produces complex effects on blood glucose homeostasis, but our findings in mice are consistent with previous works in that  $Zn^{2+}$ -deficiency is primarily associated with increased blood glucose concentrations, and they show that this is in part due to insufficient  $Zn^{2+}$ -suppression of  $Ca_v2.3$  channels. As we argue below,  $Zn^{2+}$  can likely affect release of all pancreatic peptide hormones, although the functional consequences and temporal characteristics of  $Zn^{2+}$ -suppression depend on the role of  $Ca_v2.3$  channels in affected cells and presumably on their relative location and distance to the origin of co-secreted  $Zn^{2+}$ .

##### 4.1. Role of $Ca_v2.3$ channels for (suppression of) $\alpha$ -cell glucagon secretion

Approximately 30% of net  $Ca^{2+}$  current in mouse  $\alpha$ -cells is sensitive to the R-type antagonist SNX-482 [33], and glucose-induced suppression of glucagon release is severely impaired in isolated islets from  $Ca_v2.3$ -deficient mice [16,17]. Also, SNX-482 is ineffective in suppressing glucagon release in wild-type islets at low glucose concentrations, but it inhibits glucose-induced suppression of glucagon release [16, 34], suggesting that R-type channels are more important for preventing glucagon release during hyperglycemia than for triggering it during hypoglycemia. Consistent with this notion, we found that ablation of  $Ca_v2.3$  channels impairs the coupling of glucagon release to blood glucose level rather than reducing glucagon release per se, leading to significantly higher blood glucose and glucagon levels in  $Ca_v2.3$ -deficient relative to wild-type mice. However, our findings also provide convincing evidence that this is due to insufficient  $Zn^{2+}$ -suppression of glucagon secretion, as  $Ca_v2.3$  channel ablation and  $Zn^{2+}$ -chelation in wild-type mice had very similar effects, while  $Zn^{2+}$ -chelation in  $Ca_v2.3$ -deficient mice was much less effective in increasing glucagon secretion. Considering their high  $Zn^{2+}$  sensitivity, it is reasonable to assume that  $\alpha$ -cell  $Ca_v2.3$  channels play a role for  $Zn^{2+}$ -induced paracrine suppression of glucagon secretion during hyperglycemia. In isolated mouse and rat islets and in living rats,  $Zn^{2+}$  suppresses  $\alpha$ -cell electrical

activity and cessation of  $\beta$ -cell  $Zn^{2+}$  release during hypoglycemia has been proposed as a trigger for glucagon secretion [4–6]. According to the  $Zn^{2+}$  switch-off hypothesis, glucose-induced insulin and  $Zn^{2+}$  co-secretion is associated with  $Zn^{2+}$ -induced opening of  $\alpha$ -cell  $K_{ATP}$  channels, resulting in hyperpolarization and closure of  $Ca^{2+}$  and  $Na^+$  channels (Fig. 8A). Sudden cessation of  $Zn^{2+}$  supply during hypoglycemia signals  $K_{ATP}$  channels to close and leads to  $\alpha$ -cell depolarization with successive activation of  $Ca^{2+}$  and  $Na^+$  channels (Fig. 8B). During the peak of the resulting action potential (AP), P/Q-type  $Ca^{2+}$  channels open and trigger glucagon secretion through localized  $Ca^{2+}$  influx. Due to their intermediate voltage-range for activation  $Ca_v2.3$  channels have been proposed to provide sufficient depolarization after  $K_{ATP}$  channel closure for subsequent  $Na^+$ - and L-type  $Ca^{2+}$  channel-dependent AP firing [33]. This might be especially important in mouse  $\alpha$ -cells, which have very low  $K_{ATP}$  channel densities [35,36]. The particular importance of  $Ca_v2.3$  channels for suppressing glucagon release during hyperglycemia could be explained by the fact that high glucose concentrations can directly affect  $\alpha$ -cell oxidative metabolism and thereby close  $K_{ATP}$  channels [35,37], which has led to the proposal that  $K_{ATP}$  channel dependent  $\alpha$ -cell depolarization may actually prevent secretion by inactivating  $Na^+$  and  $Ca^{2+}$  channels [34,35,37]. Thus, while electrical activity and global  $Ca^{2+}$  oscillations remain preserved in the presence of high glucose, the lower peak height of the AP associated with  $Na^+$  and  $Ca^{2+}$  channel inactivation could result in reduced P/Q-type channel dependent exocytosis.  $Ca^{2+}$  oscillations are usually indicative of low-voltage activated (LVA)  $Ca^{2+}$  channels, which support repetitive  $Ca^{2+}$  influx at negative resting membrane potentials. However, depolarization sufficient for partial  $Na^+$  channel inactivation should produce complete LVA  $Ca^{2+}$  channel inactivation, and since  $Ca_v2.3$  channels inactivate at somewhat more depolarized potentials and are well known for their involvement in neuronal pacemaking, one could speculate that they are required for maintaining  $\alpha$ -cell electrical activity in the presence of high glucose. However, there is also evidence that under physiological conditions, mouse  $\alpha$ -cells express no LVA  $Ca^{2+}$  channels [33], and the concept that  $K_{ATP}$  channel dependent  $\alpha$ -cell depolarization prevents secretion is challenged by the observation that glucose or tolbutamide-induced closure of  $K_{ATP}$  channels stimulates  $Ca^{2+}$  influx and glucagon secretion in isolated mouse and rat  $\alpha$ -cells [38–41]. Instead, the inhibitory action of glucose under hyperglycemic conditions could primarily depend on  $\beta$ -cell  $Zn^{2+}$  release and suppression of  $\alpha$ -cell  $Ca_v2.3$  channels, consistent with the observation that glucose challenge is associated with a paradoxical stimulation of glucagon secretion in  $Ca_v2.3$ -deficient mice [16]. It is also worth mentioning that SST has been shown to suppress cloned  $Ca_v2.3$  channels by a G-protein-dependent pathway [42] (Fig. 8), suggesting that their native counterparts in mouse  $\alpha$ -cells could play a role for SST suppression of glucagon secretion [34,43]. As previous studies show that SST mediates tonic but not glucose-induced inhibition of glucagon secretion [34,41], the apparent lack of SNX-482 effects on wild-type islets in low glucose could then also reflect the fact that the experimental conditions (i.e. static incubations with possible SST accumulation) are already associated with complete SST inhibition of  $Ca_v2.3$  channels.

Finally, it should be acknowledged that the relevance of  $\alpha$ -cell  $Ca_v2.3$  channels has been questioned, since  $\alpha$ -cells isolated from



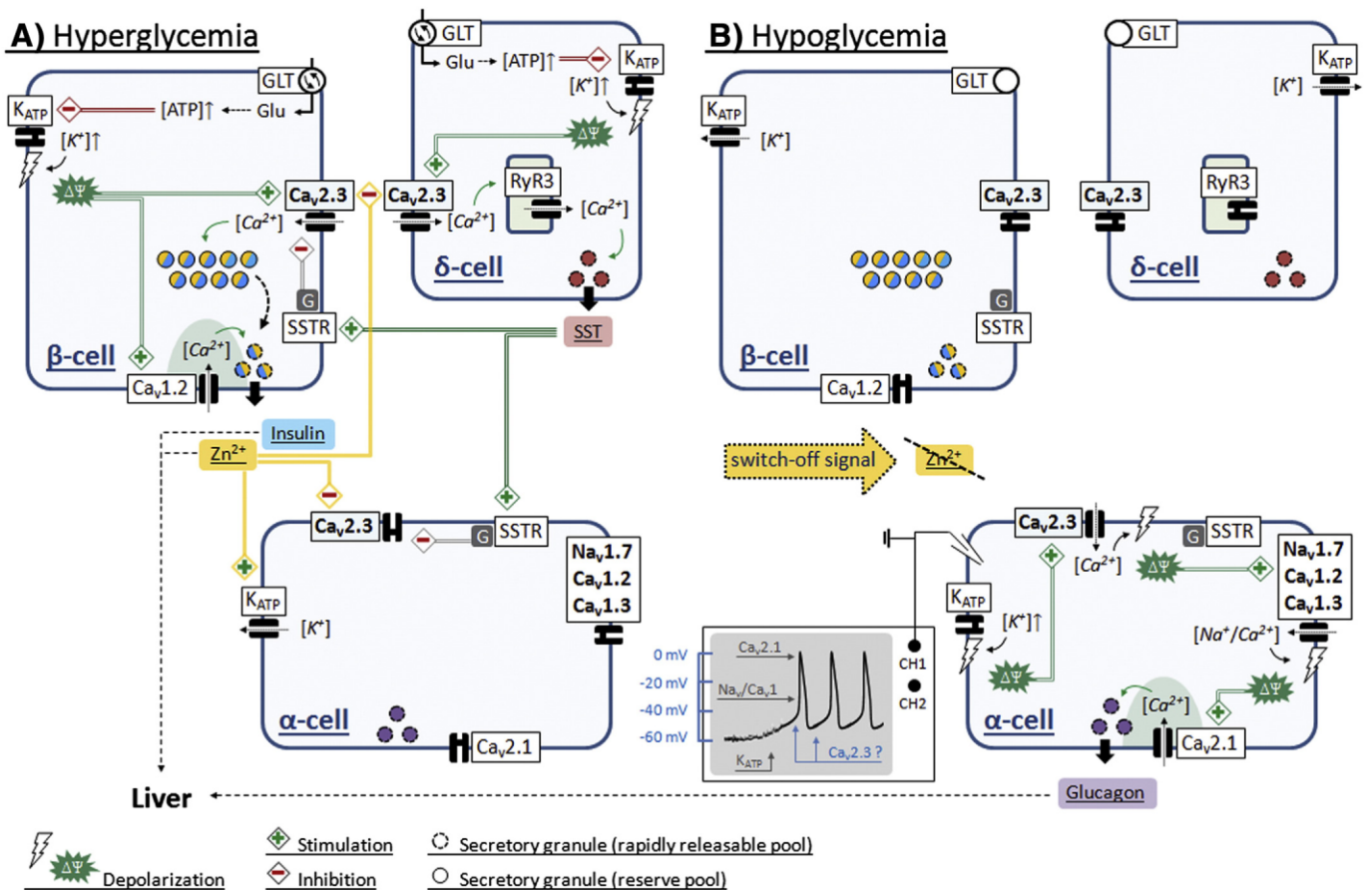


**Fig. 8.** Schema of putative  $Zn^{2+}$ -mediated functional coupling between insulin and glucagon release. A. In the presence of normal or high blood glucose concentrations, ATP level in  $\beta$ -cells increases, leading to closure of  $K_{ATP}$  channels, depolarization and co-secretion of insulin and  $Zn^{2+}$ . In downstream  $\alpha$ -cells,  $Zn^{2+}$  counteracts glucagon release by activation of  $K_{ATP}$  channels and inhibition of  $Ca_v2.3$  channels. B. Under conditions of hypoglycemia, ATP level in  $\beta$ -cells decreases, leading to disinhibition of  $K_{ATP}$  channels,  $K^+$  efflux and thus hyperpolarization with closure of voltage-gated  $Ca^{2+}$  channels. The resulting switch off of  $Zn^{2+}$  release from upstream  $\beta$ -cells is associated with closure of  $K_{ATP}$  channels and disinhibition of  $Ca_v2.3$  channels in  $\alpha$ -cells and ultimately triggers release of glucagon. For further description see text.

$Ca_v2.3$ -deficient mice were found to exhibit neither reduced whole-cell  $Ca^{2+}$  currents nor changes in single-cell glucagon exocytosis [16]. One could argue that this is due to compensatory up-regulation of other (less  $Zn^{2+}$  sensitive)  $\alpha$ -cell VGCCs. However, recent large scale patch clamp analysis of identified mouse  $\alpha$ -cells in a pancreatic slice preparation indicates that there is actually a wide range of electrophysiological properties due to heterogeneous  $\alpha$ -cell ion channel arrangement [36]. Thus, insufficient or biased  $\alpha$ -cell sampling could also explain the apparently unchanged whole-cell  $Ca^{2+}$  current as well as other inconsistencies in the reported ion channel arrangement of mouse  $\alpha$ -cells. These findings make it tempting to speculate that there are different  $\alpha$ -cell populations with distinct glucose,  $Zn^{2+}$  and SST sensitivities, which could be recruited in response to different metabolic conditions.

#### 4.2. Role of $Ca_v2.3$ channels for (suppression of) $\beta$ -cell insulin secretion

GSIS is thought to reflect interaction between a triggering pathway of fast insulin secretion (first phase insulin response), and an amplifying pathway of sustained release (second phase insulin response), which is still only poorly characterized. Here, we reaffirm earlier studies by us and others [16,17] that the sustained peripheral insulin response is significantly reduced in adult  $Ca_v2.3$ -deficient mice *in vivo*. However, our present findings also demonstrate that isolated islets from these mice exhibit normal GSIS and basal hyperinsulinemia relative to islets from wild-type mice. Increased basal insulin secretion in isolated islets could reflect  $\beta$ -cell-intrinsic functional changes, altered islet-intrinsic  $\beta$ -cell regulation or a combination of both. We are currently investigating if reduced  $Zn^{2+}$  feedback inhibition contributes to basal insulin

hypersecretion, but our present data are clearly insufficient to exclude alternative explanations. If  $Zn^{2+}$  feedback inhibition is involved, this could explain the lack of apparent effects of  $Ca_v2.3$  channel ablation on GSIS in isolated islets, since  $Zn^{2+}$  accumulation during static incubations in high glucose should prevent any contribution of these channels in wild-type mice. However as mentioned above, SST inhibits recombinant  $Ca_v2.3$  channels [42] and SNX-482 has been shown to prevent SST inhibition of insulin secretion from insulinoma cells [44]. It is therefore likely that  $Ca_v2.3$  channels are involved in tonic SST suppression of  $\beta$ -cell insulin secretion (Fig. 8), lack of which could also explain or contribute to the basal hyperinsulinemia. In any case, our findings indicate that  $\beta$ -cell  $Ca_v2.3$  channels are involved in suppression of basal insulin secretion, and that this may serve to fine-tune the glucose set-point for insulin secretion. Basal serum insulin level is only moderately but consistently increased in  $Ca_v2.3$ -deficient relative to wild-type mice [14,16,17], possibly indicating that islet-extrinsic factors counterbalance intrinsic hyperinsulinemia to keep serum insulin levels below the detrimental range. The apparent contrast between intact GSIS in isolated islets and impaired peripheral insulin response could be indicative of  $\beta$ -cell desensitization, akin to impairments of the sustained insulin response observed *in vivo* or during pancreas perfusion in diabetic rats [45,46], which are commonly reversed during islet isolation [47,48]. Alternatively, neurally mediated negative feedback loops, possibly acquired in response to elevated non-stimulated secretion (i.e. insulin feedback inhibition of GSIS), may be lost when the pancreas is denervated [49–51] or additional islet-extrinsic changes in  $Ca_v2.3$ -deficient mice (i.e. altered autonomic control of insulin secretion) may exist [15,52]. A role of



compensatory mechanisms for the effects of  $\text{Ca}_v2.3$ -deficiency on glucose homeostasis has previously been excluded based on the potent reduction of GSIS in inbred NMRI mice by SNX-482 [16]. However, this is put into question by the fact that the SNX-482 concentration used (100 nM) can affect several other ion channels as well [53, 54], which might explain why late GSIS is reduced by 80% in SNX-482-treated pancreata from NMRI mice, but only by 50% in pancreata from  $\text{Ca}_v2.3$ -deficient mice [16]. The 50% reduction of late GSIS observed during *in-situ* pancreas perfusion in  $\text{Ca}_v2.3$ -deficient mice on the other hand corresponds well with our *in vivo* data, and indicates that the impaired peripheral insulin response is not due to increased postprandial insulin clearance. Rather, our study suggests a causative role for excessive insulin release and depleted insulin stores, akin to  $\beta$ -cell exhaustion in rodent models of T2DM, where loss of GSIS is often preceded by excessive insulin secretion [55,56]. In this context, it is particularly intriguing that transiently (48 h) up-regulating insulin secretion in non-diabetic rats sufficiently to lower  $\beta$ -cell insulin content has been shown to selectively reduce the second phase insulin response by 50% [57]. In any event, our findings suggest that  $\text{Ca}_v2.3$  channel dysfunction per se is associated with basal hyperinsulinemia and possibly increased glucose sensitivity but normal glucose responsiveness of islet insulin secretion.

#### 4.3. Pathophysiological implications

Our present findings reveal that immature and young adult  $\text{Ca}_v2.3$ -deficient mice display several characteristic features of pre-diabetes, a state where glucose homeostasis is altered but glycemic control still preserved and which commonly precedes development of T2DM. Interestingly, insulin resistance seems to play no causative role in  $\text{Ca}_v2.3$ -deficient mice, as the response to insulin injection in 10 weeks old animals is unaffected [17] and as glucose tolerance is preserved<sup>3</sup> even despite markedly reduced peripheral insulin response (present investigation). We can currently not explain these findings, but adequate  $\text{Zn}^{2+}$  levels seem to be critical for preservation of normal glucose tolerance, since the response to glucose challenge is markedly impaired in  $\text{Zn}^{2+}$ -depleted  $\text{Ca}_v2.3$ -deficient mice.  $\text{Zn}^{2+}$  possesses a wide array of insulin-like effects *in vitro* [58–64], appears to be effective as insulin mimetic in adipocytes from diabetic rats and has been shown to induce normoglycemia in streptozocin-treated rats *in vivo* [65]. Hence, insulin-like  $\text{Zn}^{2+}$  effects could conceivably counterbalance the decreased peripheral insulin response of  $\text{Ca}_v2.3$ -deficient mice to glucose challenge. This could be imagined to occur through an increase in the vesicular  $\text{Zn}^{2+}$ :insulin ratio secondary to the partial depletion of insulin stores observed in isolated islets, a process which should be highly sensitive to  $\text{Zn}^{2+}$ -depletion or loss of  $\beta$ -cell function (i.e. of insulin and  $\text{Zn}^{2+}$ -cosecretion). It could thus explain the apparent age-dependent deterioration of glycemic control in  $\text{Ca}_v2.3$ -deficient mice, as reflected in the progression from reduced to elevated mean body weight (see Table 1) and fasting glucose level. This is reinforced by previous reports that  $\text{Ca}_v2.3$ -deficient mice develop symptoms of T2DM, including overweight, insulin resistance and glucose intolerance [14]. These findings are somewhat difficult to interpret, since mice of various ages (12–50 weeks) were used without appropriate age-matching or discrimination between male and female animals. The concept is nevertheless intriguing, as several studies have since linked variants in the gene encoding  $\text{Ca}_v2.3$  channels to impaired glucose homeostasis in human T2DM patients [66–68]. Most notably, the region on chromosome 1q21–25, where the human  $\text{Ca}_v2.3$  gene is located, has been linked to young-onset T2DM in Pima Indians [67]. Subjects with

<sup>3</sup> Initial reports from our lab indicated that these mice are glucose intolerant [15], but we can now state with certainty that these findings are attributable to the use of mice with different genetic backgrounds (i.e. a higher glucose tolerance of C57Bl/6 control mice) rather than to ablation of  $\text{Ca}_v2.3$  channels.

the risk allele display significantly higher blood glucose concentrations 30 min, 60 min, and 120 min after glucose challenge and higher mean fasting insulin and glucose levels than control persons [67]. Also, high fasting plasma insulin concentrations interestingly predict T2DM in Pima Indians independent of insulin resistance, suggesting a causative role of basal hyperinsulinemia [69]. Our findings indicate that  $\text{Zn}^{2+}$  supplementation could in these cases possibly preserve glucose tolerance, and that close monitoring and/or manipulation of blood  $\text{Zn}^{2+}$  levels may provide a general interventional approach for treatment in certain patient populations with T2DM.

#### 4.4. Limitations and relevance of the present work

Several approaches have been used to investigate the role of  $\text{Zn}^{2+}$  for pancreatic islet crosstalk, including single cell preparations, tissue slices, isolated islets of Langerhans and *in vivo* studies. We used  $\text{Zn}^{2+}$ -chelation in living mice, an approach which circumvents many of the problems associated with *in vitro* preparations but clearly has its own inherent limitations, resulting mainly from the complex actions of  $\text{Zn}^{2+}$  throughout the whole body. Combined with the use of genetically modified mice however, it provides the opportunity to study  $\text{Zn}^{2+}$  effects associated with a particular protein target in a physiologically relevant context. Our present study is clearly not suited nor was it intended to uncover all of the complex molecular alterations of glucose homeostasis in  $\text{Ca}_v2.3$ -deficient mice. Rather it provides first evidence for the *in vivo* relevance of  $\text{Ca}_v2.3$  channels in the context of  $\text{Zn}^{2+}$ , and a reference point for further *in vitro* and *in vivo* studies. Although DEDTC is regarded a preferential  $\text{Zn}^{2+}$ -chelator, we cannot however, exclude that chelation of other physiologically relevant metal ions, such as  $\text{Cu}^{2+}$  or  $\text{Mn}^{2+}$  may have contributed to the observed effects [70]. Due to its membrane-permeant nature, DEDTC may moreover have influenced intracellular signaling cascades or metal-dependent enzymes. However, it has been suggested that  $\text{Zn}^{2+}$  is more easily chelated by DEDTC after being released into the extracellular space [71] so that the low dose regimen used in the present study should have minimized unspecific effects, like abstraction of  $\text{Zn}^{2+}$  from metalloproteins or intracellular stores.

#### 5. Conclusion

The present study reveals that  $\text{Zn}^{2+}$  inhibition of  $\text{Ca}_v2.3$  voltage-gated  $\text{Ca}^{2+}$  channels contributes to suppression of glucagon secretion during hyperglycemia and indicates that these channels may serve as a general target for (differential) feedback inhibition of pancreatic peptide hormone secretion by  $\text{Zn}^{2+}$  and possibly SST. We also demonstrate that  $\text{Ca}_v2.3$ -deficient mice display signs of pre-diabetes followed by a progressive loss of glycemic control, making them a valuable model for certain aspects of human T2DM. Thus, our present findings indicate that maintenance of adequate  $\text{Zn}^{2+}$  levels may be critical for normal glucose tolerance in patients with T2DM linked to  $\text{Ca}_v2.3$  channel dysfunction.

#### Declaration of interest

The authors declare that they have no competing financial interests and that there are no conflicts of interest related to the research reported.

#### Authors' contribution

I.D. performed part of the *in vivo* experiments, isolated the islets, performed the *in vitro* hormone release experiments and contributed to designing the study. A.P. performed part of the *in vivo* experiments. F.N. performed the electrophysiological recordings, analyzed the data, prepared all figures and wrote the manuscript. J.H. helped to supervise the experimental activities and assisted during manuscript preparation.

T.S. initiated and designed the study, directed its implementation, and assisted during data analysis and manuscript preparation.

### Transparency document

The Transparency document associated with this article can be found, in the online version.

### Acknowledgements

We thank Prof. Dr. Edward Perez-Reyes (Charlottesville, USA) for a helpful discussion on the functional importance of zinc binding in  $\text{Ca}_v2.3$  dependent processes. We also thank Dr. B. Wagner, Mr. J. van de Burgwal, Mr. C. Spelten, and the animal keepers of the central facility, as well as Ms. Renate Clemens, Mr. Steffen Braune and Ms. Anja Hallensleben for their technical assistance. The work was financially supported by the Köln Fortune Program/Faculty of Medicine, University of Köln (Bonus 127/2012), as well as by the Deutsche Forschungsgemeinschaft for T.S. (SCHN 387/9).

### References

- [1] D.A. Scott, Crystalline insulin, *Biochem. J.* 28 (1934) 1592–1602.
- [2] S.O. Emdin, G.G. Dodson, J.M. Cutfield, S.M. Cutfield, Role of zinc in insulin biosynthesis. Some possible zinc–insulin interactions in the pancreatic B-cell, *Diabetologia* 19 (1980) 174–182.
- [3] B.J. Kim, Y.H. Kim, S. Kim, J.W. Kim, J.Y. Koh, S.H. Oh, M.K. Lee, K.W. Kim, M.S. Lee, Zinc as a paracrine effector in pancreatic islet cell death, *Diabetes* 49 (2000) 367–372.
- [4] H. Zhou, T. Zhang, J.S. Harmon, J. Bryan, R.P. Robertson, Zinc, not insulin, regulates the rat alpha-cell response to hypoglycemia in vivo, *Diabetes* 56 (2007) 1107–1112.
- [5] A.V. Gyulkhandanyan, H. Lu, S.C. Lee, A. Bhattacharjee, N. Wijesekara, J.E. Fox, P.E. MacDonald, F. Chimienti, F.F. Dai, M.B. Wheeler, Investigation of transport mechanisms and regulation of intracellular  $\text{Zn}^{2+}$  in pancreatic alpha-cells, *J. Biol. Chem.* 283 (2008) 10184–10197.
- [6] M. Slucca, J.S. Harmon, E.A. Oseid, J. Bryan, R.P. Robertson, ATP-sensitive  $\text{K}^+$  channel mediates the zinc switch-off signal for glucagon response during glucose deprivation, *Diabetes* 59 (2010) 128–134.
- [7] M. Tamaki, Y. Fujitani, A. Hara, T. Uchida, Y. Tamura, K. Takeno, M. Kawaguchi, T. Watanabe, T. Ogihara, A. Fukunaka, T. Shimizu, T. Mita, A. Kanazawa, M.O. Imaizumi, T. Abe, H. Kiyonari, S. Hojyo, T. Fukada, T. Kawauchi, S. Nagamatsu, T. Hirano, R. Kawamori, H. Watada, The diabetes-susceptible gene *SLC30A8/ZnT8* regulates hepatic insulin clearance, *J. Clin. Invest.* 123 (2013) 4513–4524.
- [8] H.S. Sun, K. Hui, D.W. Lee, Z.P. Feng,  $\text{Zn}^{2+}$  sensitivity of high- and low-voltage activated calcium channels, *Biophys. J.* 93 (2007) 1175–1183.
- [9] H.W. Kang, H.J. Moon, S.H. Joo, J.H. Lee, Histidine residues in the IS3–IS4 loop are critical for nickel-sensitive inhibition of the  $\text{Ca}_v2.3$  calcium channel, *FEBS Lett.* 581 (2007) 5774–5780.
- [10] M.T. Nelson, J. Woo, H.W. Kang, I. Vitko, P.Q. Barrett, E. Perez-Reyes, J.H. Lee, H.S. Shin, S.M. Todorovic, Reducing agents sensitize C-type nociceptors by relieving high-affinity zinc inhibition of T-type calcium channels, *J. Neurosci.* 27 (2007) 8250–8260.
- [11] H.W. Kang, I. Vitko, S.S. Lee, E. Perez-Reyes, J.H. Lee, Structural determinants of the high affinity extracellular zinc binding site on  $\text{Ca}_v3.2$  T-type calcium channels, *J. Biol. Chem.* 285 (2010) 3271–3281.
- [12] A. Shcheglovitov, I. Vitko, R.M. Lazarenko, P. Orestes, S.M. Todorovic, E. Perez-Reyes, Molecular and biophysical basis of glutamate and trace metal modulation of voltage-gated  $\text{Ca}_v2.3$  calcium channels, *J. Gen. Physiol.* 139 (2012) 219–234.
- [13] F. Neumaier, M. Dibue-Adjei, J. Hescheler, T. Schneider, Voltage-gated calcium channels: determinants of channel function and modulation by inorganic cations, *Prog. Neurobiol.* (2015) (in press).
- [14] Y. Matsuda, H. Saegusa, S. Zong, T. Noda, T. Tanabe, Mice lacking  $\text{Ca}_v2.3$  ( $\alpha1E$ ) calcium channel exhibit hyperglycemia, *Biochem. Biophys. Res. Commun.* 289 (2001) 791–795.
- [15] A. Pereverzev, M. Mikhna, R. Vajna, C. Gissel, M. Henry, M. Weiergräber, J. Hescheler, N. Smyth, T. Schneider, Disturbances in glucose-tolerance, insulin-release and stress-induced hyperglycemia upon disruption of the  $\text{Ca}_v2.3$  ( $\alpha1E$ ) subunit of voltage-gated  $\text{Ca}^{2+}$  channels, *Mol. Endocrinol.* 16 (2002) 884–895.
- [16] X. Jing, D.Q. Li, C.S. Olofsson, A. Salehi, V.V. Surve, J. Caballero, R. Ivarsson, I. Lundquist, A. Pereverzev, T. Schneider, P. Rorsman, E. Renstrom,  $\text{Ca}_v2.3$  calcium channels control second-phase insulin release, *J. Clin. Invest.* 115 (2005) 146–154.
- [17] A. Pereverzev, A. Salehi, M. Mikhna, E. Renstrom, J. Hescheler, M. Weiergräber, N. Smyth, T. Schneider, The ablation of the  $\text{Ca}_v2.3/E$ -type voltage-gated  $\text{Ca}^{2+}$  channel causes a mild phenotype despite an altered glucose induced glucagon response in isolated islets of Langerhans, *Eur. J. Pharmacol.* 511 (2005) 65–72.
- [18] Q. Zhang, M. Bengtsson, C. Partridge, A. Salehi, M. Braun, R. Cox, L. Eliasson, P.R. Johnson, E. Renström, T. Schneider, P.-O. Berggren, S. Gopel, F.M. Ashcroft, P. Rorsman, R-type calcium-channel-evoked *ClCR* regulates glucose-induced somatostatin secretion, *Nat. Cell Biol.* 9 (2007) 453–460.
- [19] M. Gotoh, T. Maki, T. Kiyozumi, S. Satomi, A.P. Monaco, An improved method for isolation of mouse pancreatic islets, *Transplantation* 40 (1985) 437–438.
- [20] O.P. Hamill, A. Marty, E. Neher, B. Sakmann, F.J. Sigworth, Improved patch-clamp techniques for high-resolution current recording from cells and cell-free membrane patches, *Pflügers Arch.* 391 (1981) 85–100.
- [21] T. Ghafghazi, M.L. McDaniel, P.E. Lacy, Zinc-induced inhibition of insulin secretion from isolated rat islets of Langerhans, *Diabetes* 30 (1981) 341–345.
- [22] R. Ferrer, B. Soria, C.M. Dawson, I. Atwater, E. Rojas, Effects of  $\text{Zn}^{2+}$  on glucose-induced electrical activity and insulin release from mouse pancreatic islets, *Am. J. Physiol.* 246 (1984) C520–C527.
- [23] C. Richards-Williams, J.L. Contreras, K.H. Berecek, E.M. Schwiebert, Extracellular ATP and zinc are co-secreted with insulin and activate multiple P2X purinergic receptor channels expressed by islet beta-cells to potentiate insulin secretion, *Purinergic Signal* 4 (2008) 393–405.
- [24] K.G. Slepchenko, C.B. James, Y.V. Li, Inhibitory effect of zinc on glucose-stimulated zinc/insulin secretion in an insulin-secreting beta-cell line, *Exp. Physiol.* 98 (2013) 1301–1311.
- [25] G. Danscher, F.M. Haug, K. Fredens, Effect of diethyldithiocarbamate (DEDTC) on sulphide silver stained boutons. Reversible blocking of Timm's sulphide silver stain for “heavy” metals in DEDTC treated rats (light microscopy), *Exp. Brain Res.* 16 (1973) 521–532.
- [26] J. Gromada, W.G. Ding, S. Barg, E. Renström, P. Rorsman, Multisite regulation of insulin secretion by cAMP-increasing agonists: evidence that glucagon-like peptide 1 and glucagon act via distinct receptors, *Pflügers Arch.* 434 (1997) 515–524.
- [27] K.M. Hope, P.O. Tran, H. Zhou, E. Oseid, E. LeRoy, R.P. Robertson, Regulation of alpha-cell function by the beta-cell in isolated human and rat islets deprived of glucose: the “switch-off” hypothesis, *Diabetes* 53 (2004) 1488–1495.
- [28] H. Zhou, P.O. Tran, S. Yang, T. Zhang, E. LeRoy, E. Oseid, R.P. Robertson, Regulation of alpha-cell function by the beta-cell during hypoglycemia in Wistar rats: the “switch-off” hypothesis, *Diabetes* 53 (2004) 1482–1487.
- [29] H. Zhou, T. Zhang, E. Oseid, J. Harmon, N. Tonooka, R.P. Robertson, Reversal of defective glucagon responses to hypoglycemia in insulin-dependent autoimmune diabetic BB rats, *Endocrinology* 148 (2007) 2863–2869.
- [30] V. Bonnevie-Nielsen, Experimental diets affect pancreatic insulin and glucagon differently in male and female mice, *Metabolism* 29 (1980) 386–391.
- [31] V. Bonnevie-Nielsen, Different effects of high glucose and high fat diet on pancreatic insulin and glucagon in female and male mice, *Diabetes Metab.* 8 (1982) 271–277.
- [32] S. Karlsson, A.J. Scheurink, B. Ahren, Gender difference in the glucagon response to glucopenic stress in mice, *Am. J. Physiol. Regul. Integr. Comp. Physiol.* 282 (2002) R281–R288.
- [33] S. Vignali, V. Leiss, R. Karl, F. Hofmann, A. Welling, Characterization of voltage-dependent sodium and calcium channels in mouse pancreatic A- and B-cells, *J. Physiol.* 572 (2006) 691–706.
- [34] S. Göpel, Q. Zhang, L. Eliasson, X.S. Ma, J. Galvanovskis, T. Kanno, A. Salehi, P. Rorsman, Capacitance measurements of exocytosis in mouse pancreatic alpha-, beta- and delta-cells within intact islets of Langerhans, *J. Physiol.* 556 (2004) 711–726.
- [35] S.O. Göpel, T. Kanno, S. Barg, X.G. Weng, J. Gromada, P. Rorsman, Regulation of glucagon release in mouse  $\alpha$ -cells by  $\text{K}_{ATP}$  channels and inactivation of TTX-sensitive  $\text{Na}^+$  channels, *J. Physiol. Lond.* 528 (2000) 509–520.
- [36] Y.C. Huang, M. Rupnik, H.Y. Gaisano, Unperturbed islet alpha-cell function examined in mouse pancreas tissue slices, *J. Physiol.* 589 (2011) 395–408.
- [37] J. Gromada, X. Ma, M. Hoy, K. Bokvist, A. Salehi, P.O. Berggren, P. Rorsman, ATP-sensitive  $\text{K}^+$  channel-dependent regulation of glucagon release and electrical activity by glucose in wild-type and *SUR1*  $-/-$  mouse alpha-cells, *Diabetes* 53 (Suppl. 3) (2004) S181–S189.
- [38] K. Bokvist, H.L. Olsen, M. Hoy, C.F. Gotfredsen, W.F. Holmes, K. Buschard, P. Rorsman, J. Gromada, Characterisation of sulphonylurea and ATP-regulated  $\text{K}^+$  channels in rat pancreatic A-cells, *Pflügers Arch.* 438 (1999) 428–436.
- [39] M. Hoy, H.L. Olsen, K. Bokvist, K. Buschard, S. Barg, P. Rorsman, J. Gromada, Tolbutamide stimulates exocytosis of glucagon by inhibition of a mitochondrial-like ATP-sensitive  $\text{K}^+$  ( $\text{K}_{ATP}$ ) conductance in rat pancreatic A-cells, *J. Physiol.* 527 (Pt 1) (2000) 109–120.
- [40] H.L. Olsen, S. Theander, K. Bokvist, K. Buschard, C.B. Wollheim, J. Gromada, Glucose stimulates glucagon release in single rat alpha-cells by mechanisms that mirror the stimulus-secretion coupling in beta-cells, *Endocrinology* 146 (2005) 4861–4870.
- [41] E. Vieira, A. Salehi, E. Gylfe, Glucose inhibits glucagon secretion by a direct effect on mouse pancreatic alpha cells, *Diabetologia* 50 (2007) 370–379.
- [42] G. Mehrke, A. Pereverzev, H. Grabsch, J. Hescheler, T. Schneider, Receptor mediated modulation of recombinant neuronal class E calcium channels, *FEBS Lett.* 408 (1997) 261–270.
- [43] K. Cejvan, D.H. Coy, S. Efendic, Intra-islet somatostatin regulates glucagon release via type 2 somatostatin receptors in rats, *Diabetes* 52 (2003) 1176–1181.
- [44] S. Mergler, V. Singh, C. Grotzinger, P. Kaczmarek, B. Wiedenmann, M.Z. Strowski, Characterization of voltage operated R-type  $\text{Ca}^{2+}$  channels in modulating somatostatin receptor subtype 2- and 3-dependent inhibition of insulin secretion from INS-1 cells, *Cell. Signal.* 20 (2008) 2286–2295.
- [45] M. Kergoat, D. Bailbe, B. Portha, Insulin treatment improves glucose-induced insulin release in rats with NIDDM induced by streptozocin, *Diabetes* 36 (1987) 971–977.
- [46] V. Grill, M. Westberg, C.G. Ostenson, B cell insensitivity in a rat model of non-insulin-dependent diabetes. Evidence for a rapidly reversible effect of previous hyperglycemia, *J. Clin. Invest.* 80 (1987) 664–669.
- [47] P.A. Halban, S. Bonner-Weir, G.C. Weir, Elevated proinsulin biosynthesis in vitro from a rat model of non-insulin-dependent diabetes mellitus, *Diabetes* 32 (1983) 277–283.



- [48] B. Portha, M.H. Giroix, P. Serradas, N. Welsh, C. Hellerstrom, A. Sener, W.J. Malaisse, Insulin production and glucose metabolism in isolated pancreatic islets of rats with NIDDM, *Diabetes* 37 (1988) 1226–1233.
- [49] D. Elahi, M. Nagulesparan, R.J. Hersheof, D.C. Muller, J.D. Tobin, P.M. Blix, A.H. Rubenstein, R.H. Unger, R. Andres, Feedback inhibition of insulin secretion by insulin: relation to the hyperinsulinemia of obesity, *N. Engl. J. Med.* 306 (1982) 1196–1202.
- [50] J. Stagner, E. Samols, K. Polonsky, w. pugh, Lack of direct inhibition of insulin secretion by exogenous insulin in the canine pancreas, *J. Clin. Invest.* 78 (1986) 1193–1198.
- [51] G. Boden, X. Chen, R. DeSantis, J. Kolaczynski, M. Morris, Evidence that suppression of insulin secretion by insulin itself is neurally mediated, *Metabolism* 42 (1993) 786–789.
- [52] A. Albillos, E. Neher, T. Moser, R-type  $Ca^{2+}$  channels are coupled to the rapid component of secretion in mouse adrenal slice chromaffin cells, *J. Neurosci.* 20 (2000) 8323–8330.
- [53] G. Arroyo, M. Aldea, J. Fuentealba, A. Albillos, Garci, and a AG, SNX482 selectively blocks P/Q  $Ca^{2+}$  channels and delays the inactivation of Na(+) channels of chromaffin cells, *Eur. J. Pharmacol.* 475 (2003) 11–18.
- [54] T. Kimm, B.P. Bean, Inhibition of A-type potassium current by the peptide toxin SNX-482, *J. Neurosci.* 34 (2014) 9182–9189.
- [55] J.L. Leahy, L.M. Bumbalo, C. Chen, Beta-cell hypersensitivity for glucose precedes loss of glucose-induced insulin secretion in 90% pancreatectomized rats, *Diabetologia* 36 (1993) 1238–1244.
- [56] M. Gadot, G. Leibowitz, E. Shafrir, E. Cerasi, D.J. Gross, N. Kaiser, Hyperproinsulinemia and insulin deficiency in the diabetic *Psammomys obesus*, *Endocrinology* 135 (1994) 610–616.
- [57] Y.A. Hosokawa, J.L. Leahy, Parallel reduction of pancreas insulin content and insulin secretion in 48-h tolbutamide-infused normoglycemic rats, *Diabetes* 46 (1997) 808–813.
- [58] L. Coulston, P. Dandona, Insulin-like effect of zinc on adipocytes, *Diabetes* 29 (1980) 665–667.
- [59] L. Coulston, P. Dandona, Zinc/insulin synergism in the rat adipocyte model, *Lancet* 1 (1980) 1200.
- [60] J.M. May, C.S. Contoreggi, The mechanism of the insulin-like effects of ionic zinc, *J. Biol. Chem.* 257 (1982) 4362–4368.
- [61] A. Yamamoto, O. Wada, T. Ono, H. Ono, S. Manabe, S. Ishikawa, Cadmium-induced stimulation of lipogenesis from glucose in rat adipocytes, *Biochem. J.* 219 (1984) 979–984.
- [62] O. Ezaki, IIb group metal ions ( $Zn^{2+}$ ,  $Cd^{2+}$ ,  $Hg^{2+}$ ) stimulate glucose transport activity by post-insulin receptor kinase mechanism in rat adipocytes, *J. Biol. Chem.* 264 (1989) 16118–16122.
- [63] I.A. Brand, J. Kleineke, Intracellular zinc movement and its effect on the carbohydrate metabolism of isolated rat hepatocytes, *J. Biol. Chem.* 271 (1996) 1941–1949.
- [64] X. Tang, N.F. Shay, Zinc has an insulin-like effect on glucose transport mediated by phosphoinositol-3-kinase and Akt in 3T3-L1 fibroblasts and adipocytes, *J. Nutr.* 131 (2001) 1414–1420.
- [65] A. Shisheva, D. Gefel, Y. Shechter, Insulinlike effects of zinc ion in vitro and in vivo. Preferential effects on desensitized adipocytes and induction of normoglycemia in streptozocin-induced rats, *Diabetes* 41 (1992) 982–988.
- [66] J. Holmkvist, D. Tojjar, P. Almgren, V. Lyssenko, C.M. Lindgren, B. Isomaa, T. Tuomi, G. Berglund, E. Renstrom, L. Groop, Polymorphisms in the gene encoding the voltage-dependent  $Ca^{2+}$  channel  $Ca_v2.3$  (CACNA1E) are associated with type 2 diabetes and impaired insulin secretion, *Diabetologia* 50 (2007) 2467–2475.
- [67] Y.L. Muller, R.L. Hanson, C. Zimmerman, I. Harper, J. Sutherland, S. Kobes, W.C. Knowler, C. Bogardus, L.J. Baier, Variants in the  $Ca_v2.3$  ( $\alpha$ 1E) subunit of voltage-activated  $Ca^{2+}$  channels are associated with insulin resistance and type 2 diabetes in Pima Indians, *Diabetes* 56 (2007) 3089–3094.
- [68] M. Trombetta, S. Bonetti, M. Boselli, F. Turrini, G. Malerba, E. Trabetti, P. Pignatti, E. Bonora, R.C. Bonadonna, CACNA1E variants affect beta cell function in patients with newly diagnosed type 2 diabetes. The Verona newly diagnosed type 2 diabetes study (VNDS) 3, *PLoS One* 7 (2012) e32755.
- [69] C. Weyer, R.L. Hanson, P.A. Tataranni, C. Bogardus, R.E. Pratley, A high fasting plasma insulin concentration predicts type 2 diabetes independent of insulin resistance: evidence for a pathogenic role of relative hyperinsulinemia, *Diabetes* 49 (2000) 2094–2101.
- [70] A. Mathie, G.L. Sutton, C.E. Clarke, E.L. Veale, Zinc and copper: pharmacological probes and endogenous modulators of neuronal excitability, *Pharmacol. Ther.* 111 (2006) 567–583.
- [71] M.I. Dominguez, J.M. Blasco-Ibanez, C. Crespo, A.I. Marques-Mari, F.J. Martinez-Guijarro, Zinc chelation during non-lesioning overexcitation results in neuronal death in the mouse hippocampus, *Neuroscience* 116 (2003) 791–806.



## 2.5. Publication 5: Journal of Neurochemistry 147(3): 310-322.

### Reciprocal modulation of Ca<sub>v</sub>2.3 voltage-gated calcium channels by copper(II) ions and kainic acid.

Felix Neumaier, Isha Akhtar-Schäfer, Jan Niklas Lüke, Maxine Dibué-Adjei, Jürgen Hescheler, Toni Schneider

#### **Abstract:**

Kainic acid (KA) is a potent agonist at non-N-methyl-D-aspartate (non-NMDA) ionotropic glutamate receptors and commonly used to induce seizures and excitotoxicity in animal models of human temporal lobe epilepsy. Among other factors, Ca<sub>v</sub>2.3 voltage-gated calcium channels have been implicated in the pathogenesis of KA-induced seizures. At physiologically relevant concentrations, endogenous trace metal ions (Cu<sup>2+</sup>, Zn<sup>2+</sup>) occupy an allosteric binding site on the domain I gating module of these channels and interfere with voltage-dependent gating. Using whole-cell patch clamp recordings in human embryonic kidney (HEK-293) cells stably transfected with human Ca<sub>v</sub>2.3d and β<sub>3</sub>-subunits, we identified a novel, glutamate receptor-independent mechanism by which KA can potently sensitize these channels. Our findings demonstrate that KA releases these channels from the tonic inhibition exerted by low nanomolar concentrations of Cu<sup>2+</sup> and produces a hyperpolarizing shift in channel voltage-dependence by about 10 mV, thereby reconciling the effects of Cu<sup>2+</sup> chelation with tricaine. When tricaine was used as a surrogate to study the receptor independent action of KA in electroretinographic recordings from the isolated bovine retina, it selectively suppressed a late b-wave component, which we have previously shown to be enhanced by genetic or pharmacological ablation of Ca<sub>v</sub>2.3 channels. Although the pathophysiological relevance remains to be firmly established, we speculate that reversal of Cu<sup>2+</sup>-induced allosteric suppression, presumably via formation of stable kainate-Cu<sup>2+</sup> complexes, could contribute to the receptor-mediated excitatory effects of KA. In addition, we discuss experimental implications for the use of KA *in vitro*, with particular emphasis on the seemingly high incidence of trace metal contamination in common physiological solutions.

#### **Contributions to Publication 5:**

I conceptualized and performed the whole-cell patch-clamp recordings, was involved in interpretation of the ERG recordings, prepared all tables and figures, wrote the manuscript and handled the submission and revision process.

ORIGINAL  
ARTICLEReciprocal modulation of Ca<sub>v</sub>2.3 voltage-gated calcium channels by copper(II) ions and kainic acidFelix Neumaier\* , Isha Akhtar-Schäfer\*†, Jan Niklas Lüke\*,  
Maxine Dibué-Adjei\*‡, Jürgen Hescheler\* and Toni Schneider\* 

\*Institute for Neurophysiology, University of Cologne, Cologne, Germany

†Department of Ophthalmology, Laboratory for Experimental Immunology of the Eye, University of Cologne, Cologne, Germany

‡Department for Neurosurgery, Medical Faculty, Heinrich Heine University, Düsseldorf, Germany

## Abstract

Kainic acid (KA) is a potent agonist at non-N-methyl-D-aspartate (non-NMDA) ionotropic glutamate receptors and commonly used to induce seizures and excitotoxicity in animal models of human temporal lobe epilepsy. Among other factors, Ca<sub>v</sub>2.3 voltage-gated calcium channels have been implicated in the pathogenesis of KA-induced seizures. At physiologically relevant concentrations, endogenous trace metal ions (Cu<sup>2+</sup>, Zn<sup>2+</sup>) occupy an allosteric binding site on the domain I gating module of these channels and interfere with voltage-dependent gating. Using whole-cell patch-clamp recordings in human embryonic kidney (HEK-293) cells stably transfected with human Ca<sub>v</sub>2.3d and β<sub>3</sub>-subunits, we identified a novel, glutamate receptor-independent mechanism by which KA can potentially sensitize these channels. Our findings demonstrate that KA releases these channels from the tonic inhibition exerted by low nanomolar concentrations of Cu<sup>2+</sup> and produces a hyperpolarizing shift in channel voltage-dependence by about 10 mV, thereby

reconciling the effects of Cu<sup>2+</sup> chelation with tricaine. When tricaine was used as a surrogate to study the receptor-independent action of KA in electroretinographic recordings from the isolated bovine retina, it selectively suppressed a late b-wave component, which we have previously shown to be enhanced by genetic or pharmacological ablation of Ca<sub>v</sub>2.3 channels. Although the pathophysiological relevance remains to be firmly established, we speculate that reversal of Cu<sup>2+</sup>-induced allosteric suppression, presumably via formation of stable kainate-Cu<sup>2+</sup> complexes, could contribute to the receptor-mediated excitatory effects of KA. In addition, we discuss experimental implications for the use of KA *in vitro*, with particular emphasis on the seemingly high incidence of trace metal contamination in common physiological solutions.

**Keywords:** endogenous Zn<sup>2+</sup> and Cu<sup>2+</sup>, excitotoxicity, kainate-induced epilepsy, R-type Ca<sup>2+</sup> channels, trace metal chelator, transition metal ions.

*J. Neurochem.* (2018) **147**, 310–322.

Alpha-kainic acid (KA) is a naturally occurring excitatory amino acid with an embedded L-glutamic acid (L-Glu) moiety. In rodents, systemic administration produces a limbic motor syndrome reminiscent of human temporal lobe epilepsy, which is characterized by recurrent limbic seizures, hippocampal sclerosis, and hyper-excitability in surviving hippocampal neurons (Wang *et al.* 2005). KA has been shown to exert its effects via activation of non-N-methyl-D-aspartate (non-NMDA) ionotropic glutamate receptors, triggering excessive Ca<sup>2+</sup>-influx with a number of detrimental cellular implications (Wang *et al.* 2005). Ca<sub>v</sub>2.3 voltage-gated Ca<sup>2+</sup>-channels (VGCCs) play a pro-ictogenic role in the pathogenesis of KA-induced seizures, which is reflected in a marked seizure resistance and neuroprotection conferred

by their genetic ablation (Weiergräber *et al.* 2007; Dibue-Adjei *et al.* 2017). These channels are widely distributed throughout the brain and involved in a number of vital physiological processes, including synaptic transmission,

Received April 12, 2018; revised manuscript received June 11, 2018; accepted July 2, 2018.

Address correspondence and reprint requests to Felix Neumaier and Toni Schneider, Institute of Neurophysiology, Robert-Koch-Str. 39, D-50931 Cologne, Germany. E-mail: felix@neumaier-net.de (or) toni.schneider@uni-koeln.de

**Abbreviations used:** Ca<sub>v</sub>2.3, ion conducting α<sub>1</sub> subunit of E-type voltage-gated Ca<sup>2+</sup> channels; HEK-293, human embryonic kidney cell line; KA, kainic acid; L-Glu, L-glutamic acid; TMIs, transition metal ions; Tn, tricaine; VGCCs, voltage-gated calcium channels.

integration, and plasticity (Magee and Johnston 1995; Magee and Carruth 1999; Gasparini *et al.* 2001; Dietrich *et al.* 2003). They are also among the most sensitive molecular targets of Zn<sup>2+</sup> and Cu<sup>2+</sup> currently known, which has been linked to a high affinity trace metal binding site that is not conserved in other high-voltage activated Ca<sup>2+</sup> channels (Castelli *et al.* 2003; Magistretti *et al.* 2003; Shcheglovitov *et al.* 2012; Neumaier *et al.* 2015). Interestingly, a recent study found that excitatory amino acids like L-glutamate (L-Glu) can significantly stimulate Ca<sub>v</sub>2.3 channels by acting as trace metal chelators and reversing suppression by Zn<sup>2+</sup> and Cu<sup>2+</sup> *in vitro* (Shcheglovitov *et al.* 2012). Although the exact role of endogenous free trace metal ions (TMI) in the brain remains controversial, their chelation has been shown to augment KA-induced neurotoxicity (Lees *et al.* 1998) and can trigger seizure activity and neuronal cell death during sub-convulsive KA over-excitation in mice (Dominguez *et al.* 2003). Given the structural similarity of KA to L-Glu and other trace metal chelating amino acids, these findings prompted us to investigate whether its application in the presence of physiologically relevant concentrations of Cu<sup>2+</sup> could also alter Ca<sub>v</sub>2.3 channel function in a receptor-independent manner. To this end, whole-cell patch-clamp recordings were performed in HEK-293 cells stably transfected with human Ca<sub>v</sub>2.3 and β<sub>3</sub> channel complexes, which allowed us to study the effects of KA without interference from glutamate receptors. Our findings confirm that KA produces a strong, Cu<sup>2+</sup>-dependent stimulation of channel gating that can be reproduced by trace metal chelation with tricaine. They also indicate that traces of other metal ions contaminating the recording solution may suffice for similar, albeit much less marked effects. When tricaine was used as a surrogate to isolate and study the receptor-independent action of KA in electroretinographic recordings from the isolated bovine retina, it selectively suppressed a late b-wave component, which we have previously shown to be carried by Ca<sub>v</sub>2.3 channels (Alnawaiseh *et al.* 2011). Although the pathophysiological relevance remains to be firmly established, we speculate that disinhibition of Ca<sub>v</sub>2.3 by chelation of endogenous transition metal ions could contribute to the receptor-independent excitotoxic effects of KA.

## Material and methods

### Cell culture

Human embryonic kidney (HEK-293) cells (RRID:CVCL\_0045) stably transfected with human Ca<sub>v</sub>2.3d and β<sub>3</sub> Ca<sup>2+</sup>-channel subunits were cultured under normal growth conditions (37°C and 5% CO<sub>2</sub>) in Dulbecco's modified Eagle medium (DMEM, Sigma, #D5796) supplemented with 10% fetal calf serum (Sigma, St Louis, MO, USA, #F0804) and antibiotics [1% penicillin-streptomycin (Sigma, #P4333) and selection markers: 1 mg/mL G-418 (Sigma, #A1720) and 200 µg/mL hygromycin B (Sigma, #H3274)]. Cells were routinely passaged twice a week. For electrophysiological recordings,

cells of intermediate passage numbers were seeded on nitric acid-washed glass coverslips in 35 mm polystyrene dishes (Falcon, Heidelberg, Germany) and used within 1–3 days after plating.

No institutional approval was required for this study. No sample calculation was performed and no randomization or blinding was performed.

### Whole-cell patch-clamp recordings

Cells were voltage-clamped using the whole-cell configuration of the patch-clamp technique (Hamill *et al.* 1981). Pipettes were prepared from thick-walled borosilicate glass capillaries (1.5/0.84 mm OD/ID; World Precision Instruments) using a P97 Micropipette puller (Sutter Instruments) and had resistances between 3 and 5 MΩ when filled with internal solution. The bath was connected to ground via 120 mM sodium chloride agar bridges. Currents were acquired at 50 kHz and filtered at 10 kHz using an EPC9 amplifier (HEKA Elektronik Dr. Schulze GmbH, Germany) controlled with HEKAs Pulse software. Leak and capacitive currents were subtracted online by use of a -P/5 protocol. Series resistance (5–15 MΩ) was compensated electronically by 75–85% and continuously monitored throughout the measurements. All experiments were performed at room temperature (15–20°C), from a holding potential of -80 mV and with cells that had a mean whole-cell capacitance of 24 ± 2 pF (*n* = 73), as estimated from the slow capacitance compensation of the amplifier.

### Recording solutions and drugs

Unless noted otherwise, reagents were purchased from Sigma-Aldrich and used without further purification. The standard external solution used to isolate Ca<sup>2+</sup>-currents contained (in mM) 120 NaCl (Carl Roth, Karlsruhe, Germany p.A. #3957.1), 5 CaCl<sub>2</sub> (Sigma, #C8106), 5 KCl (Merck, suprapure, Merck #104938), 1 MgCl<sub>2</sub> (Sigma, #M2670), 20 tetraethylammonium chloride (Sigma, #T2265), 10 glucose (Sigma, #G8270), and 10 2-(4-(2-hydroxyethyl)-1-piperazinyl)-ethanesulfonic acid (HEPES) (Carl Roth, p.A., #H3375), with the pH adjusted to 7.4 using NaOH (Sigma, #415413-1L-D). Acute effects of trace metal chelation (with or without added Cu<sup>2+</sup>) were assessed by equimolar substitution of HEPES with 10 mM *N*-[Tris(hydroxymethyl)methyl]glycine (tricaine, Sigma #RES3077T-A701X), a trace metal chelator with very similar proton buffering properties. Effects of KA in the absence of trace metal ions were analyzed in the continued presence of 2 mM tricaine to remove contaminating metal ions. Under these conditions, the predicted free trace metal concentrations for contamination with up to 40 µM Zn<sup>2+</sup> or Cu<sup>2+</sup> are <40 nM for Zn<sup>2+</sup> or <2 pM for Cu<sup>2+</sup> respectively. The intracellular solution was composed of (in mM) 130 CsCl (trace metal basis, Sigma #203025), 5 oxaloacetic acid (BioReagent, Sigma #O7753), 5 creatine (Sigma, #C3630), 5 pyruvic acid (Sigma, #107360), 10 ethyleneglycol-bis(β-aminoethyl-ether)-*N,N,N',N'*-tetraacetic acid (EGTA, Sigma, #E4378) and 10 HEPES with the pH adjusted to 7.3 using CsOH (trace metal basis, Sigma #232068). KA (Milestone PhamTech, #6M-0100) was prepared as a 1 mg/mL stock solution and kept frozen until use. Prior to the recordings, aliquots of KA were thawed and added to the standard external solution to make the final concentration given in the text. Cu<sup>2+</sup> was prepared as a 250 mM stock solution in the form of cupric sulfate (Cu(II)SO<sub>4</sub>, Merck, p.A., #102790), further diluted on the day of the experiment and added to the external solution



immediately prior to use. Solutions were applied to cells at a rate of approximately 1 mL/min using a gravity-driven 2-barreled perfusion system with two separate inlets controlled by individual precision flow regulators (Sarstedt, Nümbrecht, Germany). Recordings were not corrected for the liquid junction potential of 5.5 mV between Cs-based internal solution and the external solution (calculated using the JPCalc algorithm in pClamp 10; Molecular Devices, Sunnyvale, CA, USA), so that all voltages shown were actually 5.5 mV more negative.

#### Data analysis

Leak-subtracted current traces were directly analyzed with PulseFit (HEKA) or exported for further processing with Microsoft Excel 2010 and OriginLab Pro (version 9, OriginLab, Northampton, MA, USA). Peak current–voltage relationships determined at test potentials between -50 and 60 mV (10 mV increments) were normalized by the maximum amplitude under control conditions and fitted with a combined Ohm–Boltzmann equation:

$$I = (V_m - V_{\text{rev}}) * G_{\text{max}} / (1 + \exp(-(V_m - V_{0.5})/k)) \quad (1)$$

where  $I$  is the normalized peak current measured at the test potential  $V_m$ ,  $V_{\text{rev}}$  the apparent reversal potential,  $G_{\text{max}}$  the maximal slope conductance,  $V_{0.5}$  the voltage eliciting a half-maximal current amplitude, and  $k$  the slope factor.

The voltage-dependence of activation was determined from tail currents recorded after a brief step depolarization to potentials between -50 and 60 mV. Pre-pulse inactivation was assessed with a protocol consisting of 2 s conditioning pre-pulses at potentials between -120 mV and -10 mV, followed by a step depolarization to the voltage of maximal current activation. Activation and pre-pulse inactivation curves thus obtained were fitted with single Boltzmann equations:

$$I/I_{\text{max}} = A_2 + (A_1 - A_2) / (1 + \exp((V_m - V_{0.5})/k)) \quad (2)$$

where  $I/I_{\text{max}}$  is the normalized current at the pre-pulse potential  $V_m$ ,  $V_{0.5}$  the voltage of half-maximal activation ( $V_{0.5\text{act}}$ ) or inactivation ( $V_{0.5\text{inact}}$ ),  $k$  the activation ( $k_{\text{act}}$ ) or inactivation ( $k_{\text{inact}}$ ) slope factor and  $A_1$  and  $A_2$  the initial and final values, respectively.

Activation time constants were determined by single exponential fits to the rising phase of macroscopic currents at different test potentials according to the following equation:

$$I = a_0 + a_1 * (1 - \exp(-t/\tau_{\text{act}})) \quad (3)$$

where  $I$  is the current at the time  $t$ ,  $a_0$  the value to which the current rises,  $a_1$  a scaling factor, and  $\tau_{\text{act}}$  the time constant of activation at the corresponding test potential. Similar results were obtained when the time-course of macroscopic activation was quantified using 10–90% rise times as a measure that is unaffected by the shape of currents.

#### Bovine electroretinographic (ERG) recordings

Fresh bovine eyes were obtained immediately post-mortem from a local slaughterhouse and transported in a light-protected thermos flask containing ice-cold, serum-free oxygenated Sickel medium composed of (in mM) 120 NaCl (Carl Roth, p.A.), 2 KCl (Merck, fractopure), 0.15 CaCl<sub>2</sub>, 0.1 MgCl<sub>2</sub> (Merck, p.A.), 1.5 NaH<sub>2</sub>PO<sub>4</sub>

(Merck, p.A.), 13.5 Na<sub>2</sub>HPO<sub>4</sub> (Merck, p.A.), and 5 glucose (Merck, for microbiology), with the pH adjusted to 7.8 (Lüke *et al.* 2005b). The eyes were enucleated and hemisected under dim red light and the eye-cup divided into four pieces, from which circular elements were obtained with a 7 mm trephine. The neural retina was detached from the segments by gentle shaking in Sickel solution, mounted into a recording chamber and perfused at a rate of 1 mL min<sup>-1</sup> with oxygenated HEPES-based solution containing (in mM) 120 NaCl (Carl Roth, p.A.), 2 KCl (Merck, fractopure), 0.19 CaCl<sub>2</sub>, 0.1 MgCl<sub>2</sub> (Merck, p.A.), and 28 HEPES (Carl Roth, p.A.), with the pH adjusted to 7.8 using NaOH. Scotopic bovine electroretinograms (ERGs) were elicited at 30°C by 500 ms white flashes of light applied every 5 min and sampled at a rate of 100 Hz via two Ag/AgCl electrodes placed on both sides of the retina. Unless noted otherwise, the flash intensity was set to 6.3 mlux at the retinal surface using calibrated neutral density filters and recordings were amplified and band-limited between 1 and 300 Hz (PowerLab 8/35, Animal Bio Amp FE136, ADInstruments, Oxford, UK).

#### Data analysis

Baseline-corrected ERGs were smoothed with a 12-points symmetrical moving average filter and analyzed as shown in Fig. 5a. Briefly, a-wave amplitudes were measured from the baseline to the maximum negative trough, while b-wave amplitudes were measured from the trough of the a-wave to the consecutive maximum positive trough. Implicit times were determined as the latency between start of the light flash and maximum a- or b-wave amplitude respectively, while b-wave durations were quantified by the full width at half-maximum (FWHM). To minimize variation between individual trials, amplitudes and implicit times were always normalized by the mean value of the last four responses under control conditions.

#### Statistics

Statistical significance was assessed with OriginLab Pro 9 using a repeated measures ANOVA followed by Bonferroni's post hoc analysis when comparing mean values from the same cells or a one-way ANOVA followed by Bonferroni's post hoc analysis when comparing multiple independent mean values. Homogeneity of variances between groups was tested using Levene's test for equality of variances on the squared deviations. In the case of heteroscedastic data ( $p < 0.05$  in Levene's test and ratio of largest to smallest variance  $\geq 4$ ), statistical significance was assessed with Minitab (version 17, Minitab Inc, State College, Pennsylvania) using Welch's ANOVA and the Games-Howell multiple comparison method. All fits were performed using the Levenberg-Marquardt least-squares algorithm. Smooth curves in the figures represent fits to average data whereas values given in the text are average data from fits to individual measurements. All values in the text and figures are expressed as mean  $\pm$  SEM based on  $n$ , the number of independent experiments.

## Results

### Lack of receptor-dependent effects of KA in stably transfected HEK-293 cells

To assess potential effects of KA, we performed whole-cell patch-clamp recordings in HEK293 cells stably transfected

with human  $\text{Ca}_v2.3 + \beta_3$  channel complexes. The first set of experiments was intended to exclude an action mediated by endogenous KA-receptors. To remove traces of inhibitory metal ions typically present in physiological solutions (but see section Evidence for receptor-independent effects of KA on  $\text{Ca}_v2.3$  channels), the standard HEPES-based perfusion medium was supplemented with 2 mM of the trace metal chelator tricine (Tn). Under these conditions, addition of 27  $\mu\text{M}$  KA had no effect on peak whole-cell currents carried by 5 mM  $\text{Ca}^{2+}$  and evoked by step depolarization to 10 mV (HEPES+Tn in Fig. 1a). In addition, exposure to KA without stimulation did not elicit detectable current responses in any of a total of six cells examined and no transcripts of KA-receptor subunits could be amplified from isolated ribonucleic acid (RNA) under conditions where corresponding transcripts were easily amplified from reverse-transcribed mouse brain RNA (data not shown). Together, these findings are consistent with previous reports about the absence of functional KA-receptors in HEK-293 cells (Carver *et al.* 1996; Jones *et al.* 1997), and confirm that they provide a suitable expression system for assessing glutamate receptor-independent effects of KA.

#### Evidence for receptor-independent effects of KA on $\text{Ca}_v2.3$ channels

When tricine was omitted from the external solution, the same concentration of KA often (in 3 of 5 recordings) produced a subtle but evident stimulation of currents recorded at 10 mV, which was reversible after washout with control solution (HEPES in Fig. 1a). Similar effects were observed when whole-cell currents in the same recording solution were acquired before and after equimolar substitution of HEPES by tricine (10 mM), which should eliminate

any contaminating trace metal ions present. As shown in Fig. 1b, tricine stimulated peak  $\text{Ca}^{2+}$  currents at most test potentials examined and raised the maximum slope conductance ( $G_{\text{max}}$ ) by  $38 \pm 13\%$  ( $n = 5$ ), suggesting that it removed from the external solution traces of metal ions that tonically inhibit the channels. Application of 27  $\mu\text{M}$  KA reconciled these effects, although it was less effective and only increased  $G_{\text{max}}$  by  $20 \pm 10\%$  ( $n = 6$ ). Together with the lack of effects observed in the presence of tricine (HEPES+Tn in Fig. 1a), these findings would be consistent with a KA-induced (but incomplete) reversal of suppression by contaminating metal ions. However, candidates for trace impurity are numerous and KA only partly reproduced the effects of tricine, so that we did not try to unequivocally identify the nature of metal ions present in our solution. Importantly, the lack of tricine-induced changes in the time-course of macroscopic currents (Fig. 1c) excluded appreciable contamination with  $\text{Cu}^{2+}$ , which produces a characteristic kinetic slowing (Castelli *et al.* 2003; Shcheglovitov *et al.* 2012) (see also below). It follows that any  $\text{Cu}^{2+}$ -dependent action of KA should become evident after addition of  $\text{Cu}^{2+}$  to the recording solution as described below.

#### KA reverses allosteric suppression by physiological free $\text{Cu}^{2+}$ concentrations

When the HEPES-based external solution was spiked with 50 nM  $\text{Cu}^{2+}$  (nominal concentration), currents activated and inactivated at more depolarized test potentials and exhibited much slower rates of macroscopic activation (Table 1), which is consistent with previous reports about allosteric  $\text{Cu}^{2+}$  suppression (Shcheglovitov *et al.* 2012). Under these conditions, addition of KA produced a more pronounced, voltage-dependent stimulation of peak  $\text{Ca}^{2+}$  currents and fully

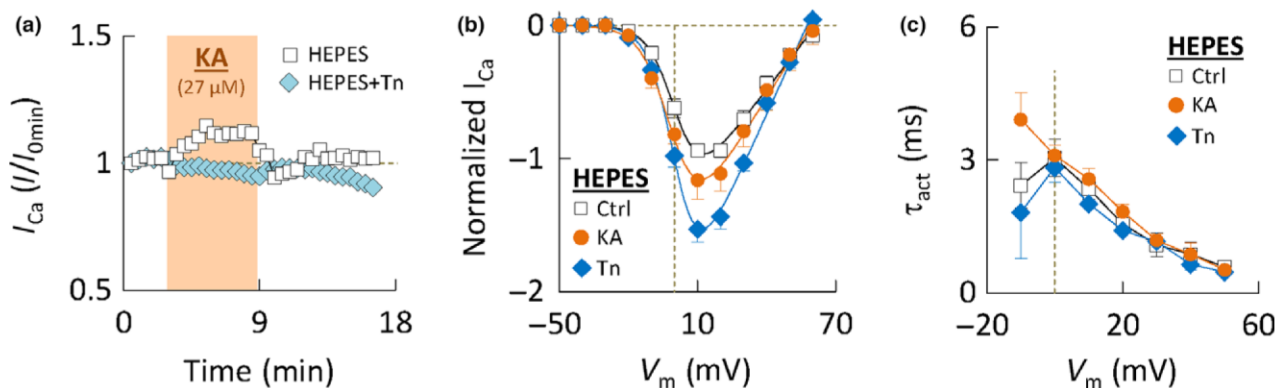


**Fig. 1** Evidence for receptor-independent effects of kainic acid on cloned  $\text{Ca}_v2.3 + \beta_3$  channels. (a) Representative time-course recordings showing changes in peak  $\text{Ca}^{2+}$  current at 10 mV induced by application of 27  $\mu\text{M}$  kainic acid (KA) in the absence (HEPES) or presence (HEPES+Tn) of 2 mM tricine to remove contaminating metal ions. (b) Effects of 27  $\mu\text{M}$  kainic acid (KA,  $n = 6$  single cells) or trace metal chelation with tricine (Tn,  $n = 5$  single cells) on normalized peak

current-voltage (IV-) relationships determined in the standard HEPES-buffered recording solution (Ctrl=pooled data from all 11 cells). (c) Effects of 27  $\mu\text{M}$  kainic acid (KA) or trace metal chelation with tricine (Tn) on activation time-constants, determined by single exponential fits to the rising phase of currents at the indicated test potentials (same cells as in B).

reconciled the effects of trace metal chelation with tricine (Fig. 2a–c). Note that there was little effect of KA or tricine at potentials that produce nearly complete macroscopic activation (e.g. 60 mV in Fig. 2b) and the changes in  $G_{\max}$  were more consistent but often less pronounced than in measurements without added  $\text{Cu}^{2+}$  (compare HEPES and  $+\text{Cu}^{2+}$  in Fig. 2d). However, IV-curves were displaced along the voltage axis (Fig. 2c), and this was due to a significant shift of channel voltage-dependence by about 10 mV to more negative test potentials (Fig. 3a and b, Table 1). Altogether, these effects are consistent with a reversal of allosteric suppression by  $\text{Cu}^{2+}$ , which has been shown to inhibit channel gating with little effect on the conduction properties (Shcheglovitov *et al.* 2012). For comparison, Fig. 3c and d contrasts the effects on half-activation voltage ( $V_{0.5\text{act}}$ ) and activation slope factor ( $dV_{\text{act}}$ ) observed in the presence and absence of  $\text{Cu}^{2+}$ . It can be seen that a subtle but significant voltage-shift by 3–4 mV was also observed without added  $\text{Cu}^{2+}$ , which may have been related to traces of  $\text{Zn}^{2+}$ ,  $\text{Ni}^{2+}$ , or other metal ions contaminating the recording solution (but see section Experimental implications). This is also supported by the fact that KA had no effect at all the shape of IV-curves or the maximum slope conductance ( $G_{\max}$ ) when recordings were performed in the continued presence of 2 mM tricine (Fig. 2d). More importantly however, most of the effects on channel voltage-dependence (Fig. 3c) and the increased voltage-sensitivity (Fig. 3d) were only observed in the presence of  $\text{Cu}^{2+}$ , confirming that they depend on pre-existing suppression by this metal ion. That KA had no effect at all on  $G_{\max}$  when recordings were performed in the continued presence of 2 mM tricine (Fig. 1a and Fig. 2d) supports the assumption that even its action without added  $\text{Cu}^{2+}$  must have relied on the presence of (contaminating) metal ions. Both KA and tricine also reversed the  $\text{Cu}^{2+}$ -induced kinetic slowing, as reflected in a significantly faster time course of macroscopic activation and a decrease of activation time constants to the values observed without added  $\text{Cu}^{2+}$  (Fig. 4a and b, Table 1). The  $\text{Cu}^{2+}$ -dependence of these effects at two different test

potentials is exemplified in Fig. 4c (10 mV) and Fig. 4d (30 mV). Finally, it should be noted that tricine but not KA produced a subtle but significant negative shift of the apparent reversal potential ( $V_{\text{rev}}$ ) by  $6 \pm 2$  mV in the presence and  $4 \pm 1$  mV in the absence of  $\text{Cu}^{2+}$  (not shown), suggesting that it altered the concentration and/or species distribution of permeant ions. As discussed in more detail in section Mechanism of  $\text{Ca}_v2.3$  channel modulation, this may have been related to the ability of tricine to weakly interact with alkaline earth metal ions like  $\text{Ca}^{2+}$ . In any case, the effects shown in Figs 2–4 are consistent with previous reports about the  $\text{Cu}^{2+}$ -induced selective suppression of  $\text{Ca}_v2.3$  channel gating and its reversal by trace metal chelation with tricine respectively (Shcheglovitov *et al.* 2012). More importantly, they provide compelling evidence that KA can potently stimulate these channels in the presence of physiological  $\text{Cu}^{2+}$  concentrations, presumably by formation of stable kainate- $\text{Cu}^{2+}$  complexes.

#### Chelation of endogenous trace metals alters retinal neurotransmission

To evaluate whether these effects of KA could also alter  $\text{Ca}_v2.3$  channel function in a native, organotypic system with transsynaptic signaling, we employed electroretinographic (ERG) recordings from the isolated and superfused neural retina (Fig. 5a).  $\text{Ca}_v2.3$  channels are involved in  $\gamma$ -aminobutyric acid (GABA)-ergic reciprocal inhibition of rod bipolar cells (Siapich *et al.* 2009), and genetic ablation or pharmacological suppression of these channels by  $\text{Zn}^{2+}$  or  $\text{Ni}^{2+}$  have been shown to selectively enhance a late component of the ERG b-wave (Lüke *et al.* 2005a; Siapich *et al.* 2010; Alnawaiseh *et al.* 2011). During initial experiments in the murine retina, we found that stable recordings in this system critically depend on the presence of several (trace metal binding) amino acids in the perfusion medium (Albanna *et al.* 2017). In addition, antagonism of KA receptors with UBP 301 (up to 20  $\mu\text{M}$  with 3–27  $\mu\text{M}$  KA) was insufficient for complete suppression of the receptor-

**Table 1** Effects of KA or tricine on  $\text{Ca}_v2.3$  channel gating in the absence and presence of  $\text{Cu}^{2+}$

		Activation			Inactivation			Kinetics (10 mV)	
		$V_{0.5\text{act}}$ [mV]	$dV_{\text{act}}$	$n$	$V_{0.5\text{inact}}$ [mV]	$dV_{\text{inact}}$	$n$	$\tau_{\text{act}}$ [ms]	$n$
HEPES	Ctrl	$12 \pm 3$	$8 \pm 1$	6	ND	ND		$2.6 \pm 0.3$	6
	Kainic acid (27 $\mu\text{M}$ )	$9 \pm 3$	$9 \pm 1$	6	ND	ND		$2.6 \pm 0.2$	6
	Ctrl	$12 \pm 1$	$10 \pm 1$	5	ND	ND		$2.1 \pm 0.2$	5
	Tricine (10 mM)	$8 \pm 1$	$9 \pm 1$	5	ND	ND		$2.0 \pm 0.1$	5
+ $\text{Cu}^{2+}$	Ctrl	$17 \pm 1$	$11 \pm 1$	9	$-71 \pm 3$	$13 \pm 1$	5	$3.9 \pm 0.8$	9
	Kainic acid (27 $\mu\text{M}$ )	$6 \pm 2$	$9 \pm 1$	9	$-87 \pm 2$	$11 \pm 1$	5	$2.6 \pm 0.5$	9
	Ctrl	$11 \pm 3$	$9 \pm 1$	6	$-61 \pm 9$	$10 \pm 1$	5	$3.9 \pm 0.6$	6
	Tricine (10 mM)	$-3 \pm 2$	$7 \pm 1$	6	$-89 \pm 5$	$9 \pm 1$	5	$2.4 \pm 0.4$	6

Recordings were performed with 5 mM  $\text{Ca}^{2+}$  as the charge carrier in the absence (HEPES) or presence ( $+\text{Cu}^{2+}$ ) of 50 nM nominal  $\text{Cu}^{2+}$ .



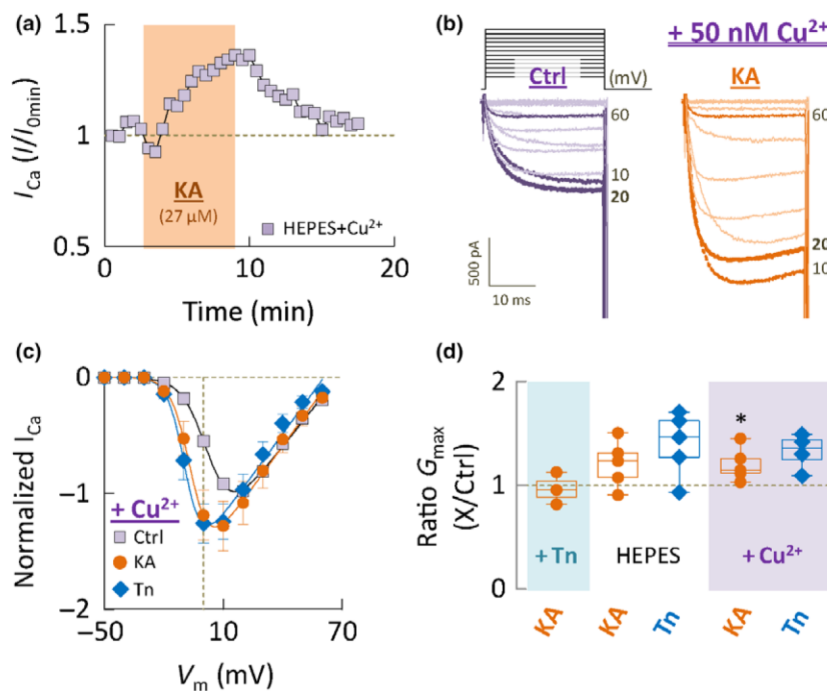


**Fig. 2** Cu<sup>2+</sup>-dependent and -independent actions of kainic acid on Ca<sub>v</sub>2.3 + β<sub>3</sub> channels. (a) Representative time-course recording showing changes in peak Ca<sup>2+</sup> current at 10 mV induced by application of 27 μM kainic acid (KA) in the presence of 50 nM nominal Cu<sup>2+</sup>. (b) Representative whole-cell currents recorded at test potentials between -50 and 60 mV (10 mV increments) before (Ctrl) and after (KA) addition of 27 μM kainic acid in the presence of 50 nM nominal Cu<sup>2+</sup>. Highlighted currents were recorded at the test potentials indicated next to the traces. (c) Effects of 27 μM kainic acid (KA, *n* = 5 single cells) or trace metal chelation with tricine (Tn, *n* = 6 single cells) on normalized peak current–voltage (IV-)relationships

determined in the presence of 50 nM nominal Cu<sup>2+</sup> (Ctrl=pooled data from all 11 cells). (d) Comparison of changes in the maximum slope conductance (*G*<sub>max</sub>) observed when kainic acid (KA) was applied in the continued presence of 2 mM tricine (+Tn, *n* = 3 single cells), when KA or tricine were applied in the nominal absence of Cu<sup>2+</sup> (HEPES, same cells as in Fig. 1b) and when KA or tricine were applied in the presence of 50 nM nominal Cu<sup>2+</sup> (+Cu<sup>2+</sup>, same cells as in c). Statistical significance refers to comparison of absolute values before and after addition of KA or Tn under the corresponding conditions. \**p* < 0.05 (One-way repeated measures ANOVA with Bonferroni's post hoc analysis).

dependent effects of KA, while application of CNQX (30 μM) resulted in a loss of basal responses to light (unpublished observation). To circumvent these problems, we employed the bovine retina, which allowed for stable recordings with a simple HEPES-based perfusion medium. In addition, we took advantage of our above findings and used tricine as a surrogate for the metal-dependent action of KA on Ca<sub>v</sub>2.3 channels. After stabilization of responses in the HEPES-based control solution, complete and stable ERGs could be recorded for several hours, which allowed us to assess the effects of tricine both in the absence (HEPES in Fig. 5b–e) and presence (+Cu<sup>2+</sup> in Fig. 5b–e) of exogenous Cu<sup>2+</sup> (for absolute values before normalization see Table 2). Finally, to examine tricine effects on isolated photoreceptor responses, recordings were repeated after a 24 h incubation of retinæ in the dark, which led to a complete loss of b-waves whereas a-waves at higher light intensities were still well preserved (Fig. 5f and g). Fig. 6a shows typical ERGs recorded before (Ctrl), during (Tn)

and after (Wash) a first application of tricine in the nominal absence of Cu<sup>2+</sup>. Under these conditions, tricine reduced both apparent a- and b-wave amplitudes (Fig. 5b and d and Fig. 6a and b) and significantly decreased b-wave implicit times (Fig. 5c and Fig. 6c), confirming that endogenous and possibly contaminating metal ions exert constitutive effects on inner transretinal signaling. Washout with control solution led to partial (amplitude) or complete (implicit times) reversal of the b-wave but not apparent a-wave effects, so that the former changes were not due to an effect on retinal phototransduction. In addition, there was no clear effect of tricine on a-wave implicit times (Figs 5e and 6c) and the changes in a-wave amplitudes were no longer observed after loss of the b-wave (Fig. 5f), suggesting that they were mostly a consequence of changes in b-wave kinetics (i.e. decreased b-wave implicit times). Note also that tricine tended to be most effective in reducing the late ERG b-wave, which was reflected in a fully reversible albeit non-significant tricine-induced

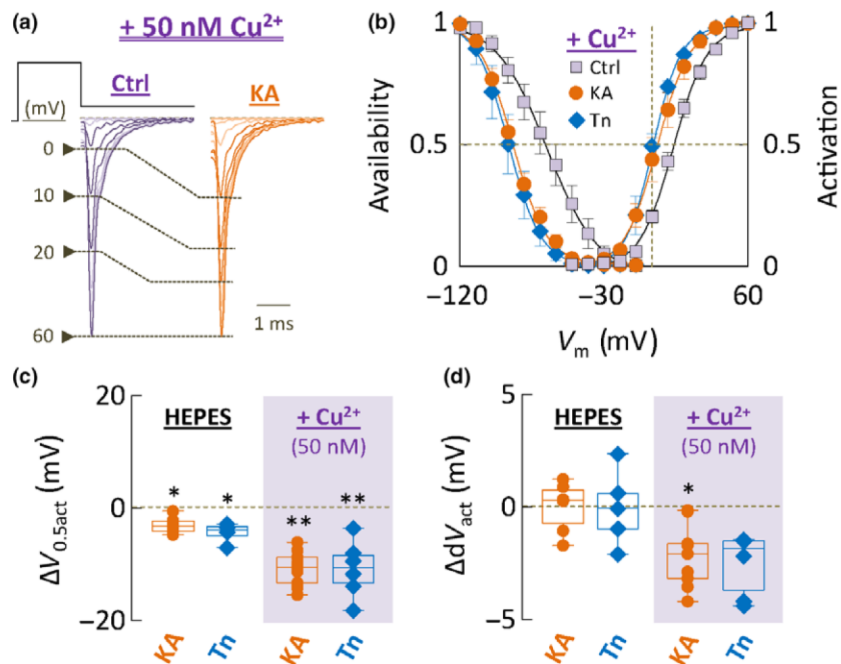


**Fig. 3**  $\text{Cu}^{2+}$ -dependent effects of kainic acid on channel voltage-dependence. (a) Representative tail-currents recorded after pre-pulses to the indicated test potentials before (Ctrl) and after (KA) addition of 27  $\mu\text{M}$  kainic acid in the presence of 50 nM nominal  $\text{Cu}^{2+}$ . They have been normalized to the tail-current amplitude at 60 mV to illustrate changes in activation voltage-dependence. (b) Effects of 27  $\mu\text{M}$  kainic acid (KA) or trace metal chelation with tricine (Tn) on the voltage-dependence of activation (right,  $n = 9$  and 6 single cells for KA and Tn respectively, Ctrl=pooled data from all 15 cells) and pre-pulse inactivation (left,  $n = 5$  single cells for each condition, Ctrl=pooled data from all 10 cells) determined in the presence of 50 nM nominal  $\text{Cu}^{2+}$ . (c) Comparison of kainic acid (KA) and tricine (Tn) effects on the

half-activation voltage ( $V_{0.5\text{act}}$ ), determined in the absence (HEPES,  $n = 6$  and 5 single cells for KA and Tn respectively) or presence ( $+\text{Cu}^{2+}$ , same cells as in b) of 50 nM nominal  $\text{Cu}^{2+}$ . Statistical significance refers to comparison of absolute values before and after addition of KA or Tn under the corresponding conditions. (d) Comparison of kainic acid (KA) and tricine (Tn) effects on the activation slope factor ( $dV_{\text{act}}$ ), determined in the absence (HEPES) or presence ( $+\text{Cu}^{2+}$ ) of 50 nM nominal  $\text{Cu}^{2+}$  (same cells as in c). Statistical significance refers to comparison of absolute values before and after addition of KA or Tn under the corresponding conditions. \* $p < 0.05$ ; \*\* $p < 0.01$  (One-way repeated measures ANOVA with Bonferroni's post hoc analysis).

decrease of b-wave durations in the nominal absence of  $\text{Cu}^{2+}$  (Fig. 7a).

### Chelation of exogenous $\text{Cu}^{2+}$ suppresses a late ERG b-wave component

Following removal of (pre-bound) endogenous free metal ions by the first tricine application and return to standard HEPES buffer, the solution was spiked with 100 nM nominal  $\text{Cu}^{2+}$ , which should be sufficient for considerable suppression of  $\text{Ca}_v2.3$  channels with little effect on most other known targets. Under these conditions, tricine produced a significant and completely reversible reduction of b-wave amplitudes (Figs 5b and 6d and e), implicit times (Figs 5c and 6d and f) and duration (Fig. 7c and d). Apparent a-wave amplitudes and implicit times did not change significantly (Figs 5d, e and 6e and f) after loss of the b-wave (Fig. 5f). Altogether, these effects are consistent with a reversal of  $\text{Cu}^{2+}$ -induced suppression of  $\text{Ca}_v2.3$  (and possibly other targets), which should increase GABAergic reciprocal

inhibition of rod bipolar cells in the transretinal network, thereby reducing late components of the ERG b-wave.

### Discussion

KA is a potent excitotoxic convulsant that exerts its action via activation of non-NMDA ionotropic glutamate receptors (Zaczek and Coyle 1982). Our findings demonstrate a novel,  $\text{Cu}^{2+}$ -dependent modulation by KA of cloned human  $\text{Ca}_v2.3 + \beta_3$  channel subunits, which can be observed in the absence of functional glutamate receptors and reconciled by  $\text{Cu}^{2+}$  chelation with tricine. Using tricine as a surrogate for the receptor-independent action of KA on inner retinal signaling, we also exemplify how modulation of  $\text{Ca}_v2.3$  and possibly other trace metal sensitive targets could alter normal function in an intact neuronal network. Below, we will address the role of trace metal chelation for KA-induced  $\text{Ca}_v2.3$  channel stimulation and briefly discuss experimental

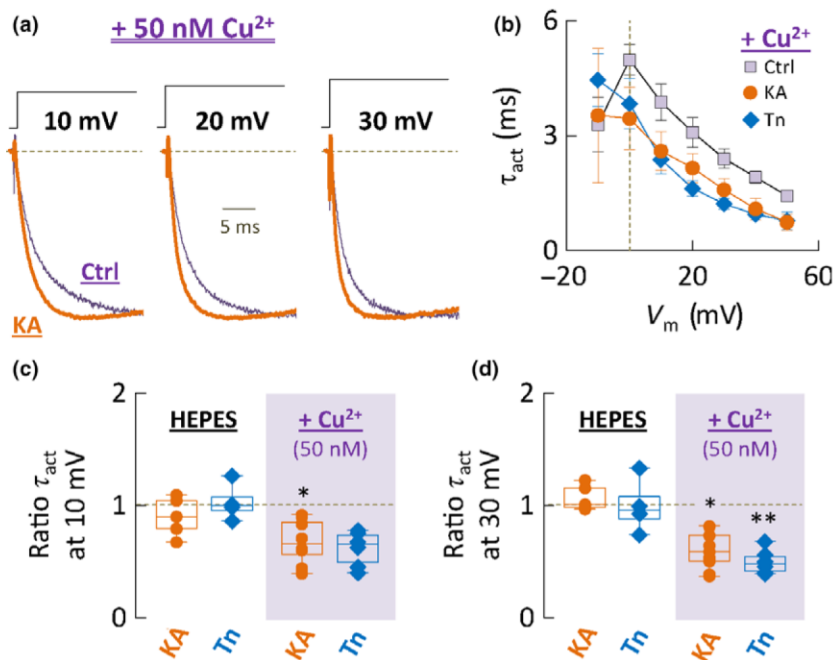


**Fig. 4** Cu<sup>2+</sup>-dependent effects of kainic acid on macroscopic current kinetics. (a) Representative whole-cell currents recorded at the indicated test potentials before (Ctrl) and after (KA) addition of 27  $\mu$ M kainic acid in the presence of 50 nM nominal Cu<sup>2+</sup>. They have been scaled to their maximum value to illustrate changes in the time-course of macroscopic activation. (b) Effects of 27  $\mu$ M kainic acid (KA,  $n = 9$  single cells) or trace metal chelation with tricine (Tn,  $n = 6$  single cells) on activation time constants in the presence of 50 nM nominal Cu<sup>2+</sup>, determined by single exponential fits to the rising phase of currents at the indicated test potentials. (c) Comparison of kainic acid (KA) and tricine (Tn) effects on activation time-constants at 10 mV,

determined in the absence (HEPES,  $n = 6$  and 5 single cells for KA and Tn respectively) or presence (+Cu<sup>2+</sup>, same cells as in b) of 50 nM nominal Cu<sup>2+</sup>. Statistical significance refers to comparison of absolute values before and after addition of KA or Tn under the corresponding conditions. (d) Comparison of kainic acid (KA) and tricine (Tn) effects on activation time-constants at 30 mV, determined in the absence (HEPES) or presence (+Cu<sup>2+</sup>) of 50 nM nominal Cu<sup>2+</sup> (same cells as in c). Statistical significance refers to comparison of absolute values before and after addition of KA or Tn under the corresponding conditions. \* $p < 0.05$ ; \*\* $p < 0.01$  (One-way repeated measures ANOVA with Bonferroni's post hoc analysis)

and potential pathophysiological implications of our findings.

#### Mechanism of Ca<sub>v</sub>2.3 channel modulation

Native and recombinant Ca<sub>v</sub>2.3 channels are a well-known target for endogenous trace metal ions (Zn<sup>2+</sup> and Cu<sup>2+</sup>), which can bind to a site in the domain I gating module and stabilize closed channel states (Shcheglovitov *et al.* 2012). We did not carry out a detailed analysis of the underlying mechanism, but our findings reaffirm that physiologically relevant Cu<sup>2+</sup> concentrations potently inhibit Ca<sub>v</sub>2.3 channel gating. More importantly, they provide compelling evidence that KA can reverse tonic suppression by Cu<sup>2+</sup> and significantly increase the response of cloned Ca<sub>v</sub>2.3 channels to depolarization. Thus, in the presence of low nanomolar extracellular free Cu<sup>2+</sup>, KA produced significant shifts of channel voltage-dependence to more negative test potentials, increased the voltage-sensitivity and accelerated the time-course of macroscopic activation. The effects depended on pre-existing inhibition by Cu<sup>2+</sup> and could be

reproduced by the trace metal chelator tricine, which reduced free Cu<sup>2+</sup> to negligible levels. In the absence of Cu<sup>2+</sup>, KA produced a more subtle and relatively variable stimulation that was not observed when it was applied in the presence of tricine, suggesting that it may also reverse suppression by certain contaminating metal ions. Together, these findings agree with previous reports that KA tightly binds Cu<sup>2+</sup> and, to a lesser extent, other trace metal ions such as Zn<sup>2+</sup>, Fe<sup>3+</sup>, or Ni<sup>2+</sup> (Robbins 1994; Burns *et al.* 2007). Also, the closely related excitatory amino acid L-Glu has been shown to reverse Ca<sub>v</sub>2.3 channel suppression by Zn<sup>2+</sup> and Cu<sup>2+</sup>, albeit at almost 10-fold higher concentrations (Shcheglovitov *et al.* 2012). Considering the higher Cu<sup>2+</sup> affinity of KA ( $\log K_{CuL} = 10.1$ ,  $\log K_{CuL2} = 7.6$ )<sup>22</sup> compared to L-Glu ( $\log K_{CuL} = 8.2$ ,  $\log K_{CuL2} = 6.4$ ) (Shuaib *et al.* 1999; Aydin and Yirikogullari 2010) or tricine ( $\log K_{CuL} = 7.8$ ) (Good *et al.* 1966; El-Roudi and Abdel-Latif 2004), it seems justified to propose that our observations are related to the formation of stable kainate-Cu<sup>2+</sup> complexes. Minor differences between the effects of KA and tricine we



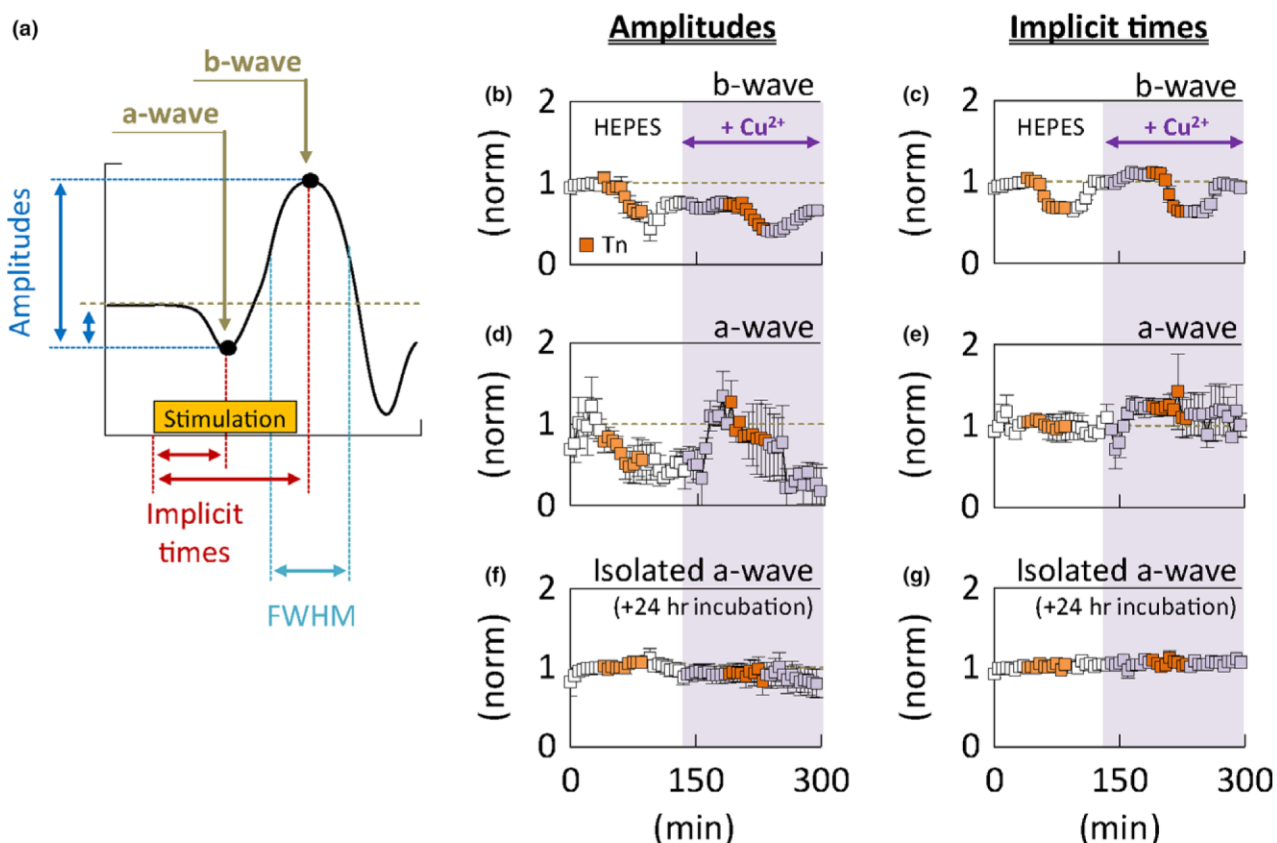


**Fig. 5** Effects of trace metal chelation on scotopic ERGs in the bovine retina. (a) Overview of ERG parameters determined to assess the effects of trace metal chelation with 5 mM tricaine on the isolated and superfused bovine retina. Apparent amplitude and latency of the a-wave were taken as a measure of changes in the photoreceptor response, while b-wave amplitude, latency, and full width at half-maximum amplitude (FWHM) provided a read-out of rod bipolar cell function and contribution to transretinal signaling. (b) Effects of trace metal chelation with tricaine (Tn, indicated by orange symbols) on b-wave amplitudes before (HEPES) and after addition of 100 nM nominal  $\text{Cu}^{2+}$  ( $+\text{Cu}^{2+}$ ) in the same retinae ( $n = 4$  individual retina segments

from four fresh retinae). (c) Effects of trace metal chelation with tricaine (Tn) on b-wave implicit times determined in the same recordings as in b. (d) Effects of trace metal chelation with tricaine (Tn) on apparent a-wave amplitudes determined in the same recordings as in b. (e) Effects of trace metal chelation with tricaine (Tn) on apparent a-wave implicit times determined in the same recordings as in b. (f) Effects of trace metal chelation with tricaine (Tn) on a-wave amplitudes determined under the same conditions as in B but after loss of the b-wave and with higher light intensities (2000 mlx). (g) Effects of trace metal chelation with tricaine (Tn) on a-wave implicit times determined under the same conditions as in F.

observed could then be accounted for by differences in their metal ion binding properties and/or concentration. For example, the reduced affinity of KA for trace metals other than  $\text{Cu}^{2+}$  together with its lower concentration compared to tricaine might explain why it was much less effective in reversing suppression by contaminating metal ions. Tricaine but not KA also affected the apparent reversal potential both in the presence and absence of added  $\text{Cu}^{2+}$ , which may have been related to its ability to weakly interact with alkaline earth metal ions like  $\text{Ca}^{2+}$  ( $\log K_{\text{CaL}}=2.4$ )<sup>26</sup> or  $\text{Mg}^{2+}$  ( $\log K_{\text{MgL}}=1.2$ )<sup>26</sup>. Thus, with 5 mM  $\text{Ca}^{2+}$  as the charge carrier and 1 mM  $\text{Mg}^{2+}$  in our external solution, tricaine (10 mM) should have lowered free  $\text{Ca}^{2+}$  and  $\text{Mg}^{2+}$  levels by about 1.2 mM and 0.2 mM respectively, which might account for subtle changes in  $V_{\text{rev}}$ .

#### Pathophysiological relevance

The exact role of endogenous free  $\text{Zn}^{2+}$  and  $\text{Cu}^{2+}$  in the brain remains controversial, but a number of previous findings indicate that they mediate anticonvulsive and neuroprotective effects (Lees *et al.* 1998). Estimated resting concentrations are sufficient for tonic suppression of  $\text{Ca}_v2.3$  channels (Shcheglovitov *et al.* 2012) and other synaptic targets (Paoletti *et al.* 1997; Nelson *et al.* 2007), so that they could serve to limit pathologic hyperexcitability mediated by excessive activation. Consistent with such a role, depletion of endogenous TMIs has been demonstrated to augment KA-induced neurotoxicity (Lees *et al.* 1998) and can trigger seizure activity and neuronal cell death during subconvulsive KA over-excitation in mice (Dominguez *et al.* 2003). Moreover, complete chelation of synaptic TMIs in

**Table 2** Effects of tricine on ERG a- and b-wave in the absence and presence of Cu<sup>2+</sup>

		ERG a-wave		ERG b-wave			n
		Amplitude [ $\mu$ V] (initial   + 24 h) <sup>1</sup>	Implicit time [ms] (initial   +24 h) <sup>1</sup>	Amplitude [ $\mu$ V]	latency [ms]	FWHM [ms]	
HEPES	Ctrl	9 $\pm$ 4   9 $\pm$ 2	309 $\pm$ 48   424 $\pm$ 73	19 $\pm$ 3	709 $\pm$ 101	546 $\pm$ 21	4
	Tricine (5 mM)	4 $\pm$ 2   10 $\pm$ 3	284 $\pm$ 43   429 $\pm$ 71	12 $\pm$ 3	483 $\pm$ 38	381 $\pm$ 25	4
	Wash	6 $\pm$ 4   9 $\pm$ 3	299 $\pm$ 57   443 $\pm$ 79	14 $\pm$ 2	746 $\pm$ 116	546 $\pm$ 31	4
+ Cu <sup>2+</sup>	Ctrl	9 $\pm$ 4   9 $\pm$ 3	356 $\pm$ 40   452 $\pm$ 79	15 $\pm$ 3	801 $\pm$ 135	537 $\pm$ 26	4
	Tricine (5 mM)	3 $\pm$ 1   9 $\pm$ 3	286 $\pm$ 41   436 $\pm$ 72	8 $\pm$ 1	444 $\pm$ 10	332 $\pm$ 10	4
	Wash	4 $\pm$ 2   8 $\pm$ 3	320 $\pm$ 32   450 $\pm$ 76	15 $\pm$ 3	680 $\pm$ 73	520 $\pm$ 64	4

<sup>1</sup>Effects on isolated photoreceptor responses, determined following complete loss of the b-wave after 24 h incubation of the same retinae in the dark.

Recordings were performed in the same retinae before (HEPES) and after (+Cu<sup>2+</sup>) addition of 100 nM nominal Cu<sup>2+</sup>.

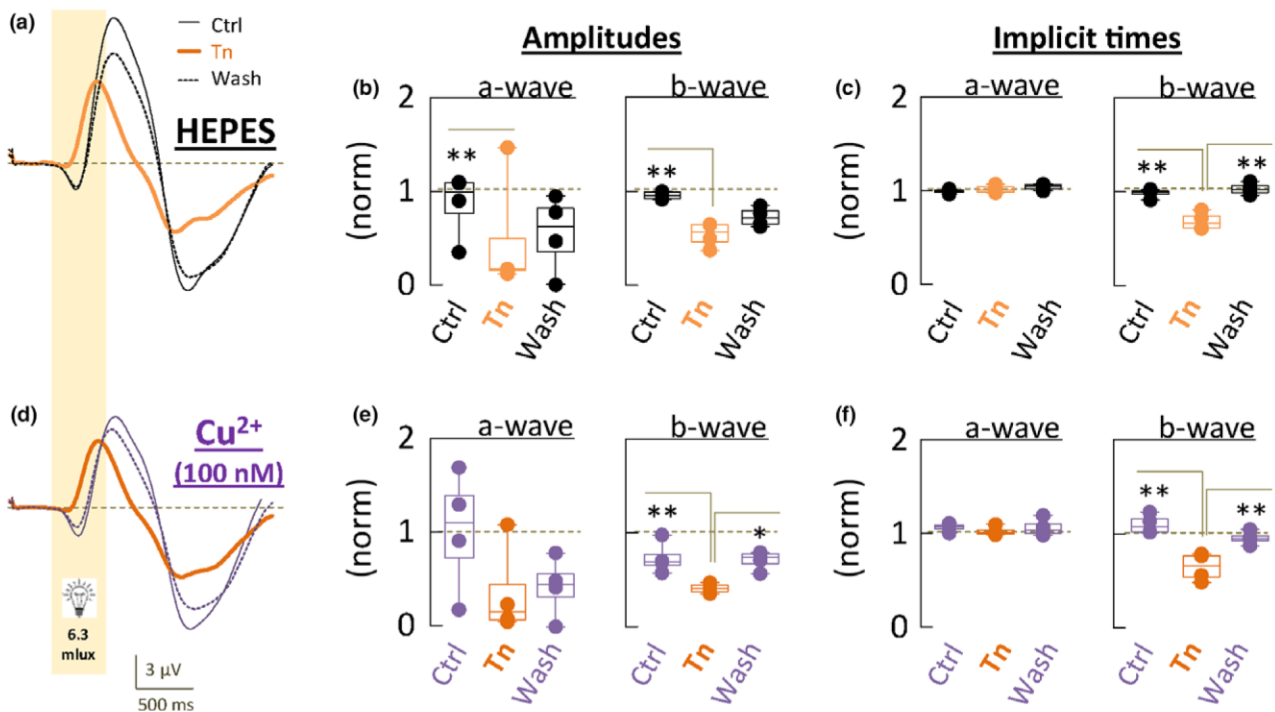


**Fig. 6** Effects of trace metal chelation before and after addition of 100 nM nominal Cu<sup>2+</sup>. (a) Representative ERGs recorded in the nominal absence of Cu<sup>2+</sup> before (Ctrl, solid black line) and after (Tn, solid orange line) trace metal chelation with tricine and after washout with control solution (wash, broken black line). (b) Comparison of tricine (Tn) effects on a- and b-wave amplitudes determined in the nominal absence of Cu<sup>2+</sup> (same recordings as in Fig. 5). (c) Comparison of tricine (Tn) effects on a- and b-wave implicit times determined in the nominal absence of Cu<sup>2+</sup> (same recordings as in Fig. 5). (d) Representative ERGs recorded in the presence of 100 nM nominal

Cu<sup>2+</sup> before (Ctrl, solid purple line) and after (Tn, solid orange line) trace metal chelation with tricine and after washout with control solution (wash, broken purple line). (e) Comparison of tricine (Tn) effects on a- and b-wave amplitudes determined in the presence of 100 nM nominal Cu<sup>2+</sup> (same recordings as in Fig. 5). (f) Comparison of tricine (Tn) effects on a- and b-wave implicit times determined in the presence of 100 nM nominal Cu<sup>2+</sup> (same recordings as in Fig. 5). \**p* < 0.05; \*\*\**p* < 0.01 (One-way repeated measures ANOVA with Bonferroni's post hoc analysis).

the hippocampus by diethyldithiocarbamate (DEDTC) induces excitotoxicity and convulsions in healthy rats, suggesting that even in the absence of other pathological phenomena, chelation of endogenous TMIs can lead to

abnormal hippocampal excitation (Blasco-Ibanez *et al.* 2004). We have previously shown that DEDTC stimulates cloned Ca<sub>v</sub>2.3 channels in the presence but not absence of micromolar Zn<sup>2+</sup> and that intraperitoneal DEDTC treatment

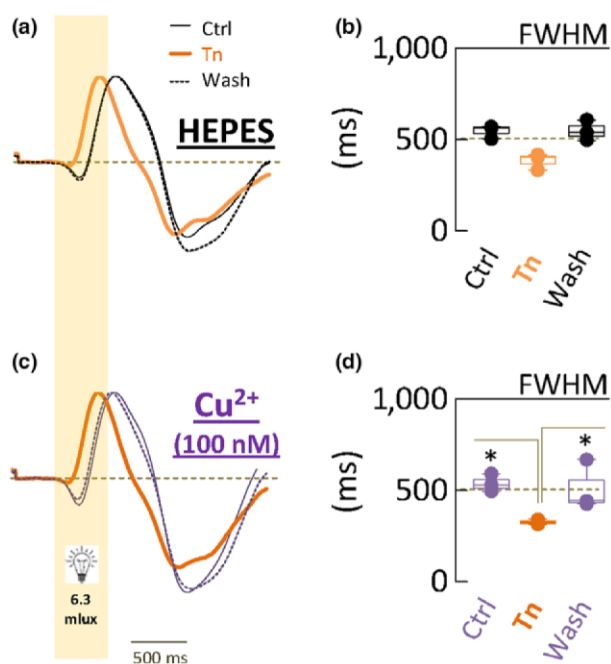


**Fig. 7** Cu<sup>2+</sup> chelation with tricine suppresses the late ERG b-wave. (a) Representative ERGs recorded in the nominal absence of Cu<sup>2+</sup> before (Ctrl, solid black line) and after (Tn, solid orange line) trace metal chelation with tricine and after washout with control solution (wash, broken black line). Recordings are the same as in Fig. 6a, but normalized by their maximum amplitude to illustrate kinetic changes. (b) Effects of trace metal chelation with tricine (Tn) on b-wave durations determined in the nominal absence of Cu<sup>2+</sup> (same recordings as in Figs 5 and 6). (c) Representative ERGs recorded in the presence of 100 nM nominal Cu<sup>2+</sup> before (Ctrl, solid purple line) and after (Tn, solid orange line) trace metal chelation with tricine and after washout with control solution (wash, broken purple line). Recordings are the same as in Fig. 6d, but normalized by their maximum amplitude to illustrate kinetic changes. (d) Effects of trace metal chelation with tricine (Tn) on b-wave durations determined in the presence of 100 nM nominal Cu<sup>2+</sup> (same recordings as in Figs 5 and 6). \**p* < 0.05 (One-way repeated measures ANOVA with Bonferroni's post hoc analysis).

significantly alters blood glucose homeostasis and peptide hormone secretion in wildtype but not Ca<sub>v</sub>2.3-deficient mice (Drobinskaya *et al.* 2015). What makes it difficult to appreciate the potential implications of our findings with regard to KA-induced seizures is that brain tissue concentrations of KA reached after systemic administration have not been established (Berger *et al.* 1986). However, KA is resistant to enzymatic degradation or reuptake, so that it could accumulate in brain regions with high KA- or AMPA-receptor densities. This in turn makes it tempting to speculate that trace metal chelation by KA itself could contribute to the substantial, tissue-specific loss of free TMIs that has been observed in the limbic system of mice following KA-induced seizures (Takeda *et al.* 2003). Indirect support for a receptor-independent mechanism of action is also provided by previous findings that  $\alpha$ -allo-kainic acid,

a C4-epimer of KA with extremely low affinity for specific [<sup>3</sup>H]-KA binding sites (*K*<sub>i</sub> > 10,000 nM) (Zaczek and Coyle 1982; Ferkany and Coyle 1983), produces significant neurotoxicity and pro-convulsive effects that exceed structure-activity relationship predictions. As such, it could provide a valuable tool to further establish the pathophysiological relevance of our findings, as the strong receptor-dependent effects of KA itself effectively prohibit direct study of Cu<sup>2+</sup>-dependent actions in native systems. Here, we followed an approach that has been employed before and used tricine as a surrogate for the receptor-independent effects of excitatory amino acids. For our experiments, we chose the neural retina because it contains all major neurotransmitter systems and represents one of the few preparations where the role of Ca<sub>v</sub>2.3 channels is relatively well established. Thus, we and others have shown that they are involved in GABAergic reciprocal inhibition of rod bipolar cells and that their genetic or pharmacologic ablation selectively enhances a late ERG b-wave component (Lüke *et al.* 2005a; Siapich *et al.* 2009; Alnawaiseh *et al.* 2011). Our present findings show that trace metal chelation produces opposite effects and inhibits the late ERG b-wave with little effect on photoreceptor responses. Although we cannot exclude a contribution of other metal ion-sensitive targets, the direction and magnitude of effects are in close agreement with increased GABAergic signaling due to a relief of metal-induced suppression of Ca<sub>v</sub>2.3 channels.

#### Experimental implications

While the *in vivo* relevance of our findings remains to be firmly established, a significant proportion of work related to KA-induced neurotoxicity is carried out in isolated tissues (brain slices or acutely dissociated primary cells), with concentrations of KA often exceeding those employed in our experiments (Gepdiremen *et al.* 1997; Oliva *et al.* 2002; Hou 2011; Smialowska *et al.* 2012). Considering the seemingly high incidence of trace metal contamination in commonly used external solutions (Paoletti *et al.* 1997; Shcheglovitov *et al.* 2012), chelation by KA could obviously contribute to the observed effects and disinherit Ca<sub>v</sub>2.3 as well as other targets tonically suppressed by low nanomolar concentrations of Cu<sup>2+</sup> or Zn<sup>2+</sup> (Ca<sub>v</sub>3.2, postsynaptic NMDA-receptors) (Spedding and Paoletti 1992; Nelson *et al.* 2007). It has also been shown that chelation by amino acids enhances cellular uptake of <sup>67</sup>[Cu<sup>2+</sup>] in hypothalamic brain slices by up to a factor of four (Barnea and Katz 1990; Barnea *et al.* 1990). Similar findings have been reported for a number of metal chelators (Jonas and Riley 1991; Chen *et al.* 2000) and linked to subsequent activation of MAPK/JNKs death signaling pathways, which are a hallmark of KA-induced apoptosis in hippocampal neurons (Faherty *et al.* 1999; Mielke *et al.* 1999). In this study, the effects of tricine (or KA) without added Cu<sup>2+</sup> were quite subtle and not associated with changes in the time-course of macroscopic



activation, so that we could exclude appreciable contamination with Cu<sup>2+</sup>. However, based on previous studies, contaminating Cu<sup>2+</sup> levels in common electrophysiological solutions can easily reach concentrations in the order of 50–100 nM. We and others have shown that this is sufficient for significant suppression of Ca<sub>v</sub>2.3 channels, so that it could also provide a pathway for receptor-independent effects of excitatory amino acids like KA or L-Glu. As long as the relevance of KA-induced trace metal chelation *in vivo* remains to be established, it may therefore be preferable if *in vitro* studies are performed under conditions that exclude formation of kainate-metal complexes. This could be achieved by pre-treatment of solutions with metal chelating resins, use of tricine-buffered solutions or addition of a small amount of some higher affinity trace metal chelator like EDTA or DTPA.

## Conclusion

Having been used for more than two decades, KA-induced seizures in rodents are one of the most widely used models of human temporal lobe epilepsy. Previous investigations have focused on high-affinity activation of non-NMDA ionotropic glutamate receptors and evaluated downstream consequences of receptor-mediated depolarization. Our observations in a heterologous expression system provide evidence for a novel, receptor-independent pathway by which KA could affect Ca<sub>v</sub>2.3 channel function in the presence of physiologically relevant concentrations of free Cu<sup>2+</sup> and possibly other metal ions. Although the relevance of trace metal chelation for the epileptogenic and neurotoxic effects of KA *in vivo* is not clear, our findings have important experimental implications. They could also help to elucidate the exact mechanisms of KA-induced excitotoxicity and (partly) explain its specificity to the hippocampus. Further investigation will be necessary to establish and rate the relevance of our findings in native systems and, if applicable, integrate them into current understanding of KA-induced seizures and hippocampal sclerosis.

## Acknowledgments and conflict of interest disclosure

We thank Renate Clemens and Simone Keil for their excellent technical assistance. This work was financially supported by the Köln Fortune Program/Faculty of Medicine, University of Cologne (259/2013) and the Deutsche Forschungsgemeinschaft (DFG, SCHN 387/21-1). The authors declare that the research was conducted in the absence of any commercial or financial relationships that could be construed as a potential conflict of interest.

All experiments were conducted in compliance with the ARRIVE guidelines.

## Author contributions statement

TS, MDA, and FN designed the experiments. FN, IAS, and JL performed the experiments. FN, IAS, and TS analyzed the data. FN and TS interpreted the results, prepared the figures, and wrote the paper. MDA and JH provided reagents or analytical tools and commented on the manuscript. All authors contributed to drafting of the final manuscript.

## References

- Albanna W., Lueke J. N., Sjapic V. *et al.* (2017) Electroretinographic assessment of inner retinal signaling in the isolated and superfused murine retina. *Curr. Eye Res.* **42**, 1518–1526.
- Alnawaiseh M., Albanna W., Chen C.-C., Campbell K. P., Hescheler J., Lüke M. and Schneider T. (2011) Two separate Ni<sup>2+</sup> sensitive voltage-gated Ca<sup>2+</sup> channels modulate transretinal signalling in the isolated murine retina. *Acta Ophthalmol.* **89**, e579–e590.
- Aydin R. and Yirikogullari A. (2010) Potentiometric study on complexation of divalent transition metal ions with amino acids and adenosine 5'-triphosphate. *J. Chem. Eng. Data* **55**, 4794–4800.
- Barnea A. and Katz B. M. (1990) Uptake of <sup>67</sup>copper complexed to <sup>3</sup>H-histidine by brain hypothalamic slices: evidence that dissociation of the complex is not the only factor determining <sup>67</sup>copper uptake. *J. Inorg. Biochem.* **40**, 81–93.
- Barnea A., Hartter D. E., Cho G., Bhasker K. R., Katz B. M. and Edwards M. D. (1990) Further characterization of the process of *in vitro* uptake of radiolabeled copper by the rat brain. *J. Inorg. Biochem.* **40**, 103–110.
- Berger M. L., Lefauconnier J. M., Tremblay E. and Ben-Ari Y. (1986) Limbic seizures induced by systemically applied kainic acid: how much kainic acid reaches the brain? *Adv. Exp. Med. Biol.* **203**, 199–209.
- Blasco-Ibanez J. M., Poza-Aznar J., Crespo C., Marques-Mari A. I., Gracia-Llanes F. J. and Martinez-Guijarro F. J. (2004) Chelation of synaptic zinc induces overexcitation in the hilar mossy cells of the rat hippocampus. *Neurosci. Lett.* **355**, 101–104.
- Burns J. M., Schock T. B., Hsia M. H., Moeller P. D. and Ferry J. L. (2007) Photostability of kainic acid in seawater. *J. Agric. Food Chem.* **55**, 9951–9955.
- Carver J. M., Mansson P. E., Cortes-Burgos L., Shu J., Zhou L. M., Howe J. R. and Giordano T. (1996) Cytotoxic effects of kainate ligands on HEK cell lines expressing recombinant kainate receptors. *Brain Res.* **720**, 69–74.
- Castelli L., Tanzi F., Taglietti V. and Magistretti J. (2003) Cu<sup>2+</sup>, Co<sup>2+</sup>, and Mn<sup>2+</sup> modify the gating kinetics of high-voltage-activated Ca<sup>2+</sup> channels in rat palaeocortical neurons. *J. Membr. Biol.* **195**, 121–136.
- Chen S. H., Liu S. H., Liang Y. C., Lin J. K. and Lin-Shiau S. Y. (2000) Death signaling pathway induced by pyrrolidine dithiocarbamate-Cu<sup>(2+)</sup> complex in the cultured rat cortical astrocytes. *Glia* **31**, 249–261.
- Dibue-Adjei M., Kamp M. A., Alpdogan S., Tevoufouet E. E., Neiss W. F., Hescheler J. and Schneider T. (2017) Ca<sub>v</sub>2.3 (R-Type) Calcium Channels are Critical for Mediating Anticonvulsive and Neuroprotective Properties of Lamotrigine *In Vivo*. *Cell. Physiol. Biochem.* **44**, 935–947.
- Dietrich D., Kirschstein T., Kukley M., Pereverzev A., von der Brölie C., Schneider T. and Beck H. (2003) Functional specialization of presynaptic Ca<sub>v</sub>2.3 Ca<sup>2+</sup> channels. *Neuron* **39**, 483–496.
- Dominguez M. I., Blasco-Ibanez J. M., Crespo C., Marques-Mari A. I. and Martinez-Guijarro F. J. (2003) Zinc chelation during non-

- lesioning overexcitation results in neuronal death in the mouse hippocampus. *Neuroscience* **116**, 791–806.
- Drobinskaya L., Neumaier F., Pereverzev A., Hescheler J. and Schneider T. (2015) Diethyldithiocarbamate-mediated zinc ion chelation reveals role of Ca<sup>v</sup>2.3 channels in glucagon secretion. *Biochim. Biophys. Acta Mol. Cell Res.* **1854**, 953–964.
- El-Roudi O. M. and Abdel-Latif S. A. (2004) Effect of ionic strength, aquo-organic solvents, and temperature on the stabilities of N-[Tris (hydroxymethyl)methyl]glycine + metal complexes. *J. Chem. Eng. Data* **49**, 1193–1196.
- Faherty C. J., Xanthoudakis S. and Smeyne R. J. (1999) Caspase-3-dependent neuronal death in the hippocampus following kainic acid treatment. *Brain Res. Mol. Brain Res.* **70**, 159–163.
- Ferkany J. W. and Coyle J. T. (1983) Kainic acid selectively stimulates the release of endogenous excitatory acidic amino acids. *J. Pharmacol. Exp. Ther.* **225**, 399–406.
- Gasparini S., Kasyanov A. M., Pietrobon D., Voronin L. L. and Cherubini E. (2001) Presynaptic R-type calcium channels contribute to fast excitatory synaptic transmission in the rat hippocampus. *J. Neurosci.* **21**, 8715–8721.
- Gepdiremen A., Sonmez S., Batat I., Esrefoglu M., Duzenli S. and Suleyman H. (1997) Nimodipine improves kainic acid induced neurotoxicity in cerebellar granular cell culture: a double-blind dose-response study. *Fundam. Clin. Pharmacol.* **11**, 117–120.
- Good N. E., Winget G. D., Winter W., Connolly T. N., Izawa S. and Singh R. M. (1966) Hydrogen ion buffers for biological research. *Biochemistry* **5**, 467–477.
- Hamill O. P., Marty A., Neher E., Sakmann B. and Sigworth F. J. (1981) Improved patch-clamp techniques for high-resolution current recording from cells and cell-free membrane patches. *Pflügers Arch.* **391**, 85–100.
- Hou C. W. (2011) Pu-Erh tea and GABA attenuates oxidative stress in kainic acid-induced status epilepticus. *J. Biomed. Sci.* **18**, 75.
- Jonas S. K. and Riley P. A. (1991) The effect of ligands on the uptake of iron by cells in culture. *Cell Biochem. Funct.* **9**, 245–253.
- Jones K. A., Wilding T. J., Huettner J. E. and Costa A. M. (1997) Desensitization of kainate receptors by kainate, glutamate and diastereomers of 4-methylglutamate. *Neuropharmacology* **36**, 853–863.
- Lees G. J., Cuajungco M. P. and Leong W. (1998) Effect of metal chelating agents on the direct and seizure-related neuronal death induced by zinc and kainic acid. *Brain Res.* **799**, 108–117.
- Lüke M., Henry M., Lingohr T., Maghsoodian M., Hescheler J., Sickel W. and Schneider T. (2005a) A Ni<sup>2+</sup>-sensitive component of the ERG-b-wave from the isolated bovine retina is related to E-type voltage-gated Ca<sup>2+</sup> channels. *Graefes Arch. Clin. Exp. Ophthalmol.* **243**, 933–941.
- Lüke M., Weiergräber M., Brand C., Siapich S. A., Banat M., Hescheler J., Lüke C. and Schneider T. (2005b) The isolated perfused bovine retina - a sensitive tool for pharmacological research on retinal function. *Brain Res. Brain Res. Protoc.* **16**, 27–36.
- Magee J. C. and Carruth M. (1999) Dendritic voltage-gated ion channels regulate the action potential firing mode of hippocampal CA1 pyramidal neurons. *J. Neurophysiol.* **82**, 1895–1901.
- Magee J. C. and Johnston D. (1995) Characterization of single voltage-gated Na<sup>+</sup> and Ca<sup>2+</sup> channels in apical dendrites of rat CA1 pyramidal neurons. *J. Physiol. (Lond.)* **487**, 67–90.
- Magistretti J., Castelli L., Taglietti V. and Tanzi F. (2003) Dual effect of Zn<sup>2+</sup> on multiple types of voltage-dependent Ca<sup>2+</sup> currents in rat palaeocortical neurons. *Neuroscience* **117**, 249–264.
- Mielke K., Brecht S., Dorst A. and Herdegen T. (1999) Activity and expression of JNK1, p38 and ERK kinases, c-Jun N-terminal phosphorylation, and c-jun promoter binding in the adult rat brain following kainate-induced seizures. *Neuroscience* **91**, 471–483.
- Nelson M. T., Woo J., Kang H. W., Vitko I., Barrett P. Q., Perez-Reyes E., Lee J. H., Shin H. S. and Todorovic S. M. (2007) Reducing agents sensitize C-type nociceptors by relieving high-affinity zinc inhibition of T-type calcium channels. *J. Neurosci.* **27**, 8250–8260.
- Neumaier F., Dibué-Adjei M., Hescheler J. and Schneider T. (2015) Voltage-gated calcium channels: Determinants of channel function and modulation by inorganic cations. *Prog. Neurobiol.* **129**, 1–36.
- Oliva A. A. Jr., Lam T. T. and Swann J. W. (2002) Distally directed dendrotoxicity induced by kainic acid in hippocampal interneurons of green fluorescent protein-expressing transgenic mice. *J. Neurosci.* **22**, 8052–8062.
- Paoletti P., Ascher P. and Neyton J. (1997) High-affinity zinc inhibition of NMDA NR1-NR2A receptors. *J. Neurosci.* **17**, 5711–5725.
- Robbins R. A. (1994) A potentiometric and spectroscopic study of metal complexes of some biologically active peptides. University of Leeds.
- Shecheglovitov A., Vitko I., Lazarenko R. M., Orestes P., Todorovic S. M. and Perez-Reyes E. (2012) Molecular and biophysical basis of glutamate and trace metal modulation of voltage-gated Ca<sup>v</sup>2.3 calcium channels. *J. Gen. Physiol.* **139**, 219–234.
- Shuaib N. M., Marafie H. M., Al-Fulajj O. and El-Ezaby M. S. (1999) Complexes of vitamin B6. 23. interaction of some tertiary ligating amino acids with the binary complexes of Ni(II) or Cu(II) and pyridoxamine. *J. Chem. Eng. Data* **44**, 1348–1354.
- Siapich S. A., Banat M., Albanna W., Hescheler J., Lüke M. and Schneider T. (2009) Antagonists of ionotropic gamma-aminobutyric acid receptors impair the NiCl<sub>2</sub>-mediated stimulation of the electroretinogram b-wave amplitude from the isolated superfused vertebrate retina. *Acta Ophthalmol.* **87**, 854–865.
- Siapich S. A., Wrubel H., Albanna W., Alnawaiseh M., Hescheler J., Weiergräber M., Lüke M. and Schneider T. (2010) Effect of ZnCl<sub>2</sub> and chelation of zinc ions by N, N-diethyldithiocarbamate (DEDTC) on the ERG b-wave amplitude from the isolated and superfused vertebrate retina. *Curr. Eye Res.* **35**, 322–334.
- Smialowska M., Golembiowska K., Kajta M., Zieba B., Dziubina A. and Domin H. (2012) Selective mGluR1 antagonist EMQMCM inhibits the kainate-induced excitotoxicity in primary neuronal cultures and in the rat hippocampus. *Neurotox. Res.* **21**, 379–392.
- Spedding M. and Paoletti R. (1992) Classification of calcium channels and the sites of action of drugs modifying channel function. *Pharmacol. Rev.* **44**, 363–376.
- Takeda A., Hirate M., Tamano H. and Oku N. (2003) Zinc movement in the brain under kainate-induced seizures. *Epilepsy Res.* **54**, 123–129.
- Wang Q., Yu S., Simonyi A., Sun G. Y. and Sun A. Y. (2005) Kainic acid-mediated excitotoxicity as a model for neurodegeneration. *Mol. Neurobiol.* **31**, 3–16.
- Weiergräber M., Henry M., Radhakrishnan K., Hescheler J. and Schneider T. (2007) Hippocampal seizure resistance and reduced neuronal excitotoxicity in mice lacking the Ca<sup>v</sup>2.3 E/R-type voltage-gated calcium channel. *J. Neurophysiol.* **97**, 3660–3669.
- Zaczek R. and Coyle J. T. (1982) Excitatory amino acid analogues: neurotoxicity and seizures. *Neuropharmacology* **21**, 15–26.

## 2.6. Publication 6: Journal of General Physiology 152(9): e202012585.

### **Zn<sup>2+</sup>-induced changes in Ca<sub>v</sub>2.3 channel function. An electrophysiological and modeling study.**

**Felix Neumaier**, Serdar Alpdogan, Jürgen Hescheler, Toni Schneider

#### **Abstract:**

Loosely bound Zn<sup>2+</sup> ions are increasingly recognized as potential modulators of synaptic plasticity and neuronal excitability under normal and pathophysiological conditions. Ca<sub>v</sub>2.3 voltage-gated Ca<sup>2+</sup> channels are among the most sensitive targets of Zn<sup>2+</sup> and are therefore likely to be involved in the neuromodulatory actions of endogenous Zn<sup>2+</sup>. Although histidine residues on the external side of domain I have been implicated in the effects on Ca<sub>v</sub>2.3 channel gating, the exact mechanisms involved in channel modulation remain incompletely understood. Here, we use a combination of electrophysiological recordings, modification of histidine residues, and computational modeling to analyze Zn<sup>2+</sup>-induced changes in Ca<sub>v</sub>2.3 channel function. Our most important findings are that multiple high- and low-affinity mechanisms contribute to the net Zn<sup>2+</sup> action, that Zn<sup>2+</sup> can either inhibit or stimulate Ca<sup>2+</sup> influx through Ca<sub>v</sub>2.3 channels depending on resting membrane potential, and that Zn<sup>2+</sup> effects may persist for some time even after cessation of the Zn<sup>2+</sup> signal. Computer simulations show that (1) most salient features of Ca<sub>v</sub>2.3 channel gating in the absence of trace metals can be reproduced by an obligatory model in which activation of two voltage sensors is necessary to open the pore; and (2) most, but not all, of the effects of Zn<sup>2+</sup> can be accounted for by assuming that Zn<sup>2+</sup> binding to a first site is associated with an electrostatic modification and mechanical slowing of one of the voltage sensors, whereas Zn<sup>2+</sup> binding to a second, lower-affinity site blocks the channel and modifies the opening and closing transitions. While still far from complete, our model provides a first quantitative framework for understanding Zn<sup>2+</sup> effects on Ca<sub>v</sub>2.3 channel function and a step toward the application of computational approaches for predicting the complex actions of Zn<sup>2+</sup> on neuronal excitability.

#### **Contributions to Publication 6:**

I independently conceptualized and performed all experiments, analyzed and interpreted the data, developed and optimized the Markov model, performed the simulations, prepared all tables and figures, wrote the manuscript and handled the submission and revision process.



ARTICLE

# Zn<sup>2+</sup>-induced changes in Ca<sub>v</sub>2.3 channel function: An electrophysiological and modeling study

Felix Neumaier , Serdar Alpdoğan , Jürgen Hescheler, and Toni Schneider 

Loosely bound Zn<sup>2+</sup> ions are increasingly recognized as potential modulators of synaptic plasticity and neuronal excitability under normal and pathophysiological conditions. Ca<sub>v</sub>2.3 voltage-gated Ca<sup>2+</sup> channels are among the most sensitive targets of Zn<sup>2+</sup> and are therefore likely to be involved in the neuromodulatory actions of endogenous Zn<sup>2+</sup>. Although histidine residues on the external side of domain I have been implicated in the effects on Ca<sub>v</sub>2.3 channel gating, the exact mechanisms involved in channel modulation remain incompletely understood. Here, we use a combination of electrophysiological recordings, modification of histidine residues, and computational modeling to analyze Zn<sup>2+</sup>-induced changes in Ca<sub>v</sub>2.3 channel function. Our most important findings are that multiple high- and low-affinity mechanisms contribute to the net Zn<sup>2+</sup> action, that Zn<sup>2+</sup> can either inhibit or stimulate Ca<sup>2+</sup> influx through Ca<sub>v</sub>2.3 channels depending on resting membrane potential, and that Zn<sup>2+</sup> effects may persist for some time even after cessation of the Zn<sup>2+</sup> signal. Computer simulations show that (1) most salient features of Ca<sub>v</sub>2.3 channel gating in the absence of trace metals can be reproduced by an obligatory model in which activation of two voltage sensors is necessary to open the pore; and (2) most, but not all, of the effects of Zn<sup>2+</sup> can be accounted for by assuming that Zn<sup>2+</sup> binding to a first site is associated with an electrostatic modification and mechanical slowing of one of the voltage sensors, whereas Zn<sup>2+</sup> binding to a second, lower-affinity site blocks the channel and modifies the opening and closing transitions. While still far from complete, our model provides a first quantitative framework for understanding Zn<sup>2+</sup> effects on Ca<sub>v</sub>2.3 channel function and a step toward the application of computational approaches for predicting the complex actions of Zn<sup>2+</sup> on neuronal excitability.

## Introduction

Voltage-gated Ca<sup>2+</sup> channels (VGCCs) participate in neuronal signaling and provide the key link between electrical signals and various nonelectrical processes, such as neurotransmitter release, transcription, and muscle contraction (Catterall, 1998; Hofmann et al., 1999; Neumaier et al., 2015). Their modulation by foreign (i.e., non-Ca<sup>2+</sup>) inorganic cations has proven instrumental in identifying the mechanisms underlying Ca<sup>2+</sup>-selective flux and may have important (patho)physiological implications. For example, the d-block metal ions Zn<sup>2+</sup> and Cu<sup>2+</sup> have been identified as endogenous modulators of neuronal transmission and synaptic plasticity and implicated in a number of pathophysiological conditions (Frederickson et al., 2000, 2005; Mathie et al., 2006). Ca<sub>v</sub>2.3 channels, which are thought to be involved in synaptic transmission (Gasparini et al., 2001), action potential burst firing, and oscillatory activity (Christie et al., 1995; Magee and Carruth, 1999), are among the most sensitive targets for Zn<sup>2+</sup> and Cu<sup>2+</sup> currently known (Kang et al., 2007; Shcheglovitov et al., 2012). In addition, these channels have an expression pattern that coincides with the

spatial distribution of loosely bound Zn<sup>2+</sup> ions in the brain (Sochivko et al., 2002; Weiergräber et al., 2006b), suggesting that they could represent a main mediator for the reported anticonvulsive effects of endogenous Zn<sup>2+</sup>. Although non-conserved histidine residues in the voltage-sensor module (VSM) of domain I have been convincingly implicated in the effects of Zn<sup>2+</sup> on Ca<sub>v</sub>2.3 channel gating (Fig. 1 A; Kang et al., 2007; Shcheglovitov et al., 2012), the exact mechanisms involved and the potential role of additional metal binding sites remain incompletely understood. Here, we have used metal ion-buffered solutions, different experimental conditions, and computational modeling to explore the effects of Zn<sup>2+</sup> on Ca<sub>v</sub>2.3 channel function over a wide range of free Zn<sup>2+</sup> concentrations. Based on our data, we have developed a Markov model that accounts for most salient features of Ca<sub>v</sub>2.3 channel gating in the absence of trace metals and also reproduces their alteration by a range of Zn<sup>2+</sup> concentrations previously estimated to be (patho)physiologically relevant. In addition, our results provide novel insights into the dependence of Zn<sup>2+</sup> effects on the ionic

University of Cologne, Faculty of Medicine and University Hospital Cologne, Institute for Neurophysiology, Cologne, Germany.

Correspondence to Felix Neumaier: [felix@neumaier-net.de](mailto:felix@neumaier-net.de).

© 2020 Neumaier et al. This article is distributed under the terms of an Attribution–Noncommercial–Share Alike–No Mirror Sites license for the first six months after the publication date (see <http://www.rupress.org/terms/>). After six months it is available under a Creative Commons License (Attribution–Noncommercial–Share Alike 4.0 International license, as described at <https://creativecommons.org/licenses/by-nc-sa/4.0/>).

Rockefeller University Press

J. Gen. Physiol. 2020 Vol. 152 No. 9 e202012585



<https://doi.org/10.1085/jgp.202012585>

1 of 25

conditions and reveal that changes in the neuronal resting membrane potential (RMP) could profoundly influence and even invert the net  $Zn^{2+}$  action from inhibition to stimulation. Taken together, our work provides a first quantitative framework for understanding  $Zn^{2+}$  effects on  $Ca_v2.3$  channel function and a step toward the application of computational approaches for understanding the complex actions of  $Zn^{2+}$  on neuronal excitability and their dependence on the prevailing neuronal properties and ionic conditions.

## Materials and methods

### Cell culture

Human embryonic kidney (HEK293) cells stably transfected with human  $Ca_v2.3d$  and  $\beta_3$   $Ca^{2+}$ -channel subunits (Mehrk et al., 1997; Nakashima et al., 1998) were cultured under normal growth conditions (37°C and 5%  $CO_2$ ) in Dulbecco's modified Eagle medium (Sigma-Aldrich) supplemented with 10% FCS and antibiotics (1% penicillin-streptomycin and selection markers; 1 mg ml<sup>-1</sup> geneticin [G-418] and 200  $\mu$ g ml<sup>-1</sup> hygromycin B). Cells were routinely passaged twice a week using 0.05% trypsin/0.02% EDTA. For electrophysiological recordings, cells were seeded on nitric acid-washed glass coverslips and used within 24–48 h after plating.

### Chemicals

HEPES (Pharmagrade), Tricine (Pharmagrade), La(III)chloride heptahydrate (99.999%), TEA chloride, Chelex 100 (sodium form), Zn(II)chloride (99.999%), pyruvic acid (98%), ATP, oxaloacetic acid, FBS, hygromycin B, geneticin, penicillin-streptomycin, hydrochloric acid (TraceSelect), and 70% nitric acid (ACS reagent) were purchased from Sigma-Aldrich. Anhydrous ethanol, diethylpyrocarbonate (high purity), sodium hydroxide 30% solution (suprapur), sodium chloride (puratronic, 99.999%; AlfaAesar), potassium chloride (puratronic, 99.997%; AlfaAesar) cesium chloride (99.999%; AlfaAesar), calcium chloride (99.99%; AlfaAesar), 50% cesium hydroxide solution (99.9%; AlfaAesar), D-glucose (AnalaR Normapur), and potassium hydroxide (99.98%) were purchased from VWR. 1,000 mM stock solutions of diethyl pyrocarbonate (DEPC) in anhydrous ethanol were prepared on the day of the experiments, kept on ice, and diluted into standard external solution immediately before use.

### Preparation of buffered $Zn^{2+}$ solutions

To avoid trace metal contamination and reduce uncertainties with regard to free metal ion concentrations in our recording solutions, we employed suitable labware and sample handling procedures, which have been outlined in detail in a previous publication (Neumaier et al., 2017). Briefly, all solutions were prepared using type 1 ultrapure water (Purelab Flex 2 by ELGA Labwater), metal-free pipette tips, and reagents of the highest purity available (see previous section). All containers used for preparation and storage were made from polymethylpentene, polystyrene, or low-density polyethylene and pretreated by a comprehensive cleaning procedure that involved rinses with alcohol, successive soaking in dilute (10%) hydrochloric and nitric acid, and extensive washes with type 1 ultrapure water.

Before the addition of multivalent cations or chelators, all solutions were treated with the metal-chelating ion exchange resin Chelex 100 to remove adventitious metal ions. For most experiments, Tricine (10 mM) was used as a dual proton and metal ion buffer to prepare buffered  $Zn^{2+}$  solutions (solutions 1–3A in Table S1). Free  $Zn^{2+}$  concentrations above the useful range for buffering with Tricine were prepared in a HEPES-buffered background solution (solutions 1–3B in Table S1). There was no difference in the electrophysiological properties recorded in Tricine- versus HEPES-buffered solutions, suggesting that our methods were sufficient to reduce trace metal contamination below the limits for detection. To facilitate fast and complete reversal of metal ion effects during washout, however, the HEPES-buffered solution used for control recordings and washout was supplemented with 0.1 mM of the trace metal chelator diethylenetriaminepentaacetic acid. In all cases, pH-, temperature-, and ionic strength-corrected free metal ion concentrations were calculated with the general-purpose speciation software Visual MINTEQ and constants reported previously (Mohamed, 2007; Goldberg et al., 2002; Khalil et al., 2009). Apart from  $Zn^{2+}$  binding by Tricine, these calculations took into account the formation of hydroxide species and the (weak) binding by Tricine of  $Ca^{2+}$  ions so as to ensure that the estimated free  $Ca^{2+}$  concentration was the same in HEPES- and Tricine-buffered solutions.

### Ionic and gating current recordings

Cells were voltage clamped using the whole-cell configuration of the patch-clamp technique (Hamill et al., 1981). Pipettes were prepared from thick-walled borosilicate glass capillaries (1.5/0.84 mm OD/ID; World Precision Instruments) using a P97 Micropipette puller (Sutter Instruments). Resistance of the resulting electrodes was between 1.5 and 6.5 M $\Omega$  when filled with standard internal solution. The bath was connected to ground via 140 mM sodium chloride agar bridges. Currents were sampled at 20 or 50 kHz and filtered at 10 kHz using an EPC9 amplifier (HEKA) controlled with HEKA's Pulse software. Leak and capacitive currents were subtracted online using a -P/5 (for ionic currents) or -P/8 (for gating currents) protocol. Series resistance was compensated electronically by  $\leq 90\%$  and continuously monitored throughout the measurements. All experiments were performed at room temperature (20–22°C) and, unless noted otherwise, from a holding potential of -80 mV for ionic current recordings or -100 mV for gating current recordings. During the experiments, cells were constantly perfused with external solution at a rate of  $\sim 2$ –4 ml min<sup>-1</sup> using a gravity-driven perfusion system controlled by manual precision flow regulators (Sarstedt). The standard external solution for ionic current recordings contained (in mM) 120 NaCl, 5 KCl, 20 TEA chloride, 10 D-glucose, 10 Tricine, and 2.8/5.8  $CaCl_2$  or 10 HEPES and 2.3/4.5  $CaCl_2$  (= 2/4 mM free  $Ca^{2+}$ ; for details, see Table S1) with the pH adjusted to 7.4 using NaOH or HCl and osmolarity of 297–314 mOsm. Gating currents were recorded in the same HEPES-buffered solution but with 4 mM free  $MgCl_2$  (instead of  $CaCl_2$ ) and 0.1 mM free  $La^{3+}$  (0.2 mM  $LaCl_3$  + 0.1 mM EDTA) to block ionic currents.  $Ca^{2+}$  substitution by  $Mg^{2+}$  did not alter channel voltage dependence (Fig. S1 A), whereas 100  $\mu$ M

free  $\text{La}^{3+}$  shifted it by  $8.3 \pm 0.7$  mV ( $n = 6$  cells) to more depolarized test potentials (Fig. S1 B), which was taken into account by assuming a 10-mV shift during fitting.

The standard internal solution was composed of (in mM) 130 CsCl, 5 oxaloacetic acid, 5 creatine, 5 pyruvic acid, 10 EGTA, 10 HEPES, and 4 MgATP with the pH adjusted to 7.3 using CsOH and osmolarity of 275–295 mOsm. It was filtered through 0.2- $\mu\text{m}$  surfactant-free cellulose acetate membranes (Corning) and kept on ice between the recordings. The liquid junction potential between internal and external solution (calculated using the JPCalc algorithm in pClamp 10; Molecular Devices) was  $\sim 5$  mV. Since no correction for the liquid junction potential was done, all voltages shown were actually 5 mV more negative.

### Whole-cell protocols

During the experiments, currents were routinely monitored by application at 0.03 Hz of a 30-ms test pulse to +10 mV followed by 10-ms repolarization at -50 mV to record well-resolved tail currents. To construct steady-state I-V relationships, peak currents recorded with a protocol consisting of 25-ms test pulses to potentials between -80 mV and +60 mV (10-mV increments at 0.1 Hz) were normalized by the cell capacitance or maximum current amplitude under control conditions and plotted as a function of the test-pulse potential. Tail-current amplitudes recorded during repolarization to -50 mV at the end of the voltage steps were normalized to the maximum tail-current amplitude and plotted as a function of the prepulse potential to construct isochronous activation curves. Gating currents were recorded with the same protocol, except that the holding potential was -100 mV, the test pulse duration was reduced to 20 ms, and repolarization was also to -100 mV.

Instantaneous I-V (II-V) relationships were obtained with a protocol consisting of a fixed 10-ms prepulse to +60 mV followed by 40-ms test pulses to potentials between -80 mV and +60 mV (10-mV increments at 0.1 Hz). Instantaneous (tail) current amplitudes recorded during the test pulses were normalized by the cell capacitance or maximum tail current amplitude under control conditions and plotted as a function of the test-pulse potential.

The fraction of channels available for activation from different holding potentials was assessed by a protocol consisting of 2-s conditioning prepulses at potentials between -120 mV and +10 mV (10-mV increments at 0.1 Hz) followed by a fixed 35-ms test pulse to +10 mV. To construct prepulse inactivation (PPI) curves, peak current amplitudes recorded during the test pulse were normalized by the maximum amplitude and plotted as a function of the prepulse potential.

### Data analysis and statistics

Leak-subtracted current traces were directly analyzed with PulseFit (HEKA) or exported for further processing with Microsoft Excel 2010 and OriginLab Pro (version 9; OriginLab).

I-V relationships were fitted with a combined Ohm-Boltzmann equation:

$$I = (V_m - V_{rev}) \times G_{max} / \{1 + \exp[-(V_m - V_{0.5})/k]\}, \quad (1)$$

where  $I$  is the (normalized) peak current density measured at the test potential  $V_m$ ,  $V_{rev}$  the apparent reversal potential,  $G_{max}$

the maximum slope conductance,  $V_{0.5}$  the voltage eliciting half-maximal inward currents, and  $k$  the slope factor. Isochronous activation and PPI curves were fitted with single Boltzmann equations:

$$I/I_{max} = A_2 + (A_1 - A_2) / \{1 + \exp[(V_m - V_{0.5})/k]\}, \quad (2)$$

where  $I/I_{max}$  is the normalized current corresponding to the prepulse potential  $V_m$ ,  $V_{0.5}$  is the voltage of half-maximal activation ( $V_{0.5act}$ ) or inactivation ( $V_{0.5inact}$ ),  $k$  the activation ( $k_{act}$ ) or inactivation ( $k_{inact}$ ) slope factor, and  $A_1$  and  $A_2$  the initial and final values, respectively. Activation time constants were determined by single exponential functions fit to the rising phase of currents, which started when the current amplitude had reached 20% of its final value. Inactivation during 400-ms voltage steps was biexponential, but the slower time constant was often too slow to be determined reliably ( $\tau_{slow} > 200$ –700 ms depending on the test potential), so that inactivation time constants were determined using a single exponential function with variable offset fitted to the decaying phase of currents. Tail current decay over a wide voltage range was quantified by the sum of up to three exponential functions, where the two faster time constants presumably reflect deactivation and the third, slowest time constant corresponds to inactivation. Weighted deactivation time constants were calculated according to the following equation:

$$\tau_w = (A_1 \times \tau_1 + A_2 \times \tau_2) / (A_1 + A_2), \quad (3)$$

where  $\tau_w$  is the weighted time-constant,  $A_1$  and  $\tau_1$  are the relative amplitude and time-constant of the first exponential component and  $A_2$  and  $\tau_2$  the relative amplitude and time-constant of the second exponential component. All fits were performed using the Levenberg-Marquardt least-squares algorithm and the goodness of fits was judged based on residual plots and adjusted  $\chi^2$  values. Smooth curves in the figures represent fits to average data whereas values given in the text are average data from fits to individual measurements. Values in the text and figures are expressed as mean  $\pm$  SEM based on  $n$ , the number of independent experiments. Boxplots show median, upper and lower quartiles (box), minimum and maximum values (whiskers), and individual data points (dots). Numerical values for the parameters characterizing monotonic concentration-response curves were obtained from fits of the data with a standard sigmoid saturation curve of the form:

$$Y = A_1 + (A_2 - A_1) / \left\{ 1 + 10^{[(\log K_{Zn} - X) \times h]} \right\}, \quad (4a)$$

where  $X$  is the logarithm of the free  $\text{Zn}^{2+}$  concentration that produces the effect  $Y$ ,  $A_1$  is the bottom asymptote,  $A_2$  the top asymptote or maximum effect ( $E_{max}$ ),  $K_{Zn}$  the free  $\text{Zn}^{2+}$  concentration producing 50% of the  $E_{max}$  (= apparent dissociation constant for  $\text{Zn}^{2+}$ ), and  $h$  the Hill slope. Biphasic concentration-response curves were fitted with a combination of two sigmoid saturation curves of the form

$$Y = A_1 + (A_2 - A_1) \left\{ \frac{p}{1 + 10^{[(\log K_{Zn1} - X) \times h1]}} + \frac{1 - p}{1 + 10^{[(\log K_{Zn2} - X) \times h2]}} \right\}, \quad (4b)$$

where  $X$  is the logarithm of the free  $\text{Zn}^{2+}$  concentration that produces the effect  $Y$ ,  $A_1$  and  $A_2$  are the bottom and top



asymptotes,  $K_{Zn1}$  and  $K_{Zn2}$  the free  $Zn^{2+}$  concentrations producing 50% of the  $E_{max}$  is mediated by the two components,  $h_1$  and  $h_2$  the corresponding Hill slopes, and  $p$  the proportion of maximum response due to the more potent component. Unless noted otherwise, the Hill slopes were fixed to 1 (but see Limitations).

To indicate experimental uncertainty, we assumed a Gaussian distribution of the fit parameters and used 84% confidence intervals (CIs), so that the probability that two CIs abut or overlap if there really is no difference should be roughly equal to or smaller than  $P = 0.05$ , respectively (Austin and Hux, 2002). In all other cases, statistical significance was assessed with OriginLab Pro 9 using a repeated-measures ANOVA followed by Bonferroni's post hoc analysis when comparing mean values from the same cells or a one-way ANOVA followed by Bonferroni's post hoc analysis when comparing multiple independent mean values. Homogeneity of variances between groups was tested using Levene's test for equality of variances on the squared deviations. In the case of heteroscedastic data ( $P < 0.05$  in Levene's test and ratio of largest to smallest variance  $\geq 4$ ), statistical significance was assessed with Minitab (version 17; Minitab) using Welch's ANOVA and the Games-Howell multiple comparison method.

### Modeling and simulations

Model development, optimization, and simulations were performed using the NEURON version 7.6.2 simulation environment (Carnevale and Hines, 2006). Kinetic equations were written and solved directly using KINETIC methods of the NMODL language in NEURON.

The rates of  $Zn^{2+}$  interaction with different sites were defined in terms of a simple, bimolecular reaction:

$$k_{on} = [Zn] \times d_{zn} \quad (5a)$$

and

$$k_{off} = d_{zn} \times K_{zn}, \quad (5b)$$

where  $[Zn]$  is the free  $Zn^{2+}$  concentration,  $d_{zn}$  is the rate of complex formation between  $Zn^{2+}$  and the site, and  $K_{zn}$  is the affinity of the site for  $Zn^{2+}$ .

For parameter optimization and whole-cell simulations, we constructed an *in silico* one-compartmental model of a HEK293 cell with diameter and length of 21.851  $\mu\text{m}$ , which corresponds to a sphere with surface area of 1,500  $\mu\text{m}^2$ . Temperature, specific membrane capacitance, and cytoplasmic resistivity were set to 22°C, 1  $\mu\text{F}/\text{cm}^2$ , and 60  $\Omega \times \text{cm}$ , respectively. All simulations were performed using the default integration strategy with an implicit fixed time step of 25  $\mu\text{s}$ .

For kinetic modeling, mean current traces (in pA/pF) were calculated from all control recordings performed with the voltage protocols shown in Fig. 15, C-F and converted to mA/cm<sup>2</sup> assuming a specific membrane capacitance of 1  $\mu\text{F}/\text{cm}^2$ . The model shown in Fig. 15 A was then simultaneously fitted to the whole set of experimental traces using the nonlinear least-squares minimization method included in NEURON (Multiple Run Fitter [MRF] subroutine), which is based on the principal axis method described by Brent (1976). Approximately equal

weighting of current traces recorded with different protocols was achieved by scaling the error values reported by each MRF generator until it was close to the value reported by all other MRF generators.

Macroscopic ion currents (in mA/cm<sup>2</sup>) were calculated according to

$$I_{ion} = P_o \times n \times p \times ghk(V_m, Ca_i, Ca_o), \quad (6)$$

where  $P_o$  is the fraction of channels in the four open states,  $n$  is the number of channels per square centimeter,  $p$  is the single-channel permeability, and  $ghk$  is the Goldman-Hodgkin-Katz current equation. The single-channel permeability was assumed to be  $7.5 \times 10^{-14} \text{ cm}^3\text{s}^{-1}$ , and the number of channels per square centimeter was set to values between  $1.15 \times 10^{10}$  and  $1.40 \times 10^{10}$  to account for differences in expression levels between experiments performed with the different voltage protocols.

Macroscopic gating currents were calculated as the product of the number of channels and the sum, over all pairs of states, of the charge movement between states times the fraction of channels in each state times the transition rate between the states. Some of the optimizations were run on the Neuroscience Gateway (Sivagnanam et al., 2013). Source code for the model reported in this paper and several scripts for running simulations are available in ModelDB (McDougal et al., 2017) at <http://modeldb.yale.edu/261714>.

### Online supplemental material

Fig. S1 shows the effects of  $Ca^{2+}$  substitution with  $Mg^{2+}$  or 100  $\mu\text{M}$  free  $La^{3+}$  on  $Ca_v2.3$  channel voltage dependence. Fig. S2 shows evidence for fast and slow components of charge movement observed in our gating current recordings. Fig. S3 compares experimental and simulated  $Ca_v2.3$  channel biophysical properties in the absence of metal ions. Table S1 lists the composition of all external solutions used in the electrophysiological recordings. Table S2 presents the absolute effects of 5.4  $\mu\text{M}$  free  $Zn^{2+}$  on  $Ca_v2.3$  channel gating under different experimental conditions. Table S3 lists the relative effects of various free  $Zn^{2+}$  concentrations on  $Ca_v2.3$  channel gating under different experimental conditions. Table S4 shows  $E_{max}$  and  $K_{zn}$  values obtained from  $Zn^{2+}$  concentration-response data under different experimental conditions. Table S5 shows global  $K_{zn}$  values for high-affinity shift and slowing.

## Results

We reassessed the action of  $Zn^{2+}$  on  $Ca_v2.3$  channel function under near-physiological ionic conditions with either 2 or 4 mM free  $Ca^{2+}$  as the charge carrier and at two different pH values. To identify gating effects caused by binding to the putative metal binding site in domain I, some recordings were performed after carbethoxylation of extracellular histidine residues with DEPC (Fig. 1 B). Unless noted otherwise, all recordings were performed at room temperature (20–22°C) and from a holding potential of –80 mV. The key electrophysiological properties as a function of the experimental conditions in the absence of  $Zn^{2+}$  or other trace metals (control recordings with Tricine or HEPES + diethylenetriaminepentaacetic acid) are summarized in Table 1. In the

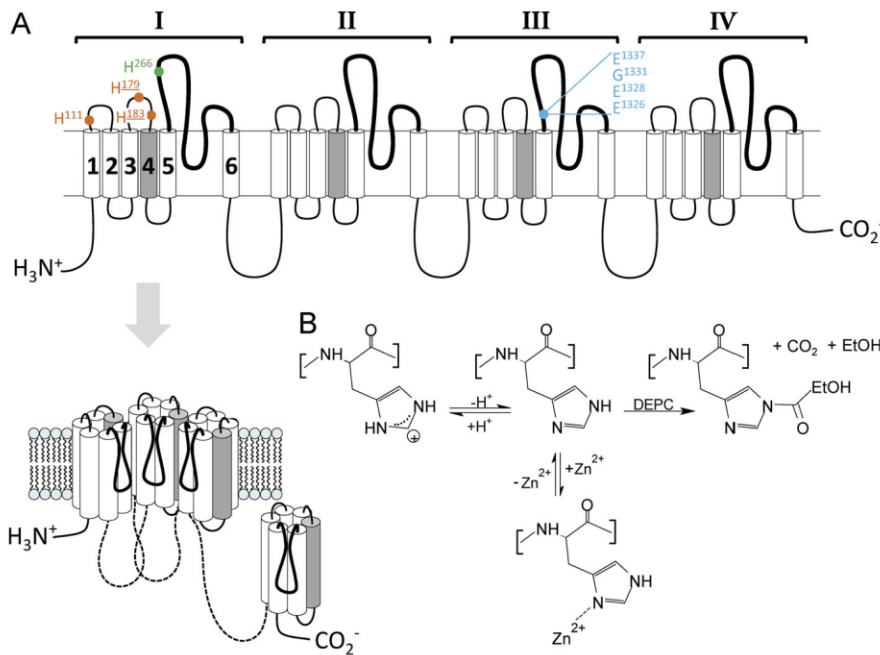


**Figure 1. General structure and potential Zn<sup>2+</sup>-binding sites in Ca<sub>v</sub>2.3 channels.** (A) General structure and transmembrane topology of Ca<sub>v</sub>2.3 channels along with residues that have been implicated in the effects of Zn<sup>2+</sup> and/or protons. Three nonconserved histidine residues in domain I (indicated in orange) have been linked to gating modulation by Zn<sup>2+</sup>, other d-block metal ions, and (for underlined residues) protons (Cens et al., 2011; Shcheglovitov et al., 2012; Kang et al., 2007). A nonconserved histidine residue in the p-loop of domain I (indicated in green) has been linked to proton-induced changes in single-channel conductance (Cens et al., 2011). An EF hand-like motif in the S5-H5 region of domain III (indicated in light blue) that is present in all HVA channels has been implicated in their differential sensitivity to Zn<sup>2+</sup> (Sun et al., 2007). (B) Scheme illustrating possible reactions of histidine residues with protons (left), Zn<sup>2+</sup> ions (bottom), or DEPC (right).

first part of the Results, we will briefly describe the hallmarks of Ca<sub>v</sub>2.3 channel modulation by low micromolar Zn<sup>2+</sup> levels and their dependence on time, voltage, ionic conditions, and Zn<sup>2+</sup> interaction with histidine residues. In the second and third parts, we will summarize their rather complex dependence on Zn<sup>2+</sup> concentration and try to delineate effects mediated by high- and low-affinity binding. The fourth part briefly describes the development of a model for Ca<sub>v</sub>2.3 channel gating in the absence of trace metals, while the last part deals with our approach to model the major Zn<sup>2+</sup> effects on Ca<sub>v</sub>2.3 channel gating.

**Ca<sub>v</sub>2.3 channel modulation by low micromolar Zn<sup>2+</sup> concentrations**

Fig. 2 exemplifies the effects of 5.4 μM Zn<sup>2+</sup> on macroscopic currents carried by 4 mM free Ca<sup>2+</sup> at pH 7.4. Currents were evoked by step depolarization to different test potentials and repolarization to -50 mV (Fig. 2 A, I-V protocol), a fixed test pulse following 2-s prepulses at different conditioning potentials (Fig. 2 B, PPI protocol), or repolarization to different test potentials following a fixed depolarizing prepulse to open the channels (Fig. 2 C, II-V protocol). Zn<sup>2+</sup>-induced suppression was strong and steeply voltage dependent when recorded with the I-V protocol, as reflected in a shift of the I-V curve to more depolarized test potentials (Fig. 2, A and D). The same concentration of Zn<sup>2+</sup> produced almost no changes in currents measured with the II-V protocol (Fig. 2, C and E).

**Zn<sup>2+</sup> shifts and alters channel voltage dependence**

Fig. 2 F shows isochronous activation and inactivation curves, constructed from tail currents recorded with the I-V protocol or from the fraction of current available for activation recorded with the PPI protocol, respectively. Application of 5.4 μM Zn<sup>2+</sup> produced a depolarizing shift of both activation and inactivation voltage dependence by almost 10 mV (Fig. 2 G), which was

completely reversed during washout with Zn<sup>2+</sup>-free solution (Fig. 2 F). The shift was paralleled by a decreased slope of the activation curve, as reflected in a moderate but significant and selective increase of the activation slope factor by ~10–15% (Fig. 2 H).

**Zn<sup>2+</sup> slows macroscopic current kinetics**

Apart from altering channel voltage dependence, Zn<sup>2+</sup> produced a dramatic slowing of current kinetics that is most evident when inspecting scaled I-V current traces (Fig. 3 A). Fig. 4 A summarizes the effects of 5.4 μM Zn<sup>2+</sup> on the time course of macroscopic activation (right) and deactivation (left) at various test potentials, quantified by fitting exponential functions to the rising phase of I-V currents (Fig. 2 A and Fig. 3 A) or the decaying phase of II-V currents (Fig. 2 C and Fig. 3 B), respectively. It can be seen that the effects on activation kinetics were much more pronounced than would be expected based on the voltage shift described above. Thus, after correction for the expected effects of a 10-mV shift on activation kinetics, 5.4 μM Zn<sup>2+</sup> still slowed current activation almost twofold and over the whole voltage range examined.

On the other hand, Zn<sup>2+</sup> had no effects on deactivation time constants except for a minor increase at intermediate test potentials (Fig. 4 A), which could reflect the depolarizing shift in channel voltage dependence. Interestingly, inspection of scaled II-V current traces near the threshold voltage for macroscopic activation still revealed a clear acceleration of tail-current decay (Fig. 3 B), which was related to neither changes in deactivation time constants nor faster inactivation (Fig. 4 B). Instead, the faster tail-current decay in the presence of Zn<sup>2+</sup> appeared to result almost entirely from a depolarizing shift in the relative amplitude of both processes, which markedly increased the apparent contribution of deactivation to total tail-current decay at depolarized test potentials (Fig. 4 C). Indeed, when the time

Table 1. Electrophysiological properties of Ca<sub>v</sub>2.3 channels in the absence of metal ions

	V <sub>0.5act</sub> [mV]	k <sub>act</sub>	n	τ <sub>act(10 mV)</sub> [ms]	τ <sub>deact(-50 mV)</sub> [ms]	n
4 Ca, pH 7.4	-2.3 ± 0.3	6.8 ± 0.1	87	1.3 ± 0.1	0.38 ± 0.01	95
4 Ca, pH 7.0	-0.2 ± 0.4 <sup>a</sup>	6.6 ± 0.1	51	1.6 ± 0.1 <sup>b</sup>	0.40 ± 0.01	66
2 Ca, pH 7.4	-3.1 ± 0.4	7.7 ± 0.2 <sup>a</sup>	37	1.3 ± 0.1	0.37 ± 0.01	63
4 Ca, pH 7.4 (DEPC)	-11.4 ± 0.8 <sup>a</sup>	8.7 ± 0.3 <sup>a</sup>	34	1.1 ± 0.1 <sup>c</sup>	0.42 ± 0.01	63

<sup>a</sup>P < 0.001 versus 4 Ca, pH 7.4 (Welch ANOVA and Games-Howell analysis).  
<sup>b</sup>P < 0.05 versus 4 Ca, pH 7.4 (Welch ANOVA and Games-Howell analysis).  
<sup>c</sup>P < 0.01 versus 4 Ca, pH 7.4 (Welch ANOVA and Games-Howell analysis).

course of inactivation was examined using 400-ms voltage steps, Zn<sup>2+</sup> actually slowed down both fast and slow components of current decay recorded near the half-activation voltage (Fig. 3 A). However, there was no effect on the limiting decay rate reached at depolarized test potentials (Fig. 4 D) or on the time constants for recovery from inactivation at -80 mV (data not shown), suggesting that the underlying microscopic inactivation rates were unaffected. Because macroscopic inactivation is thought to derive most of its voltage dependence from the voltage dependence of activation, the observed shift in inactivation voltage dependence might have been a consequence of the Zn<sup>2+</sup>-induced changes in activation gating (but see Modeling the effects of Zn<sup>2+</sup> on Ca<sub>v</sub>2.3 channel gating).

**Zn<sup>2+</sup> effects depend on the holding potential**

Regardless of the underlying mechanism, the shift of the inactivation curve (Fig. 2 F) suggested that Zn<sup>2+</sup> increases the availability for activation after prepulses at intermediate test potentials, in which case its effects could be influenced by the RMP. To test this assumption, we compared the effects of Zn<sup>2+</sup> on currents evoked by step depolarization from different holding potentials. As illustrated in Fig. 5, Ca<sup>2+</sup> currents evoked from voltages that provide full availability (i.e., less than or equal to -80 mV) were rapidly inhibited and slowed by application of 5.4 μM free Zn<sup>2+</sup> and quickly returned to their control amplitude and kinetics during washout (Fig. 5, A, B, and D), indicating that Zn<sup>2+</sup> application and washout were complete in <30 s. Currents

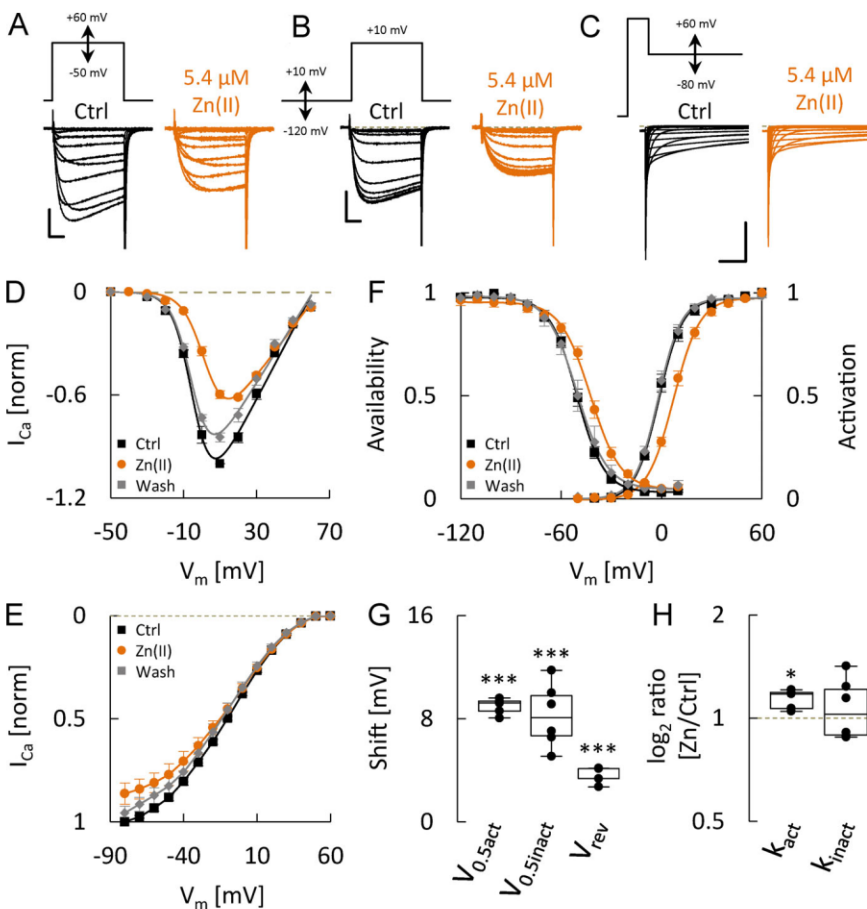
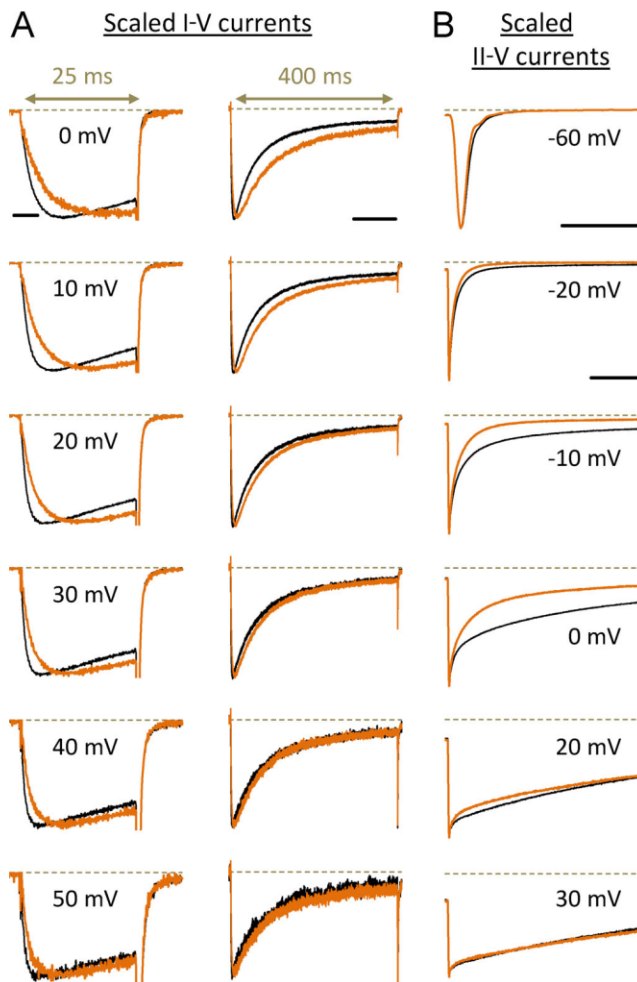


Figure 2. Effects of Zn<sup>2+</sup> on Ca<sub>v</sub>2.3 channel voltage dependence. (A–C) Families of mean current traces carried by 4 mM free Ca<sup>2+</sup> and recorded with the protocols depicted above in the absence (black) and presence (orange) of 5.4 μM free Zn<sup>2+</sup> at pH 7.4 (n = 5 cells in A and C, and 6 cells in B). Scale bar corresponds to 5 ms and 20 pA/pF in A, 5 ms and 50 pA/pF in B, or 10 ms and 200 pA/pF in C. (D) I–V relationships determined with the protocol in A before (black squares), during (orange circles), and after (gray diamonds) application of 5.4 μM free Zn<sup>2+</sup> (same cells as in A). (E) I–V relationships determined with the protocol in C before (black squares), during (orange circles), and after (gray diamonds) application of 5.4 μM free Zn<sup>2+</sup> (same cells as in C). (F) Isochronous activation (right) and PPI (left) curves determined from tail currents recorded with the protocol in A or peak currents recorded with the protocol in B, respectively, before (open squares), during (orange circles), and after (gray squares) application of 5.4 μM free Zn<sup>2+</sup> (same cells as in A and B). (G) Boxplots comparing the Zn<sup>2+</sup>-induced shifts in half-activation voltage (V<sub>0.5act</sub>), half-inactivation voltage (V<sub>0.5inact</sub>), and apparent V<sub>rev</sub>. (H) Boxplots comparing the Zn<sup>2+</sup>-induced changes in activation slope factor (k<sub>act</sub>) and inactivation slope factor (k<sub>inact</sub>). \*, P < 0.05; \*\*\*, P < 0.001 (one-way repeated-measures ANOVA).





**Figure 3. Effects of  $Zn^{2+}$  on the shape of macroscopic  $Ca^{2+}$  currents.** (A) Mean I-V current traces recorded in response to 25-ms (left) or 400-ms (right) voltage steps to the indicated test potentials in the absence (black) and presence (orange) of  $5.4 \mu M$  free  $Zn^{2+}$  at pH 7.4. They have been scaled to their maximum amplitude to highlight kinetic changes. Scale bars correspond to 10 and 100 ms for short and long voltage steps, respectively. (B) Mean I-V current traces recorded at the indicated test potentials in the absence (black) and presence (orange) of  $5.4 \mu M$  free  $Zn^{2+}$  at pH 7.4. They have been scaled to their maximum amplitude to highlight kinetic changes. Scale bars correspond to 2 ms for the tail current at  $-60$  mV and 10 ms for all other test potentials.

evoked from more depolarized holding potentials displayed the same rapid slowing, but suppression was diminished and followed by a paradoxical increase of current amplitudes in the maintained presence of  $Zn^{2+}$  (Fig. 5 A), during which the kinetic slowing persisted (Fig. 5 B). For example, currents evoked from a holding potential of  $-60$  mV were reduced to  $85 \pm 3\%$  of their initial amplitude 30 s after application of  $5.4 \mu M$   $Zn^{2+}$  but then progressively increased to reach a steady-state level at  $128 \pm 7\%$  of their control amplitude after 240 s in the maintained presence of  $Zn^{2+}$  (Fig. 5, A and C). Subsequent washout of  $Zn^{2+}$  rapidly restored the normal activation kinetics (Fig. 5 B) and led to overrecovery of current amplitudes beyond their initial level, which was followed by a gradual return toward the control

amplitude. The same but less pronounced effects were observed when the free  $Zn^{2+}$  concentration was reduced to  $2.3 \mu M$  (data not shown). In principle,  $Zn^{2+}$ -induced stimulation that gets evident as the holding potential becomes more depolarized would be consistent with a shift in the voltage dependence of inactivation, which should increase availability near the voltage of half-maximal inactivation. However, considering the slow time course of current increase, most of the observed stimulation could not be explained by the increase in availability measured after 2-s prepulses. To roughly separate the two opposing effects of  $Zn^{2+}$ , the difference in peak current amplitudes between the last test pulse delivered in the presence of  $Zn^{2+}$  and the first test pulse delivered after starting washout was taken as a measure for the degree of  $Zn^{2+}$ -induced suppression and used to correct the original peak current amplitudes measured in the presence of  $Zn^{2+}$ . Fig. 6 A illustrates the magnitude and time course of current stimulation thus obtained at different holding potentials (top) and also indicates the estimated magnitude of suppression (bottom), which showed no dependence on holding potential. Fig. 6 B compares the current increase after 240 s in the presence of  $Zn^{2+}$  from Fig. 6 A with the increase in availability determined using the PPI protocol. Both effects exhibited the bell-shaped voltage dependence that would be expected for a shift in inactivation, but the slow changes peaked at  $\sim 30$  mV more negative holding potentials. A possible explanation for these findings could be that  $Zn^{2+}$  also shifts a process like ultraslow voltage-dependent inactivation, which occurs at more negative holding potentials and with time constants for development and recovery in the order of minutes (Boyett et al., 1994; Yasuda et al., 2004). True steady-state inactivation curves that reflect such processes could not be obtained, as the long prepulse durations necessary were neither practical nor tolerated by the cells. However, a testable prediction of the above assumption is that the time course of recovery from inactivation produced by a hyperpolarizing shift in holding potential equivalent to the  $Zn^{2+}$ -induced depolarizing shift in activation voltage dependence should roughly match that of  $Zn^{2+}$ -induced stimulation at the same holding potential. Fig. 6 C shows data from a recording where the holding potential was changed from  $-60$  mV to  $-70$  mV and back to  $-60$  mV as indicated. Neither the time course (Fig. 6 D) nor the degree (Fig. 6 E) of current increase were significantly different from the values for  $Zn^{2+}$ -induced stimulation at the same holding potential, suggesting that the latter effect was also due to slow recovery from holding potential-dependent inactivation.

#### $Zn^{2+}$ effects depend on histidine residues

Previous studies have linked both pH- and metal-induced changes in  $Ca_v2.3$  channel gating to histidine residues making up the proposed metal binding site in domain I (Fig. 1 A; Cens et al., 2011; Kang et al., 2007; Shcheglovitov et al., 2012). Because divalent cations often compete with each other and protons for binding to the histidine imidazole ring, one of our aims was to assess how changes in the ionic conditions or histidine modification influence  $Zn^{2+}$ -induced modulation. As illustrated in Fig. 7, A–D and Table S2, reducing the concentration of  $Ca^{2+}$  (from 4 to 2 mM) or moderate acidification

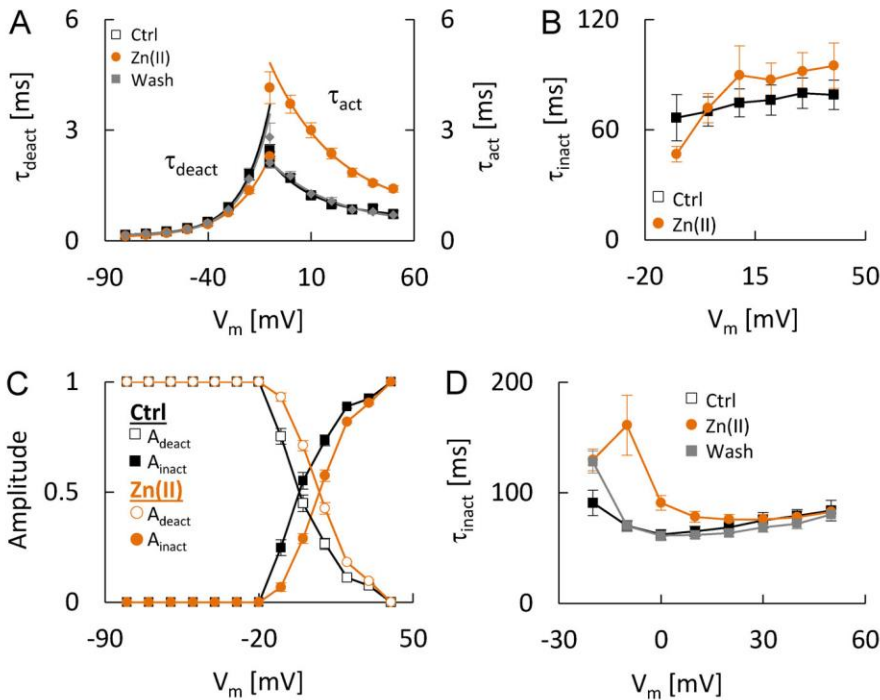


**Figure 4. Effects of Zn<sup>2+</sup> on macroscopic activation, deactivation, and inactivation kinetics.** (A) Activation (right) and deactivation (left) time-constants, determined from exponential fits to I-V or II-V currents carried by 4 mM free Ca<sup>2+</sup> and recorded before (black squares), during (orange circles), and after (gray diamonds) application of 5.4 μM free Zn<sup>2+</sup> at pH = 7.4. Note that deactivation time-constants reflect a weighted τ comprising fast and intermediate components of tail-current decay. (B) Inactivation time constants determined from exponential fits to II-V current decay at the indicated test potentials in the absence (black squares) and presence (orange circles) of 5.4 μM Zn<sup>2+</sup> (same cells as in A). (C) Contribution of deactivation (open symbols) and inactivation (filled symbols) to total II-V current decay in the absence (black squares) and presence (orange circles) of 5.4 μM Zn<sup>2+</sup> (same cells as in A and B). (D) Inactivation time constants, determined from exponential fits to the decaying phase of currents recorded during 400-ms voltage steps to the indicated test potentials before (open squares), during (orange circles), and after (gray squares) application of 5.4 μM Zn<sup>2+</sup>.

(from pH 7.4 to 7.0) significantly increased or decreased, respectively, the changes in activation voltage dependence and kinetics produced by 5.4 μM Zn<sup>2+</sup>, suggesting that Ca<sup>2+</sup> and protons both counteract the effects of Zn<sup>2+</sup> on gating. The pH

reduction also significantly slowed and shifted activation under control conditions (Table 1), indicating that protonation of residues in the Zn<sup>2+</sup> site could produce gating effects similar to Zn<sup>2+</sup> binding.

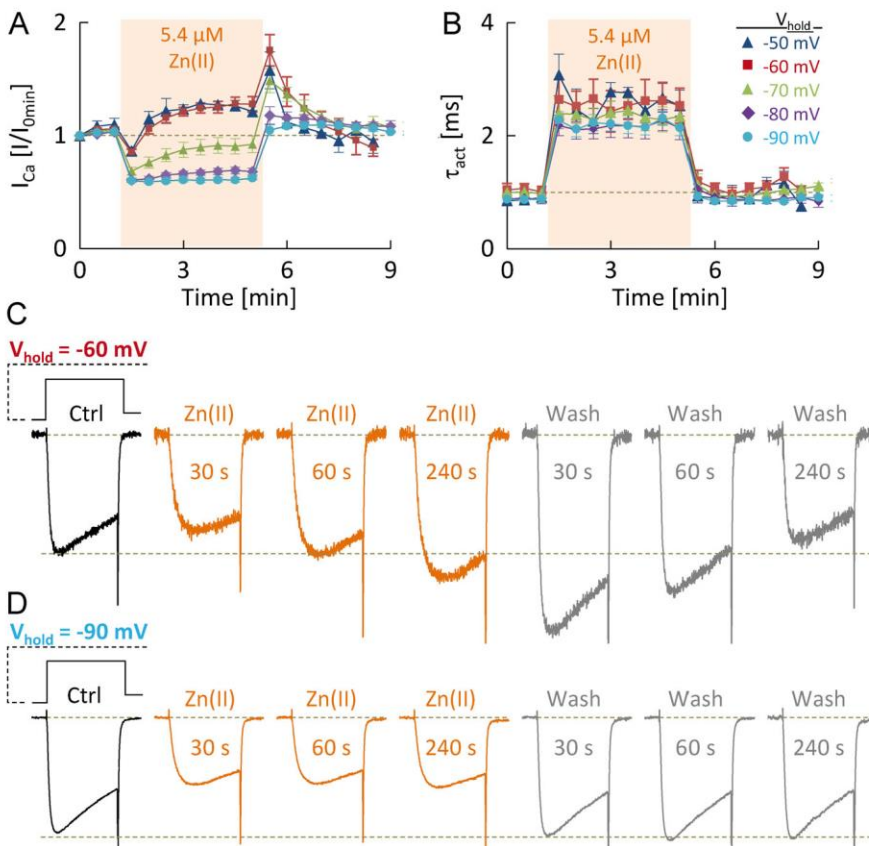


**Figure 5. Kinetics of Zn<sup>2+</sup>-induced modulation at different holding potentials.** (A) Time course of Zn<sup>2+</sup>-induced changes in peak currents carried by 4 mM free Ca<sup>2+</sup> and evoked by voltage steps to 10 mV from the indicated holding potentials (*n* = 6–9 cells per holding potential). (B) Time course of Zn<sup>2+</sup>-induced changes in activation time constants determined in the same cells as in A. (C) Mean current traces recorded at the indicated time points before, during, and after Zn<sup>2+</sup>-application from a holding-potential of -60 mV (*n* = 8 cells). (D) Mean current traces recorded as in B but from a holding potential of -90 mV (*n* = 8 cells).



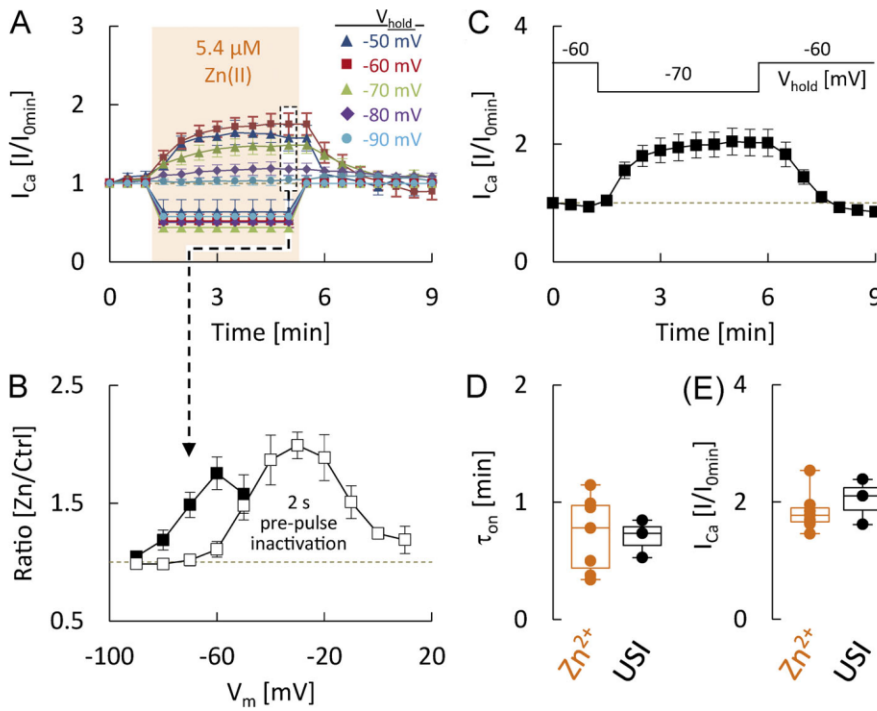


**Figure 6. Zn<sup>2+</sup>-induced stimulation and the role of ultraslow inactivation gating.** (A) Time course and degree of stimulation (top) and suppression (bottom) during application of 5.4 μM free Zn<sup>2+</sup> at different holding potentials after separation of the opposing effects as described in the text (same cells as in Fig. 5). (B) Comparison of the relative Zn<sup>2+</sup>-induced increase of currents at 10 mV determined from the data in Fig. 2 F (i.e., after 2-s prepulses at the indicated test potentials, open squares) or A (i.e., 240 s after addition of Zn<sup>2+</sup> at the indicated holding potentials, black squares). (C) Slow holding potential-dependent recovery from and development of inactivation induced by switching the holding potential from -60 mV to -70 mV and back to -60 mV in the absence of trace metal ions (*n* = 3 cells). (D) Comparison of time constants determined by exponential fits to the development of Zn<sup>2+</sup>-induced stimulation at a holding potential of -60 mV in A (Zn<sup>2+</sup>, orange) or to the recovery from holding potential-dependent inactivation in C (USI, black). (E) Comparison of the magnitude of current increase during Zn<sup>2+</sup>-induced stimulation at a holding potential of -60 mV (Zn<sup>2+</sup>, orange) and during recovery from holding potential-dependent inactivation (USI; black).

Pretreatment with the histidine-modifying agent DEPC almost completely prevented the Zn<sup>2+</sup>-induced shift (Fig. 7 C) and slowing (Fig. 7, B and D), confirming that both effects are related to interaction with histidine residues, presumably located in the proposed metal ion binding site. In addition, DEPC produced gating effects opposite to those exerted by Zn<sup>2+</sup> and selectively stimulated Ca<sub>v</sub>2.3 channel activation in the absence of trace metal ions, as reflected in a significant shift of the activation

curve by ~9 mV toward more negative test potentials and accelerated activation kinetics under control conditions (Table 1).

Finally, DEPC pretreatment also prevented the Zn<sup>2+</sup>-induced increase of the activation slope factor (Fig. 7 E), but several observations indicated that the underlying mechanism may differ from that mediating the shift and slowing. First, pH reduction reproduced the other gating effects of Zn<sup>2+</sup> as described above but had no effect on the slope of the activation

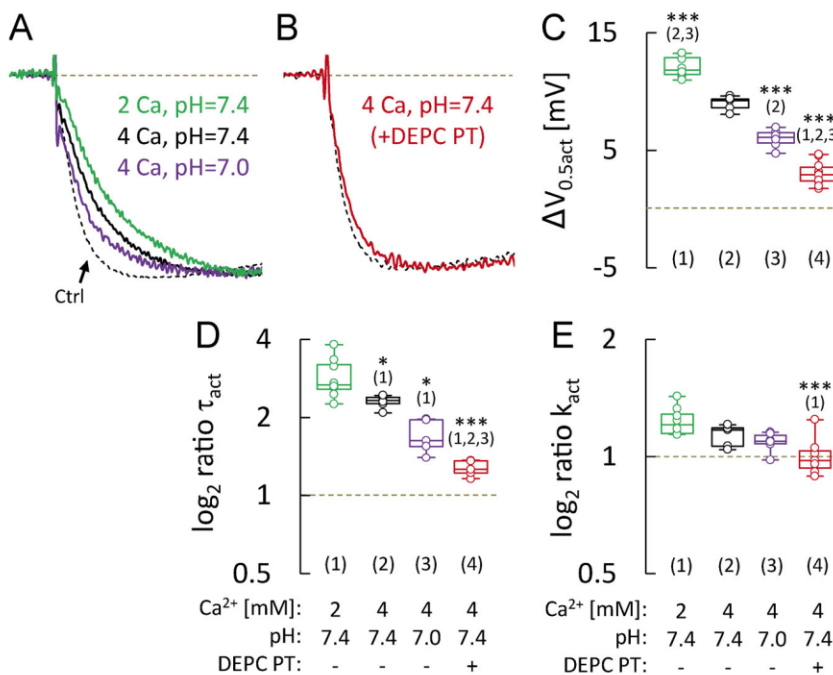


**Figure 7. Dependence of Zn<sup>2+</sup> effects on extracellular Ca<sup>2+</sup> concentration, pH, and histidine residues.** (A–E) Comparison of normalized mean current traces (A and B) and changes in half-activation voltage ( $V_{0.5act}$ ; C), activation time constants at 10 mV ( $\tau_{act}$ ; D), and activation slope factor ( $k_{act}$ ; E) produced by application of 5.4 μM free Zn<sup>2+</sup> under the experimental conditions indicated below (*n* = 5–8 cells per experimental condition). \*, *P* < 0.05; \*\*\*, *P* < 0.001 (one-way ANOVA with Bonferroni post hoc test). DEPC PT, DEPC pretreatment.



under control conditions (Table 1). Second, manipulation of the  $\text{Ca}^{2+}$  concentration or of the pH of the extracellular solution significantly altered the other gating effects of  $\text{Zn}^{2+}$  (Fig. 7, A–D) but had no effect on the  $\text{Zn}^{2+}$ -induced changes in  $k_{\text{act}}$  (Fig. 7 E). Third, while DEPC pretreatment produced effects opposite to the shift and slowing, it reproduced  $\text{Zn}^{2+}$ -induced changes in the slope of the activation curve, as reflected in a significant increase of  $k_{\text{act}}$  in pretreated cells under control conditions (Table 1).

### Concentration dependence of $\text{Zn}^{2+}$ -induced gating changes

To further corroborate and extend the above findings, we performed additional experiments with a wide range of free  $\text{Zn}^{2+}$  levels. Fig. 8 A, Fig. 9 A, and Fig. 10 A show concentration-response curves, which were constructed by plotting the indicated  $\text{Zn}^{2+}$ -induced gating changes as a function of the logarithm of the free  $\text{Zn}^{2+}$  concentration and fitted with one (Eq. 4a) or a combination of two (Eq. 4b) sigmoid saturation curves. Best-fit values and CIs for apparent dissociation constants ( $K_{\text{Zn}}$ ) and  $E_{\text{max}}$  values obtained under the different experimental conditions are summarized below each plot (Fig. 8, B and C; Fig. 9, B and C; and Fig. 10, B and C) and in Table S4.

### Micromolar $\text{Zn}^{2+}$ concentrations slow and shift by multiple mechanisms

The concentration-response curves for the  $\text{Zn}^{2+}$ -induced shift in activation voltage dependence were clearly biphasic under all experimental conditions examined, revealing the existence of two separable components with vastly different affinities (Fig. 8). They could be well described by a combination of two simple saturation curves with Hill slopes of 1 (Eq. 4b), indicating that  $\text{Zn}^{2+}$  may exert its effects through interaction with at least two independent sites. The concentration dependence for changes in inactivation voltage dependence (not shown, but see Table S4) and for the (shift-corrected)  $\text{Zn}^{2+}$ -induced slowing (Fig. 9) had a very similar overall appearance, comprising both high- and low-affinity components. On the other hand, effects on the slope of the activation curve showed a less complex dependence on  $\text{Zn}^{2+}$  concentration that could be well described by a single saturation curve (Fig. 10; Eq. 4a). To better delineate the various effects and their differential dependence on  $\text{Zn}^{2+}$  concentration, Fig. 11 A compares high- and low-affinity  $K_{\text{Zn}}$  values for shift and slowing and the  $K_{\text{Zn}}$  value for changes in the slope of the activation curve obtained with 4 mM free  $\text{Ca}^{2+}$  (pH 7.4). It can be seen that there was no significant difference between the  $K_{\text{Zn}}$  values for high-affinity shift and slowing, supporting the notion that both effects reflect  $\text{Zn}^{2+}$  binding to a common site. To obtain a single apparent dissociation constant, we simultaneously refitted the effects on channel voltage dependence and kinetics with a global  $K_{\text{Zn}}$  value for the high-affinity component (high-affinity 1 in Fig. 11 A) and all other parameters fixed to the values shown in Table S4. The  $\text{Zn}^{2+}$  concentration for half-maximal shift and slowing thus obtained for recordings performed with 4 mM  $\text{Ca}^{2+}$  was 4.4  $\mu\text{M}$ , with an 84% CI ranging from 4.2 to 4.6  $\mu\text{M}$  (Fig. 11, A and B; and Table S5). Under the same experimental conditions, the apparent  $K_{\text{Zn}}$  value was approximately four times higher for effects on the slope of the

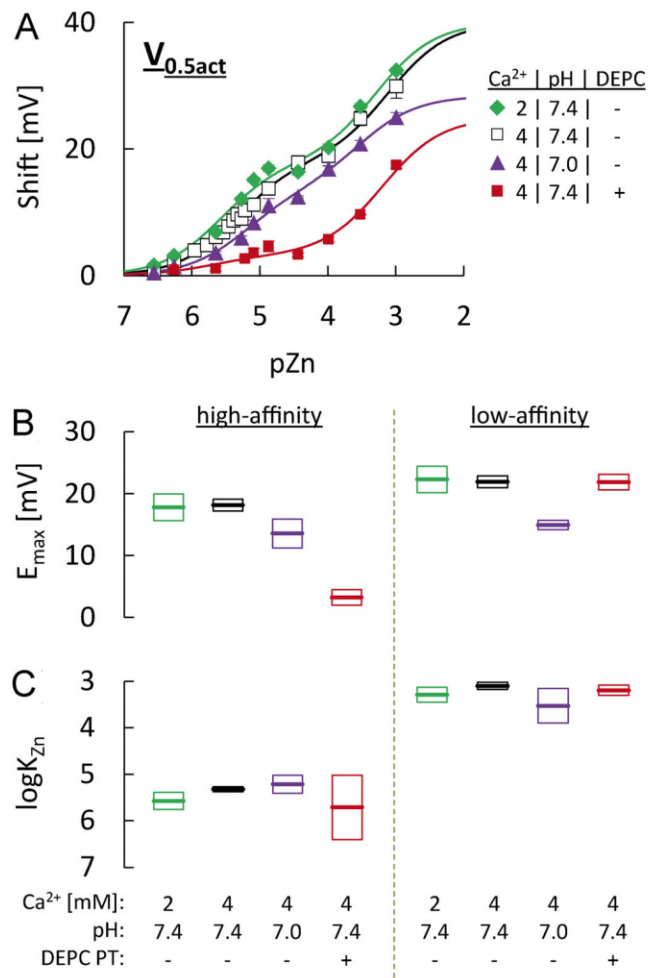
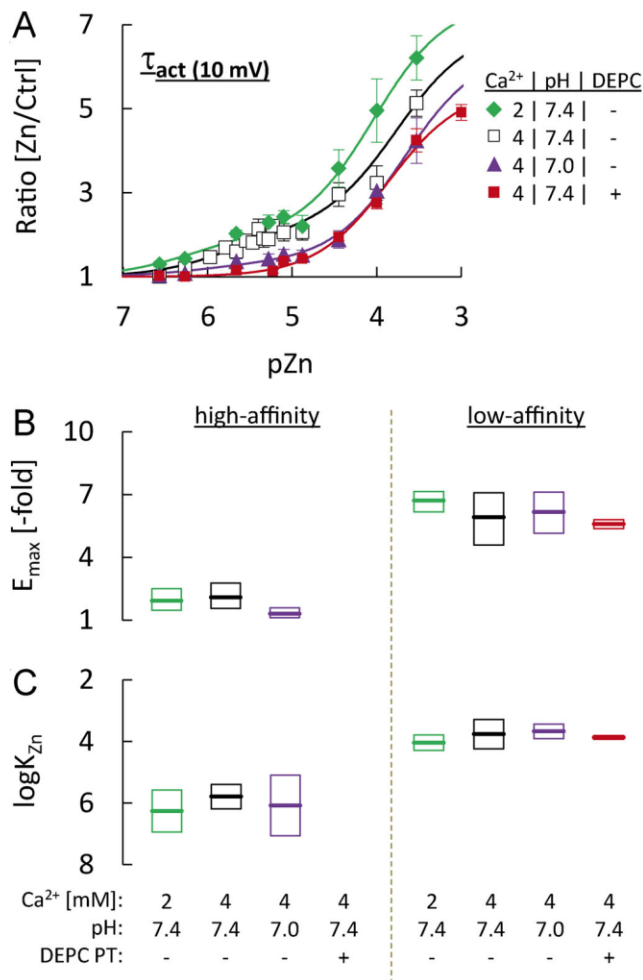


Figure 8. **Concentration dependence for  $\text{Zn}^{2+}$  effects on activation voltage dependence.** (A) Concentration dependence for the shift in half-activation voltage ( $V_{0.5\text{act}}$ ) determined with 4 mM free  $\text{Ca}^{2+}$  as the charge carrier at pH 7.4 without (open squares,  $n = 5\text{--}12$  cells per  $\text{Zn}^{2+}$  concentration) or with DEPC pretreatment (red squares,  $n = 5\text{--}11$  cells per  $\text{Zn}^{2+}$  concentration), 2 mM free  $\text{Ca}^{2+}$  as the charge carrier at pH 7.4 (green diamonds,  $n = 5\text{--}8$  cells per  $\text{Zn}^{2+}$  concentration), or 4 mM free  $\text{Ca}^{2+}$  as the charge carrier at pH 7.0 (purple triangles,  $n = 5\text{--}11$  cells per  $\text{Zn}^{2+}$  concentration). Solid lines are the combination of two binding isotherms for simple bimolecular reactions. (B and C) Extrapolated maximum shift ( $E_{\text{max}}$ ; B) and logarithm of apparent dissociation constants ( $\log K_{\text{Zn}}$ ; C) for the high-affinity (left) and low-affinity (right) components obtained from fits to the data in A. Shown are best-fit values and 84% CIs.

activation curve (high-affinity 2 in Fig. 11, A and C; and ratio  $k_{\text{act}}$  in Table S4), >40 times higher for the low-affinity slowing (low-affinity 1 in Fig. 11, A and D; and low-affinity ratio  $\tau_{\text{act}}$  in Table S4), and ~200 times higher for the low-affinity shift in channel voltage dependence (low-affinity 2 in Fig. 11, A and E; and low-affinity  $\Delta V_{0.5\text{act}}$  and  $\Delta V_{0.5\text{inact}}$  in Table S4), indicating that there are either multiple  $\text{Zn}^{2+}$  sites and/or differences in the coupling between  $\text{Zn}^{2+}$  binding and its various functional consequences.

### Hallmarks of high-affinity shift and slowing

Pretreatment with DEPC completely eliminated the high-affinity slowing (Fig. 9) and significantly decreased the maximum shift



**Figure 9. Concentration dependence for Zn<sup>2+</sup> effects on activation kinetics.** (A) Concentration dependence for the slowing of activation time constants at 10 mV ( $\tau_{act(10mV)}$ ) determined with 4 mM free Ca<sup>2+</sup> as the charge carrier at pH 7.4 without (open squares,  $n = 5-12$  cells per Zn<sup>2+</sup> concentration) or with DEPC pretreatment (red squares,  $n = 5-11$  cells per Zn<sup>2+</sup> concentration), 2 mM free Ca<sup>2+</sup> as the charge carrier at pH 7.4 (green diamonds,  $n = 5-8$  cells per Zn<sup>2+</sup> concentration) or 4 mM free Ca<sup>2+</sup> as the charge carrier at pH 7.0 (purple triangles,  $n = 5-11$  cells per Zn<sup>2+</sup> concentration). Solid lines are the combination of two binding isotherms for simple bimolecular reactions. (B and C) Extrapolated maximum slowing ( $E_{max}$ ; B) and logarithm of apparent dissociation constants ( $\log K_{Zn}$ ; C) for the high-affinity (left) and low-affinity (right) components obtained from fits to the data in A. Shown are best-fit values and 84% CIs.

mediated by the high-affinity component, which produced, at most, a 3-mV shift (Fig. 8) in pretreated cells. Based on these two findings, DEPC pretreatment antagonized high-affinity Zn<sup>2+</sup> binding noncompetitively, which is consistent with a disruption of the putative metal binding site by irreversible carbethoxylation of one or more histidine residues.

Reducing the concentration of Ca<sup>2+</sup> or moderate acidification significantly decreased or increased respectively, the global apparent  $K_{Zn}$  value for high-affinity shift and slowing (Fig. 8, Fig. 9, and Fig. 11 B; and Table S5), supporting the notion that there is competition for binding among Zn<sup>2+</sup>, Ca<sup>2+</sup>, and protons. In addition, the increase in proton concentration was associated

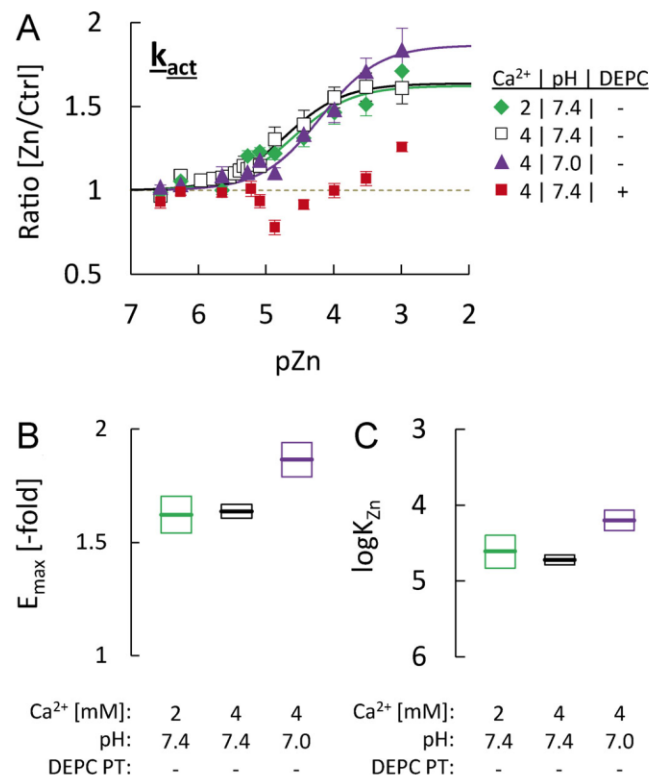


**Figure 10. Concentration dependence for Zn<sup>2+</sup> effects on activation voltage sensitivity.** (A) Concentration dependence for the increase in activation slope factor ( $k_{act}$ ) determined under the experimental conditions indicated on the right (same cells as in Fig. 8). Solid lines are binding isotherms for a simple bimolecular reaction. (B and C) Extrapolated maximum increase ( $E_{max}$ ; B) and logarithm of apparent dissociation constants ( $\log K_{Zn}$ ; C) obtained from fits to the data in A. Shown are best-fit values and 84% CIs.

with a significant decrease of the  $E_{max}$  values for high-affinity shift and slowing (Fig. 8, Fig. 9, and Fig. 11 B). The latter could only partly be accounted for by the moderate gating effects of pH reduction observed under control conditions (~2-mV shift and 1.2-fold slowing; Table 1), suggesting that protonation of the high-affinity site is either less effective than Zn<sup>2+</sup>-binding in altering channel gating (i.e., protons could act as weak partial agonists, possibly due to their lower charge) or that protons also reduce Zn<sup>2+</sup> binding noncompetitively.

On the other hand, reducing the Ca<sup>2+</sup> concentration had no clear effects on the maximum gating changes mediated by high-affinity binding (Fig. 8, Fig. 9, and Fig. 11 B) or activation gating under control conditions (Table 1), suggesting that Ca<sup>2+</sup> acts as competitive antagonist that binds to the high-affinity site and displaces Zn<sup>2+</sup> ions without altering channel gating.

DEPC pretreatment also prevented and partly reversed the direction of changes in  $k_{act}$ , but this effect differed from the shift and slowing in that it was completely unaffected by changes in the concentration of Ca<sup>2+</sup> (Fig. 10 and Fig. 11 C). It was also more sensitive to moderate acidification, which significantly increased the apparent dissociation constant for effects on  $k_{act}$  approximately threefold but also significantly increased the  $E_{max}$  (Fig. 10, B and C).



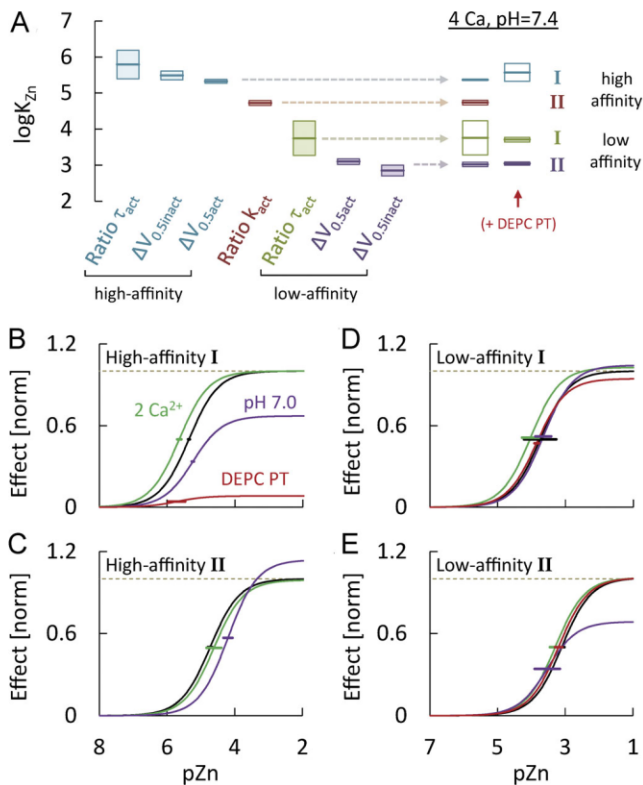


**Figure 11. Concentration dependencies for high- and low-affinity Zn<sup>2+</sup>-induced gating effects.** (A) Comparison of best-fit logK<sub>Zn</sub> values and confidence limits for the indicated gating changes obtained in recordings with 4 mM Ca<sup>2+</sup> at pH 7.4. Note that some of the values shown on the right were obtained by globally fitting the high-affinity shift and slowing (high-affinity I) or the low affinity shift (low-affinity II) with shared K<sub>Zn</sub> values as described in the text. (B) Concentration–response curves, reconstructed from best-fit values obtained by globally fitting the changes in channel voltage dependence ( $\Delta V_{0.5act}$ ,  $\Delta V_{0.5inact}$ ) and kinetics (Ratio  $\tau_{act}$ ) under the indicated conditions with a single, shared K<sub>Zn</sub> for the high-affinity component and all other values fixed to the values shown in Table S4. For comparison, the extrapolated E<sub>max</sub> values were normalized by the E<sub>max</sub> values observed with 4 mM Ca<sup>2+</sup> at pH 7.4 (black line). (C–E) Concentration–response curves reconstructed from best-fit values for the changes in activation slope factor (Ratio  $k_{act}$ ; C), the low-affinity changes in activation kinetics (Ratio  $\tau_{act}$ ; D), and the low-affinity changes in channel voltage dependence (E). For comparison, the extrapolated E<sub>max</sub> values were normalized as in B.

**Low-affinity shift and slowing have distinct concentration dependencies**

Low-affinity shift and slowing were much less affected by DEPC pretreatment (Fig. 8, Fig. 9, and Fig. 11, D and E; and Table S4), suggesting that histidine residues are not involved in these effects. The apparent K<sub>Zn</sub> value for the shift obtained in recordings performed with 4 mM Ca<sup>2+</sup> was 790 μM (CI, 660–950 μM), which is significantly higher than the K<sub>Zn</sub> value for low-affinity slowing of 180 μM (CI, 60–530 μM). For comparison, the corresponding values after pretreatment with DEPC were 640 μM (CI, 500–820 μM) for the low-affinity shift and 140 μM (CI, 120–160 μM) for the low-affinity slowing, respectively (Fig. 11 A). The two effects were also differently affected by moderate acidification, which significantly reduced the K<sub>Zn</sub> and E<sub>max</sub> values for low-affinity shift (Fig. 8 and Fig. 11 E), but not slowing

(Fig. 9 and Fig. 11 D). Reducing the concentration of Ca<sup>2+</sup> affected neither the low-affinity shift nor the low-affinity slowing (Fig. 8, Fig. 9, and Fig. 11, D–E). Taken together, these findings are in good agreement with previous studies showing that Zn<sup>2+</sup> and other d-block metal ions slow activation, often without altering channel voltage dependence, in several VGCCs lacking critical histidine residues in domain I (Magistretti et al., 2001, 2003; Castelli et al., 2003; Park et al., 2015). Interestingly, most of these studies also found a less marked but significant metal-induced slowing of I<sub>Ca</sub> deactivation speed (Magistretti et al., 2003; Castelli et al., 2003), an effect that was also observed in the present study (Fig. 12). Under normal conditions (i.e., 2 or 4 mM Ca<sup>2+</sup>, pH 7.4), a clear slowing was only visible at the highest free Zn<sup>2+</sup> concentrations examined (Fig. 12 B), most likely because the Zn<sup>2+</sup>-induced depolarizing shift tended to accelerate deactivation at a given test potential, thereby counteracting and masking any potential slowing. Thus, as illustrated in Fig. 12, A and B, the deactivation slowing became much more pronounced and evident already at low micromolar Zn<sup>2+</sup> levels after DEPC pretreatment and, to some extent, pH reduction, both of which strongly reduced the shift in channel voltage dependence.

**Concentration dependence of Zn<sup>2+</sup>-induced changes in permeation**

While the site of action for high-affinity shift and slowing of Ca<sub>v</sub>2.3 channel currents by Zn<sup>2+</sup>, Ni<sup>2+</sup>, and Cu<sup>2+</sup> is relatively well established, much less is known about the location of additional, lower-affinity sites for d-block metal ions, which appear to be present in most or all high-voltage activated (HVA) Ca<sup>2+</sup> channels (Neumaier et al., 2015). Since all of these cations can more or less effectively obstruct the ion-conducting pore, and Ca<sup>2+</sup> channel gating is well known to be influenced by the permeability of charge-carrying ions, it has been proposed that the slowing is independent of the time course and voltage dependence of pore block per se (i.e., not a consequence of time- and voltage-dependent unblock during the test pulses) but related to an allosteric modification of channel gating, induced by binding of metals to their blocking site (Castelli et al., 2003). Block of single HVA Ca<sup>2+</sup> channels has been shown to occur on a rapid timescale (Winegar et al., 1991), so that II-V current suppression should provide a reasonable measure for the degree of pore block. To assess the apparent voltage dependence of Ca<sub>v</sub>2.3 channel block by Zn<sup>2+</sup>, we therefore determined apparent K<sub>Zn</sub> values for II-V current suppression and plotted them as a function of the test potential (Fig. 13, A and B; but see below). As a simple voltage-independent measure for the degree of “instantaneous” block, we also quantified Zn<sup>2+</sup> effects on II-V currents in terms of the slope conductance between –40 and +20 mV (G<sub>II-V</sub>; Fig. 13 C and Table S4). Finally, for comparison with previous work, the degree of “steady-state” block measured with the I-V protocol was quantified based on changes in G<sub>max</sub> (Table S4).

Although the concentration dependencies exhibited some clear discontinuities at intermediate Zn<sup>2+</sup> concentrations, they could be reasonably well approximated by a combination of two simple saturation isotherms, the best-fit values of which are



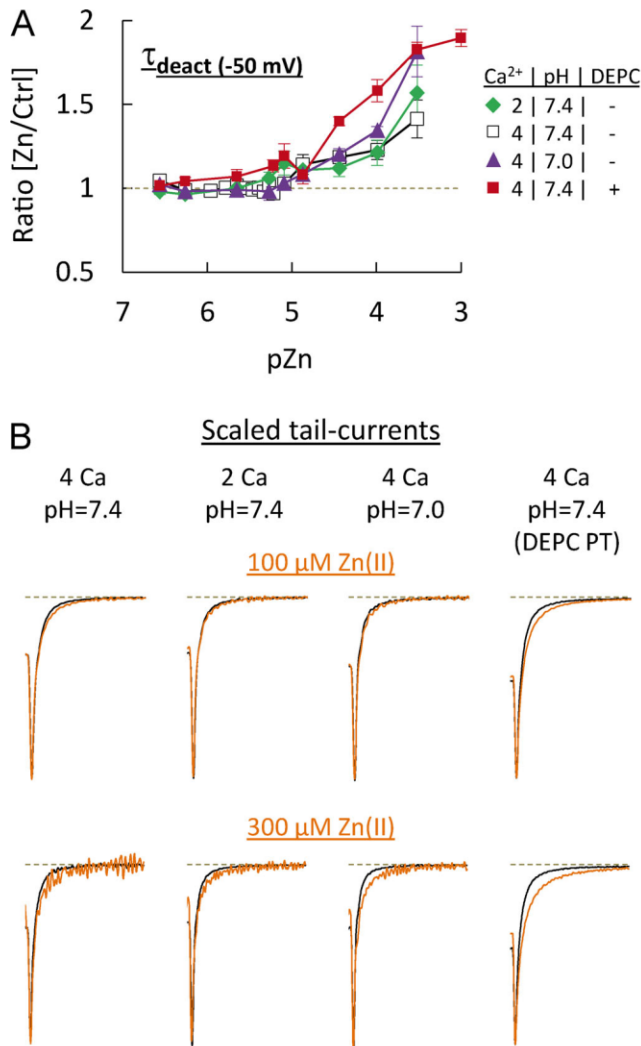


Figure 12. **Concentration dependence for Zn<sup>2+</sup> effects on tail-current kinetics.** (A) Concentration dependence for the increase in deactivation time-constants at -50 mV ( $\tau_{deact(-50\text{ mV})}$ ), determined under the experimental conditions indicated on the right (same cells as in Fig. 9). (B) Mean tail-current traces recorded under the experimental conditions indicated above in the absence (black) and presence (orange) of 100  $\mu\text{M}$  (top) or 300  $\mu\text{M}$  (bottom) free Zn<sup>2+</sup>. They have been scaled to their maximum amplitude to highlight kinetic changes.

shown in Table S4 and described in more detail in the following sections.

**High-affinity binding to histidine residues may also affect conduction**

Apparent dissociation constants for high-affinity II-V current suppression showed no clear dependence on the test potential and could be well described with a single, shared  $K_{Zn}$  value of 16  $\mu\text{M}$  (CI, 14–20  $\mu\text{M}$ ; Fig. 13 A, right), which is in good agreement with the high-affinity  $K_{Zn}$  value 12  $\mu\text{M}$  (CI, 9–17  $\mu\text{M}$ ; Table S4) obtained when the effects were quantified in terms of changes in  $G_{II-V}$ . Suppression mediated by high-affinity binding was incomplete at all test potentials examined (Fig. 13 B), indicating that it is not related to physical obstruction of the ion-conducting pore. In addition, its contribution to total

Neumaier et al.

Complex Zn<sup>2+</sup> effects on Ca<sub>v</sub>2.3 channel function

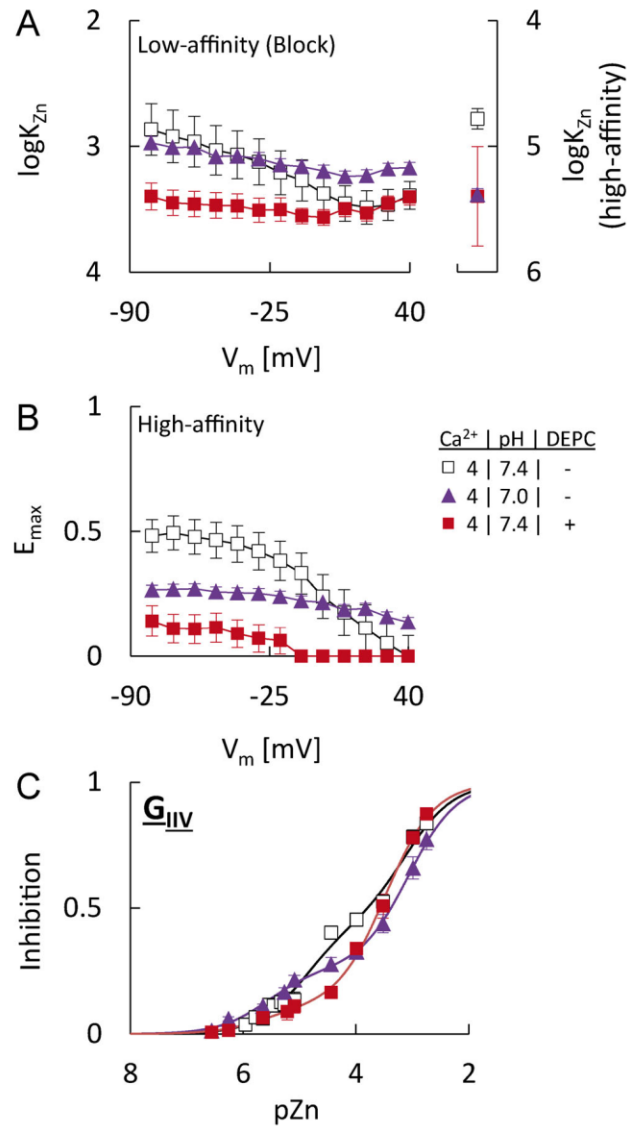


Figure 13. **Voltage and concentration dependence for Zn<sup>2+</sup> effects on instantaneous (II-V) currents.** (A) Voltage dependence of the logarithm of apparent dissociation constants ( $\log K_{Zn}$ ) for low-affinity Zn<sup>2+</sup>-induced suppression/block of II-V currents under the conditions indicated in B. Also shown in the middle are the voltage-independent  $\log K_{Zn}$  values for the high-affinity component of II-V current suppression. Note the different scaling of the vertical axis. (B) Maximum suppression of II-V currents mediated by the high-affinity component. (C) Concentration dependence of II-V current suppression quantified in terms of the slope conductance between -40 and 20 mV ( $G_{II-V}$ ).

suppression was sensitive to acidification or DEPC pretreatment (Fig. 13 B), suggesting an involvement of histidine residues and possibly other protonation sites. However, while slower activation and faster deactivation due to the Zn<sup>2+</sup>-induced gating changes may have contributed to a scaling down of instantaneous currents, high-affinity II-V current suppression per se could not be explained by the shift and slowing alone, since it was most prominent at Zn<sup>2+</sup> concentrations where activation at the prepulse voltage was still complete in under 10 ms (which was the duration of the activating prepulse). In addition, the corresponding  $K_{Zn}$  value was significantly higher than the  $K_{Zn}$

Downloaded from https://jgp.physiology.org/ at University of California, San Diego on June 20, 2020

for shift and slowing but almost identical to that for the changes in  $k_{act}$  (Table S4; see also next section), possibly pointing to a common site of action.

### Evidence for a link between pore block and low-affinity changes in gating

$K_{Zn}$  values for low-affinity II-V current suppression were much higher and exhibited a shallow voltage dependence matching the expectations for  $Ca^{2+}$  channel block by d-block metal ions (Fig. 13 A). For example, under our standard recording conditions, the logarithm of the  $K_{Zn}$  values between  $-80$  and  $10$  mV could be well described by a straight line  $K_{Zn}(V_m) = 443 \times \exp(-0.015 \times V_m)$ , indicating that block decreased approximately e-fold per 77 mV with hyperpolarization. In the context of a model where blocking  $Zn^{2+}$  ions enter the electric field (compare Woodhull, 1973), the intercept of the line should provide the zero-voltage  $K_{Zn}$  value ( $443 \mu M$ ; CI, 299–592) and the slope should be equal to  $z\delta F/RT$ , where  $z$  is blocker valence (i.e., +2 for  $Zn^{2+}$ ) and  $\delta$  is the fraction of the voltage drop at the blocking site. The value of  $\delta = 0.19$  obtained from the above equations corresponds to a blocking site located at  $\sim 20\%$  of the potential drop from the membrane surface, which is in good agreement with previous findings on the voltage dependence of  $Zn^{2+}$  block in native HVA  $Ca^{2+}$  channels (Winegar et al., 1991). At test potentials more depolarized than  $10$  mV however, block started to decrease with depolarization, indicating that the voltage dependence is more complex. Moreover, DEPC pretreatment or moderate acidification increased or decreased, respectively, the  $Zn^{2+}$  affinity at zero voltage, while both reduced the apparent voltage dependence of block (Fig. 13 A). A more important observation is illustrated in Fig. 14, which compares  $\log K_{Zn}$  values for the various  $Zn^{2+}$ -induced gating changes (left) with those for block at  $-50$  mV (i.e., the test potential where tail currents for activation curves were determined) or  $10$  mV (i.e., the test potential where the activation slowing was quantified) and that for high-affinity (voltage-independent) suppression of II-V currents. It can be seen that  $K_{Zn}$  values for low-affinity shift and slowing were not significantly different from the  $K_{Zn}$  values for block at  $-50$  mV or  $10$  mV, respectively. Hence, while the low-affinity gating effects could clearly not be accounted for by the shallow voltage dependence of block per se, it seems conceivable that they could be linked to occupation of the blocking site by  $Zn^{2+}$ . Also note that, as described in the preceding section, the voltage-independent  $K_{Zn}$  value for high-affinity II-V current suppression was almost identical to that obtained for the  $Zn^{2+}$ -induced changes in  $k_{act}$ .

### A Markov model of $Ca_v2.3$ channel gating in the absence of trace metals

To better resolve and separate specific effects of  $Zn^{2+}$  on channel gating, we developed a Markov model for  $Ca_v2.3$  channels as described below and applied a global fitting procedure, whereby the model was simultaneously fitted to the whole set of recordings obtained under control conditions ( $4$  mM  $Ca^{2+}$  at pH 7.4). Because ionic currents alone provide little information on transitions between closed states, the model was further constrained with gating currents (Fig. S2 A), recorded after blocking ion conduction by substitution of  $Ca^{2+}$  with  $Mg^{2+}$  and addition of

$200 \mu M La^{3+} + 100 \mu M EDTA$  (i.e.,  $100 \mu M$  free  $La^{3+}$ ). The total dataset used for fitting included gating currents recorded at 15 different test potentials, short I-V currents ( $25$  ms) recorded at 15 different test potentials, long I-V currents ( $400$  ms) recorded at 10 different test potentials, II-V currents recorded at 13 different test potentials, and PPI currents recorded at 14 different test potentials.

The topology of the model (Fig. 15 A) was chosen based on the following structural and functional considerations: VGCCs are heterotetrameric proteins composed of four nonidentical VSMs and a central pore region (Fig. 1 A). Optical tracking of voltage-sensor movement by voltage-clamp fluorometry (VCF) in voltage-gated sodium and calcium channels indicates that activation of the individual VSMs is probabilistic in nature and largely governed by their respective steady-state and kinetic properties (Chanda and Bezanilla, 2002; Pantazis et al., 2014). To reflect these findings, horizontal transitions in Fig. 15 A are voltage dependent and correspond to movement of the four nonidentical voltage sensors (rows 1–4 in Fig. 15 B) and pore opening or closing (row 5 in Fig. 15 B), respectively. The voltage sensors operate in parallel and are independent of each other, with one simplifying assumption as described below. The rates for voltage-dependent transitions between two states were expressed in terms of the transition-state theory and are given by

$$k_{fw} = k_{eq} \times \exp[z \times x \times (V_m - V_{eq}) \times F/RT] \quad (7a)$$

and

$$k_{bw} = k_{eq} \times \exp[-z \times (1 - x) \times (V_m - V_{eq}) \times F/RT], \quad (7b)$$

where  $k_{fw}$  and  $k_{bw}$  are the values of the forward and backward rates at the test potential  $V_m$ ,  $k_{eq}$  is the value of the forward and backward rates at the test potential  $V_{eq}$ ,  $z$  is the effective valence of the gating charge associated with the transition,  $x$  is the relative position of the energy barrier in the membrane, and  $F$ ,  $R$ , and  $T$  have their usual thermodynamic meaning (Brog-Graham, 1991).

In voltage-gated sodium channels, activation of the VSMs in domain I–III is associated with rapid charge movement and obligatorily precedes channel opening (Chanda and Bezanilla, 2002), while activation of the VSM in domain I–V is correlated with a slow component of charge movement and gives rise to a short-lived second open state that precedes inactivation (Chen et al., 1996; Capes et al., 2013; Goldschen-Ohm et al., 2013). Much less is known about VGCCs, but mutational studies (Beyl et al., 2016; García et al., 1997) and optical tracking of voltage-sensor movement by VCF (Pantazis et al., 2014; Savalli et al., 2016; Flucher, 2016) indicate that activation of two or three VSMs may be sufficient for pore opening. Consistent with these findings,  $Ca_v2.3$  channel gating currents showed a significant fraction of charge movement that was too slow to be associated with channel opening (Fig. S2 B). We tested obligatory models in which activation of 2–4 VSMs is required for channel opening and found that the whole set of ionic and gating current recordings could only be described by a model where activation of two VSMs is obligatory for channel opening, with the simplifying assumption that these VSMs activate in a specific sequence. Based on the role of the VSM that activates first for simulated  $Zn^{2+}$ -induced modulation (see next section), we have tentatively assigned these two VSMs the numbers 1 and 2, noting

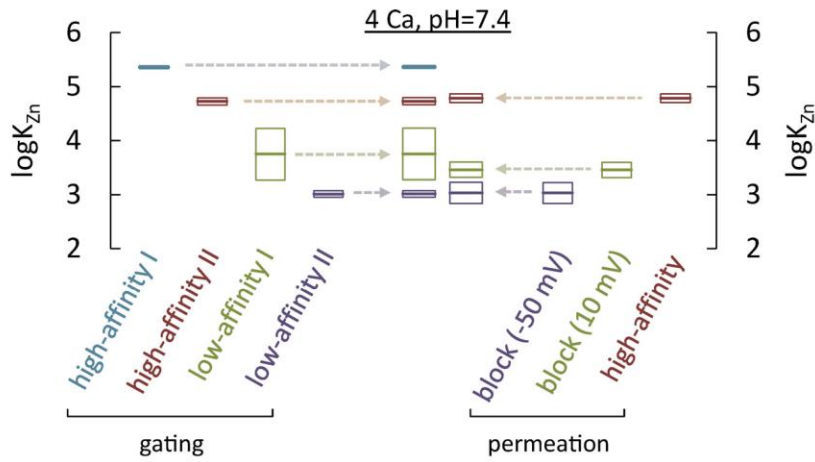


Figure 14. **Concentration dependencies for block and high-affinity suppression of II-V currents.** Comparison of best-fit  $\log K_{Zn}$  values and 84% confidence limits for the  $Zn^{2+}$ -induced high- and low-affinity gating changes (left; for definition, see Fig. 11 A) with the values obtained for the low-affinity component of II-V current suppression/block at  $-50$  mV or  $10$  mV and the high-affinity voltage-independent component of II-V current suppression (right).

that our data are not sufficient to conclusively relate them to specific protein domains (but see A model of  $Ca_v2.3$  channel gating and  $Zn^{2+}$ -induced modulation and Limitations). The resulting model has a total of four conductive states, which is consistent with experimental evidence for multiple  $Ca^{2+}$  channel open states (Fass and Levitan, 1996; Schneider et al., 1994; Nakayama and Brading, 1993). In analogy to sodium channels, the VSMs not obligatory for channel opening have been proposed to play a role for coupling of activation to voltage-

dependent inactivation (Pantazis et al., 2014; Flucher, 2016), a process that has been shown or is thought to be state rather than truly voltage dependent in VGCCs (Neumaier et al., 2015). Therefore, vertical transitions in the model are voltage independent and correspond to entry into and return from fast (Fig. 15 A, middle) and slow (Fig. 15 A, bottom) inactivated states. As the VSMs in the model could not be related to specific domains of the channel protein and data on the coupling between voltage-sensor movement and voltage-dependent inactivation is not available, the

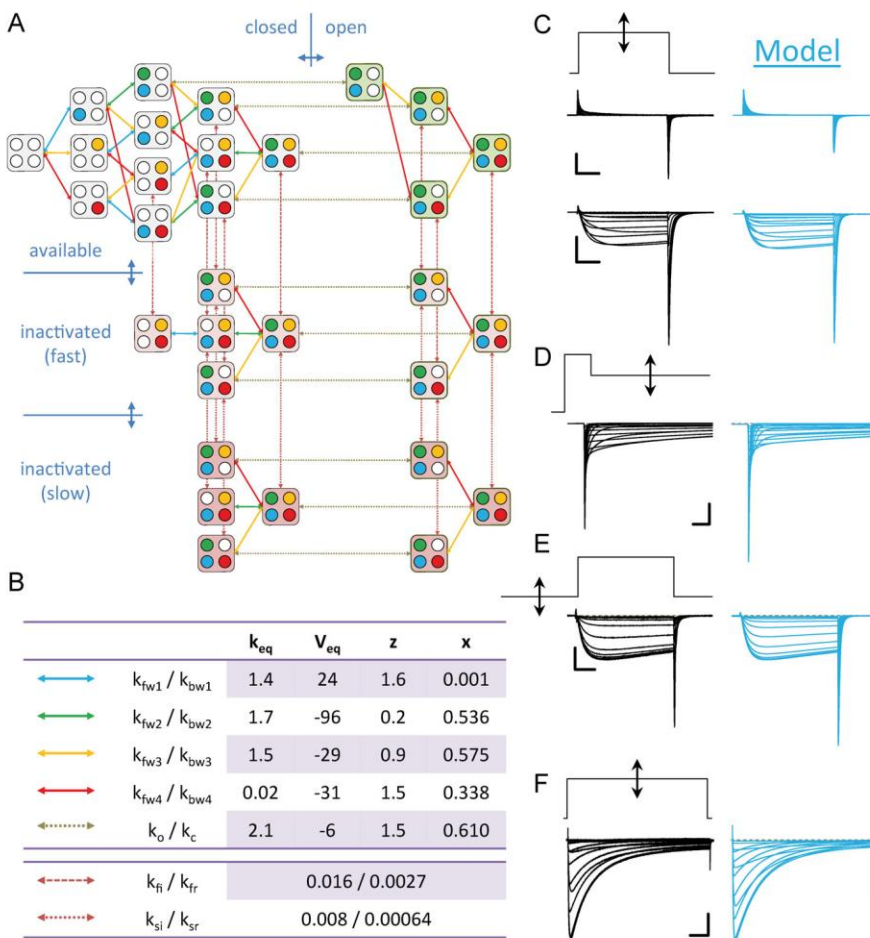


Figure 15. **A Markov model of  $Ca_v2.3$  channel gating.** (A) Topology of a Markov model that accounts for most salient features of  $Ca_v2.3$  channel gating under control conditions. Horizontal transitions are voltage dependent and correspond to movement of four nonidentical voltage sensors and channel opening or closing, with rate constants expressed in terms of the transition state theory (for details, see text). Vertical transitions are voltage independent and correspond to entry into and return from fast (middle) and slow (bottom) inactivated states. Transitions between inactivated states are identical to the parallel transitions between closed and open states. (B) Overview of individual transitions of the model and optimized parameter values obtained by globally fitting the model to the whole set of control recordings obtained with  $4$  mM  $Ca^{2+}$  at pH  $7.4$ . (C-F) Comparison of recorded (black) and simulated (turquoise) families of current traces evoked with the protocols depicted above. Source code for the model is available in ModelDB (McDougal et al., 2017) at <http://modeldb.yale.edu/261714>.



state dependence of inactivation was determined empirically by fixing fast and slow inactivation and deinactivation time constants to experimentally determined values and adding or removing inactivated states until the model reproduced both the time-course and steady-state voltage dependence of inactivation. Microscopic reversibility was imposed by defining transition rates between inactivated states as being identical to those of the (parallel) transitions between closed states.

The individual transitions of the model and optimized parameter values obtained from fits to the control recordings are listed in Fig. 15 B. Fig. 15, C-F compare recorded families of current traces evoked with the voltage protocols depicted above (black) and simulations (blue) performed with the optimized parameter values. For further comparison, the simulated currents were analyzed in the same way as the experimental data, and the results are plotted together in Fig. S3. The model accounted for all salient features of the control data, including the time course of macroscopic current activation, deactivation, and inactivation (Fig. 15, C-F); the shape and position of the I-V curve (Fig. S3 A); the relatively sharp separation between voltage-dependent activation and inactivation (Fig. S3 B); the bell-shaped voltage dependence of activation and deactivation time constants (Fig. S3 D); and the fast and slow gating current components (Fig. 15 C, top).

### Modeling the effects of Zn<sup>2+</sup> on Ca<sub>v</sub>2.3 channel gating

Lacking data from, for example, VCF, the voltage sensors in our model could obviously not be related to specific domains in the channel protein. However, preliminary tests with the model showed that only manipulation of one set of voltage-dependent transitions (i.e.,  $k_{fw1}/k_{bw1}$  in Fig. 15 B) could qualitatively reproduce the selective slowing of activation gating observed experimentally, while changes in the other transition had either little effect on activation kinetics ( $k_{fw3}/k_{bw3}$  and  $k_{fw4}/k_{bw4}$ ) or affected the deactivation kinetics in a way that was inconsistent with the experimental data ( $k_{fw2}/k_{bw2}$  and  $k_o/k_c$ ). With this in mind, we first extended our model by including Zn<sup>2+</sup> binding to a first site (site 1) with a resulting modification of voltage sensor 1 in the model to simulate the Zn<sup>2+</sup>-induced high-affinity changes in activation gating.

To this end, each state in the model was connected to a corresponding Zn-bound state, with rates for binding ( $k_{on1}$ ) and unbinding ( $k_{off1}$ ) at site 1 defined in terms of a simple, bimolecular reaction (Eq. 5a and Eq. 5b). To simulate Zn<sup>2+</sup>-induced changes in gating rates, we adopted the shift and scaling procedure first introduced by Elinder and Arhem (2003) and assumed that the rate constants for movement of voltage sensor 1 in metal-bound channels can be expressed by modification of Eq. 7a and Eq. 7b into

$$k_{fw1} = A_{off1} \times k_{eq} \times \exp [z_1 \times x_1 \times (V_m - V_{eq1} - V_{off1}) \times F/RT] \quad (8a)$$

and

$$k_{bw1} = A_{off1} \times k_{eq} \times \exp [-z_1 \times (1 - x_1) \times (V_m - V_{eq1} - V_{off1}) \times F/RT], \quad (8b)$$

where  $V_{off1}$  is a voltage offset that accounts for the electrostatic effects of a bound metal ion on the local electric field at sensor 1 and  $A_{off}$  is a slowing factor that accounts for the mechanical

Table 2. Parameters used for simulation of Zn<sup>2+</sup> effects in Figs. 16, 17, 18, and 19

Parameter	Site 1	Site 2
$K_{Zn1}$ [mM <sup>-1</sup> ]	0.003	0.1
$d_{zn}$ [mM <sup>-1</sup> ms <sup>-1</sup> ]	100	100
$A_{off}$	0.05	0.3
$V_{off}$ [mV]	50	-

effects of a bound metal ion on sensor 1 and corresponds to adding an energy barrier of  $\Delta W = kT \times \ln(A_{off}^{-1})$ .

Pore block and the low-affinity slowing of activation and deactivation were implemented by including a second, lower-affinity Zn<sup>2+</sup> blocking site, with rates for binding ( $k_{on2}$ ) and unbinding ( $k_{off2}$ ) defined as above (Eq. 5a and Eq. 5b). Channels with Zn<sup>2+</sup> bound to site 2 were assumed to be nonconductive (i.e., blocked) and their rates for opening and closing slowed by an unidentified allosteric mechanism implemented as slowing factor  $A_{off2}$ . For simplicity, block was assumed to be voltage independent and restricted to activated closed and open channel states.

Fig. 16, Fig. 17, and Fig. 18 show results from simulations for a Zn<sup>2+</sup> concentration of 5.4  $\mu$ M performed with the extended model and parameter values shown in Table 2. It can be seen that, despite the many simplifying assumptions, the model reproduced almost exactly the corresponding experimental data, with much stronger suppression of I-V versus II-V currents (Fig. 16, A and C-E), a depolarizing shift of the activation voltage dependence (Fig. 16 F), a dramatic slowing of macroscopic activation with little change in deactivation time constants (Fig. 17, A and B; and Fig. 18 A), and an apparent acceleration of tail-current decay measured with the II-V protocol at depolarized test potentials (Figs. 17 B and 18 C). In addition, simulated Zn<sup>2+</sup>-modified currents showed the same apparent slowing of inactivation kinetics near the half-activation voltage as observed experimentally (Fig. 17 A; and Fig. 18, B and D) and a similar shift of the inactivation voltage dependence (Fig. 16 F), supporting the assumption that these effects could result from activation-inactivation coupling rather than Zn<sup>2+</sup>-induced changes in the microscopic inactivation rates. The model underestimated the magnitude of II-V current suppression at low Zn<sup>2+</sup> concentrations and overestimated it at high Zn<sup>2+</sup> concentrations, which is not surprising given that we have neglected the voltage dependence of block and the high-affinity component of II-V current suppression. However, the predicted concentration dependence of I-V current suppression, quantified in terms of the  $G_{max}$ , was in good agreement with the experimental data (Fig. 16 G). Even more importantly, the model qualitatively and quantitatively reproduced the concentration dependence of Zn<sup>2+</sup> effects on activation voltage dependence (Fig. 19 A), macroscopic activation (Fig. 19 B), and deactivation kinetics (Fig. 19 D) in the range of physiologically relevant Zn<sup>2+</sup> concentrations. Interestingly, the model also reproduced the small but significant and Zn<sup>2+</sup>-concentration-dependent increase in apparent  $V_{rev}$  (Fig. 19 C), indicating that this effect was not related to true changes in,

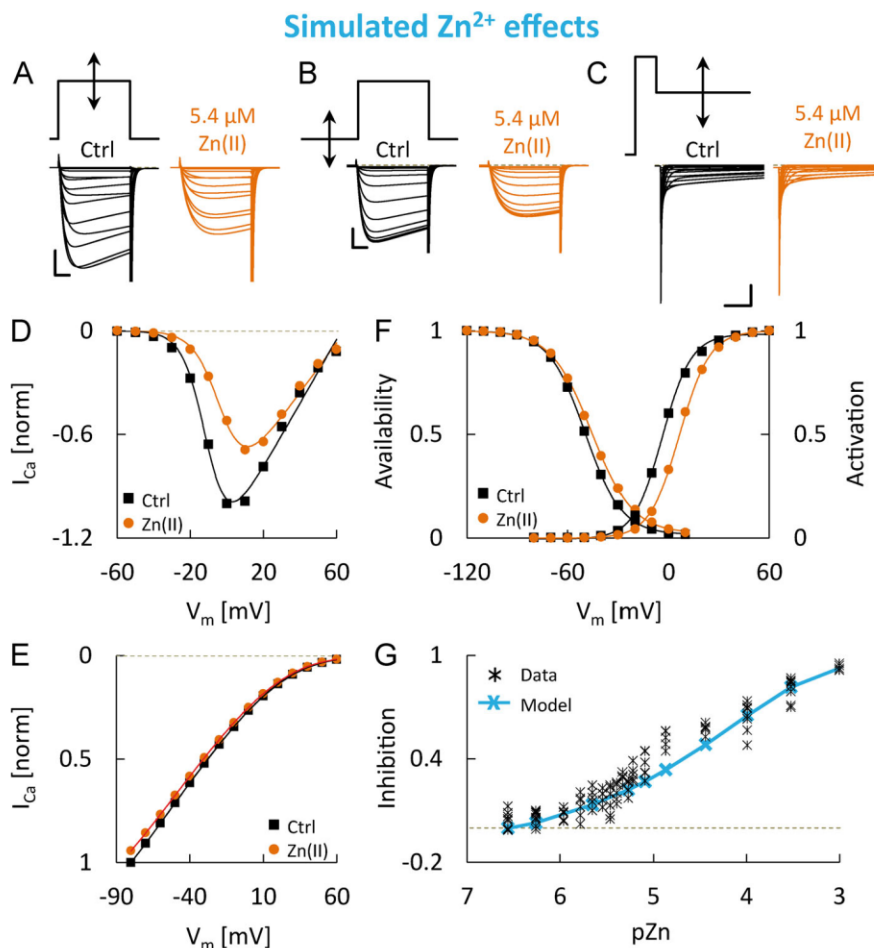


Figure 16. **Simulated Zn<sup>2+</sup> effects on Ca<sub>v</sub>2.3 channel voltage dependence.** (A–C) Families of simulated current traces evoked with the protocols depicted above (for details, see Fig. 2), with the free Zn<sup>2+</sup> concentration set to 0 (black) or 5.4 μM (orange). Scale bar corresponds to 5 ms and 20 pA/pF in A, 5 ms and 50 pA/pF in B, or 10 ms and 200 pA/pF in C. (D) I-V relationships determined from the simulated currents shown in A. (E) I-V relationships determined from the simulated currents shown in C. (F) Isochronous activation (right) and PPI (left) curves determined from the simulated tail currents in A or the simulated peak currents in B, respectively. (G) Concentration dependence of simulated Zn<sup>2+</sup>-induced suppression, quantified in terms of changes in G<sub>max</sub> of simulated currents observed when the free Zn<sup>2+</sup> concentration was increased from 0 to 1,000 μM.

for example, equilibrium potentials or selectivity and highlighting the ineptness of  $V_{rev}$  as a measure for true  $V_{rev}$  values under conditions that alter channel voltage dependence. It also qualitatively reproduced the concentration dependence of changes in inactivation voltage dependence, although it did underestimate the degree of shift (Fig. 19 E), which could reflect the arbitrary state dependence of inactivation and/or the disregard of ultraslow inactivation processes. On the other hand, the model did clearly not account for the reduced steepness of the activation curve (Fig. 19 F), even though it did predict a minor increase of  $k_{act}$  at the highest free Zn<sup>2+</sup> concentration. Taken together, this is consistent with our findings that the mechanism underlying the changes in  $k_{act}$  is somewhat different from that involved in the shift and slowing.

## Discussion

Endogenous, loosely bound Zn<sup>2+</sup> ions are increasingly recognized as potential modulators of neuronal excitability, and Zn<sup>2+</sup> dis-homeostasis has been implicated in a number of pathological conditions (Frederickson et al., 2000, 2005; Mathie et al., 2006). Owing to a high-affinity trace metal-binding site in their domain I VSM (Fig. 1 A), which is not conserved in other HVA VGCCs, Ca<sub>v</sub>2.3 channels are among the

most sensitive targets for Zn<sup>2+</sup> and certain other trace metals currently known (Kang et al., 2007; Shcheglovitov et al., 2012). Here, we performed an in-depth assessment of Zn<sup>2+</sup>-induced modulation of cloned human Ca<sub>v</sub>2.3 + β<sub>3</sub> channels over a wide range of Zn<sup>2+</sup> concentrations and used a preliminary Markov model to test whether the results can be accounted for by different biophysical mechanisms. Our most important and novel findings are (1) that low micromolar Zn<sup>2+</sup> concentrations could both inhibit or stimulate Ca<sup>2+</sup> influx through Ca<sub>v</sub>2.3 channels depending on RMP (Figs. 5 and 6); (2) that multiple high- and low-affinity mechanisms of Zn<sup>2+</sup> action exist, which can be distinguished based on their concentration dependence, sensitivity to the experimental conditions, and correlation with pore block (Figs. 7, 8, 9, 10, 11, 12, 13, and 14); and (3) that most, but not all, of the observed effects can be described by a simplified model that involves Zn<sup>2+</sup> binding to a first site with an associated electrostatic modification and mechanical slowing of one of the voltage sensors and Zn<sup>2+</sup> binding to a second, lower-affinity site, which blocks the channel and modifies the opening and closing transitions (Figs. 16, 17, 18, and 19). In the following sections, we will try to reconcile our findings with previous results and discuss potential implications with regard to the underlying sites, briefly consider our proposed model and potential (patho)physiological implications, and finally address some inherent limitations of our work.

Neumaier et al.

Complex Zn<sup>2+</sup> effects on Ca<sub>v</sub>2.3 channel function

Journal of General Physiology

https://doi.org/10.1085/jgp.202012585

17 of 25

## Simulated Zn<sup>2+</sup> effects

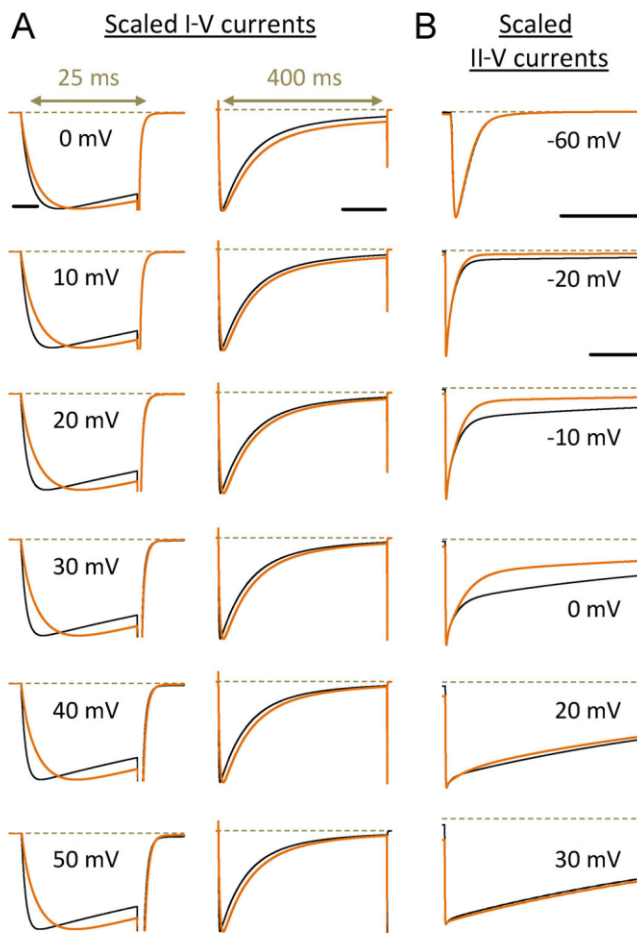


Figure 17. **Simulated Zn<sup>2+</sup> effects on the shape of macroscopic Ca<sup>2+</sup> currents.** (A) Simulated I-V current traces evoked in response to 25 ms (left) or 400 ms (right) voltage steps to the indicated test potentials, with the free Zn<sup>2+</sup> concentration set to 0 (black) or 5.4 μM (orange). They have been scaled to their maximum amplitude to highlight kinetic changes. Scale bars correspond to 10 and 100 ms for short and long voltage steps, respectively. (B) Simulated II-V current traces evoked at the indicated test potentials, with the free Zn<sup>2+</sup> concentration set to 0 (black) or 5.4 μM (orange). They have been scaled to their maximum amplitude to highlight kinetic changes. Scale bars correspond to 2 ms for the tail current at -60 mV and 10 ms for all other test potentials.

### Evidence for multiple mechanisms of Zn<sup>2+</sup> action

Various previous studies have investigated the effects of Zn<sup>2+</sup> and other trace metals on native or cloned VGCCs, all of which are thought to be more or less potently blocked by these cations. With regard to cloned Ca<sub>v</sub>2.3 channels, (sub)micromolar concentrations of Zn<sup>2+</sup>, Cu<sup>2+</sup>, and Ni<sup>2+</sup> have also been shown to produce depolarizing shifts in channel voltage dependence, a reduced sensitivity toward depolarization, and a pronounced slowing of macroscopic activation (Zamponi et al., 1996; Shcheglovitov et al., 2012; Kang et al., 2007), resembling their action on native R-type currents in cortical (Castelli et al., 2003; Magistretti et al., 2003) and dorsal root ganglion neurons (Shcheglovitov et al., 2012). Our present findings reveal that the Zn<sup>2+</sup>-induced gating changes can be separated into multiple

components with distinct concentration dependencies, which comprise a common high-affinity component for shift and slowing ( $K_{Zn} \sim 2\text{--}3 \mu\text{M}$  with 2 mM Ca<sup>2+</sup>), a second high-affinity component for the changes in activation voltage sensitivity ( $K_{Zn} \sim 15\text{--}40 \mu\text{M}$  with 2 mM Ca<sup>2+</sup>), and two lower-affinity components for shift ( $K_{Zn} > 500 \mu\text{M}$  with 2 mM Ca<sup>2+</sup>) and slowing ( $K_{Zn} \sim 50\text{--}170 \mu\text{M}$  with 2 mM Ca<sup>2+</sup>).

### High-affinity shift and slowing

To delineate effects mediated by Zn<sup>2+</sup> binding to histidine residues, we used DEPC pretreatment, which effectively prevented the high-affinity shift and slowing. This is consistent with molecular cloning studies showing that the effects of Zn<sup>2+</sup>, Cu<sup>2+</sup>, and Ni<sup>2+</sup> are all diminished by mutation of histidine residues located in the IS1-IS2 (His<sup>111</sup>) and IS3-IS4 (His<sup>179</sup> and His<sup>183</sup>) loops (Fig. 1 A; Kang et al., 2007; Shcheglovitov et al., 2012). In particular, substitution of two loop histidines has previously been shown to reduce the activation shift induced by 7 μM Zn<sup>2+</sup> from 13 mV in WT channels to 3 mV in mutant channels (with 1 mM Ca<sup>2+</sup>; Shcheglovitov et al., 2012). Considering that interpolation of our own data to the same free Zn<sup>2+</sup> concentration gives a shift of 11 or 13 mV (with 4 or 2 mM Ca<sup>2+</sup>) for untreated and 3 mV (with 4 mM Ca<sup>2+</sup>) for DEPC-treated channels, it seems justified to conclude that high-affinity shift and slowing reflect Zn<sup>2+</sup> interaction with the proposed metal binding site and that DEPC mainly acted by modification of histidine residues in the same site (but see Limitations). Moderate acidification significantly reduced apparent Zn<sup>2+</sup> affinity and maximum Zn<sup>2+</sup> effects and produced gating changes similar to Zn<sup>2+</sup> under control conditions, which is consistent with previous results showing that metal ions and protons both alter Ca<sub>v</sub>2.3 channel gating by interaction with the known loop histidines (Cens et al., 2011; Shcheglovitov et al., 2012). In view of our findings, protons could act as partial agonists that are less effective than Zn<sup>2+</sup> in altering channel gating, whereas the effects of Ca<sup>2+</sup> on apparent Zn<sup>2+</sup> affinity are consistent with a competitive antagonism.

Unexpectedly, low micromolar Zn<sup>2+</sup> concentrations also stimulated Ca<sub>v</sub>2.3 channel currents evoked from moderately depolarized holding potentials, which may have important (patho)physiological implications (see (Patho)physiological implications). Development and reversal of this effect were much slower than Zn<sup>2+</sup>-induced suppression but could be reproduced by a change in holding potential approximately equal to the shift in channel voltage dependence, suggesting that they reflect equilibration of a slow coupled inactivation process rather than slow Zn<sup>2+</sup> binding/unbinding at a distinct, stimulatory site.

### High-affinity changes in slope factor

Another unexpected finding was that the  $K_{Zn}$  for high-affinity shift and slowing (4.2–4.6 μM) is roughly four times smaller than the  $K_{Zn}$  for changes in voltage sensitivity (16–22 μM), even though both effects were sensitive to histidine modification. In principle, this could reflect the fact that Zn<sup>2+</sup> preferentially affects the charge movement of only one of the four pseudosubunits. However, we also found that (1) DEPC produces effects opposite to the Zn<sup>2+</sup>-induced shift and slowing but mimics Zn<sup>2+</sup> effects on the activation slope factor under control conditions,



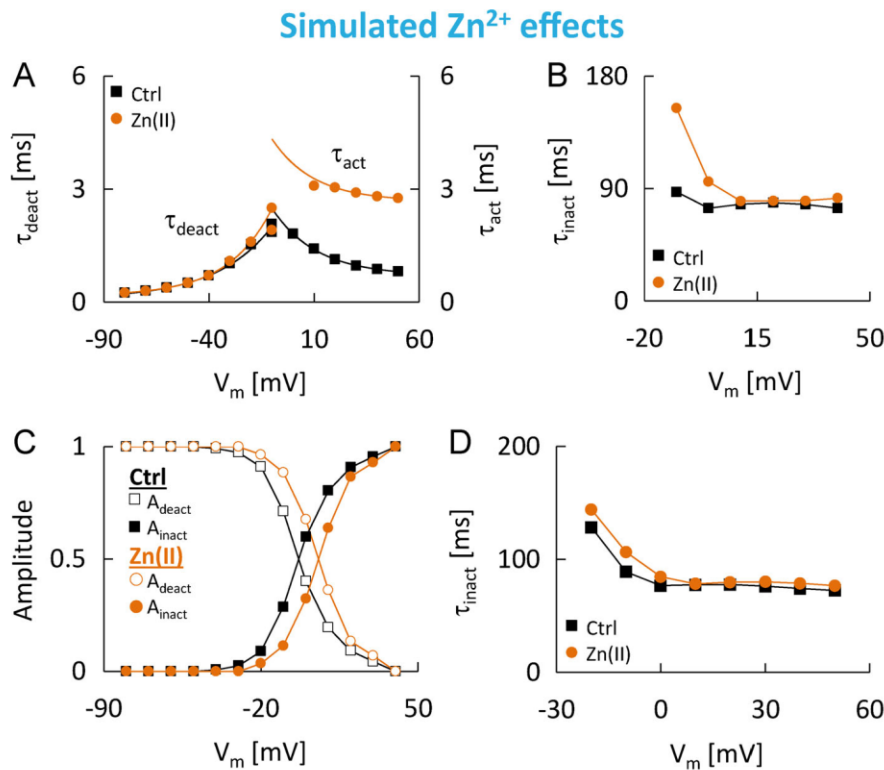


Figure 18. **Simulated Zn<sup>2+</sup> effects on macroscopic activation, deactivation, and inactivation kinetics.** (A) Activation (right) and deactivation (left) time constants, determined by exponential fits to the rising phase of simulated I-V currents or the decaying phase of simulated II-V currents, with the free Zn<sup>2+</sup> concentration set to 0 (black squares) or 5.4 μM (orange circles). (B) Inactivation time constants determined from exponential fits to the decay of simulated II-V currents at depolarized test potentials, with the free Zn<sup>2+</sup> concentration set to 0 (black squares) or 5.4 μM (orange circles). (C) Contribution of deactivation (open symbols) and inactivation (filled symbols) to total decay of simulated II-V currents, with the free Zn<sup>2+</sup> concentration set to 0 (black squares) or 5.4 μM (orange circles). (D) Inactivation time constants, determined by fitting a single exponential function with variable offset to the decaying phase of simulated currents evoked by 400-ms voltage steps to the indicated test potentials, with the free Zn<sup>2+</sup> concentration set to 0 (open squares) or 5.4 μM (orange circles).

(2) shift and slowing show a different dependence on the experimental conditions than the changes in the slope of the activation curve, and (3) the proposed model quantitatively accounts for the shift and slowing, but not for the increase in slope factor. In addition, the  $K_{Zn}$  for changes in slope factor coincided almost exactly with the  $K_{Zn}$  for a voltage-independent decrease of II-V currents (14–20 μM) that was also sensitive to DEPC pretreatment. The underlying mechanism remains to be firmly established, but it is tempting to speculate that Zn<sup>2+</sup> mimics the proton-induced decrease in Ca<sub>v</sub>2.3 channel unitary conductance described in a previous study, which has been linked to a histidine residue in one of the pore loops (Fig. 1 A) and is also accompanied by an increased slope factor (Cens et al., 2011). However, DEPC sensitivity alone does not necessarily prove a role of histidine residues, and the fact that acidification actually increased the maximum changes in slope factor could point to the involvement of other amino acid residues (see Limitations). In any case, the moderate magnitude of the slope changes even at saturating Zn<sup>2+</sup> concentrations (~1.7-fold increase in  $k_{act}$ ) suggests that reduced voltage sensitivity does not significantly contribute to the net Zn<sup>2+</sup> action, which is also supported by our modeling results.

### Low-affinity slowing

Our findings also indicate that an unidentified, DEPC-resistant site with lower Zn<sup>2+</sup> affinity contributes to the slowing observed at higher free Zn<sup>2+</sup> levels and that the same site could be involved in Zn<sup>2+</sup>-induced block measured with the II-V protocol.  $K_{Zn}$  values for the low-affinity slowing were ~150 μM and well separated from those for the low-affinity shift. Interestingly,

Zn<sup>2+</sup> and other trace metal ions have been shown to slow activation of several native HVA Ca<sup>2+</sup> channels lacking critical histidine residues in domain I (Magistretti et al., 2001, 2003; Castelli et al., 2003), so that the site involved in the slowing could be shared with other members of the family. Because Ca<sup>2+</sup> channel block and permeation are thought to be governed by the same principles, and Ca<sup>2+</sup> channel gating is well known to be affected by the nature of permeating ions (for review, see Neumaier et al., 2015), the metal-induced slowing has been proposed to reflect an allosteric effect linked to occupation of the pore (Castelli et al., 2003), an idea that is reinforced by our electrophysiological and modeling results (see A model of Ca<sub>v</sub>2.3 channel gating and Zn<sup>2+</sup>-induced modulation). Based on the shallow voltage dependence of low-affinity II-V current suppression, the putative Zn<sup>2+</sup>-blocking site in Ca<sub>v</sub>2.3 channels could reside in or at a superficial part of the pore near the outer vestibule rather than deep within the electric field, which is consistent with a number of previous studies on VGCC block by d-block metal ions (Winegar et al., 1991; Díaz et al., 2005; Lopin et al., 2012). As such, one promising candidate site appears to be a putative EF-hand motif located external to the selectivity filter EEEE-locus and outside of the narrow pore region (Fig. 1 A), which is present in all HVA Ca<sup>2+</sup> channels and has previously been implicated in their differential sensitivity to Zn<sup>2+</sup> block (Sun et al., 2007). Lack of this site in low-voltage activated channels could explain why the effects of Zn<sup>2+</sup> on these channels appear to be much less uniform, with several studies in different preparations reporting inconsistent or even contradictory findings (Cataldi et al., 2007; Traboulsie et al., 2007; Sun et al., 2007; Noh et al., 2010).

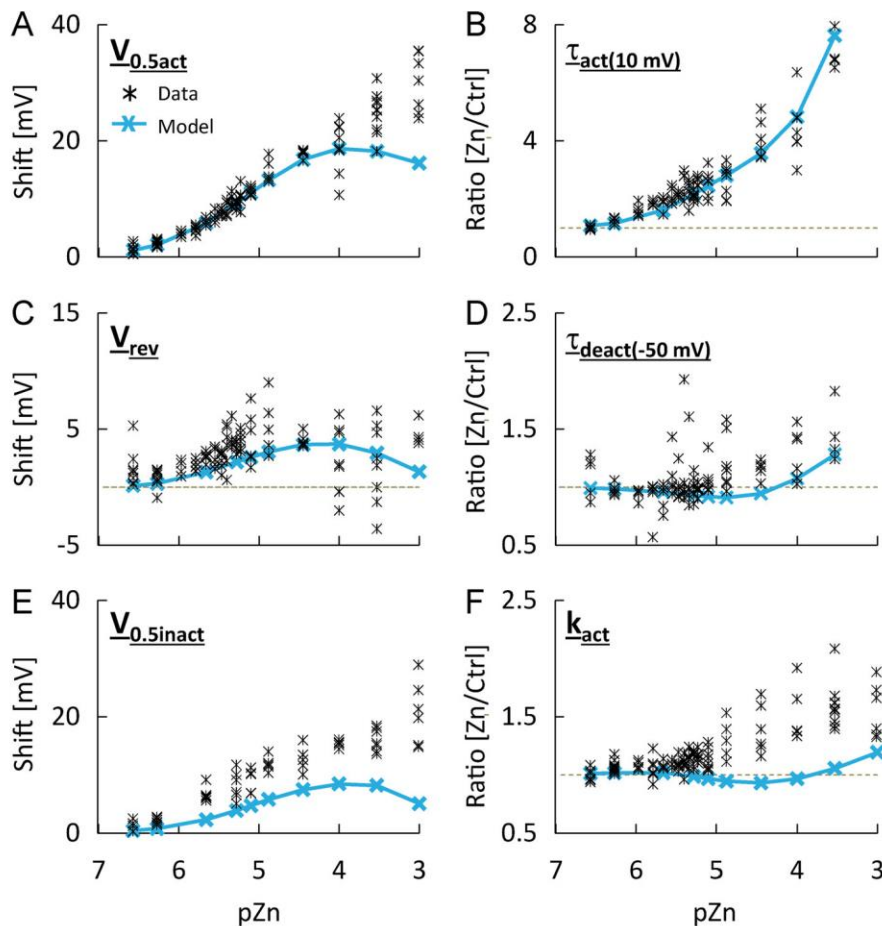


Figure 19. **Concentration dependence of simulated  $Zn^{2+}$  effects on  $Ca_v2.3$  channels.** (A–F) Comparison of measured and simulated concentration dependencies for  $Zn^{2+}$ -induced changes in half-activation voltage (A), activation time constant at 10 mV (B), apparent  $V_{rev}$  (C), deactivation time constant at –50 mV (D), half-inactivation voltage (E), and activation slope factor (F).

### Low-affinity shift

$K_{Zn}$  values for the low-affinity shift were  $>500\ \mu\text{M}$  and similar for activation and inactivation voltage dependence. The concentration dependence suggested that this effect might also be related to block measured with the II-V protocol, but because it is unlikely to ever become significant under (patho)physiological conditions, we have neglected it in our modeling study.

### A model of $Ca_v2.3$ channel gating and $Zn^{2+}$ -induced modulation

Gating models provide quantitative predictions that can be used to test hypotheses about molecular mechanisms and understand the role of voltage-gated ion channels in electrical excitability and cell signaling. Here, we developed a preliminary Markov model for  $Ca_v2.3$  channel voltage-dependent gating that is consistent with the available data on channel structure and accurately reproduces most salient features of ionic and gating currents under near-physiological ionic conditions. Voltage-sensor activation in the model is probabilistic in nature and only governed by the respective steady-state and kinetic properties, with the simplifying assumption that two of the VSMs activate in a specific sequence. The latter is at odds with a VCF study on  $Ca_v1.2$  channels, where fluorescent changes in all four domains occurred without a discernible lag (Pantazis et al., 2014), but it has been shown that sequential and parallel activation models may not always be resolvable from each other in

electrophysiological recordings (Chanda and Bezanilla, 2002). The model also incorporates recent findings that activation of only two VSMs may be obligatory for  $Ca^{2+}$  channel opening (Pantazis et al., 2014), an idea that is reinforced by (1) a slow component of charge movement observed in our own and previous  $Ca^{2+}$  channel gating current recordings (Josephson and Varadi, 1996; Josephson, 1997), (2) evidence for multiple  $Ca^{2+}$  channel open states (Fass and Levitan, 1996; Schneider et al., 1994; Nakayama and Brading, 1993), and (3) the success of HH  $m^2h$ -type models in describing  $Ca^{2+}$  channel ionic currents (Sala, 1991; Kostyuk et al., 1977; Kay and Wong, 1987; Benison et al., 2001).

In addition, our model provides insight into potential mechanisms of  $Zn^{2+}$ -induced modulation and shows that electrostatic modification and mechanical slowing of a single VSM mediated by  $Zn^{2+}$  binding to a common site could quantitatively account for the high-affinity shift and slowing and also explain the observed changes in macroscopic inactivation if the process is state dependent and coupled to activation.

The low-affinity slowing was modeled as an allosteric effect that results from occupation by  $Zn^{2+}$  of a pore blocking site, which could well account for the experimental data, even though we made several simplifying assumptions. As such, the modeling results also confirm that slower opening of blocked channels could result in slower macroscopic currents even though only nonblocked channels contribute to these currents,



which might account for the fact that many inorganic blockers also alter  $\text{Ca}^{2+}$  channel gating (Neumaier et al., 2015). Given that we have only circumstantial evidence for an intrapore location of the site involved in low-affinity slowing, other models could almost certainly account for these findings as well, albeit at the cost of more complicated model structures with additional binding sites. In addition, until exact VCF data on  $\text{Ca}_v2.3$  channel voltage-sensor movement become available, structural interpretation of the model in terms of specific protein domains remains problematic (see also Limitations). Regardless of its physical interpretation, however, our model faithfully reproduces  $\text{Ca}_v2.3$  channel gating in the absence of trace metals and most hallmarks of  $\text{Zn}^{2+}$ -induced suppression as well as their dependence on  $\text{Zn}^{2+}$  concentration. It is freely available at ModelDB (accession number 261714) and can be readily integrated into existing cell models, making it a useful tool for future studies on the physiological role of  $\text{Ca}_v2.3$  channels and/or the effects of synaptic  $\text{Zn}^{2+}$  release on electrical excitability and cell signaling.

### (Patho)physiological implications

Although some have questioned that synaptic  $\text{Zn}^{2+}$  can exceed  $1 \mu\text{M}$  (Erreger and Traynelis, 2005; Vergnano et al., 2014), most studies suggest that physiological peak cleft concentrations at  $\text{Zn}^{2+}$  enriched synapses could reach at least low micromolar levels, especially during intense, LTP-inducing stimulation (Aniksztejn et al., 1987; Assaf and Chung, 1984; Besser et al., 2009; Howell et al., 1984; Kodirov et al., 2006; Qian and Noebels, 2005, 2006; Vogt et al., 2000; Ueno et al., 2002; Komatsu et al., 2005; Li et al., 2001; Quinta-Ferreira et al., 2016). One of our most important findings may therefore be that low micromolar  $\text{Zn}^{2+}$  concentrations could inhibit or stimulate  $\text{Ca}^{2+}$  influx through  $\text{Ca}_v2.3$  channels depending on RMP. In addition, slow reversal of the stimulation during washout at depolarized RMP could result in a paradoxical increase of  $\text{Ca}^{2+}$  influx above the control level that persists for some time after cessation of the  $\text{Zn}^{2+}$  signal. The latter is especially interesting, because rises in synaptic  $\text{Zn}^{2+}$  concentrations during neuronal activity have been shown or are thought to be transient in nature (Vergnano et al., 2014; Quinta-Ferreira et al., 2016). As such, it could potentially provide a link between  $\text{Zn}^{2+}$  signals and certain plasticity processes like presynaptic LTP at hippocampal mossy fiber synapses, which is in part mediated by  $\text{Ca}_v2.3$  channels (Dietrich et al., 2003) and has been shown to depend on synaptic  $\text{Zn}^{2+}$  release in brain slice recordings (Pan et al., 2011). In principle, the holding potential dependence of  $\text{Zn}^{2+}$  effects could also be involved in the reported proictogenic role of  $\text{Ca}_v2.3$  channels (Weiergräber et al., 2006a, 2007; Dibué-Adjei et al., 2017), since depolarization of the neuronal RMP due to, for example, spreading depolarization or paroxysmal depolarizing shifts might lead to a decrease in the inhibitory action or even reverse the direction of  $\text{Zn}^{2+}$  effects. Considering that even very small changes in ion channel function (Thomas et al., 2009) and synaptic gain (Du et al., 2019) can lead to seizure-like activity, reduced  $\text{Ca}_v2.3$  channel suppression by  $\text{Zn}^{2+}$  could conceivably contribute to the ictogenic processes when the brain moves into a pro seizure state.

Because maximum  $\text{Zn}^{2+}$  cleft concentrations have not been established with sufficient certainty, the potential relevance of low-affinity  $\text{Zn}^{2+}$ -induced modulation in the brain remains ambiguous. However, the slowing effect could be important in certain tissues outside of the brain, such as in pancreatic islets of Langerhans, where local  $\text{Zn}^{2+}$  concentrations during cosecretion of  $\text{Zn}^{2+}$  and insulin have been estimated to reach several hundred micromoles (Kim et al., 2000). Animal studies have linked  $\text{Ca}_v2.3$  channels to  $\alpha$ -cell glucagon (Pereverzev et al., 2005),  $\beta$ -cell insulin (Jing et al., 2005; Matsuda et al., 2001; Pereverzev et al., 2002), and  $\delta$ -cell somatostatin (Zhang et al., 2007) secretion and we have previously shown that they are involved in intra-islet paracrine  $\text{Zn}^{2+}$  signaling (Drobinskaya et al., 2015). However, further studies will clearly be required to firmly establish whether the low-affinity effects described here are physiologically relevant or simply phenomena that must be taken into account when studying the high-affinity effects. Additional studies will also be necessary to determine the kinetics, magnitude and direction of  $\text{Zn}^{2+}$  effects on native  $\text{Ca}_v2.3$  channels in different cells under physiological conditions, as they could be influenced by a number of factors such as RMP, subunit-composition or alternative splicing. For example,  $\text{Ca}_v\beta$ -subunits have been shown to differentially modify the time course of  $\text{Ca}_v2.3$  channel recovery from inactivation at depolarized test potentials (Jeziorski et al., 2000) as well as the gating effects of  $\text{Ni}^{2+}$  on cloned  $\text{Ca}_v2.1$  channels (Zamponi et al., 1996), suggesting that auxiliary subunits could directly or indirectly influence trace metal-induced VGCC modulation.

### Limitations

There are some important limitations and inherent assumptions of our work that need to be addressed. First of all, to reduce uncertainty with regard to the  $K_{\text{Zn}}$  and  $E_{\text{max}}$  values we analyzed all of the concentration-response relationships using a Hill slope of unity, which assumes simple, bimolecular reactions. With regard to the high-affinity shift and slowing, this assumption seems justified based on the proposed structure of the trace metal binding site. Moreover, when the data were fitted with unconstrained Hill slopes, the values obtained for the high-affinity component were always close to 1 (i.e., 0.7–1.2). Likewise, the Hill slope obtained for the low-affinity slowing after DEPC pretreatment was 0.9 (CI, 0.7–1.0). The low-affinity shift could often be equally well described using different values for the Hill slope, possibly because full saturation of this effect was not consistently observed and/or nonspecific surface charge effects contributed to the net  $\text{Zn}^{2+}$  action (but see below). However, by fixing the Hill slope to 1, we still obtained visibly good fits, adjusted  $\chi^2$  values close to 1, and consistent results for the  $E_{\text{max}}$  values, suggesting that the plateau phase was sufficiently well defined by the data.

Second, we used DEPC to probe the role of histidine residues for high-affinity  $\text{Zn}^{2+}$  binding, which is frequently employed for this purpose (Choi and Lipton, 1999; Bancila et al., 2005; Harvey et al., 1999) but has no perfect target specificity and can also react with other amino acid residues (Mendoza and Vachet, 2008; Limpikirati et al., 2019). Protons often compete with  $\text{Zn}^{2+}$  for binding to the histidine imidazole ring, so that their



effects on  $Zn^{2+}$ -induced modulation can to some extent support or oppose an action at histidine residues. For example, moderate acidification reduced the  $K_{Zn}$  and  $E_{max}$  values for high-affinity shift and slowing and produced effects similar to  $Zn^{2+}$  under control conditions, which is consistent with an effect mediated by the known loop histidines. Also, neither DEPC nor acidification altered the concentration dependence of low-affinity slowing, suggesting that histidine residues are not involved and that  $Zn^{2+}$  binding to the underlying site was unaffected. On the other hand, DEPC pretreatment completely prevented and partly reversed the  $Zn^{2+}$ -induced changes in activation slope factor, while moderate acidification only slightly reduced apparent  $Zn^{2+}$  affinity and even increased the maximum  $Zn^{2+}$  effects. Likewise, DEPC and protons both reduced the voltage dependence of block/low-affinity II-V current suppression, but DEPC did so by increasing apparent  $Zn^{2+}$  affinity at negative test potentials, while protons reduced apparent  $Zn^{2+}$  affinity at positive test potential. As such, further studies will clearly be required for firm conclusions with regard to the exact identity of residues that could be directly or indirectly involved in some of the more complex  $Zn^{2+}$ -induced effects and their modification by DEPC and protons.

We have also neglected any contribution of nonspecific surface charge screening or binding to the observed effects, which might have introduced some error, especially at the highest free  $Zn^{2+}$  levels examined. However, divalent cation concentrations in our recording solutions were relatively high even before addition of  $Zn^{2+}$ , and there was no significant difference in channel voltage dependence between recordings performed with 2 versus 4 mM  $Ca^{2+}$  or 4 mM  $Ca^{2+}$  versus  $Mg^{2+}$ , suggesting that the contribution of nonspecific surface charge effects was small.

Finally, although our Markov model for  $Ca_v2.3$  channel gating and  $Zn^{2+}$ -induced modulation describes well many qualitative and quantitative features of the experimental data, it should be considered preliminary for several reasons. First of all, our model obviously represents a considerable simplification, and the available data are insufficient for a detailed physical interpretation or full validation of the underlying assumptions. The most important limitation in its current form is that the VSMs in the model cannot be related to specific domains in the channel protein, even though its success in modeling the high-affinity  $Zn^{2+}$  effects makes it tempting to propose that VSM 1 in the model could correspond to the VSM in domain I. Another related shortcoming of our model is that the state dependence of inactivation had to be determined from the data using an empirical approach. While somewhat arbitrary, this approach was sufficient to demonstrate that  $Zn^{2+}$ -induced changes in activation gating alone could bring about the observed changes in inactivation kinetics and voltage dependence if inactivation is state dependent and coupled to activation. Moreover, once exact fluorescence data on  $Ca_v2.3$  channel voltage-sensor movement and activation inactivation coupling become available, it should be possible to revise and extend the model structure accordingly.

Lastly, our model in its current form does not reproduce the kinetics of recovery from inactivation or the process of ultraslow inactivation, which we have shown here to be of potential importance for the time course and direction of slow  $Zn^{2+}$  effects at

depolarized RMPs. Despite all these limitations, we think it is useful to present our model at this time, since it may provide a basis for further investigation of trace metal effects on  $Ca_v2.3$  channel function and could be extended based on future findings to ultimately help predict the intricate effects of endogenous  $Zn^{2+}$  on neuronal excitability.

## Conclusion

The present study performed a comprehensive assessment of the modulation of  $Ca_v2.3$  channel electrophysiological properties by a wide range of  $Zn^{2+}$  concentrations and reveals how the degree and even direction of effects could be influenced by the prevailing neuronal properties and ionic conditions. While still far from complete, the model developed provides a first quantitative framework for understanding  $Zn^{2+}$  effects on  $Ca_v2.3$  channel function and a step toward the application of computational approaches for predicting the complex actions of  $Zn^{2+}$  on neuronal excitability.

## Acknowledgments

Christopher J. Lingle served as editor.

We thank Renate Clemens for her excellent technical assistance.

This work was financially supported by the Köln Fortune Program/Faculty of Medicine, University of Cologne (259/2013) and the Deutsche Forschungsgemeinschaft (SCHN 387/21-1 and SCHN 387/21-2).

The authors declare no competing financial interests.

Author contributions: F. Neumaier was involved in conceptualization, formal analysis, funding acquisition, investigation, methodology, visualization, and writing (original draft, review, and editing). T. Schneider was involved in conceptualization, funding acquisition, project administration, supervision, and writing (review and editing). S. Alpdogan and J. Hescheler contributed resources.

Submitted: 7 February 2020

Revised: 30 April 2020

Accepted: 19 May 2020

## References

- Aniksztejn, L., G. Charton, and Y. Ben-Ari. 1987. Selective release of endogenous zinc from the hippocampal mossy fibers in situ. *Brain Res.* 404: 58–64. [https://doi.org/10.1016/0006-8993\(87\)91355-2](https://doi.org/10.1016/0006-8993(87)91355-2)
- Assaf, S.Y., and S.-H. Chung. 1984. Release of endogenous  $Zn^{2+}$  from brain tissue during activity. *Nature.* 308:734–736. <https://doi.org/10.1038/308734a0>
- Austin, P.C., and J.E. Hux. 2002. A brief note on overlapping confidence intervals. *J. Vasc. Surg.* 36:194–195. <https://doi.org/10.1067/mva.2002.125015>
- Bancila, V., T. Cens, D. Monnier, F. Chanson, C. Faure, Y. Dunant, and A. Bloc. 2005. Two SUR1-specific histidine residues mandatory for zinc-induced activation of the rat  $K_{ATP}$  channel. *J. Biol. Chem.* 280:8793–8799. <https://doi.org/10.1074/jbc.M413426200>
- Benison, G., J. Keizer, L.M. Chalupa, and D.W. Robinson. 2001. Modeling temporal behavior of postnatal cat retinal ganglion cells. *J. Theor. Biol.* 210:187–199. <https://doi.org/10.1006/jtbi.2000.2289>
- Besser, L., E. Chorin, I. Sekler, W.F. Silverman, S. Atkin, J.T. Russell, and M. Hershinkel. 2009. Synaptically released zinc triggers metabotropic

- signaling via a zinc-sensing receptor in the hippocampus. *J. Neurosci.* 29: 2890–2901. <https://doi.org/10.1523/JNEUROSCI.5093-08.2009>
- Beyl, S., A. Hohaus, S. Andranovits, E. Timin, and S. Hering. 2016. Upward movement of IS4 and III54 is a rate-limiting stage in  $Ca_v1.2$  activation. *Pflugers Arch.* 468:1895–1907. <https://doi.org/10.1007/s00424-016-1895-5>
- Boyett, M.R., H. Honjo, S.M. Harrison, W.-J. Zang, and M.S. Kirby. 1994. Ultra-slow voltage-dependent inactivation of the calcium current in guinea-pig and ferret ventricular myocytes. *Pflugers Arch.* 428:39–50. <https://doi.org/10.1007/BF00374750>
- Brent, R.. 1976. A New Algorithm for Minimizing a Function of Several Variables without Calculating Derivatives. In *Algorithms for Minimization without Derivatives*. Prentice Hall, Englewood Cliffs, NJ. pp. 200–248.
- Brog-Graham, L.J.. 1991. Modeling the Nonlinear Conductances of Excitable Membranes. In *Cellular and Molecular Neurobiology: A Practical Approach*. H. Wheal, and J. Chad, editors. Oxford University Press, New York. pp. 247–275.
- Capes, D.L., M.P. Goldschen-Ohm, M. Arcisio-Miranda, F. Bezanilla, and B. Chanda. 2013. Domain IV voltage-sensor movement is both sufficient and rate limiting for fast inactivation in sodium channels. *J. Gen. Physiol.* 142:101–112. <https://doi.org/10.1085/jgp.201310998>
- Carnevale, N.T., and M.L. Hines. 2006. *The NEURON Book*. Cambridge University Press, Cambridge, UK. 742 pp. <https://doi.org/10.1017/CBO9780511541612>
- Castelli, L., F. Tanzi, V. Taglietti, and J. Magistretti. 2003.  $Cu^{2+}$ ,  $Co^{2+}$ , and  $Mn^{2+}$  modify the gating kinetics of high-voltage-activated  $Ca^{2+}$  channels in rat palaeocortical neurons. *J. Membr. Biol.* 195:121–136. <https://doi.org/10.1007/s00232-003-0614-2>
- Cataldi, M., V. Lariccia, V. Marzaioli, A. Cavaccini, G. Curia, D. Viggiano, L.M.T. Canzoniero, G. di Renzo, M. Avoli, and L. Annunziato. 2007.  $Zn^{2+}$  slows down  $Ca_v1.3$  gating kinetics: implications for thalamocortical activity. *J. Neurophysiol.* 98:2274–2284. <https://doi.org/10.1152/jn.00889.2006>
- Catterall, W.A.. 1998. Structure and function of neuronal  $Ca^{2+}$  channels and their role in neurotransmitter release. *Cell Calcium.* 24:307–323. [https://doi.org/10.1016/S0143-4160\(98\)90055-0](https://doi.org/10.1016/S0143-4160(98)90055-0)
- Gens, T., M. Rousset, and P. Charvet. 2011. Two sets of amino acids of the domain I of  $Ca_v2.3$   $Ca^{2+}$  channels contribute to their high sensitivity to extracellular protons. *Pflugers Arch.* 462:303–314. <https://doi.org/10.1007/s00424-011-0974-x>
- Chanda, B., and F. Bezanilla. 2002. Tracking voltage-dependent conformational changes in skeletal muscle sodium channel during activation. *J. Gen. Physiol.* 120:629–645. <https://doi.org/10.1085/jgp.20028679>
- Chen, L.Q., V. Santarelli, R. Horn, and R.G. Kallen. 1996. A unique role for the S4 segment of domain 4 in the inactivation of sodium channels. *J. Gen. Physiol.* 108:549–556. <https://doi.org/10.1085/jgp.108.6.549>
- Choi, Y.-B., and S.A. Lipton. 1999. Identification and mechanism of action of two histidine residues underlying high-affinity  $Zn^{2+}$  inhibition of the NMDA receptor. *Neuron.* 23:171–180. [https://doi.org/10.1016/S0896-6273\(00\)80763-1](https://doi.org/10.1016/S0896-6273(00)80763-1)
- Christie, B.R., L.S. Eliot, K. Ito, H. Miyakawa, and D. Johnston. 1995. Different  $Ca^{2+}$  channels in soma and dendrites of hippocampal pyramidal neurons mediate spike-induced  $Ca^{2+}$  influx. *J. Neurophysiol.* 73:2553–2557. <https://doi.org/10.1152/jn.1995.73.6.2553>
- Díaz, D., R. Bartolo, D.M. Delgado, F. Higueldo, and J.C. Gomora. 2005. Contrasting effects of  $Ca^{2+}$  and  $Co^{2+}$  on the blocking/unblocking of human  $Ca_v3$  channels. *J. Membr. Biol.* 207:91–105. <https://doi.org/10.1007/s00232-005-0804-1>
- Dibué-Adjei, M., M.A. Kamp, S. Alpdogan, E.E. Tevoufouet, W.F. Neiss, J. Hescheler, and T. Schneider. 2017.  $Ca_v2.3$  (R-type) calcium channels are critical for mediating anticonvulsive and neuroprotective properties of lamotrigine in vivo. *Cell. Physiol. Biochem.* 44:935–947. <https://doi.org/10.1159/000485361>
- Dietrich, D., T. Kirschstein, M. Kukley, A. Pereverzev, C. von der Brélie, T. Schneider, and H. Beck. 2003. Functional specialization of presynaptic  $Ca_v2.3$   $Ca^{2+}$  channels. *Neuron.* 39:483–496. [https://doi.org/10.1016/S0896-6273\(03\)00430-6](https://doi.org/10.1016/S0896-6273(03)00430-6)
- Drobinskaya, I., F. Neumaier, A. Pereverzev, J. Hescheler, and T. Schneider. 2015. Diethyldithiocarbamate-mediated zinc ion chelation reveals role of  $Ca_v2.3$  channels in glucagon secretion. *Biochim. Biophys. Acta.* 1853: 953–964. <https://doi.org/10.1016/j.bbamcr.2015.01.001>
- Du, J., V. Vegh, and D.C. Reutens. 2019. Small changes in synaptic gain lead to seizure-like activity in neuronal network at criticality. *Sci. Rep.* 9:1097. <https://doi.org/10.1038/s41598-018-37646-9>
- Elinder, F., and P. Arhem. 2003. Metal ion effects on ion channel gating. *Q. Rev. Biophys.* 36:373–427. <https://doi.org/10.1017/S0033583504003932>
- Erreger, K., and S.F. Traynelis. 2005. Allosteric interaction between zinc and glutamate binding domains on NR2A causes desensitization of NMDA receptors. *J. Physiol.* 569:381–393. <https://doi.org/10.1113/jphysiol.2005.095497>
- Fass, D.M., and E.S. Levitan. 1996. L-type  $Ca^{2+}$  channels access multiple open states to produce two components of Bay K 8644-dependent current in GH3 cells. *J. Gen. Physiol.* 108:13–26. <https://doi.org/10.1085/jgp.108.1.13>
- Flucher, B.E.. 2016. Specific contributions of the four voltage-sensing domains in L-type calcium channels to gating and modulation. *J. Gen. Physiol.* 148:91–95. <https://doi.org/10.1085/jgp.201611663>
- Frederickson, C.J., S.W. Suh, D. Silva, C.J. Frederickson, and R.B. Thompson. 2000. Importance of zinc in the central nervous system: the zinc-containing neuron. *J. Nutr.* 130(5S, Suppl):1471S–1483S. <https://doi.org/10.1093/jn/130.5.1471S>
- Frederickson, C.J., J.-Y. Koh, and A.I. Bush. 2005. The neurobiology of zinc in health and disease. *Nat. Rev. Neurosci.* 6:449–462. <https://doi.org/10.1038/nrn1671>
- García, J., J. Nakai, K. Imoto, and K.G. Beam. 1997. Role of S4 segments and the leucine heptad motif in the activation of an L-type calcium channel. *Biophys. J.* 72:2515–2523. [https://doi.org/10.1016/S0006-3495\(97\)78896-9](https://doi.org/10.1016/S0006-3495(97)78896-9)
- Gasparini, S., A.M. Kasyanov, D. Pietrobon, L.L. Voronin, and E. Cherubini. 2001. Presynaptic R-type calcium channels contribute to fast excitatory synaptic transmission in the rat hippocampus. *J. Neurosci.* 21:8715–8721. <https://doi.org/10.1523/JNEUROSCI.21-22-08715.2001>
- Goldberg, R.N., N. Kishore, and R.M. Lennen. 2002. Thermodynamic quantities for the ionization reaction of buffers. *J. Phys. Chem. Ref. Data.* 31: 231–370. <https://doi.org/10.1063/1.1416902>
- Goldschen-Ohm, M.P., D.L. Capes, K.M. Oelstrom, and B. Chanda. 2013. Multiple pore conformations driven by asynchronous movements of voltage sensors in a eukaryotic sodium channel. *Nat. Commun.* 4:1350. <https://doi.org/10.1038/ncomms2356>
- Hamill, O.P., A. Marty, E. Neher, B. Sakmann, and F.J. Sigworth. 1981. Improved patch-clamp techniques for high-resolution current recording from cells and cell-free membrane patches. *Pflugers Arch.* 391:85–100. <https://doi.org/10.1007/BF00656997>
- Harvey, R.J., P. Thomas, C.H. James, A. Wilderspin, and T.G. Smart. 1999. Identification of an inhibitory  $Zn^{2+}$  binding site on the human glycine receptor  $\alpha_1$  subunit. *J. Physiol.* 520:53–64. <https://doi.org/10.1111/j.1469-7793.1999.00053.x>
- Hofmann, F., L. Lacinová, and N. Klugbauer. 1999. Voltage-Dependent Calcium Channels: From Structure to Function. In *Reviews of Physiology, Biochemistry and Pharmacology*. Vol. Vol. 139. Springer-Verlag, Berlin, Heidelberg. pp. 33–87.
- Howell, G.A., M.G. Welch, and C.J. Frederickson. 1984. Stimulation-induced uptake and release of zinc in hippocampal slices. *Nature.* 308:736–738. <https://doi.org/10.1038/308736a0>
- Jeziorski, M.C., R.M. Greenberg, and P.A.V. Anderson. 2000. Calcium channel  $\beta$  subunits differentially modulate recovery of the channel from inactivation. *FEBS Lett.* 483:125–130. [https://doi.org/10.1016/S0014-5793\(00\)02098-6](https://doi.org/10.1016/S0014-5793(00)02098-6)
- Jing, X., D.-Q. Li, C.S. Olofsson, A. Salehi, V.V. Surve, J. Caballero, R. Ivarsson, I. Lundquist, A. Pereverzev, T. Schneider, et al. 2005.  $Ca_v2.3$  calcium channels control second-phase insulin release. *J. Clin. Invest.* 115: 146–154. <https://doi.org/10.1172/JCI200522518>
- Josephson, I.R.. 1997. Kinetic components of the gating currents of human cardiac L-type  $Ca^{2+}$  channels. *Pflugers Arch.* 433:321–329. <https://doi.org/10.1007/s004240050283>
- Josephson, I.R., and G. Varadi. 1996. The beta subunit increases  $Ca^{2+}$  currents and gating charge movements of human cardiac L-type  $Ca^{2+}$  channels. *Biophys. J.* 70:1285–1293. [https://doi.org/10.1016/S0006-3495\(96\)79685-6](https://doi.org/10.1016/S0006-3495(96)79685-6)
- Kang, H.-W., H.J. Moon, S.H. Joo, and J.-H. Lee. 2007. Histidine residues in the IS3-IS4 loop are critical for nickel-sensitive inhibition of the  $Ca_v2.3$  calcium channel. *FEBS Lett.* 581:5774–5780. <https://doi.org/10.1016/j.febslet.2007.11.045>
- Kay, A.R., and R.K. Wong. 1987. Calcium current activation kinetics in isolated pyramidal neurones of the Cal region of the mature guinea-pig hippocampus. *J. Physiol.* 392:603–616. <https://doi.org/10.1113/jphysiol.1987.sp016799>
- Khalil, M.M., A.M. Radalla, and A.G. Mohamed. 2009. Potentiometric investigation on complexation of divalent transition metal ions with some zwitterionic buffers and triazoles. *J. Chem. Eng. Data.* 54:3261–3272. <https://doi.org/10.1021/je9002459>
- Kim, B.J., Y.H. Kim, S. Kim, J.W. Kim, J.-Y. Koh, S.H. Oh, M.K. Lee, K.W. Kim, and M.S. Lee. 2000. Zinc as a paracrine effector in pancreatic islet cell death. *Diabetes.* 49:367–372. <https://doi.org/10.2337/diabetes.49.3.367>

- Kodirov, S.A., S. Takizawa, J. Joseph, E.R. Kandel, G.P. Shumyatsky, and V.Y. Bolshakov. 2006. Synaptically released zinc gates long-term potentiation in fear conditioning pathways. *Proc. Natl. Acad. Sci. USA*. 103: 15218–15223. <https://doi.org/10.1073/pnas.0607131103>
- Komatsu, K., K. Kikuchi, H. Kojima, Y. Urano, and T. Nagano. 2005. Selective zinc sensor molecules with various affinities for Zn<sup>2+</sup>, revealing dynamics and regional distribution of synaptically released Zn<sup>2+</sup> in hippocampal slices. *J. Am. Chem. Soc.* 127:10197–10204. <https://doi.org/10.1021/ja050301e>
- Kostyuk, P.G., O.A. Krishtal, and Y.A. Shakhvalov. 1977. Separation of sodium and calcium currents in the somatic membrane of mollusc neurones. *J. Physiol.* 270:545–568. <https://doi.org/10.1113/jphysiol.1977.sp011968>
- Li, Y., C.J. Hough, S.W. Suh, J.M. Sarvey, and C.J. Frederickson. 2001. Rapid translocation of Zn<sup>2+</sup> from presynaptic terminals into postsynaptic hippocampal neurons after physiological stimulation. *J. Neurophysiol.* 86:2597–2604. <https://doi.org/10.1152/jn.2001.86.5.2597>
- Limpikirati, P., X. Pan, and R.W. Vachet. 2019. Covalent labeling with Diethylpyrocarbonate: Sensitive to the residue microenvironment, providing improved analysis of protein higher order structure by mass spectrometry. *Anal. Chem.* 91:8516–8523. <https://doi.org/10.1021/acs.analchem.9b01732>
- Lopin, K.V., I.P. Gray, C.A. Obejero-Paz, F. Thévenod, and S.W. Jones. 2012. Fe<sup>2+</sup> block and permeation of Ca<sub>v</sub>3.1 (α1G) T-type calcium channels: candidate mechanism for non-transferrin-mediated Fe<sup>2+</sup> influx. *Mol. Pharmacol.* 82:1194–1204. <https://doi.org/10.1124/mol.112.080184>
- Magee, J.C., and M. Carruth. 1999. Dendritic voltage-gated ion channels regulate the action potential firing mode of hippocampal CA1 pyramidal neurons. *J. Neurophysiol.* 82:1895–1901. <https://doi.org/10.1152/jn.1999.82.4.1895>
- Magistretti, J., S. Brevi, and M. de Curtis. 2001. Ni<sup>2+</sup> slows the activation kinetics of high-voltage-activated Ca<sup>2+</sup> currents in cortical neurons: evidence for a mechanism of action independent of channel-pore block. *J. Membr. Biol.* 179:243–262. <https://doi.org/10.1007/s002320010050>
- Magistretti, J., L. Castelli, V. Taglietti, and F. Tanzi. 2003. Dual effect of Zn<sup>2+</sup> on multiple types of voltage-dependent Ca<sup>2+</sup> currents in rat palaeocortical neurons. *Neuroscience*. 117:249–264. [https://doi.org/10.1016/S0306-4522\(02\)00865-5](https://doi.org/10.1016/S0306-4522(02)00865-5)
- Mathie, A., G.L. Sutton, C.E. Clarke, and E.L. Veale. 2006. Zinc and copper: pharmacological probes and endogenous modulators of neuronal excitability. *Pharmacol. Ther.* 111:567–583. <https://doi.org/10.1016/j.pharmthera.2005.11.004>
- Matsuda, Y., H. Saegusa, S. Zong, T. Noda, and T. Tanabe. 2001. Mice lacking Ca<sub>v</sub>2.3 (α1E) calcium channel exhibit hyperglycemia. *Biochem. Biophys. Res. Commun.* 289:791–795. <https://doi.org/10.1006/bbrc.2001.6051>
- McDougal, R.A., T.M. Morse, T. Carnevale, L. Marengo, R. Wang, M. Migliore, P.L. Miller, G.M. Shepherd, and M.L. Hines. 2017. Twenty years of ModelDB and beyond: building essential modeling tools for the future of neuroscience. *J. Comput. Neurosci.* 42:1–10. <https://doi.org/10.1007/s10827-016-0623-7>
- Mehrke, G., A. Pereverzev, H. Grabsch, J. Hescheler, and T. Schneider. 1997. Receptor-mediated modulation of recombinant neuronal class E calcium channels. *FEBS Lett.* 408:261–270. [https://doi.org/10.1016/S0014-5793\(97\)00437-7](https://doi.org/10.1016/S0014-5793(97)00437-7)
- Mendoza, V.L., and R.W. Vachet. 2008. Protein surface mapping using diethylpyrocarbonate with mass spectrometric detection. *Anal. Chem.* 80: 2895–2904. <https://doi.org/10.1021/ac701999b>
- Mohamed, M.M.A.. 2007. Complex formation reactions of lanthanum(III), cerium(III), thorium(IV), dioxouranyl(IV) complexes with tricine. *Ann. Chim.* 97:759–770. <https://doi.org/10.1002/adic.200790059>
- Nakashima, Y.M., S.M. Todorovic, A. Pereverzev, J. Hescheler, T. Schneider, and C.J. Lingle. 1998. Properties of Ba<sup>2+</sup> currents arising from human α1E and α1Eβ2.3 constructs expressed in HEK293 cells: physiology, pharmacology, and comparison to native T-type Ba<sup>2+</sup> currents. *Neuropharmacology*. 37:957–972. [https://doi.org/10.1016/S0028-3908\(98\)00097-5](https://doi.org/10.1016/S0028-3908(98)00097-5)
- Nakayama, S., and A.F. Brading. 1993. Evidence for multiple open states of the Ca<sup>2+</sup> channels in smooth muscle cells isolated from the guinea-pig detrusor. *J. Physiol.* 471:87–105. <https://doi.org/10.1113/jphysiol.1993.sp019892>
- Neumaier, F., M. Dibué-Adjei, J. Hescheler, and T. Schneider. 2015. Voltage-gated calcium channels: Determinants of channel function and modulation by inorganic cations. *Prog. Neurobiol.* 129:1–36. <https://doi.org/10.1016/j.pneurobio.2014.12.003>
- Neumaier, F., S. Alpdogan, J. Hescheler, and T. Schneider. 2017. A practical guide to the preparation and use of metal ion-buffered systems for physiological research. *Acta Physiol. (Oxf.)*. 12988. <https://doi.org/10.1111/apha.12988>
- Noh, J., M.K. Kim, and J.M. Chung. 2010. A novel mechanism of zinc block on α1G-like low-threshold T-type Ca<sup>2+</sup> channels in a rat thalamic relay neuron. *Neurosci. Res.* 66:353–358. <https://doi.org/10.1016/j.neures.2009.12.005>
- Pan, E., X.-A. Zhang, Z. Huang, A. Krezel, M. Zhao, C.E. Tinberg, S.J. Lippard, and J.O. McNamara. 2011. Vesicular zinc promotes presynaptic and inhibits postsynaptic long-term potentiation of mossy fiber-CA3 synapse. *Neuron*. 71:1116–1126. <https://doi.org/10.1016/j.neuron.2011.07.019>
- Pantazis, A., N. Savalli, D. Sigg, A. Neely, and R. Olcese. 2014. Functional heterogeneity of the four voltage sensors of a human L-type calcium channel. *Proc. Natl. Acad. Sci. USA*. 111:18381–18386. <https://doi.org/10.1073/pnas.1411127112>
- Park, S.-J., S.-H. Min, H.-W. Kang, and J.-H. Lee. 2015. Differential zinc permeation and blockage of L-type Ca<sup>2+</sup> channel isoforms Ca<sub>v</sub>1.2 and Ca<sub>v</sub>1.3. *Biochim. Biophys. Acta*. 1848(10, Pt A):2092–2100. <https://doi.org/10.1016/j.bbame.2015.05.021>
- Pereverzev, A., M. Mikhna, R. Vajna, C. Gissel, M. Henry, M. Weiergräber, J. Hescheler, N. Smyth, and T. Schneider. 2002. Disturbances in glucose-tolerance, insulin-release, and stress-induced hyperglycemia upon disruption of the Ca<sub>v</sub>2.3 (α<sub>1E</sub>) subunit of voltage-gated Ca<sup>2+</sup> channels. *Mol. Endocrinol.* 16:884–895. <https://doi.org/10.1210/mend.16.4.0801>
- Pereverzev, A., A. Salehi, M. Mikhna, E. Renström, J. Hescheler, M. Weiergräber, N. Smyth, and T. Schneider. 2005. The ablation of the Ca<sub>v</sub>2.3/E-type voltage-gated Ca<sup>2+</sup> channel causes a mild phenotype despite an altered glucose induced glucagon response in isolated islets of Langerhans. *Eur. J. Pharmacol.* 511:65–72. <https://doi.org/10.1016/j.ejphar.2005.01.044>
- Qian, J., and J.L. Noebels. 2005. Visualization of transmitter release with zinc fluorescence detection at the mouse hippocampal mossy fibre synapse. *J. Physiol.* 566:747–758. <https://doi.org/10.1113/jphysiol.2005.089276>
- Qian, J., and J.L. Noebels. 2006. Exocytosis of vesicular zinc reveals persistent depression of neurotransmitter release during metabotropic glutamate receptor long-term depression at the hippocampal CA3-CA1 synapse. *J. Neurosci.* 26:6089–6095. <https://doi.org/10.1523/JNEUROSCI.0475-06.2006>
- Quinta-Ferreira, M.E., F.D.S. Sampaio Dos Aidos, C.M. Matias, P.J. Mendes, J.C. Dionísio, R.M. Santos, L.M. Rosário, and R.M. Quinta-Ferreira. 2016. Modelling zinc changes at the hippocampal mossy fiber synaptic cleft. *J. Comput. Neurosci.* 41:323–337. <https://doi.org/10.1007/s10827-016-0620-x>
- Sala, F.. 1991. Activation kinetics of calcium currents in bull-frog sympathetic neurones. *J. Physiol.* 437:221–238. <https://doi.org/10.1113/jphysiol.1991.sp018592>
- Savalli, N., A. Pantazis, D. Sigg, J.N. Weiss, A. Neely, and R. Olcese. 2016. The α<sub>2</sub>δ<sub>1</sub> subunit remodels Ca<sub>v</sub>1.2 voltage sensors and allows Ca<sup>2+</sup> influx at physiological membrane potentials. *J. Gen. Physiol.* 148:147–159. <https://doi.org/10.1085/jgp.201611586>
- Schneider, T., X. Wei, R. Olcese, J.L. Costantin, A. Neely, P. Palade, E. Perez-Reyes, N. Qin, J. Zhou, G.D. Crawford, et al. 1994. Molecular analysis and functional expression of the human type E neuronal Ca<sup>2+</sup> channel alpha 1 subunit. *Receptors Channels*. 2:255–270.
- Shcheglovitov, A., I. Vitko, R.M. Lazarenko, P. Orestes, S.M. Todorovic, and E. Perez-Reyes. 2012. Molecular and biophysical basis of glutamate and trace metal modulation of voltage-gated Ca<sub>v</sub>2.3 calcium channels. *J. Gen. Physiol.* 139:219–234. <https://doi.org/10.1085/jgp.201110699>
- Sivagnanam, S., A. Majumdar, K. Yoshimoto, V. Astakhov, and A. Bandrowski. M.M. E., and N.T. Carnevale. 2013. Introducing the Neuroscience Gateway. In *CEUR Workshop Proceedings*. Vol. 993.
- Sochivko, D., A. Pereverzev, N. Smyth, C. Gissel, T. Schneider, and H. Beck. 2002. The Ca<sub>v</sub>2.3 Ca<sup>2+</sup> channel subunit contributes to R-type Ca<sup>2+</sup> currents in murine hippocampal and neocortical neurones. *J. Physiol.* 542:699–710. <https://doi.org/10.1113/jphysiol.2002.020677>
- Sun, H.-S., K. Hui, D.W.K. Lee, and Z.-P. Feng. 2007. Zn<sup>2+</sup> sensitivity of high- and low-voltage activated calcium channels. *Biophys. J.* 93:1175–1183. <https://doi.org/10.1529/biophysj.106.103333>
- Thomas, E.A., C.A. Reid, S.F. Berkovic, and S. Petrou. 2009. Prediction by modeling that epilepsy may be caused by very small functional changes in ion channels. *Arch. Neurol.* 66:1225–1232. <https://doi.org/10.1001/archneurol.2009.219>
- Traboulsi, A., J. Chemin, M. Chevalier, J.-F. Quignard, J. Nargeot, and P. Lory. 2007. Subunit-specific modulation of T-type calcium channels by zinc. *J. Physiol.* 578:159–171. <https://doi.org/10.1113/jphysiol.2006.114496>
- Ueno, S., M. Tsukamoto, T. Hirano, K. Kikuchi, M.K. Yamada, N. Nishiyama, T. Nagano, N. Matsuki, and Y. Ikegaya. 2002. Mossy fiber Zn<sup>2+</sup> spillover



- modulates heterosynaptic N-methyl-D-aspartate receptor activity in hippocampal CA3 circuits. *J. Cell Biol.* 158:215–220. <https://doi.org/10.1083/jcb.200204066>
- Vergnano, A.M., N. Rebola, L.P. Savtchenko, P.S. Pinheiro, M. Casado, B.L. Kieffer, D.A. Rusakov, C. Mülle, and P. Paoletti. 2014. Zinc dynamics and action at excitatory synapses. *Neuron*. 82:1101–1114. <https://doi.org/10.1016/j.neuron.2014.04.034>
- Vogt, K., J. Mellor, G. Tong, and R. Nicoll. 2000. The actions of synaptically released zinc at hippocampal mossy fiber synapses. *Neuron*. 26:187–196. [https://doi.org/10.1016/S0896-6273\(00\)81149-6](https://doi.org/10.1016/S0896-6273(00)81149-6)
- Weiergräber, M., M. Henry, A. Krieger, M. Kamp, K. Radhakrishnan, J. Hescheler, and T. Schneider. 2006a. Altered seizure susceptibility in mice lacking the Ca<sub>v</sub>2.3 E-type Ca<sup>2+</sup> channel. *Epilepsia*. 47:839–850. <https://doi.org/10.1111/j.1528-1167.2006.00541.x>
- Weiergräber, M., M.A. Kamp, K. Radhakrishnan, J. Hescheler, and T. Schneider. 2006b. The Ca<sub>v</sub>2.3 voltage-gated calcium channel in epileptogenesis—shedding new light on an enigmatic channel. *Neurosci. Biobehav. Rev.* 30:1122–1144. <https://doi.org/10.1016/j.neubiorev.2006.07.004>
- Weiergräber, M., M. Henry, K. Radhakrishnan, J. Hescheler, and T. Schneider. 2007. Hippocampal seizure resistance and reduced neuronal excitotoxicity in mice lacking the Ca<sub>v</sub>2.3 E/R-type voltage-gated calcium channel. *J. Neurophysiol.* 97:3660–3669. <https://doi.org/10.1152/jn.01193.2006>
- Winegar, B.D., R. Kelly, and J.B. Lansman. 1991. Block of current through single calcium channels by Fe, Co, and Ni. Location of the transition metal binding site in the pore. *J. Gen. Physiol.* 97:351–367. <https://doi.org/10.1085/jgp.97.2.351>
- Woodhull, A. M. 1973. Ionic blockage of sodium channels in nerve. *J. Gen. Physiol.* 61(6):687–708. <https://doi.org/10.1085/jgp.61.6.687>
- Yasuda, T., R.J. Lewis, and D.J. Adams. 2004. Overexpressed Ca<sub>v</sub>β<sub>3</sub> inhibits N-type (Ca<sub>v</sub>2.2) calcium channel currents through a hyperpolarizing shift of ultra-slow and closed-state inactivation. *J. Gen. Physiol.* 123:401–416. <https://doi.org/10.1085/jgp.200308967>
- Zamponi, G.W., E. Bourinet, and T.P. Snutch. 1996. Nickel block of a family of neuronal calcium channels: subtype- and subunit-dependent action at multiple sites. *J. Membr. Biol.* 151:77–90. <https://doi.org/10.1007/s002329900059>
- Zhang, Q., M. Bengtsson, C. Partridge, A. Salehi, M. Braun, R. Cox, L. Eliasson, P.R.V. Johnson, E. Renström, T. Schneider, et al. 2007. R-type Ca<sup>2+</sup>-channel-evoked CICR regulates glucose-induced somatostatin secretion. *Nat. Cell Biol.* 9:453–460. <https://doi.org/10.1038/ncb1563>

## Supplemental material

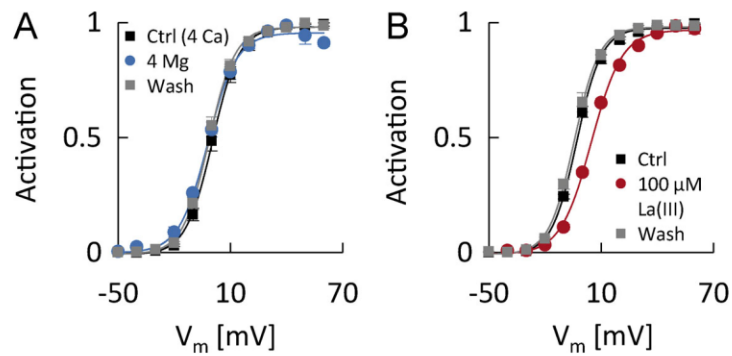


Figure S1. **Effects of  $\text{Ca}^{2+}$  substitution by  $\text{Mg}^{2+}$  or ionic block by  $\text{La}^{3+}$  on  $\text{Ca}_v2.3$  channel voltage dependence.** (A) Isochronous activation curves constructed from  $\text{Ca}_v2.3$  channel currents before (black squares), during (blue circles), and after (gray squares) substitution of 4 mM free  $\text{Ca}^{2+}$  as the charge carrier by 4 mM free  $\text{Mg}^{2+}$  ( $n = 5$  cells). (B) Isochronous activation curves constructed from  $\text{Ca}_v2.3$  channel currents carried by 4 mM free  $\text{Ca}^{2+}$  before (black squares), during (red circles), and after (gray squares) application of 100  $\mu\text{M}$  free  $\text{La}^{3+}$  ( $n = 6$  cells).

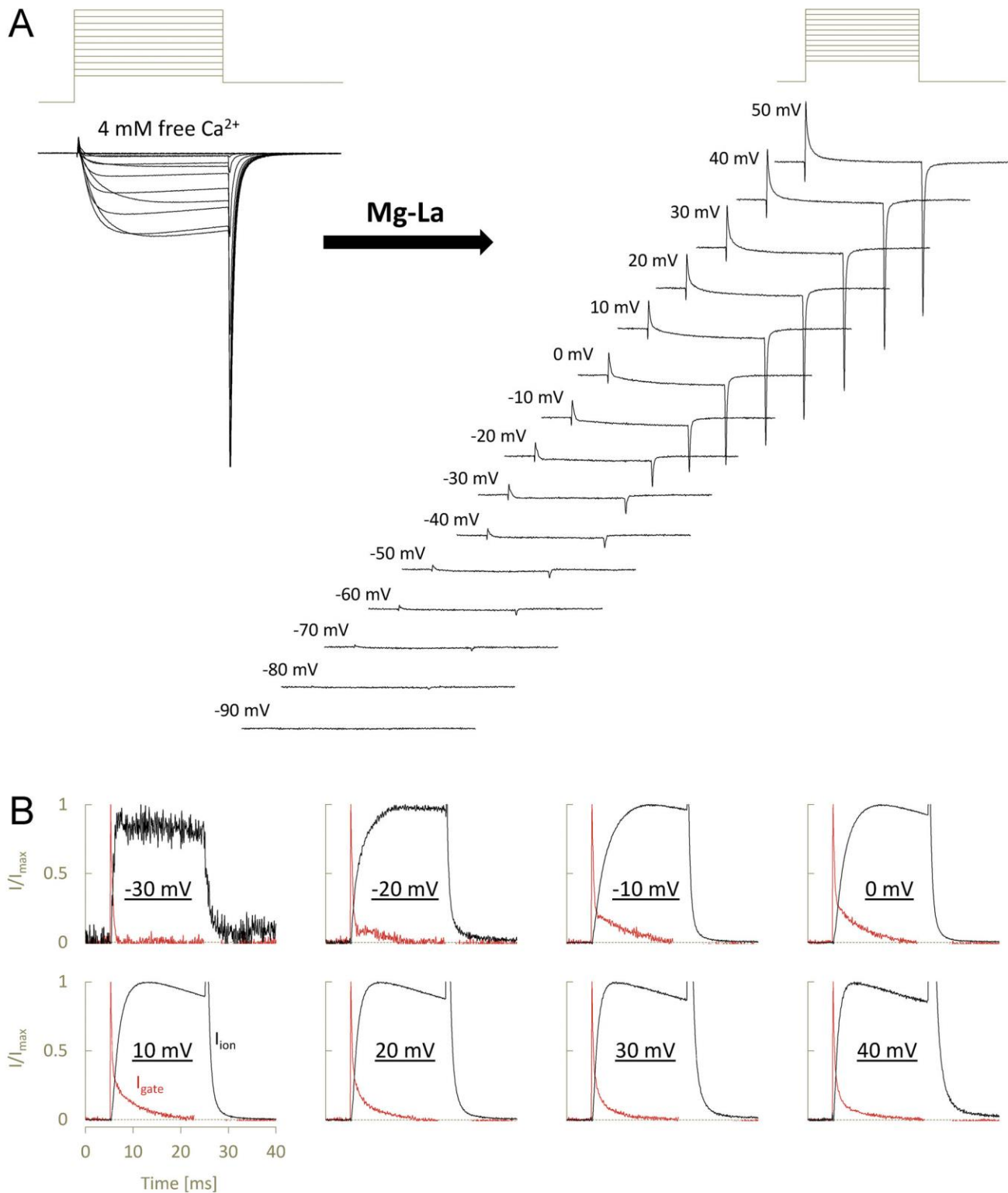


Figure S2. **Ca<sub>v</sub>2.3 channel ionic and gating currents.** (A) Mean ionic (left) and gating (right) current traces recorded from the same cells before and after  $\text{Ca}^{2+}$  substitution by  $\text{Mg}^{2+}$  and addition of  $100 \mu\text{M}$  free  $\text{La}^{3+}$  ( $n = 18$ ). Test potentials indicated next to the gating current traces have been corrected for the shift in channel voltage dependence produced by the  $\text{La}^{3+}$  used to suppress ionic currents. (B) Comparison of mean ionic (black) and gating (red) current traces after normalization by their maximum amplitudes to show that there was a significant fraction of charge movement that is too slow to be associated with channel opening (same cells as in A).



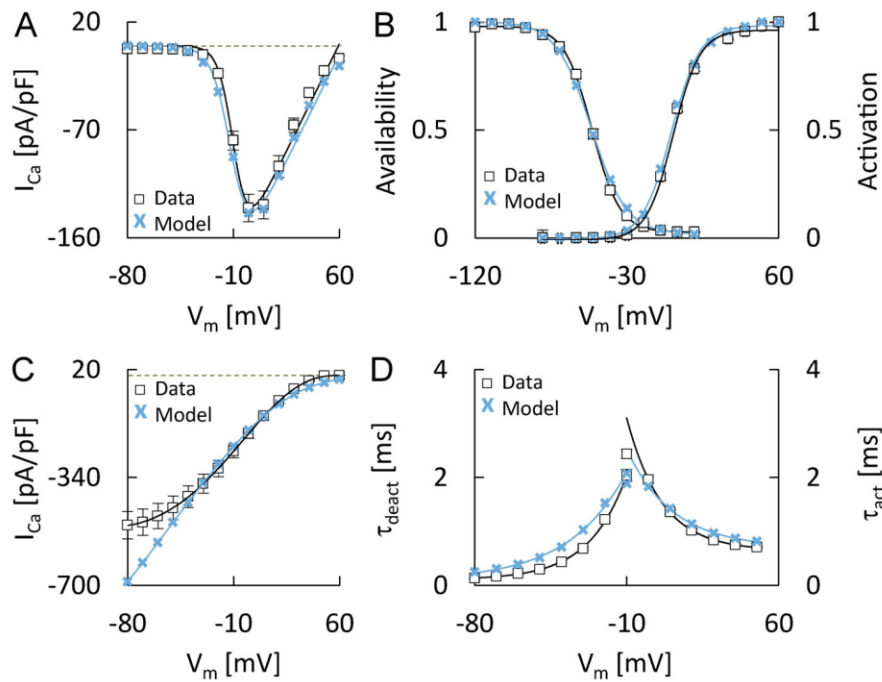


Figure S3. **Modeling  $Ca_v2.3$  channel gating under control conditions.** Comparison of I-V relationships (A), activation and PPI curves (B), II-V relationships (C), and activation and deactivation time constants (D), determined in the same way from either experimental control recordings with 4 mM  $Ca^{2+}$  as the charge carrier (open squares) or from currents simulated with the model shown in Fig. 15 (turquoise crosses).

Tables S1, S2, S3, S4, and S5 are provided online as separate files. Table S1 lists the composition of different external solutions used in electrophysiological recordings. Table S2 shows the absolute effects of 5.4  $\mu M$  free  $Zn^{2+}$  on  $Ca_v2.3$  channel gating under different experimental conditions. Table S3 lists the effects of different free  $Zn^{2+}$  concentrations on  $Ca_v2.3$  channel gating. Table S4 provides the  $E_{max}$  and  $K_{Zn}$  values obtained from  $Zn^{2+}$  concentration-response data under different experimental conditions. Table S5 provides the global  $K_{Zn}$  values for high-affinity shift and slowing.

### 3. Discussion

The exact role of Ca<sub>v</sub>2.3 channel modulation by endogenous Zn<sup>2+</sup> and Cu<sup>2+</sup> remains elusive, but our results provide evidence for a potential (patho)physiological relevance. For example, the findings in publication 4 indicate that Ca<sub>v</sub>2.3 channels are critically involved in the Zn<sup>2+</sup>-induced suppression of glucagon secretion and that glucose tolerance in Ca<sub>v</sub>2.3-deficient mice is highly sensitive to Zn<sup>2+</sup> chelation, so that dysfunction of these channels under conditions of Zn<sup>2+</sup>-deficiency could lead to severe disturbances in glucose homeostasis. In addition, in publication 5 we show that the excitatory amino acid KA can reverse suppression by physiological Cu<sup>2+</sup> concentrations *in vitro* and stimulate Ca<sup>2+</sup> influx through cloned Ca<sub>v</sub>2.3 channels even in the absence of functional glutamate receptors. These and other findings prompted us to re-assess the effects Zn<sup>2+</sup> as a prototype redox-inert trace metal ion on Ca<sub>v</sub>2.3 channel function. The results described in publication 6 reveal that Zn<sup>2+</sup>-induced Ca<sub>v</sub>2.3 channel modulation is complex and inconsistent with a single mechanism of action, that it can be either inhibitory or stimulatory and that it may persist for several minutes even after cessation of the Zn<sup>2+</sup> signal. To account for these findings, we have developed a preliminary Markov model that describes well many qualitative and quantitative features of the experimental data and could provide a starting point for future studies on the intricate effects of endogenous Zn<sup>2+</sup> (and Cu<sup>2+</sup>) on Ca<sub>v</sub>2.3 channel function in neuronal, neuroendocrine and possibly other tissues. Below, I will briefly summarize our findings with regard to the mechanisms of Ca<sub>v</sub>2.3 channel modulation by trace metal ions and trace metal chelators and discuss potential implications for Ca<sub>v</sub>2.3 channel function in the brain and endocrine pancreas.

#### 3.1. Mechanisms of Ca<sub>v</sub>2.3 channel modulation by Zn<sup>2+</sup> and Cu<sup>2+</sup>

(Sub)micromolar concentrations of Zn<sup>2+</sup>, Cu<sup>2+</sup> or Ni<sup>2+</sup> produce depolarizing shifts in the voltage-dependence of cloned Ca<sub>v</sub>2.3 channel gating, a reduced slope of the activation curve, a pronounced slowing of activation and a decrease in the maximum macroscopic conductance (Drobinskaya et al., 2015; Kang et al., 2007; Neumaier et al., 2018a; Shcheglovitov et al., 2012; Zamponi et al., 1996). Although histidine residues in the domain I VSM have been implicated in the shift and slowing (Kang et al., 2007; Shcheglovitov et al., 2012), the underlying mechanisms, their dependence on the experimental conditions and the potential role of additional metal binding sites remain incompletely understood. We have addressed some of these questions in publication 6, the results of which indicate that multiple sites contribute to the effects of Zn<sup>2+</sup>. For example, concentration-response curves for the shift and slowing obtained under near-physiological ionic conditions revealed separable high- and low-affinity components, which could also be distinguished based on their sensitivity to histidine modification by DEPC. With 4 mM free Ca<sup>2+</sup> as the charge carrier, the high-affinity effects were half-maximal at Zn<sup>2+</sup> concentrations in the order of 4.2-4.6 μM and produced, at most, a shift by approximately 20 mV and a two- to three-fold slowing of activation. These effects were reduced or prevented by histidine-modification with DEPC, suggesting that they result from Zn<sup>2+</sup> binding to the putative metal binding site. Consistent with this assumption, computer simulations showed that both effects could be

well described by assuming that a single, bimolecular reaction between  $\text{Zn}^{2+}$  and a site on the channel results in electrostatic modification and mechanical slowing of one of the voltage-sensors. Moderate acidification (from pH 7.4 to 7.0) or a decrease in the extracellular  $\text{Ca}^{2+}$  concentration (from 4 to 2 mM) significantly increased or decreased respectively, the apparent  $K_{\text{Zn}}$  value for high-affinity shift and slowing, indicating that there is competition for binding between  $\text{Zn}^{2+}$ ,  $\text{Ca}^{2+}$  and protons. However, while  $\text{Ca}^{2+}$  concentrations neither affected the maximum effects mediated by high-affinity binding, nor activation under control conditions (i.e.  $\text{Ca}^{2+}$  appeared to antagonize  $\text{Zn}^{2+}$  binding competitively), acidification reduced the maximum  $\text{Zn}^{2+}$  action and produced effects similar to  $\text{Zn}^{2+}$  under control conditions. The latter is consistent with previous findings that protons affect  $\text{Ca}_v2.3$  channel gating by interaction with histidine residues in the proposed metal binding site (Cens et al., 2011) and indicates that they are less effective than  $\text{Zn}^{2+}$ , possibly because of their lower charge. Protons have also been shown to reduce the slope of the activation curve and to decrease the unitary conductance, which has been linked to a histidine residue in one of the pore loops of domain I (Cens et al., 2011). Our findings indicate that  $\text{Zn}^{2+}$  could act in a similar manner, since histidine-modification also prevented the  $\text{Zn}^{2+}$ -induced slope reduction and a voltage-independent component of instantaneous current suppression, both of which became half-maximal at  $\text{Zn}^{2+}$  concentrations four to five times higher than the shift and slowing ( $K_{\text{Zn}} \sim 20 \mu\text{M}$ ) and were not reproduced by the model described above. Higher concentrations of  $\text{Zn}^{2+}$  also produced an additional shift and up to 5-fold slowing of activation and a weakly voltage-dependent block of instantaneous currents, which became half-maximal at  $\text{Zn}^{2+}$  concentrations in excess of 100  $\mu\text{M}$  and were largely insensitive to acidification or histidine-modification. In principle, all of these effects could reflect time- and voltage- or state-dependent unblock, in which case re-block of channels upon repolarization should have accelerated macroscopic deactivation. However, depolarization actually increased the degree of block and high concentrations of  $\text{Zn}^{2+}$  produced a subtle but significant deceleration of channel deactivation, indicating that the slowing was not directly related to intrinsically voltage- or state-dependent block. Based on circumstantial evidence and a previously proposed mechanism, we have instead assumed that  $\text{Zn}^{2+}$ -binding to a low affinity, superficial intra-pore site could block the channel and allosterically modify the opening and closing transitions. Computer simulations based on this idea are in reasonable agreement with the experimental data for free  $\text{Zn}^{2+}$  concentrations up to approximately 300  $\mu\text{M}$ , but other models could almost certainly account for the slowing as well. As  $\text{Zn}^{2+}$ -induced slowing of activation appears to be a common feature of all HVA but not LVA VGCCs, the underlying site may be conserved in other members of the family. For example, all HVA channels contain a putative EF-hand like motif that has previously been implicated in their differential sensitivity to  $\text{Zn}^{2+}$  block and is located external to the selectivity filter EEEE-locus (Sun et al., 2007), so that it could also account for the shallow voltage-dependence of block.



### 3.2. Trace metal chelators as functional Ca<sub>v</sub>2.3 channel agonists

Amino acids like histidine, cysteine or L-glutamic acid (L-Glu) have long been known for their ability to bind trace metal ions like Zn<sup>2+</sup> and Cu<sup>2+</sup>. More recently, L-Glu was identified as a potential agonist for Ca<sub>v</sub>2.3 channels that acts by reversing Zn<sup>2+</sup>- or Cu<sup>2+</sup>-induced suppression (Shcheglovitov et al., 2012). Transient relief of tonic Ca<sub>v</sub>2.3 channel inhibition by these metal ions following release of L-Glu into the synaptic cleft has been proposed to affect synaptic transmission and plasticity in the brain. In line with these observations, the results from publication 5 indicate that KA, a conformationally restricted analogue of L-Glu, is capable of reversing tonic Cu<sup>2+</sup>-induced suppression of cloned Ca<sub>v</sub>2.3 channels, presumably by formation of stable kainate-Cu<sup>2+</sup> complexes (Neumaier et al., 2018a). Thus, KA stimulated Ca<sub>v</sub>2.3 channels in the presence of 50 nM nominal Cu<sup>2+</sup> by shifting channel voltage-dependence to more negative test potentials, increasing their voltage-sensitivity and accelerating the time-course of activation, consistent with a reversal of trace metal-induced suppression. In addition, the effects were independent of the presence of functional glutamate receptors but depended on pre-existing suppression by Cu<sup>2+</sup> and could be reproduced by Cu<sup>2+</sup> chelation with tricine. In brain slice recordings from the hippocampal area, co-administration of the related neurotoxin domoic acid with Zn<sup>2+</sup> or Cd<sup>2+</sup> has also been shown to result in the formation of trace metal-neurotoxin complexes (Hoedemaker et al., 2005), supporting the experimental relevance of our findings in *in vitro* systems. In addition, when tricine was used as a surrogate for the receptor-independent action of KA in the isolated bovine retina, it produced effects consistent with increased GABAergic reciprocal inhibition of rod bipolar cells due to reversal of Ca<sub>v</sub>2.3 channel suppression in amacrine cells (Neumaier et al., 2018a). Brain tissue concentrations of KA reached after systemic administration have not been established (Berger et al., 1986), but are likely to be much lower than the millimolar concentrations of L-Glu that may be transiently reached in the synaptic cleft. However, KA is resistant to enzymatic degradation or reuptake, binds Cu<sup>2+</sup> much more tightly ( $\log K_{CuL}=10.1$  &  $\log K_{CuL2}=7.6$  compared to  $\log K_{CuL}=8.2$  &  $\log K_{CuL2}=6.4$  for L-Glu) (Aydin and Yirikogullari, 2010; Burns et al., 2007; Shuaib et al., 1999) and effectively reversed Cu<sup>2+</sup>-induced suppression at concentrations 10-times lower than L-Glu (Neumaier et al., 2018a). As such, the pathophysiological relevance of our observations in *in vivo* animal models of KA-induced seizures remains to be established, but they support and extend previous findings that endogenous or exogenous trace metal-binding compounds could profoundly alter excitability by indirectly modifying the function of Ca<sub>v</sub>2.3 and numerous other metal-sensitive targets (Boldyrev, 2001; Coddou et al., 2002; Eimerl and Schramm, 1993; Nelson et al., 2007; Shcheglovitov et al., 2012; Thio and Zhang, 2006; Trombley et al., 1998; Wakita et al., 2014).

### 3.3. Ca<sub>v</sub>2.3 channel modulation by endogenous brain Zn<sup>2+</sup> and Cu<sup>2+</sup>

The conditions under which vesicular Zn<sup>2+</sup> and Cu<sup>2+</sup> are released during synaptic activity and their exact functional significance remain enigmatic, making it difficult to predict the implications of Zn<sup>2+</sup>- or Cu<sup>2+</sup>-induced Ca<sub>v</sub>2.3 channel modulation for neuronal transmission. However, a remarkable consequence of the parallel changes in activation and inactivation

voltage-dependence described in publication 6 is that, depending on the resting membrane potential (RMP) of a cell,  $Zn^{2+}$  could both, inhibit or stimulate  $Ca^{2+}$  influx via  $Ca_v2.3$  channels. For example, currents were inhibited by application of  $5.4 \mu M$  free  $Zn^{2+}$  when they were evoked from a holding potential of  $-80$  mV, but potentiated by the same free  $Zn^{2+}$  concentration when they were evoked from a holding potential of  $-60$  mV. Washout of  $Zn^{2+}$  resulted in a further transient current stimulation that was followed by a progressive decline back to the control level, presumably due to time-dependent entry into one or more inactivated states. Hence, even though rises in the synaptic free or loosely-bound  $Zn^{2+}$  concentration during neuronal activity are likely to be transient, they could endow  $Ca_v2.3$  channels with a form of 'short-term memory' that alters their properties even after cessation of the  $Zn^{2+}$  signal. This could provide a mechanism to transiently increase their availability following release of  $Zn^{2+}$  into the synaptic cleft, with potential implications for certain forms of synaptic sensitization or plasticity. The holding potential-dependence of  $Zn^{2+}$  effects could also be involved in the pro-ictogenic role of  $Ca_v2.3$  channels observed in previous studies (Dibué-Adjei et al., 2017; Weiergräber et al., 2007, 2006a), since depolarization of the neuronal RMP due to e.g. spreading depolarization or paroxysmal depolarizing shifts could lead to a decrease in the inhibitory action or even reverse the direction of  $Zn^{2+}$  effects from inhibition to stimulation. In addition, our findings in publications 4-6 show that mild acidosis, as typically observed during seizures, or trace metal chelation by endogenous (i.e. L-Glu, carnosine, glutathione) or exogenous (i.e. KA, DEDTC) agents could significantly reduce the effects of  $Zn^{2+}$  or  $Cu^{2+}$  on  $Ca_v2.3$  channel gating regardless of the holding potential. Since even very small changes in ion channel function (Thomas et al., 2009) and synaptic gain (Du et al., 2019) can lead to seizure-like activity, it seems conceivable that reduced  $Ca_v2.3$  channel suppression by  $Zn^{2+}$  could contribute to the ictogenic processes when the brain moves into a pro-seizure state. However, further studies on  $Zn^{2+}$ -induced  $Ca_v2.3$  channel modulation will clearly be required to firmly establish the kinetics, magnitude and direction of  $Zn^{2+}$  effects on native  $Ca_v2.3$  channels in different cells, as they could be influenced by a number of factors such as subunit-composition or alternative splicing. For example,  $Ca_v\beta$ -subunits have been shown to differentially modify the time-course of  $Ca_v2.3$  channel recovery from inactivation at depolarized test potentials (Jeziorski et al., 2000), which could in turn alter the dynamics of  $Zn^{2+}$ -induced modulation. Likewise, co-expression of different  $Ca_v\beta$ -subunits has been shown differentially affect the gating effects of  $Ni^{2+}$  on cloned  $Ca_v2.1$  channels (Zamponi et al., 1996), suggesting that auxiliary subunits could also directly influence trace metal-induced VGCC modulation.

### **3.4. $Ca_v2.3$ channels as a target for paracrine $Zn^{2+}$ signals in the pancreas**

The two most important findings of our study on the role of  $Ca_v2.3$  channels for blood glucose homeostasis are that (i) fasting glucose and glucagon levels are significantly higher in  $Ca_v2.3$ -deficient compared to wildtype mice, while (ii) the correlated increase of blood glucose and serum glucagon levels observed during  $Zn^{2+}$ -chelation in wildtype mice is severely blunted in  $Ca_v2.3$ -deficient mice (Drobinskaya et al., 2015). Thus,  $Ca_v2.3$ -deficiency

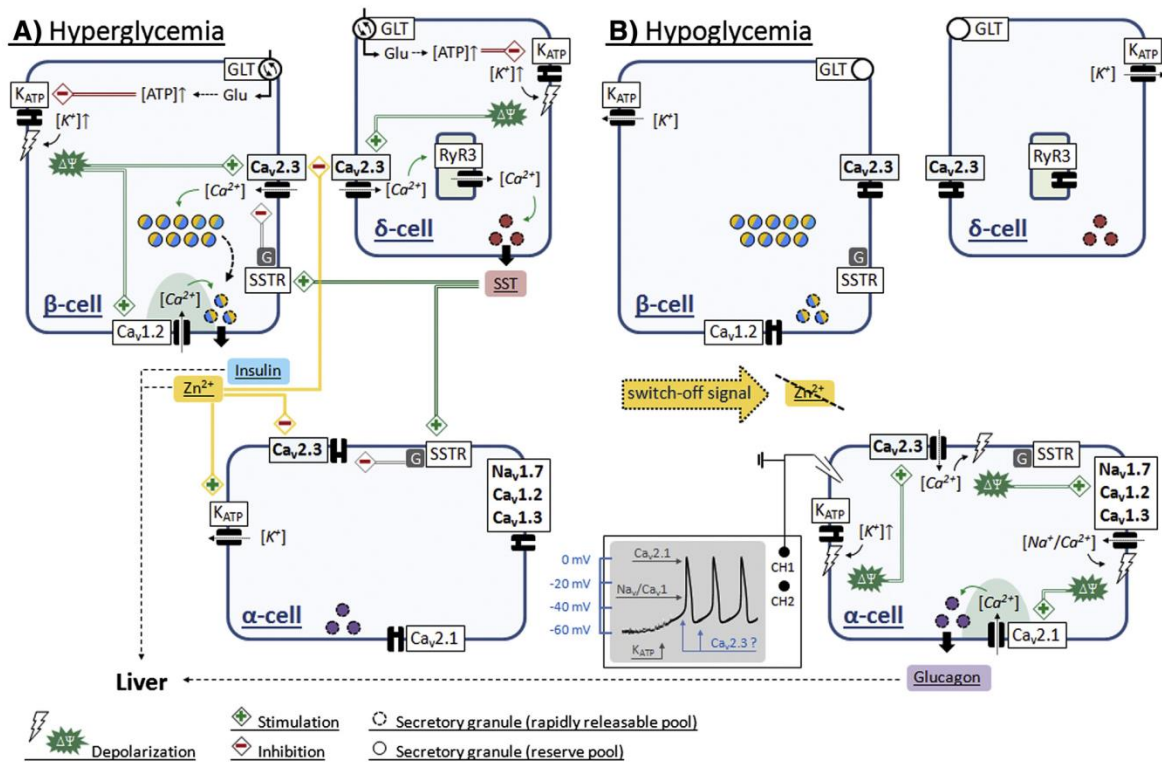


**Figure 5.** Schema of putative  $Zn^{2+}$ -mediated functional coupling between insulin and glucagon release. **(A)** In the presence of normal or high blood glucose concentrations, ATP level in  $\beta$ -cells increases, leading to closure of  $K_{ATP}$  channels, depolarization and co-secretion of insulin and  $Zn^{2+}$ . In downstream  $\alpha$ -cells,  $Zn^{2+}$  counteracts glucagon release by activation of  $K_{ATP}$  channels and inhibition of  $Ca_v2.3$  channels. **(B)** Under conditions of hypoglycemia, ATP level in  $\beta$ -cells decreases, leading to disinhibition of  $K_{ATP}$  channels,  $K^+$  efflux and thus hyperpolarization with closure of voltage-gated  $Ca^{2+}$  channels. The resulting switch off of  $Zn^{2+}$  release from upstream  $\beta$ -cells is associated with closure of  $K_{ATP}$  channels and disinhibition of  $Ca_v2.3$  channels in  $\alpha$ -cells, which ultimately leads to release of glucagon. Reprinted with permission from (Drobinskaya et al., 2015).

appears to impair the coupling between blood glucose levels and glucagon secretion rather than reducing glucagon release per se, which could explain previous findings that glucose challenge produces a paradoxical stimulation of glucagon release in  $Ca_v2.3$ -deficient mice (Jing et al., 2005). According to the  $Zn^{2+}$  switch-off hypothesis,  $Zn^{2+}$  co-secreted with insulin during hyperglycemia could hyperpolarize  $\alpha$ -cells by opening  $K_{ATP}$  channels, leading to closure of  $Na^+$  and  $Ca^{2+}$  channels and suppression of glucagon release (**Fig. 5A**) (Gyulkhandanyan et al., 2008; Slucca et al., 2010; Zhou et al., 2007). Sudden cessation of  $Zn^{2+}$  release during hypoglycemia could conversely depolarize  $\alpha$ -cells through closure of  $K_{ATP}$  channels, leading to  $Na^+$  and L-type  $Ca^{2+}$  channel-dependent action potential firing and (during the peak of the AP) local  $Ca^{2+}$  influx through P/Q-type channels, which then mediates glucagon secretion (**Fig. 5B**). Considering their intermediate threshold for activation,  $Ca_v2.3$  channel disinhibition upon cessation of  $Zn^{2+}$  supply could conceivably serve to amplify the effects of  $K_{ATP}$  channel closure, providing sufficient depolarization for subsequent  $Na^+$  and L-type  $Ca^{2+}$  channel-dependent AP firing. However, the fact that  $Ca_v2.3$ -deficiency did not reduce overall glucagon release indicates that  $Ca_v2.3$  channel opening per



se may not be a critical requirement for  $\alpha$ -cell secretion, but could instead alter P/Q-type channel-dependent exocytosis by e.g. modifying the threshold or peak height of the APs. This would be consistent with their proposed role for fine-tuning of rhythmogenesis in oscillatory networks (Schneider et al., 2015) and with the fact that  $\text{Ca}_v2.3$  channel inactivation at typical  $\alpha$ -cell membrane potentials would be predicted to limit their contribution to  $\text{Ca}^{2+}$  influx and thus secretion. On the other hand, the  $\text{Zn}^{2+}$ -induced changes in inactivation voltage-dependence described in publication 6 could significantly increase their availability at rest. Upon cessation of  $\text{Zn}^{2+}$ -supply, rapid reversal of  $\text{Zn}^{2+}$ -induced suppression could allow for a brief burst of  $\text{Ca}^{2+}$  influx before time-dependent inactivation would again limit the number of channels available for activation. Given the synchronous nature of basal insulin and glucagon secretion, it is tempting to speculate that (cessation of)  $\text{Zn}^{2+}$  release from pancreatic  $\beta$ -cells could provide some kind of impulse generator for pulsatile  $\alpha$ -cell glucagon secretion, possibly triggered by  $\text{Ca}_v2.3$  channels, which synchronizes the release of both peptide hormones. However, it has also been proposed that the suppression of glucagon secretion during hyperglycemia is independent of  $\text{Zn}^{2+}$  and results from  $\alpha$ -cell glucose metabolism and closure of  $\text{K}_{\text{ATP}}$  channels, which depolarizes the cell sufficiently to inactivate  $\text{Na}^+$  and L-type  $\text{Ca}^{2+}$  channels (Göpel et al., 2004, 2000; Gromada et al., 2004). In this view, electrical activity and global  $\text{Ca}^{2+}$  oscillations remain preserved during hyperglycemia, but the lower AP peak height associated with  $\text{Na}^+$  and L-type  $\text{Ca}^{2+}$  channel inactivation reduces P/Q-type  $\text{Ca}^{2+}$  channel mediated exocytosis. Here a  $\text{Zn}^{2+}$ -induced depolarizing shift in the voltage-dependence of  $\alpha$ -cell  $\text{Ca}_v2.3$  channels could allow them to remain active during hyperglycemia, where they might be involved in maintaining electrical activity and global  $\text{Ca}^{2+}$  oscillations. Further studies will therefore be required to define both, the direction of  $\text{Zn}^{2+}$  effects on  $\alpha$ -cell  $\text{Ca}_v2.3$  channels during hyperglycemia, and their exact role for regulating glucagon secretion.

Another interesting observation of our study was that isolated islets from  $\text{Ca}_v2.3$ -deficient mice exhibit increased basal insulin secretion and reduced insulin content but normal GSIS, while the peripheral insulin response *in vivo* was significantly reduced by about 50% in  $\text{Ca}_v2.3$ -deficient mice (Drobinskaya et al., 2015). A similar 50% decrease of second phase insulin secretion was previously observed during *in situ* perfusion of pancreata from  $\text{Ca}_v2.3$ -deficient mice (Jing et al., 2005), suggesting that it is not related to increased postprandial insulin clearance. Instead,  $\text{Ca}_v2.3$  channels could also be involved in  $\text{Zn}^{2+}$ -induced autocrine feedback inhibition of basal insulin secretion, so that their ablation results in excessive insulin release and depleted insulin stores, akin to  $\beta$ -cell exhaustion in rodent models of type 2 diabetes mellitus (T2DM) (Grill et al., 1987; Kergoat et al., 1987). In non-diabetic rats, transient upregulation of insulin release with tolbutamide to lower  $\beta$ -cell insulin contents has been shown to selectively reduce the second phase insulin response by about 50% (Hosokawa and Leahy, 1997). Basal *in vivo* insulin secretion is only moderately increased in  $\text{Ca}_v2.3$ -deficient compared to wildtype mice (Jing et al., 2005; Matsuda et al., 2001; Pereverzev et al., 2005), suggesting that neurally mediated feedback loops or other islet-extrinsic factors could partly counter-balance intrinsic hyperinsulinemia to keep insulin

levels below the detrimental range. Interestingly however, we also observed that  $\text{Ca}_v2.3$ -deficient mice exhibit signs of pre-diabetes followed by a progressive loss of glycemic control, which is consistent with previous reports that these animals may develop symptoms of T2DM, such as insulin resistance, glucose intolerance and overweight (Matsuda et al., 2001). As such, they could be a valuable model for certain aspects of human T2DM, an idea that is reinforced by several studies linking variants in the gene encoding  $\text{Ca}_v2.3$  channels to impaired glucose homeostasis in human T2DM patients (Holmkvist et al., 2007; Muller et al., 2007; Trombetta et al., 2012). In particular, in Pima Indians, where a variant of the human  $\text{Ca}_v2.3$  gene has been linked young-onset T2DM (Muller et al., 2007), high fasting plasma insulin concentrations predicted T2DM independent of insulin resistance, pointing to a causative role of basal hyperinsulinemia (Weyer et al., 2000). Based on our findings,  $\text{Zn}^{2+}$  supplementation could possibly preserve glucose tolerance in these patients and provide a general interventional approach for certain patient populations with T2DM.

### **3.5. Conclusion**

Endogenous trace metal ions are increasingly recognized as potential modulators of neuronal transmission and neuroendocrine function and have been implicated in a number of pathophysiological conditions. Our findings confirm and extend previous findings about the high sensitivity of  $\text{Ca}_v2.3$  channels to physiologically relevant concentrations of  $\text{Zn}^{2+}$  or  $\text{Cu}^{2+}$  and indicate that multiple metal binding sites are likely to be involved in the action of trace metal ions on these channels. In addition, they provide evidence for a potential pathophysiological relevance of  $\text{Zn}^{2+}$ -induced  $\text{Ca}_v2.3$  channel modulation in the context of T2DM and possibly epilepsy. Finally, we have developed a preliminary model that reproduces most salient features of  $\text{Ca}_v2.3$  channel currents in the absence of trace metals and can also account for the hallmarks of  $\text{Zn}^{2+}$ -induced  $\text{Ca}_v2.3$  channel modulation. While still far from complete, our model provides a quantitative framework for understanding  $\text{Zn}^{2+}$  effects on  $\text{Ca}_v2.3$  channel function and a first step towards the application of computational approaches for predicting the complex effects of  $\text{Zn}^{2+}$  on neuronal excitability.

## 4. References

- Aiba, I., Carlson, A.P., Sheline, C.T., Shuttleworth, C.W., 2012. Synaptic release and extracellular actions of Zn<sup>2+</sup> limit propagation of spreading depression and related events *in vitro* and *in vivo*. *J. Neurophysiol.* 107, 1032–1041. <https://doi.org/10.1152/jn.00453.2011>
- Albanna, W., Lüke, J.N., Schubert, G.A., Dibué-Adjei, M., Kotliar, K., Hescheler, J., Clusmann, H., Steiger, H.-J., Hänggi, D., Kamp, M.A., Schneider, T., Neumaier, F., 2019. Modulation of Ca<sub>v</sub>2.3 channels by unconjugated bilirubin (UCB) – Candidate mechanism for UCB-induced neuromodulation and neurotoxicity. *Mol. Cell. Neurosci.* 96, 35–46. <https://doi.org/10.1016/j.mcn.2019.03.003>
- Albanna, W., Neumaier, F., Lüke, J.-N., Kotliar, K., Conzen, C., Lindauer, U., Hescheler, J., Clusmann, H., Schneider, T., Schubert, G.A., 2017. Unconjugated bilirubin modulates neuronal signaling only in wild-type mice, but not after ablation of the R-type/Ca<sub>v</sub>2.3 voltage-gated calcium channel. *CNS Neurosci. Ther.* 2017, 1–9. <https://doi.org/10.1111/cns.12791>
- Almers, W., McCleskey, E.W., 1984. Non-selective conductance in calcium channels of frog muscle: Calcium selectivity in a single-file pore. *J. Physiol.* 353, 585–608. <https://doi.org/10.1113/jphysiol.1984.sp015352>
- Almog, M., Korngreen, A., 2009. Characterization of voltage-gated Ca<sup>2+</sup> conductances in layer 5 neocortical pyramidal neurons from rats. *PLoS One* 4, e4841. <https://doi.org/10.1371/journal.pone.0004841>
- Alnawaiseh, M., Albanna, W., Chen, C.-C., Campbell, K.P., Hescheler, J., Lüke, M., Schneider, T., 2011. Two separate Ni<sup>2+</sup>-sensitive voltage-gated Ca<sup>2+</sup> channels modulate transretinal signalling in the isolated murine retina. *Acta Ophthalmol.* 89, e579-90. <https://doi.org/10.1111/j.1755-3768.2011.02167.x>
- Anastassov, I.A., Ripps, H., Chappell, R.L., 2014. Cytoprotection by endogenous zinc in the vertebrate retina. *J. Neurochem.* 129, 249–255. <https://doi.org/10.1111/jnc.12627>
- Anastassov, I.A., Shen, W., Ripps, H., Chappell, R.L., 2013. Zinc modulation of calcium activity at the photoreceptor terminal: A calcium imaging study. *Exp. Eye Res.* 112, 37–44. <https://doi.org/10.1016/j.exer.2013.04.011>
- Anzellotti, A.I., Farrell, N.P., 2008. Zinc metalloproteins as medicinal targets. *Chem. Soc. Rev.* 37, 1629. <https://doi.org/10.1039/b617121b>
- Armstrong, C.M., Neyton, J., 1991. Ion permeation through calcium channels. A one-site model. *Ann. N. Y. Acad. Sci.* 635, 18–25. <https://doi.org/10.1111/j.1749-6632.1991.tb36477.x>
- Assaf, S.Y., Chung, S.-H., 1984. Release of endogenous Zn<sup>2+</sup> from brain tissue during activity. *Nature* 308, 734–736. <https://doi.org/10.1038/308734a0>
- Aydin, R., Yirikogullari, A., 2010. Potentiometric study on complexation of divalent transition metal ions with amino acids and adenosine 5'-triphosphate. *J. Chem. Eng. Data* 55, 4794–4800. <https://doi.org/10.1021/je100402a>
- Banarar, S., McGregor, V.P., Cryer, P.E., 2002. Intraislet hyperinsulinemia prevents the glucagon response to hypoglycemia despite an intact autonomic response. *Diabetes* 51, 958–965. <https://doi.org/10.2337/diabetes.51.4.958>
- Becq, F., 1996. Ionic channel rundown in excised membrane patches. *Biochim. Biophys. Acta - Rev. Biomembr.* 1286, 53–63. [https://doi.org/10.1016/0304-4157\(96\)00002-0](https://doi.org/10.1016/0304-4157(96)00002-0)
- Belles, B., Malécot, C.O., Hescheler, J., Trautwein, W., 1988. “Run-down” of the Ca current during long whole-cell recordings in guinea pig heart cells: Role of phosphorylation and



- intracellular calcium. *Pflügers Arch. Eur. J. Physiol.* 411, 353–360. <https://doi.org/10.1007/BF00587713>
- Benquet, P., Guen, J. Le, Dayanithi, G., Pichon, Y., Tiaho, F., 1999.  $\omega$ -AgaIVA-sensitive (P/Q-type) and -resistant (R-type) high-voltage-activated  $\text{Ba}^{2+}$  currents in embryonic cockroach brain neurons. *J. Neurophysiol.* 82, 2284–2293. <https://doi.org/10.1152/jn.1999.82.5.2284>
- Berger, M.L., Lefauconnier, J.-M., Tremblay, E., Ben-Ari, Y., 1986. Limbic seizures induced by systemically applied kainic acid: How much kainic acid reaches the brain?, in: *Excitatory Amino Acids and Epilepsy. Advances in Experimental Medicine and Biology* Vol. 203. Springer, Boston, MA, pp. 199–209. [https://doi.org/10.1007/978-1-4684-7971-3\\_15](https://doi.org/10.1007/978-1-4684-7971-3_15)
- Beyl, S., Hohaus, A., Andranovits, S., Timin, E., Hering, S., 2016. Upward movement of IS4 and IIIS4 is a rate-limiting stage in  $\text{Ca}_v1.2$  activation. *Pflügers Arch. - Eur. J. Physiol.* 468, 1895–1907. <https://doi.org/10.1007/s00424-016-1895-5>
- Birnbaumer, L., Campbell, K.P., Catterall, W.A., Harpold, M.M., Hofmann, F., Horne, W.A., Mori, Y., Schwartz, A., Snutch, T.P., Tanabe, T., Tsien, R.W., 1994. The naming of voltage-gated calcium channels. *Neuron* 13, 505–506. [https://doi.org/10.1016/0896-6273\(94\)90021-3](https://doi.org/10.1016/0896-6273(94)90021-3)
- Blasco-Ibáñez, J.M., Poza-Aznar, J., Crespo, C., Marqués-Marí, A.I., Gracia-Llanes, F.J., Martínez-Guijarro, F.J., 2004. Chelation of synaptic zinc induces overexcitation in the hilar mossy cells of the rat hippocampus. *Neurosci. Lett.* 355, 101–104. <https://doi.org/10.1016/j.neulet.2003.10.053>
- Bloodgood, B.L., Sabatini, B.L., 2007. Nonlinear regulation of unitary synaptic signals by  $\text{Ca}_v2.3$  voltage-sensitive calcium channels located in dendritic spines. *Neuron* 53, 249–260. <https://doi.org/10.1016/j.neuron.2006.12.017>
- Boldyrev, A., 2001. Carnosine as a modulator of endogenous  $\text{Zn}^{2+}$  effects. *Trends Pharmacol. Sci.* 22, 112–113. [https://doi.org/10.1016/S0165-6147\(00\)01648-5](https://doi.org/10.1016/S0165-6147(00)01648-5)
- Bourinet, E., Zamponi, G.W., Stea, A., Soong, T.W., Lewis, B.A., Jones, L.P., Yue, D.T., Snutch, T.P., 1996. The  $\alpha_{1E}$  calcium channel exhibits permeation properties similar to low-voltage-activated calcium channels. *J. Neurosci.* 16, 4983–4993. <https://doi.org/10.1523/jneurosci.16-16-04983.1996>
- Budde, T., Meuth, S., Pape, H.-C., 2002. Calcium-dependent inactivation of neuronal calcium channels. *Nat. Rev. Neurosci.* 3, 873–883. <https://doi.org/10.1038/nrn959>
- Burarei, Z., Yang, J., 2013. Structure and function of the  $\beta$  subunit of voltage-gated  $\text{Ca}^{2+}$  channels. *Biochim. Biophys. Acta - Biomembr.* 1828, 1530–1540. <https://doi.org/10.1016/j.bbamem.2012.08.028>
- Burns, J.M., Schock, T.B., Hsia, M.H., Moeller, P.D.R., Ferry, J.L., 2007. Photostability of kainic acid in seawater. *J. Agric. Food Chem.* 55, 9951–9955. <https://doi.org/10.1021/jf072362x>
- Büsselberg, D., Platt, B., Michael, D., Carpenter, D.O., Haas, H.L., 1994. Mammalian voltage-activated calcium channel currents are blocked by  $\text{Pb}^{2+}$ ,  $\text{Zn}^{2+}$ , and  $\text{Al}^{3+}$ . *J. Neurophysiol.* 71, 1491–1497. <https://doi.org/10.1152/jn.1994.71.4.1491>
- Cadetti, L., Thoreson, W.B., Piccolino, M., 2004. Pre- and post-synaptic effects of manipulating surface charge with divalent cations at the photoreceptor synapse. *Neuroscience* 129, 791–801. <https://doi.org/10.1016/j.neuroscience.2004.08.043>
- Carbone, E., Lux, H.D., 1987. Single low-voltage-activated calcium channels in chick and rat sensory neurones. *J. Physiol.* 386, 571–601. <https://doi.org/10.1113/jphysiol.1987.sp016552>

- Carbone, E., Lux, H.D., 1984. A low voltage-activated, fully inactivating Ca channel in vertebrate sensory neurones. *Nature* 310, 501–502. <https://doi.org/10.1038/310501a0>
- Carvill, G.L., 2019. Calcium channel dysfunction in epilepsy: Gain of CACNA1E. *Epilepsy Curr.* 19, 199–201. <https://doi.org/10.1177/1535759719845324>
- Castelli, L., Tanzi, F., Taglietti, V., Magistretti, J., 2003. Cu<sup>2+</sup>, Co<sup>2+</sup>, and Mn<sup>2+</sup> modify the gating kinetics of high-voltage-activated Ca<sup>2+</sup> channels in rat palaeocortical neurons. *J. Membr. Biol.* 195, 121–136. <https://doi.org/10.1007/s00232-003-0614-2>
- Catterall, W.A., 2011. Voltage-gated calcium channels. *Cold Spring Harb. Perspect. Biol.* 3, a003947–a003947. <https://doi.org/10.1101/cshperspect.a003947>
- Catterall, W.A., Striessnig, J., Snutch, T.P., Perez-Reyes, E., 2003. International Union of Pharmacology. XL. Compendium of voltage-gated ion channels: Calcium channels. *Pharmacol. Rev.* 55, 579–581. <https://doi.org/10.1124/pr.55.4.8>
- Cens, T., Rousset, M., Charnet, P., 2011. Two sets of amino acids of the domain I of Ca<sub>v</sub>2.3 Ca<sup>2+</sup> channels contribute to their high sensitivity to extracellular protons. *Pflügers Arch. Eur. J. Physiol.* 462, 303–314. <https://doi.org/10.1007/s00424-011-0974-x>
- Cens, T., Rousset, M., Kajava, A., Charnet, P., 2007. Molecular determinant for specific Ca/Ba selectivity profiles of low and high threshold Ca<sup>2+</sup> channels. *J. Gen. Physiol.* 130, 415–425. <https://doi.org/10.1085/jgp.200709771>
- Cerda, O., Baek, J.-H., Trimmer, J.S., 2011. Mining recent brain proteomic databases for ion channel phosphosite nuggets. *J. Gen. Physiol.* 137, 3–16. <https://doi.org/10.1085/jgp.201010555>
- Chad, J.E., Eckert, R., 1986. An enzymatic mechanism for calcium current inactivation in dialysed Helix neurones. *J. Physiol.* 378, 31–51. <https://doi.org/10.1113/jphysiol.1986.sp016206>
- Charton, G., Rovira, C., Ben-Ari, Y., Leviel, V., 1985. Spontaneous and evoked release of endogenous Zn<sup>2+</sup> in the hippocampal mossy fiber zone of the rat *in situ*. *Exp. Brain Res.* 58. <https://doi.org/10.1007/BF00238969>
- Christie, B.R., Eliot, L.S., Ito, K.-I., Miyakawa, H., Johnston, D., 1995. Different Ca<sup>2+</sup> channels in soma and dendrites of hippocampal pyramidal neurons mediate spike-induced Ca<sup>2+</sup> influx. *J. Neurophysiol.* 73, 2553–7. <https://doi.org/10.1152/jn.1995.73.6.2553>
- Cibulsky, S.M., Sather, W.A., 2000. The EEEE locus is the sole high-affinity Ca<sup>2+</sup> binding structure in the pore of a voltage-gated Ca<sup>2+</sup> channel: Block by Ca<sup>2+</sup> entering from the intracellular pore entrance. *J. Gen. Physiol.* 116, 349–362. <https://doi.org/10.1085/jgp.116.3.349>
- Coddou, C., Villalobos, C., González, J., Acuña-Castillo, C., Loeb, B., Huidobro-Toro, J.P., 2002. Formation of carnosine-Cu(II) complexes prevents and reverts the inhibitory action of copper in P2X<sub>4</sub> and P2X<sub>7</sub> receptors. *J. Neurochem.* 80, 626–633. <https://doi.org/10.1046/j.0022-3042.2001.00732.x>
- Cohen, R., Buttke, D.E., Asano, A., Mukai, C., Nelson, J.L., Ren, D., Miller, R.J., Cohen-Kutner, M., Atlas, D., Travis, A.J., 2014. Lipid modulation of calcium flux through Ca<sub>v</sub>2.3 regulates acrosome exocytosis and fertilization. *Dev. Cell* 28, 310–321. <https://doi.org/10.1016/j.devcel.2014.01.005>
- Colvin, R.A., Fontaine, C.P., Laskowski, M., Thomas, D., 2003. Zn<sup>2+</sup> transporters and Zn<sup>2+</sup> homeostasis in neurons. *Eur. J. Pharmacol.* 479, 171–185. <https://doi.org/10.1016/j.ejphar.2003.08.067>
- Colvin, R.A., Holmes, W.R., Fontaine, C.P., Maret, W., 2010. Cytosolic zinc buffering and muffling: Their role in intracellular zinc homeostasis. *Metallomics* 2, 306. <https://doi.org/10.1039/b926662c>

- Cota, G., 1986. Calcium channel currents in pars intermedia cells of the rat pituitary gland. Kinetic properties and washout during intracellular dialysis. *J. Gen. Physiol.* 88, 83–105. <https://doi.org/10.1085/jgp.88.1.83>
- Curtis, B.M., Catterall, W.A., 1986. Reconstitution of the voltage-sensitive calcium channel purified from skeletal muscle transverse tubules. *Biochemistry* 25, 3077–3083. <https://doi.org/10.1021/bi00359a002>
- Curtis, B.M., Catterall, W.A., 1984. Purification of the calcium antagonist receptor of the voltage-sensitive calcium channel from skeletal muscle transverse tubules. *Biochemistry* 23, 2113–2118. <https://doi.org/10.1021/bi00305a001>
- Dang, T.X., McCleskey, E.W., 1998. Ion channel selectivity through stepwise changes in binding affinity. *J. Gen. Physiol.* 111, 185–193. <https://doi.org/10.1085/jgp.111.2.185>
- Day, N.C., Shaw, P.J., McCormack, A.L., Craig, P.J., Smith, W., Beattie, R., Williams, T.L., Ellis, S.B., Ince, P.G., Harpold, M.M., Lodge, D., Volsen, S.G., 1996. Distribution of  $\alpha_{1A}$ ,  $\alpha_{1B}$  and  $\alpha_{1E}$  voltage-dependent calcium channel subunits in the human hippocampus and parahippocampal gyrus. *Neuroscience* 71, 1013–1024. [https://doi.org/10.1016/0306-4522\(95\)00514-5](https://doi.org/10.1016/0306-4522(95)00514-5)
- Dibué-Adjei, M., Kamp, M.A., Alpdogan, S., Tevoufouet, E.E., Neiss, W.F., Hescheler, J., Schneider, T., 2017. Cav2.3 (R-type) calcium channels are critical for mediating anticonvulsive and neuroprotective properties of lamotrigine *in vivo*. *Cell. Physiol. Biochem.* 44, 935–947. <https://doi.org/10.1159/000485361>
- Dietrich, D., Kirschstein, T., Kukley, M., Pereverzev, A., Brelie, C. Von Der, Schneider, T., Beck, H., 2003. Functional specialization of presynaptic Cav2.3 Ca<sup>2+</sup> channels. *Neuron* 39, 1–20. [https://doi.org/10.1016/s0896-6273\(03\)00430-6](https://doi.org/10.1016/s0896-6273(03)00430-6)
- Doering, P., Stoltenberg, M., Penkowa, M., Rungby, J., Larsen, A., Danscher, G., 2010. Chemical blocking of zinc ions in CNS increases neuronal damage following traumatic brain injury (TBI) in mice. *PLoS One* 5, e10131. <https://doi.org/10.1371/journal.pone.0010131>
- Domínguez, M.I., Blasco-Ibáñez, J.M., Crespo, C., Marqués-Marí, A.I., Martínez-Guijarro, F.J., 2003. Zinc chelation during non-lesioning overexcitation results in neuronal death in the mouse hippocampus. *Neuroscience* 116, 791–806. [https://doi.org/10.1016/S0306-4522\(02\)00731-5](https://doi.org/10.1016/S0306-4522(02)00731-5)
- Drobinskaya, I., Neumaier, F., Pereverzev, A., Hescheler, J., Schneider, T., 2015. Diethyldithiocarbamate-mediated zinc ion chelation reveals role of Cav2.3 channels in glucagon secretion. *Biochim. Biophys. Acta - Mol. Cell Res.* 1853, 953–964. <https://doi.org/10.1016/j.bbamcr.2015.01.001>
- Du, J., Vegh, V., Reutens, D.C., 2019. Small changes in synaptic gain lead to seizure-like activity in neuronal network at criticality. *Sci. Rep.* 9, 1097. <https://doi.org/10.1038/s41598-018-37646-9>
- Eimerl, S., Schramm, M., 1993. Potentiation of <sup>45</sup>Ca uptake and acute toxicity mediated by the N-methyl-D-aspartate receptor: The effect of metal binding agents and transition metal ions. *J. Neurochem.* 61, 518–525.
- Elhamdani, A., Bossu, J.-L., Feltz, A., 1995. ADP exerts a protective effect against rundown of the Ca<sup>2+</sup> current in bovine chromaffin cells. *Pflügers Arch. Eur. J. Physiol.* 430, 401–409. <https://doi.org/10.1007/BF00373916>
- Elhamdani, A., Bossu, J.-L., Feltz, A., 1994. Evolution of the Ca<sup>2+</sup> current during dialysis of isolated bovine chromaffin cells: Effect of internal calcium. *Cell Calcium* 16, 357–366. [https://doi.org/10.1016/0143-4160\(94\)90029-9](https://doi.org/10.1016/0143-4160(94)90029-9)
- Elinder, F., Arhem, P., 2003. Metal ion effects on ion channel gating. *Q. Rev. Biophys.* 36,



- 373–427. <https://doi.org/10.1017/S0033583504003932>
- Ellinor, P.T., Yang, J., Sather, W.A., Zhang, J.-F., Tsien, R.W., 1995. Ca<sup>2+</sup> channel selectivity at a single locus for high-affinity Ca<sup>2+</sup> interactions. *Neuron* 15, 1121–1132. [https://doi.org/10.1016/0896-6273\(95\)90100-0](https://doi.org/10.1016/0896-6273(95)90100-0)
- Ellis, S., Williams, M., Ways, N., Brenner, R., Sharp, A., Leung, A., Campbell, K., McKenna, E., Koch, W., Hui, A., Et, A., 1988. Sequence and expression of mRNAs encoding the  $\alpha_1$  and  $\alpha_2$  subunits of a DHP-sensitive calcium channel. *Science* 241, 1661–1664. <https://doi.org/10.1126/science.2458626>
- Emdin, S.O., Dodson, G.G., Cutfield, J.M., Cutfield, S.M., 1980. Role of zinc in insulin biosynthesis. Some possible zinc-insulin interactions in the pancreatic  $\beta$ -cell. *Diabetologia* 19, 174–182. <https://doi.org/10.1007/BF00275265>
- Ertel, E.A., Campbell, K.P., Harpold, M.M., Hofmann, F., Mori, Y., Perez-Reyes, E., Schwartz, A., Snutch, T.P., Tanabe, T., Birnbaumer, L., Tsien, R.W., Catterall, W.A., 2000. Nomenclature of voltage-gated calcium channels. *Neuron* 25, 533–535. <https://doi.org/10.1080/13518040701205365>
- Flockerzi, V., Oeken, H.-J., Hofmann, F., Pelzer, D., Cavalié, A., Trautwein, W., 1986. Purified dihydropyridine-binding site from skeletal muscle t-tubules is a functional calcium channel. *Nature* 323, 66–68. <https://doi.org/10.1038/323066a0>
- Franklin, I., Gromada, J., Gjinovci, A., Theander, S., Wollheim, C.B., 2005.  $\beta$ -cell secretory products activate  $\alpha$ -cell ATP-dependent potassium channels to inhibit glucagon release. *Diabetes* 54, 1808–1815. <https://doi.org/10.2337/diabetes.54.6.1808>
- Frederickson, C.J., Giblin, L.J., Krezel, A., McAdoo, D.J., Muelle, R.N., Zeng, Y., Balaji, R. V., Masalha, R., Thompson, R.B., Fierke, C.A., Sarvey, J.M., de Valdenebro, M., Prough, D.S., Zornow, M.H., 2006. Concentrations of extracellular free zinc (pZn)<sub>e</sub> in the central nervous system during simple anesthetization, ischemia and reperfusion. *Exp. Neurol.* 198, 285–293. <https://doi.org/10.1016/j.expneurol.2005.08.030>
- Frederickson, C.J., Hernandez, M.D., Goik, S.A., Morton, J.D., McGinty, J.F., 1988. Loss of zinc staining from hippocampal mossy fibers during kainic acid induced seizures: A histofluorescence study. *Brain Res.* 446, 383–386. [https://doi.org/10.1016/0006-8993\(88\)90899-2](https://doi.org/10.1016/0006-8993(88)90899-2)
- Frederickson, C.J., Koh, J.-Y., Bush, A.I., 2005. The neurobiology of zinc in health and disease. *Nat. Rev. Neurosci.* 6, 449–462. <https://doi.org/10.1038/nrn1671>
- Frederickson, Christopher J., Suh, S.W., Silva, D., Frederickson, Cathy J., Thompson, R.B., 2000. Importance of zinc in the central nervous system: The zinc-containing neuron. *J. Nutr.* 130, 1471S–83S. <https://doi.org/10.1093/jn/130.5.1471S>
- Galetin, T., Tevoufouet, E.E., Sandmeyer, J., Matthes, J., Nguemo, F., Hescheler, J., Weiergräber, M., Schneider, T., 2013. Pharmacoresistant Ca<sub>v</sub>2.3 (E-type/R-type) voltage-gated calcium channels influence heart rate dynamics and may contribute to cardiac impulse conduction. *Cell Biochem. Funct.* 31, 434–449. <https://doi.org/10.1002/cbf.2918>
- García, J., Nakai, J., Imoto, K., Beam, K.G., 1997. Role of S4 segments and the leucine heptad motif in the activation of an L-type calcium channel. *Biophys. J.* 72, 2515–2523. [https://doi.org/10.1016/S0006-3495\(97\)78896-9](https://doi.org/10.1016/S0006-3495(97)78896-9)
- Gasparini, S., Kasyanov, A.M., Pietrobon, D., Voronin, L.L., Cherubini, E., 2001. Presynaptic R-type calcium channels contribute to fast excitatory synaptic transmission in the rat hippocampus. *J. Neurosci.* 21, 8715–21. <https://doi.org/10.1523/JNEUROSCI.21-22-08715.2001>
- Göpel, S., Zhang, Q., Eliasson, L., Ma, X.-S., Galvanovskis, J., Kanno, T., Salehi, A., Rorsman, P., 2004. Capacitance measurements of exocytosis in mouse pancreatic  $\alpha$ -,  $\beta$ - and  $\delta$ -cells

- within intact islets of Langerhans. *J. Physiol.* 556, 711–726. <https://doi.org/10.1113/jphysiol.2003.059675>
- Göpel, S.O., Kanno, T., Barg, S., Weng, X.-G., Gromada, J., Rorsman, P., 2000. Regulation of glucagon release in mouse  $\alpha$ -cells by  $K_{ATP}$  channels and inactivation of TTX-sensitive  $Na^+$  channels. *J. Physiol.* 528, 509–520. <https://doi.org/10.1111/j.1469-7793.2000.00509.x>
- Grabsch, H., Pereverzev, A., Weiergräber, M., Schramm, M., Henry, M., Vajna, R., Beattie, R.E., Volsen, S.G., Klöckner, U., Hescheler, J., Schneider, T., 1999. Immunohistochemical detection of  $\alpha_{1E}$  voltage-gated  $Ca^{2+}$  channel isoforms in cerebellum, INS-1 cells, and neuroendocrine cells of the digestive system. *J. Histochem. Cytochem.* 47, 981–994. <https://doi.org/10.1177/002215549904700802>
- Grill, V., Westberg, M., Ostenson, C.G., 1987.  $\beta$ -cell insensitivity in a rat model of non-insulin-dependent diabetes. Evidence for a rapidly reversible effect of previous hyperglycemia. *J. Clin. Invest.* 80, 664–669. <https://doi.org/10.1172/JCI113119>
- Gromada, J., Ma, X., Hoy, M., Bokvist, K., Salehi, A., Berggren, P.-O., Rorsman, P., 2004. ATP-sensitive  $K^+$  channel-dependent regulation of glucagon release and electrical activity by glucose in wild-type and  $SUR1^{-/-}$  mouse-cells. *Diabetes* 53, S181–S189. [https://doi.org/10.2337/diabetes.53.suppl\\_3.S181](https://doi.org/10.2337/diabetes.53.suppl_3.S181)
- Gurnett, C.A., De Waard, M., Campbell, K.P., 1996. Dual function of the voltage-dependent  $Ca^{2+}$  channel  $\alpha_{2\delta}$  subunit in current stimulation and subunit interaction. *Neuron* 16, 431–440. [https://doi.org/10.1016/S0896-6273\(00\)80061-6](https://doi.org/10.1016/S0896-6273(00)80061-6)
- Gyulkhandanyan, A. V., Lu, H., Lee, S.C., Bhattacharjee, A., Wijesekara, N., Fox, J.E.M., MacDonald, P.E., Chimienti, F., Dai, F.F., Wheeler, M.B., 2008. Investigation of transport mechanisms and regulation of intracellular  $Zn^{2+}$  in pancreatic  $\alpha$ -cells. *J. Biol. Chem.* 283, 10184–10197. <https://doi.org/10.1074/jbc.M707005200>
- Hainsworth, A.H., McNaughton, N.C.L., Pereverzev, A., Schneider, T., Randall, A.D., 2003. Actions of sipatrigine, 202W92 and lamotrigine on R-type and T-type  $Ca^{2+}$  channel currents. *Eur. J. Pharmacol.* 467, 77–80. [https://doi.org/10.1016/S0014-2999\(03\)01625-X](https://doi.org/10.1016/S0014-2999(03)01625-X)
- Hao, L.-Y., Kameyama, A., Kameyama, M., 1999. A cytoplasmic factor, calpastatin and ATP together reverse run-down of  $Ca^{2+}$  channel activity in guinea-pig heart. *J. Physiol.* 514, 687–699. <https://doi.org/10.1111/j.1469-7793.1999.687ad.x>
- Hartter, D.E., Barnea, A., 1988. Evidence for release of copper in the brain: Depolarization-induced release of newly taken-up  $^{67}Cu$ . *Synapse* 2, 412–415. <https://doi.org/10.1002/syn.890020408>
- Hawkins, B.E., Frederickson, C.J., DeWitt, D.S., Prough, D.S., 2012. Fluorophilia: Fluorophore-containing compounds adhere non-specifically to injured neurons. *Brain Res.* 1432, 28–35. <https://doi.org/10.1016/j.brainres.2011.11.009>
- Helbig, K.L., Lauerer, R.J., Bahr, J.C., Souza, I.A., Myers, C.T., Uysal, B., Schwarz, N., Gandini, M.A., Huang, S., Keren, B., Mignot, C., Afenjar, A., Billette de Villemeur, T., Héron, D., Nava, C., Valence, S., Buratti, J., Fagerberg, C.R., Soerensen, K.P., Kibaek, M., Kamsteeg, E.-J., Koolen, D.A., Gunning, B., Schelhaas, H.J., Kruer, M.C., Fox, J., Bakhtiari, S., Jarrar, R., Padilla-Lopez, S., Lindstrom, K., Jin, S.C., Zeng, X., Bilguvar, K., Papavasileiou, A., Xing, Q., Zhu, C., Boysen, K., Vairo, F., Lanpher, B.C., Klee, E.W., Tillema, J.-M., Payne, E.T., Cousin, M.A., Kruisselbrink, T.M., Wick, M.J., Baker, J., Haan, E., Smith, N., Sadeghpour, A., Davis, E.E., Katsanis, N., Corbett, M.A., MacLennan, A.H., Gecz, J., Biskup, S., Goldmann, E., Rodan, L.H., Kichula, E., Segal, E., Jackson, K.E., Asamoah, A., Dimmock, D., McCarrier, J., Botto, L.D., Filloux, F., Tvrđik, T., Cascino, G.D., Klingerman, S., Neumann, C., Wang, R., Jacobsen, J.C., Nolan, M.A., Snell, R.G., Lehnert, K., Sadleir, L.G., Anderlid, B.-M., Kvarnung, M., Guerrini, R., Friez,

- M.J., Lyons, M.J., Leonhard, J., Kringlen, G., Casas, K., El Achkar, C.M., Smith, L.A., Rotenberg, A., Poduri, A., Sanchis-Juan, A., Carss, K.J., Rankin, J., Zeman, A., Raymond, F.L., Blyth, M., Kerr, B., Ruiz, K., Urquhart, J., Hughes, I., Banka, S., Hedrich, U.B.S., Scheffer, I.E., Helbig, I., Zamponi, G.W., Lerche, H., Mefford, H.C., Allori, A., Angrist, M., Ashley, P., Bidegain, M., Boyd, B., Chambers, E., Cope, H., Cotten, C.M., Curington, T., Davis, E.E., Ellestad, S., Fisher, K., French, A., Gallentine, W., Goldberg, R., Hill, K., Kansagra, S., Katsanis, N., Katsanis, S., Kurtzberg, J., Marcus, J., McDonald, M., Mikati, M., Miller, S., Murtha, A., Perilla, Y., Pizoli, C., Purves, T., Ross, S., Sadeghpour, A., Smith, E., Wiener, J., 2018. De Novo pathogenic variants in CACNA1E cause developmental and epileptic encephalopathy with contractures, macrocephaly, and dyskinesias. *Am. J. Hum. Genet.* 103, 666–678. <https://doi.org/10.1016/j.ajhg.2018.09.006>
- Hell, J.W., Yokoyama, C.T., Breeze, L.J., Chavkin, C., Catterall, W.A., 1995. Phosphorylation of presynaptic and postsynaptic calcium channels by cAMP-dependent protein kinase in hippocampal neurons. *EMBO J.* 14, 3036–44. <https://doi.org/10.1002/j.1460-2075.1995.tb07306.x>
- Hering, S., Berjukow, S., Sokolov, S., Marksteiner, R., Weiß, R.G., Kraus, R., Timin, E.N., 2000. Molecular determinants of inactivation in voltage-gated Ca<sup>2+</sup> channels. *J. Physiol.* 528, 237–249. <https://doi.org/10.1111/j.1469-7793.2000.t01-1-00237.x>
- Hescheler, J., Mieskes, G., Rüegg, J.C., Takai, A., Trautwein, W., 1988. Effects of a protein phosphatase inhibitor, okadaic acid, on membrane currents of isolated guinea-pig cardiac myocytes. *Pflügers Arch. Eur. J. Physiol.* 412, 248–252. <https://doi.org/10.1007/BF00582504>
- Hess, P., Lansman, J.B., Tsien, R.W., 1986. Calcium channel selectivity for divalent and monovalent cations. Voltage and concentration dependence of single channel current in ventricular heart cells. *J. Gen. Physiol.* 88, 293–319. <https://doi.org/10.1085/jgp.88.3.293>
- Hess, P., Tsien, R.W., 1984. Mechanism of ion permeation through calcium channels. *Nature* 309, 453–456. <https://doi.org/10.1038/309453a0>
- Hilaire, C., Diochot, S., Desmadryl, G., Richard, S., Valmier, J., 1997. Toxin-resistant calcium currents in embryonic mouse sensory neurons. *Neuroscience* 80, 267–276. [https://doi.org/10.1016/S0306-4522\(97\)00101-2](https://doi.org/10.1016/S0306-4522(97)00101-2)
- Hille, B., 1992. *Ionic Channels of Excitable Membranes.*, 2nd ed. Sinauer Associates, Inc., Sunderland, Massachusetts. <https://doi.org/10.1149/1.2100457>
- Hoedemaker, J.R., Peake, B.M., Kerr, D.S., 2005. Reduction in functional potency of the neurotoxin domoic acid in the presence of cadmium and zinc ions. *Environ. Toxicol. Pharmacol.* 20, 175–181. <https://doi.org/10.1016/j.etap.2004.12.061>
- Holmkvist, J., Tojjar, D., Almgren, P., Lyssenko, V., Lindgren, C.M., Isomaa, B., Tuomi, T., Berglund, G., Renström, E., Groop, L., 2007. Polymorphisms in the gene encoding the voltage-dependent Ca<sup>2+</sup> channel Cav2.3 (CACNA1E) are associated with type 2 diabetes and impaired insulin secretion. *Diabetologia* 50, 2467–2475. <https://doi.org/10.1007/s00125-007-0846-2>
- Hosokawa, Y.A., Leahy, J.L., 1997. Parallel reduction of pancreas insulin content and insulin secretion in 48-h tolbutamide-infused normoglycemic rats. *Diabetes* 46, 808–813. <https://doi.org/10.2337/diab.46.5.808>
- Ishiguro, M., Wellman, G.C., 2008. Cellular basis of vasospasm: Role of small diameter arteries and voltage-dependent Ca<sup>2+</sup> channels., in: *Cerebral Vasospasm. Acta Neurochirurgica Supplementum*, Vol 104. Springer Vienna, Vienna, pp. 95–98. [https://doi.org/10.1007/978-3-211-75718-5\\_18](https://doi.org/10.1007/978-3-211-75718-5_18)
- Ishiguro, M., Wellman, T.L., Honda, A., Russell, S.R., Tranmer, B.I., Wellman, G.C., 2005.



- Emergence of a R-type  $\text{Ca}^{2+}$  channel ( $\text{Ca}_v2.3$ ) contributes to cerebral artery constriction after subarachnoid hemorrhage. *Circ. Res.* 96, 419–426. <https://doi.org/10.1161/01.RES.0000157670.49936.da>
- Ishihara, H., Maechler, P., Gjinovci, A., Herrera, P.-L., Wollheim, C.B., 2003. Islet  $\beta$ -cell secretion determines glucagon release from neighbouring  $\alpha$ -cells. *Nat. Cell Biol.* 5, 330–335. <https://doi.org/10.1038/ncb951>
- Jeong, S.-W., Park, B.-G., Park, J.-Y., Lee, J.-W., Lee, J.-H., 2003. Divalent metals differentially block cloned T-type calcium channels. *Neuroreport* 14, 1537–1540. <https://doi.org/10.1097/00001756-200308060-00028>
- Jeziorski, M.C., Greenberg, R.M., Anderson, P.A. V., 2000. Calcium channel  $\beta$  subunits differentially modulate recovery of the channel from inactivation. *FEBS Lett.* 483, 125–130. [https://doi.org/10.1016/S0014-5793\(00\)02098-6](https://doi.org/10.1016/S0014-5793(00)02098-6)
- Jing, X., Li, D.-Q., Olofsson, C.S., Salehi, A., Surve, V. V., Caballero, J., Ivarsson, R., Lundquist, I., Pereverzev, A., Schneider, T., Rorsman, P., Renström, E., 2005.  $\text{Ca}_v2.3$  calcium channels control second-phase insulin release. *J. Clin. Invest.* 115, 146–154. <https://doi.org/10.1172/JCI200522518.146>
- Jones, S.W., 1998. Overview of voltage-dependent calcium channels. *J. Bioenerg. Biomembr.* 30, 299–312. <https://doi.org/10.1023/A:1021977304001>
- Kang, H.-W., Moon, H.J., Joo, S.H., Lee, J.-H., 2007. Histidine residues in the IS3-IS4 loop are critical for nickel-sensitive inhibition of the  $\text{Ca}_v2.3$  calcium channel. *FEBS Lett.* 581, 5774–5780. <https://doi.org/10.1016/j.febslet.2007.11.045>
- Kardos, J., Kovács, I., Hajós, F., Kálmán, M., Simonyi, M., 1989. Nerve endings from rat brain tissue release copper upon depolarization. A possible role in regulating neuronal excitability. *Neurosci. Lett.* 103, 139–144. [https://doi.org/10.1016/0304-3940\(89\)90565-X](https://doi.org/10.1016/0304-3940(89)90565-X)
- Kavalali, E.T., Zhuo, M., Bito, H., Tsien, R.W., 1997. Dendritic  $\text{Ca}^{2+}$  channels characterized by recordings from isolated hippocampal dendritic segments. *Neuron* 18, 651–663. [https://doi.org/10.1016/S0896-6273\(00\)80305-0](https://doi.org/10.1016/S0896-6273(00)80305-0)
- Kerchner, G.A., Canzoniero, L.M.T., Yu, S.P., Ling, C., Choi, D.W., 2000.  $\text{Zn}^{2+}$  current is mediated by voltage-gated  $\text{Ca}^{2+}$  channels and enhanced by extracellular acidity in mouse cortical neurones. *J. Physiol.* 528 Pt 1, 39–52. <https://doi.org/10.1111/j.1469-7793.2000.00039.x>
- Kergoat, M., Bailbe, D., Portha, B., 1987. Insulin treatment improves glucose-induced insulin release in rats with NIDDM induced by streptozocin. *Diabetes* 36, 971–977. <https://doi.org/10.2337/diab.36.8.971>
- Kim, B.J., Kim, Y.H., Kim, S., Kim, J.W., Koh, J.-Y., Oh, S.H., Lee, M.K., Kim, K.W., Lee, M.S., 2000. Zinc as a paracrine effector in pancreatic islet cell death. *Diabetes* 49, 367–372. <https://doi.org/10.2337/diabetes.49.3.367>
- Kim, M.-S., Morii, T., Sun, L.-X., Imoto, K., Mori, Y., 1993. Structural determinants of ion selectivity in brain calcium channel. *FEBS Lett.* 318, 145–148. [https://doi.org/10.1016/0014-5793\(93\)80009-J](https://doi.org/10.1016/0014-5793(93)80009-J)
- Kimm, T., Bean, B.P., 2014. Inhibition of A-type potassium current by the peptide toxin SNX-482. *J. Neurosci.* 34, 9182–9189. <https://doi.org/10.1523/JNEUROSCI.0339-14.2014>
- Krężel, A., Maret, W., 2006. Zinc-buffering capacity of a eukaryotic cell at physiological pZn. *JBIC J. Biol. Inorg. Chem.* 11, 1049–1062. <https://doi.org/10.1007/s00775-006-0150-5>
- Kubota, M., Murakoshi, T., Saegusa, H., Kazuno, A., Zong, S., Hu, Q., Noda, T., Tanabe, T., 2001. Intact LTP and fear memory but impaired spatial memory in mice lacking  $\text{Ca}_v2.3$  ( $\alpha_{1E}$ ) channel. *Biochem. Biophys. Res. Commun.* 282, 242–248. <https://doi.org/10.1006/bbrc.2001.4572>

- Kuzmiski, J.B., Barr, W., Zamponi, G.W., MacVicar, B.A., 2005. Topiramate inhibits the initiation of plateau potentials in CA1 neurons by depressing R-type calcium channels. *Epilepsia* 46, 481–489. <https://doi.org/10.1111/j.0013-9580.2005.35304.x>
- Lacinová, L., 2005. Voltage-dependent calcium channels. *Gen. Physiol. Biophys.* 24 Suppl 1, 1–78. <https://doi.org/10.1002/jcp.1041460203>
- Lacinová, L., Klugbauer, N., Hofmann, F., 1999. Absence of modulation of the expressed calcium channel  $\alpha_{1G}$  subunit by  $\alpha_{2\delta}$  subunits. *J. Physiol.* 516, 639–645. <https://doi.org/10.1111/j.1469-7793.1999.0639u.x>
- Lambert, R.C., Maulet, Y., Mouton, J., Beattie, R., Volsen, S., De Waard, M., Feltz, A., 1997. T-type  $\text{Ca}^{2+}$  current properties are not modified by  $\text{Ca}^{2+}$  channel  $\beta$  subunit depletion in nodosus ganglion neurons. *J. Neurosci.* 17, 6621–8. <https://doi.org/10.1523/jneurosci.17-17-06621.1997>
- Lee, J.-Y., Cole, T.B., Palmiter, R.D., Koh, J.-Y., 2000. Accumulation of zinc in degenerating hippocampal neurons of  $\text{ZnT}_3$ -null mice after seizures: Evidence against synaptic vesicle origin. *J. Neurosci.* 20, RC79. <https://doi.org/20004230> [pii]
- Lee, S.-C., Choi, S., Lee, T., Kim, H.-L., Chin, H., Shin, H.-S., 2002. Molecular basis of R-type calcium channels in central amygdala neurons of the mouse. *Proc. Natl. Acad. Sci. U. S. A.* 99, 3276–3281. <https://doi.org/10.1073/pnas.052697799>
- Leuranguer, V., Bourinet, E., Lory, P., Nargeot, J., 1998. Antisense depletion of  $\beta$ -subunits fails to affect T-type calcium channels properties in a neuroblastoma cell line. *Neuropharmacology* 37, 701–708. [https://doi.org/10.1016/S0028-3908\(98\)00060-4](https://doi.org/10.1016/S0028-3908(98)00060-4)
- Li, Y. V., 2014. Zinc and insulin in pancreatic  $\beta$ -cells. *Endocrine* 45, 178–189. <https://doi.org/10.1007/s12020-013-0032-x>
- Li, Y., Hough, C.J., Frederickson, C.J., Sarvey, J.M., 2001. Induction of mossy fiber  $\rightarrow$  CA3 long-term potentiation requires translocation of synaptically released  $\text{Zn}^{2+}$ . *J. Neurosci.* 21, 8015–8025. <https://doi.org/10.1523/jneurosci.21-20-08015.2001>
- Llinás, R., Sugimori, M., Hillman, D.E., Cherksey, B., 1992. Distribution and functional significance of the P-type, voltage-dependent  $\text{Ca}^{2+}$  channels in the mammalian central nervous system. *Trends Neurosci.* 15, 351–355. [https://doi.org/10.1016/0166-2236\(92\)90053-B](https://doi.org/10.1016/0166-2236(92)90053-B)
- Lüke, M., Henry, M., Lingohr, T., Maghsoodan, M., Hescheler, J., Weiergräber, M., Sickel, W., Schneider, T., 2005. A  $\text{Ni}^{2+}$ -sensitive component of the ERG b-wave from the isolated bovine retina is related to E-type voltage-gated  $\text{Ca}^{2+}$  channels. *Graefes Arch. Clin. Exp. Ophthalmol.* 243, 933–941. <https://doi.org/10.1007/s00417-005-1145-6>
- Lux, H.-D., Carbone, E., Zucker, H., 1990.  $\text{Na}^+$  currents through low-voltage-activated  $\text{Ca}^{2+}$  channels of chick sensory neurones: Block by external  $\text{Ca}^{2+}$  and  $\text{Mg}^{2+}$ . *J. Physiol.* 430, 159–188. <https://doi.org/10.1113/jphysiol.1990.sp018287>
- Magee, J.C., Carruth, M., 1999. Dendritic voltage-gated ion channels regulate the action potential firing mode of hippocampal CA1 pyramidal neurons. *J. Neurophysiol.* 82, 1895–901. <https://doi.org/10.1152/jn.1999.82.4.1895>
- Magee, J.C., Johnston, D., 1995. Characterization of single voltage-gated  $\text{Na}^+$  and  $\text{Ca}^{2+}$  channels in apical dendrites of rat CA1 pyramidal neurons. *J. Physiol.* 487, 67–90. <https://doi.org/10.1113/jphysiol.1995.sp020862>
- Magistretti, J., Castelli, L., Taglietti, V., Tanzi, F., 2003. Dual effect of  $\text{Zn}^{2+}$  on multiple types of voltage-dependent  $\text{Ca}^{2+}$  currents in rat palaeocortical neurons. *Neuroscience* 117, 249–264. [https://doi.org/10.1016/S0306-4522\(02\)00865-5](https://doi.org/10.1016/S0306-4522(02)00865-5)
- Martini, M., Rossi, M.L., Rubbini, G., Rispoli, G., 2000. Calcium currents in hair cells isolated from semicircular canals of the frog. *Biophys. J.* 78, 1240–1254.

- [https://doi.org/10.1016/S0006-3495\(00\)76681-1](https://doi.org/10.1016/S0006-3495(00)76681-1)
- Maruyama, H., Hisatomi, A., Orci, L., Grodsky, G.M., Unger, R.H., 1984. Insulin within islets is a physiologic glucagon release inhibitor. *J. Clin. Invest.* 74, 2296–2299. <https://doi.org/10.1172/JCI111658>
- Mathie, A., Sutton, G.L., Clarke, C.E., Veale, E.L., 2006. Zinc and copper: Pharmacological probes and endogenous modulators of neuronal excitability. *Pharmacol. Ther.* 111, 567–583. <https://doi.org/10.1016/j.pharmthera.2005.11.004>
- Matsuda, Y., Saegusa, H., Zong, S., Noda, T., Tanabe, T., 2001. Mice lacking  $Ca_v2.3$  ( $\alpha_{1E}$ ) calcium channel exhibit hyperglycemia. *Biochem. Biophys. Res. Commun.* 289, 791–795. <https://doi.org/10.1006/bbrc.2001.6051>
- McDonald, T.F., Pelzer, S., Trautwein, W., Pelzer, D.J., 1994. Regulation and modulation of calcium channels in cardiac, skeletal, and smooth muscle cells. *Physiol. Rev.* 74, 365–507. <https://doi.org/10.1152/physrev.1994.74.2.365>
- Mehrke, G., Pereverzev, A., Grabsch, H., Hescheler, J., Schneider, T., 1997. Receptor-mediated modulation of recombinant neuronal class E calcium channels. *FEBS Lett.* 408, 261–270. [https://doi.org/10.1016/S0014-5793\(97\)00437-7](https://doi.org/10.1016/S0014-5793(97)00437-7)
- Mergler, S., Singh, V., Grötzinger, C., Kaczmarek, P., Wiedenmann, B., Strowski, M.Z., 2008. Characterization of voltage operated R-type  $Ca^{2+}$  channels in modulating somatostatin receptor subtype 2- and 3-dependent inhibition of insulin secretion from INS-1 cells. *Cell. Signal.* 20, 2286–2295. <https://doi.org/10.1016/j.cellsig.2008.08.015>
- Mironov, S.L., 1992. Conformational model for ion permeation in membrane channels: A comparison with multi-ion models and applications to calcium channel permeability. *Biophys. J.* 63, 485–496. [https://doi.org/10.1016/S0006-3495\(92\)81628-4](https://doi.org/10.1016/S0006-3495(92)81628-4)
- Mironov, S.L., Lux, H.D., 1991. Calmodulin antagonists and protein phosphatase inhibitor okadaic acid fasten the “run-up” of high-voltage activated calcium current in rat hippocampal neurones. *Neurosci. Lett.* 133, 175–178. [https://doi.org/10.1016/0304-3940\(91\)90563-9](https://doi.org/10.1016/0304-3940(91)90563-9)
- Muller, Y.L., Hanson, R.L., Zimmerman, C., Harper, I., Sutherland, J., Kobes, S., Diabetes, T., Knowler, W.C., Bogardus, C., Baier, L.J., 2007. Variants in the  $Ca_v2.3$  ( $\alpha_{1E}$ ) subunit of voltage-activated  $Ca^{2+}$  channels are associated with insulin resistance and type 2 diabetes in Pima Indians. *Diabetes* 56, 3089–3094. <https://doi.org/10.2337/db07-0587>.Additional
- Nelson, M.T., Woo, J., Kang, H.-W., Vitko, I., Barrett, P.Q., Perez-Reyes, E., Lee, J.-H., Shin, H.-S., Todorovic, S.M., 2007. Reducing agents sensitize C-type nociceptors by relieving high-affinity zinc inhibition of T-type calcium channels. *J. Neurosci.* 27, 8250–8260. <https://doi.org/10.1523/jneurosci.1800-07.2007>
- Neumaier, F., Akhtar-Schäfer, I., Lüke, J.N., Dibué-Adjei, M., Hescheler, J., Schneider, T., 2018a. Reciprocal modulation of  $Ca_v2.3$  voltage-gated calcium channels by copper(II) ions and kainic acid. *J. Neurochem.* 147, 310–322. <https://doi.org/10.1111/jnc.14546>
- Neumaier, F., Alpdogan, S., Hescheler, J., Schneider, T., 2018b. Protein phosphorylation maintains the normal function of cloned human  $Ca_v2.3$  channels. *J. Gen. Physiol.* 150, jgp.201711880. <https://doi.org/10.1085/jgp.201711880>
- Neumaier, F., Dibué-Adjei, M., Hescheler, J., Schneider, T., 2015. Voltage-gated calcium channels: Determinants of channel function and modulation by inorganic cations. *Prog. Neurobiol.* 129, 1–36. <https://doi.org/10.1016/j.pneurobio.2014.12.003>
- Nowycky, M.C., Fox, A.P., Tsien, R.W., 1985. Three types of neuronal calcium channel with different calcium agonist sensitivity. *Nature* 316, 440–443. <https://doi.org/10.1038/316440a0>



- Ono, S.-I., Cherian, M.G., 1999. Regional distribution of metallothionein, zinc, and copper in the brain of different strains of rats. *Biol. Trace Elem. Res.* 69, 151–159. <https://doi.org/10.1007/BF02783866>
- Pan, E., Zhang, X.-A., Huang, Z., Krezel, A., Zhao, M., Tinberg, C.E., Lippard, S.J., McNamara, J.O., 2011. Vesicular zinc promotes presynaptic and inhibits postsynaptic long term potentiation of mossy fiber-CA3 synapse. *Neuron* 71, 1116–1126. <https://doi.org/10.1016/j.biotechadv.2011.08.021>. Secreted
- Pantazis, A., Savalli, N., Sigg, D., Neely, A., Olcese, R., 2014. Functional heterogeneity of the four voltage sensors of a human L-type calcium channel. *Proc. Natl. Acad. Sci.* 111, 18381–18386. <https://doi.org/10.1073/pnas.1411127112>
- Pereverzev, A., Mikhna, M., Vajna, R., Gissel, C., Henry, M., Hescheler, J., Smyth, N., Schneider, T., 2002a. Disturbances in glucose-tolerance, insulin-release, and stress-induced hyperglycemia upon disruption of the  $Ca_v2.3$  ( $\alpha_{1E}$ ) subunit of voltage-gated  $Ca^{2+}$  channels. *Mol. Endocrinol.* 16, 884–895. <https://doi.org/10.1210/mend.16.4.0801>
- Pereverzev, A., Salehi, A., Mikhna, M., Renström, E., Hescheler, J., Weiergräber, M., Smyth, N., Schneider, T., 2005. The ablation of the  $Ca_v2.3/E$ -type voltage-gated  $Ca^{2+}$  channel causes a mild phenotype despite an altered glucose induced glucagon response in isolated islets of Langerhans. *Eur. J. Pharmacol.* 511, 65–72. <https://doi.org/10.1016/j.ejphar.2005.01.044>
- Pereverzev, A., Vajna, R., Pfitzer, G., Hescheler, J., Klöckner, U., Schneider, T., 2002b. Reduction of insulin secretion in the insulinoma cell line INS-1 by overexpression of a  $Ca_v2.3$  ( $\alpha_{1E}$ ) calcium channel antisense cassette. *Eur. J. Endocrinol.* 146, 881–889. <https://doi.org/10.1530/eje.0.1460881>
- Ramracheya, R., Ward, C., Shigeto, M., Walker, J.N., Amisten, S., Zhang, Q., Johnson, P.R., Rorsman, P., Braun, M., 2010. Membrane potential-dependent inactivation of voltage-gated ion channels in  $\alpha$ -cells inhibits glucagon secretion from human islets. *Diabetes* 59, 2198–2208. <https://doi.org/10.2337/db09-1505>
- Randall, A., Tsien, R.W., 1995. Pharmacological dissection of multiple types of  $Ca^{2+}$  channel currents in rat cerebellar granule neurons. *J. Neurosci.* 15, 2995–3012. <https://doi.org/10.1523/jneurosci.15-04-02995.1995>
- Ravier, M.A., Rutter, G.A., 2005. Glucose or insulin, but not zinc ions, inhibit glucagon secretion from mouse pancreatic  $\alpha$ -cells. *Diabetes* 54, 1789–1797. <https://doi.org/10.2337/diabetes.54.6.1789>
- Reuter, H., 1979. Properties of two inward membrane currents in the heart. *Annu. Rev. Physiol.* 41, 413–424. <https://doi.org/10.1146/annurev.ph.41.030179.002213>
- Reuter, H., 1967. The dependence of slow inward current in Purkinje fibres on the extracellular calcium-concentration. *J. Physiol.* 192, 479–492. <https://doi.org/10.1113/jphysiol.1967.sp008310>
- Robertson, R.P., Zhou, H., Slucca, M., 2011. A role for zinc in pancreatic islet  $\beta$ -cell cross-talk with the  $\alpha$ -cell during hypoglycaemia. *Diabetes, Obes. Metab.* 13, 106–111. <https://doi.org/10.1111/j.1463-1326.2011.01448.x>
- Saegusa, H., Kurihara, T., Zong, S., Minowa, O., Kazuno, A., Han, W., Matsuda, Y., Yamanaka, H., Osanai, M., Noda, T., Tanabe, T., 2000. Altered pain responses in mice lacking  $\alpha_{1E}$  subunit of the voltage-dependent  $Ca^{2+}$  channel. *Proc. Natl. Acad. Sci.* 97, 6132–6137. <https://doi.org/10.1073/pnas.100124197>
- Sato, M., Ohtomo, K., Daimon, T., Sugiyama, T., Iijima, K., 1994. Localization of copper to afferent terminals in rat locus ceruleus, in contrast to mitochondrial copper in cerebellum. *J. Histochem. Cytochem.* 42, 1585–1591.

<https://doi.org/10.1177/42.12.7983358>

- Schneider, T., Dibué-Adjei, M., Neumaier, F., Akhtar, I., Hescheler, J., Kamp, M.A., Tevoufouet, E.E., 2015. R-type voltage-gated Ca<sup>2+</sup> channels in cardiac and neuronal rhythogenesis. *Curr. Mol. Pharmacol.* 8. <https://doi.org/10.2174/1874467208666150507093845>
- Schneider, T., Wei, X., Olcese, R., Costantin, J.L., Neely, A., Palade, P., Perez-Reyes, E., Qin, N., Zhou, J., Crawford, G.D., 1994. Molecular analysis and functional expression of the human type E neuronal Ca<sup>2+</sup> channel  $\alpha_1$  subunit. *Receptors Channels* 2, 255–70.
- Shcheglovitov, A., Vitko, I., Lazarenko, R.M., Orestes, P., Todorovic, S.M., Perez-Reyes, E., 2012. Molecular and biophysical basis of glutamate and trace metal modulation of voltage-gated Ca<sub>v</sub>2.3 calcium channels. *J. Gen. Physiol.* 139, 219–234. <https://doi.org/10.1085/jgp.2011106991395c>
- Shuaib, N.M., Marafie, H.M., Al-Fulajj, O., El-Ezaby, M.S., 1999. Complexes of vitamin B<sub>6</sub>. 23. Interaction of some tertiary ligating amino acids with the binary complexes of Ni(II) or Cu(II) and pyridoxamine. *J. Chem. Eng. Data* 44, 1348–1354. <https://doi.org/10.1021/je990056c>
- Shuba, Y.M., 2014. Models of calcium permeation through T-type channels. *Pflügers Arch. Eur. J. Physiol.* 466, 635–644. <https://doi.org/10.1007/s00424-013-1437-3>
- Siapich, S.A., Banat, M., Albanna, W., Hescheler, J., Lüke, M., Schneider, T., 2009. Antagonists of ionotropic  $\gamma$ -aminobutyric acid receptors impair the NiCl<sub>2</sub>-mediated stimulation of the electroretinogram b-wave amplitude from the isolated superfused vertebrate retina. *Acta Ophthalmol.* 87, 854–865. <https://doi.org/10.1111/j.1755-3768.2008.01387.x>
- Siapich, S.A., Wrubel, H., Albanna, W., Alnawaiseh, M., Hescheler, J., Weiergräber, M., Lüke, M., Schneider, T., 2010. Effect of ZnCl<sub>2</sub> and chelation of zinc ions by N,N-diethyldithiocarbamate (DEDTC) on the ERG b-wave amplitude from the isolated superfused vertebrate retina. *Curr. Eye Res.* 35, 322–334. <https://doi.org/10.3109/02713680903509410>
- Slucca, M., Harmon, J.S., Oseid, E.A., Bryan, J., Robertson, R.P., 2010. ATP-sensitive K<sup>+</sup> channel mediates the zinc switch-off signal for glucagon response during glucose deprivation. *Diabetes* 59, 128–134. <https://doi.org/10.2337/db09-1098>
- Snutch, T.P., Leonard, J.P., Gilbert, M.M., Lester, H.A., Davidson, N., 1990. Rat brain expresses a heterogeneous family of calcium channels. *Proc. Natl. Acad. Sci.* 87, 3391–3395. <https://doi.org/10.1073/pnas.87.9.3391>
- Snutch, T.P., Reiner, P.B., 1992. Ca<sup>2+</sup> channels: Diversity of form and function. *Curr. Opin. Neurobiol.* 2, 247–253. [https://doi.org/10.1016/0959-4388\(92\)90111-W](https://doi.org/10.1016/0959-4388(92)90111-W)
- Sochivko, D., Pereverzev, A., Smyth, N., Gissel, C., Schneider, T., Beck, H., 2002. The Ca<sub>v</sub>2.3 Ca<sup>2+</sup> channel subunit contributes to R-type Ca<sup>2+</sup> currents in murine hippocampal and neocortical neurones. *J. Physiol.* 542, 699–710. <https://doi.org/10.1113/jphysiol.2002.020677>
- Soong, T.W., Stea, A., Hodson, C.D., Dubel, S.J., Vincent, S.R., Snutch, T.P., 1993. Structure and functional expression of a member of the low voltage-activated calcium channel family. *Science* 260, 1133–1136. <https://doi.org/10.1126/science.8388125>
- Stotz, S.C., Hamid, J., Spaetgens, R.L., Jarvis, S.E., Zamponi, G.W., 2000. Fast inactivation of voltage-dependent calcium channels. A hinged-lid mechanism? *J. Biol. Chem.* 275, 24575–24582. <https://doi.org/10.1074/jbc.M000399200>
- Stotz, S.C., Jarvis, S.E., Zamponi, G.W., 2004. Functional roles of cytoplasmic loops and pore lining transmembrane helices in the voltage-dependent inactivation of HVA calcium

- channels. *J. Physiol.* 554, 263–273. <https://doi.org/10.1113/jphysiol.2003.047068>
- Sun, H.-S., Hui, K., Lee, D.W.K., Feng, Z.-P., 2007. Zn<sup>2+</sup> sensitivity of high- and low-voltage activated calcium channels. *Biophys. J.* 93, 1175–1183. <https://doi.org/10.1529/biophysj.106.103333>
- Takeda, A., Hirate, M., Tamano, H., Nisibaba, D., Oku, N., 2003. Susceptibility to kainate-induced seizures under dietary zinc deficiency. *J. Neurochem.* 85, 1575–1580. <https://doi.org/10.1046/j.1471-4159.2003.01803.x>
- Takeda, A., Tamano, H., Nagayoshi, A., Yamada, K., Oku, N., 2005. Increase in hippocampal cell death after treatment with kainate in zinc deficiency. *Neurochem. Int.* 47, 539–544. <https://doi.org/10.1016/j.neuint.2005.07.009>
- Talavera, K., Staes, M., Janssens, A., Klugbauer, N., Droogmans, G., Hofmann, F., Nilius, B., 2001. Aspartate residues of the Glu-Glu-Asp-Asp (EEDD) pore locus control selectivity and permeation of the T-type Ca<sup>2+</sup> Channel  $\alpha_{1C}$ . *J. Biol. Chem.* 276, 45628–45635. <https://doi.org/10.1074/jbc.M103047200>
- Tanabe, T., Takeshima, H., Mikami, A., Flockerzi, V., Takahashi, H., Kangawa, K., Kojima, M., Matsuo, H., Hirose, T., Numa, S., 1987. Primary structure of the receptor for calcium channel blockers from skeletal muscle. *Nature* 328, 313–318. <https://doi.org/10.1038/328313a0>
- Tang, S., Mikala, G., Bahinski, A., Yatani, A., Varadi, G., Schwartz, A., 1993. Molecular localization of ion selectivity sites within the pore of a human L-type cardiac calcium channel. *J. Biol. Chem.* 268, 13026–9.
- Thio, L.L., Zhang, H.X., 2006. Modulation of inhibitory glycine receptors in cultured embryonic mouse hippocampal neurons by zinc, thiol containing redox agents and carnosine. *Neuroscience* 139, 1315–1327. <https://doi.org/10.1016/j.neuroscience.2006.01.013>
- Thomas, E.A., Reid, C.A., Berkovic, S.F., Petrou, S., 2009. Prediction by modeling that epilepsy may be caused by very small functional changes in ion channels. *Arch. Neurol.* 66. <https://doi.org/10.1001/archneurol.2009.219>
- Tiaho, F., Nargeot, J., Richard, S., 1993. Repriming of L-type calcium currents revealed during early whole-cell patch-clamp recordings in rat ventricular cells. *J. Physiol.* 463, 367–389. <https://doi.org/10.1113/jphysiol.1993.sp019599>
- Trombetta, M., Bonetti, S., Boselli, M., Turrini, F., Malerba, G., Trabetti, E., Pignatti, P., Bonora, E., Bonadonna, R.C., 2012. CACNA1E variants affect  $\beta$ -cell function in patients with newly diagnosed type 2 diabetes. The verona newly diagnosed type 2 diabetes study (VNDS) 3. *PLoS One* 7. <https://doi.org/10.1371/journal.pone.0032755>
- Trombley, P.Q., Horning, M.S., Blakemore, L.J., 1998. Carnosine modulates zinc and copper effects on amino acid receptors and synaptic transmission. *Neuroreport* 9, 3503–3507.
- Tsien, R.W., Fox, A.P., Hess, P., McCleskey, E.W., Nilius, B., Nowycky, M.C., Rosenberg, R.L., 1987. Multiple types of calcium channel in excitable cells. *Soc. Gen. Physiol. Ser.* 41, 167–87.
- Vajna, R., Schramm, M., Pereverzev, A., Arnhold, S., Grabsch, H., Klöckner, U., Perez-Reyes, E., Hescheler, J., Schneider, T., 1998. New isoform of the neuronal Ca<sup>2+</sup> channel  $\alpha_{1E}$  subunit in islets of Langerhans and kidney - Distribution of voltage-gated Ca<sup>2+</sup> channel  $\alpha_1$  subunits in cell lines and tissues. *Eur. J. Biochem.* 257, 274–285. <https://doi.org/10.1046/j.1432-1327.1998.2570274.x>
- Vargas, E., Yarov-Yarovoy, V., Khalili-Araghi, F., Catterall, W.A., Klein, M.L., Tarek, M., Lindahl, E., Schulten, K., Perozo, E., Bezanilla, F., Roux, B., 2012. An emerging consensus on voltage-dependent gating from computational modeling and molecular



- dynamics simulations. *J. Gen. Physiol.* 140, 587–94. <https://doi.org/10.1085/jgp.201210873>
- Vogt, K., Mellor, J., Tong, G., Nicoll, R., 2000. The actions of synaptically released zinc at hippocampal mossy fiber synapses. *Neuron* 26, 187–196. [https://doi.org/10.1016/S0896-6273\(00\)81149-6](https://doi.org/10.1016/S0896-6273(00)81149-6)
- Wakamori, M., Niidome, T., Furutama, D., Furuichi, T., Mikoshiba, K., Fujita, Y., Tanaka, I., Katayama, K., Yatani, A., Schwartz, A., 1994. Distinctive functional properties of the neuronal BII (class E) calcium channel. *Receptors Channels* 2, 303–14.
- Wakita, M., Kotani, N., Kogure, K., Akaike, N., 2014. Inhibition of excitatory synaptic transmission in hippocampal neurons by levetiracetam involves Zn<sup>2+</sup>-dependent GABA type A receptor-mediated presynaptic modulation. *J. Pharmacol. Exp. Ther.* 348, 246–59. <https://doi.org/10.1124/jpet.113.208751>
- Weiergräber, M., Henry, M., Krieger, A., Kamp, M.A., Radhakrishnan, K., Hescheler, J., Schneider, T., 2006a. Altered seizure susceptibility in mice lacking the Ca<sub>v</sub>2.3 E-type Ca<sup>2+</sup> channel. *Epilepsia* 47, 839–850. <https://doi.org/10.1111/j.1528-1167.2006.00541.x>
- Weiergräber, M., Henry, M., Radhakrishnan, K., Hescheler, J., Schneider, T., 2007. Hippocampal seizure resistance and reduced neuronal excitotoxicity in mice lacking the Ca<sub>v</sub>2.3 E/R-type voltage-gated calcium channel. *J. Neurophysiol.* 97, 3660–3669. <https://doi.org/10.1152/jn.01193.2006>
- Weiergräber, M., Henry, M., Südkamp, M., de Vivie, E.R., Hescheler, J., Schneider, T., 2005. Ablation of Ca<sub>v</sub>2.3 / E-type voltage-gated calcium channel results in cardiac arrhythmia and altered autonomic control within the murine cardiovascular system. *Basic Res. Cardiol.* 100, 1–13. <https://doi.org/10.1007/s00395-004-0488-1>
- Weiergräber, M., Kamp, M.A., Radhakrishnan, K., Hescheler, J., Schneider, T., 2006b. The Ca<sub>v</sub>2.3 voltage-gated calcium channel in epileptogenesis - Shedding new light on an enigmatic channel. *Neurosci. Biobehav. Rev.* 30, 1122–1144. <https://doi.org/10.1016/j.neubiorev.2006.07.004>
- Wennemuth, G., Westenbroek, R.E., Xu, T., Hille, B., Babcock, D.F., 2000. Ca<sub>v</sub>2.2 and Ca<sub>v</sub>2.3 (N- and R-type) Ca<sup>2+</sup> channels in depolarization-evoked entry of Ca<sup>2+</sup> into mouse sperm. *J. Biol. Chem.* 275, 21210–21217. <https://doi.org/10.1074/jbc.M002068200>
- Weyer, C., Hanson, R.L., Tataranni, P.A., Bogardus, C., Pratley, R.E., 2000. A high fasting plasma insulin concentration predicts type 2 diabetes independent of insulin resistance: Evidence for a pathogenic role of relative hyperinsulinemia. *Diabetes* 49, 2094–2101. <https://doi.org/10.2337/diabetes.49.12.2094>
- Williams, M.E., Marubio, L.M., Deal, C.R., Hans, M., Brust, P.F., Philipson, L.H., Miller, R.J., Johnson, E.C., Harpold, M.M., Ellis, S.B., 1994. Structure and functional characterization of neuronal  $\alpha_{1E}$  calcium channel subtypes. *J. Biol. Chem.* 269, 22347–22357.
- Williamson, A., Spencer, D., 1995. Zinc reduces dentate granule cell hyperexcitability in epileptic humans. *Neuroreport* 6, 1562–1564. <https://doi.org/10.1097/00001756-199507310-00024>
- Winegar, B.D., Lansman, J.B., 1990. Voltage-dependent block by zinc of single calcium channels in mouse myotubes. *J. Physiol.* 425, 563–578. <https://doi.org/10.1113/jphysiol.1990.sp018118>
- Yang, J., Ellinor, P.T., Sather, W.A., Zhang, J.-F., Tsien, R.W., 1993. Molecular determinants of Ca<sup>2+</sup> selectivity and ion permeation in L-type Ca<sup>2+</sup> channels. *Nature* 363. <https://doi.org/10.1038/366158a0>
- Yasuda, R., Sabatini, B.L., Svoboda, K., 2003. Plasticity of calcium channels in dendritic spines. *Nat. Neurosci.* 6, 948–955. <https://doi.org/10.1038/nn1112>
- Yokoyama, C.T., Westenbroek, R.E., Hell, J.W., Soong, T.W., Snutch, T.P., Catterall, W.A.,

1995. Biochemical properties and subcellular distribution of the neuronal class E calcium channel  $\alpha_1$  subunit. *J. Neurosci.* 15, 6419–32. <https://doi.org/10.1523/jneurosci.15-10-06419.1995>
- Zamponi, G.W., Bourinet, E., Snutch, T.P., 1996. Nickel block of a family of neuronal calcium channels: Subtype- and subunit-dependent action at multiple sites. *J. Membr. Biol.* 151, 77–90. <https://doi.org/10.1007/s002329900059>
- Zhang, Q., Bengtsson, M., Partridge, C., Salehi, A., Braun, M., Cox, R., Eliasson, L., Johnson, P.R. V., Renström, E., Schneider, T., Berggren, P.-O., Göpel, S., Ashcroft, F.M., Rorsman, P., 2007. R-type  $\text{Ca}^{2+}$ -channel-evoked CICR regulates glucose-induced somatostatin secretion. *Nat. Cell Biol.* 9, 453–460. <https://doi.org/10.1038/ncb1563>
- Zhen, X., Xie, C., Fitzmaurice, A., Schoonover, C.E., Orenstein, E.T., Yang, J., 2005. Functional architecture of the inner pore of a voltage-gated  $\text{Ca}^{2+}$  channel. *J. Gen. Physiol.* 126, 193–204. <https://doi.org/10.1085/jgp.200509292>
- Zhou, H., Zhang, T., Harmon, J.S., Bryan, J., Robertson, R.P., 2007. Zinc, not insulin, regulates the rat  $\alpha$ -cell response to hypoglycemia *in vivo*. *Diabetes* 56, 1107–1112. <https://doi.org/10.2337/db06-1454>

## 5. Declaration

Ich versichere, dass ich die von mir vorgelegte Dissertation selbständig angefertigt, die benutzten Quellen und Hilfsmittel vollständig angegeben und die Stellen der Arbeit – einschließlich Tabellen, Karten und Abbildungen –, die anderen Werken im Wortlaut oder dem Sinn nach entnommen sind, in jedem Einzelfall als Entlehnung kenntlich gemacht habe; dass diese Dissertation noch keiner anderen Fakultät oder Universität zur Prüfung vorgelegen hat; dass sie – abgesehen von unten angegebenen Teilpublikationen – noch nicht veröffentlicht worden ist, sowie, dass ich eine solche Veröffentlichung vor Abschluss des Promotionsverfahrens nicht vornehmen werde. Die Bestimmungen der Promotionsordnung sind mir bekannt. Die von mir vorgelegte Dissertation ist von Prof. Dr. Toni Schneider und Prof. Dr. Ludwig Eichinger betreut worden.

### Publikationen:

- Neumaier F., Dibué-Adjei M., Hescheler J., Schneider T. (2015) Voltage-gated calcium channels: Determinants of channel function and modulation by inorganic cations. *Prog. Neurobiol.* **129**: 1–36. (<https://doi.org/10.1016/j.pneurobio.2014.12.003>)
- Drobinskaya I., Neumaier F., Pereverzev A., Hescheler J., Schneider T. (2015) Diethyldithiocarbamate-mediated zinc ion chelation reveals role of Ca<sub>v</sub>2.3 channels in glucagon secretion. *Biochim. Biophys. Acta - Mol. Cell Res.* **1853**(5): 953–964. (<https://doi.org/10.1016/j.bbamcr.2015.01.001>)
- Neumaier F., Alpdogan S., Hescheler J., Schneider T. (2017) A practical guide to the preparation and use of metal ion-buffered systems for physiological research. *Acta Physiol.* **222**(3): e12988. (<https://doi.org/10.1111/apha.12988>)
- Neumaier F., Akhtar-Schäfer I., Lüke J.N., Dibué-Adjei M., Hescheler J., Schneider T. (2018) Reciprocal modulation of Ca<sub>v</sub>2.3 voltage-gated calcium channels by copper(II) ions and kainic acid. *J. Neurochem.* **147**(3): 310–322. (<https://doi.org/10.1111/jnc.14546>)
- Neumaier F., Alpdogan S., Hescheler J., Schneider T. (2018) Protein phosphorylation maintains the normal function of cloned human Ca<sub>v</sub>2.3 channels. *J. Gen. Physiol.* **150**(3): 491–510. (<https://doi.org/10.1085/jgp.201711880>)
- Neumaier, F., Alpdogan, S., Schneider, T., Hescheler, J. (2020) Zn<sup>2+</sup>-induced changes in Ca<sub>v</sub>2.3 channel function. An electrophysiological and modeling study. *J. Gen. Physiol.* **152**(9): e202012585. (<https://doi.org/10.1085/jgp.202012585>)

Ich versichere, dass ich alle Angaben wahrheitsgemäß nach bestem Wissen und Gewissen gemacht habe und verpflichte mich, jedmögliche, die obigen Angaben betreffenden Veränderungen, dem Promotionsausschuss unverzüglich mitzuteilen.

Köln, den 25.06.2020

\_\_\_\_\_  
(Felix Neumaier)



## 6. Curriculum vitae



Jabachstraße 17  
50354 Hürth



+49-2233-70595



+49-172-6754246



felix@neumaier-net.de

**Felix Neumaier**  <https://orcid.org/0000-0002-6376-6391>

Neuroscientist with a focus on electrophysiology, metalloneurochemistry, multi-modal imaging and computational neuroscience.



### Research experience

11/2014 - 01/2020

#### ◆ Research associate

*Institute for Neurophysiology, University of Cologne*

Performed *in vitro*, *in vivo* and *in silico* studies on Ca<sup>2+</sup> channel modulation by trace metal ions and trace metal chelators (DFG Project 278832231), blood degradation products and intracellular factors.

08/2012 - 09/2012

#### ◆ Internship student

*Institute for Pharmacology, University of Cologne*

Investigated atherosclerosis-associated changes in murine Ca<sup>2+</sup> channels with single-channel patch-clamp recordings.

10/2010 - 03/2011

#### ◆ Internship student

*Institute for Neurophysiology, University of Cologne*

Isolated, cultured and characterized murine cardiac ganglion cells with whole-cell patch-clamp recordings.

04/2009 - 09/2009

#### ◆ Internship student

*Max-Planck Institute for Neurological Research*

Developed a system for determination of hearing thresholds in rats using auditory-evoked potentials.

11/2014 - 04/2020



### Education

#### ◆ Dr. rer. nat. (Doctorate in natural sciences)

*Institute for Neurophysiology, University of Cologne*

- Graduated with summa cum laude
- Dissertation: Modulation of Ca<sub>v</sub>2.3 voltage-gated calcium channels by trace metal ions and trace metal chelators.

04/2011 - 11/2013

#### ◆ M.Sc. in Experimental and Clinical Neuroscience

*University of Cologne*

- Graduated with ECTS-Grade A (1.3)
- Supported by a scholarship of the Hans-Boeckler foundation
- Thesis: Reciprocal modulation of recombinant Ca<sub>v</sub>2.3 voltage-gated Ca<sup>2+</sup>-channels by copper(II) ions and kainic acid.

10/2007 - 09/2010

#### ◆ B.Sc. in Neuroscience

*University of Cologne*

- Graduated with ECTS-Grade A (1.2)
- Supported by a scholarship of the Hans-Boeckler foundation
- Thesis: Chemical preconditioning with 3-nitropropionic acid: A  $\mu$ PET investigation of metabolism and cerebral blood flow in stroke-tolerant rat brains.

2012 - 2019



## Teaching activity

### ◆ Instructor

Topic: Role of  $Zn^{2+}$  and  $Cu^{2+}$  in the central nervous system.  
(Course M-Neuro-B13: (Patho-)biochemistry and (patho-)physiology of the nervous system. B.Sc. Neuroscience, University of Cologne.)

2012 - 2019

### ◆ Instructor

Topic: Investigation of voltage-gated ion channels with the patch-clamp technique.  
(Course M-Neuro-AM5: Examination techniques for neurons and nerve tissue. M.Sc. Neuroscience, University of Cologne.)

2012 - 2014

### ◆ Instructor

Topic: *In vivo* and *in vitro* imaging techniques.  
(Course M-Neuro-B16: Graduates teach Undergraduates. B.Sc. Neuroscience, University of Cologne.)



## Language skills

- ◆ **German:** first language
- ◆ **English:** fluent in written and spoken
- ◆ **French:** school knowledge



## Additional skills

- ◆ **Software for data acquisition and processing:** extensive hands-on experience with Excel, OriginLab, DasyLab, Vinci, MiniTab, Pulse and more
- ◆ **Software for data presentation:** extensive hands-on experience with Word, PowerPoint, Illustrator and more
- ◆ **Software for modeling and simulation:** extensive hands-on experience with PyMol and NEURON simulation environment
- ◆ **Laboratory animal science:** expert knowledge (FELASA Type B)
- ◆ **Experience in DFG grant proposal development, writing and revision**



## Professional memberships

- ◆ **Gesellschaft für Biochemie und Molekularbiologie (GBM)**
- ◆ **Neurowissenschaftliche Gesellschaft (NWG)**



## Publications

- 2014 ◆ Dibué M, Kamp MA, **Neumaier F**, Steiger HJ, Hänggi D, Hescheler J, Schneider T (2014) Cardiac phenomena during kainic-acid induced epilepsy and lamotrigine antiepileptic therapy. *Epilepsy Research* 108(4):666-74.
- 2015 ◆ Drobinskaya I\*, **Neumaier F\***, Pereverzev A, Hescheler J, Schneider T (2015) Diethyldithiocarbamate-mediated zinc ion chelation reveals role of Ca<sub>v</sub>2.3 channels in glucagon secretion. *Biochim Biophys Acta Mol Cell Res.* 1853(5):953-964.
- ◆ **Neumaier F**, Dibué-Adjei M, Hescheler J, Schneider T (2015) Voltage-gated calcium channels: Determinants of channel function and modulation by inorganic cations. *Progress in Neurobiology* 129:1-36.
- 2017 ◆ Tevoufouet EE, Nembo EN, Distler F, **Neumaier F**, Hescheler, Nguemo F, Schneider T (2017) Multiple nickel-sensitive targets elicit cardiac arrhythmia in isolated mouse hearts after pituitary adenylate cyclase-activating polypeptide-mediated chronotropy. *Pharmacological Research* 117:140-147.
- ◆ **Neumaier F**, Paterno M, Alpdogan S, Tevoufouet EE, Schneider T, Hescheler J, Albanna W (2017) Surgical approaches in psychiatry: A survey of the world literature on psychosurgery. *World Neurosurgery* 97:603–634.
- ◆ Albanna W, Lüke JN, Sjapic V, Kotliar K, Hescheler J, Clusmann H, Sjapic S, Alpdogan S, Schneider T, Schubert GA, **Neumaier F** (2017) Electoretinographic assessment of inner retinal signaling in the isolated and superfused murine retina. *Current Eye Research* 42:1518–1526.
- ◆ **Neumaier F**, Alpdogan S, Hescheler J, Schneider T (2017) A practical guide to the preparation and use of metal ion-buffered systems for physiological research. *Acta Physiologica* 222(3).
- 2018 ◆ Albanna W\*, **Neumaier F\***, Lüke JN, Kotliar K, Conzen C, Lindauer U, Hescheler J, Clusmann H, Schneider T\*, Schubert GA\* (2018) Unconjugated bilirubin modulates neuronal signaling only in wild-type mice, but not after ablation of the R-type/Ca<sub>v</sub>2.3 voltage-gated calcium channel. *CNS Neuroscience & Therapeutics* 24(3).
- ◆ **Neumaier F**, Alpdogan S, Hescheler J, Schneider T (2018) Protein phosphorylation maintains the normal function of cloned human Ca<sub>v</sub>2.3 channels. *Journal of General Physiology* 150(3): 491-510.
- ◆ **Neumaier F**, Akhtar-Schäfer I, Lüke JN, Dibué-Adjei M, Hescheler J, Schneider T (2018) Reciprocal modulation of Ca<sub>v</sub>2.3 voltage-gated calcium channels by copper(II) ions and kainic acid. *Journal of Neurochemistry* 147: 310-322.
- ◆ **Neumaier F**, Paterno M, Alpdogan S, Tevoufouet EE, Schneider T, Hescheler J, Albanna W (2018) In Reply to "Corpus Callosotomy for Drug-Resistant Schizophrenia; Novel Treatment Based on Pathophysiology". *World Neurosurgery* 116: 485.
- ◆ Schneider T, Alpdogan S, Hescheler J, **Neumaier F** (2018) *In vitro* and *in vivo* phosphorylation of the Ca<sub>v</sub>2.3 voltage-gated R-type calcium channel. *Channels* 12(1): 326-334.
- 2019 ◆ Albanna W, Lüke JN, Schubert GA, Dibué-Adjei M, Kotliar K, Hescheler J, Clusmann H, Steiger HJ, Hänggi D, Kamp MA, Schneider T, **Neumaier F** (2019) Modulation of Ca<sub>v</sub>2.3 channels by unconjugated bilirubin (UCB) - Candidate mechanism for UCB-induced neuromodulation and neurotoxicity. *Molecular and Cellular Neuroscience* 96: 35-46.

\* equal contribution



2020

- ◆ Alpdogan S, **Neumaier F**, Dibué M, Hescheler J, Schneider T (2019) Intracerebroventricular administration of histidine reduces kainic acid-induced convulsive seizures in mice. *Experimental Brain Research* 237: 2481-2493.
- ◆ Alpdogan S, **Neumaier F**, Hescheler J, Albanna W, Schneider T (2020) Experimentally induced convulsive seizures are modulated in part by zinc ions through the pharmacoresistant Ca<sub>v</sub>2.3 calcium channel. *Cellular Physiology and Biochemistry* 54: 180-194.
- ◆ Müller-Thomsen L, Borgmann D, Morcinek K, Schröder S, Dengler B, Moser N, **Neumaier F**, Schneider T, Schröder H, Huggenberger S (2020) Consequences of hyperphosphorylated tau on the morphology and excitability of hippocampal neurons in aged tau transgenic mice. *Neurobiology of Aging* (in press).
- ◆ Lüke JN, **Neumaier F**, Alpdogan S, Hescheler J, Schneider T, Albanna W, Akhtar-Schäfer I (2020) Submicromolar copper(II) ions stimulate transretinal signaling in the isolated retina from wildtype but not from Ca<sub>v</sub>2.3-deficient mice. *BMC Ophthalmology* 20(1): 182.
- ◆ **Neumaier F**, Alpdogan S, Hescheler J, Schneider T (2020) Zn<sup>2+</sup>-induced changes in Ca<sub>v</sub>2.3 channel function: An electrophysiological and modeling study. *Journal of General Physiology* 152(9): e202012585.
- ◆ Zlatopolskiy BD, **Neumaier F**, Rüngeler T, Drewes B, Kolks N, Neumaier B (2020) Preparation of a first <sup>18</sup>F-labeled agonist for M<sub>1</sub> muscarinic acetylcholine receptors. *Molecules* 25(12): 2880.



## Talks and posters

2011

- ◆ Tevoufouet E, Galetin T, **Neumaier F**, Hescheler J, Schneider T (2011) Pharmacoresistant voltage-gated Ca<sup>2+</sup> channels in the murine heart. 90. *Jahrestagung der Deutschen Physiologischen Gesellschaft*, 26.03.-29.03.2011. Regensburg, Deutschland.

2014

- ◆ **Neumaier F**, Dibué M, Steiger HJ, Schneider T, Kamp MA, Hänggi D (2014) Modulation of recombinant human Ca<sub>v</sub>2.3 calcium channels by hemolysate and bilirubin. 65. *Jahrestagung der Deutschen Gesellschaft für Neurochirurgie*, 11.05.-14.05.2014. Dresden, Deutschland.
- ◆ Schneider T, **Neumaier F**, Tevoufouet E, Hescheler J, Kamp MA, Dibué M (2014) Kainate – Role of pharmacoresistant Ca<sub>v</sub>2.3 calcium channels: functional and pathophysiological implications. *FENS 2014*, 05.07.-09.07.2014. Milan, Italien.
- ◆ Morcinek K, Dengler B, **Neumaier F**, Schneider T, Walkowiak W, Schröder H, Götz J, Huggenberger S (2014) Preliminary electrophysiological characterization of hippocampal CA1 neurons in a mouse model of tauopathy. *Neuroscience 2014*, 15.12-19.12.2014. Washington DC, USA.

2015

- ◆ Akhtar I, **Neumaier F**, Hescheler J, Schneider T (2015) Effects of endogenous and exogenous d-block metal ions on neuronal transmission in the isolated and perfused vertebrate retina. 66. *Mosbacher Kolloquium*, 26.03.-28.03.2015. Mosbach, Deutschland.
- ◆ **Neumaier F**, Akhtar I, Dibué-Adjei M, Hescheler J, Schneider T (2015) Reciprocal modulation of recombinant Ca<sub>v</sub>2.3 voltage-gated calcium channels by copper(II) ions and kainic acid. 11. *Jahrestagung der Deutschen Neurowissenschaftlichen Gesellschaft*. 18.03.-21.03.2015. Göttingen, Deutschland.